Hydrothermal Alteration and Lithogeochemistry of the Boundary Volcanogenic Massive Sulfide (VMS) Deposit, Central Newfoundland, Canada

By Michael Buschette

A Thesis submitted to the School of Graduate Studies

in partial fulfillment of the requirements for the degree of

Master of Science, Department of Earth Sciences

Memorial University of Newfoundland

March 2015

St. John’s, Newfoundland and Labrador

Abstract

The Boundary volcanogenic massive sulfide (VMS) deposit (0.45 Mt @ 3.4% Cu, 4.0% Zn, 1.0 % Pb, 34 g/t Ag) is located in the Tally Pond group (~510 Ma), central Newfoundland, Canada. The deposit is hosted by rhyolitic rocks that are interpreted to have formed within a rifted continental arc on the leading edge of Ganderia. Mineralization consists of massive pyrite, chalcopyrite, and sphalerite lenses. The basal portion of these lenses contain lapilli tuff clasts indicative of replacement style mineralization. Three hydrothermal alteration assemblages are recognized at Boundary: quartz-sericite, chlorite-sericite, and intense chlorite. Lithogeochemical data are useful in identifying key element associations and alteration assemblages. Short-wave infrared (SWIR) spectroscopy data provide an effective vector for Zn mineralization and correlate with whole rock geochemistry. Lithogeochemical and SWIR data have been used to recreate a three-dimensional alteration model of the Boundary deposit that may be useful in further mineral exploration.

Acknowledgments

This thesis has been immensely improved through the help of many. First and foremost, I would like to thank my advisor, Dr. Stephen Piercey for his endless guidance and support. His enthusiasm and relentless sense of humor helped make this an extremely enjoyable project. I would like to thank Dr. Derek Wilton for being on my committee and reviewing this manuscript. Suggested revisions from external examiners, Dr. Graham Layne and Dr. John Hinchey, are also greatly appreciated. The following people provided valuable advice and a number of extremely insightful conversations: Jean-Luc Pilote, Stefanie Lode, Jonathan Cloutier, Shannon Guffey, Praise Nyade and Shannon Gill.

This project was made possible by Teck Resources, who provided logistical support and allowed me to study the Boundary deposit. Teck Resources also provided me with countless resources and valuable experience. Specifically, I'd like to thank Gerry Squires, Darren Hennessey, and Andrew Sheppard.

Financial support for this project was provided by Dr. Piercey through a Natural Sciences and Engineering Research Council (NSERC) Discovery Grant and the NSERC-Altius Industrial Research Chair in Mineral Deposits Supported by NSERC, Altius Resources Inc., and the Research and Development Corporation of Newfoundland and Labroador. Secondary funding was provided by a Society of Economic Geologists (SEG) Fellowship and SEG Research Grant.

Last but certainly not least, I would like to thank my friends and family back home for their never-ending support. My parents, John and Rae, and siblings, Kady and Josh, have provided me with the drive and motivation to pursue a graduate degree. And most of all, I'd like to thank my fiancé, Stephanie, whose unwavering confidence and patience has allowed me dedicate the time needed to complete this project.

Table of Contents

List of Tables

Chapter 1

Chapter 2

List of Figures

Chapter 1

Chapter 2

List of Abbreviations

AAT	Annieopsquotch Accretionary Tract
AI	Hashimoto alteration index
Alt	Alteration
A.N.D. Co.	Anglo Newfoundland Development Company
Ana	Anatase
aq	Aqueous
Arg	Argillite
Ave	Average
BBL	Baie Verte Brompton Line
BX	Breccia
BVOT	Baie Verte Oceanic Tract
Carb	Carbonate
CC	Chaotic carbonate
Ccp	Chalcopyrite
CCPI	Chlorite-carbonate-pyrite alteration index
Chl	Chlorite
cm	Centimeter
CREAIT	Core Research Equipment and Instrument Training
DBL	Dog Bay Line
DF	Dover Fault
EDX	Energy Dispersive X-Ray
Eq	Equation
EPMA	Electron probe microanalysis
Fig(s)	Figure(s)
Frag(s)	Fragment(s)
FW	Footwall
g/t	Grams per ton
Gal	Galena
GBF	Green Bay fault
Gpa	Giga pascal
HFSE	High field strength elements
Hg-FIMS	Mercury-flow injection mercury system
HREE	Heavy rare earth elements

HW	Hanging wall
ICP-ES	Inductively coupled emission-mass spectroscopy
ICP-MS	Inductively coupled plasma-mass spectrometry
Int	Intrusion
Int Chl	Intense chlorite
km	Kilometer
Kspar, K-feldspar	Potassium feldspar
LBOT	Lushs Bight Oceanic Tract
LCF	Lobster Cove fault
LFSE	Light field strength elements
LOI	Loss on ignition
LREE	Light rare earth elements
LRF	Lloyds River fault
Lt	Lapilli tuff
m	Meters
mm	Millimeter
Mon	Monazite
MS	Massive sulfide
Mt	Million tonnes
nm	Nanometers
PCA	Principal component analysis
Pheno(s)	Phenocryst(s)
ppb	Parts per billion
ppm	Parts per million
Py	Pyrite
Qtz	Quartz
REE	Rare earth elements
RIL	Red Indian Line
SEM-BSE	Scanning electron microscope back scatter electron
Ser	Sericite
Sph	Sphalerite
SWIR	Short-wave infrared
VMS	Volcanogenic massive sulfide
WL	wavelength
wt %	Weight percent
Xcutting	Crosscutting
2D, 3D	Two, three dimensional

List of Appendices

Chapter 1: Introduction to the Boundary volcanogenic massive sulfide deposit, central Newfoundland, Canada

The Exploits Subzone represents the peri-Gondwanan remnants of the ancient Iapetus Ocean and is composed of continental and intra-oceanic, arc-back arc, and ophiolite complexes (Williams et al., 1988). The subzone is host to a number of volcanogenic massive sulfide (VMS) deposits in a region known as the Victoria Lake Supergroup, in central Newfoundland (Williams, et al., 1988; Swinden, 1991; Evans and Kean, 2002; Piercey and Hinchey 2012). Within the Victoria Lake supergroup, the Tally Pond group hosts the Duck Pond and Boundary bimodal felsic VMS deposits (combined tonnage of 4.1 Mt @ 3.3% Cu, 5.7% Zn, 0.9% Pb, 59 g/t Ag, and 0.8 g/t Au; Squires and Moore, 2004; Piercey and Hinchey, 2012; Piercey et al., 2014). Various regional and deposit scale studies have been undertaken on these deposits, mostly focusing on the general setting and stratigraphy of mineralization (i.e., Squires et al., 2001; Squires and Moore, 2004; Piercey et al., 2014). Despite the regional and deposit-specific research, no detailed study of the petrology, chemostratigraphy, and 2D-3D alteration, alteration mineralogy, or lithogeochemistry has been undertaken. This is the primary objective of this thesis. The following sections provide background information on the exploration history of the area, regional tectonic and geological setting, local geology, and a review of the geology of VMS deposits.

1.1-Exploration History

In 1871 Alexander Murray of the Geological Survey of Newfoundland undertook a general geological survey of the area. The findings of Murray's survey were followed up by the Anglo Newfoundland Development Company (A.N.D.Co.) who, in 1905, secured a 99-year resource lease that included timber, water, and mineral rights to an area over 3,700 km^2 (Evans and Kean, 2002). Intense exploration by A.N.D.Co and partners led to the discovery of the Buchans Mine and several other promising prospects in the early 1900s. Through a series of partnerships and acquisitions, Noranda entered into a joint exploration agreement with Abitibi-Price in 1979, and this led to the discovery of the Boundary (1981) and Duck Pond (1987) VMS deposits (Evans and Kean, 2002). In 1993 Noranda purchased the mineral rights to both the Duck Pond and Boundary deposits along with many other prospects in the region. After five years of further exploration, Noranda gave up its rights to low mineral potential properties and sold the more promising prospects to several junior exploration companies (Evans and Kean, 2002). Thundermin Resources purchased the rights to the Duck Pond and Boundary deposits in March 1999. Upon the completion of feasibility studies for both deposits, Thundermin Resources sold the rights of Duck Pond and Boundary to Aur Resources in 2002, which began mining Duck Pond in 2007 (Evans and Kean, 2002; Mineral Information, 2007). Later in 2007, Teck Cominco (now Teck Resources) purchased 93% of Aur Resources (Teck News Release 2007) and is the current owner of the Duck Pond and Boundary deposits, which are now undergoing closure and reclamation.

1.2 Tectonic Evolution and Regional Geology

The Appalachian orogeny in Newfoundland is divided into four tectonostratigraphic zones based upon rock type, age, geophysical signatures, and metallogeny (Wiliams, 1979; Williams et al., 1988; Williams, 1995). From west to east, these zones are the Humber Zone, Dunnage Zone, Gander Zone, and the Avalon Zone (Fig. 1.1). These zones represent a sequence of arcs, back arcs, ophiolite sequences, and rifted blocks generated by the opening and closing of both the Iapetus and Rheic oceans during the Taconic, Penobscot, Salinic, Acadian, and Neo-Acadian orogenies (Williams, 1979; Swinden, 1991; van Staal et al., 1998; Zagorevski et al., 2010).

The Taconic Orogeny is divided into three separate events, which took place from the late Cambrian (~500 Ma) until the late Ordovician (~450 Ma), and occured within the Laurentian Humber Zone and the peri-Laurentian side of the Dunnage Zone (Fig. 1.2)(van Staal et al., 2007). The first event (500-493 Ma) was the accretion of the Lushs Bight Oceanic Tract (LBOT) onto the Dashwoods microcontinent as the Taconic Seaway closed (van Staal et al., 2007). This was followed by the obduction of the Baie Verte Oceanic Tract (BVOT) onto the Humber margin as the Taconic Seaway finished closing (~488-460 Ma). The third event (~460-450 Ma) involved the collision the Annieopsquotch Accretionary Tract (AAT), which represents the leading edge of the peri-Laurentian margin, with the Victoria Arc, the leading edge of peri-Gondwana margin (van Staal et al., 2007; Zagorevski et al., 2007b).

The Penobscot Orogeny roughly coincided with the Taconic Orogeny though there is no direct link between the two orogenic events as there were over 2,500 km separating peri-Gondwanan and peri-Laurentian crustal fragments on opposite sides of the Iapetus Ocean (van Staal and Zagorevski, 2012). Extension resulted in the separation of the Penobscot arc from the edge of Gondwana (~509-501 Ma), which created the Rheic Ocean (Neuman, 1967; Colman-Sadd et al., 1992; van Staal and Zagorevski, 2012). The Penobscot arc then began to undergo back-arc extension (~500-485 Ma), which separated the Penobscot arc from the Gander margin until terminal closure (486-478 Ma)(Fig. 1.3)(Colman-Sadd et al., 1992; Zagorevski, et al., 2010).

As subduction continued to close the Iapetus Ocean, a collision between the younger, more buoyant Victoria Arc and the older, denser Penobscot Arc left the Victoria Arc emplaced above the Penobscot Arc (van Staal et al., 2007; Zagorevski, 2007b). Further subduction closed the Iapetus Ocean permanently as the peri-Laurentian AAT collided with the peri-Gondwanan Victoria Arc (460-455 Ma)(van Staal et al., 2007).

The Dunnage Zone of the Appalachians represents the vestiges of the Iapetus Ocean and remnants of continental and intra-oceanic, arc, back-arc, and ophiolite complexes that developed during the third Taconic event and the Penobscot Orogeny (Williams et al., 1988; Swinden, 1991; Zagorevski et al., 2007a). It is divided into two subzones: the Notre Dame Subzone (peri-Laurentian margin) and the Exploits Subzone (peri-Gondwanan margin)(Williams et al., 1988; Williams, 1995; Zagorevski, 2007b). These subzones are juxtaposed against one another along the Red Indian Line, a suture that represents the accretion of peri-Gondwanan and peri-Laurentian elements (~460-455 Ma)(van Staal et al., 1998; van Staal et al., 2007; Zagorevski, 2007a; Zagorevski, 2007b).

The Victoria Lake supergroup is situated east of the Red Indian Line within the Exploits Subzone (Fig. 1.4). It is bound to the east by the Noel Paul's Line, and to the northeast, it is overlain or in fault contact with Ordovician to Silurian sedimentary rocks of the Badger Group (Zagorevski et al., 2007b). Initially the Victoria Lake supergroup was divided into two main volcanic belts: the Tally Pond and Tulks volcanic belts; however, more detailed geochronological, lithological, and geochemical studies have resulted in the division into six fault-bound packages (Kean and Jayasinghe, 1980; van Rogers et al., 2005; Zagorevski et al., 2007b; Zagorevski et al., 2010). From west to east, these groups are the Wigwam Brook group (~453 Ma)(Zagorevski et al., 2007b), the Pats Pond group (~488 Ma)(Zagorevski et al., 2007b), the Sutherlands Pond group (~462 Ma)(Dunning et al., 1987), the Tulks group (~498 Ma)(Evans et al., 1990; Evans and Kean, 2002), the Long Lake group (~506 Ma)(Zagorevski, et al., 2007b), and the Tally Pond group (~513-509 Ma) (Dunning et al., 1991; McNicoll et al., 2010).

The Tally Pond group, host to the Boundary deposit, is further broken down into two separate formations: the Lake Ambrose formation and Bindon's Pond formation (Fig. 1.5)(Evans and Kean, 2002; Rogers and van Staal, 2002; Squires and Moore, 2004). The Lake Ambrose formation (~513 Ma) is a sequence of basalt-dominated pillowed and massive flows with minor felsic and sedimentary rocks (Evans and Kean, 2002; McNicoll et al, 2010; Piercey et al., 2014). The Bindon's Pond formation (~509 Ma) is predominantly comprised of felsic breccia, tuffs, quartz porphyry, crystal tuff, and flow-banded rhyolite and hosts the Duck Pond, Boundary, and Lemarchant VMS deposits

(Evans and Kean, 2002; Rogers and van Staal, 2002; Squires and Moore, 2004; Rogers et al., 2005).

1.3 Volcanogenic Massive Sulfide (VMS) Deposits

Volcanogenic massive sulfide (VMS) deposits are accumulations of Zn-Pb-Cu-(Ag-Au)-bearing sulfide deposits that form at or near the seafloor and are associated with contemporaneous, submarine volcanism in a subaqueous environment (Franklin et al., 1981, 2005; Lydon 1984, 1988; Large, 1992; Barrie and Hannington, 1999; Galley et al., 2007). They form in a variety of tectonic environments, including mid-ocean ridges, intraoceanic and continental arcs, and back-arc basins; and in all cases, they form in extensional environments associated with high heat flow (Franklin et al., 1981, 2005; Lydon 1984, 1988; Large, 1992; Barrie and Hannington, 1999; Galley et al. 2007). The deposits typically occur as polymetallic, massive sulfide lenses containing Cu, Zn, Pb, Au, and Ag that form through the precipitation of metals from heated hydrothermal fluids as they mix with cool seawater (i.e., Franklin et al., 1981, 2005; Lydon 1984, 1988; Large, 1992; Barrie and Hannington, 1999; Galley et al., 2007). In addition to typical exhalative-type deposition, the Boundary deposit exhibits textures indicative subseafloor replacement deposition (Piercey et al., 2014).

Volcanogenic massive sulfide deposits are divided into six groups based on the lithology of the main volcanic or sedimentary units present at the time of deposition (Table 1; Barrie and Hannington, 1999; Franklin et al., 2005; Galley et al., 2007; Gibson et al., 2007). The Boundary deposit is a bimodal-felsic VMS deposit (Fig. 1.6), as are many deposits within the Dunnage Subzone (Piercey, 2007, McNicoll et al., 2008;

Piercey and Hinchey, 2012). Bimodal-felsic deposits are polymetallic and typically exhibit high base metal grades, especially for Zn and Pb (Galley et al., 2007; Franklin et al., 2005). The Boundary and Duck Pond deposits also show elevated Cu concentrations, up to 3.3%, in comparison to other Canadian bimodal felsic VMS deposits (Table 1).

Volcanogenic massive sulfide deposits have extensive zones of hydrothermal alteration that vary in mineralogy, shape, and size. Alteration mineralogy and composition varies with proximity to mineralization. Hydrothermal alteration associated with bimodal-felsic deposits can be divided into pipe-like or discordant alteration and semi-conformable or recharge-related alteration (Riverin and Hodgson, 1980; Franklin et al., 1981, 2005; Gemmell and Large, 1992; Large, 1992; Galley, 1993, Piercey, 2009).

Semi-conformable alteration results from lateral fluid flow as seawater is drawn down through fractures. As the water is heated, it interacts with footwall rocks leaching metals and certain other elements at different temperatures (Galley, 1993). The stacking of hydrothermal alteration zones with different mineralogy is a function of the geothermal gradient, often forming zones of spilitization, silicification, epidote-quartz, and carbonatization/potassic alteration (Galley, 2003; Piercey, 2009). Semi-conformable alteration is generally patchy but can extend laterally up to a couple hundred kilometers (Galley, 1993; Franklin et al., 2005).

Pipe-like alteration develops as heated hydrothermal fluids are discharged through vents and crosscuts stratigraphy (Fig. 1.6)(Riverin and Hodgson, 1980; Franklin et al., 1981; Piercey, 2007). The resulting alteration zone is often constrained to only a few hundred meters wide and is controlled by synvolcanic fault structures (Riverin and

Hodgson, 1979; Lydon, 1984, 1988; Gemmell and Large, 1992; Franklin et al., 2005; Galley et al., 2007; Piercey 2007). Chlorite-quartz alteration makes up the innermost zone that gives way to a middle chlorite-sericite zone, and eventually grades to an outer sericite-quartz zone (Riverin and Hodgson, 1980; Franklin et al., 1981, 2005; Lydon, 1984; Lydon, 1988; Galley et al., 2007).

1.4 Deposit Geology

The Boundary deposit consists of three separate sulfide lenses, the North zone, South zone, and Southeast zone and contains approximately 0.45 Mt grading 3.5% Cu, 4.0% Zn, 1.0% Pb, and 34.0 g/t Ag (Fig. 1.7)(Squires and Moore, 2004; Piercey and Hinchey, 2012; Piercey et al., 2014). Regional studies and recent airborne magnetic studies show that the North zone and South zone lenses are separated by the Wagner fault (Wagner, 1993; Hennessey, pers. comm.).

Stratigraphically, the Boundary deposit occurs at the contact between an impermeable hanging wall consisting of flow-banded rhyolite flows and breccia, and a permeable footwall made up primarily of felsic lapilli tuff and lesser tuff (Piercey and Hinchey 2012; Piercey et al., 2014). Below the lapilli tuff are interlayered, aphyric rhyolite flows, flow breccias, and aphyric rhyolite jigsaw-fit breccias. The jigsaw-fit breccias are similar to those found in the Duck Pond deposit (Squires and Moore, 2004; Piercey et al., 2014). Deeper in the stratigraphy, pillow basalts are interlayered with aphyric rhyolites and breccias (Piercey and Hinchey, 2012; Piercey et al., 2014). An altered, quartz-feldspar porphyritic intrusion cross-cuts all units in a similar manner as observed at the Duck Pond deposit (Piercey and Hinchey 2012; Piercey et al., 2014).

Mineralization in each of the three lenses is relatively consistently comprised of Cu-Zn massive sulfide mineralization, dominated by chalcopyrite and sphalerite, with variable pyritic sulfides and minor galena (McNicoll et al., 2010; Piercey and Hinchey 2012; Piercey et al., 2014). The mineralization occurs at the hanging wall-footwall contact and locally extends into the porous lapilli tuff for approximately 10 meters (Piercey and Hinchey 2012; Piercey et al., 2014). The lenses are comprised of a series of conformable to semi-conformable stacked sheets that center around synvolcanic structures, resulting in a tree-branch-type morphology (Piercey and Hinchey 2012; Piercey et al., 2014). Mineralization displays five main facies (Piercey and Hinchey 2012; Piercey et al., 2014):

1) stringer sulfides with clasts;
2) clast-rich massive sulfides;
3) massive pyritic sulfides with chalcopyrite stringers;
4) chalcopyrite-sphalerite-rich massive sulfide;
5) bedded sulfides

The abundance of clast-rich mineralization has led to the interpretation that mineralization formed by both replacement and exhalation processes (Squires and Moore, 2004; McNicoll et al., 2010, Piercey and Hinchey 2012; Piercey et al., 2014).

Alteration consists predominantly of chlorite, variably intense quartz-sericite, and carbonate that occurs in both the hanging wall and footwall (McNicoll et al., 2010; Piercey and Hinchey 2012; Piercey et al., 2014). The footwall exhibits all three types of alteration. The lapilli tuff unit provides the best measure of alteration as it ranges from being relatively fresh, to quartz-sericite altered, to quartz-sericite-chlorite altered, to intense chlorite altered with "chaotic carbonate" or dolomite (Piercey and Hinchey 2012; Piercey et al., 2014). Intense chlorite alteration occurs in discrete vertical zones thought to represent feeder pipes running along the synvolcanic structures that fed the replacement style mineralization (Piercey and Hinchey 2012; Piercey et al., 2014). The hanging wall alteration is less diverse and is dominated by patchy quartz-sericite alteration with minor chlorite (Piercey and Hinchey 2012; Piercey et al., 2014). Spotty iron carbonate alteration is found throughout the region, in the Boundary, Duck Pond, and Lemarchant deposits as an overprint thought to be related to either a late VMS hydrothermal activity or a younger regional metamorphism (van Staal et al, 2007; Piercey and Hinchey 2012; Piercey et al., 2014).

Limited lithochemical analyses have been performed on the Boundary deposit rocks. The most recent by Piercey et al. (2014) consisted of two downhole lithogeochemical profiles from holes thought to be representative of the hydrothermal alteration. A majority of the samples show strong Na_2O depletions along with high Hashimoto and chlorite-carbonate-pyrite indices (Piercey and Hinchey, 2012; Piercey et al., 2014). The "Duck Pond alteration signature" (Collins, 1989), defined by anomalous Hg contents and high Hg/Na_2O and Ba/Sr, is also present at the Boundary deposit (Piercey et al., 2014). Limited immobile element analyses revealed signatures of LREE enrichment, flat HREE, and negative Nb, Ti, and Eu anomalies, petrogenetic signatures common in arc environments or re-melted arc basement (Piercey, 2011; Piercey et al., 2014).

1.5 Thesis Objectives

Though the Boundary deposit was discovered over thirty years ago, a complete thorough study of this deposit's alteration signature has never been undertaken. An in-depth study of the stratigraphy, alteration type and distribution, and lithogeochemistry will be used herein to understand the controls on alteration and deposit formation in order to create a detailed deposit model. The main objectives are as follows:

1) build upon the stratigraphic work of Piercey et al. (2014) and study the lithofacies and their relationship to various alteration zones;
2) document the mineralogy and spatial distribution of alteration within the deposit through graphic core logging, petrography, lithogeochemistry, and infrared spectroscopy. This will lead to a constrained hydrothermal alteration distribution model for the deposit;
3) map mineralogical variations and compositional variations among micas and chlorite by utilizing short-wave infrared (SWIR) spectroscopy;
4) understand textural and compositional variations among the different alteration facies to gain a better understanding of alteration history and ore deposition;
5) utilize lithogeochemistry to obtain a chemostratigraphy for the deposit. This can be used to calculate mass changes and quantify elemental gains and losses associated with individual alteration zones;

6) combine all the above to create 2D and 3D representations of the deposit that may be used to create custom alteration indices for other mineralized zones within the Tally Pond belt;
7) determine what factors influenced ore formation. This will aid in understanding why alteration is more heavily concentrated in certain areas and why sulfides were deposited where they were; and
8) use the stratigraphic findings and textural evidence to determine the order of events that led to the deposition of the Boundary deposit.

1.6 Methods

A comprehensive model of the Boundary deposit will be defined using the following methods: 1) identification of stratigraphic units and alteration assemblages documented in drill core; 2) careful sample selection that encompasses all alteration types and lithologies followed by thin section petrography and scanning electron microscope (SEM) analyses, major and trace element analyses, and hyperspectral analysis; 3) 2D-3D modeling of the alteration and lithogeochemistry of the Boundary deposit. A detailed description of each analysis is described below.

1.6.1 Core Logging

Detailed drill hole logging took place during August-September 2013 and June 2014 at the Duck Pond core storage area. A total of 62 holes were logged in a manner that allowed for complete coverage of the North and South zones (Fig. 1.7). Entire holes were logged (~50 m) in which lithology, mineralization, and alteration were documented. Hand-drawn core logs were created in the field with detailed notes and photographs.

Core logs were later digitized using Adobe Illustrator software (Appendix A). A series of 2-D fence diagrams was also created in which the alteration was extrapolated between holes in order to gain a better understanding of the alteration surrounding the Boundary deposit (Chapter 2).

A total of 237 samples from 51 drill holes were selected based on major lithology or alteration intensity/assemblage changes. Samples (~10 cm) were halved using a water-cooled rock saw in the Core Research Equipment and Instrument Training (CREAIT)-TERRA facility at Memorial University and subsequently photographed before being cut to size for thin sections and geochemistry. All samples also underwent hyperspectral analyses. The results are discussed in Chapter 2.

1.6.2 Lithogeochemistry

All samples were analyzed for major elements and trace elements, rare earth elements, base metals, and trace metals. Samples were sent to Actlabs in Ancaster, Ontario to analyze major oxides and select trace elements. Prior to shipment, the samples were cut to size and washed to avoid cross-contamination. Samples were crushed and pulverized using mild steel at Actlabs. The samples were analyzed using a pre-analysis lithium metaborate/tetraborate fusion, dissolution of the fused bead in nitric acid, and subsequent analysis using inductively coupled plasma emission spectroscopy (ICP-ES). Mercury analyses were also undertaken at Actlabs using cold vapor flow injection mercury spectrometer (CV-FIMS) where a sample is digested with aqua regia to leach out soluble compounds and then analyzed by CV-FIMS. Other trace elements, including rare earth elements, high field strength elements, and volatile metals were obtained at

Memorial University using multi-acid digestion and sodium peroxide dissolution with subsequent analyses of solutions by inductively coupled plasma mass spectrometry (ICP-MS)(see Chapter 2).

1.6.3 Petrography and Scanning Electron Microscopy

A total of 45 samples were cut down to standard microscope slide size (25 mm x 45 mm) before being sent to Vancouver Petrographics, in October 2013, for polished thin sections to be made. Polished thin sections were fabricated for samples that exhibited unique textures and representative lithologies or alteration types. Petrographic work was carried out using a Nikon LV100POL polarizing microscope at Memorial University. Basic petrography, mineral assemblages, and textures were documented using reflected and transmitted light. Scanning electron microscope (SEM) analyses were used to document finer scale textures, trace minerals, and semi-quantitative chemical information and textural relationships for sulfide phases. SEM analyses were undertaken at Memorial University's CREAIT-Micro-Analysis Facility, Bruneau Innovation Centre (MAF-IIC) using the FEI MLA 650F SEM. Characteristic mineral phases and textures were identified using backscatter electron imaging, whereas semi-quantitative compositional data were collected using point analyses and Energy Dispersive X-Ray (EDX) analysis mapping. The SEM analyses were critical in identifying all the mineral phases present within the Boundary deposit (Appendix E).

1.6.4 Short-wave Infrared (SWIR) Spectroscopy

Hyperspectral analysis using short wave infrared (SWIR) spectroscopy was used to map mineralogical variations in drill core samples and compositional variations in micas and chlorite throughout the deposit. Analyses were completed at Memorial University using a Terraspec™ mineral spectrometer with a Hi-Brite Muglight. Minimal sample preparation was needed as SWIR absorption spectra were collected from fresh drill core that had been recently cut and cleaned. Optimization and white references were collected every ~20 samples or 40 min to avoid drifts in data calibration. Analyses were only performed in a naturally sunlit room to avoid any interference from artificial lighting. Reference sample measurements were made after each optimization and white reference calibration to measure both precision and accuracy. Reflectance spectra were collected using the RS^3 Spectral Acquisition software. The resultant spectra were processed using The Spectral Geologist Hotcore (TSG) v 7.1.55 software in which the hull correction was applied. Hyperspectral scalars were calculated using a fourth order polynomial fitting curve applied over the ranges 2120-2245 nm (focused at 2180-2230 nm) for the AlOH wavelengths and 2230-2270 nm (focused at 2240-2260 nm) for FeOH. Spectral depth filters were applied to remove background noise: 0.015% for AlOH and 0.010% for FeOH. Due to the variable clast-matrix mineralogy, a minimum of three analyses per sample were made to ensure representative measurements. The SWIR absorption data for each sample are also reported in Appendix B.

1.6.5 Modeling of 2D-3D Alteration

Stratigraphy, lithofacies, and alteration zones were modeled in 2D and 3D. Additional lithogeochemical analyses (elemental gains and losses, metallurgical assays, alteration indices, etc.) were included to identify unique relationships throughout the deposit. Modeling was initially performed using the program Geosoft Target linked to

ArcGIS. Final models were produced using Leapfrog Geo^{TM}. Lithofacies zones were created using the logged drill hole data, ore zones used assay data, mass change interpolants used the mass change data from Appendix C. Hyperspectral data points are from Appendix B.

1.7 Co-Authorship Statement

The design of this research project is attributed to Dr. Stephen J. Piercey. The author conducted the primary research, which includes core logging, sample collection, and optical microscopy. The hyperspectral analysis, Geosoft Target, and Leapfrog Geo aspects of the project were conducted by the author with valuable assistance provided by Jonathan Cloutier. The Principal Component Analysis (PCA) was carried out by the author with assistance from Praise Nyade. Scanning electron microscopy was conducted by the author under the supervision of David Grant. The primary editor of this manuscript is Dr. Stephen J. Piercey, with secondary editing performed by Dr. Graham Layne and Dr. John Hinchey.

1.8 Thesis Presentation

This thesis consists of three chapters plus supplementary appendices. Chapter 1 serves as an introductory chapter that presents the purpose and format of this thesis by providing background information about the exploration history, regional and local geology, previous work on the deposit, and the methods used in this study.

Chapter 2 is the main body of the thesis and is intended for publication in *Economic Geology* or a similar scientific journal. This chapter contains detailed descriptions of the lithology and alteration assemblages. Through the use of various geochemical techniques and hyperspectral analysis, this chapter presents evidence pertaining to the tectonic setting, a complete deposit alteration model, and details on the Boundary deposit's evolution.

Chapter 3 is a summary of the conclusions drawn from Chapter 2 in addition to additional information provided in the appendices. This chapter also summarizes unresolved questions and directions for future research.

The appendices provide supplementary material not included in Chapter 2. They include digitized drill logs, complete geochemical and hyperspectral datasets, and a compilation of scanning electron microscope (SEM) analyses.

References

Aur Resources, Ltd. 2007. Duck Pond Mine, Official Ceremony, May 9, 2007. Company brochure. [For updated information see Teck Resources website — www.teck.com]

Barrie, C.T. and Hannington, M.D., 1999, Classification of volcanic-associated massive sulfide deposits based on host-rock composition: Reviews in Economic Geology, v. 8, p. 1-11.

Collins, C. J., 1989, Report on lithogeochemical study of the Tally Pond Volcanics and associated alteration and mineralization, Unpublished Report for Noranda Exploration Company Limited (Assessment File 012A/1033 Newfoundland Department of Mines and Energy, Mineral Lands Division): St. John's, Newfoundland, p. 87.

Colman-Sadd, S.P., Dunning, G.R., and Dec, T., 1992, Dunnage-Gander relationships and Ordovician orogeny in central Newfoundland: a sediment provenance and U/Pb study: American Journal of Science, v. 292, p. 317-355.

Doyle, M.G., and Allen, R.L., 2003, Subsea-floor replacement in volcanic-hosted massive sulfide deposits: Ore Geology Reviews, v. 23, p. 183-222.

Dunning, G.R., Kean, B.F., Thurlow, J.G. and Swinden, H.S., 1987, Geochronology of the Buchans, Roberts Arm, and Victoria Lake groups and Mansfield Cove Complex, Newfoundland: Canadian Journal of Earth Sciences, v. 24, p. 1175-1184.

Dunning, G.R., Swinden, H.S., Kean, B.F., Evans, D.T.W. and Jenner, G.A., 1991, A Cambrian island arc in Iapetus; geochronology and geochemistry of the Lake Ambrose volcanic belt, Newfoundland Appalachians: Geological Magazine, v. 128, p. 1-17.

Evans, D.T.W., and Kean, B.F., 2002, The Victoria Lake Supergroup, central Newfoundland - its definition, setting and volcanogenic massive sulphide mineralization, Newfoundland and Labrador Department of Mines and Energy, Geological Survey, Open File NFLD/2790, p. 68.

Evans, D.T.W., Kean, B.F., and Dunning, G.R., 1990, Geological Studies, Victoria Lake Group, Central Newfoundland. In Current Research, Newfoundland Department of Mines and Energy, Geological Survey Branch, Report 90-1, p. 131-144.

Franklin, J.M., Gibson, H.L., Jonasson, I.R., and Galley, A.G., 2005, Volcanogenic massive sulfide deposits: Economic Geology, 100th Anniversary Volume, p. 523–560.

Franklin, J.M., Lydon, J.W., and Sangster, D.F., 1981, Volcanic-associated massive sulfide deposits; in Skinner, B.J., ed., Economic Geology 75th Anniversary Volume: Society of Economic Geologists, p. 485-627.

Galley, A.G., 1993, Characteristics of semi-conformable alteration zones associated with volcanogenic massive sulphide districts: Journal of Geochemical Exploration, v. 48, p. 175-200.

Galley, A.G., Hannington, M.D. and Jonasson, I.R., 2007, Volcanogenic massive sulfide deposits: In Contributions to Mineral Resources of Canada: A Synthesis of Major Deposit Types, District Metallogeny, the Evolution of Geological Provinces, and Exploration Methods. Edited by W.D. Goodfellow and I.M. Kjarsgaard. Mineral Deposits Division, Geological Association of Canada.

Galley, A.G., and Jonasson, I.R., 2003, Classification and tectonic environments of VMS deposits in the Flin Flon mining camp, Manitoba: Geological Association of Canada/Mineralogical Association of Canada Annual General Meeting, Program with Abstracts (CD-ROM).

Gemmell, J.B., and Large, R.R., 1992, Stringer system and alteration zones underlying the Hellyer volcanic-hosted massive sulfide deposit, Tasmania, Australia: ECONOMIC GEOLOGY v. 87, p. 620–649.

Gibson, H.L., Allen, R.L., Riverin, G., Lane, T.E., 2007, The VMS Model: Advances and Application to Exploration Targeting. Plenary Session: Ore Deposits and Exploration Technology. Fifth Decennial International Conference on Mineral Exploration, p. 713-730.

Kean, B.F., and Jayasinghe, N.R., 1980, Geology of the Lake Ambrose (12-A/10)-Noel Paul's Brook (12-A/9) Map Areas, Central Newfoundland: Government of Newfoundland and Labrador, Department of Mines and Energy, Mineral Development Division, Report 80-02, 33 p., 2 maps.

Large, R.R. 1992, Australian volcanic-hosted massive sulfide deposits: Features, styles, and genetic models: ECONOMIC GEOLOGY, v. 87, p. 471–510.

Lydon, J.W., 1984, Volcanogenic sulphide deposits, Part 1, A descriptive model; Geoscience Canada, v. 11, p. 195-202.

Lydon, J.W., 1988, Ore deposit models: Volcanogenic massive sulfide deposits. Part 2: Genetic models: Geoscience Canada, v. 15, p. 43–65.

McNicoll, V., Squires, G.C., Kerr, A., Moore, P.J., 2008, Geological and Metallogenic Implications of U-Pb Zircon Geochronological Data from the Tally Pond Area, Central Newfoundland, Current Research, Report 08-1: Newfoundland and Labrador Department of Natural Resources, Geological Survey, p.173-192.

McNicoll, V., Squires, G.C., Kerr, A., Moore, P.J., 2010, The Duck Pond and Boundary Cu-Zn deposits, Newfoundland: new insights into the ages of host rocks and the timing of VHMS mineralization: Canadian Journal of Earth Science, v. 47, p 1481-1506.

Mineral Information, 2007. Department of Natural Resources: Mines Branch, Newfoundland and Labrador, v. 13, no. 1.

Moore, P. J., 2003, Stratigraphic implications for mineralization; preliminary findings of a metallogenic investigation of the Tally Pond Volcanics, central Newfoundland, in Pereira, C. P. G., Walsh, D. G., and Kean, B. F., eds., Current Research, Report 03-1: St. John's, NL, Geological Survey Branch, p. 241-257.

Neuman, R.B., 1967, Bedrock geology of the Shin Pond and Stacyville quadrangles, Maine. U.S. Geological Survey, Professional Paper 524-1, 47 pages.

Piercey, S. J., 2007, Volcanogenic massive sulphide (VMS) deposits of the Newfoundland Appalachians: An overview of their setting, classification, grade-tonnage data, and unresolved questions, in Pereira, C.P.G., and Walsh, D. G., eds., Current Research, Report 07-01: St. John's, NL, Geological Survey Branch, p. 169-178.

Piercey, S.J., 2009, Lithogeochemistry of volcanic rocks associated with volcanogenic massive sulphide deposits and applications to exploration, in Submarine Volcanism and Mineralization: Modern through Ancient, (eds.) B. Cousens and S.J. Piercey; Geological Association of Canada, Short Course 29-30 May 2008, Quebec City, Canada, p. 15-40.

Piercey, S.J., 2011, The setting, style, and role of magmatism in the formation of volcanogenic massive sulfide deposits: Mineralium Deposita, v. 46, p. 449-471.

Piercey, S.J., and Hinchey, J., 2012, Volcanogenic Massive Sulphide (VMS) Deposits of the Central Mobile Belt, Newfoundland, Geologic Association of Canada-Mineral Association of Canada. Field Trip Guidebook-B4, 56p.

Piercey, S.J., Squires, G.C., and Brace, T.D., 2014, Lithostratigraphic, hydrothermal, and tectonic setting of the Boundary volcanogenic massive sulfide deposit, Newfoundland Appalachians, Canada: Formation by subseafloor replacement in a Cambrian rifted arc: Economic Geology, v. 109, p. 661–87.

Riverin, G. and Hodgson, C.J., 1980, Wall-rock alteration at the Millenbach Cu-Zn mine, Noranda, Quebec: Economic Geology, v. 75, p. 424-444.

Rogers, N., and van Staal, C. R., 2002, Toward a Victoria Lake Supergroup; a provisional stratigraphic revision of the Red Indian to Victoria lakes area, central Newfoundland: Current Research - Newfoundland Geological Survey Branch, Report: 02-1, pp.185-195, Mar 2002.

Rogers, N., van Staal, C.R., Pollock, J., and Zagorevski, A., 2005, Geology, Lake Ambrose and Part of Buchans, Newfoundland (NTS 12-A/10 and Part of 12-A/15): Geological Survey of Canada Open-File 4544, scale 1:50,000.

Squires, G.C., Brace, T.D., and Hussey, A.M., 2001, Newfoundland's polymetallic Duck Pond deposit: Earliest Iapetan VMS mineralization formed within a sub-seafloor, carbonate-rich alteration system, *in* Evans, D.T.W., and Kerr, A., eds., Geology and mineral deposits of the northern Dunnage zone, Newfoundland Appalachians: St. John's, Newfoundland, Geological Association of Canada-Mineralogical Association of Canada, Field Trip Guide A2, p. 167–187.

Squires, G.C., and Moore, P.J., 2004, Volcanognic massive sulphide environments of the Tally Pond Volcanics and adjacent area; geological, lithogeochemical, and geochronological results, in Pereira, C. P. G., Walsh, D. G., and Kean, B. F., eds., Current Research, Report 04-1: St.John's, NL, Geological Survey Branch, p. 63-91.

Swinden, H.S., 1991, Paleotectonic settings of volcanogenic massive sulphide deposits in the Dunnage Zone, Newfoundland Appalachians: Canadian Institute of Mining and Metallurgy Bulletin, v. 84, p. 59-89.

Teck Cominco Ltd., 2007, Teck Cominco Acquires Approximately 93% of Aur Resources Common Shares. External News Release August 22, 2007. [For updated information see Teck Resources website-www.teck.com]

van Staal, C.R., Dewey, J.F., MacNiocaill, C., and McKerrow, S., 1998, The Cambrian-Silurian tectonic evolution of the northern Appalachians: history of a complex, southwest Pacific-type segment of Iapetus, in Blundell, D.J., and Scott, A.C., eds., Lyell: the Past is the Key to the Present: Geological Society, Special Publication 143, p. 199-242.

van Staal, C.R., and Zagorevski, A., 2012, Accreted Terranes of the Appalachian Orogen in Newfoundland: in the Footsteps of Hank Williams: Geologic Association of Canada-Mineral Association of Canada. Field Trip Guidebook –A1, 99p.

van Staal, C.R., Whalen, J.B., McNicoll, V.J., Pehrsson, S., Lissenberg, C.J., Zagorevski, A., van Breemen, O. and Jenner, G.A., 2007, The Notre Dame Arc and the Taconic Orogeny in Newfoundland. In 4-D Framework of Continental Crust. Edited by R.D. Hatcher, Jr., M.P. Carlson, J.H. McBride and J.R. Martinez Catalan. Geological Society of America Memoirs, v. 200, p. 511-552.

Wagner, D.W., 1993, Volcanic stratigraphy and hydrothermal alteration associated with the Duck Pond and Boundary volcanogenic massive sulphide deposits, Central Newfoundland: Unpublished MSc. thesis, Ottawa, Ontario, Canada, Carleton University, 430 p.

Williams, H., 1979, Appalachian Orogen in Canada: Canadian Journal of Earth Sciences, v. 16, p. 792-807.

Williams, H., 1995, Geology of the Appalachian-Caledonian Orogen in Canada and Greenland: Geological Survey of Canada, Geology of Canada No. 6, 952 p.

Williams, H., Colman-Sadd, S.P., and Swinden, H.S., 1988, Tectonostratigraphic subdivisions of central Newfoundland: Geological Survey of Canada, Current Research, Part B, Paper 88-1B, p. 91-98

Zagorevski, A., van Staal, C. R., and McNicoll, V. J., 2007a, Distinct Taconic, Salinic, and Acadian deformation along the Iapetus suture zone, Newfoundland Appalachians: Canadian Journal of Earth Sciences, v. 44, p. 1567-1585.

Zagorevski, A., van Staal, C. R., McNicoll, V. J., and Rogers, N., 2007b, Upper Cambrian to Upper Ordovician peri-Gondwanan island arc activity in the Victoria Lake Supergroup, central Newfoundland; tectonic development of the northern Ganderian margin: American Journal of Science, v. 307, p. 339-370.

Zagorevski, A., van Staal, C. R., Rogers, N., McNicoll, V. J., and Pollock, J., 2010, Middle Cambrian to Ordovician arc-backarc development on the leading edge of Ganderia, Newfoundland Appalachians: Geological Society of America Memoirs, v. 206, p. 367-396.

Table 1.1 Classification, type associations, and setting of VMS deposits

Type	Lithology	Tectonic Setting	Ore Grade*	Examples
Pelitic-Mafic	Mature back-arc successions with mafic sills (up to 25%). Less than 5% felsic volcanic rocks.	Sedimented mid-ocean ridges, transforms, or back-arcs	Cu: 1.6% Zn: 2.6% Pb: 0.36% Ag: 29 g/t Au: <0.9 g/t	Windy Craggy, Canada; Besshi district Japan
Back-Arc Mafic	Dominantly mafic flows with up to 10% felsic flows/domes. Mafic sills and dikes are common.	Mature intra-oceanic back-arcs	Cu: 3.2% Zn: 1.9% Pb: 0.0% Ag: 15 g/t Au: 2.5 g/t	South Urals, Russia; Semail, Oman
Bimodal-Mafic	Dominantly mafic flows with up to 25% felsic volcanic rocks.	Rifted oceanic arcs	Cu: 1.7% Zn 5.1% Pb: 0.6% Ag: 45 g/t Au: 1.4 g/t	Flin Flon, Canada; Tambo Grande, Peru
Bimodal-Felsic	Felsic volcanic rocks with 10-40% mafic flows and sills. Less than 10% terrigenous sediment. May exhibit subaerial or shallow water facies.	Continental margin arcs and related back-arcs	Cu: 1.3% Zn: 6.1% Pb: 1.8% Ag: 123 g/t Au: 2.2 g/t	Boundary, Newfoundland, Canada; Pontides, Turkey
Felsic Siliciclastitc	Siliciclastic rocks up to 75% with felsic volcanic rocks (up to 25%). Less than 10% mafic flows and sills. May exhibit subaerial or shallow water facies.	Mature epicontinental back-arcs	Cu: 1.0% Zn: 4.7% Pb: 2.0% Ag: 53 g/t Au: 0.9 g/t	Bathurst, Canada; Iberian Pyrite Belt, Spain
Hybrid Bimodal-Felsic	Felsic volcaniclastic and siliciclastic rocks.	Combinations of shallow water VMS and epithermal mineralization	NA	Manus Basin, Pacific Ocean

*Average Canadian ore grade

Table data compiled from Franklin et al., (2005); Gibson et al., (2007); Galley et al., (2007); and references therein.

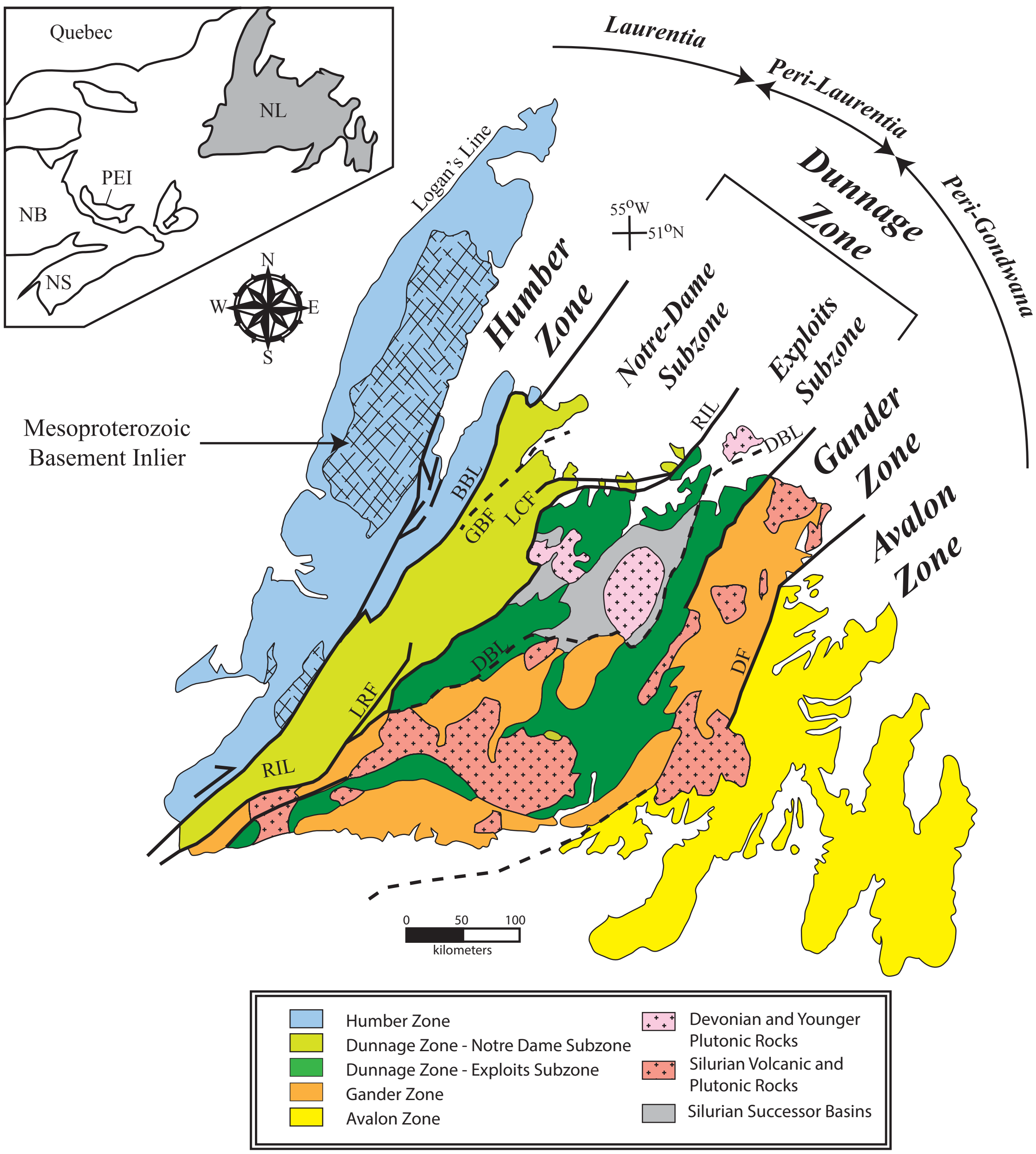

Figure 1.1 Geological map of the Newfoundland Appalachians with tectonostratigraphic zones, accretionary tracts, and associated belts. Tectonostratigraphic divisions modified from van Stall (2007), and van Staal and Barr (2012). Abbreviations: BBL=Baie Verte Brompton Line; DF=Dover Fault; DBL=Dog Bay Line; GBF=Green Bay fault; LCF=Lobster Cove fault; LRF=Lloyds River fault; RIL=Red Indian Line.

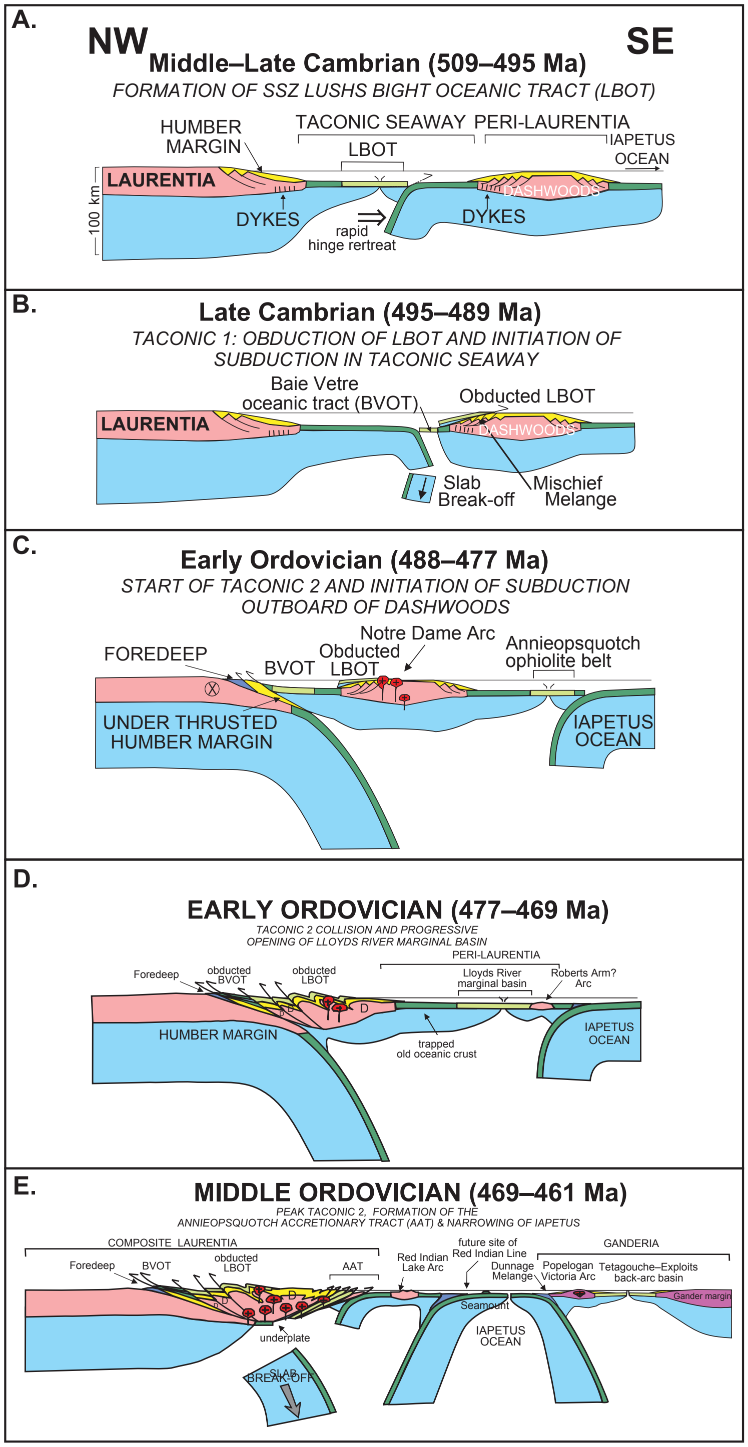

Figure 1.2 Evolution of the Taconic Orogeny. The first two events are related to the closure of the Taconic/Humber seaway, which caused the obduction of the Lushs Bight Oceanic Tract onto the Dashwoods (A,B; Taconic 1) and the Baie Verte Oceanic Tract onto the Humber margin (C,D; Taconic 2). Taconic 3 (E) involves the formation of the Annieopsquotch Accretionary Tract (AAT) and the location of the eventual collison between the AAT and Victoria Arc, marked by the Red Indian Line (modified from van Staal and Barr, 2012; van Staal et al., 2007).

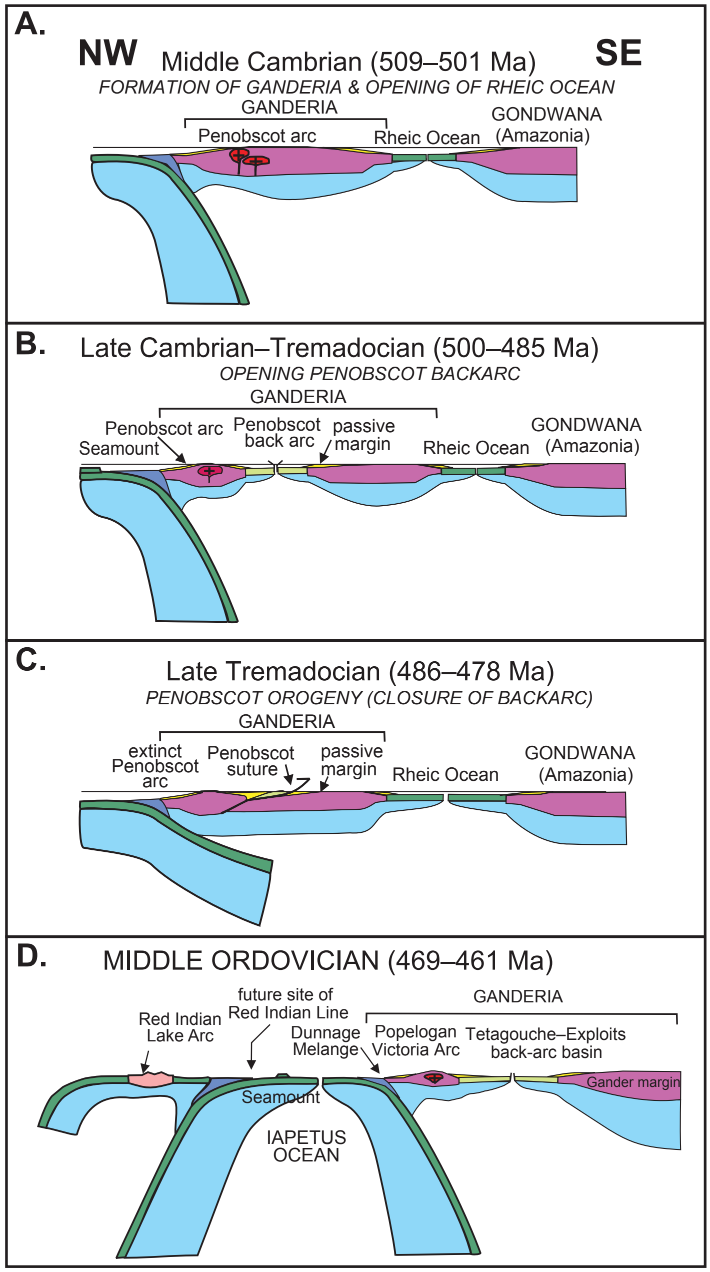

Figure 1.3 Evolution of the Penobscot and Victoria arc systems. Development of the Penobscot arc-back arc system (A,B). The closure of the Penobscot back-arc led to the Penobscot Orogeny (C). Further closure of the Iapetus ocean (D) prompted the formation of the Popelogan Victoria arc and the corresponding Tetagouche-Exploits back-arc basin (modified from van Staal and Barr, 2012; Zagorevski et al., 2010).

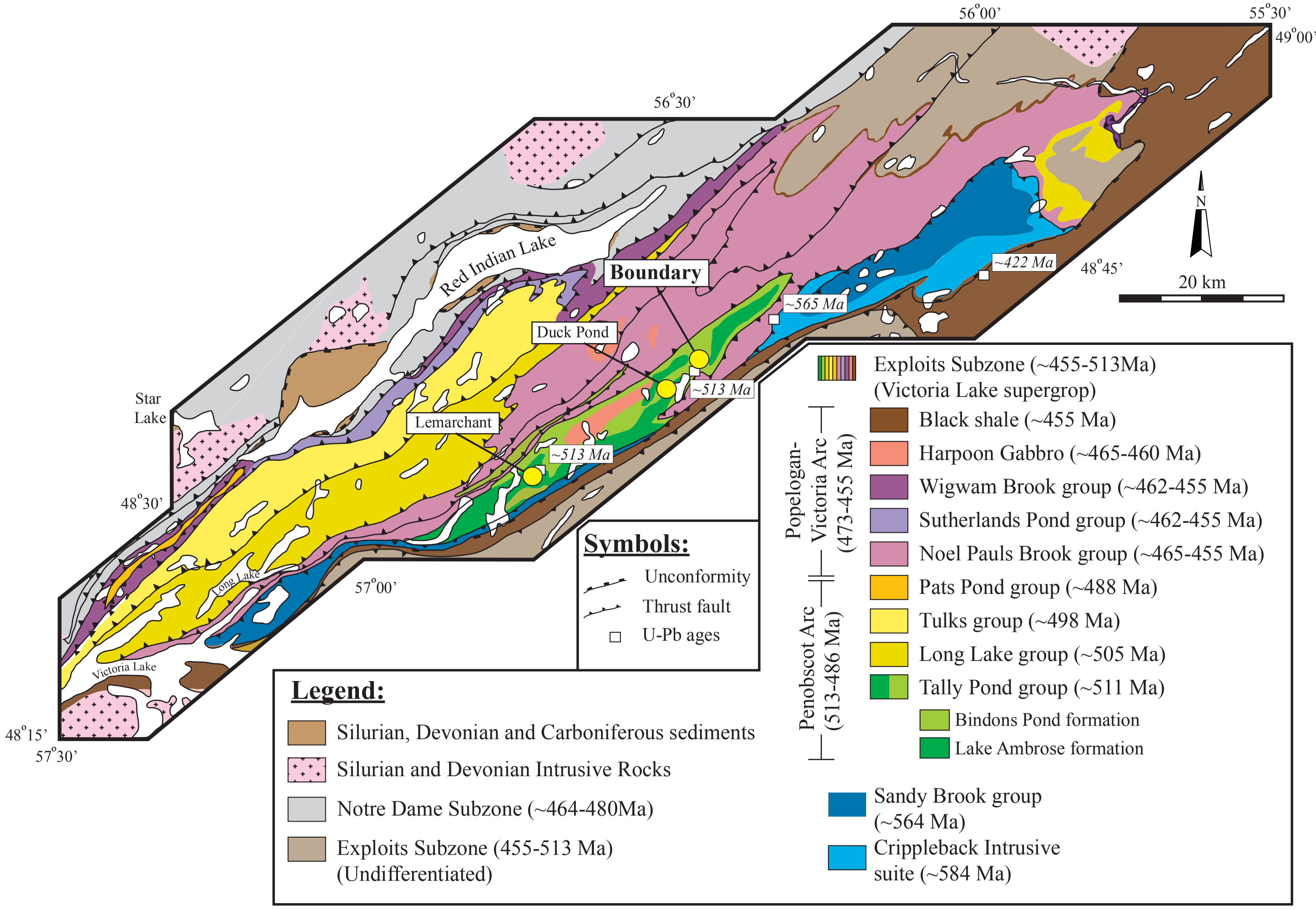

Figure 1.4 Detailed geological map of the Victoria Lake supergroup and the Tally Pond deposits: Boundary, Duck Pond, and Lemarchant (modified from McNicoll et al., 2010; Piercey et al., 2014).

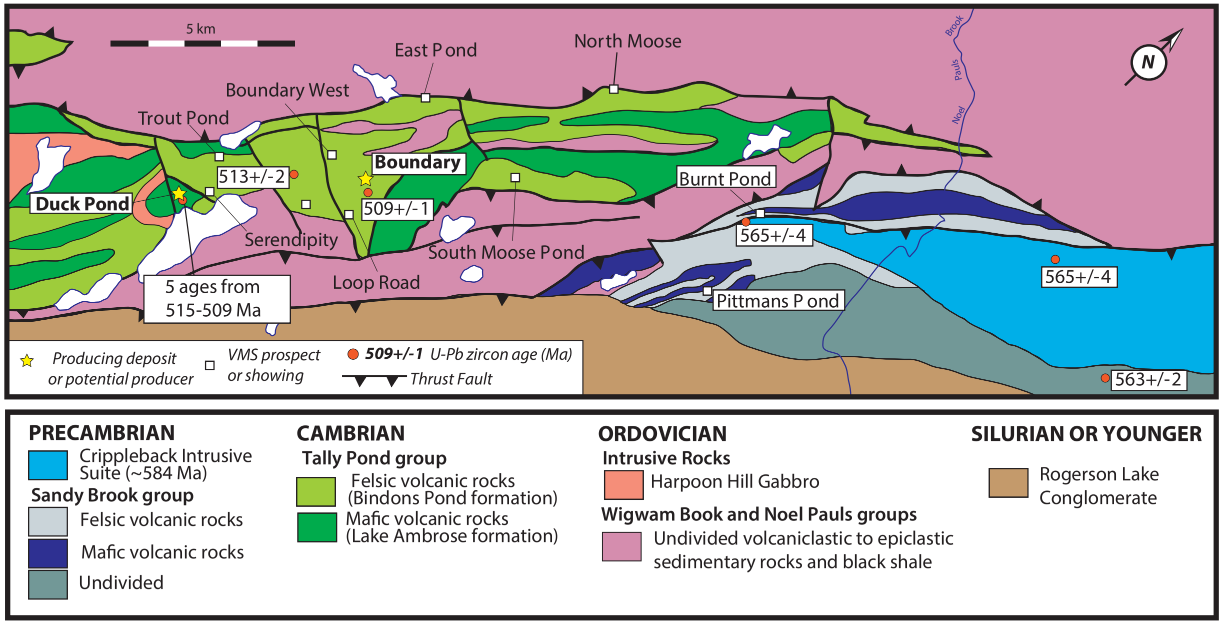

Figure 1.5 Geology of the Tally Pond group and related rocks. Thrust faults, U-Pb zircon age dates, and mines/prospects are shown (modified from Piercey et al., 2014; McNicoll et al., 2010).

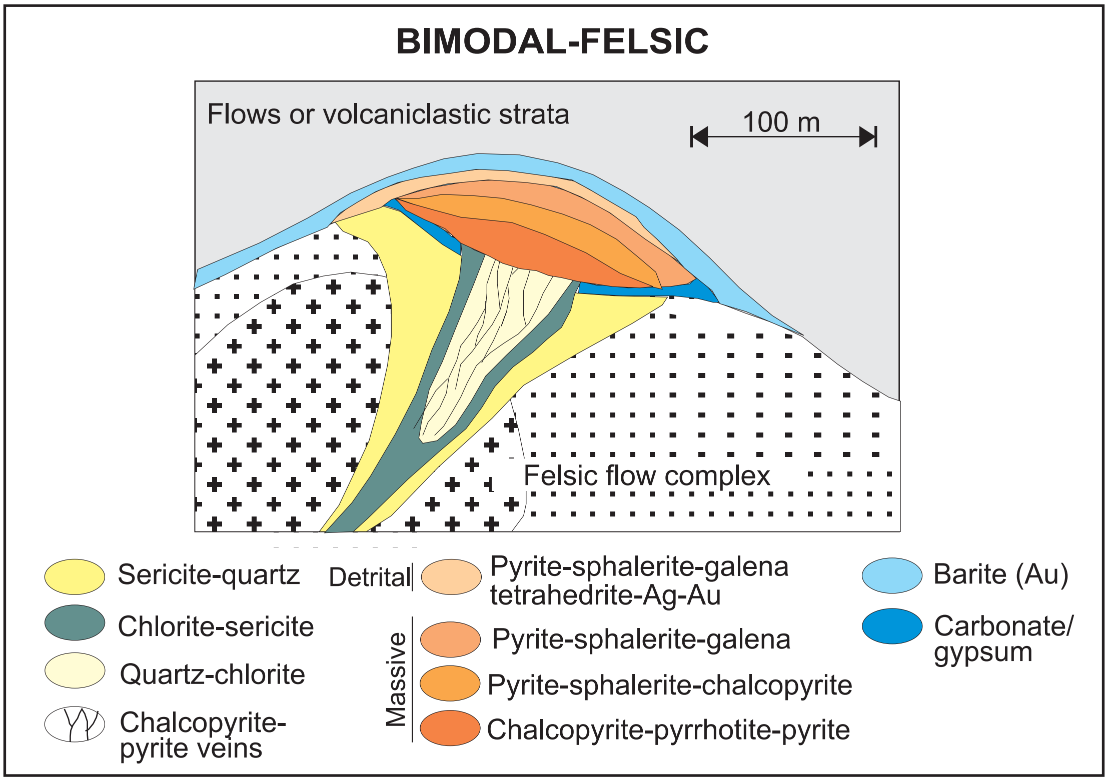

Figure 1.6 Ideal cross section of a bimodal-felsic VMS deposit (modified from Galley et al., 2007).

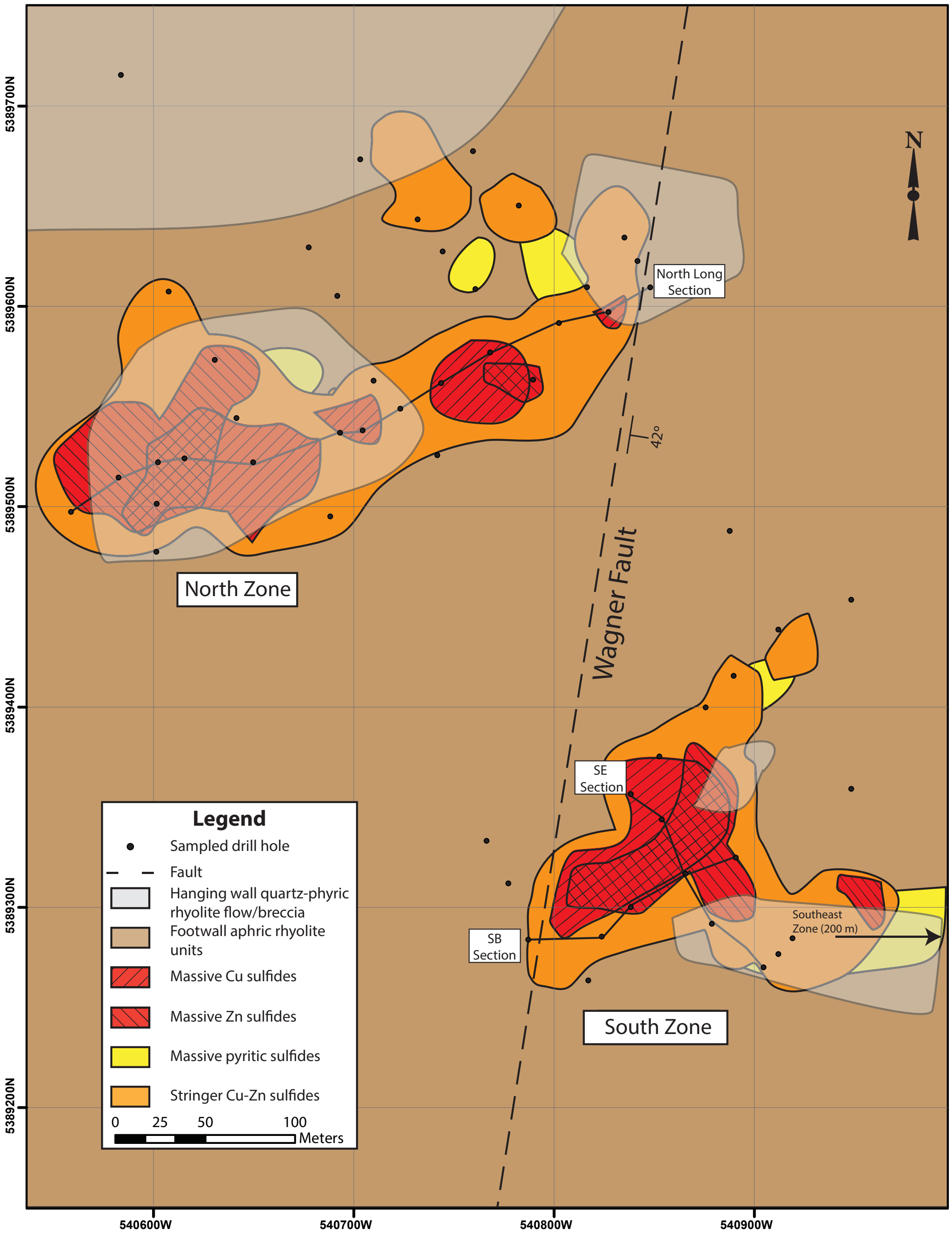

Figure 1.7 Boundary deposit surface geology plan map with distribution of sulfide mineralization. Modified from Hennessey (2013)(Unpublished).

Chapter 2: Hydrothermal Alteration and Lithogeochemistry of the Boundary Volcanogenic Massive Sulfide (VMS) Deposit, central Newfoundland, Canada

2.1 Abstract

The Boundary volcanogenic massive sulfide (VMS) deposit (0.45 Mt @ 3.4% Cu, 4.0% Zn, 1.0% Pb, 34 g/t Ag) is hosted by the Tally Pond group (~510 Ma) of the Victoria Lake supergroup, central Newfoundland, Canada. The Boundary deposit is a type example of a subseafloor replacement-style VMS deposit. The deposit has a felsic hanging wall composed of flow banded, quartz-phyric flows and breccias. The immediate footwall consists of aphyric, felsic lapilli tuff that contains interlayered aphyric, felsic flow breccias and massive flows. Mineralization predominantly occurs within the upper ten meters of the footwall and at the hanging wall-footwall contact. It consists of a broad pyrite lens and smaller individual chalcopyrite and sphalerite lenses. The basal portions of these lenses commonly contain clasts of the host lapilli tuff, typical of replacement-type mineralization. Three distinct hydrothermal alteration assemblages are present at Boundary: quartz-sericite, chlorite-sericite, and intense or pervasive chlorite. The intense chlorite assemblage occurs within the footwall lapilli tuff as both discordant pipes and conformable sheets underlying the ore. The chlorite-sericite assemblage typically forms around the periphery of the intense chlorite assemblage and occurs within all lithofacies, though rarely in the hanging wall. The quartz-sericite

assemblage occurs throughout the deposit, but its intensity increases proximal to Zn-rich mineralization.

The hanging wall and footwall rhyolites have no significant immobile element differences, suggesting a common petrological history. The rhyolites have FIIIa signatures, transitional Zr/Y ratios (2.8-4.5), low Nb/Y ratios, low Zr contents (Zr<200ppm), and low upper crust-normalized La/Sm ratios (<1) consistent with the formation of felsic rocks derived from melting of juvenile to weakly evolved crust within an extensional rift environment. When coupled with previous Nd-Pb isotopic data and zircon inheritance patterns, these immobile element data suggest that the Boundary host rocks were formed in a rifted peri-continental arc environment.

All rocks at the Boundary deposit are altered and contain elevated alteration indices, including high Ba/Sr, Hg/Na_2O, chlorite-carbonate-pyrite index (CCPI), and Hashimoto alteration index (AI) values. Mass changes and principal component analysis (PCA) identify key element associations related to mineralization and alteration. Intense chlorite alteration exhibits significant mass gains in MgO and Cu, variable Fe_2O_3 and SiO_2 behavior, and depletions in K_2O and Ba. The quartz-sericite assemblage has mass gains in SiO_2, K_2O, Ba, and Fe_2O_3, but no significant enrichment in Cu or MgO. Chlorite-sericite alteration contains variable gains and losses of SiO_2, K_2O, Ba, MgO, and Fe_2O_3 depending on the dominant matrix mineral phase (i.e., chlorite vs. sericite). The principal component analysis shows key element associations that include those involved with high temperature mineralization (Cu, Co, Bi, Mo, As, MgO, W, LOI, Fe_2O_3) and low temperature mineneralization (Zn, Pb, Sn, Hg). Short-wave infrared

(SWIR) spectroscopic data, particularly AlOH and FeOH absorption hulls, differentiate alteration styles and correlate with lithogeochemical results. The AlOH wavelengths increase in length (>2208 nm) proximal to Zn mineralization, and the wavelength variations correspond with relative abundances for sericite and chlorite. Collectively, these data have been used to reconstruct a three-dimensional alteration model of the Boundary deposit.

2.2 Introduction

Volcanogenic massive sulfide (VMS) deposits are important global resources of base and precious metals and one of the best understood mineral deposit types (e.g., Franklin et al., 1981, 2005; Lydon, 1984, 1988; Large, 1992; Franklin, 1995; Barrie and Hannington, 1999; Galley et al., 2007). They are well represented in the ancient record and our understanding of these deposits has been greatly enhanced by observations on the modern seafloor (e.g., Herzig and Hannington, 1995; de Ronde et al., 2005; Wysoczanski, et al., 2012; Gruen et al., 2014; Petersen et al., 2014; de Ronde et al., 2014). Modern seafloor deposits are associated with venting of hydrothermal fluids in black (and white) smokers, and observed mineralization is predominantly exhalative in nature (Hekinian et al., 1980; Lydon, 1988; Herzig and Hannington, 1995; Hannington and Barrie, 1999, German and Von Damm, 2003; Berkenbosch et al., 2012; de Ronde et al., 2014; Petersen et al., 2014). In the ancient record there are also exhalative deposits, but a sub-class of deposits is interpreted to have formed via replacement of host strata near or slightly below the seafloor (Doyle and Huston, 1999; Doyle and Allen, 2003). Replacement-style VMS deposits are also recognized as some of the largest/highest grade

VMS deposits globally (Squires et al., 1991, 2001; Galley et al., 1993, 1995; Doyle and Huston, 1999; Hannington et al., 1999; Doyle and Allen, 2003; Bradshaw et al., 2008). Despite their significance and importance, the processes of subseafloor replacement are incompletely understood. Furthermore, detailed studies of the alteration mineralogy and lithogeochemistry and the associated 2D-3D distribution of these variables in replacement deposits are lacking.

The Boundary volcanogenic massive sulfide (VMS) deposit (~0.5 Mt @ 3.5% Cu, 4% Zn, and 1% Pb, 34.0 g /t Ag) in the Canadian Appalachians is an outstanding example of a replacement-style VMS deposit and is one of the best preserved replacement deposits in the geological record (Piercey et al., 2014). The deposit, while small, is flat lying, contains excellent textural and alteration preservation, and lacks a metamorphic overprint found in many ancient replacement systems, therefore making it an ideal location to study alteration, lithogeochemistry, and mineralogy in VMS deposits. The goal of this paper is to build upon the previous work undertaken on the Boundary deposit by Moore (2003), Squires and Moore (2004), Piercey and Hinchey (2012), and Piercey et al. (2014). To build on our knowledge of the Boundary deposit we have undertaken a detailed study of the alteration distribution, alteration assemblage mineralogy, and lithogeochemistry, in both 2D and 3D. The research includes utilization of immobile elements to understand the tectonic setting of deposit formation and the genesis of the host volcanic facies present at Boundary. Mobile element geochemistry, mass balance calculations, and short wave infrared (SWIR) spectroscopy are utilized to construct an alteration model and provide insight into the key controls and processes involved with alteration and genesis of the Boundary deposit. These results provide both descriptive and genetic insight into subseafloor replacement alteration processes that have implications for similar deposits both in the Appalachians and globally.

2.3 Geological Setting

The Newfoundland Appalachians are divided into four tectonostratigraphic zones (Fig. 2.1): the Humber, Dunnage, Gander and Avalon zones (Williams, 1979; Williams et al., 1988). The Dunnage Zone hosts the Boundary deposit and is comprised of arc, back-arc, and ophiolitic rocks that formed along the margins of Laurentia (Notre Dame Subzone) and Gondwana (Exploits Subzone) from the Cambrian to Ordovician (Swinden et al., 1989; Swinden, 1991; Kean et al., 1995; van Staal and Colman-Sadd, 1997; Evans and Kean, 2002; Rogers and van Staal, 2002; Rogers et al., 2006, 2007; van Staal, 2007). The closure of the Iapetus Ocean resulted in the accretion of the Notre Dame Subzone onto the Laurentian margin during the Taconic orogeny (500-450 Ma), whereas the Exploits Subzone was accreted to the Gondwanan margin during the Penobscot orogeny (486-478 Ma)(van Staal, 2007; Zagorevski et al., 2007a, 2010). The two subzones were juxtaposed against each other during the final stages of the Taconic orogeny and created a suture between the two subzones termed the Red Indian Line (Fig. 2.1) (van Staal, 2007; Zagorevski et al., 2007b, 2010, van Staal and Barr, 2012).

Within the Exploits Subzone, the Boundary deposit is hosted by the Tally Pond group (~513-509 Ma; Dunning et al., 1991; McNicoll et al., 2010), one of six fault bounded packages that make up the Victoria Lake supergroup (Fig. 2.2; Evans and Kean, 2002; Zagorevski et al., 2007b, 2010; McNicoll et al., 2010; Piercey et al, 2014). In addition to the Boundary deposit, the Tally Pond group hosts the Duck Pond and Lemarchant VMS deposits, as well as several other prospects (Squires et al., 1991, 2001; Wagner, 1993; Evans and Kean, 2002; Squires and Moore, 2004; Piercey et al., 2014). The Tally Pond group is divided further into two informal formations: Lake Ambrose formation and the Bindons Pond formation (Rogers and van Staal, 2002; Rogers et al., 2006; Piercey et al., 2014). The Lake Ambrose formation (~513 Ma; Dunning et al., 1991) is predominantly basalt, consisting of massive and pillow flows, volcaniclastic rocks, and lesser felsic and sedimentary rocks (Kean and Evans, 1986; Evans and Kean, 2002, Rogers and van Staal, 2002; Rogers et al., 2006). The Lake Ambrose formation underlies the younger Bindons Pond formation (509 Ma; McNicoll et al., 2010). The Bindons Pond formation, a felsic-dominated unit that consists of felsic flows, volcaniclastic rocks, and carbonaceous clastic sedimentary rocks, hosts the Duck Pond, Lemarchant, and Boundary deposits (Kean and Evans, 1986; Squires et al., 1991; Evans and Kean, 2002; Rogers and van Staal, 2002; Squires and Moore, 2004, Rogers et al., 2006).

2.4 Deposit Geology

The Boundary deposit is located approximately 4 km NE of the Duck Pond deposit. It occurs in two fault-separated lenses, the North zone and the South zone (Fig. 2.3) (Wagner, 1993; Piercey et al., 2014). A third lens, the Southeast zone, occurs as an extension of the South zone but was not a focus in this study. The hanging wall rocks exposed at or near the surface below a few meters of till and consist of a quartz-phyric assemblage of massive and flow-banded rhyolite flows and breccias (Fig. 2.4a-b). The hanging wall is partially preserved in the North zone, whereas in the South zone, it has been mostly eroded, thus exposing massive sulfides at surface. The footwall consists of aphyric lapilli tuff with minor breccia and tuff underlain by aphyric breccias and flows (flow banded to massive) (Fig. 2.4c-f). The top of the footwall is comprised of a thin (<10 cm) tuff that has mostly been replaced by sulfides (G. Squires, pers. comm.). The aphyric lapilli tuff makes up the majority of the footwall and is generally clast-supported with 1-3 cm clasts; however, the unit becomes more matrix supported with depth. Bedded tuffs and aphyric rhyolite breccias are interlayered throughout the lapilli tuff. Deeper within the footwall, aphyric rhyolite flows and breccias underlie the lapilli tuff. Intrusions at Boundary are rare; only one quartz-porphyry intrusion has been recognized just east of the South zone, where it crosscuts all units. The lithofacies and stratigraphic successions are shown in cross section in Figures 2.5a and 2.5b.

The Boundary deposit is essentially structurally intact with two exceptions that involve post-mineralization faulting. The first is the N-S trending Wagner fault, which offsets the North zone from the South zone (Fig. 2.3; Wagner, 1993; G. Squires pers. comm.). This fault is easily recognized in drill holes that occur distal from the deposit as intense, friable sericite zones. The second involves thrust faulting in the western portion of the North zone. Shallow, meter-scale thrust faults have resulted in apparent stacked massive sulfide lenses within the hanging wall; however, detailed core logging reveals that faulting took place at the hanging wall-ore contact and imbricated the ore horizon (Fig. 2.5a).

2.5 Mineralization and Alteration

2.5.1 Mineralization

In both zones, mineralization occurs as a series of semi-conformable, discontinuous lenses, most of which occur below the contact between the hanging wall quartz-phyric rhyolite flows and breccias and the footwall aphyric rhyolite lapilli tuff (Fig. 2.4A-C, 2.5A-B; Appendix A; Squires and Moore, 2004; Piercey et al., 2014). At the hanging wall-footwall contact, the lenses (up to 50 meters in diameter, ~1-5 meters thick) consist primarily of massive Cu-Zn sulfide cores surrounded by massive pyrite. The contact between the hanging wall and these lenses is typically sharp; however, locally mineralization consists of pyrite-chalcopyrite and displays relict hanging wall flow textures. The basal portions of these large lenses commonly contain lapilli tuff fragments within a sulfide matrix. Bedded sulfides are also present at the hanging wall-footwall contact along the southern edges of both zones and consist of mm- to cm-scale bands of pyrite, chalcopyrite, and sphalerite. Smaller lenses (~10s of meters, usually 1-2 meters thick) consisting of massive to clast-rich chalcopyrite and pyrite occur less than 10 meters below the hanging wall-footwall contact within the footwall lapilli tuff. Deeper in the footwall, pyrite stringers occur within the inter-fragment space of the flows and breccias. The hanging wall in the South zone has mostly been eroded, with massive sulfides exposed near surface. These near surface sulfides have variable degrees of supergene enrichment and contain surface staining and veinlets of chalcocite, bornite, and covellite.

2.5.2 Alteration

Three main alteration assemblages are present in the Boundary deposit: quartz-sericite, chlorite-sericite, and intense chlorite (Figs. 2.6-2.8). The most abundant, least intense quartz-sericite alteration assemblage occurs throughout the deposit, both proximal (within meters) and distal (>100 meters) to mineralization. It extends into the uppermost levels of the remnant hanging wall and deep into the footwall aphyric rhyolitic flows and breccias (Fig. 2.5a -b). Quartz-sericite alteration may be varying shades of grey, as well as white, purple or black. The black quartz-sericite assemblage sometimes occurs near massive to semi-massive sulfide (Fig. 2.6b). The black color does not appear to be caused by any compositional abnormalities or inclusions within the sericite. Clasts and flows are typically dominated by quartz alteration, whereas the matrix contains variable sericite, quartz, and minor epidote (Fig. 2.6c). Chlorite is rare in the quartz-sericite assemblage, but occurs as small pods in heavily sericite altered, relict feldspar grains, or along the edges of sulfides (Fig. 2.6d). In the more intensely quartz-sericite altered parts of the stratigraphy, chlorite becomes a minor matrix constituent (~5%). Disseminated pyrite is the dominant sulfide phase with lesser sphalerite and galena. Chalcopyrite is present as chalcopyrite disease in sphalerite (Fig. 2.6e; Large, 1992) or as crosscutting veins.

The chlorite-sericite assemblage forms around the intense chlorite assemblage (see below), usually within a few meters of mineralization (Fig. 2.7). Samples from this assemblage contain quartz (50-70%), sericite (20-30%), and chlorite (20-30%). Texturally, the alteration manifests itself with zoned lapilli tuff clasts that have quartz altered rims and slightly sericite altered cores (Fig. 2.7a-b), whereas the matrix is dominated by fine-grained chlorite and sericite (Fig. 2.7c-d). The accompanying sulfide mineralogy consists of pyrite, chalcopyrite (± Bi-Te-sulfides), sphalerite, and trace galena.

The intense chlorite assemblage occurs in close association with massive and clast-rich sulfides, commonly as semi-conformable sheets that form thin envelopes (< 2 m) around the sulfides (Fig. 2.8). It also defines discordant alteration pipes that crosscut stratigraphy (Fig. 2.5). Within the intense chlorite assemblage, most if not all, of the original host rock has been replaced by chlorite and sulfides (Fig. 2.8a-b). The intense chlorite assemblage consists predominantly of Mg-chlorite (60-80%), quartz (20-40%), and occasional chaotic carbonate (dolomite; ~5%); the latter of which is a feature more common in the neighboring Duck Pond mine (Squires et al., 2001; Squires and Moore, 2004; Piercey et al., 2014). The sulfide mineralogy in this assemblage includes pyrite, chalcopyrite (+/- Bi-Te-sulfides), and minor sphalerite and Co-rich arsenopyrite.

Accessory minerals such as anatase, apatite, and monazite are found in all three zones, whereas xenotime is present only in the quartz-sericite assemblage. Also common throughout the Boundary deposit are mm-scale Fe-Mg-(+/-Mn) carbonate spots (e. g. Fig 2.6a-b; Fig. 2.7a; and Fig. 2.8b). This type of alteration occurs throughout the Tally Pond group and is interpreted to be the result of regional metamorphism during the late Silurian (van Staal, 2007; Piercey et al., 2014).

2.6 Lithogeochemistry

2.6.1 Methods

A total of 237 samples from the Boundary deposit were selected from 51 diamond drill holes during the 2013 field season. Samples were selected every ~5 meters or wherever there was a major change in the alteration assemblage. Samples included the hanging wall flows and breccias as well as footwall tuff, lapilli tuff, breccias, and flows from both the North and South zones. Samples that exhibited evidence for faulting such as fractured core or extensive quartz veining were avoided.

All samples were analyzed for major element oxides (SiO_2, Al_2O_3, Fe_2O_3, MnO, MgO, CaO, Na_2O, K_2O, TiO_2, P_2O_5) and select trace elements (Ba, Sr, Y, Sc, Zr, Be, V, Hg) at Activation Laboratories Ltd. (Actlabs) in Ancaster, ON, Canada. At Actlabs, samples were crushed and pulverized using mild steel before undergoing lithium metaborate/tetraborate fusion followed by HF-HNO_3 dissolution and subsequent analysis by inductively coupled emission-mass spectroscopy (ICP-ES). Separate Hg concentrations were determined via cold vapor flow injection mercury system (Hg-FIMS).

Additional trace elements, including trace metals, low field strength elements (LFSE), rare earth elements (REE), and high field strength elements (HFSE), were analyzed at the Department of Earth Sciences at Memorial University. Base metals (Cu, Zn, Pb), transition metals (Sc, Ti, V, Cr, Mn, Co, Ni), volatile elements (As, Cd, Sn, Sb), and the LFSE (Sr, Ba, Th) were determined by multi-acid dissolution and analyzed by inductively coupled plasma-mass spectrometry (ICP-MS). The whole-rock dissolution process was a modified version of that described by Jenner (1990) and Longerich et al., (1990) and is described in detail by Lode et al. (in review). The REE and HFSE were determined by means of sodium peroxide (Na_2O_2) sinter and analyzed using the same ICP-MS at Memorial University by the following procedure: sintering of a 0.2 g sample aliquot with Na_2O_2, dissolution of the sinter cake by addition of deionized water and subsequent REE precipitate formation, separation by centrifuge, and acid dissolution of precipitate prior to ICP-MS analysis. The complete method can be found in Longerich et al., (1990). Precision and accuracy of the various methods have been previously reported in Piercey and Colpron (2009) for Actlabs, Jenner et al. (1990) and Lode et al. (in review) for multi-acid dissolution, and Longerich et al. (1990) for Na_2O_2 sinter. Representative values are displayed in Table 1 (see Appendix B for complete results).

2.6.2 Results

All samples from the Boundary deposit exhibit some degree of hydrothermal alteration, which means most major elements (except Al_2O_3 and TiO_2), base metals, volatile metals, and the low field strength elements (LFSE) are considered to have been mobile (Spitz and Darling, 1978; Saeki and Date, 1980; Barrett and MacLean, 1994; Jenner, 1996; Large et al, 2001). The high field strength elements (HFSE) and the REE (except Eu) are often regarded as being immobile, but may become mobile (especially the LREE) during intense hydrothermal alteration (e.g., MacLean, 1988). In extremely altered samples, Y and LREE mobility can be characterized by “fan-shaped” REE patterns (e.g., MacLean, 1988) and anomalous Y/Zr and La/Zr ratios relative to the more robust Nb/Zr and Yb/Zr ratios (Barrett et al., 2008).

Despite the potential for element mobility in intensely altered samples, elements considered immobile are useful in determining primary chemostratigraphic and petrologic attributes such as magmatic affinity or tectonic environments. The mobile elements, in contrast, provide insight into alteration and mineralization processes. Collectively, these data can also be used to undertake quantitative mass balance calculations to understand absolute element mobility.

2.6.3 Affinity Monitors

Elements such as Zr, Ti, La, Yb, and Nb have been used extensively to determining primary chemostratigraphic and petrologic attributes in altered volcanic terranes due to their immobility during hydrothermal alteration (MacLean and Kranidiotis, 1987; MacLean and Barrett, 1993; Barrett and MacLean, 1994). In a Zr/Ti versus Nb/Y plot (Fig. 2.9a), most samples fall within the rhyolite/dacite field with the exception of two significantly altered lapilli tuff samples. Most samples also exhibit Zr/Y ratios between 2.8 and 4.5, indicating the rocks have transitional affinities (Fig. 2.9b)(Ross and Bedard, 2009). Samples that do not fall within this Zr/Y range have intense chlorite/sericite alteration and plot both above and below the transitional field. This is likely due to the mobilization of Y during intense hydrothermal alteration and is discussed in the Mass Changes section. The Zr/Y ratios and the low Nb/Y ratios (Fig. 2.9c) of most Boundary deposit samples support their formation in an arc environment or from re-melted arc crust (Lentz, 1998; Piercey et al., 2014). Low Zr contents (Zr<200 ppm; Fig. 2.9d) and upper crust–normalized La/Sm ratios of <1 (Fig. 2.9e) are consistent with the formation of felsic rocks from sources less evolved than upper continental crust (e.g., post-Archean, juvenile crust; Piercey, 2009, 2011). Nearly all samples fall within the FIIIa field of a felsic volcanic discriminant diagram (Fig. 2.9f), indicating that partial melting likely took place at relatively shallow levels in the crust (<10km) (Lesher et al., 1986; Hart et al., 2004).

2.6.4 Rare Earth Element Plots

REE patterns for both the hanging wall and footwall samples are shown in Figure 2.10a-b, and have been normalized to the chondrite values of McDonough and Sun (1995). Both hanging wall and footwall sample patterns display slight LREE-enrichment with flat HREE patterns; however, the hanging wall samples have much tighter patterns with less dispersion in REE abundances. The variation displayed by the footwall rocks (Fig. 2.10b) is due to either mass/volume changes and/or the actual mobility of the REE during hydrothermal alteration. The addition of Si and Fe during alteration results in a net mass gain, which can dilute the overall immobile REE concentration; conversely, a net mass loss (e.g., chlorite or sericite alteration) can result in apparent increase of REE concentrations (Fig. 2.10c)(Barrett et al., 2008). The effects of mass changes should result in a uniform shift; however, the observed LREE contents in highly altered samples have likely been influenced by element mobility, resulting in decreased LREE, without losses in HREE (Fig. 2.10d). The mobility of REE are further investigated in the Mass Change Calculations section below.

2.6.5 Mobile Element Lithogeochemistry

Regardless of lithology, all samples from the Boundary deposit have pronounced depletions in Na_2O (often Na_2O <0.6%) and high Spitz-Darling index values

(Al_2O_3/Na_2O>40; Fig. 2.11a). High Hashimoto index values [$AI=100(MgO+K_2O)/(MgO+K_2O+CaO+Na_2O)$] (Ishikawa et al., 1976) and chlorite-carbonate-pyrite index values [$CCPI=100(MgO+Fe_2O_3)/(MgO+Fe_2O_3+CaO+Na_2O)$] (Large et al., 2001) are also characteristic of these samples, with the intense chlorite altered samples plotting near the chlorite-pyrite node and quartz/sericite altered samples plotting near the sericite node (Fig. 2.11b). The three alteration assemblages are most easily differentiated using MgO/Al_2O_3 and K_2O/Al_2O_3 ratios (Fig. 2.11c-d).

Select trace elements also increase towards mineralization (e.g., Large et al., 2001), including Hg/Na_2O and Ba/Sr which are elevated in all alteration assemblages, with the exception of those that display very intense chlorite and chaotic carbonate alteration (Ba/Sr <10 and Hg/Na_2O >10) (Fig. 2.11e; Collins, 1989). Increasing Hg/Na_2O ratios also correlate with increasing Zn contents (Fig. 2.11f), but not Cu contents, and thus likely mirror the edge of high temperature mineralization/alteration.

2.6.6 Mass Change Calculations

Although raw lithogeochemical data can illustrate useful alteration trends, the absolute gains and losses of mobile elements yield true alteration dimensions and take into account mass and volume changes during alteration in addition to elemental changes (e.g., Gresens, 1967; Grant, 1986; MacLean, 1990). By plotting pairs of immobile elements against one another, samples from an originally homogeneous protolith will plot along a single line that passes through the origin, whereas those from multiple sources will form additional trend lines (MacLean and Kranidiotis, 1987; Barrett and MacLean, 1991; MacLean and Barrett, 1993). Samples from the Boundary deposit all plot along a single trend line (Fig. 2.12) indicating that mass changes can be determined by using a single-precursor method (this paper employs the single precursor method of MacLean (1990)). Correlation coefficients calculated for immobile-compatible and immobile-incompatible element pairs are reported in Appendix C. The element pair with the highest correlation coefficient between an immobile compatible element (e.g., Al_2O_3, TiO_2) and an immobile incompatible element (e.g., Nb, Zr) was used in determining the mass changes, in this case Al_2O_3-Zr. Enrichment factors for each sample were calculated using Al_2O_3 in comparison with the least altered sample. The reconstructed compositions of each sample were then calculated using the enrichment factor, and mass changes for each sample was calculated by subtracting the precursor composition from each of the reconstructed compositions. The least altered precursor composition (Table 2.1-hanging wall sample H501278) was selected based on the sample's low loss on ignition (LOI) and base metal values, minimal Na_2O depletion, and relatively minor alteration mineral content. The calculated mass changes are shown in Appendix C, plotted in Figure 2.13, and discussed in detail below.

SiO_2: Gains and losses in SiO_2 are the primary causes for mass/volume changes in the Boundary deposit, and they mirror the total mass changes in each sample. Most samples show small to moderate SiO_2 gains, especially those from the footwall lapilli tuff and breccias that exhibit chlorite-sericite alteration. The greatest mass loss is observed in the intense chlorite altered footwall lapilli tuffs (50% loss) and in the chlorite-sericite altered hanging wall flows and breccias (~20% loss)(Fig. 2.13a-b; Appendix C.2).

Na_2O, CaO: The alkali components, Na_2O and CaO, behave differently from each other. Throughout the Boundary deposit, Na_2O is nearly completely depleted from all samples (1-2% Na_2O losses). Only in the least altered samples does Na_2O appear to be slightly less depleted (0-0.5 Na_2O% losses). Conversely, no change or only moderate mass gains are observed for CaO within the footwall lapilli tuff and breccias. Calcium gains are present in samples that have undergone carbonate alteration (i.e., contain chaotic carbonate, carbonate spot overprinting) within the chlorite-sericite and intense chlorite assemblages (1-3%; Appendix C.2).

K_2O: The less altered quartz-sericite assemblage generally displays ~1% K_2O increase independent of lithology. The chlorite-sericite assemblage displays variable mass changes (most showing either a 1% gain or 1-2% loss) in accordance with the dominant observed matrix mineral (gains=sericite; losses=chlorite). The intense chlorite altered samples all show a 1-3% K_2O loss (Fig. 2.13a).

MgO, Fe_2O_3: MgO gains in the Boundary deposit mirror the presence of chlorite alteration. The quartz-sericite assemblage has very little change (± 3%); the chlorite-sericite assemblage has slight gains in MgO (1-5%), predominantly within the hanging wall breccia and within the footwall lapilli tuff and breccia; and the intense chlorite altered samples exhibit gains of 5-20% of MgO. Because Fe_2O_3 is not only a major constituent of chlorite but also of the sulfide phases present, Fe_2O_3 gains range from 5-50%, with the highest gains present in the footwall lapilli tuff (Fig. 13c).

Transition Metals (Sc, Ti, V, Cr, Mn, Co, Ni): Overall, all Boundary samples show some degree of transition metal enrichment (Appendix C.2). The greatest enrichments occur in the footwall lapilli tuff and tuff units. Manganese and Co show significant enrichments within the intense chlorite altered lapilli tuff that underlies the Cu-rich lenses (gains up to 0.8% MnO and ~270 ppm Co). Titanium, V, Cr, and Ni tend to show moderate enrichments (20-50 ppm) in the footwall lapilli tuff, tuff, and breccias within no preferred alteration assemblage. Scandium displays little to no mass change throughout the deposit.

Base Metals (Cu, Zn, Pb): Chlorite-sericite and intensely altered chlorite samples within the footwall lapilli tuffs and breccias show significant Cu and Zn gains. Zinc and Pb exhibit gains within the hanging wall flows and breccias as well as the footwall lapilli tuff. Minor depletions in base metal content occur at distances greater than 50 meters from the main ore lenses.

Other LFSE (Th, Sr, Ba): No substantial mass changes of Th are observed amongst the Boundary samples. Strontium losses are common throughout the deposit (~10 ppm), with the exception of footwall units below the South ore zones that display no change or slight gains (~10 ppm). Because the least altered sample contains some degree of sericite alteration, Ba contents are higher than would be expected for a completely unaltered sample. The Ba contents of the least altered sample are ~1,400 ppm. Keeping this in mind, all lithologies show significant Ba mass gains and losses (±1000 ppm). The hanging wall breccias show the highest Ba gains relative to the other lithologies. The footwall flows and breccia exhibit moderate depletions within the chlorite-sericite samples, whereas the quartz-sericite assemblage generally shows moderate to significant enrichments (500-1000 ppm). The intense chlorite samples display significant losses (~1,000 ppm).

HFSE (Y, Nb, Hf, Ta): Amongst the HFSE, Y displays the most significant mass changes throughout the Boundary deposit (Appendix C). Yttrium gains and losses are generally on the order of ~8 ppm in both the hanging wall and footwall flows and breccias. Significant Y gains (~10 ppm) occur proximal to Cu-rich mineralized zones. Hafnium and Nb both exhibit minor mass changes (generally ±3 ppm) with slightly greater changes in the more intensely chlorite altered samples (-7 to +10 ppm). Tantalum does not exhibit any significant changes.

Volatile Elements (As, Cd, Sn, Sb, Hg): Tin and Sb generally exhibit minor gains and losses (±10 ppm) throughout the Boundary deposit (Appendix C.2). Gains in As (75-100 ppm) and Cd (~20 ppm) are common within the chlorite-sericite samples surrounding Zn ore zones but depletions are present in samples overlying and underlying these Zn-rich zones. Significant Hg gains (>1 ppm) are present in the upper ten meters of the quartz-sericite altered lapilli tuff and in hanging wall units.

REE (La-Lu): In general, the REE do not display significant mass changes with the exception of La, Ce, and Nd (Fig. 2.14a), which exhibit exceedingly large gains and losses in a set of 12 samples that are found within footwall lapilli tuff (matrix supported) and tuff samples; however, the gains and losses are not tied to a specific alteration assemblage.

The mobility of REE in VMS deposits has been documented in a number of studies (e.g., MacLean and Kranidiotis, 1987; MacLean, 1988; Barrett and MacLean, 1994; Barrett et al., 2008), and this appears to be the case as well at Boundary, especially in the footwall (Fig. 2.10b, Fig. 2.14a). However, once the effects of volume change are taken into account, the REE values are very similar to those of the least altered sample (Fig. 2.14b-c). All three alteration assemblages show minor LREE depletions and relatively unchanged HREE (Fig. 2.14b). Maclean (1988) attributes sample/precursor ratios between 1-3 to strong REE mobility, whereas the ratios in this study are less than 0.25 for both the LREE and HREE. The intense chlorite assemblage displays the greatest depletions in the LREE, all of which occurs in the footwall lapilli tuff unit. The chlorite-sericite and quartz-sericite assemblages have similar REE patterns with the exception of Eu, which is liberated and removed as plagioclase breaks down (Sverjensky, 1984). Compared to the footwall (Fig 2.14c), the hanging wall samples show slightly greater REE depletions. However, given that the majority of the hanging wall has been eroded, this is likely a function of proximity to the ore horizon, as all of the hanging wall samples were taken from the bottom ten meters of the unit. The footwall samples display lower depletion levels for two reasons: 1) higher number of distal, less altered samples decrease the effect of the intense chlorite samples; and 2) the LREE removed from the intense chlorite zones were probably redistributed among the less altered zones as evidenced by the precipitation of apatite, monazite, and xenotime, especially within the heavily sericite altered samples (high K_2O wt.%).

2.6.7 Principal Component Analysis

A principal component analysis (PCA) was carried out on the major and trace element dataset listed in Appendix B. Elements that contained a high percentage of censored values (i.e., values below or close to detection limit), such as Be and Se, were not included in the analysis due to the false components generated based on censored values. Since the REE and HFSE were deemed essentially immobile, one REE (Lu) and one HFSE (Y) was included in the analysis to represent these groups in order to maximize the correlations between the mobile elements. Lutetium was chosen because it represents the least mobile REE and HFSE elements (from mass change section). Yttruim was chosen because it exhibited the most significant changes amongst the HFSE REE (including the LREE). A subsequent PCA analysis was carried out with the entire dataset, and all REE and HFSE produced similar results to the representative elements choses. Figure 2.15a is an ordered plot of eigenvalues and their relative significance for each component. Determining the number of significant components can be done a number of ways (e.g., “elbow” of the screeplot, components <5%, eigen values<1). In this analysis only the first four components are considered, because any component after four represents <5% of the variance in the dataset and often contains redundant element associations with, only one or two differing elements from one of the four major principal components. Further PCA information is given in Appendix D.

This approach discriminated four components that account for ~55% of the total geochemical variability (Table 2). The first component accounts for 20% of the variation in the Boundary dataset and is reflects the inverse relationship between elements associated with intense chlorite alteration and mineralization (Fe_2O_3, LOI, Co, Mo, Cu, W, Bi, MgO, As) and those associated with quartz-sericite alteration (SiO_2, K_2O, Ba). The second component accounts for 18% of dataset variance and contains only positive scores for MgO, Sc, TiO_2, Al_2O_3, Lu, Y, P_2O_5, K_2O, and Ba; these elements represent less intense sericite and chlorite alteration. The lack of scores for Cu, Zn, Pb, Fe_2O_3, CaO, MnO, and SiO_2 indicates that, while these elements are indicative of intense alteration/mineralization/silicification, they also occur throughout the deposit in variable amounts. The third component (10% dataset variance), exhibits significant scores for Pb, Zn, Hg, and Sn; which represents that low temperature mineralization is present throughout the deposit regardless of alteration assemblage. The fourth component (7% variance) reflects carbonate alteration (LOI, P_2O_5, MnO, CaO, MgO, and Sr) versus quartz-sericite alteration (SiO_2, K_2O, and Ba). Figure 2.15b displays components one and two plotted in eigenvector space to illustrate the observed clustering of elemental scores.

2.7 Shortwave Infrared (SWIR) Spectroscopy

A total of 237 samples from both the hanging wall flows and breccias and the footwall tuff, lapilli tuff, breccia, and flows were analyzed at Memorial University using a Terraspec™ mineral spectrometer with a Hi-Brite Muglight. Minimal sample preparation was needed as SWIR absorption spectra were collected from fresh drill core that had been recently cut and cleaned. Optimization and white references were collected every ~20 analyses or 40 min to avoid significant drifts in data. Analyses were only performed in a naturally sunlit room to avoid any interference from artificial lighting. Reference sample measurements were made after each optimization and white reference to measure both precision and accuracy. Reference sample measurements for pyrophyllite and kaolinite indicate that the Terraspec™ was consistently within 1 nm of the accepted values. Reflectance spectra were collected using the RS^3 Spectral Acquisition software. The resultant spectra were processed using The Spectral Geologist Hotcore v 7.1.55 software in which the hull correction was applied. Hyperspectral scalars were calculated using a fourth order polynomial fitting curve applied over the ranges 2120-2245 nm (focused at 2180-2230 nm) for the AlOH wavelengths and 2230-2270 nm (focused at 2240-2260 nm) for FeOH. Spectral depth filters were applied to remove background noise with filters of 0.015% for AlOH and 0.010% for FeOH. Reported spectra with trough depths less than the filter value were dismissed. The simple mineralogy and absence of weathering products, as determined through petrographic studies and SEM analyses (Appendix E), generally produced diagnostic absorption features and made for clear mineral identification. Due to the variable clast-matrix mineralogy, a minimum of three analyses per sample were made to ensure representative measurements. The complete SWIR absorption data are also reported in Appendix B.

Shortwave infrared (SWIR) spectrometry subjects a sample to a light source and measures the wavelengths of light that are absorbed by certain bonds within minerals (AusSpect International, 2008). Most absorption features are generated by OH, H_2O, CO_3, NH_4, AlOH, FeOH, and MgOH bonds and are represented as minima in the reflectance spectrum over a specified range (AusSpect International, 2008). Two of the most commonly used features in mineral deposit exploration are the AlOH absorption feature between 2190-2225 nm and the FeOH absorption feature between 2,245-2,260 nm which correspond to white mica (sericite) and chlorite compositions at the Boundary deposit, respectively (Fig. 2.16)(AusSpect International, 2008).

Theoretical absorption features for chlorite (FeOH bonds) and white mica (AlOH bonds) are shown in Fig. 2.16. The diagnostic absorption feature for white mica is a deep absorption feature between 2,180-2,228 nm. The exact wavelength at which the absorption feature occurs is directly related to the composition (e.g., Velde, 1978; Besson and Drits, 1997a&b; Guidotti and Sassi, 1998; Herrmann et al., 2001). Shorter wavelengths (2,180-2,195 nm) are characteristic of sodium bearing mica (paragonite), whereas longer wavelengths (2,210-2,228 nm) are typically diagnostic of Fe-Mg mica (phengite) (Herrmann et al., 2001; Yang et al., 2011). Typical potassic mica (muscovite) produces absorption features between 2,200 and 2,204. Intermediate wavelengths are the result of intermediate compositions or multiple white mica phases (Herrmann et al., 2001). Chlorite spectra contain two diagnostic absorption features that represent FeOH (2,235-2,260 nm) and MgOH (2,320-2,360 nm) bonds (Herrmann et al., 2001). Both the FeOH and MgOH bonds wavelengths have been illustrated to increase with iron content (McLeod and Stanton., 1984; Pontual et al, 1997). The MgOH absorption feature occurs over the same range of wavelengths as CO_3 (Fig. 2.16). Due to the varying degree of carbonate spot overprinting in the Boundary samples and overlap with the MgOH range, the measured MgOH wavelengths were not used in this study.

2.7.1 Results

The AlOH wavelengths of white mica within the Boundary deposit range from 2,190-2,213 nm, with the majority of samples falling in the range of 2,200-2,205 (Fig. 2.17a). The FeOH wavelengths range from 2,248-2,257 and display a normal distribution centered at 2,252 nm (Fig. 2.17b). For ease of description, samples that exhibit AlOH wavelengths ≤ 2,205 nm are designated as muscovitic mica, whereas those with wavelengths ≥ 2,210 nm are termed phengitic mica. FeOH wavelengths can be used to estimate chlorite compositions (e.g., McLeod and Stanton, 1984; Pontual et al., 1997; Jones et al., 2005), in which longer FeOH wavelengths correlate to Fe-rich chlorite. The FeOH wavelengths from the Boundary deposit rocks do increase with decreasing Mg number (100*MgO/[MgO+FeO])(Fig. 2.18). Samples that contain higher amounts of Fe- and Mg-bearing minerals (i.e., pyrite, chalcopyrite, carbonate) plot further from the regression line (Fig. 2.18).

2.8 Discussion

2.8.1 Rhyolite Formation and Tectonic Implications

Rhyolites from the Boundary deposit have FIIIa chemical signatures (Fig. 2.9f). Rocks with FIIIa signatures are interpreted to have formed via partial melting of either continental or oceanic crust due to basaltic underplating during rifting (Lesher et al., 1986; Barrie et al., 1993; Hart et al., 2004; Piercey, 2011). Hart et al. (2004) further argued that FIIIa rhyolites form at shallow depths (<10 km), due to low pressure (<0.5 Gpa) and high temperature (900-1000°C) melting. Melts generated under such conditions typically have negative Ti-Nb anomalies and weakly depleted HREE, Y, and Eu, implying formation at shallow levels and at high temperatures, and these are features present in the rhyolitic rocks of the Boundary deposit (this study and Piercey et al., 2014),

Previous studies have argued that the Tally Pond group formed as the result of continental arc magmatism based on U-Pb geochronology and evolved Nd and Pb isotopic signatures (e.g., Swinden and Thorpe, 1984; Dunning et al., 1991; Pollock, 2004, Rogers et al., 2006; McNicoll et al., 2010). However, rhyolites from the Boundary deposit have signatures that are more akin to those that have formed in post-Archean, juvenile environments (e.g., Figs. 2.9-2.10; Hart et al., 2004; Piercey, 2011; Piercey et al., 2014). These data therefore suggest that the Boundary deposit host rocks could not have formed from solely continental crustal sources and must have had input from sources more juvenile than typical, evolved upper continental crust. Additionally, the Tally Pond group is predominantly bimodal, a characteristic commonly observed in continental rift environments in which felsic rocks are produced by partial melting of overlying crust by basaltic underplating (Barrie et al., 1993; Wright et al., 1996; Smith et al., 2003) as opposed to the full volcanic spectrum (basalt-andesite-dacite-rhyolite) produced by continuous fractionation in continental arc environments (Arculus, 1994; Lentz, 1998; Hart et al., 2004).

Zagorevski et al. (2010) and Piercey et al. (2014) provided tectonic models that incorporate both the juvenile rift and continental arc signatures present within the Tally Pond group, inferring a rifted continental arc on the Iapetus-side of Ganderia. A rift environment would result in crustal thinning and asthenospheric mantle upwelling leading to basaltic underplating of the overlying arc crust (Hart et al., 2004, Zagorevski et al., 2010, Piercey et al., 2014). Shallow (<10 km) partial melting of this crust would result in the production of the bimodal volcanic rocks present at the Boundary deposit (Zagoreveski et al., 2010, Piercey et al., 2014). Furthermore, the partial melting of arc crust would have resulted in rhyolitic melts with hybrid geochemical signatures containing a juvenile component from the basaltic underplating and a crustal signature from the arc crust.

The rifted arc model also explains the VMS endowment in the Tally Pond group, as arc rifting creates a geodynamic environment favorable to VMS formation (i.e., Franklin et al., 2005; Galley et al., 2007). In particular, as rifting occurs, the thinning of the overlying crust and upwelling of asthenospheric mantle allow for shallow emplacement of heat sources (magma chambers, intrusions, etc.) needed to drive the convection of hydrothermal fluids (e.g., Lesher et al., 1986; Lentz, 1998; Hart et al., 2004; Piercey, 2009, 2011). In addition, rifting increases the fracture permeability and porosity, which creates hydrothermal fluid pathways necessary for constant discharge and recharge of seawater-based hydrothermal fluids (e.g., Franklin et al., 1981, 2005; Lydon, 1984, 1988; Large, 1992; Lentz, 1998; Barrie and Hannington, 1999; Galley et al., 2007; Piercey, 2009, 2011).

2.8.2 Characteristics and Controls on Hydrothermal Alteration

Because the Boundary deposit has not undergone any significant metamorphism and has remained mostly structurally intact, most, if not all of the hydrothermal alteration features are extremely well preserved and close to their original distribution. Whereas most VMS deposits only exhibit classic discordant, pipe-like alteration (e.g., Riverin and Hodgson, 1980; Gemmell and Large, 1992; Franklin et al., 2005), Boundary exhibits both discordant alteration and laterally extensive alteration, especially near the ore body. Laterally extensive alteration is interpreted to be a product of upflow rather than semi-conformable alteration associated with hydrothermal recharge (e.g., Galley, 1993;

Franklin et al., 2005). Its stratigraphic, semi-conformable geometry is a function of unfocused discharge into relatively unconsolidated and porous volcaniclastic rocks, which make up the footwall that were overlain by an impermeable (to semi-permeable), flow-dominated hanging wall (Doyle and Allen, 2003; Gibson, 2005; Franklin et al., 2005). This stratigraphic and hydrothermal architecture was also responsible for the development of the replacement-type mineralization and alteration preserved in the Boundary deposit (Piercey et al., 2014).

The intense depletion of Na_2O throughout both the hanging wall and footwall (Fig. 2.11a) is due to the destruction of feldspar and zoisite during hydrothermal alteration (e.g., Riverin and Hodgson, 1980; Knuckey et al., 1982; Date et al., 1983; Barrett and MacLean, 1994), which is likely the result of one or more of the following reactions (Riverin and Hodgson, 1980; Barrett and MacLean, 1994):

$$(1)\quad \underset{\text{Albite}}{3NaAlSi_3O_8} + 2K^+_{(aq)} + 2H^+_{(aq)} = \underset{\text{Muscovite}}{KAl_3Si_3O_{10}(OH)_2} + \underset{\text{Quartz}}{6SiO_{2(aq)}} + 3Na^+_{(aq)}$$

$$(2)\quad \underset{\text{Andesine}}{2Ca_{0.5}Na_{0.5}Al_{1.5}Si_{2.5}O_8} + 4.48Al(OH)_4^-{}_{(aq)} + 1.16K^+_{(aq)} + 2.23H^+_{(aq)} =$$

$$\underset{\text{Muscovite}}{1.16KAl_3Si_3O_{10}(OH)_2} + \underset{\text{Quartz}}{1.5SiO_{2(aq)}} + Na^+_{(aq)} + Ca^{2+}_{(aq)}$$

$$(3)\quad \underset{\text{Zoisite}}{Ca_2Al_2Si_3O_{12}(OH)} + K^+_{(aq)} = \underset{\text{Muscovite}}{KAl_3Si_3O_{10}(OH)_2} + \underset{\text{Quartz}}{6SiO_{2(aq)}} + 3Na^+_{(aq)}$$

$$(4)\ \underset{\text{Albite}}{2NaAlSi_3O_8} + 5Mg^{2+}_{(aq)} + 8H_2O = \underset{\text{Chlorite}}{Mg_5Al_2Si_3(OH)_8} + \underset{\text{Quartz}}{3SiO_{2(aq)}} + 2Na^{+}_{(aq)} + 2H^{+}_{(aq)}$$

These reactions result in the loss of Na (and Ca) and gains in K and Si (and Mg in Eq. 4), which are illustrated by the mass changes for the quartz-sericite zone (Table 3, Fig. 2.13a). This zone does not show significant Mg gains; however, the alteration of albite to chlorite does take place (Fig. 2.6d; Eq. 4). The formation of chlorite in the chlorite-sericite and intense chlorite assemblages, is due to the destruction of (previously formed) white mica (Riverin and Hodgson, 1980; Knuckey et al., 1982):

$$(5)\ \underset{\text{Muscovite}}{2K(Al_3Si_3O_{10})(OH)_2} + 3H_4SiO_{4(aq)} + 9Fe^{2+}_{(aq)} + 6Mg^{2+}_{(aq)} + 18H_2O =$$

$$\underset{\text{Chlorite}}{3Mg_2Fe_3Al_2Si_3O_{10}(OH)_8} + 2K^{+}_{(aq)} + 28H^{+}_{(aq)}$$

$$(6)\ \underset{\text{Phengite}}{K_2(Fe^{2+}, Mg)Al_3Si_7AlO_{20}(OH)_4} + 9FeCl_{2(aq)} + 16H_2O =$$

$$\underset{\text{Chlorite}}{(Fe^{2+},Mg)_{10}Al_2Si_6Al_2O_{20}(OH)_{16}} + H_4SiO_{4(aq)} + 2KCl_{(aq)} + 16HCl_{(aq)}$$

These reactions result in a net gain of Mg and Fe, whereas K (±Si) is lost from the system, which is observed in the mass changes within the chlorite-altered assemblages (Table 3, Fig. 2.13a-b). However, samples within the chlorite-sericite assemblage show varying degrees of K_2O losses, depending on the abundance of sericite relative to chlorite in the rocks. Losses of SiO_2 are greatest in the intense chlorite samples, which also exhibit losses of K_2O (Fig. 2.13a). Despite reactions 5 and 6 accounting for gains of both MgO and Fe_2O_3, the gains in these elements are amplified by additional gains of MgO associated with chaotic carbonate alteration, and Fe_2O_3 associated with pyrite stringers commonly found within the quartz-sericite assemblage (Fig. 2.13c).

A series of 3D models representing the Boundary deposit, including the main lithologic contacts, ore zones, Wagner fault, and key alteration features are shown in Figure 2.19. The mineralized horizon is comprised of the upper ~30m of lapilli tuff and tuff, where the lower footwall contact (Fig. 2.19a) contact marks the first significant (>2m) aphyric flow or flow breccia. Massive pyrite zones are those with >15% assayed Fe and have been cross-checked with drill logs and cross sections. As expected, the CCPI (Fig.2.19b) systematically increases towards zones underlying both the pyrite and Cu-rich zones, reflective of the Mg-Fe-enrichment in these areas. These high Mg-Fe zones are also mirrored by low AlOH and high FeOH SWIR absorption depth values (Fig. 2.19c-d); the higher AlOH and lower FeOH correspond to sericite-rich zones proximal to high Zn-rich zones (Fig. 2.19), a relationship also observed in other VMS deposits (e.g., Jones et al. 2005; Yang et al. 2011). The deepest FeOH absorption features correlate with the highest CCPI values, which underlie the South zone and the Cu-rich areas of the North zone. This not only suggests that these areas have been offset by the Wagner fault, but also that they represent primary, hydrothermal vent locations (i.e., upflow zones)(Fig. 2.19d).

The results above are also reflected in the 3D distribution of mass change results, particularly gains and losses in MgO, K_2O, and SiO_2. The interpreted hydrothermal upflow zones contain mass gains in K_2O and MgO, with >3% MgO gains near the center and ~2% MgO and >0.5% K_2O gains near the outer edge of the upflow zone; each upflow zone broadly coincides with Cu-enrichment above it and coincident losses in SiO_2 (Fig. 2.19e).

The alteration patterns, and the chemical attributes thereof, as outlined above are controlled by two factors: 1) the host volcanic facies; and 2) the hydrothermal fluid conditions (i.e., temperature, composition, pH). The relatively simple stratigraphy of the Boundary deposit makes documenting the type and intensity of alteration straightforward. Flows and breccias are more crystalline and resistant to hydrothermal alteration, whereas lapilli tuff and tuff units are typically glassy and more susceptible to alteration (e.g., McPhie et al., 1993; Large et al., 2001). This is evident at the Boundary deposit as the flows and breccias are far less altered than the lapilli tuff and tuff units. Furthermore, the porosity and permeability of these units differ due to their fabric. Alteration in the flows and breccias would have been dependent on fracture-controlled porosity and permeability, which include quench fractures or cooling joints (Large et al., 2001). In both footwall and hanging wall breccias (and flow-banded rhyolite flows) only the inter-fragment regions show alteration, whereas the coherent fragments and massive flows display little to no alteration (Fig. 2.4a-b,e-f), implying fracture controlled fluid flow and alteration. Conversely, the permeability and porosity of the lapilli tuff and tuff was controlled by inter-clast and inter-particle pore space (e.g., McPhie et al., 1993; Large et al., 2001). The lapilli tuff at the Boundary deposit are generally clast-supported (Fig. 2.4c), which provided an extremely porous matrix consisting of loosely packed ash and/or void space. Consequently, hydrothermal fluids were able to move along numerous paths, rather than just through a single synvolcanic structure, thus resulting in much more widespread and intense fluid-rock interaction and alteration. This relationship has been observed at the Boundary deposit (e.g., Figs. 2.5a-b), and is also recorded as much greater mass changes and the subtle mobility of the LREE of the lapilli tuff relative to the more coherent flows and breccias (Fig. 2.13).

The physicochemical conditions of fluid rock interaction also play a key role in the alteration zoning and chemistry of footwall alteration (e.g., Riverin and Hodgson, 1979; Lydon, 1984, 1988; Gemmell and Large, 1992; Large et al., 2001; Schardt et al., 2001; Franklin et al., 2005; Galley et al., 2007). The well-developed zoning from distal quartz-sericite, to chlorite-sericite, to intense chlorite reflects changing fluid-rock interaction, and fluid temperatures and pH. Schardt et al. (2001) demonstrated that in Cu-Zn systems, the inner, intense chlorite alteration generally forms at higher temperatures (250-350°C) and at moderate pH levels (4.5-5.5). As Mg is fixed within the main upflow zones through the formation of chlorite, the fluids on the periphery of the vent are not only cooler, but become more acidic and form the chlorite-sericite and quartz-sericite alteration assemblages. Increased fluid-rock interactions reduce some of the pH lowering effects of Mg fixation and allow chlorite to form in some areas of the quartz-sericite alteration assemblage (Fig. 2.6d). Additionally, this process explains the absence of chlorite alteration within the hanging wall above the peripheral vent structures. By the time the fluids reached the hanging wall, nearly all the Mg had been fixed within the chloritic pipe leaving only acidic (and cooler) fluids, which created the intense quartz-sericite alteration within the hanging wall.

2.8.3 Relationships between Short Wave Infrared Spectroscopy, Alteration Mineralogy and Lithogeochemistry

The SWIR data show clear distinctions among the alteration assemblages (Table 3). Notably, the intense chlorite samples have AlOH absorption wavelengths ~2,196 nm, indicative of sodium bearing white mica (paragonite). The presence of paragonite within the intense alteration pipe is likely the result of a late stage overprint during the waning stages of hydrothermal activity, in which unmodified Na-rich seawater flushed through the hydrothermal system, forming sodic mica (e.g., Date et al., 1983; Green et al., 1983). The chlorite-sericite and quartz-sericite samples exhibit longer wavelengths, the longest of which occur in samples proximal to the Zn-ore zones, indicative of phengite (Fig. 2.20). These samples also contain elevated Zn, Pb, Hg, and Sn (e.g., elements of PCA component 3; Table 2).

The relative proportions of white mica and chlorite is often difficult to determine macroscopically and can be time consuming to determine petrologically. However, in comparison with the whole rock geochemistry, the AlOH depth shows a weak correlation with K_2O (sericite; Fig. 21a), as does FeOH depth with MgO (chlorite; Fig. 2.21b). Despite the weak correlation, the absorption depth feature (Fig. 21c) does appear to correspond to the relative abundance of sericite and chlorite. The scatter in Figure 2.21, is attributed to the presence of other K_2O- and MgO-bearing minerals (e.g., K-feldspar, carbonate), in addition to sericite and chlorite.

Huston et al. (1997) and Herrmann et al. (2001) demonstrated that sericite/chlorite ratios can be estimated semi-quantitatively using the ratio of AlOH to FeOH absorption depths in SWIR spectra (i.e., AlOH/FeOH). The AlOH/FeOH depth ratios in Boundary samples show a distinct correlation with decreasing AlOH/FeOH depths as CCPI increases (Fig. 2.21c). The high CCPI values generally correlate with the intensely altered chlorite pipes that underlie the Cu-rich ore zones, therefore implying that the AlOH/FeOH depth ratio could be used to identify prospective chlorite and Cu-rich alteration zones. In contrast, the best indicator for Zn-rich zones is AlOH wavelength, particularly values greater than 2208 nm (Fig. 2.20). The distribution and variation of the AlOH and FeOH absorption features at the Boundary provide an effective method in tracing fluid pathways and potential vectors to mineralization as summarized in Figure 2.22).

2.8.4 Ore Deposition Mechanism: Exhalative or Replacement

The dominant ore deposition mechanism is difficult to determine at the Boundary deposit. Bedded sulfides along the southern edges of both ore zones provide evidence for exhalative formation, whereas clast-rich sulfides (Fig. 2.7b) and relict hanging wall flow textures indicate replacement processes also took place. The massive sulfides, which can form from either process (e.g., Doyle and Allen, 2003), occur at both the hanging wall-footwall contact and as discrete lenses solely within the lapilli tuff. Although both forms of mineralization are present, a few key lines of evidence provide insight as to which mechanism was the dominant mineralization process.

1) Hanging wall-footwall contact massive sulfides- In non-mineralized zones, the 10 cm, fine-grained tuff layer found at the top of the aphyic lapilli tuff is directly overlain by the hanging wall quartz-phyric flows and breccia. The tuff layer is traceable throughout most of the deposit, including below the massive sulfide lenses at the hanging wall-footwall contact. The hanging wall contact with the ore lenses typically sharp and hanging wall replacement textures absent throughout the lenses except near the top in rare cases. The sulfide lenses found above this tuff layer with sharp hanging wall contacts indicate that they were likely deposited prior to the deposition of the hanging wall. The bedded sulfides that occur directly above the tuff layer, distal to the main alteration pipes also indicate exhalative process and contain drop stones of lapilli tuff.
2) Hanging wall alteration/mineralization- As stated previously the hanging wall fabric is not favorable for replacement processes to take place. The limited porosity and permeability inhibited hydrothermal fluid flow and mineralization. However, moderate sericite and minor chlorite alteration, determined petrographically and geochemically (2.11b-d; 2.13a-c), shows that hydrothermal fluids were able to somewhat affect the hanging wall. Furthermore, replacement style mineralization (relict flow textures) is found

within the hanging wall, though it does not extend more than a couple meters and is very uncommon.

3) Footwall alteration/mineralization- The footwall lapilli tuff and tuff unit is far more conducive for hydrothermal fluid flow given the host rock properties. The intensity of hydrothermal alteration, as demonstrated by the geochemistry and mass change calculations, is far greater than in the hanging wall. Although this does not prove replacement mineralization, it does show that the footwall interacted with far more hydrothermal fluids. The main evidence for replacement within the footwall lapilli tuff and tuff unit is the clast-rich massive sulfides, in which the ash tuff matrix has been replaced by sulfides (e.g., Fig. 2.7b). Both the basal portions of the hanging wall-footwall contact massive sulfides and the smaller footwall sulfide lenses are clast-rich, a feature indicative of replacement in the Boundary deposit (Piercey et al., 2014).

The massive sulfides that occur at the hanging wall-footwall and corresponding bedded sulfides were deposited via exhalative processes, whereas the hanging wall sulfides, basal portion of the hanging wall-footwall contact massive sulfides, and footwall lapilli tuff and tuff sulfides were all deposited via replacement processes. Although mineralization by stratigraphic position cannot be calculated, replacement mineralization appears to be the dominant mechanism. The replacement footwall lapilli tuff mineralization accounts for the majority of mineralization at the Boundary deposit

(Appendix A), followed by the exhalative hanging wall-footwall contact sulfides (massive and bedded) and hanging wall replacement mineralization.

2.8.5 The Boundary Replacement Model

Piercey et al. (2014) demonstrated that the Boundary deposit meets the criteria set forth by Doyle and Allen (2003) for replacement-style VMS deposits. However, prior to subseafloor replacement processes, Boundary was initially a seafloor VMS (Fig. 2.23a). The main alteration pipe formed along a single synvolcanic structure within the coherent footwall flows and breccias before entering the highly permeable and porous upper lapilli tuff unit that allowed the formation of multiple vent structures (Fig. 2.23a). Given the size of these vent structures, the primary alteration would have been relatively limited, consisting of a chlorite (reaction 4) or sericite (reaction 1-3) depending on the size of the vent.

As hydrothermal activity progressed, alteration in the main upflow zones broadened (Fig. 2.23b). The main upflow zones became well defined and early sericite alteration was altered to chlorite alteration (e.g., reactions 5 and 6). Smaller offshoots of the main upflow zones would have contained chlorite, but after the precipitation of chlorite and progressive cooling, these smaller zones would have become dominated by sericite. Initially, these fluids were hot (~300°C) and depleted of Mg due to chlorite formation; thus, white mica precipitation would be minimal and muscovitic in composition. As the fluids rose towards the seafloor, they became cooler and Mg-rich through the drawdown of unmodified seawater, which created alteration pipes of increasingly phengitic mica. Precipitation of sulfides occurred primarily at the seafloor and minor amounts may have formed below as a result of mixing with unmodified seawater (e.g., Doyle and Allen, 2003). Sulfides also precipitated lower in the offshoot upflow zones as these fluids cooled faster than those in the central upflow zones.

Following the deposition of the hanging wall units (~509 Ma; Fig. 2.23c), the internal behavior of the Boundary hydrothermal system would have been greatly altered. The impermeable hanging wall would have forced fluids to move more laterally though the porous lapilli tuff both at the hanging wall contact and within the alteration pipe(s). As the alteration pipes expanded laterally, preexisting sericite was converted to chlorite (reactions 5-6); incomplete conversion of sericite resulted in the formation of the chlorite-sericite zones. Additionally, the lateral fluid flow resulted in the replacement of the lapilli tuff by sulfide mineralization that underlies parts of the massive sulfides (Fig. 2.7b). As Figure 2.11 illustrates, very few hanging wall samples display even moderate chlorite alteration, and those that do occur directly over the main ore lenses. Although hanging wall alteration is evident both visually (i.e., sericite, disseminated pyrite) and geochemically (e.g., SiO_2, K_2O mass gains, Na_2O depletions), the intensity is limited, primarily occurring as quartz-sericite alteration, likely due to the limited permeability of the hanging wall.

The deposition of the hanging wall likely marked the decline of hydrothermal activity at Boundary; however, its life may have been temporarily prolonged during the emplacement of the quartz-porphyry intrusion (Figs. 2.4g and 2.23c). Although only two samples were taken from the intrusion, they display similar immobile element and alteration patterns (e.g., Figs. 2.9a-f, 2.10a, and 2.11a-f) to both the hanging wall and footwall. It is uncertain as to whether or not the intrusion contributed heat and fluids/metals, especially near the South zone. Further work is required to decipher the relationship between this intrusion and the Boundary alteration and mineralization. As the hydrothermal activity came to an end, Na-bearing seawater was circulated though the main upflow zones, which resulted in the formation of the minute amounts of paragonite identified by SWIR spectroscopy within the intense chlorite and chlorite-sericite samples. (Table 3, Fig. 2.22).

2.9 Conclusions

The main conclusion of this manuscript include:

1. The Boundary deposit formed on the leading edge of Ganderia in rhyolitic rocks within a rifted continental arc. This is supported by immobile element geochemistry and is consistent with previous studies within the Tally Pond group.
2. The Boundary deposit contains three dominant alteration assemblages: quartz-sericite, chlorite-sericite, and intense chlorite, each which have distinct geochemical and hyperspectral signatures. These alteration assemblages are predominantly controlled by the host rock permeability and porosity in addition to hydrothermal fluid conditions.
3. Alteration indices, such as CCPI, and element gains (e.g., Cu, MgO, MnO, Fe_2O_3) provide useful vectors for Cu-mineralization; whereas, Hg/Na_2O and Hg, Zn, Pb, Cd, and Ba increase in proximity to Zn mineralization.

4. Mass changes among the major oxides (e.g., SiO_2, MgO, Fe_2O_3, K_2O), base metals, transition metals (e.g., Ba, Sr) vary with each alteration assemblage. Other elements, such as the REEs and high field strength elements, are largely immobile throughout the deposit.
5. Hyperspectral data reveal distinct trends that correlate with alteration assemblages and geochemistry: A) AlOH absorption hull depths loosely correspond with the K_2O wt% and the wavelengths increase proximal to Zn-rich mineralization; B) FeOH wavelengths correlate with whole rock Mg number and indicate a high abundance of Mg-rich chlorite in the intense chlorite assemblage; and C) the absorption hull depths for both AlOH and FeOH are useful in differentiating between assemblages and the ratio of the two (AlOH depth/FeOH depth) correlates strongly with the CCPI.
6. The Boundary deposit formed as a result of both exhalative and replacement mechanisms. The majority of the mineralization, including the clast-rich basal portions of the massive sulfides, footwall mineralization, and the relict flow band mineralization, was formed through replacement processes. Only the massive and bedded mineralization at the hanging wall-footwall contact, which accounts for a lesser portion of mineralization at the Boundary deposit, formed through exhalative processes.

Acknowledgements

Financial and logistical support for this project was provided by Teck Resources Ltd., a Natural Sciences and Engineering Research Council of Canada (NSERC) Discovery grant to Piercey, and SEG Graduate Fellowship and Research Grant to Buschette. Piercey is also funded by the NSERC-Altius Industrial Research Chair at Memorial University, which is supported by NSERC, Altius Resources Inc., and the Research and Development Corporation of Newfoundland and Labrador. Numerous discussions with the staff of the Duck Pond mine, particularly Gerry Squires and Darren Hennessey are gratefully acknowledged. Additionally, the Terraspec™ and Leapfrog Geo™ training as well as numerous discussions and reviews by Jonathan Cloutier of Memorial University is greatly appreciated. Lab assistance provided by Pam King and Lakmali Hewa of CREAIT at Memorial University is appreciatively acknowledged.

References

Arculus, R.J., 1994, Aspects of magma genesis in arcs: Lithos, v. 33, p. 189-208.

AusSpec International, 2008, Spectral Interpretation Field Manual: GMEX, Edition 3, Volumes 1-10.

Barrett, T.J., and MacLean, W.H., 1991, Chemical, mass, and oxygen isotope changes during extreme hydrothermal alteration of an Archean rhyolite, Noranda, Quebec: Economic Geology, v. 86, p. 406-414.

Barrett, T.J., and MacLean, W.H., 1994, Chemostratigraphy and hydrothermal alteration in exploration for VHMS deposits in greenstones and younger rocks: in Lentz, D. R., ed., Alteration and Alteration Processes Associated with Ore-Forming Systems, Short Course Notes Volume 11, Geological Association of Canada, p. 433-467.

Barrett, T.J., Dawson, G.L., and MacLean, W.H., 2008, Volcanic stratigraphy, alteration, and sea-floor setting of the Paleozoic Feitais massive sulfide deposit, Aljustrel, Portugal: Economic Geology, v. 103, p. 215–39.

Barrie, C.T., 1995, Zircon thermometry of high-temperature rhyolites near volcanic associated massive sulfide deposits, Abitibi subprovince, Canada: Geology, v. 23, p. 169-172.

Barrie, C.T., and Hannington, M.D., 1999, Introduction: classification of VMS deposits based on host rock composition, in volcanic-associated massive sulfide deposits: processes and examples in modern and ancient environments, (eds.) C.T. Barrie and M.D. Hannington; Society of Economic Geologists, Reviews in Economic Geology, v. 8, p. 2-10.

Barrie, C.T., Ludden, J.N., and Green, T.H., 1993, Geochemistry of volcanic rocks associated with Cu-Zn and Ni-Cu deposits in the Abitibi Subprovince: Economic Geology, v. 88, p. 1341-1358.

Berkenbosch, H.A., de Ronde, C.E.J., Gemmell, J.B., McNeill, A.W., and Goeman, K., 2012, Mineralogy and formation of black smoker chimneys from Brothers submarine volcano, Kermadec arc: ECONOMIC GEOLOGY, v. 107, p. 1613-1633.

Besson, G., and Drits, V.A., 1997a, Refined relationships between chemical composition of dioctahedral fine-grained micaceous minerals and their infrared spectra within the OH stretching region. Part 1: Identification of the OH stretching band: Clays and Clay Minerals, v. 45, p. 158-169.

Besson G., and Drits V.A., 1997b, Refined relationships between chemical composition of dioctahedral fine-grained micaceous minerals and their infrared spectra within the OH stretching region. Part II: The main factors affecting OH vibrations and quantitative analysis: Clays and Clay Minerals, v. 45, p. 170-183.

Bradshaw, G.D., Rowins, S.M., Peter, J.M., and Taylor, B.E., 2008, Genesis of the Wolverine volcanic sediment-hosted massive sulfide deposit, Finlayson Lake district, Yukon, Canada: Mineralogical, mineral chemical, fluid inclusion, and sulfur isotope evidence: Economic Geology, v. 103, p. 35–60.

Collins, C.J., 1989, Report on lithogeochemical study of the Tally Pond Volcanics and associated alteration and mineralization: Unpublished Report for Noranda Exploration Company Limited (Assessment File 012A/1033 Newfoundland Department of Mines and Energy, Mineral Lands Division): St. John’s, Newfoundland, 87 p.

Date, J., Watanabe, Y., and Saeki, Y., 1983, Zonal alteration around the Fukazawa Kuroko deposits, Akita Prefecture, northern Japan: Economic Geology Monograph 5, p. 365-386.

de Ronde, C.E.J., Hannington, M.D., Stoffers, P., 2005, Evolution of a submarine magmatic-hydrothermal system: Brothers volcano, southern Kermadec arc, New Zealand: Economic Geology, v. 100, p.1097-1133.

de Ronde, C.E.J., Walker, S.L., Ditchburn, R.G., Caratori Tontini, F., Hannington, M.D., Merle, S.G., Timm, C., Handler, M.R., Wysoczanski, R.J., Dekov, V.M., Kamenov, G.D., Baker, E.T., Embley, R.W., Lupton, J.E., and Stoffers, P., 2014, The anatomy of a buried submarine hydrothermal system, Clark volcano, Kermadec arc, New Zealand: ECONOMIC GEOLOGY, v. 109, p. 2261-2292.

Deer, W.A., Howie, R.A., and Zussman, J., 1992, Introduction to the rock- forming minerals, 2nd ed.: New York, Longman Scientific and Technical, 696 p.

Doyle, M.G., and Allen R.L., 2003, Subsea-floor replacement in volcanic-hosted massive sulfide deposits: Ore Geology Reviews, v. 23, p. 183–222.

Doyle, M.G., and Huston, D.L., 1999, The subsea-floor replacement origin of the Ordovician Highway-Reward VMS deposit, Mount Windsor Subprovince, northern Queensland: Economic Geology, v. 94, 825–844.

Dunning, G.R., Swinden, H.S., Kean, B.F., Evans, D.T.W., and Jenner, G.A., 1991, A Cambrian island arc in Iapetus: Geochronology and geochemistry of the Lake

Ambrose volcanic belt, Newfoundland Appalachians: Geological Magazine, v. 128, p. 1–17.

Evans, D.T.W., and Kean, B.F., 2002, The Victoria Lake Supergroup, central Newfoundland: Its definition, setting and volcanogenic massive sulfide mineralization: Newfoundland and Labrador Department of Mines and Energy, Geological Survey, Open File NFLD/2790, 68 p.

Franklin, J.M., 1995, Volcanic-associated massive sulfide base metal: Geological Survey of Canada, Geology of Canada, no.8, p. 158–183.

Franklin, J.M., Gibson, H.L., Galley, A.G., and Jonasson, I.R., 2005, Volcanogenic massive sulfide deposits: Economic Geology 100th Anniversary Volume, p. 523-560.

Franklin, J.M., Lydon, J.W., and Sangster, D.F., 1981, Volcanic-associated massive sulfide deposits: Economic Geology 75th Anniversary Volume, p. 485–627.

Galley, A.G., 1993, Characteristics of semi-conformable alteration zones associated with volcanogenic massive sulphide districts: Journal of Geochemical Exploration, v. 48, p. 175–200.

Galley, A.G., Hannington, M.D., and Jonasson, I.R., 2007, Volcanogenic massive sulphide deposits: In mineral deposits of Canada: A synthesis of major deposit types, district metallogeny, the evolution of geological provinces, and exploration methods, Geolocial Association of Canada, Mineral Deposits Division, Special Publication No. 5.

Galley, A.G., Watkinson, D.H., Jonasson, I.R., and Riverin, G., 1995, The subsea-floor formation of volcanic-hosted massive sulfide: Evidence from the Ansil deposit, Rouyn-Noranda, Canada: Economic Geology, v. 90, p. 2006–2017.

Gemmell, J.B., and Fulton, F., 2001, Geology, genesis, and exploration implications of the footwall and hanging-wall alteration associated with the Hellyer volcanic-hosted massive sulfide deposit, Tasmania, Australia: Economic Geology, v. 96, p. 1003–1035.

Gemmell, J.B., and Large, R.R., 1992, Stringer system and alteration zones underlying the Hellyer volcanic-hosted massive sulfide deposit, Tasmania, Australia: Economic Geology v. 87, p. 620–649.

German, C.R., and Von Damm, K.L., 2003, Hydrothermal systems. In: Elderfield H (ed.): Treatise on Geochemistry-The Oceans, v. 6, p. 181-222.

Gibson, H.L., 2005, Volcanic-hosted ore deposits, in Marti, J., and Ernst, G.G.J., eds., Volcanoes in the environment: New York, Cambridge University Press, p. 332–386.

Grant, J. A., 1986, The isocon diagram - a simple solution to Gresens' equation for metasomatic alteration. Economic Geology, 81, p. 1976-1982.

Green, G.R., Ohmoto, H., Date, J., Takahashi, T., 1983, Whole-rock oxygen isotope distribution in the Fukazawa-Kosaka area, Hokuroku District, Japan, and its potential application to mineral exploration: Economic Geology Monolith, v. 5, p. 395-411.

Gresens, R.L., 1967, Composition-volume relationships of metasomatism. Chemical Geology, 2, p. 47-55.

Gruen, G., Weis, P., Driesner, T., Heinrich, C.A., and de Ronde, C.E.J., 2014, Hydrodynamic modeling of magmatic-hydrothermal activity at submarine arc volcanoes with implications for ore deposit formation: Earth and Planetary Science Letters, v. 404, p. 307-318.

Guidotti, C.V., Sassi, F.P., 1998, Petrogenetic significance of Na–K white mica mineralogy: recent advances for metamorphic rocks: European Journal of Mineralogy, v. 10, p. 815–854.

Hannington, M.D., Barrie, C.T., and Bleeker, W., 1999, The giant Kidd Creek volcanogenic massive sulfide deposit, western Abitibi subprovince, Canada: Preface and introduction: Economic Geology Monograph 10, p. 1–30.

Hart, T.R., Gibson, H.L., and Lesher, C.M., 2004, Trace element geochemistry and petrogenesis of felsic volcanic rocks associated with volcanogenic massive Cu-Zn-Pb sulphide deposits, Economic Geology, v. 99, p. 1003–1013.

Hekinian, R., Fevrier, M., Bischoff, J.L., Picot, P., and Shanks, W.C., 1980, Sulfide deposits from the East Pacific Rise near 21°N: Science, v. 207, p.1433-1444.

Herrmann, W., Blake, M., Doyle, M., Huston, D., Kamprad, J., Merry, N. and Pontual, S., 2001, Short wavelength infrared (SWIR) spectral analysis of hydrothermal alteration zones associated with base metal sulfide deposits at Rosebery and Western Tharsis, Tasmania, and Highway-Reward, Queensland: Economic Geology, v. 96, p. 939–955.

Herzig, P.M., and Hannington, M.D., 1995, Polymetallic massive sulfides at the modern seafloor-a review: Ore Geology, v. 10, p. 95-115.

Huston, D.L., Kamprad, J., and Brauhart, C., 1997, Preliminary results of PIMA analysis of the alteration zone underlying the Sulphur Springs deposit, Panorama district, Pilbara block, Western Australia: Australian Geological Survey Organization Record 1997/14, 36 p.

Ishikawa, Y., Sawaguchi, T., Ywaya, S., and Horiuchi, M., 1976, Delineation of prospecting targets for Kuroko deposits based on modes of volcanism of underlying dacite and alteration halos: Mining Geology, v. 26, p. 105-117.

Jenner, G.A., 1996, Trace element geochemistry of igneous rocks: Geochemical nomenclature and analytical geochemistry: in Wyman, D.A., ed., Trace Element Geochemistry of Volcanic Rocks: Applications for Massive Sulfide Exploration: Geological Association of Canada, Short Course Notes, v. 12, p. 51–77.

Jenner, G.A., Longerich, H.P., Jackson, S.E., and Fryer, B.J., 1990, ICP-MS – A powerful tool for high-precision trace element analysis in Earth sciences: Evidence from analysis of selected U.S.G.S. reference samples: Chemical Geology, v. 83, p. 133-148.

Jones, S., 2005, Short wavelength infrared spectral characteristics of the HW horizon: Implications for exploration in the Myra Falls volcanic-hosted massive sulfide camp, Vancouver Island, British Columbia, Canada: Economic Geology, v. 100, p. 273–94.

Kean, B.F. and Evans, D.T.W. 1986, Metallogeny of the Tulks Hill volcanics, Victoria Lake Group, central Newfoundland: Report—Government of Newfoundland and Labrador, Department of Mines and Energy, Mineral Development Division, v. 86-1, p. 51-57.

Kean, B.F., Evans, D.T.W., and Jenner, G.A., 1995, Geology and mineralization of the Lushs Bight Group: St. John's, Newfoundland, Geological Survey of Newfoundland and Labrador, Mineral Development Division, Report 95-05, 204 p.

Knuckey, M.J., Comba, C.D.A., and Riverin, G., 1982, Structure, metal zoning and alteration at the Millenbach Deposit, Noranda, Quebec: Special Paper – Geological Association of Canada, v. 25, p. 255-295.

Large, R.R. 1992, Australian volcanic-hosted massive sulfide deposits: Features, styles, and genetic models: Economic Geology, v. 87, p. 471–510.

Large, R.R., Gemmell, J.B., Paulick, H., and Huston, D.L., 2001, The alteration box plot: A simple approach to understanding the relationships between alteration mineralogy and lithogeochemistry associated with VHMS deposits: Economic Geology, v. 96, p. 957–971.

Lentz, D.R., 1998, Petrogenetic evolution of felsic volcanic sequences associated with Phanerozoic volcanic-hosted massive sulphide systems: The role of extensional geodynamics: Ore Geology Reviews, v. 12, p. 289–327.

Lentz, D., and Wilson, R.A., 1997, Chemostratigraphic analysis of the volcanic and sedimentary rocks in the Heath Steele B-B5 zone area, Bathurst camp, New Brunswick: Stratigraphic and structural implications: Current Research - Geological Survey of Canada, Report 1997-D, p. 21–33.

Lesher, C.M., Goodwin, A.M., Campbell, I.H., and Gorton, M.P., 1986, Trace-element geochemistry of ore-associated and barren, felsic metavol- canic rocks in the Superior province, Canada: Canadian Journal of Earth Sciences, v. 23, p. 222–237.

Lode, S., Piercey, J.S., Devine, C.A., in review. Geology, Mineralogy, and Lithogeochemistry of Hydrothermal Exhalites Associated with the Lemarchant Volcanogenic Massive Sulfide (VMS) Deposit, Tally Pond Belt, Central Newfoundland. Economic Geology.

Longerich, H.P., Jenner, G.A., Fryer, B.J., and Jackson, S.E., 1990, Inductively coupled plasma-mass spectrometric analysis of geological samples: A critical evaluation based on case studies: Chemical Geology, v. 83, p.105-118.

Luff, W.M., Goodfellow, W.D., and Juras, S.J., 1992, Evidence for a feeder pipe and associated alteration at the Brunswick No. 12 massive sulphide deposit: Exploration and Mining Geology, v. 1, p. 167–185.

Lydon, J.W., 1984, Volcanogenic sulphide deposits, Part 1, A descriptive model; Geoscience Canada, v. 11, p. 195-202.

Lydon, J.W., 1988, Volcanogenic massive sulphide deposits; Part 2, Genetic models: Geoscience Canada, v. 15, p. 43-65.

MacLean, W.H., 1988, Rare earth element mobility at constant inter-REE ratios in the alteration zone at the Phelps Dodge massive sulphide deposit, Matagami, Quebec: Mineralium Deposita, v. 23, p. 231–38.

MacLean, W.H., 1990, Mass change calculations in altered rock series: Mineralium Deposita, v. 25, p. 44-49.

MacLean, W.H., and Kranidiotis, P., 1987, Immobile elements as monitors of mass transfer in hydrothermal alteration: Phelps Dodge massive sulfide deposit, Matagami, Quebec: Economic Geology, v. 82, p. 951–62.

MacLean, W.H., and Barrett, T.J., 1993, Lithogeochemical techniques using immobile elements: Journal of Geochemical Exploration, v. 48, p. 109–33.

McDonough, W.F., and Sun, S., 1995, Composition of the earth: Chemical Geology, v. 120, p. 223-253.

McLeod, R.L., and Stanton, R.L., 1984, Phyllosilicates and associated minerals in some Paleozoic stratiform sulfide deposits of southeastern Australia: Economic Geology, v. 79, p. 1–21.

McNicoll, V., Squires, G., Kerr, A., and Moore, P.J., 2010, The Duck Pond and Boundary Cu–Zn deposits, Newfoundland: New insights into the ages of host rocks and the timing of VHMS mineralization: Canadian Journal of Earth Sciences, v. 47, p. 1481–1506.

McPhie, J., Doyle, M., and Allen, R.L., 1993, Volcanic textures: A guide to the interpretation of textures in volcanic rocks: Hobart, Australia, Centre for Ore Deposit and Exploration Studies, University of Tasmania, 198 p.

Moore, P.J., 2003, Stratigraphic implications for mineralization: Preliminary findings of a metallogenic investigation of the Tally Pond volcanics, central Newfoundland, in Pereira, C.P.G., Walsh, D.G., and Kean, B.F., ends., Current Research Report 03-1: St. John’s, Newfoundland, Geological Survey Branch, p. 241-257.

Petersen, S., Monecke, T., Westhues, A., Hannington, M.D., Gemmell, J.B., Sharpe, R., Peters, M., Strauss, H., Lackschewitz, K., Augustin, N., Gibson, H., and Kleeberg, R., 2014, Drilling shallow-water massive sulfides at the Palinuro volcanic complex, Aeolian island arc, Italy: ECONOMIC GEOLOGY, v. 109, p. 2129-2157.

Piercey, S.J., 2009, Lithogeochemistry of volcanic rocks associated with volcanogenic massive sulfide deposits and applications to exploration, *in* Submarine Volcanism and Mineralization: Modern through ancient, (eds.) B. Cousens and S.J. Piercey; Geological Association of Canada, Short Course 29-30 May 2008, Quebec City, Canada, p. 15-40.

Piercey, S., 2011, The setting, style, and role of magmatism in the formation of volcanogenic massive sulfide deposits: Mineralium Deposita, v. 46, p. 449–471

Piercey, S., and Colpron., 2009, Composition and provenance of the Snowcap assemblage, basement to the Yukon-Tanana terrane, northern Cordillera: Implications for Cordilleran crustal growth: Geosphere, v. 5, p. 439-464.

Piercey, S.J. and Hinchey, J. 2012: Volcanogenic massive sulphide (VMS) deposits of the Central Mineral Belt, Newfoundland. Geological Association of Canada–Mineralogical Association of Canada Joint Annual Meeting, Field Trip Guidebook B4. Newfoundland and Labrador Department of Natural Resources, Geological Survey, Open File NFLD/3173, 56 pages.

Piercey, S.J., Squires, G.C., and Brace, T.D., 2014, Lithostratigraphic, hydrothermal, and tectonic setting of the Boundary volcanogenic massive sulfide deposit, Newfoundland Appalachians, Canada: Formation by subseafloor replacement in a Cambrian rifted arc: Economic Geology, v. 109, p. 661–87.

Pollock, J., 2004, Geology and paletectonic history of the Tally Pond Group, Dunnage zone, Newfoundland Appalachians: An integrated geochemical, geochronological, metallogenic and isotopic study of a Cambrian island arc along the Peri-Gondwanan margin of Iapetus: Unpublished M.Sc. thesis, St. John's, Newfoundland, Memorial University, 420 p.

Pontual, S., Merry, N., and Gamson, P., 1997, G-Mex Vol. 1, Spectral interpretation field manual: Kew, Victoria 3101, Australia, Ausspec International Pty. Ltd., p. 169.

Riverin, G., and Hodgson, C.J., 1980, Wall-rock alteration at the Millenbach Cu-Zn mine, Noranda, Quebec: Economic Geology, v. 75, p. 424-444.

Roberts, R. G., and Reardon, E.J., 1978, Alteration and ore-forming processeast Mattagami Lake mine,Quebec: Canadian Journal of Earth Sciences, v. 15, p. 1-21.

Rogers, N., van Staal, C.R., McNicoll, V., Pollock, J., Zagorevski, A., and Whalen, J., 2006, Neoproterozoic and Cambrian arc magmatism along the eastern margin of the Victoria Lake Supergroup: A remnant of Ganderian basement in central Newfoundland?: Precambrian Research, v. 147, p. 320–341.

Rogers, N., and van Staal, C.R., 2002, Toward a Victoria Lake Supergroup: A provisional stratigraphic revision of the Red Indian to Victoria Lakes area, central Newfoundland: Current Research–Newfoundland, Geological Survey Branch, Report 02-1, p.185–195.

Rogers, N., van Staal, C., Zagorevski, A., Skulski, T., Piercey, S.J., and McNicoll, V., 2007, Timing and tectonic setting of volcanogenic massive sulfide bearing terranes within the Central Mobile belt of the Canadian Appalachians, in Milkereit, B., ed., Proceedings of Exploration 07: Toronto, Fifth Decennial International Conference on Mineral Exploration, September 9-12, 2007, p. 1199–1205.

Ross, P.-S., and Bedard, J.H., 2009, Magmatic affinity of modern and ancient subalkaline volcanic rocks determined from trace-element discriminant diagrams: Canadian Journal of Earth Sciences, v. 46, p. 823-839.

Rucks, T.W., Piercey, S.J., Ryan, J.J., Villeneuve, M.E., and Creaser, R.A., 2006, Mid- to late Paleozoic K-feldspar augen granitoids of the Yukon-Tanana terrane, Yukon, Canada: Implications for crustal growth and tectonic evolution of the northern Cordillera: Geologic Society of America Bulletin, v. 118, p. 1212-1231.

Saeki, Y., and Date, J., 1980, Computer application to the alteration data of the footwall dacite lava at the Ezuri Kuroko deposits, Akito Prefecture: Mining Geology, v. 30, p. 241–250.

Sangster, D.F., 1972, Precambrian volcanogenic massive sulphide deposits in Canada: A review: Canada Geological Survey Paper 72-22, p. 44.

Schardt, C., Cooke, D.R., Gemmell, J.B., and Large, R.R., 2001, Geochemical modeling of the zoned footwall alteration pipe, Hellyer volcanic-hosted massive sulfide deposit, Western Tasmania, Australia: Economic Geology, v. 96, p. 1037–1054.

Shukuno, H., Tamura, Y., Tani, K., Chang, Q., Suzuki, T., and Fiske, R.S., 2006, Origin of silicic magmas and the compositional gap at Sumisu submarine caldera, Izu-Bonin arc, Japan: Journal of Volcanology and Geothermal Research, v. 156, p. 187–216

Smith, I., Worthington, T.J., Stewart, R.B., Price, R.C., and Gamble, J.A., 2003, Felsic volcanism in the Kermadec Arc, SW Pacific: Crustal recycling in an oceanic setting: Geological Society, London, Special Publications, v. 219, p. 99–118.

Spitz, G., and Darling, R., 1978, Major and minor element lithogeochemical anomalies surrounding the Louvem copper deposit, Val d'Or, Quebec: Canadian Journal of Earth Sciences, v. 15, p. 1161–1169.

Squires, G.C., and Moore, P.J., 2004, Volcanogenic massive sulfide environments of the Tally Pond Volcanics and adjacent area: Geological, lithogeochemical and geochronological results, in Pereira, C.P.G., Walsh, D.G., and Kean, B.F., eds., Current Research Report 04-1: St. John's, Newfoundland, Geological Survey Branch, p. 63-91.

Squires, G.C., Brace, T.D., and Hussey, A.M., 2001, Newfoundland's polymetallic Duck Pond deposit: Earliest Iapetan VMS mineralization formed within a sub-seafloor, carbonate-rich alteration system, *in* Evans, D.T.W., and Kerr, A., eds., Geology and mineral deposits of the northern Dunnage zone, Newfoundland Appalachians: St. John's, Newfoundland, Geological Association of Canada-Mineralogical Association of Canada, Field Trip Guide A2, p. 167–187.

Squires, G.C., MacKenzie, A.C., and MacInnis, D., 1991, Geology and genesis of the Duck Pond volcanogenic massive sulfide deposit, *in* Swinden, H.S., Evans, D.T.W., and Kean, B.F., eds., Metallogenic framework of base and precious metal deposits, central and western Newfoundland: Geological Survey of Canada Open File 2156, p. 56–64.

Swinden, H.S., 1991, Paleotectonic settings of volcanogenic massive sulfide deposits in the Dunnage zone, Newfoundland Appalachians: Canadian Institute of Mining and Metallurgy Bulletin, v. 84, p. 59–89

Swinden, H.S., Jenner, G.A., Kean, B.F., and Evans, D.T.W., 1989, Volcanic rock geochemistry as a guide for massive sulfide exploration in central Newfoundland: Newfoundland Department of Mines, Current Research Report 89-1, p. 201–219.

Swinden, H.S., and Thorpe, R.I., 1984, Variations in style of volcanism and massive sulfide deposition in Early to Middle Ordovician island-arc sequences of the Newfoundland Central Mobile belt: Economic Geology, v. 79, p. 1596–1619.

Sverjensky, D.A., 1984, Europium redox equilibria in aqueous solutions: Earth and Planetary Science Letters, v. 67, p. 70-78.

van Staal, C.R., 2007, Pre-Carboniferous tectonic evolution and metallogeny of the Canadian Appalachians, in Goodfellow, W.D., ed., Mineral deposits of Canada: A synthesis of major deposit types, district metallogeny, the evolution of geological provinces, and exploration methods: Geological Association of Canada, Mineral Deposits Division Special Publication 5, p. 793–818

van Staal, C.R. and Barr, S.M., 2012, Lithospheric architecture and tectonic evolution of the Canadian Appalachians and associated Atlantic margin. Chapter 2 In Tectonic Styles in Canada: the LITHOPROBE Perspective. Edited by J.A. Percival, F.A. Cook, and R.M. Clowes. Geological Association of Canada, Special Paper 49, pp.

van Staal, C.R., and Colman-Sadd, S.P., 1997, The Central Mobile belt of the northern Appalachians: Oxford Monographs on Geology and Geophysics, v. 35, p. 747–760.

Velde, B.,1978, Infrared spectra of synthetic micas in the series muscovite-MgAl celadonite: American Mineralogist, v. 63, p. 341-349.

Wagner, D.W., 1993, Volcanic stratigraphy and hydrothermal alteration associated with the Duck Pond and Boundary volcanogenic massive sulphide deposits, Central Newfoundland: Unpublished MSc. thesis, Ottawa, Ontario, Canada, Carleton University, 430 p.

Williams, H., 1979, Appalachian orogen in Canada: Canadian Journal of Earth Sciences, v. 16, p. 792–807.

Williams, H., Colman-Sadd, S.P., and Swinden, H.S., 1988, Tectonostratigraphic subdivisions of central Newfoundland: Geological Survey of Canada, Current Research, Part B, Paper 88-1B, p. 91–98.

Wright, I., Parson, L.M., and Gamble, J.A., 1996, Evolution and interaction of migrating cross-arc volcanism and backarc rifting: An example from the Southern Havre Trough (35°20′–37°S): Journal of Geophysical Research, v. 101, p. 22071–22086.

Wysoczanski, R.J., Handler, M.R., Schipper, C.I., Leybourne, M.I., Creech, J., Rotella, M.D., Nicols, A.R.L., Wilson, C.J.N., and Stewart, R.B., 2012, The tectonomagmatic source of ore metals and volatile elements in the southern Kermadec arc: ECONOMIC GEOLOGY, v. 107, p. 1539-1556.

Yang, K., Huntington, J.F., Gemmell, J.B., Scott, K.M., 2011, Variations in composition and abundance of white mica in the hydrothermal alteration system at Hellyer, Tasmania, as revealed by infrared reflectance spectroscopy: Journal of Geochemical Exploration, v. 108, p. 143-156.

Zagorevski, A., van Staal, C.R., McNicoll, V.J., and Rogers, N., 2007, Upper Cambrian to Upper Ordovician peri-Gondwanan island arc activity in the Victoria Lake Supergroup, central Newfoundland: Tectonic development of the northern Ganderian margin: American Journal of Science, v. 307, p. 339–370.

Zagorevski, A., van Staal, C.R., Rogers, N., McNicoll, V.J., and Pollock, J., 2010, Middle Cambrian to Ordovician arc-backarc development on the leading edge of Ganderia, Newfoundland Appalachians: Geological Society of America Memoir, v. 206, p. 367–396.

Table 2.1 Representative Whole-rock Analyses for Boundary Samples

Sample ID	H501278	H500680	H501213	H501317	H501222	H501217	H500663
Hole ID	BD10-11	BD10-87	BD10-40	BD10-6	BD10-50	BD10-98	BD10-102
Depth (m)	4	17.9	9.5	7.3	9	13.7	25.1
HW or FW	HW	FW	HW	FW	HW	FW	FW
Lithology	Flow	Lapill Tuff	Breccia	Lapilli Tuff	Flow	Lapilli Tuff	Lapilli Tuff
Alteration	Least altered	Qtz-Ser	Qtz-Ser	Chl-Ser	Chl-Ser	Int Chl	Int Chl
SiO_2 (wt %)	73.94	70.79	65.39	65.02	54.83	21.26	52.08
Al_2O_3	11.79	11.14	12.23	11.35	13.1	18.1	6.05
Fe_2O_3(T)	2.34	8.06	7.94	8.49	13.69	24.73	21.35
MnO	0.095	0.045	0.185	0.164	0.07	0.233	0.073
MgO	2.46	3	2.41	3.11	4.75	16.23	5.47
CaO	0.16	0.05	0.07	0.04	0.05	0.09	0.06
Na_2O	1.97	0.2	0.28	0.08	0.22	0.61	0.03
K_2O	2.29	2.06	3.01	2.56	2.41	0.71	0.12
TiO_2	0.144	0.169	0.156	0.14	0.162	0.242	0.095
P_2O_5	0.01	< 0.01	0.02	0.01	0.01	0.01	0.01
LOI	2.93	5.42	6.85	6.14	9.44	17.88	11.66
Total	98.15	100.9	98.54	97.1	98.73	100.1	97
Hg (ppb)	12	11	9	1580	333	68	100
Ba (ppm)	1408	811	1367	1776	1441	391	46
Sr	22	11	12	5	12	34	4
Y	39	43	45	36	46	70	23
Sc	10	10	11	11	13	17	7
Zr	145	126	153	120	158	250	86
Be	1	< 1	1	1	< 1	< 1	< 1
V	< 5	8	7	22	< 5	11	6
Cr	<8.9	<8.9	32.25	12.73	<8.9	<8.9	14.01
Co	1.11	15.34	3.11	18.74	6.04	16.42	133.23
Ni	<10	<10	<10	<10	<10	<10	<10
Cu	83.36	<19	55.96	2252.77	108.98	198.95	16898.55
Zn	150.64	58.08	287.07	5509.07	151.30	1109.40	167.78
As	2.12	1.96	9.96	183.87	17.89	79.21	31.47
Se	<26.7	<26.7	<26.7	<26.7	<26.7	<26.7	61.22
Br	176.10	247.70	257.37	267.29	142.76	240.93	162.60
Mo	<1	18.77	8.96	18.90	7.57	3.10	27.15
Ag	<1	<1	<1	9.78	<1	<1	2.13
Cd	<0.9	<0.9	<0.9	15.47	<0.9	3.14	<0.9
Sn	5.61	4.11	3.92	13.47	4.47	3.46	4.25
Sb	0.82	0.64	1.39	25.57	7.16	1.29	2.33
Te	<4.3	<4.3	<4.3	<4.3	<4.3	<4.3	45.98
I	<37	<37	<37	<37	<37	<37	<37
W	1.32	6.89	3.41	3.32	1.71	6.01	15.59
Pb	<25.3	<25.3	<25.3	1331.20	<25.3	<25.3	<25.3
Bi	0.30	2.09	1.34	9.38	5.33	4.02	44.03
Nb	6.07	6.03	7.58	5.04	8.10	15.55	3.00
La	20.65	33.51	21.14	16.75	19.53	27.67	9.32
Ce	43.88	71.84	43.82	34.47	40.85	55.42	19.28
Pr	5.49	9.16	5.50	4.35	5.35	6.86	2.41
Nd	23.07	40.38	23.26	18.36	22.78	29.77	10.36
Sm	5.55	9.22	5.97	4.48	5.62	7.36	2.36
Eu	1.19	1.10	1.15	1.41	1.12	1.19	0.25
Tb	1.04	1.29	1.22	0.87	1.20	1.73	0.55
Dy	6.72	8.20	8.12	5.80	8.00	11.70	3.75
Ho	1.48	1.69	1.69	1.25	1.61	2.45	0.83
Er	4.53	4.87	5.20	3.92	5.05	7.50	2.53
Tm	0.68	0.70	0.75	0.58	0.74	1.13	0.38
Yb	4.80	4.49	5.29	4.04	4.91	7.87	2.65
Lu	0.74	0.65	0.80	0.62	0.79	1.20	0.40
Hf	4.70	3.04	5.15	3.77	6.26	7.09	2.03
Ta	0.25	0.22	0.32	0.21	0.31	0.58	0.13
Th	5.59	4.62	5.87	4.18	6.37	12.23	2.68
AlOH WL (nm)	2,213	2,198	2,202	2,209	2,196	2,190	NA
AlOH Depth (%)	14.85%	13.28%	7.52%	10.41%	2.16%	3.08%	NA
FeOH WL (nm)	2,252	2,254	NA	2,253	2,252	2,252	2,251
FeOH Depth (%)	2.42%	6.02%	NA	3.39%	2.94%	4.24%	2.45%
AlOH depth/FeOH depth	6.14	2.21	NA	3.07	0.73	0.73	NA

Abbreviations: HW=Hanging wall; FW=Footwal; Qtz-Ser= Quartz-sericite; Chl-Ser=Chlorite-sericite; Int Chl= Intense chlorite; WL=wavelength

Table 2.2 Principal Component Analysis Components

Component	Variance	Positive Scores	Negative Scores
1	20%	Fe_2O_3, LOI, Co, Mo, Cu, W, Bi, MgO, As	SiO_2, K_2O, Ba
2	18%	MgO, Sc, TiO_2, Al_2O_3, Lu, Y, P_2O_5, MnO, CaO, Sr, V, K_2O, Ba	
3	10%	Pb, Zn, Hg, Sn	
4	7%	LOI, P_2O_5, MnO, CaO, MgO, Sr	SiO_2, K_2O, Ba

Table 2.3 Alteration Characteristics

Average Values	Quartz-Sericite	Chlorite-Sericite	Intense Chlorite
SiO_2 (wt. %)	72.11	63.1	40.11
Δ SiO_2 (wt. %)	3.56	2.39	-31.13
K_2O(wt. %)	2.96	1.98	0.36
Δ K_2O (wt. %)	0.77	-0.08	-1.99
MgO (wt. %)	1.95	3.98	13.01
Δ MgO (wt. %)	-0.47	1.99	9.82
Ba/Sr	157	140	32
Hg/Na_2O	1248	2152	5624
CCPI	66	86	98
AI	94	95	97
AlOH Wavelength (nm)	2204	2202	2196
AlOH Depth	0.12	0.07	0.04
FeOH Wavelength (nm)	2253	2252	2250
FeOH Depth	0.02	0.04	0.06
AlOH Depth/FeOH Depth	6.83	2.73	0.59

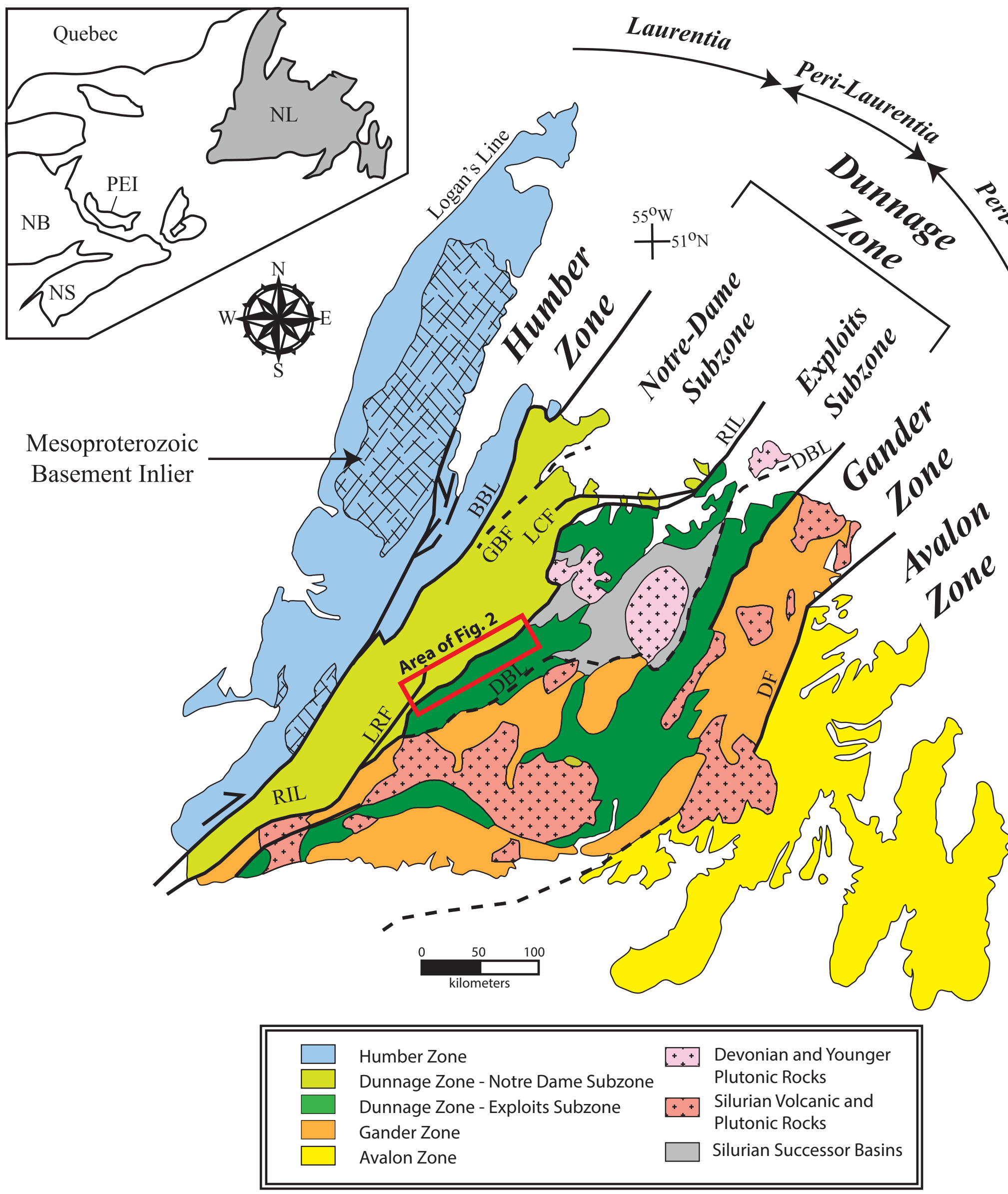

Figure 2.1 Geological map of the Newfoundland Appalachians with tectonostratigraphic zones, accretionary tracts, and associated belts. Tectonostratigraphic divisions modified from van Stall (2007), and van Staal and Barr (2012). Abbreviations: BBL=Baie Verte Brompton Line; DF=Dover Fault; DBL=Dog Bay Line; GBF=Green Bay fault; LCF=Lobster Cove fault; LRF=Lloyds River fault; RIL=Red Indian Line.

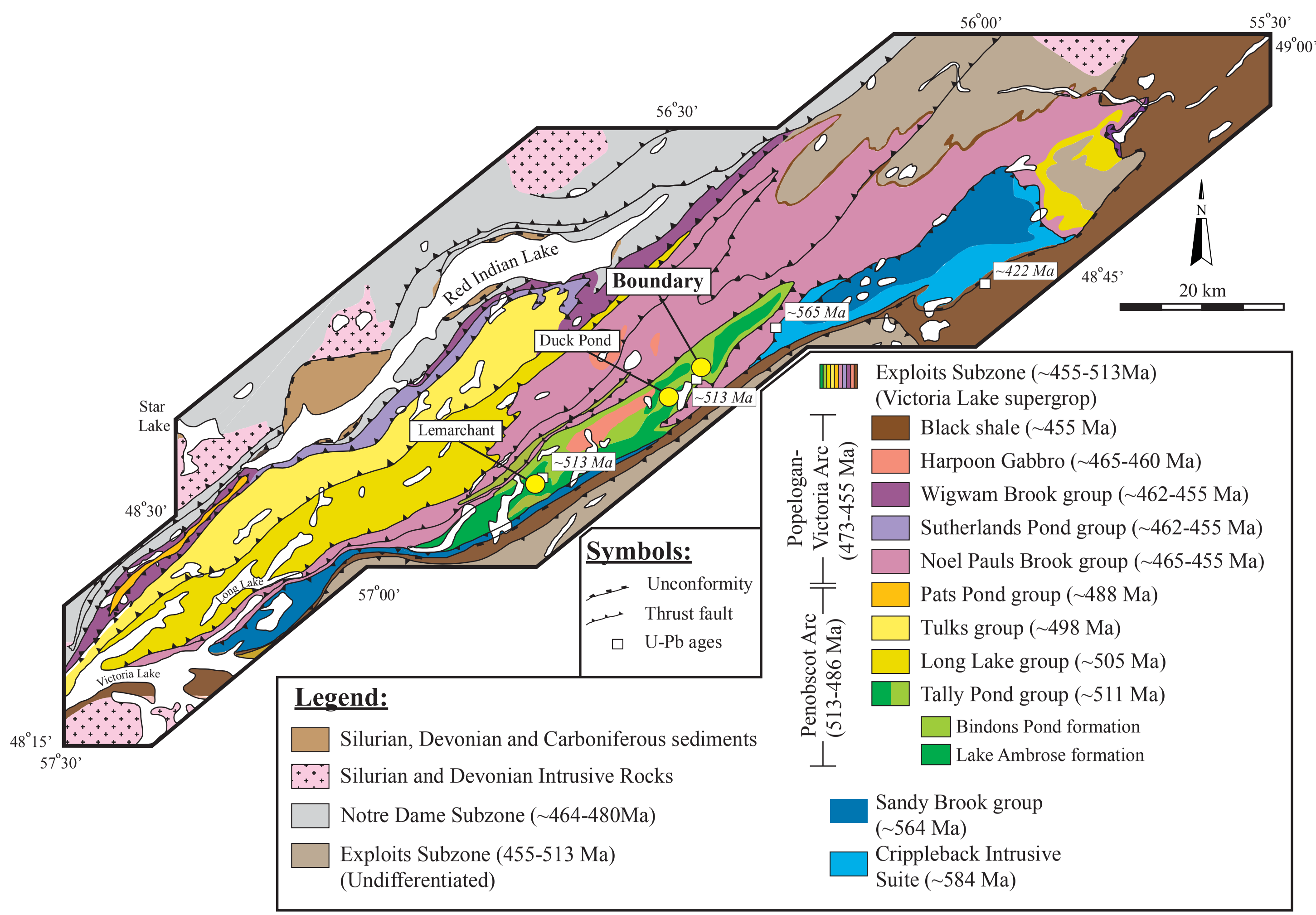

Figure 2.2 Geological setting of the Victoria Lake supergroup and the Tally Pond group, displaying the Boundary deposit and the neighboring Duck Pond and Lemarchant deposits. Modified from McNicoll et al. (2010) and Piercey et al. (2014).

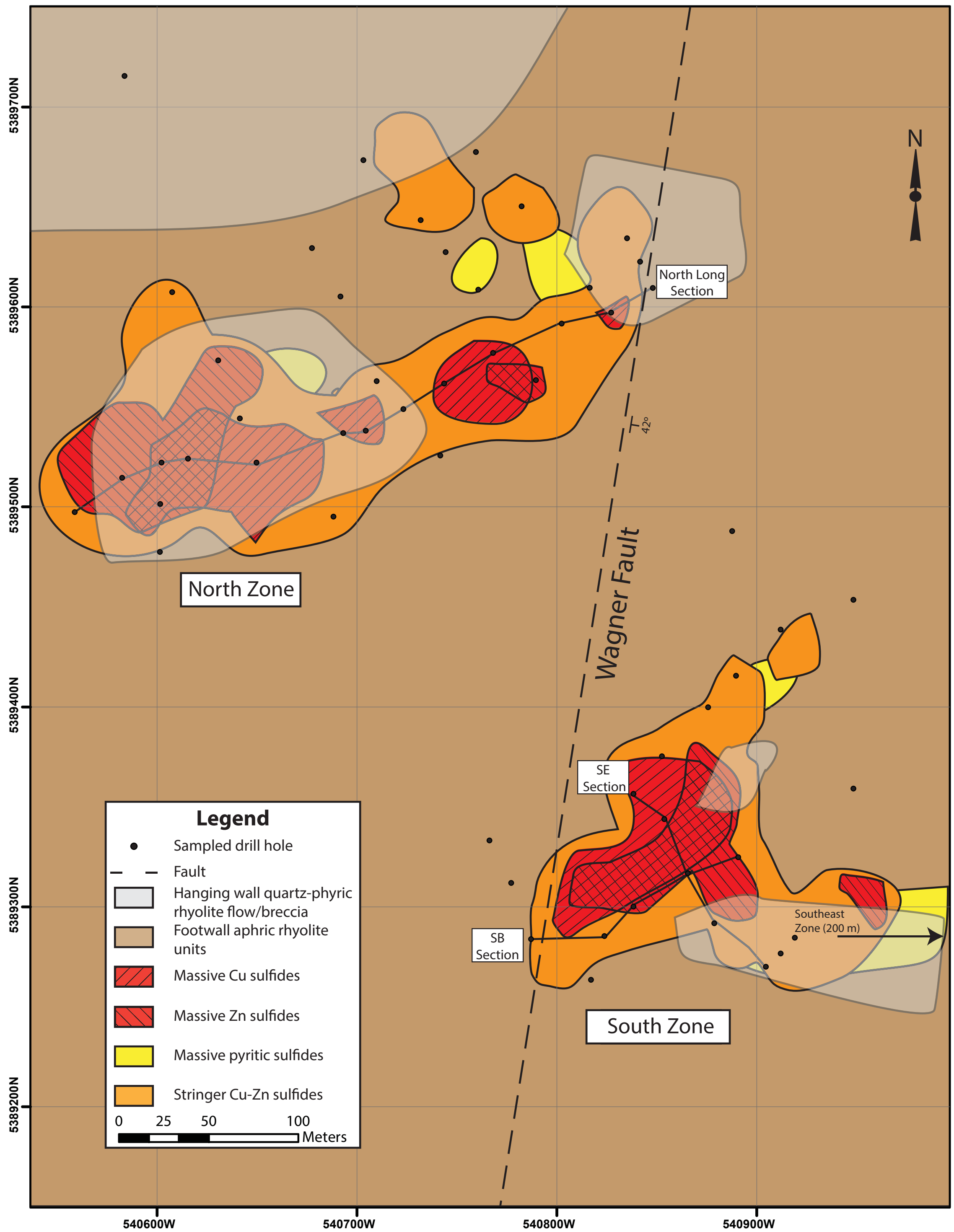

Figure 2.3 Boundary deposit surface geology plan map with distribution of sulfide mineralization and locations of sections in Figure 5a-b. Modified from Hennessey (2013) (Unpublished).

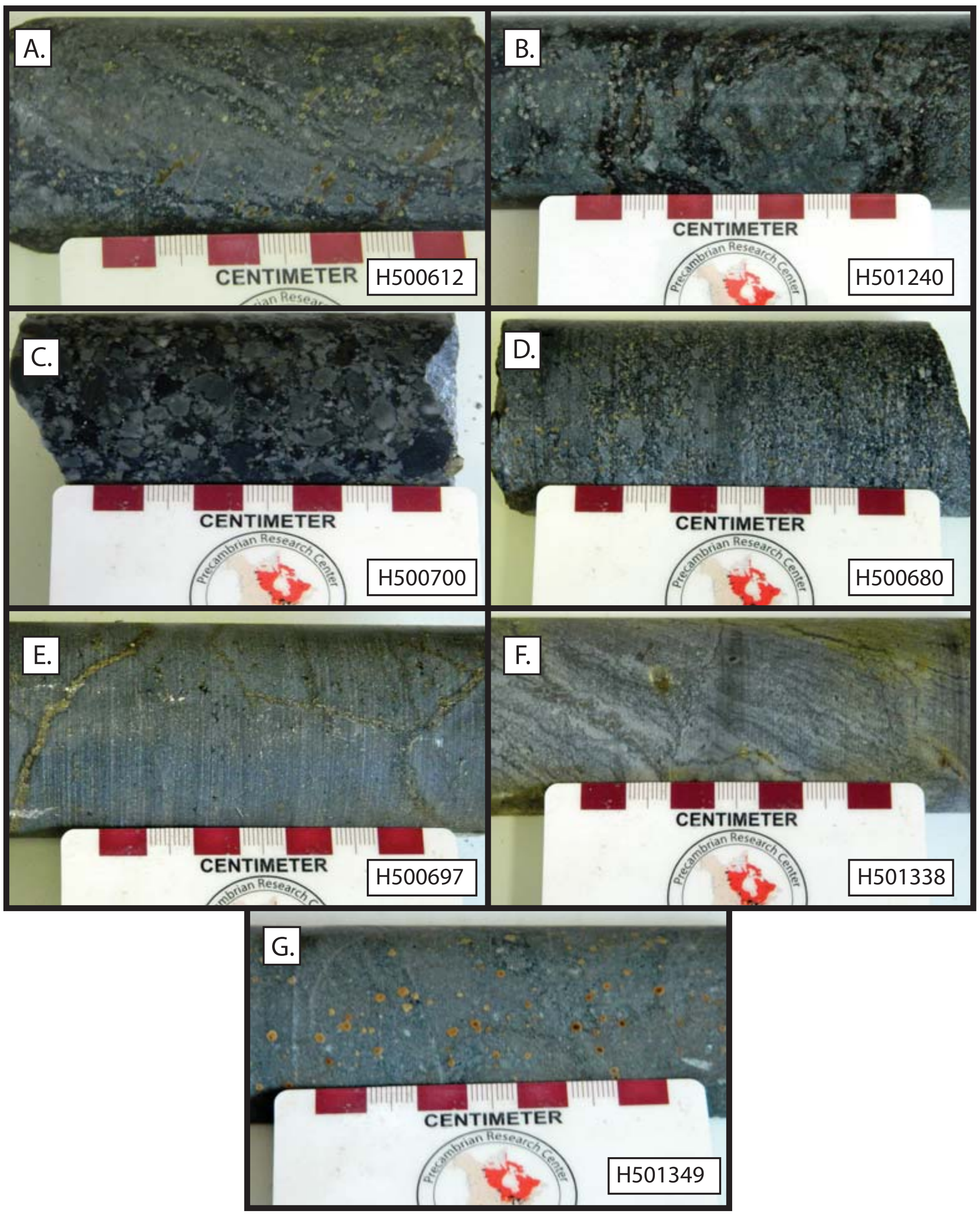

Figure 2.4 Lithologies of the Boundary deposit. A) Hanging wall flow-banded rhyolite. B) Hanging wall hyaloclastite breccia. C) Footwall lapilli tuff. D) Footwall tuff. E) Footwall jig-saw breccia. F) Footwall flow-banded rhyolite. G) Quartz-porphyry intrusion.

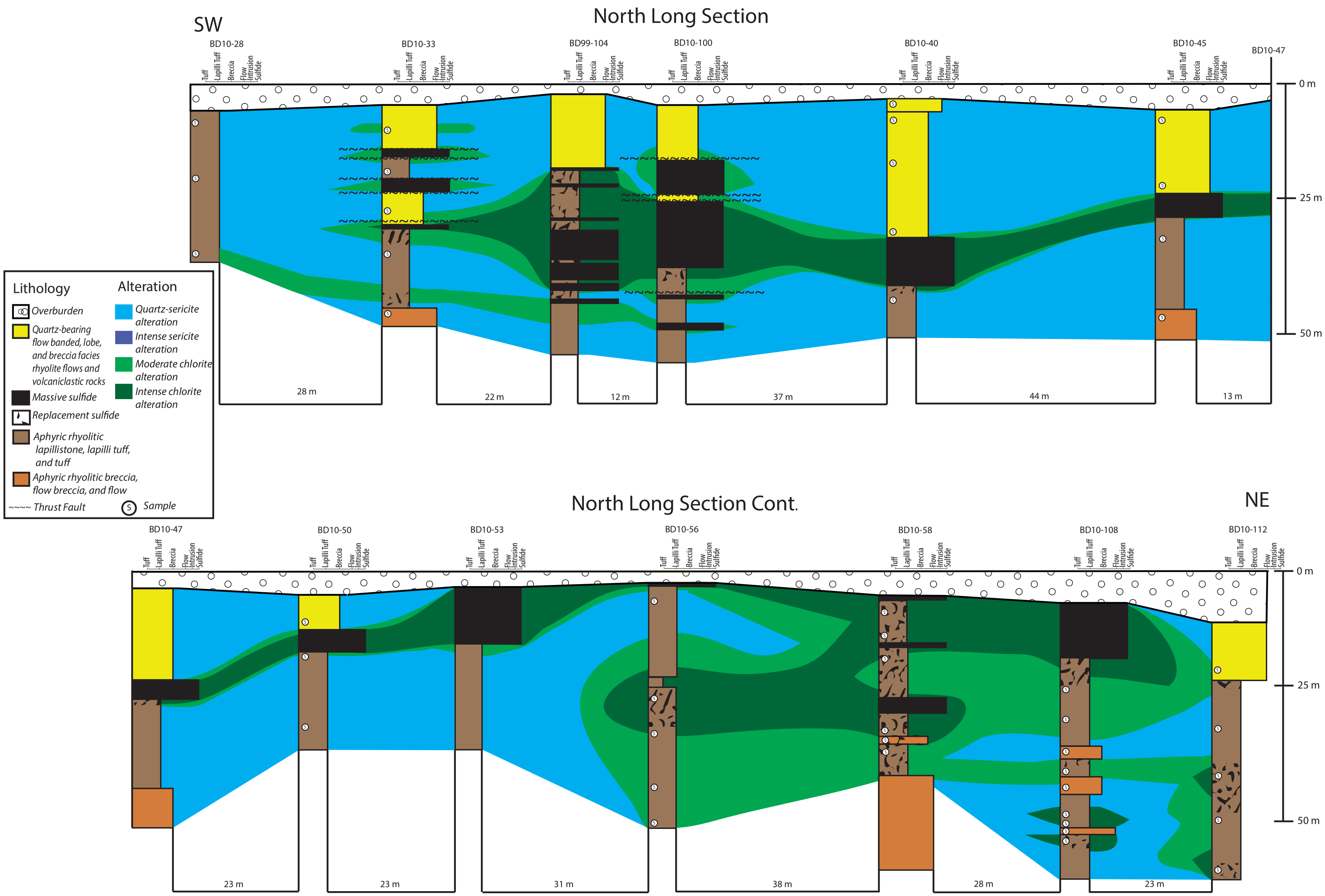

Figure 2.5 A) Alteration cross section through the North zone of the Boundary deposit. Location of section shown on Figure 3.

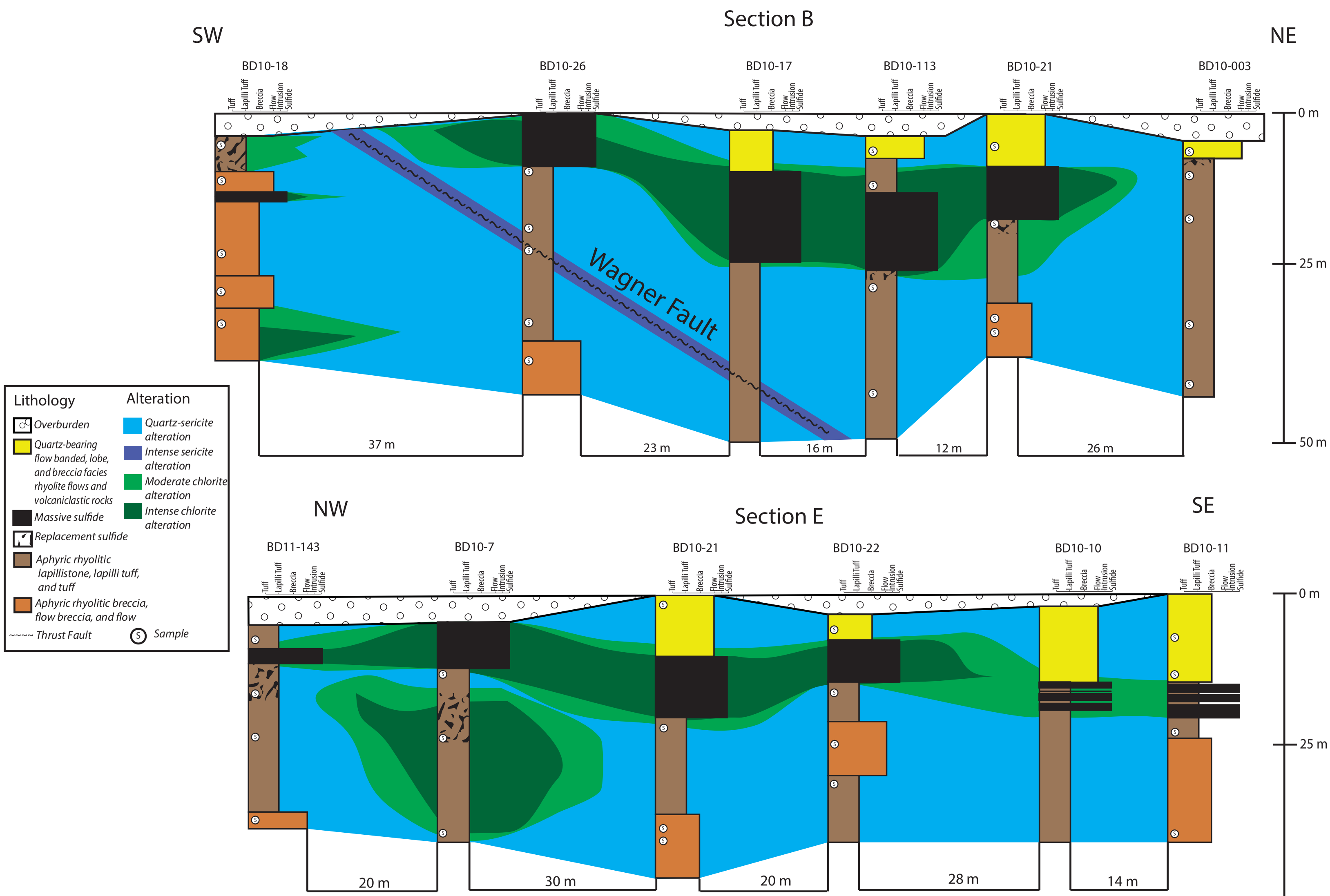

Figure 2.5 B) Alteration cross sections through the South zone of the Boundary deposit. Location of sections shown on Figure 3.

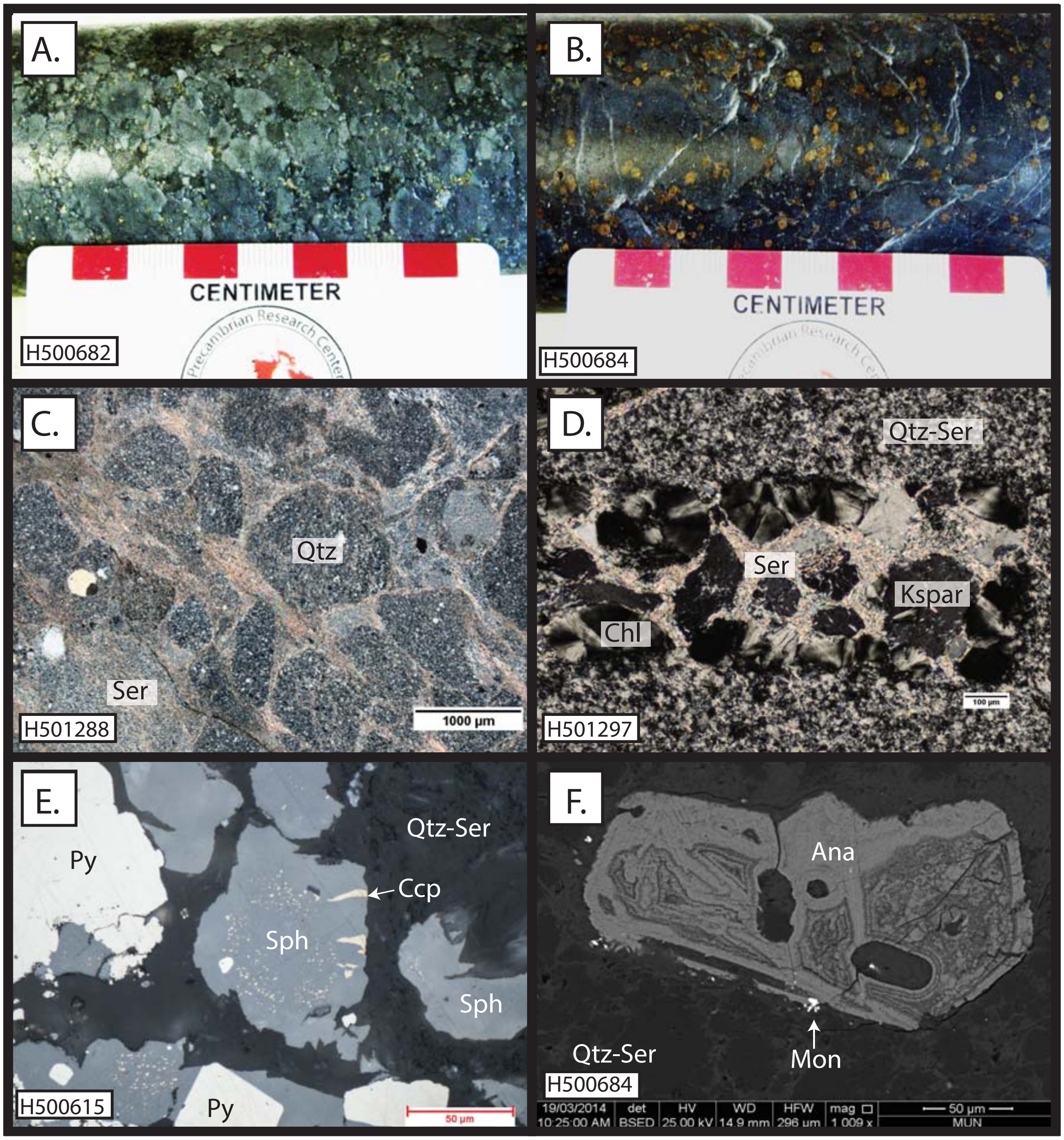

Figure 2.6 Photographs and photomicrographs of quartz-sericite alteration. A) Gray, relatively unaltered lapilli tuff with tan carbonate spots. B) Black, quartz-sericite altered lapilli tuff with dark red carbonate spots. C) Photomicrograph of quartz altered clasts with sericite replaced matrix (cross-polarized light). D) Photomicrograph of relict feldspar grain altered to fine grained sericite and chlorite pockets (cross-polarized light). E) Photomicrograph of chalcopyrite disease in sphalerite (reflected light). F) Scanning electron microscope back scatter electron (SEM-BSE) image of anatase and minor monazite in quartz-sericite matrix. Ser = sericite; Qtz = quartz; Chl = chlorite; Kspar = potassium feldspar; Py = pyrite, Sph = sphalerite; Ccp = chalcopyrite; Ana = anatase (rutile); Mon = monazite.

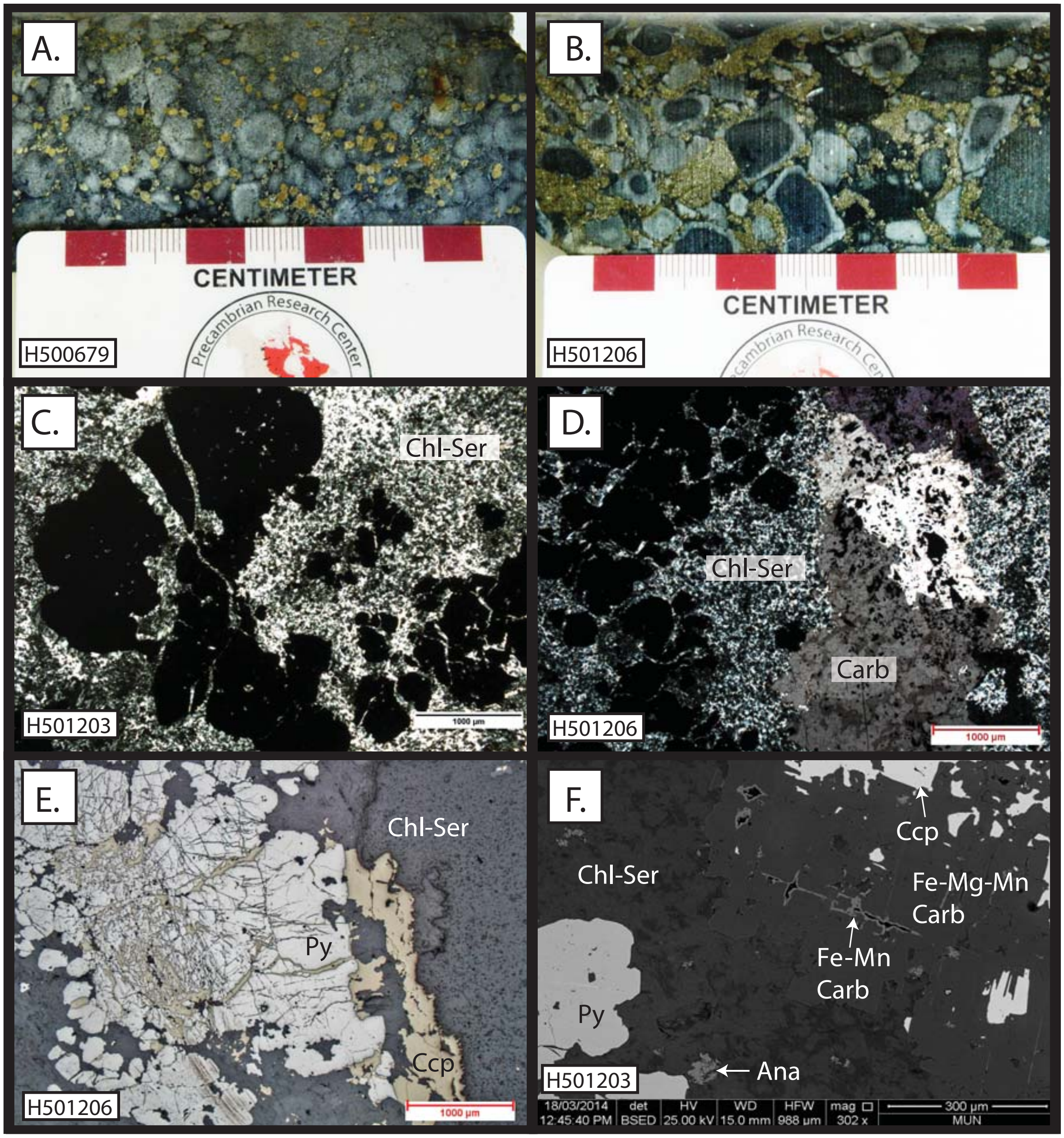

Figure 2.7 Photographs and photomicrographs of chlorite-sericite alteration. A) Gray, chlorite-sericite altered lapilli tuff. B) Zoned lapilli clasts in chlorite-sericite-chalcopyrite matrix. C) Photomicrograph of chlorite-sericite matrix (cross-polarized light). D) Photomicrograph of chlorite-sericite matrix with Fe-Mg-Mn carbonate spot (cross-polarized light). E) Photomicrograph of fractured pyrite with chalcopyrite infill (reflected light). F) SEM-BSE image of Mn-Mg-Fe zoned carbonate spot. Carb = carbonate.

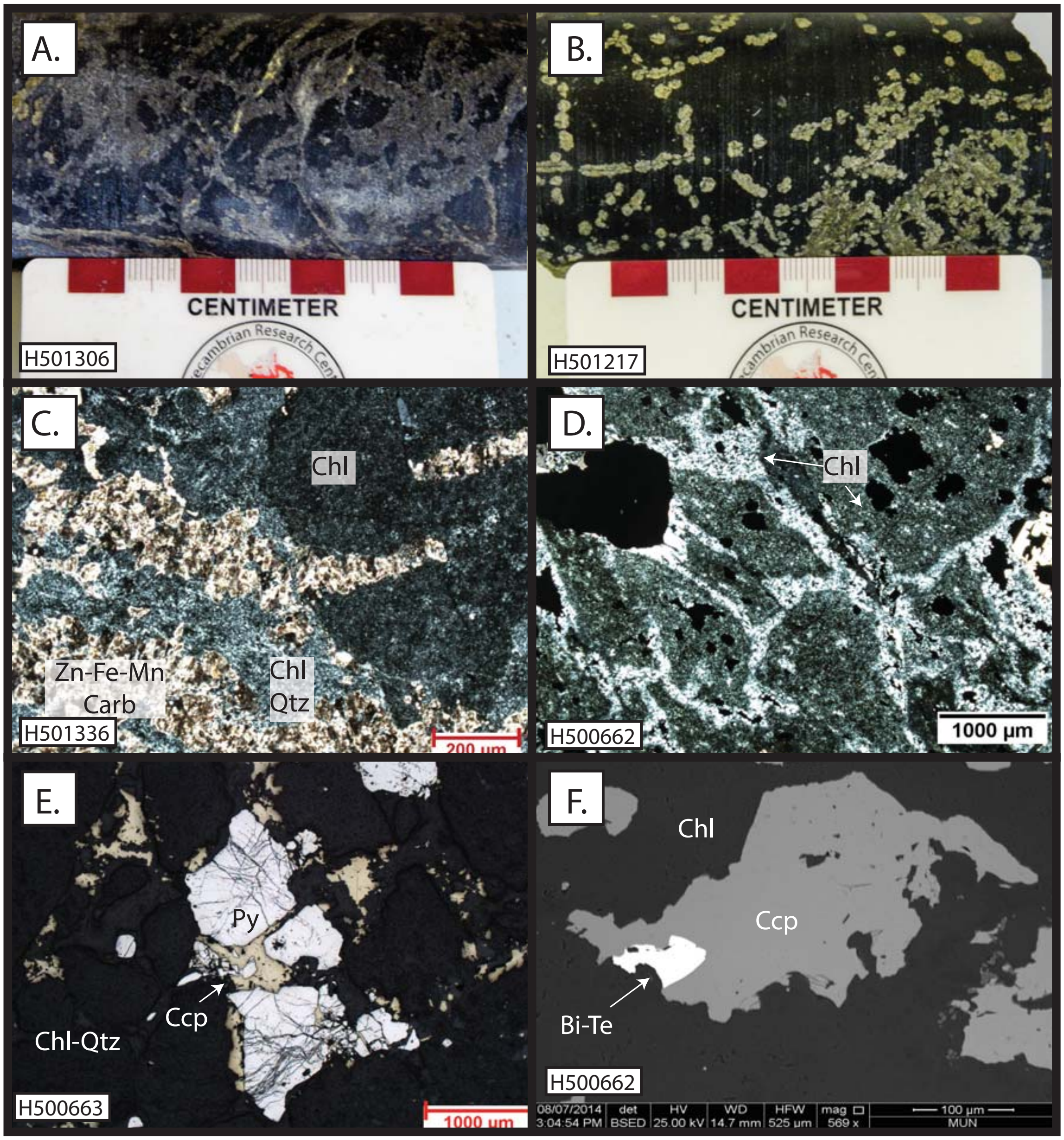

Figure 2.8 Photographs and photomicrographs of intense chlorite alteration. A) Intense chlorite alteration with chaotic carbonate alteration. B) Intense chlorite alteration with carbonate spots. C) Photomicrograph of chaotic carbonate in chlorite-quartz matrix (cross-polarized light). D) Photomicrograph of chlorite replaced lapilli clasts in coarse grained chlorite matrix (cross-polarized light). E) Photomicrograph of fractured pyrite with chalcopyrite infill (reflected light). F) SEM-BSE image of chalcopyrite and Bi-Te sulfide in chlorite matrix.

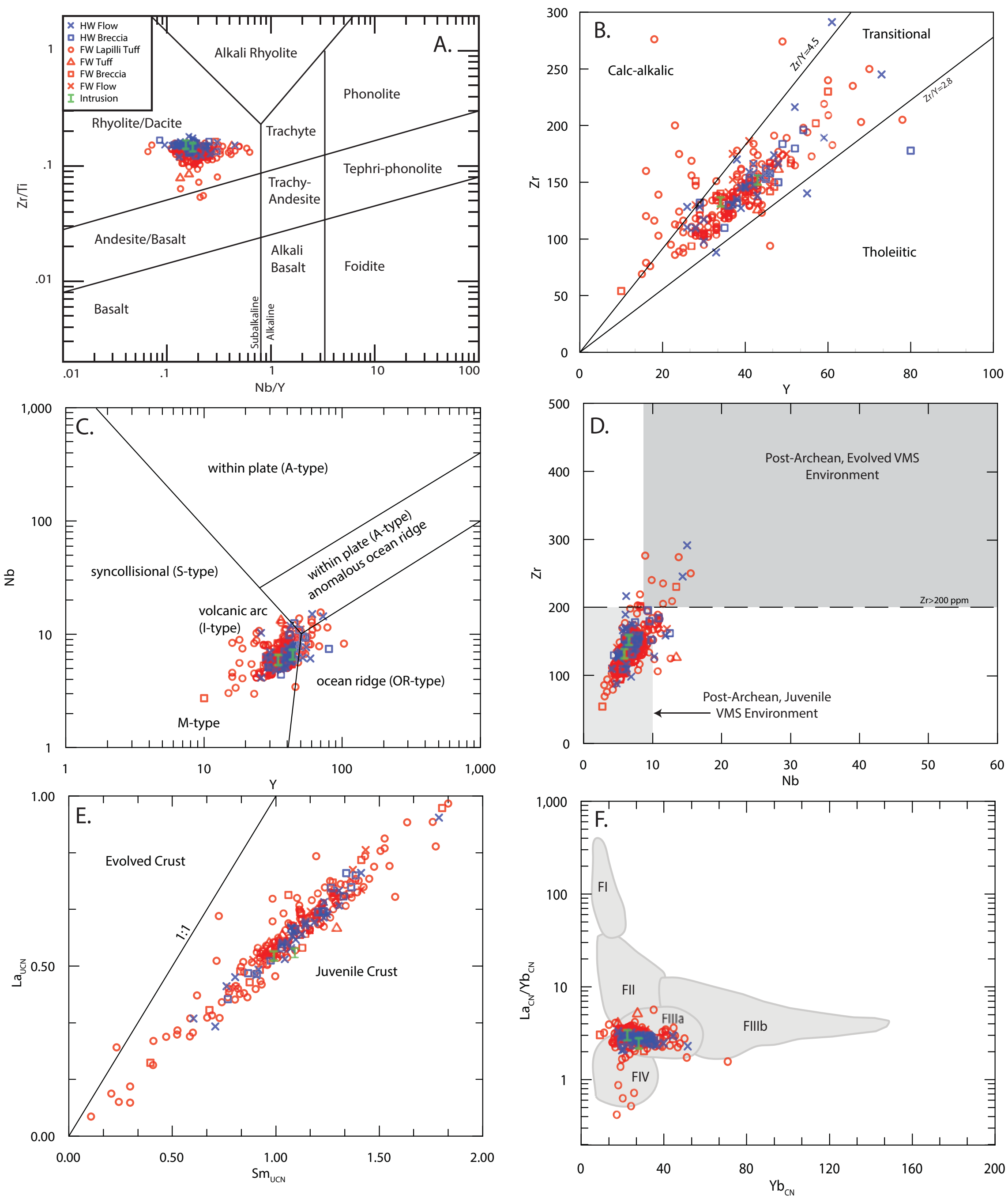

Figure 2.9 Immobile element plots for rhyolitic rocks from the Boundary VMS deposit. A) Modified Winchester and Floyd (1977) Zr/TiO_2-Nb/Y discrimination diagram for rock classification (from Pearce, 1996). B) Zr-Y diagram for discriminating magma affinity (from Ross and Bedard, 2009). C) Nb-Y tectonic discrimination diagram (from Pearce et al., 1984). D) Zr-Nb diagram useful for discriminating juvenile environments from evolved environments (modified from Piercey, 2009). E) Upper-crust normalized (UCN) La-Sm diagram (upper-crust values from Taylor and McLennan, 1985; from Piercey and Colpron, 2009). F) La/Ybcn-Ybcn FI-FIV rhyolite discrimination diagram (chondrite normalized values (CN) McDonough and Sun, 1995; diagrams from Lesher et al., 1986; and Hart et al., 2004).

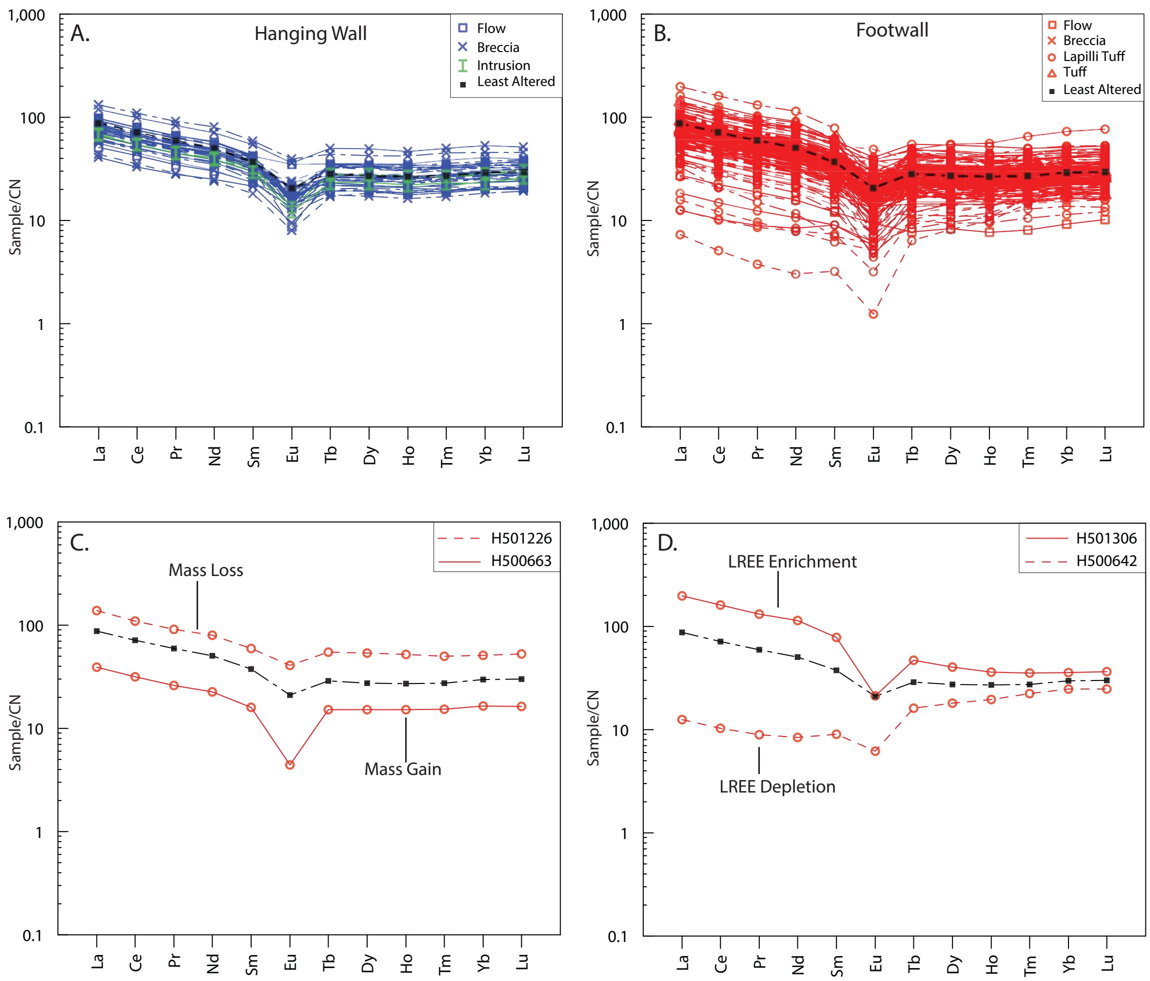

Figure 2.10 REE plots of the Boundary deposit (chondrite-normalized (CN) to the values of McDonough and Sun, 1995). A) Hanging wall. B) Footwall. C) Mass change effects on REE signature. D) REE mobility effects on signature.

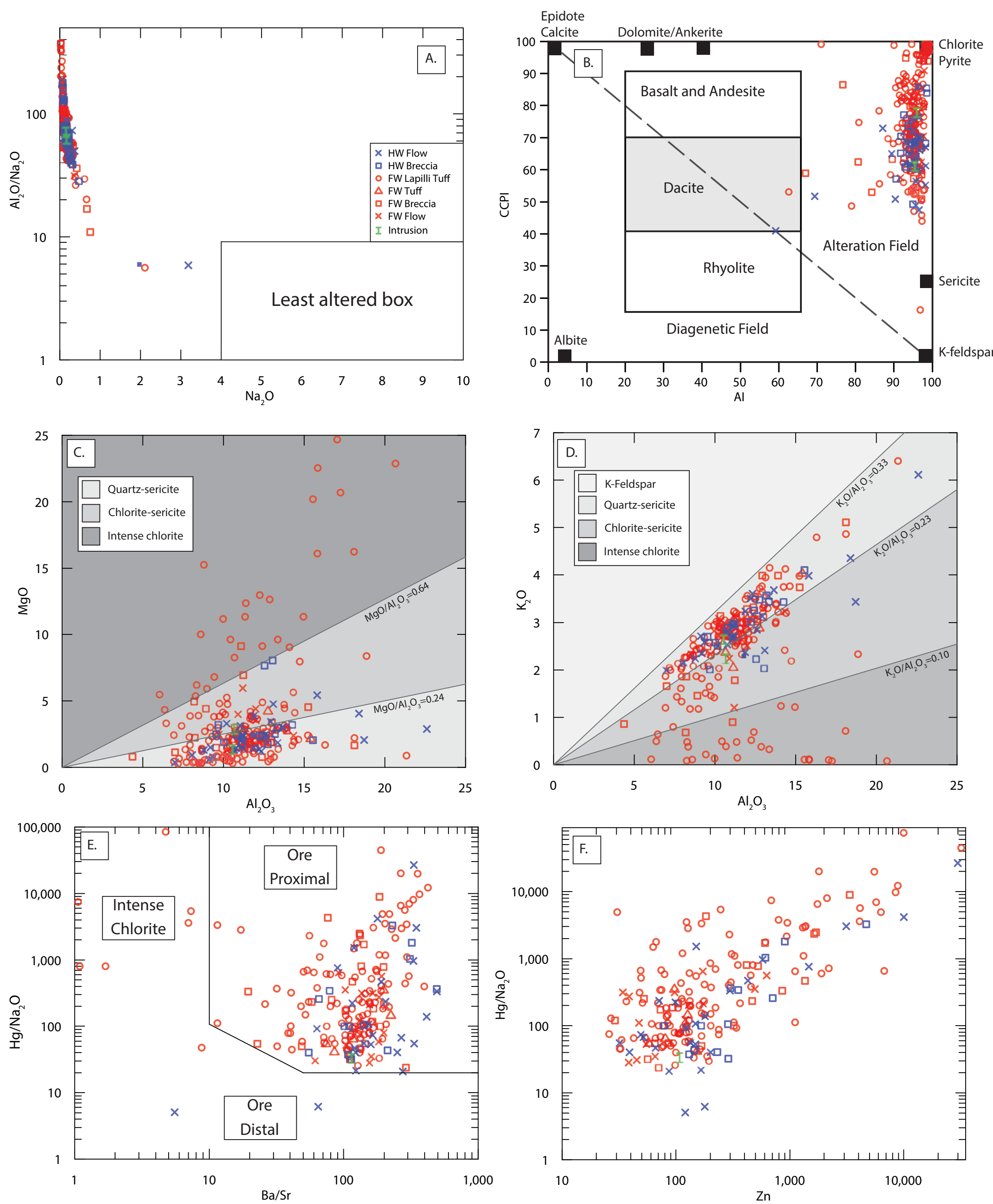

Figure 2.11 Mobile element plots for rhyolitic rocks from the Boundary VMS deposit. A) Spitz-Darling (Spitz and Darling, 1978) index versus Na_2O (diagram after Ruks et al., 2006). B) Alteration box plot with the Hashimoto alteration index (AI; Ishikawa et al., 1976) plotted against the chlorite-carbonate-pyrite index (CCPI) (CCPI and diagram from Large et al. 2001). C) Diagram of MgO plotted against Al_2O_3. D) Diagram of K_2O plotted against Al_2O_3. E) Hg/Na_2O-Ba/Sr plot of the "Duck Pond index" (modified from Collins, 1989). F) Hg/Na_2O plotted against Zn.

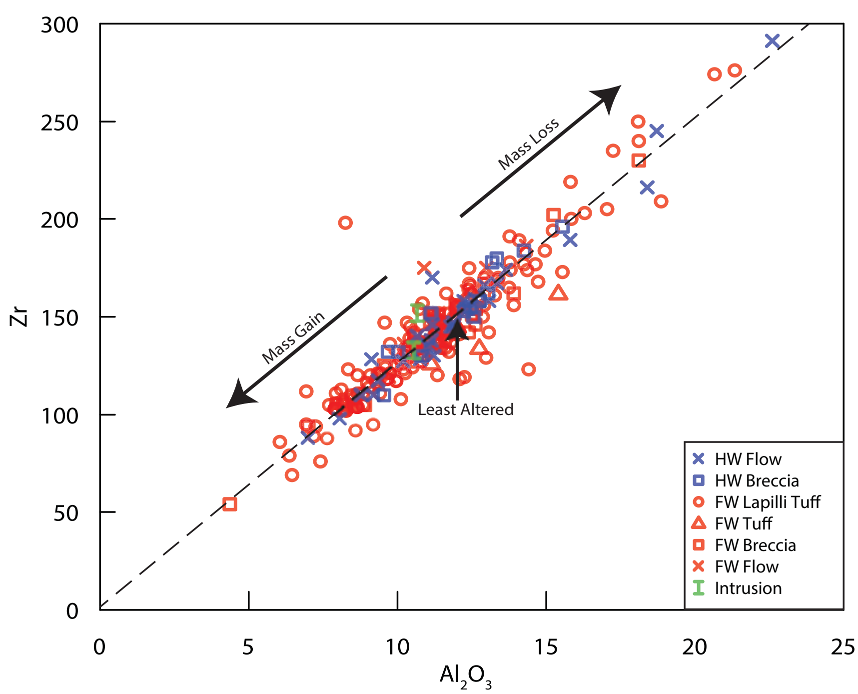

Figure 2.12 Linear immobile trend line for the Boundary deposit. Mass loss and gain of mobile elements have shifted the relative amounts of Al_2O_3 and Zr in the shown directions.

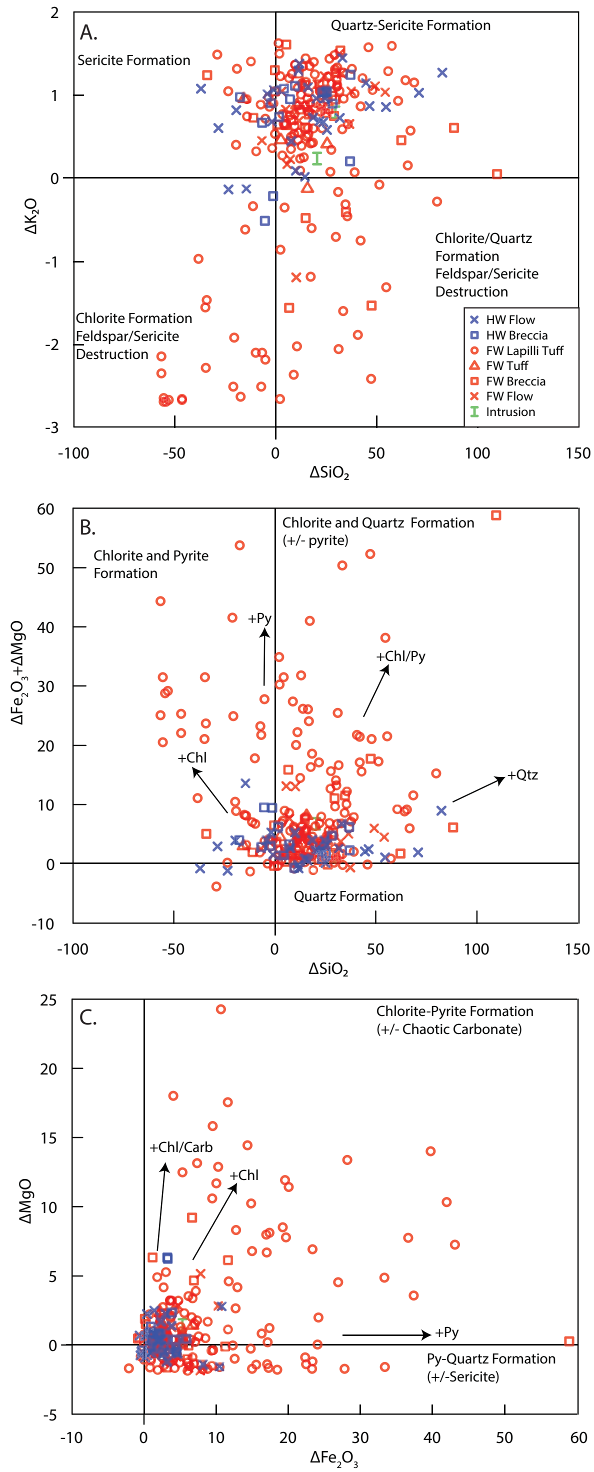

Figure 2.13 Mass change plots showing gains and losses of key alteration elements. A) Mass change of K_2O versus SiO_2 showing the formation of quartz and sericite. B) Mass change plot of Fe_2O_3+MgO versus SiO_2 showing the formation of quartz, chlorite, and pyrite. C) Mass change plot of MgO vs Fe_2O_3 differentiating between the formation of pyrite, chlorite, and carbonate. Chl=chlorite, Py=pyrite, Qtz=quartz, Carb=carbonate

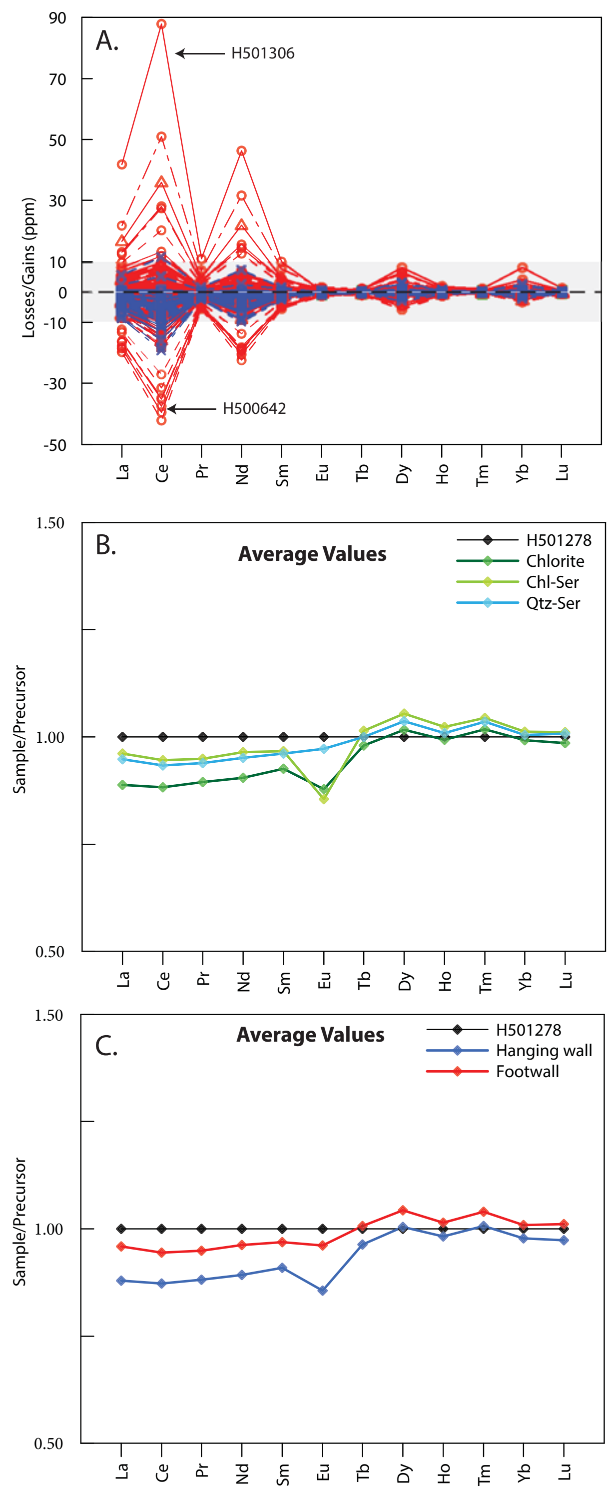

Figure 2.14 REE mass balance changes. Concentrations are compared to that of a least altered sample (H501278; Table 2.1). A) Absolute mass gains and losses in ppm. B) Plot of average reconstructed REE values/precursor values by alteration assemblage. C) Plot of average reconstructed REE values/precursor values by hanging wall and footwall.

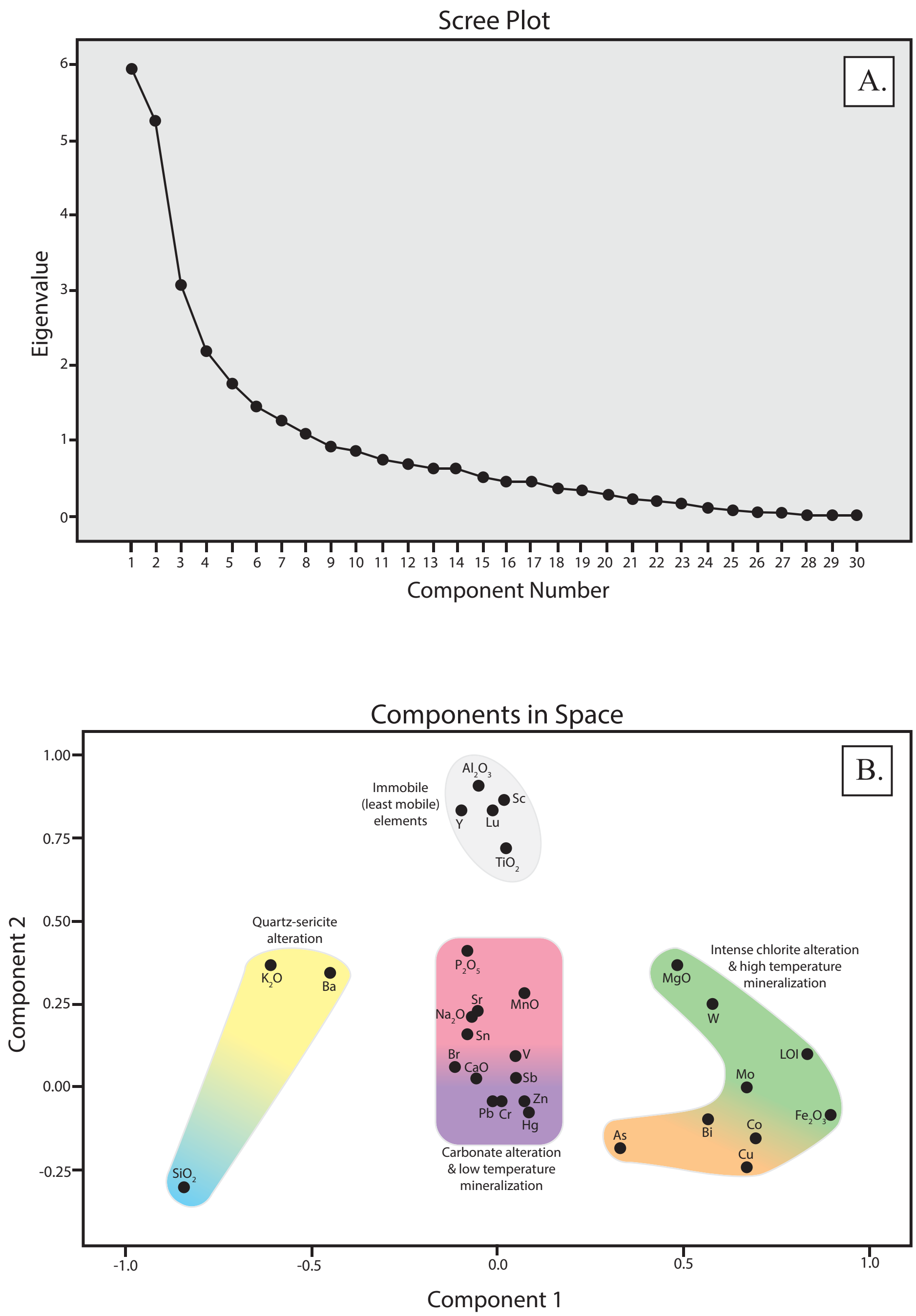

Figure 2.15 Principle component analysis results. A) Screeplot showing the significance of each component. B) Component 1 plotted against Component 2.

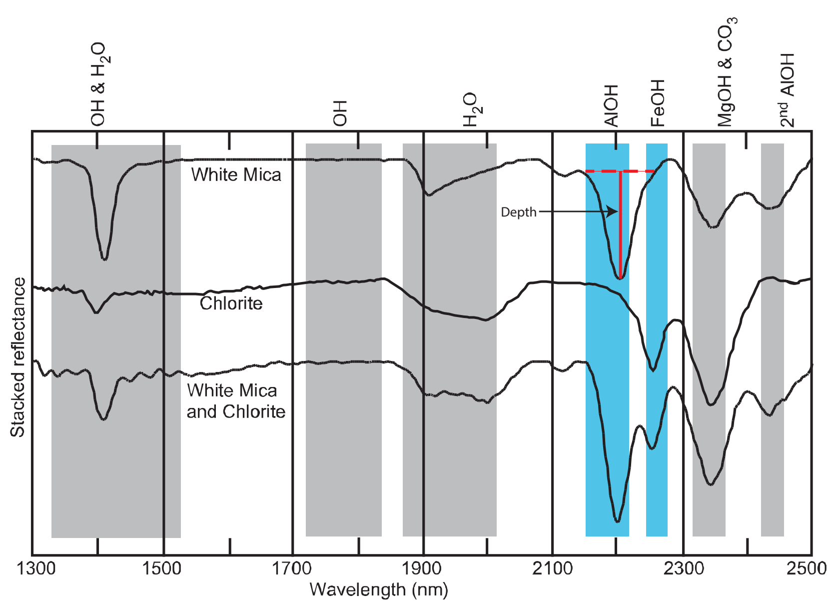

Figure 2.16 Typical SWIR absorption features of white mica and chlorite highlighted in blue with the ranges of other key hydroxyl groups shaded in gray. Figure modified from Jones et al. (2005) and Herrmann et al. (2001).

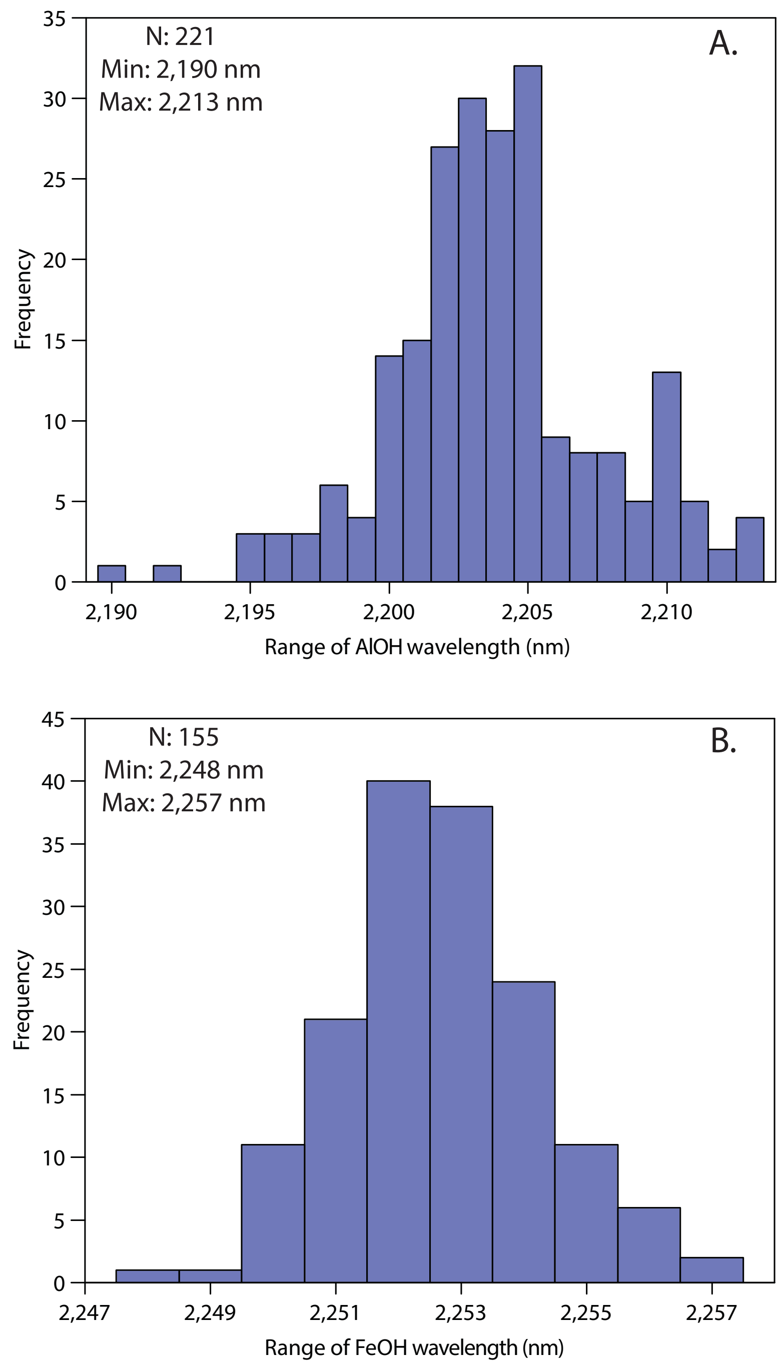

Figure 2.17 SWIR results. A) Histogram of the AlOH wavelengths present at Boundary. B) Histogram of FeOH wavelengths.

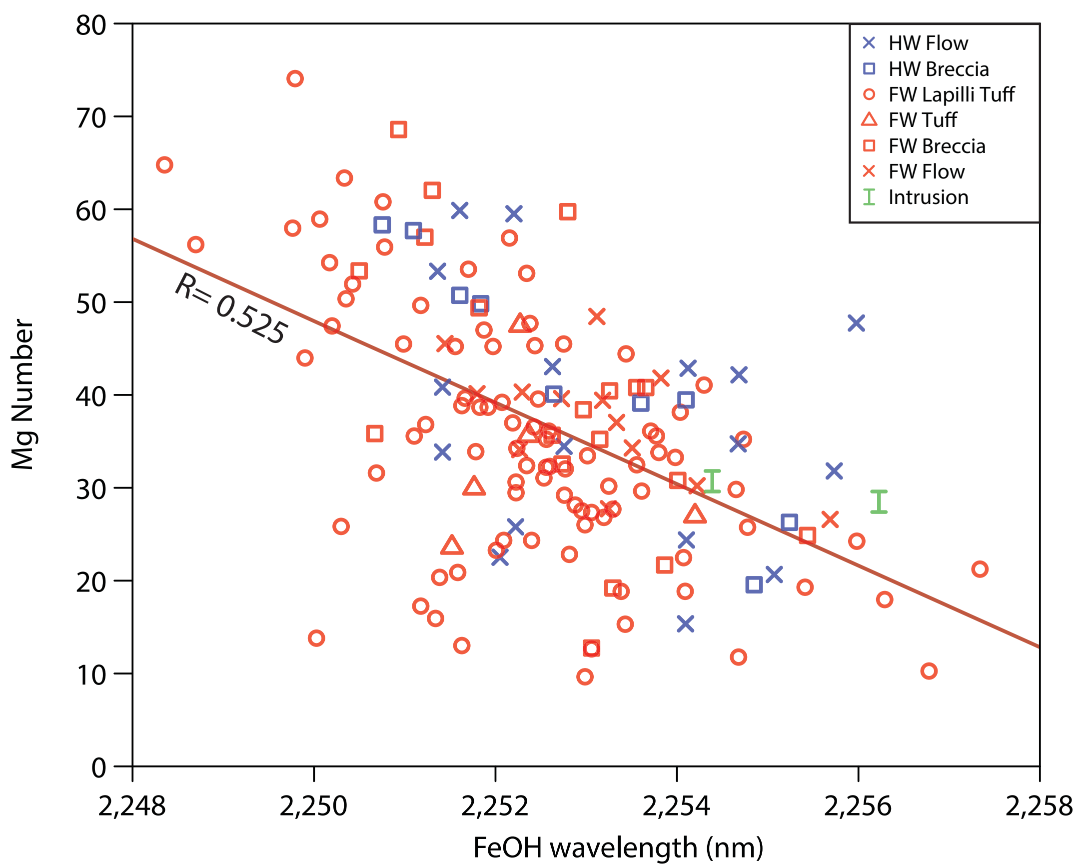

Figure 2.18 Plot of whole-rock Mg number (100*MgO/(MgO+Fe_2O_3) versus FeOH wavelength.

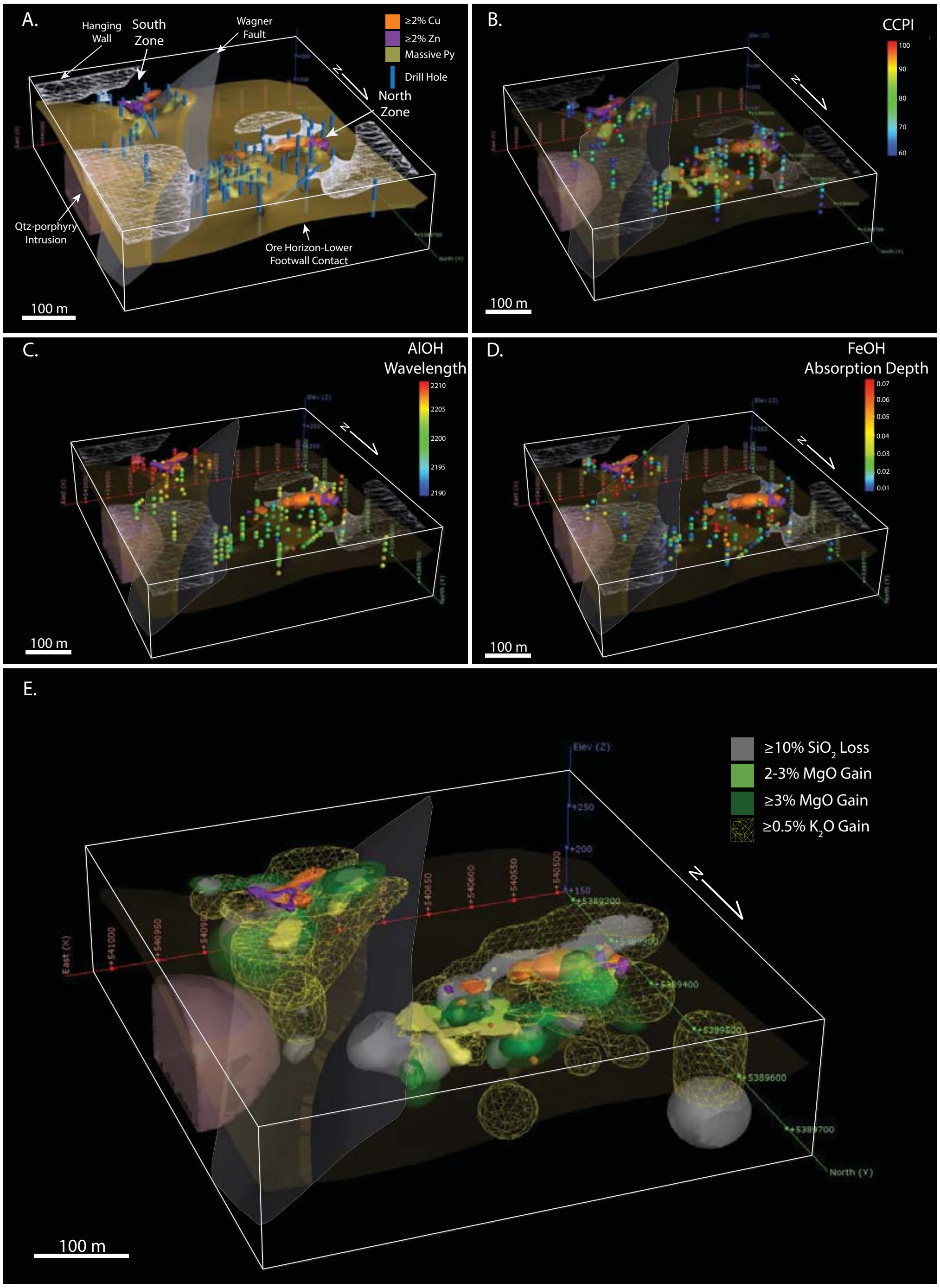

Figure 2.19 Series of 3D models of the Boundary deposit. A) Model showing key lithological contacts, major sulfide zones, and drill holes used to determine alteration extents. Ore zones are defined by assays from additional drill holes not shown. B) Model showing CCPI values in relationship to major ore zones. C) Model showing AlOH wavelengths. Note that wavelengths are significantly longer in the South zone. Long wavelengths in the North zone only occur on the western end of the deposit. D) Model showing FeOH absorption depth. The higher values occur within the same samples of the high CCPI samples from Figure 19B. E) Alteration model of the Boundary deposit based on mass balance changes. The major chlorite gains correlate with the high CCPI values (2.19B) and FeOH absorption values (2.19D).

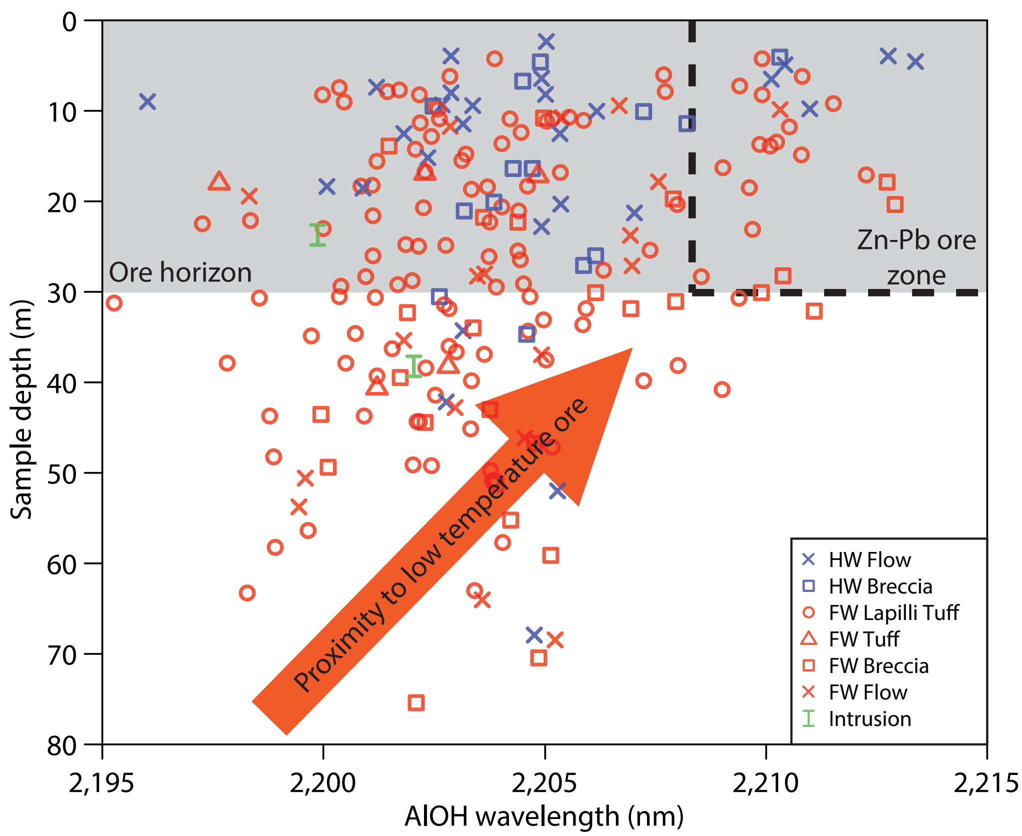

Figure 2.20 Plot of sample depth vs. AlOH wavelength of samples from the chlorite-sericite and quartz-sericite zones.

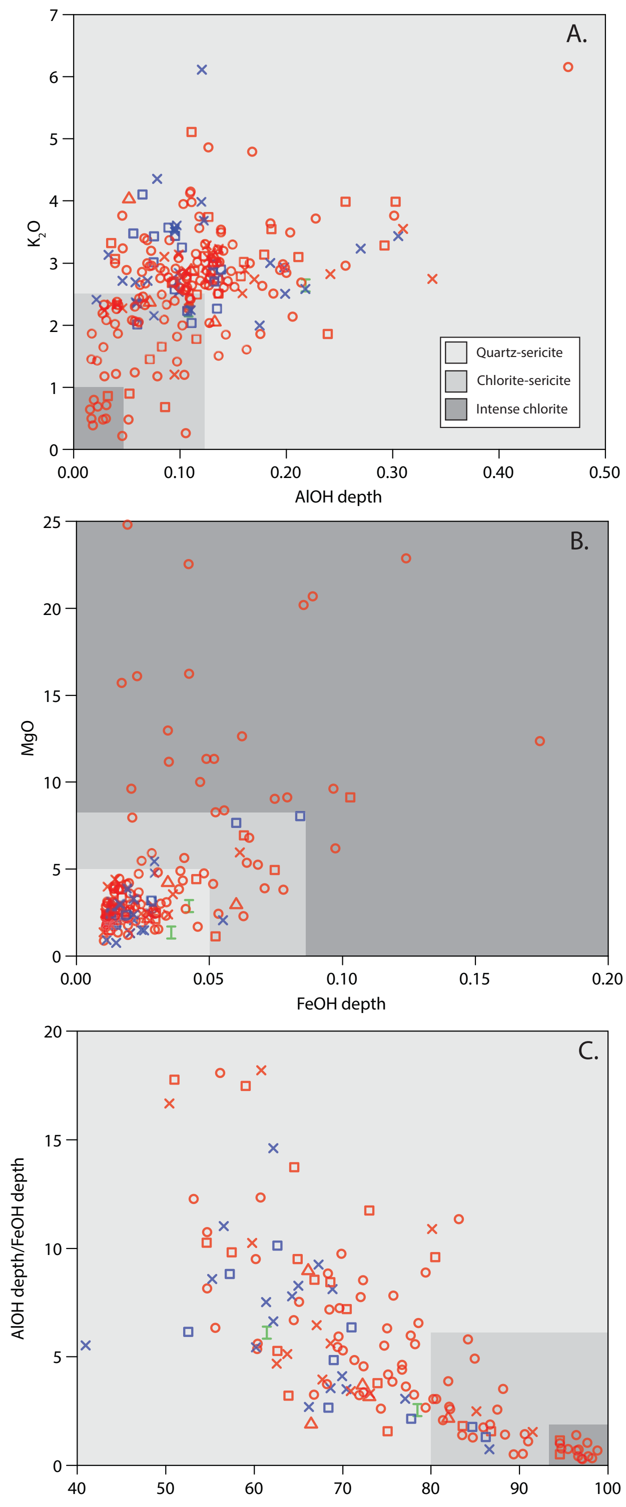

Figure 2.21 SWIR and geochemistry. A) Plot of K_2O versus AlOH absorption depth. B) Plot of MgO versus FeOH absorption depth. C) Plot of the AlOH absorption depth/FeOH absorption depth versus CCPI.

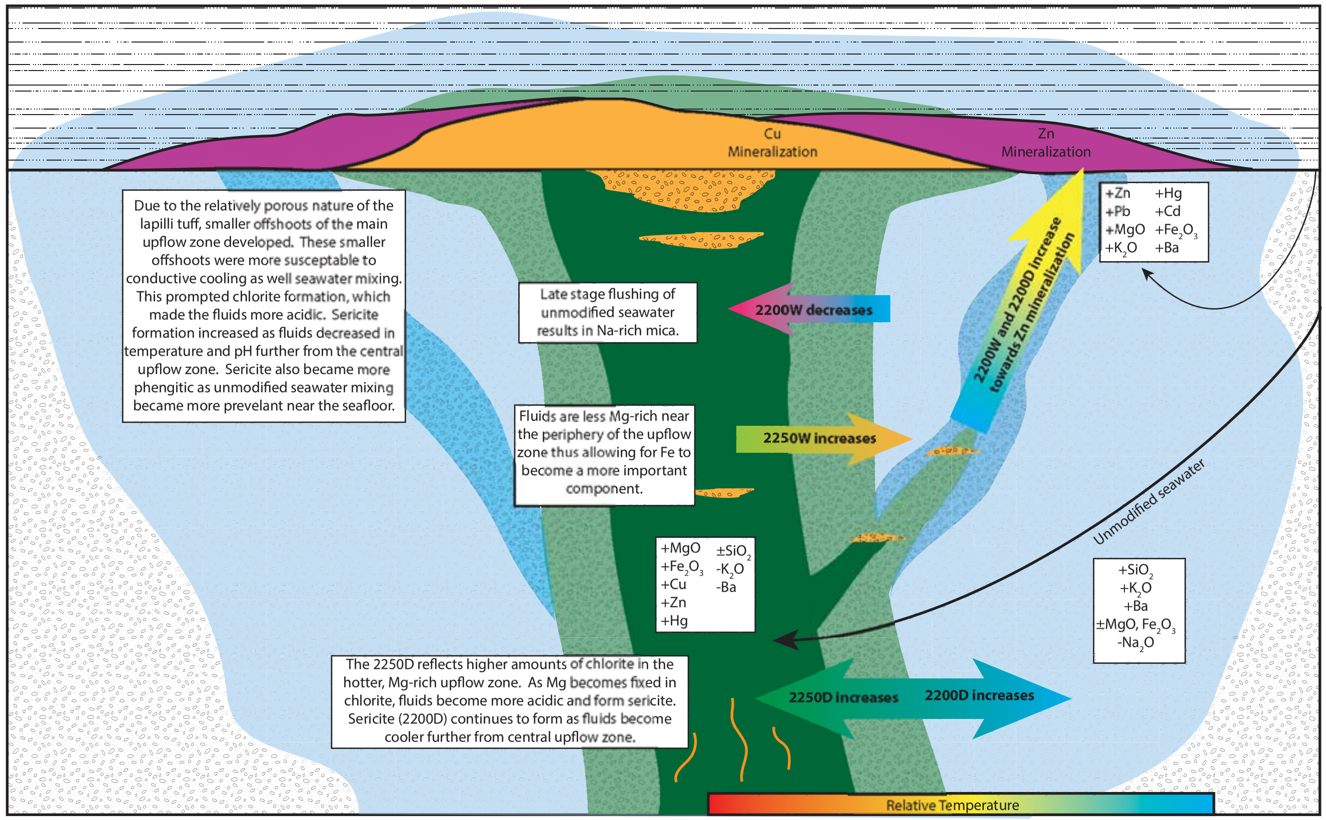

Figure 2.22 Schematic diagram showing the SWIR data variation and mass changes with geologic explanations. Although the alteration distribution is primarily controlled by the host rock permeability and porosity, the SWIR variation is heavily dependent on the addition of unmodified seawater, temperature, and pH. The central upflow zone exhibits gains in elements related to chlorite formation (MgO, Fe_2O_3) and mineralization (Cu, Zn, Hg,Fe_2O_3) and hyperspectral signatures indicating abundant Mg-chlorite content (shorter FeOH wavelength and increasing absorption depth). The offshoot of the main upflow zone exhibits gains in low temperature minrealization (Zn, Pb, Hg), minor chlorite (MgO, Fe_2O_3), and increasing sericite (K_2O,Ba). The hyperspectral signatures indicate an increase in phengitic white mica (longer AlOH wavelengths and increasing absorption depth) near the top of the lapilli tuff unit.

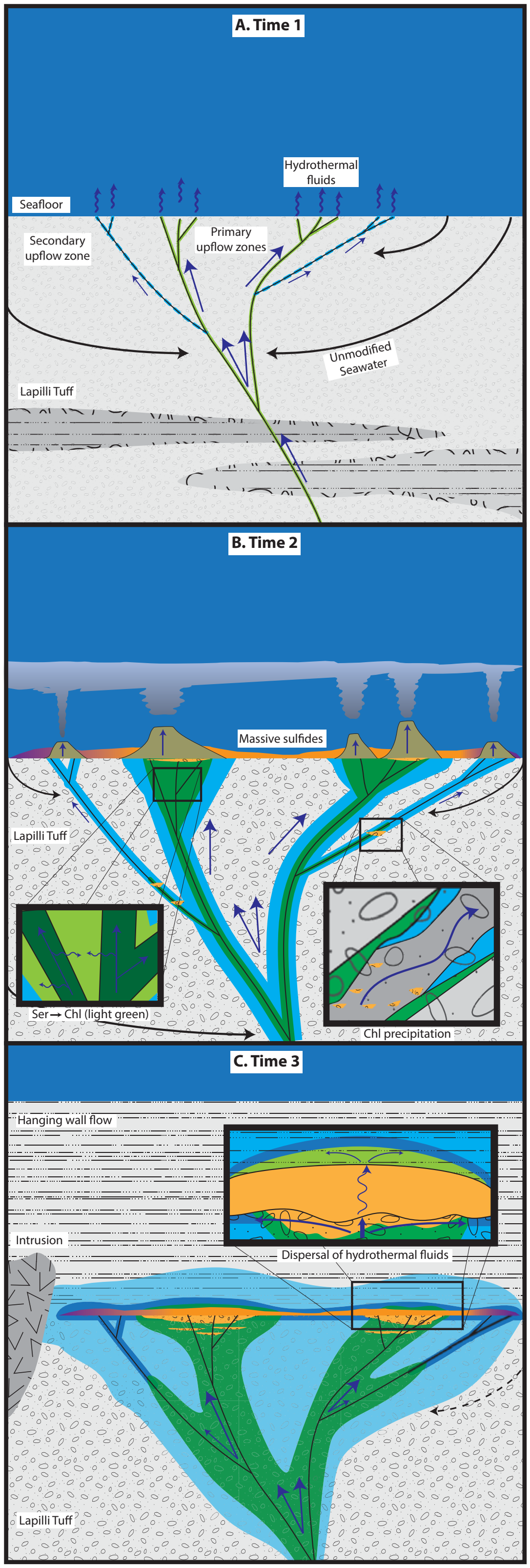

Figure 2.23 Schematic diagram showing the evolution of the Boundary deposit (see text for details; not to scale). Light green=moderate chlorite alteration; Dark green=intense chlorite alteration; Light blue=sericite alteration, Dark blue=intense sericite alteration. Orange=Cu mineralization; Purple=Zn mineralization; Blue arrows=hydrothermal fluids (size relative to fluid abundance); black arrows=unmodified seawater.

Chapter 3: Summary and Future Research

3.1 Summary

The bimodal felsic Zn-Cu-Pb Boundary VMS deposit is hosted within the Cambrian Tally Pond group Newfoundland, Canada, and is an example of a replacement-style VMS deposit. The lack of metamorphic overprint and structural integrity make this deposit an ideal location to study the distribution of mineralization and alteration in subseafloor replacement-type VMS deposits. Furthermore, geochemical and hyperspectral data provide insight into the genesis of the Boundary deposit and its hydrothermal alteration system. The major conclusions from this study are as follows:

1. The Boundary deposit formed on the leading edge of Ganderia in rhyolitic host rocks within a rifted continental arc. This is supported by immobile element geochemistry and is consistent with previous studies within the Tally Pond group.
2. The Boundary deposit contains three alteration assemblages: quartz-sericite, chlorite-sericite, and intense chlorite, each which have distinct geochemical and hyperspectral signatures. These alteration assemblages are predominantly controlled by the host rock permeability and porosity in addition to hydrothermal fluid conditions.
3. Alteration indices, such as CCPI, and element gains (e.g., Cu, MgO, MnO, Fe_2O_3) provide useful vectors for Cu-mineralization; whereas, Hg/Na_2O and Hg, Zn, Pb, Cd, and Ba increase in proximity to Zn mineralization.

4. Mass changes among the major oxides (e.g., SiO_2, MgO, Fe_2O_3, K_2O), base metals, transition metals (e.g., Ba, Sr) vary with each alteration assemblage. Other elements, such as the REEs and high field strength elements, are predominantly immobile throughout the deposit.
5. Hyperspectral data reveal distinct trends that correlate with alteration assemblages and geochemistry: A) AlOH absorption hull depths correspond with the K_2O wt% and the wavelengths increase proximal to Zn-rich mineralization; B) the FeOH wavelengths correlate with whole rock Mg number and indicate a high abundance of Mg-rich chlorite in the intense chlorite assemblage; and C) the absorption hull depths for both AlOH and FeOH are useful in differentiating between assemblages and the ratio of the two (AlOH depth/FeOH depth) correlates strongly with the CCPI.
6. The evolution of the Boundary deposit led to the unique replacement features present in both the hanging wall and footwall. The formation of Boundary took place in three main stages: 1) initial faulting: formation of the main upflow zones for hydrothermal fluids to travel through. Lower footwall lapilli tuff and flow units were more resilient than the upper lapilli tuff, which was more heavily fractured creating numerous fluid pathways; 2) initiation of hydrothermal activity: deposition of typical VMS mineralization (i.e., massive Py-Ccp-Sph, bedded sulfides). Some of the smaller upflow zones cooled faster are dominated by sericite alteration and typically underlay Zn-mineralization; and 3) deposition of the hanging wall: fluids were forced to flow laterally

beneath the hanging wall causing replacement of tuff matrix with sulfide mineralization. This also led to moderate hanging wall alteration (generally chlorite-sericite or quartz-sericite) and some restricted hanging wall mineralization.

3.2 Future Research

Although the Boundary and Duck Pond mine site is now entering the reclamation phase, there are a number of unanswered questions that would greatly benefit the understanding of the Boundary deposit. Potential areas of interest for future research include: 1) the carbonate distribution, both within the Boundary deposit and throughout Tally Pond group, to test if the carbonate compositions vary in proximity to known mineralization; 2) a detailed study of the mineralization that includes the use of sulfur and lead isotopes to determine the main sources of metals and fluids in the deposit; 3) detailed mineralogy, mineral chemistry, stable isotope, and physicochemical modeling of the sulfides and associated hydrothermal fluids to determine fluid and metal origins, temperatures, and conditions of formation; 4) an electron probe microanalysis (EPMA) study of the sericite and chlorite at Boundary to compare compositions with Terraspec™ measurements and determine more precisely how wavelengths are related to composition.

References

Arculus, R.J., 1994, Aspects of magma genesis in arcs: Lithos, v. 33, p. 189-208.

Aur Resources, Ltd. 2007. Duck Pond Mine, Official Ceremony, May 9, 2007, Company brochure. [For updated information see Teck Resources website — www.teck.com]

AusSpec International, 2008, Spectral Interpretation Field Manual: GMEX, Edition 3, Volumes 1-10.

Barrett, T.J., and MacLean, W.H., 1991, Chemical, mass, and oxygen isotope changes during extreme hydrothermal alteration of an Archean rhyolite, Noranda, Quebec: Economic Geology, v. 86, p. 406-414.

Barrett, T.J., and MacLean, W.H., 1994, Chemostratigraphy and hydrothermal alteration in exploration for VHMS deposits in greenstones and younger rocks: in Lentz, D. R., ed., Alteration and Alteration Processes Associated with Ore-Forming Systems, Short Course Notes Volume 11, Geological Association of Canada, p. 433-467.

Barrett, T.J., Dawson, G.L., and MacLean, W.H., 2008, Volcanic stratigraphy, alteration, and sea-floor setting of the Paleozoic Feitais massive sulfide deposit, Aljustrel, Portugal: Economic Geology, v. 103, p. 215–39.

Barrie, C.T., 1995, Zircon thermometry of high-temperature rhyolites near volcanic associated massive sulfide deposits, Abitibi subprovince, Canada: Geology, v. 23, p. 169-172.

Barrie, C.T., and Hannington, M.D., 1999, Introduction: classification of VMS deposits based on host rock composition, in volcanic-associated massive sulfide deposits: processes and examples in modern and ancient environments, (eds.) C.T. Barrie and M.D. Hannington; Society of Economic Geologists, Reviews in Economic Geology, v. 8, p. 2-10.

Barrie, C.T., Ludden, J.N., and Green, T.H., 1993, Geochemistry of volcanic rocks associated with Cu-Zn and Ni-Cu deposits in the Abitibi Subprovince: Economic Geology, v. 88, p. 1341-1358.

Berkenbosch, H.A., de Ronde, C.E.J., Gemmell, J.B., McNeill, A.W., and Goeman, K., 2012, Mineralogy and formation of black smoker chimneys from Brothers submarine volcano, Kermadec arc: ECONOMIC GEOLOGY, v. 107, p. 1613-1633.

Besson, G., and Drits, V.A., 1997a, Refined relationships between chemical composition of dioctahedral fine-grained micaceous minerals and their infrared spectra within the OH stretching region. Part 1: Identification of the OH stretching band: Clays and Clay Minerals, v. 45, p. 158-169.

Besson G., and Drits V.A., 1997b, Refined relationships between chemical composition of dioctahedral fine-grained micaceous minerals and their infrared spectra within the OH stretching region. Part II: The main factors affecting OH vibrations and quantitative analysis: Clays and Clay Minerals, v. 45, p. 170-183.

Bradshaw, G.D., Rowins, S.M., Peter, J.M., and Taylor, B.E., 2008, Genesis of the Wolverine volcanic sediment-hosted massive sulfide deposit, Finlayson Lake district, Yukon, Canada: Mineralogical, mineral chemical, fluid inclusion, and sulfur isotope evidence: Economic Geology, v. 103, p. 35–60.

Collins, C.J., 1989, Report on lithogeochemical study of the Tally Pond Volcanics and associated alteration and mineralization: Unpublished Report for Noranda Exploration Company Limited (Assessment File 012A/1033 Newfoundland Department of Mines and Energy, Mineral Lands Division): St. John’s, Newfoundland, 87 p.

Colman-Sadd, S.P., Dunning, G.R., and Dec, T., 1992, Dunnage-Gander relationships and Ordovician orogeny in central Newfoundland: a sediment provenance and U/Pb study: American Journal of Science, v. 292, p. 317-355.

Date, J., Watanabe, Y., and Saeki, Y., 1983, Zonal alteration around the Fukazawa Kuroko deposits, Akita Prefecture, northern Japan: Economic Geology Monograph 5, p. 365-386.

de Ronde, C.E.J., Hannington, M.D., Stoffers, P., 2005, Evolution of a submarine magmatic-hydrothermal system: Brothers volcano, southern Kermadec arc, New Zealand: Economic Geology, v. 100, p.1097-1133.

de Ronde, C.E.J., Walker, S.L., Ditchburn, R.G., Caratori Tontini, F., Hannington, M.D., Merle, S.G., Timm, C., Handler, M.R., Wysoczanski, R.J., Dekov, V.M., Kamenov, G.D., Baker, E.T., Embley, R.W., Lupton, J.E., and Stoffers, P., 2014, The anatomy of a buried submarine hydrothermal system, Clark volcano, Kermadec arc, New Zealand: ECONOMIC GEOLOGY, v. 109, p. 2261-2292.

Deer, W.A., Howie, R.A., and Zussman, J., 1992, Introduction to the rock- forming minerals, 2nd ed.: New York, Longman Scientific and Technical, 696 p.

Doyle, M.G., and Allen R.L., 2003, Subsea-floor replacement in volcanic-hosted massive sulfide deposits: Ore Geology Reviews, v. 23, p. 183–222.

Doyle, M.G., and Huston, D.L., 1999, The subsea-floor replacement origin of the Ordovician Highway-Reward VMS deposit, Mount Windsor Subprovince, northern Queensland: Economic Geology, v. 94, 825–844.

Dunning, G.R., Kean, B.F., Thurlow, J.G. and Swinden, H.S., 1987, Geochronology of the Buchans, Roberts Arm, and Victoria Lake groups and Mansfield Cove Complex, Newfoundland: Canadian Journal of Earth Sciences, v. 24, p. 1175-1184.

Dunning, G.R., Swinden, H.S., Kean, B.F., Evans, D.T.W., and Jenner, G.A., 1991, A Cambrian island arc in Iapetus: Geochronology and geochemistry of the Lake Ambrose volcanic belt, Newfoundland Appalachians: Geological Magazine, v. 128, p. 1–17.

Evans, D.T.W., and Kean, B.F., 2002, The Victoria Lake Supergroup, central Newfoundland: Its definition, setting and volcanogenic massive sulfide mineralization: Newfoundland and Labrador Department of Mines and Energy, Geological Survey, Open File NFLD/2790, 68 p.

Evans, D.T.W., Kean, B.F., and Dunning, G.R., 1990, Geological Studies, Victoria Lake Group, Central Newfoundland: In Current Research, Newfoundland Department of Mines and Energy, Geological Survey Branch, Report 90-1, p. 131-144.

Franklin, J.M., 1995, Volcanic-associated massive sulfide base metal: Geological Survey of Canada, Geology of Canada, no.8, p. 158–183.

Franklin, J.M., Gibson, H.L., Galley, A.G., and Jonasson, I.R., 2005, Volcanogenic massive sulfide deposits: Economic Geology 100th Anniversary Volume, p. 523-560.

Franklin, J.M., Lydon, J.W., and Sangster, D.F., 1981, Volcanic-associated massive sulfide deposits: Economic Geology 75th Anniversary Volume, p. 485–627.

Galley, A.G., 1993, Characteristics of semi-conformable alteration zones associated with volcanogenic massive sulphide districts: Journal of Geochemical Exploration, v. 48, p. 175–200.

Galley, A.G., Hannington, M.D., and Jonasson, I.R., 2007, Volcanogenic massive sulphide deposits: In mineral deposits of Canada: A synthesis of major deposit types, district metallogeny, the evolution of geological provinces, and exploration methods, Geolocial Association of Canada, Mineral Deposits Division, Special Publication No. 5.

Galley, A.G., and Jonasson, I.R., 2003, Classification and tectonic environments of VMS deposits in the Flin Flon mining camp, Manitoba: Geological Association of Canada/Mineralogical Association of Canada Annual General Meeting, Program with Abstracts (CD-ROM).

Galley, A.G., Watkinson, D.H., Jonasson, I.R., and Riverin, G., 1995, The subsea-floor formation of volcanic-hosted massive sulfide: Evidence from the Ansil deposit, Rouyn-Noranda, Canada: Economic Geology, v. 90, p. 2006–2017.

Gemmell, J.B., and Fulton, F., 2001, Geology, genesis, and exploration implications of the footwall and hanging-wall alteration associated with the Hellyer volcanic-hosted massive sulfide deposit, Tasmania, Australia: Economic Geology, v. 96, p. 1003–1035.

Gemmell, J.B., and Large, R.R., 1992, Stringer system and alteration zones underlying the Hellyer volcanic-hosted massive sulfide deposit, Tasmania, Australia: Economic Geology v. 87, p. 620–649.

German, C.R., and Von Damm, K.L., 2003, Hydrothermal systems. In: Elderfield H (ed.): Treatise on Geochemistry-The Oceans, v. 6, p. 181-222.

Gibson, H.L., 2005, Volcanic-hosted ore deposits, in Marti, J., and Ernst, G.G.J., eds., Volcanoes in the environment: New York, Cambridge University Press, p. 332–386.

Gibson, H.L., Allen, R.L., Riverin, G., Lane, T.E., 2007, The VMS Model: Advances and Application to Exploration Targeting. Plenary Session: Ore Deposits and Exploration Technology. Fifth Decennial International Conference on Mineral Exploration, p. 713-730.

Grant, J. A., 1986, The isocon diagram - a simple solution to Gresens' equation for metasomatic alteration. Economic Geology, 81, p. 1976-1982.

Green, G.R., Ohmoto, H., Date, J., Takahashi, T., 1983, Whole-rock oxygen isotope distribution in the Fukazawa-Kosaka area, Hokuroku District, Japan, and its potential application to mineral exploration: Economic Geology Monolith, v. 5, p. 395-411.

Gresens, R.L., 1967, Composition-volume relationships of metasomatism. Chemical Geology, 2, p. 47-55.

Gruen, G., Weis, P., Driesner, T., Heinrich, C.A., and de Ronde, C.E.J., 2014, Hydrodynamic modeling of magmatic-hydrothermal activity at submarine arc volcanoes with implications for ore deposit formation: Earth and Planetary Science Letters, v. 404, p. 307-318.

Guidotti, C.V., Sassi, F.P., 1998, Petrogenetic significance of Na–K white mica mineralogy: recent advances for metamorphic rocks: European Journal of Mineralogy, v. 10, p. 815–854.

Hannington, M.D., Barrie, C.T., and Bleeker, W., 1999, The giant Kidd Creek volcanogenic massive sulfide deposit, western Abitibi subprovince, Canada: Preface and introduction: Economic Geology Monograph 10, p. 1–30.

Hart, T.R., Gibson, H.L., and Lesher, C.M., 2004, Trace element geochemistry and petrogenesis of felsic volcanic rocks associated with volcanogenic massive Cu-Zn-Pb sulphide deposits, Economic Geology, v. 99, p. 1003–1013.

Hekinian, R., Fevrier, M., Bischoff, J.L., Picot, P., and Shanks, W.C., 1980, Sulfide deposits from the East Pacific Rise near 21°N: Science, v. 207, p.1433-1444.

Herrmann, W., Blake, M., Doyle, M., Huston, D., Kamprad, J., Merry, N. and Pontual, S., 2001, Short wavelength infrared (SWIR) spectral analysis of hydrothermal alteration zones associated with base metal sulfide deposits at Rosebery and Western Tharsis, Tasmania, and Highway-Reward, Queensland: Economic Geology, v. 96, p. 939–955.

Herzig, P.M., and Hannington, M.D., 1995, Polymetallic massive sulfides at the modern seafloor-a review: Ore Geology, v. 10, p. 95-115.

Huston, D.L., Kamprad, J., and Brauhart, C., 1997, Preliminary results of PIMA analysis of the alteration zone underlying the Sulphur Springs deposit, Panorama district, Pilbara block, Western Australia: Australian Geological Survey Organization Record 1997/14, 36 p.

Ishikawa, Y., Sawaguchi, T., Ywaya, S., and Horiuchi, M., 1976, Delineation of prospecting targets for Kuroko deposits based on modes of volcanism of underlying dacite and alteration halos: Mining Geology, v. 26, p. 105-117.

Jenner, G.A., 1996, Trace element geochemistry of igneous rocks: Geochemical nomenclature and analytical geochemistry: in Wyman, D.A., ed., Trace Element Geochemistry of Volcanic Rocks: Applications for Massive Sulfide Exploration: Geological Association of Canada, Short Course Notes, v. 12, p. 51–77.

Jenner, G.A., Longerich, H.P., Jackson, S.E., and Fryer, B.J., 1990, ICP-MS – A powerful tool for high-precision trace element analysis in Earth sciences: Evidence from analysis of selected U.S.G.S. reference samples: Chemical Geology, v. 83, p. 133-148.

Jones, S., 2005, Short wavelength infrared spectral characteristics of the HW horizon: Implications for exploration in the Myra Falls volcanic-hosted massive sulfide camp, Vancouver Island, British Columbia, Canada: Economic Geology, v. 100, p. 273–94.

Kean, B.F., and Jayasinghe, N.R., 1980, Geology of the Lake Ambrose (12-A/10)-Noel Paul's Brook (12-A/9) Map Areas, Central Newfoundland: Government of Newfoundland and Labrador, Department of Mines and Energy, Mineral Development Division, Report 80-02, 33 p., 2 maps.

Kean, B.F. and Evans, D.T.W. 1986, Metallogeny of the Tulks Hill volcanics, Victoria Lake Group, central Newfoundland: Report—Government of Newfoundland and Labrador, Department of Mines and Energy, Mineral Development Division, v. 86-1, p. 51-57.

Kean, B.F., Evans, D.T.W., and Jenner, G.A., 1995, Geology and mineralization of the Lushs Bight Group: St. John's, Newfoundland, Geological Survey of Newfoundland and Labrador, Mineral Development Division, Report 95-05, 204 p.

Knuckey, M.J., Comba, C.D.A., and Riverin, G., 1982, Structure, metal zoning and alteration at the Millenbach Deposit, Noranda, Quebec: Special Paper – Geological Association of Canada, v. 25, p. 255-295.

Large, R.R. 1992, Australian volcanic-hosted massive sulfide deposits: Features, styles, and genetic models: Economic Geology, v. 87, p. 471–510.

Large, R.R., Gemmell, J.B., Paulick, H., and Huston, D.L., 2001, The alteration box plot: A simple approach to understanding the relationships between alteration mineralogy and lithogeochemistry associated with VHMS deposits: Economic Geology, v. 96, p. 957–971.

Lentz, D.R., 1998, Petrogenetic evolution of felsic volcanic sequences associated with Phanerozoic volcanic-hosted massive sulphide systems: The role of extensional geodynamics: Ore Geology Reviews, v. 12, p. 289–327.

Lentz, D., and Wilson, R.A., 1997, Chemostratigraphic analysis of the volcanic and sedimentary rocks in the Heath Steele B-B5 zone area, Bathurst camp, New

Brunswick: Stratigraphic and structural implications: Current Research - Geological Survey of Canada, Report 1997-D, p. 21–33.

Lesher, C.M., Goodwin, A.M., Campbell, I.H., and Gorton, M.P., 1986, Trace-element geochemistry of ore-associated and barren, felsic metavol- canic rocks in the Superior province, Canada: Canadian Journal of Earth Sciences, v. 23, p. 222–237.

Lode, S., Piercey, J.S., Devine, C.A., in review. Geology, Mineralogy, and Lithogeochemistry of Hydrothermal Exhalites Associated with the Lemarchant Volcanogenic Massive Sulfide (VMS) Deposit, Tally Pond Belt, Central Newfoundland. Economic Geology.

Longerich, H.P., Jenner, G.A., Fryer, B.J., and Jackson, S.E., 1990, Inductively coupled plasma-mass spectrometric analysis of geological samples: A critical evaluation based on case studies: Chemical Geology, v. 83, p.105-118.

Luff, W.M., Goodfellow, W.D., and Juras, S.J., 1992, Evidence for a feeder pipe and associated alteration at the Brunswick No. 12 massive sulphide deposit: Exploration and Mining Geology, v. 1, p. 167–185.

Lydon, J.W., 1984, Volcanogenic sulphide deposits, Part 1, A descriptive model; Geoscience Canada, v. 11, p. 195-202.

Lydon, J.W., 1988, Volcanogenic massive sulphide deposits; Part 2, Genetic models: Geoscience Canada, v. 15, p. 43-65.

MacLean, W.H., 1988, Rare earth element mobility at constant inter-REE ratios in the alteration zone at the Phelps Dodge massive sulphide deposit, Matagami, Quebec: Mineralium Deposita, v. 23, p. 231–38.

MacLean, W.H., 1990, Mass change calculations in altered rock series: Mineralium Deposita, v. 25, p. 44-49.

MacLean, W.H., and Kranidiotis, P., 1987, Immobile elements as monitors of mass transfer in hydrothermal alteration: Phelps Dodge massive sulfide deposit, Matagami, Quebec: Economic Geology, v. 82, p. 951–62.

MacLean, W.H., and Barrett, T.J., 1993, Lithogeochemical techniques using immobile elements: Journal of Geochemical Exploration, v. 48, p. 109–33.

McDonough, W.F., and Sun, S., 1995, Composition of the earth: Chemical Geology, v. 120, p. 223-253.

McLeod, R.L., and Stanton, R.L., 1984, Phyllosilicates and associated minerals in some Paleozoic stratiform sulfide deposits of southeastern Australia: Economic Geology, v. 79, p. 1–21.

McNicoll, V., Squires, G.C., Kerr, A., Moore, P.J., 2008, Geological and Metallogenic Implications of U-Pb Zircon Geochronological Data from the Tally Pond Area, Central Newfoundland, Current Research, Report 08-1: Newfoundland and Labrador Department of Natural Resources, Geological Survey, p.173-192.

McNicoll, V., Squires, G., Kerr, A., and Moore, P.J., 2010, The Duck Pond and Boundary Cu–Zn deposits, Newfoundland: New insights into the ages of host rocks and the timing of VHMS mineralization: Canadian Journal of Earth Sciences, v. 47, p. 1481–1506.

McPhie, J., Doyle, M., and Allen, R.L., 1993, Volcanic textures: A guide to the interpretation of textures in volcanic rocks: Hobart, Australia, Centre for Ore Deposit and Exploration Studies, University of Tasmania, 198 p.

Mineral Information, 2007. Department of Natural Resources: Mines Branch, Newfoundland and Labrador, v. 13, no. 1

Moore, P.J., 2003, Stratigraphic implications for mineralization: Preliminary findings of a metallogenic investigation of the Tally Pond volcanics, central Newfoundland, in Pereira, C.P.G., Walsh, D.G., and Kean, B.F., ends., Current Research Report 03-1: St. John’s, Newfoundland, Geological Survey Branch, p. 241-257.

Neuman, R.B., 1967, Bedrock geology of the Shin Pond and Stacyville quadrangles, Maine. U.S. Geological Survey, Professional Paper 524-1, 47 pages.

Petersen, S., Monecke, T., Westhues, A., Hannington, M.D., Gemmell, J.B., Sharpe, R., Peters, M., Strauss, H., Lackschewitz, K., Augustin, N., Gibson, H., and Kleeberg, R., 2014, Drilling shallow-water massive sulfides at the Palinuro volcanic complex, Aeolian island arc, Italy: ECONOMIC GEOLOGY, v. 109, p. 2129-2157.

Piercey, S.J., 2007, Volcanogenic massive sulphide (VMS) deposits of the Newfoundland Appalachians: An overview of their setting, classification, grade-tonnage data, and unresolved questions, in Pereira, C. P. G., and Walsh, D. G., eds., Current Research, Report 07-01: St. John's, NL, Geological Survey Branch, p. 169-178.

Piercey, S.J., 2009, Lithogeochemistry of volcanic rocks associated with volcanogenic massive sulfide deposits and applications to exploration, *in* Submarine Volcanism and Mineralization: Modern through ancient, (eds.) B. Cousens and S.J. Piercey;

Geological Association of Canada, Short Course 29-30 May 2008, Quebec City, Canada, p. 15-40.

Piercey, S.J., 2011, The setting, style, and role of magmatism in the formation of volcanogenic massive sulfide deposits: Mineralium Deposita, v. 46, p. 449–471

Piercey, S., and Colpron., 2009, Composition and provenance of the Snowcap assemblage, basement to the Yukon-Tanana terrane, northern Cordillera: Implications for Cordilleran crustal growth: Geosphere, v. 5, p. 439-464.

Piercey, S.J. and Hinchey, J. 2012: Volcanogenic massive sulphide (VMS) deposits of the Central Mineral Belt, Newfoundland. Geological Association of Canada–Mineralogical Association of Canada Joint Annual Meeting, Field Trip Guidebook B4. Newfoundland and Labrador Department of Natural Resources, Geological Survey, Open File NFLD/3173, 56 pages.

Piercey, S.J., Squires, G.C., and Brace, T.D., 2014, Lithostratigraphic, hydrothermal, and tectonic setting of the Boundary volcanogenic massive sulfide deposit, Newfoundland Appalachians, Canada: Formation by subseafloor replacement in a Cambrian rifted arc: Economic Geology, v. 109, p. 661–87.

Pollock, J., 2004, Geology and paletectonic history of the Tally Pond Group, Dunnage zone, Newfoundland Appalachians: An integrated geochemical, geochronological, metallogenic and isotopic study of a Cambrian island arc along the Peri-Gondwanan margin of Iapetus: Unpublished M.Sc. thesis, St. John’s, Newfoundland, Memorial University, 420 p.

Pontual, S., Merry, N., and Gamson, P., 1997, G-Mex Vol. 1, Spectral interpretation field manual: Kew, Victoria 3101, Australia, Ausspec International Pty. Ltd., p. 169.

Riverin, G., and Hodgson, C.J., 1980, Wall-rock alteration at the Millenbach Cu-Zn mine, Noranda, Quebec: Economic Geology, v. 75, p. 424-444.

Roberts, R. G., and Reardon, E.J., 1978, Alteration and ore-forming processeast Mattagami Lake mine,Quebec: Canadian Journal of Earth Sciences, v. 15, p. 1-21.

Rogers, N., and van Staal, C.R., 2002, Toward a Victoria Lake Supergroup: A provisional stratigraphic revision of the Red Indian to Victoria Lakes area, central Newfoundland: Current Research–Newfoundland, Geological Survey Branch, Report 02-1, p.185–195.

Rogers, N., van Staal, C.R., McNicoll, V., Pollock, J., Zagorevski, A., and Whalen, J., 2006, Neoproterozoic and Cambrian arc magmatism along the eastern margin of the

Victoria Lake Supergroup: A remnant of Ganderian basement in central Newfoundland?: Precambrian Research, v. 147, p. 320–341.

Rogers, N., van Staal, C.R., Pollock, J., and Zagorevski, A., 2005, Geology, Lake Ambrose and Part of Buchans, Newfoundland (NTS 12-A/10 and Part of 12-A/15): Geological Survey of Canada Open-File 4544, scale 1:50,000.

Rogers, N., van Staal, C., Zagorevski, A., Skulski, T., Piercey, S.J., and McNicoll, V., 2007, Timing and tectonic setting of volcanogenic massive sulfide bearing terranes within the Central Mobile belt of the Canadian Appalachians, in Milkereit, B., ed., Proceedings of Exploration 07: Toronto, Fifth Decennial International Conference on Mineral Exploration, September 9-12, 2007, p. 1199–1205.

Ross, P.-S., and Bedard, J.H., 2009, Magmatic affinity of modern and ancient subalkaline volcanic rocks determined from trace-element discriminant diagrams: Canadian Journal of Earth Sciences, v. 46, p. 823-839.

Rucks, T.W., Piercey, S.J., Ryan, J.J., Villeneuve, M.E., and Creaser, R.A., 2006, Mid- to late Paleozoic K-feldspar augen granitoids of the Yukon-Tanana terrane, Yukon, Canada: Implications for crustal growth and tectonic evolution of the northern Cordillera: Geologic Society of America Bulletin, v. 118, p. 1212-1231.

Saeki, Y., and Date, J., 1980, Computer application to the alteration data of the footwall dacite lava at the Ezuri Kuroko deposits, Akito Prefecture: Mining Geology, v. 30, p. 241–250.

Sangster, D.F., 1972, Precambrian volcanogenic massive sulphide deposits in Canada: A review: Canada Geological Survey Paper 72-22, p. 44.

Schardt, C., Cooke, D.R., Gemmell, J.B., and Large, R.R., 2001, Geochemical modeling of the zoned footwall alteration pipe, Hellyer volcanic-hosted massive sulfide deposit, Western Tasmania, Australia: Economic Geology, v. 96, p. 1037–1054.

Shukuno, H., Tamura, Y., Tani, K., Chang, Q., Suzuki, T., and Fiske, R.S., 2006, Origin of silicic magmas and the compositional gap at Sumisu submarine caldera, Izu-Bonin arc, Japan: Journal of Volcanology and Geothermal Research, v. 156, p. 187–216

Smith, I., Worthington, T.J., Stewart, R.B., Price, R.C., and Gamble, J.A., 2003, Felsic volcanism in the Kermadec Arc, SW Pacific: Crustal recycling in an oceanic setting: Geological Society, London, Special Publications, v. 219, p. 99–118.

Spitz, G., and Darling, R., 1978, Major and minor element lithogeochemical anomalies surrounding the Louvem copper deposit, Val d'Or, Quebec: Canadian Journal of Earth Sciences, v. 15, p. 1161–1169.

Squires, G.C., and Moore, P.J., 2004, Volcanogenic massive sulfide environments of the Tally Pond Volcanics and adjacent area: Geological, lithogeochemical and geochronological results, in Pereira, C.P.G., Walsh, D.G., and Kean, B.F., eds., Current Research Report 04-1: St. John's, Newfoundland, Geological Survey Branch, p. 63-91.

Squires, G.C., Brace, T.D., and Hussey, A.M., 2001, Newfoundland's polymetallic Duck Pond deposit: Earliest Iapetan VMS mineralization formed within a sub-seafloor, carbonate-rich alteration system, *in* Evans, D.T.W., and Kerr, A., eds., Geology and mineral deposits of the northern Dunnage zone, Newfoundland Appalachians: St. John's, Newfoundland, Geological Association of Canada-Mineralogical Association of Canada, Field Trip Guide A2, p. 167–187.

Squires, G.C., MacKenzie, A.C., and MacInnis, D., 1991, Geology and genesis of the Duck Pond volcanogenic massive sulfide deposit, *in* Swinden, H.S., Evans, D.T.W., and Kean, B.F., eds., Metallogenic framework of base and precious metal deposits, central and western Newfoundland: Geological Survey of Canada Open File 2156, p. 56–64.

Swinden, H.S., 1991, Paleotectonic settings of volcanogenic massive sulfide deposits in the Dunnage zone, Newfoundland Appalachians: Canadian Institute of Mining and Metallurgy Bulletin, v. 84, p. 59–89

Swinden, H.S., Jenner, G.A., Kean, B.F., and Evans, D.T.W., 1989, Volcanic rock geochemistry as a guide for massive sulfide exploration in central Newfoundland: Newfoundland Department of Mines, Current Research Report 89-1, p. 201–219.

Swinden, H.S., and Thorpe, R.I., 1984, Variations in style of volcanism and massive sulfide deposition in Early to Middle Ordovician island-arc sequences of the Newfoundland Central Mobile belt: Economic Geology, v. 79, p. 1596–1619.

Sverjensky, D.A., 1984, Europium redox equilibria in aqueous solutions: Earth and Planetary Science Letters, v. 67, p. 70-78.

Teck Cominco Ltd., 2007, Teck Cominco Acquires Approximately 93% of Aur Resources Common Shares. External News Release August 22, 2007. [For updated information see Teck Resources website-www.teck.com] van Staal, C.R., 2007, Pre-Carboniferous tectonic evolution and metallogeny of the Canadian Appalachians, in Goodfellow, W.D., ed., Mineral deposits of Canada: A synthesis of major deposit types, district metallogeny, the evolution of geological provinces, and exploration methods: Geological Association of Canada, Mineral Deposits Division Special Publication 5, p. 793–818

van Staal, C.R. and Barr, S.M., 2012, Lithospheric architecture and tectonic evolution of the Canadian Appalachians and associated Atlantic margin. Chapter 2 In Tectonic Styles in Canada: the LITHOPROBE Perspective. Edited by J.A. Percival, F.A. Cook, and R.M. Clowes. Geological Association of Canada, Special Paper 49, pp.

van Staal, C.R., and Colman-Sadd, S.P., 1997, The Central Mobile belt of the northern Appalachians: Oxford Monographs on Geology and Geophysics, v. 35, p. 747–760.

van Staal, C.R., Dewey, J.F., MacNiocaill, C., and McKerrow, S., 1998, The Cambrian-Silurian tectonic evolution of the northern Appalachians: history of a complex, southwest Pacific-type segment of Iapetus, in Blundell, D.J., and Scott, A.C., eds., Lyell: the Past is the Key to the Present: Geological Society, Special Publication 143, p. 199-242.

van Staal, C.R., and Zagorevski, A., 2012, Accreted Terranes of the Appalachian Orogen in Newfoundland: in the Footsteps of Hank Williams: Geologic Association of Canada-Mineral Association of Canada. Field Trip Guidebook –A1, 99p.

van Staal, C.R., Whalen, J.B., McNicoll, V.J., Pehrsson, S., Lissenberg, C.J., Zagorevski, A., van Breemen, O. and Jenner, G.A., 2007, The Notre Dame Arc and the Taconic Orogeny in Newfoundland. In 4-D Framework of Continental Crust. Edited by R.D. Hatcher, Jr., M.P. Carlson, J.H. McBride and J.R. Martinez Catalan. Geological Society of America Memoirs, v. 200, p. 511-552.

Velde, B.,1978, Infrared spectra of synthetic micas in the series muscovite-MgAl celadonite: American Mineralogist, v. 63, p. 341-349.

Wagner, D.W., 1993, Volcanic stratigraphy and hydrothermal alteration associated with the Duck Pond and Boundary volcanogenic massive sulphide deposits, Central Newfoundland: Unpublished MSc. thesis, Ottawa, Ontario, Canada, Carleton University, 430 p.

Williams, H., 1979, Appalachian orogen in Canada: Canadian Journal of Earth Sciences, v. 16, p. 792–807.

Williams, H., 1995, Geology of the Appalachian-Caledonian Orogen in Canada and Greenland: Geological Survey of Canada, Geology of Canada No. 6, 952 p.

Williams, H., Colman-Sadd, S.P., and Swinden, H.S., 1988, Tectonostratigraphic subdivisions of central Newfoundland: Geological Survey of Canada, Current Research, Part B, Paper 88-1B, p. 91–98.

Wright, I., Parson, L.M., and Gamble, J.A., 1996, Evolution and interaction of migrating cross-arc volcanism and backarc rifting: An example from the Southern Havre Trough (35°20′–37°S): Journal of Geophysical Research, v. 101, p. 22071–22086.

Wysoczanski, R.J., Handler, M.R., Schipper, C.I., Leybourne, M.I., Creech, J., Rotella, M.D., Nicols, A.R.L., Wilson, C.J.N., and Stewart, R.B., 2012, The tectonomagmatic source of ore metals and volatile elements in the southern Kermadec arc: ECONOMIC GEOLOGY, v. 107, p. 1539-1556.

Yang, K., Huntington, J.F., Gemmell, J.B., Scott, K.M., 2011, Variations in composition and abundance of white mica in the hydrothermal alteration system at Hellyer, Tasmania, as revealed by infrared reflectance spectroscopy: Journal of Geochemical Exploration, v. 108, p. 143-156.

Zagorevski, A., van Staal, C. R., and McNicoll, V. J., 2007a, Distinct Taconic, Salinic, and Acadian deformation along the Iapetus suture zone, Newfoundland Appalachians: Canadian Journal of Earth Sciences, v. 44, p. 1567-1585.

Zagorevski, A., van Staal, C. R., McNicoll, V. J., and Rogers, N., 2007b, Upper Cambrian to Upper Ordovician peri-Gondwanan island arc activity in the Victoria Lake Supergroup, central Newfoundland; tectonic development of the northern Ganderian margin: American Journal of Science, v. 307, p. 339-370.

Zagorevski, A., van Staal, C.R., Rogers, N., McNicoll, V.J., and Pollock, J., 2010, Middle Cambrian to Ordovician arc-backarc development on the leading edge of Ganderia, Newfoundland Appalachians: Geological Society of America Memoir, v. 206, p. 367–396.

Appendix A: Graphic Logs

A.1-Graphic Logs

Preliminary fieldwork at the Boundary deposit consisted of detailed logging and sampling of the hanging wall, ore horizon, and upper 100 m of the footwall in diamond drill core. Drill core logs focused predominantly on lithology, alteration assemblages, and general mineralization at the Boundary deposit. Fieldwork took place during August-September 2013 and June 2014 at the Duck Pond mine site just outside of Millertown, Newfoundland. A total of 62 drill holes were logged and 237 samples (from 51 drill holes) were taken. A total of 45 thin sections were made from these samples.

Below is the Abbreviation Key and Legend (Appendix A.2) for the 62 drill hole logs (Appendix A.3). Drill holes are labeled using the following nomenclature: BDXX-YYY, where BD stands for Boundary Deposit, XX stands for the last two numbers in the year the hole was drilled, and YYY represents the hole number drilled in that year's drilling program (i.e. BD10-45 was drilled at the Boundary deposit in 2010 and is the 45th hole drilled that year). As most holes are relatively short and vertical, these logs represent the true depth with the exception of a few longer holes and those drilled at dips other than 90°.

The logs contain the field interpretation of alteration. In some locations, this is not the true alteration determined through geochemistry and petrography, in which case a note has been made in the description section. Because carbonate spot alteration is present throughout the deposit, only non-carbonate spot alteration (e.g., veins, chaotic carbonate) is represented by the carbonate alteration field. Spot features are sometimes noted in the description if needed. Sulfide occurrences have their own lithology and symbols. Only disseminated sulfide amounts are represented in the alteration field.

A.2-Abbreviation Key and Legend for Graphic Logs

Table A.2.1-Abbreviation Key for Graphic Logs

General	
E	Easting
m	Meter
N	Northing
UTM	Universal Transverse Mercator
Alteration Types	
Carb	Carbonate
Chl	Chlorite
Qtz	Quartz
Ser	Sericite
Sulf	Sulfide

Host Rock Facies	
Arg	Argillite
BX	Breccia
Flow	Volcanic flow
Int	Intrusion
Lap	Lapilli tuff
MS	Massive sulfide
Tuff	Tuff
Descriptions	
alt.	Alteration
CC	Chaotic carbonate
Ccp	Chalcopyrite
Dia.	Diameter
Dis.	Disseminated
Fe	Iron
frag(s)	Fragment(s)
FW	Footwall
HW	Hanging wall
Hyalo	Hyaloclastite
int. chl	Intense chlorite
mod.	Moderate
Pheno(s)	Phenocryst(s)
Po	Pyrrhotite
Py	Pyrite
Sph	Sphalerite
Zn	Zinc

Table A.2.2-Legend for Graphic Logs

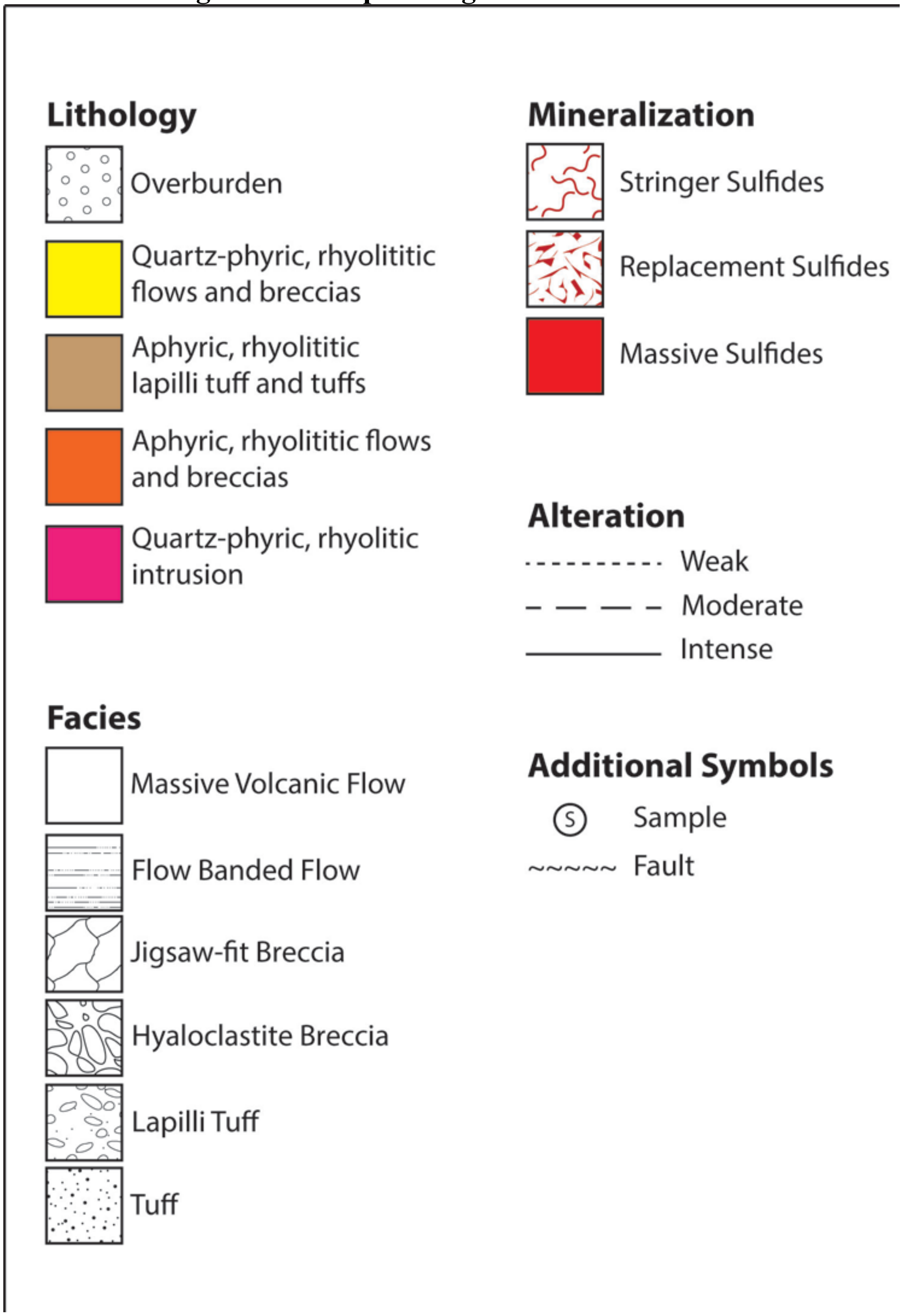

A.3-Compilation of Graphic Logs

Project: Boundary Diamond Drill Hole: BD07-199 Date: 8-15-2013	UTM 540816.00E 5389653.00N	Azimuth: 339 Dip: -90 Length: 30.1 m

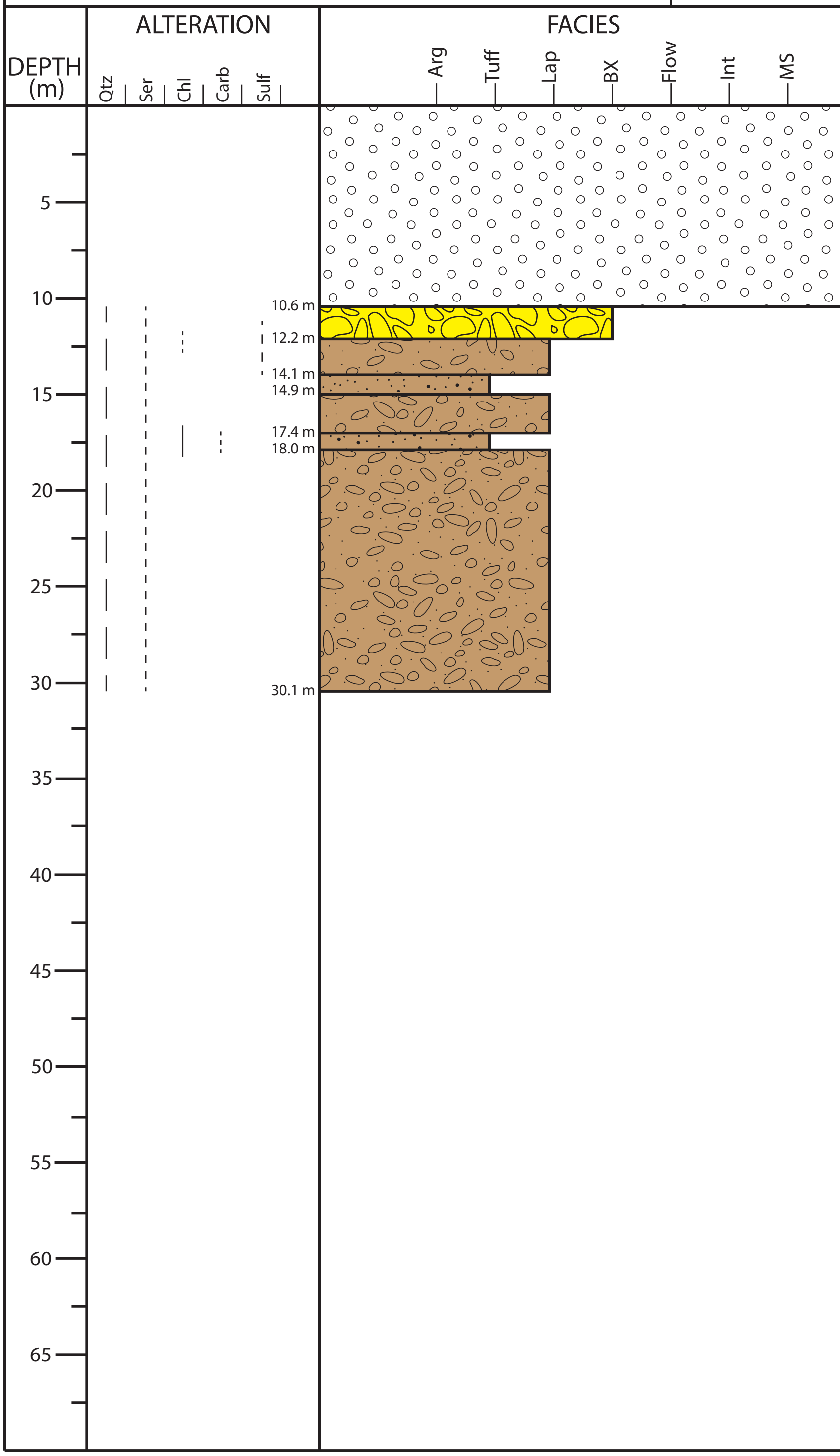

DESCRIPTION

Dark gray, qtz-phyric hyaloclastite with slight chl alteration near contact.

LT and tuff layers are relatively unaltered. Except the 17.4-18.0 m interval where tuff is intensely chl altered. LT units are all similar light-medium gray color. Clasts are more so matrix supported in the upper two LT units but become clasts supported in the third unit. Clasts also increase in size from ~1 cm in diameter in the top two and become bimodal in the third (2-4 cm and <0.5 cm). May be potential fault/shear ~17 m. Dis. Py is only sulfide in hole.

Project: Boundary Diamond Drill Hole: BD10-003 Date: 8-23-2013	UTM 540889.45E 5389325.32N	Azimuth: 360 Dip:-90 Length: 41

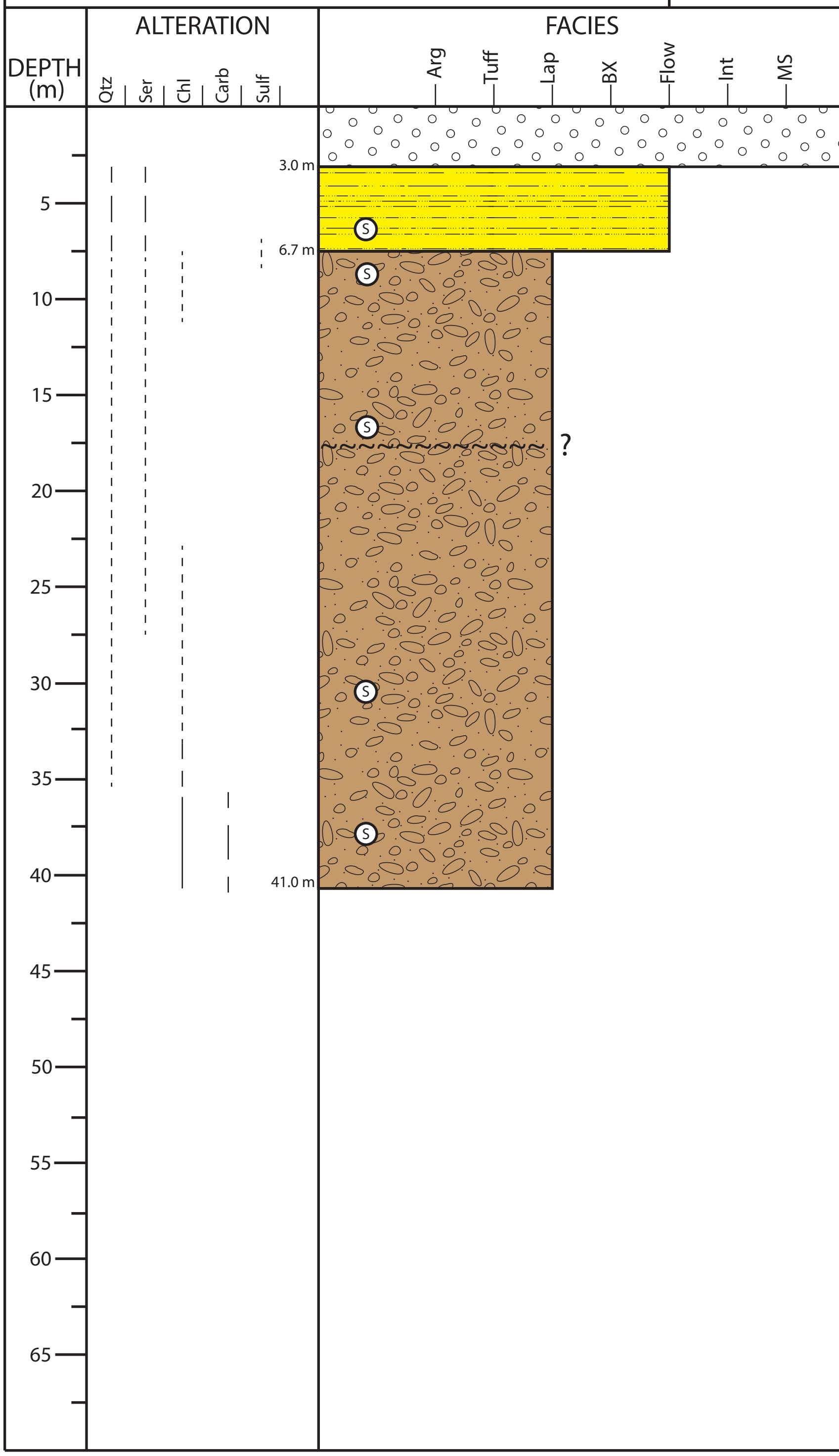

DESCRIPTION

Sample: H501332
Green/yellow-grey flow banded with minor carbonate spots and Fe pits. Dis. Py increases near the sharp HW-FW contact.

Sample: H501333
Minor dis-stringer Py in upper meter or so. Once stringer Py ends, ser alteration becomes more prevalent. Clasts are generally gray-white and bimodal in size in upper portion (~1cm and ~4 cm).

Sample: H501334
Most clasts are ~1-2 cm in diameter and generally varying shades of gray. Small sections (1-2m in length) appear to have elongate orientation: may be signs of faulting/shear?

Sample: H501335
Clasts again bimodal like upper portion of unit. Sericite alteration dies out as chl alteration begins. Unit appears to be becoming more matrix supported. Small zones of pink clasts occur sporadically.

Sample: H501336
Lower 5 meters of hole is intense chlorite and chaotic carbonate is present. Original LS not discernable. CC is varying shades of brown and white: probably different compos. No sulfides really visible.

Project: Boundary Diamond Drill Hole: BD10-006 Date: 8-22-2013	UTM 540924.63E 5389280.33N	Azimuth: 360 Dip: -90 Length: 35 m

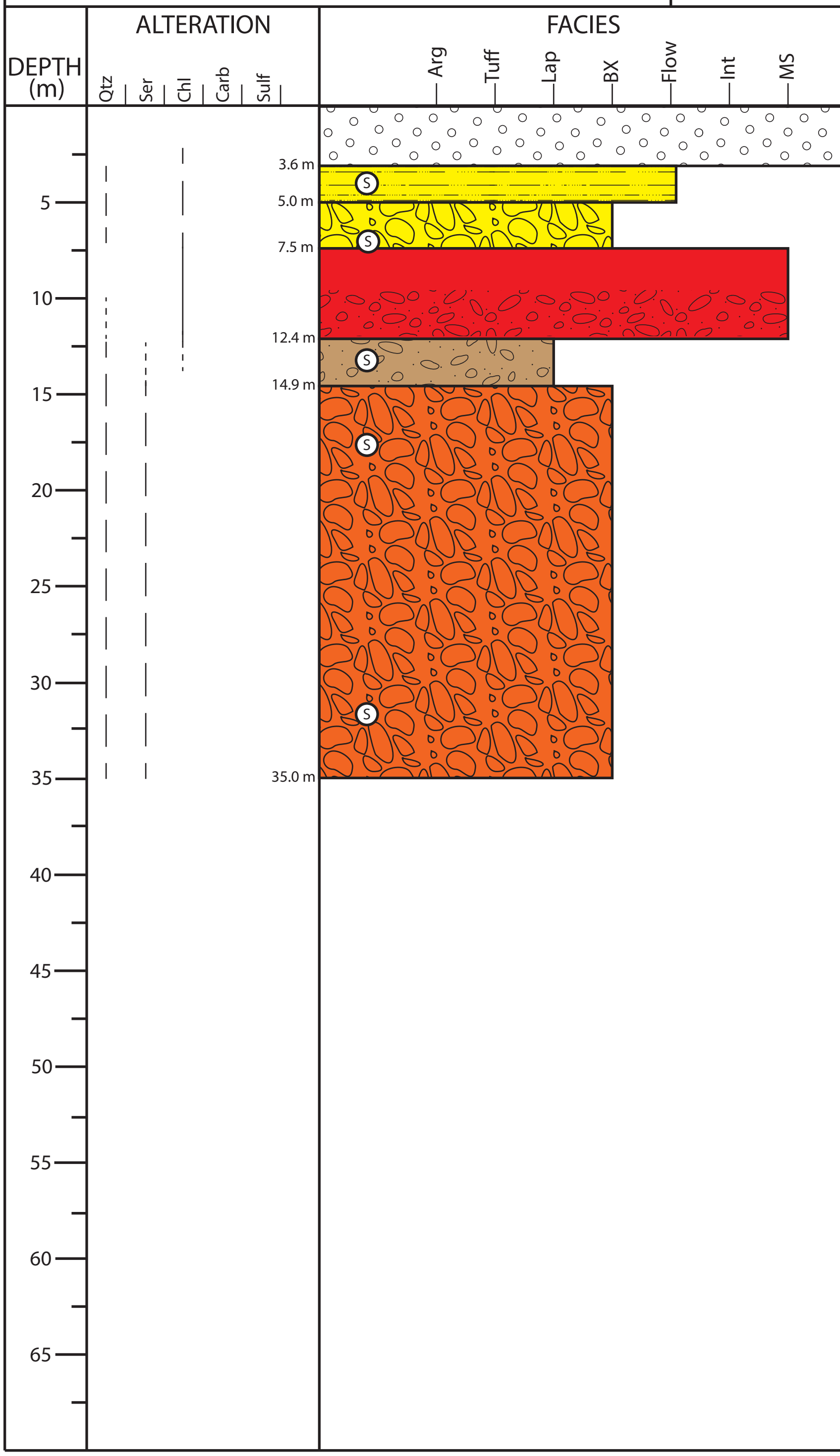

DESCRIPTION

Sample: H501316

Both flow and breccia are black and white. The BX frags are chl while matrix has been completely replaced by qtz. (?)

Sample: H501317

Massive sulfide is Py with minor Ccp and Sph. Also contains bedded Py-Sph with xcutting Ccp veins. Lower half of unit is LS clast rich. Pretty sharp alt. contact-once sulfides end, so does chl alt. within the LS.

Sample: H501318

LS clasts are light gray to white and generally ~1cm or less. Contains several small (<10cm) graded tuff beds. Clast supported.

Sample: H501319

The breccia contains large flow frags (some are flow banded). Most are between 5 and 8 cm in diameter and have white rims (~0.5 cm) with light gray centers. Generally clast supported but also matrix supported locally. Matrix is dark gray-black and contains a tuff size frags. Sericite alteration is greater here than seen in the North zone. No sulfides in this unit.

Sample: H501320

Project: Boundary Diamond Drill Hole: BD10-007 Date: 8-20-2013	UTM 540854.96E 5389344.86N	Azimuth: 360 Dip: -90 Length: 30

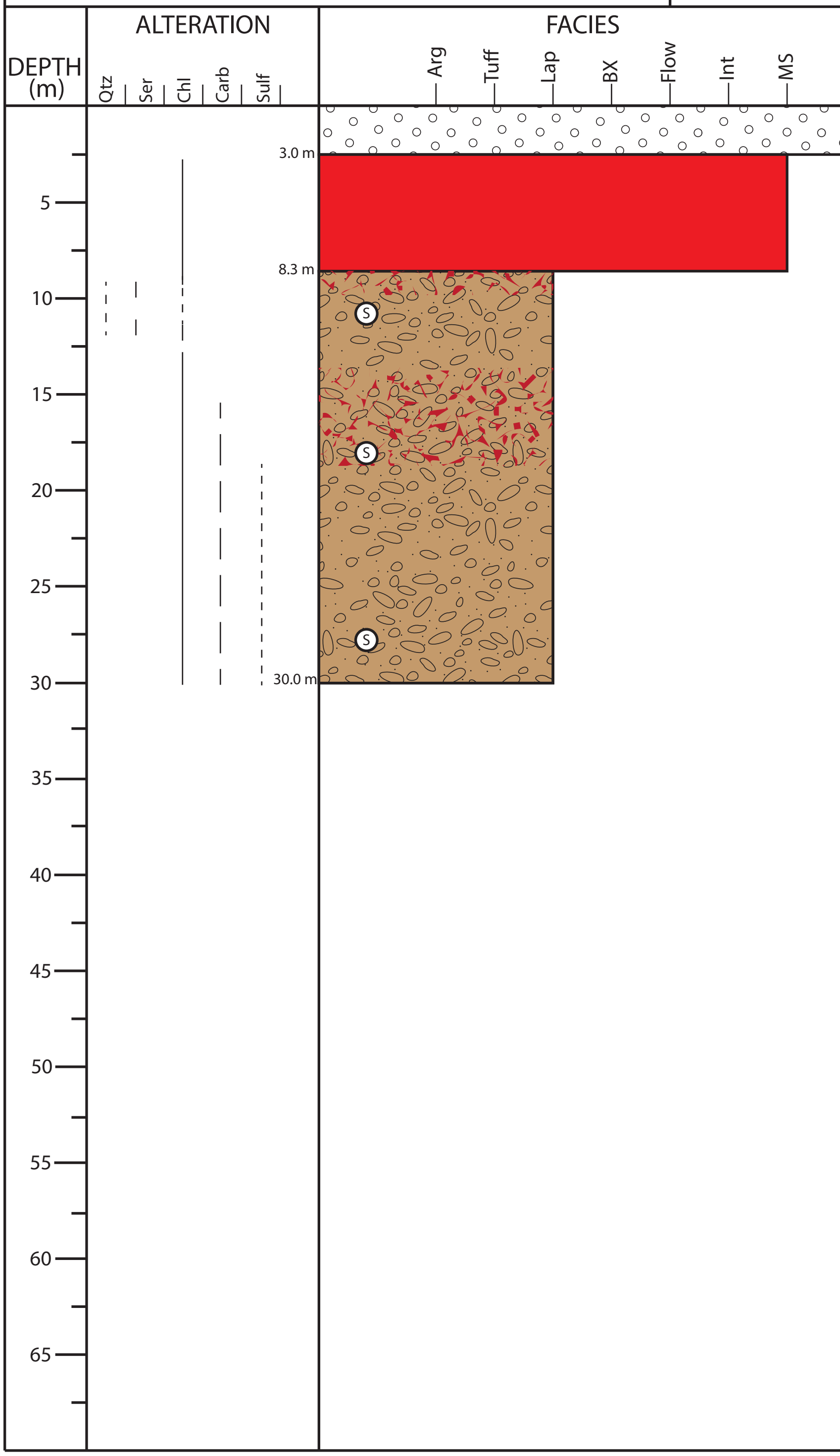

DESCRIPTION

Massive sulfides include Py, Ccp, and Sph (+maybe some galena?). Upper portion is mostly Py rich but becomes more Sph and Ccp rich near the bottom. Sharp contact with int. chl zone below + minor replacement sulfides.

Sample: H501268

LS quickly goes from complete black chlorite alteration to mod-int qtz-ser alteration for about 3 meters. Unit is clast supported and bimodal in clast size. In the qtz-ser zone clasts are yellow/white (ser) or gray (qtz). At ~13m, unit quickly becomes mod-int chlorite altered again. Clasts become difficult to make out. Small zone of replacement sulfides. Bottom of hole contains minor dis. sulfides and maybe some chaotic carbonate? Carbonate occurs as spots but in high abundance.

Sample: H501269

Project: Boundary Diamond Drill Hole: BD10-009 Date: 8-20-2013	UTM 540915.52E 5389274.98N	Azimuth: 360 Dip: -90 Length: 30.4

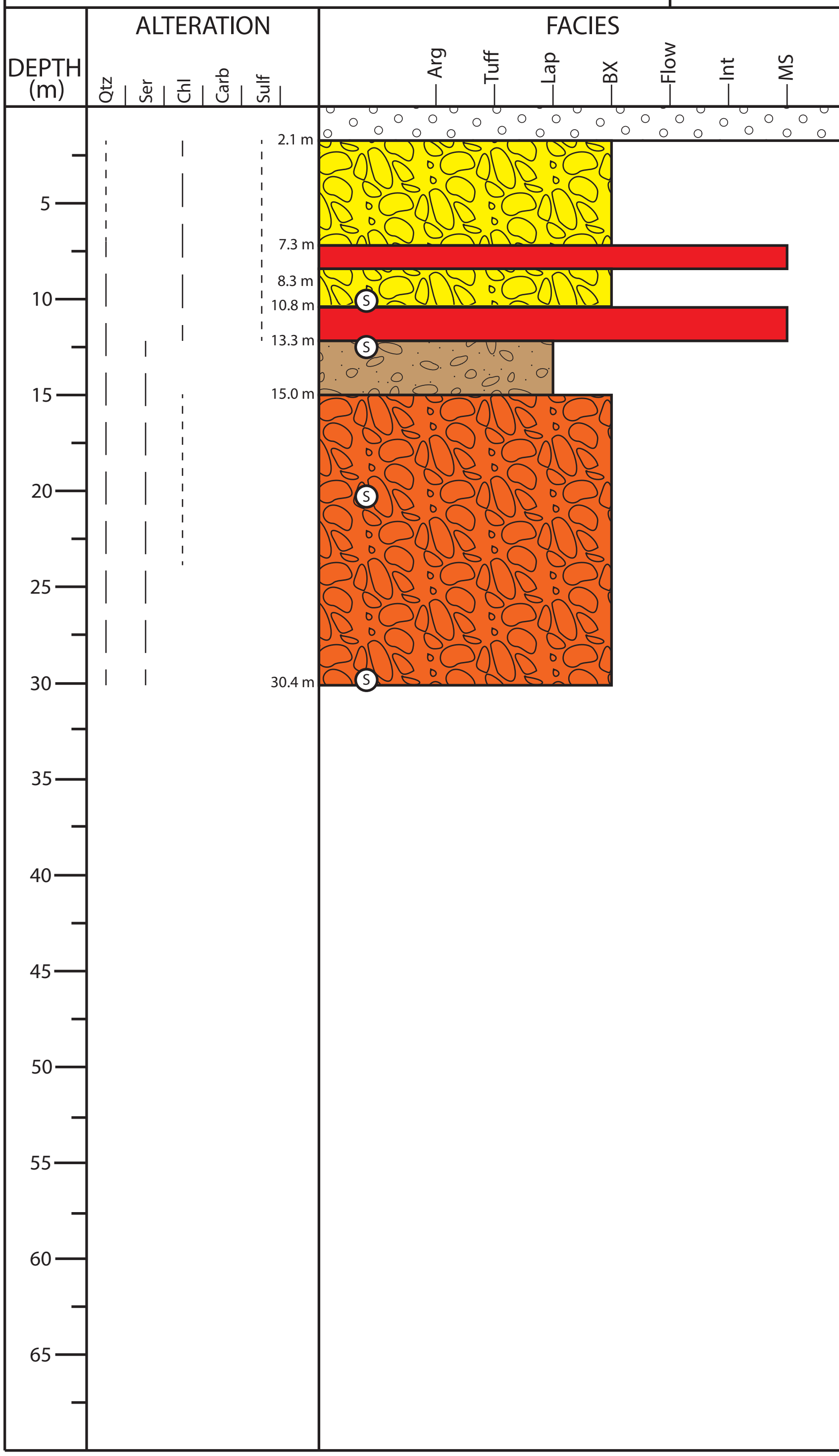

DESCRIPTION

Bx frags are dark gray and matrix is black chlorite. Appears to be LS mixed in? May be a thin thrust faulting as seen in North zone (would explain HW and sulfides. High amount of carbonate spots. Massive sulfide are dominantly Py-Sph with small blebs of Ccp. Sulfides are massive, bedded, and contain LS clasts. Some clasts look like dropstones that have fallen into bedded sulfides.

Sample: H501363

Sample: H501275

LS clasts are light grey-white/yellow. Clasts are characteristic bimodal sizes with very little matrix. May be link between the sericite alteration and zinc rich ores?

Sample: H501276

Most of the BX is white/yellow with large fragments (<5cm). In some of the more brecciated areas the matrix is visible and contains minor chl alteration and small tuff sized fragments. Lower in the hole, unit becomes more milky white and contains flow banded fragments.

Sample: H501277

Project: Boundary
Diamond Drill Hole: BD10-010
Date: 6-13-14

UTM
540895.47E
5389280.14N

Azimuth: 360
Dip: -90
Length: 30 m

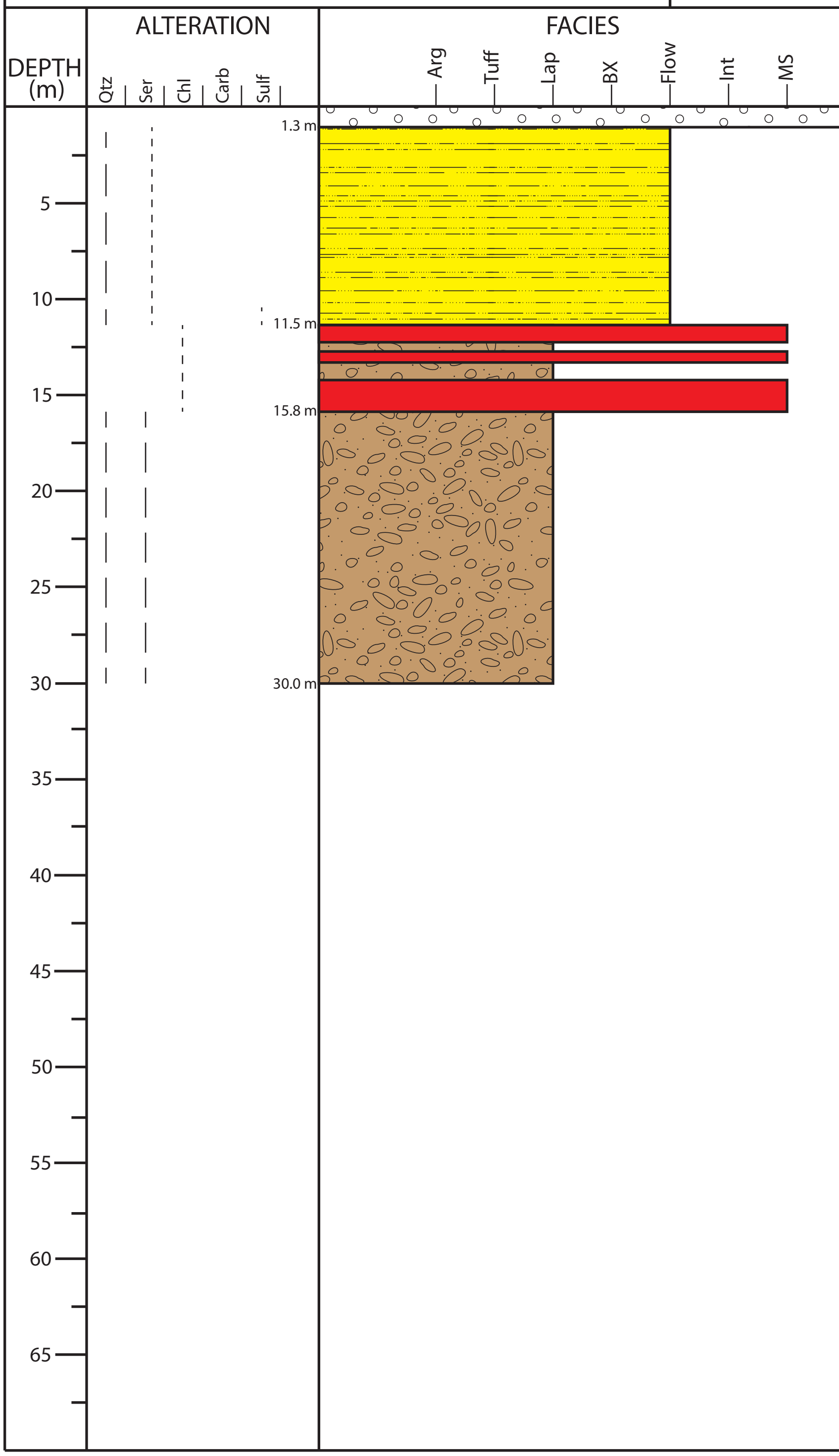

DESCRIPTION

The HW flow is flow banded and is white-gray in color. Contains carbonate spots.

From 11.5-15.8 m, interval consists of a series of bedded MS (Py-Sph) and LT. The bedded sulfides show soft sediment deformation as lapilli clasts appear as dropstones in some bed layers. Some Ccp veins crosscut the bedded layers.

LT unit has a sharp contact with overlying MS bed. LT ranges from white-gray-green and clasts are bimodal in size (~1 and 3 cm). Sericite alteration is present in both clasts and matrix. Clasts increase in size deeper in hole (near 4cm) and are either white or green (ser).

Project: Boundary Diamond Drill Hole: BD10-011 Date: 8-20-2013	UTM 540904.87E 5389269.62N	Azimuth: 360 Dip: -90 Length: 30 m

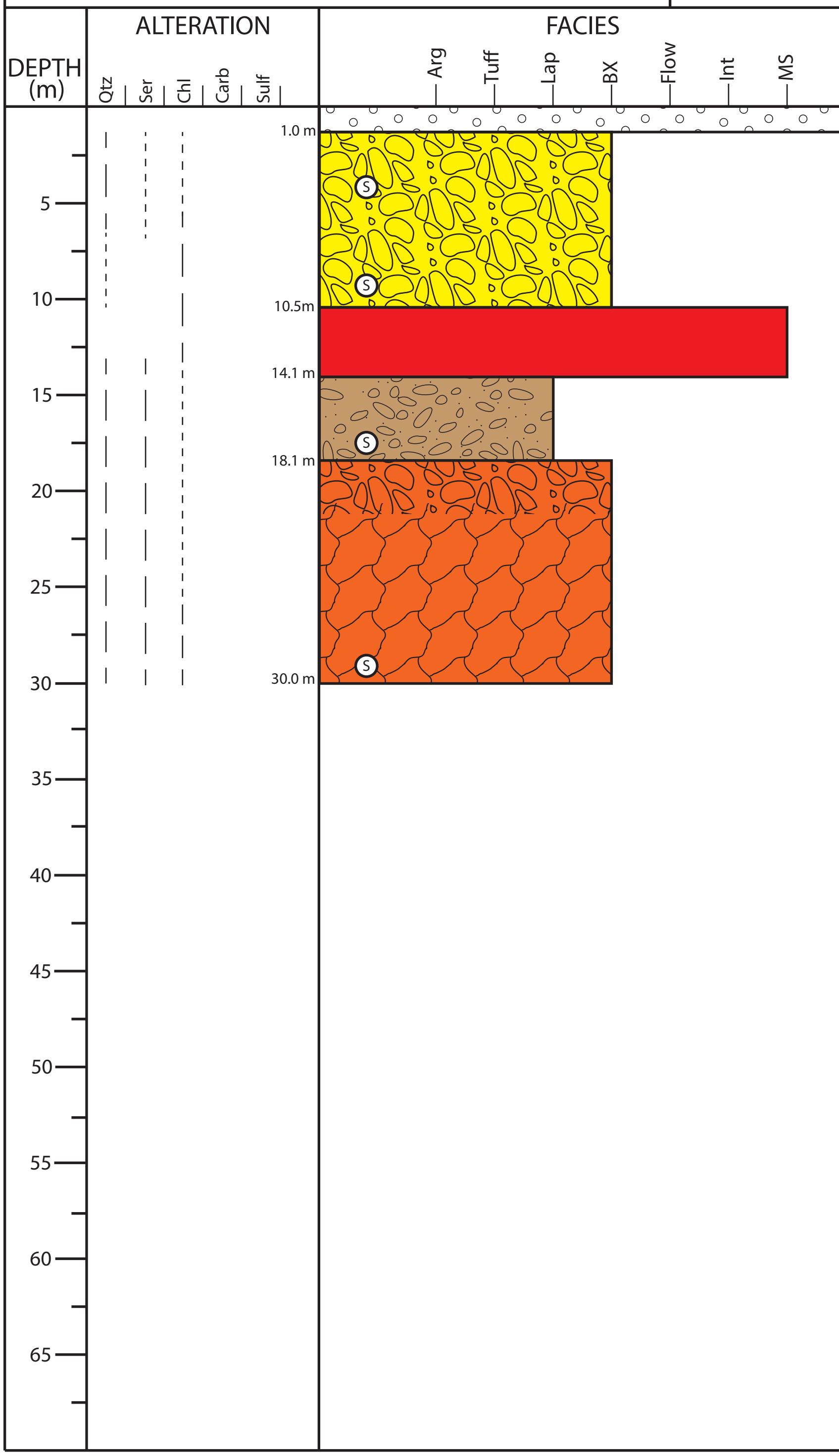

DESCRIPTION

Sample: H501278
Gray breccia, nearly massive flow in some sections but appears to be hyaloclastite or flow margins for the most part. Fracture are often filled with dark chlorite or sericite. Lower in hole becomes more altered and only large fragments remain. Those appear more qtz-ser altered with matrix chl altered.
Sample: H501279

Most of the core is missing, but whats left appears to be bedded sulfides (Teck logs indicate Py). Little to no Ccp or Sph visible.

Large (>3cm), white-gray rimmed clasts in what appears to be semi chlorite altered ash tuff? Matrix supported and most clasts are bleached white>>Qtz-ser alteration.

Sample: H501280
Upper portion of this unit appears to be hyaloclastite then grades into jigsaw fit bx. Qtz-ser alteration remains strong. Higher in hole rock is white like above LS but becomes gray deeper in hole. Chl alteration intensifies near bottom within fracture of jigsaw pieces.

Sample: H501281

Project: Boundary Diamond Drill Hole: BD10-017 Date: 6-13-14	UTM 540839.28E 5389301.61N	Azimuth: 360 Dip: -90 Length: 47 m

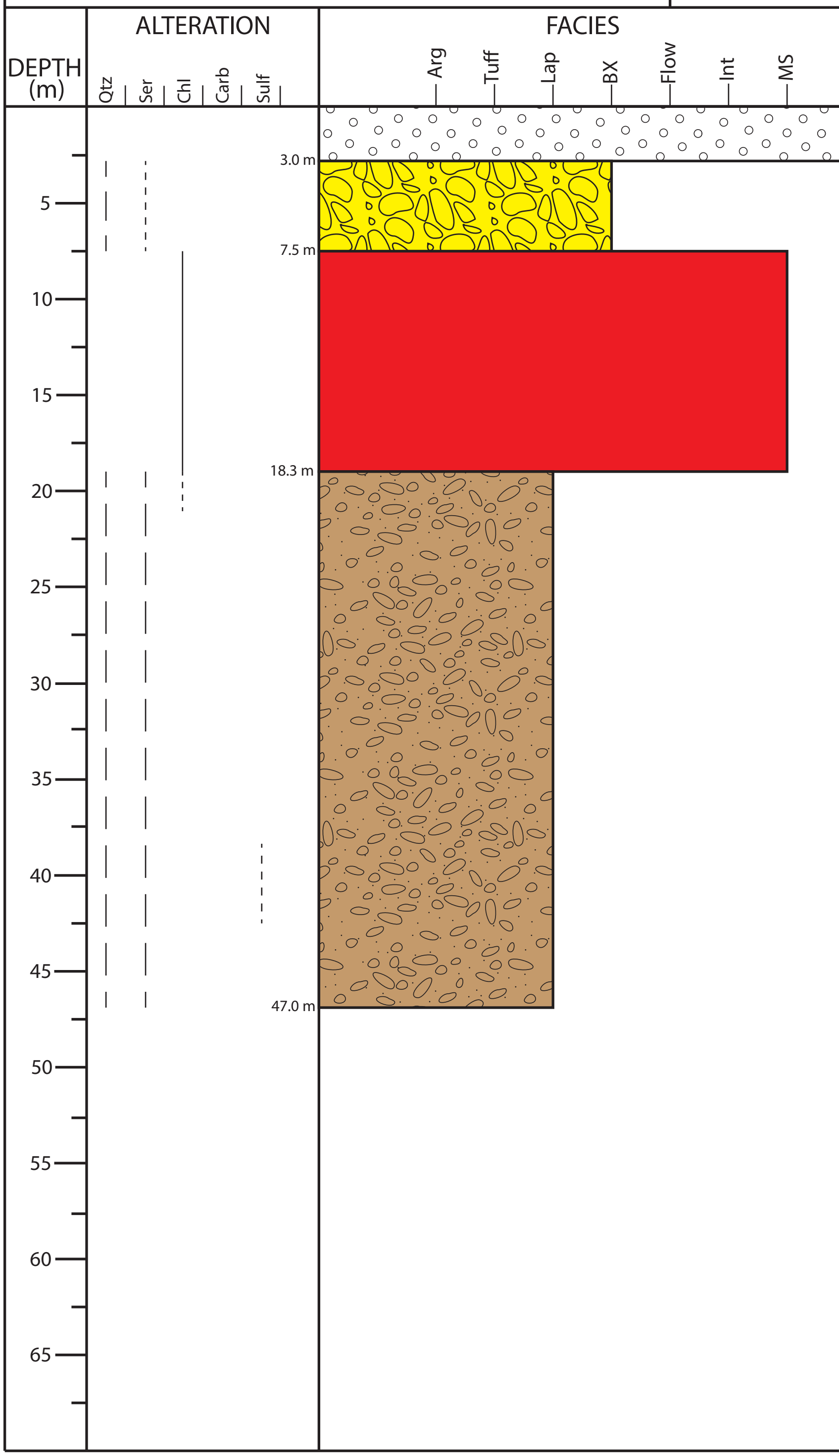

DESCRIPTION

BX is light gray-green (ser). No sulfides in matrix. Matrix is dark gray-green (ser). Chl alteration slightly increases near contact.

Massive Py-Ccp-Sph. Top of MS is Py-Ccp and grades into Py-Sph-Ccp after ~14m. Ccp occurs as wisps and blebs. Sph occurs as ~1cm blobs. MS is moderately fractured and contains chalcocite coatings.

Top ~10 m of LT is a mix of large (3-5 cm) and small (<0.5 cm). Clasts are matrix supported and are gray-green. Matrix is soft and dark (ser) and does not contain sulfides.

From 30 m and down, clasts become smaller (1-3 cm). Clasts become yellowish in color but matrix is still dark gray. Some clasts are flow banded.

Small zone of dis. Ccp-Py and lesser Sph. Ser alteration slightly increases on either side.

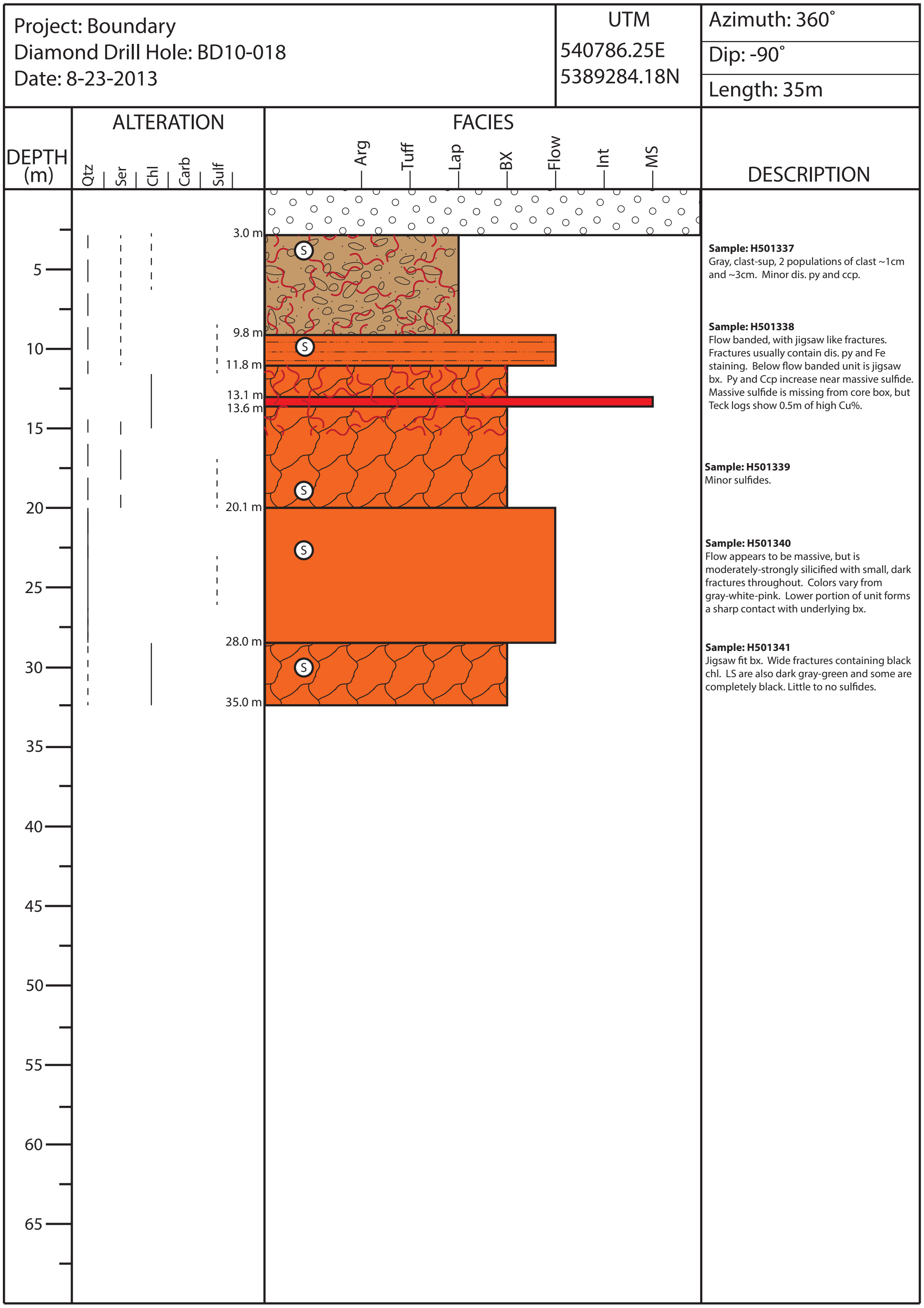
Project: Boundary
Diamond Drill Hole: BD10-018
Date: 8-23-2013
UTM
540786.25E
5389284.18N
Azimuth: 360˚
Dip: -90˚
Length: 35m
DEPTH (m)
ALTERATION
Qtz
Ser
Chl
Carb
Sulf
FACIES
Arg
Tuff
Lap
BX
Flow
Int
MS
DESCRIPTION
3.0 m
9.8 m
11.8 m
13.1 m
13.6 m
20.1 m
28.0 m
35.0 m
5
10
15
20
25
30
35
40
45
50
55
60
65
S
Sample: H501337
Gray, clast-sup, 2 populations of clast ~1cm and ~3cm. Minor dis. py and ccp.
Sample: H501338
Flow banded, with jigsaw like fractures. Fractures usually contain dis. py and Fe staining. Below flow banded unit is jigsaw bx. Py and Ccp increase near massive sulfide. Massive sulfide is missing from core box, but Teck logs show 0.5m of high Cu%.
Sample: H501339
Minor sulfides.
Sample: H501340
Flow appears to be massive, but is moderately-strongly silicified with small, dark fractures throughout. Colors vary from gray-white-pink. Lower portion of unit forms a sharp contact with underlying bx.
Sample: H501341
Jigsaw fit bx. Wide fractures containing black chl. LS are also dark gray-green and some are completely black. Little to no sulfides.

Project: Boundary Diamond Drill Hole: BD10-21 Date: 8-20-2013	UTM 540864.68E 5389316.36N	Azimuth: 360 Dip: -90 Length: 35 m

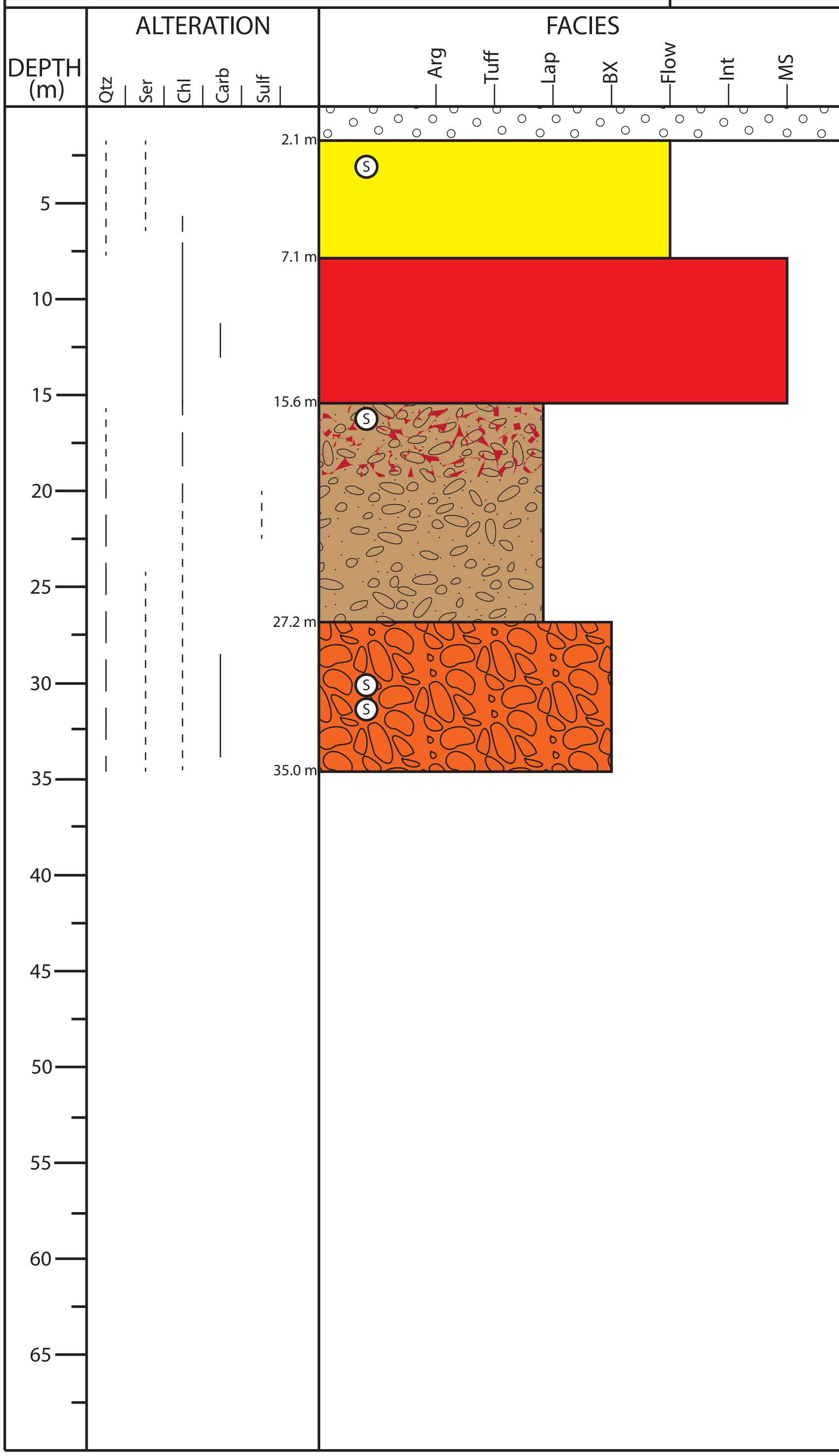

DESCRIPTION

Sample: H501282
Massive, grey qtz-phyric flow. Very little alteration in terms of black chl/ser anywhere. Not many fractures or breaks either.

Massive sulfide appears to be mostly Py with minor Ccp and purple splotches of Sph, especially near the bottom of the sulfide lense. Below the lens, sulfides replace matrix around clasts.

Sample: H501283
LS contains large clasts (often around 4 cm) and is matrix supported. Matrix is often chl or Py replaced. Clasts are generally less altered and don't show rims.

Lower portion of the unit becomes more clast supported and shows typical bimodal clast sizes (1cm and 3 cm).

Sample: H501284
Sample: H501285
Relatively sharp contact with overlying LS. BX is pale grey/blue/green with brown Fe-carbonate staining. Matrix around margins of hyaloclastite appears to be chl/ser.

Project: Boundary
Diamond Drill Hole: BD10-022
Date: 8-20-2013

UTM
540878.39E
5389302.36N

Azimuth: 360
Dip: -90
Length: 30

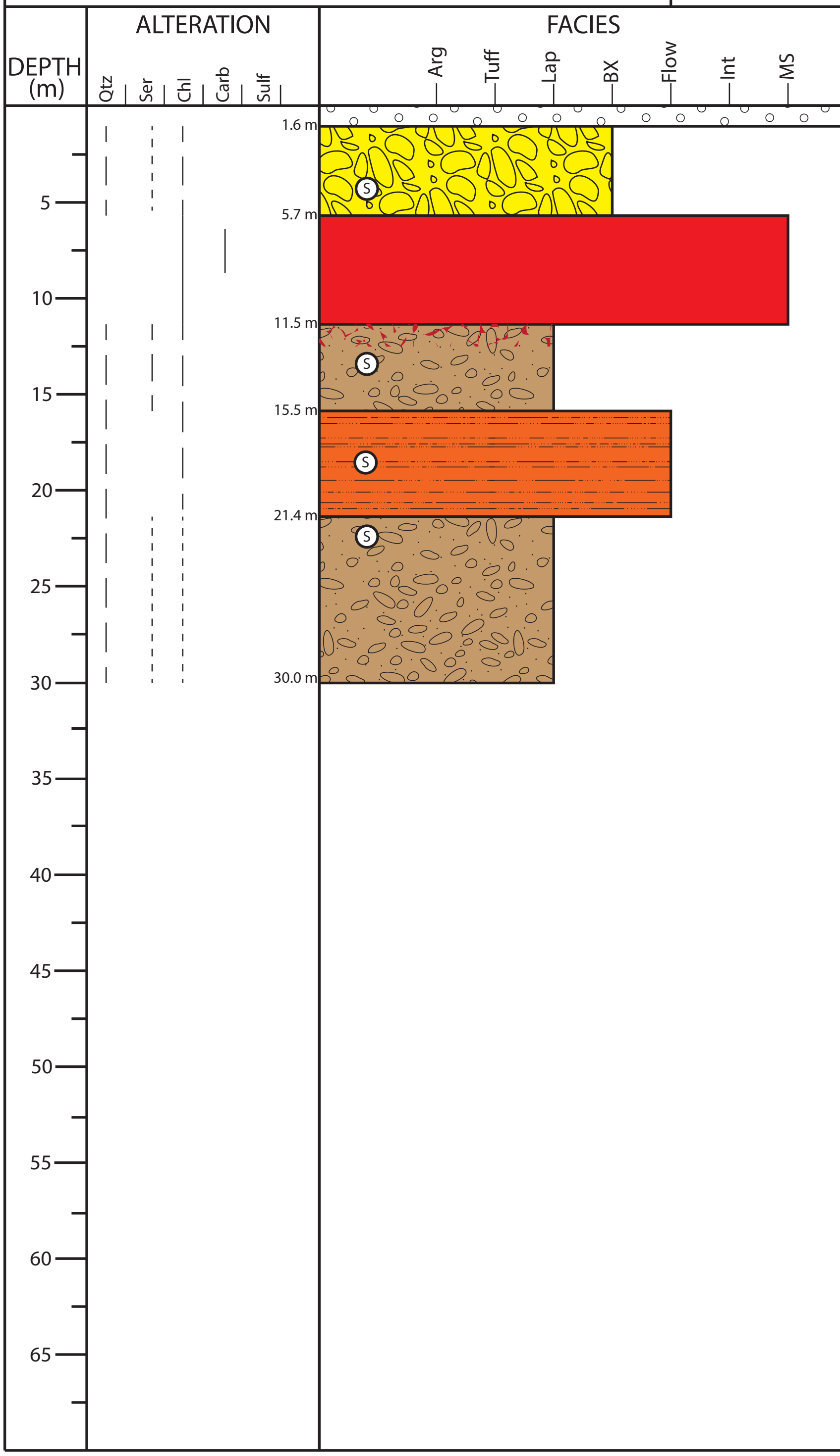

DESCRIPTION

Sample: H501270
Appears to be qtz-phyric hyaloclastite. Fragments are grey to white in color, some frags are flow banded. Matrix is black (chl) but no sulfides until <0.25m from MS.

Top of MS section is Py-Ccp-Sph right then grades down to massive Sph. Sulfides occur in discrete lenses within LT. Multiple locations of core loss, but can still make out some zones. Replacement sulfides occur in the LT between lenses and below.

Sample: H501271
Clasts (2-5cm) are mostly matrix supported. Matrix has been replaced by chlorite while clasts themselves are mostly white rimmed with gray cores.

Sample: H501272
Sharp contact. Unit is flow banded. Bands alternate between white silicified bands and chl/ser? altered bands. No sulfides. Lower contact is also sharp.

Sample: H501273
Lapilli tuff look like the typical bimodal (1 and 3cm) clasts. Clast supported. Most clasts are varying shades of gray a few are white but show no rims like upper LT section. Some fragments are flow banded. Bottom of hole looks chewed up: may be fault or just end of hole fragmentation.

Project: Boundary Diamond Drill Hole: BD10-026 Date: 8-20-2013	UTM 540824.22E 5389284.90N	Azimuth: 360 Dip: -90 Length: 41 m

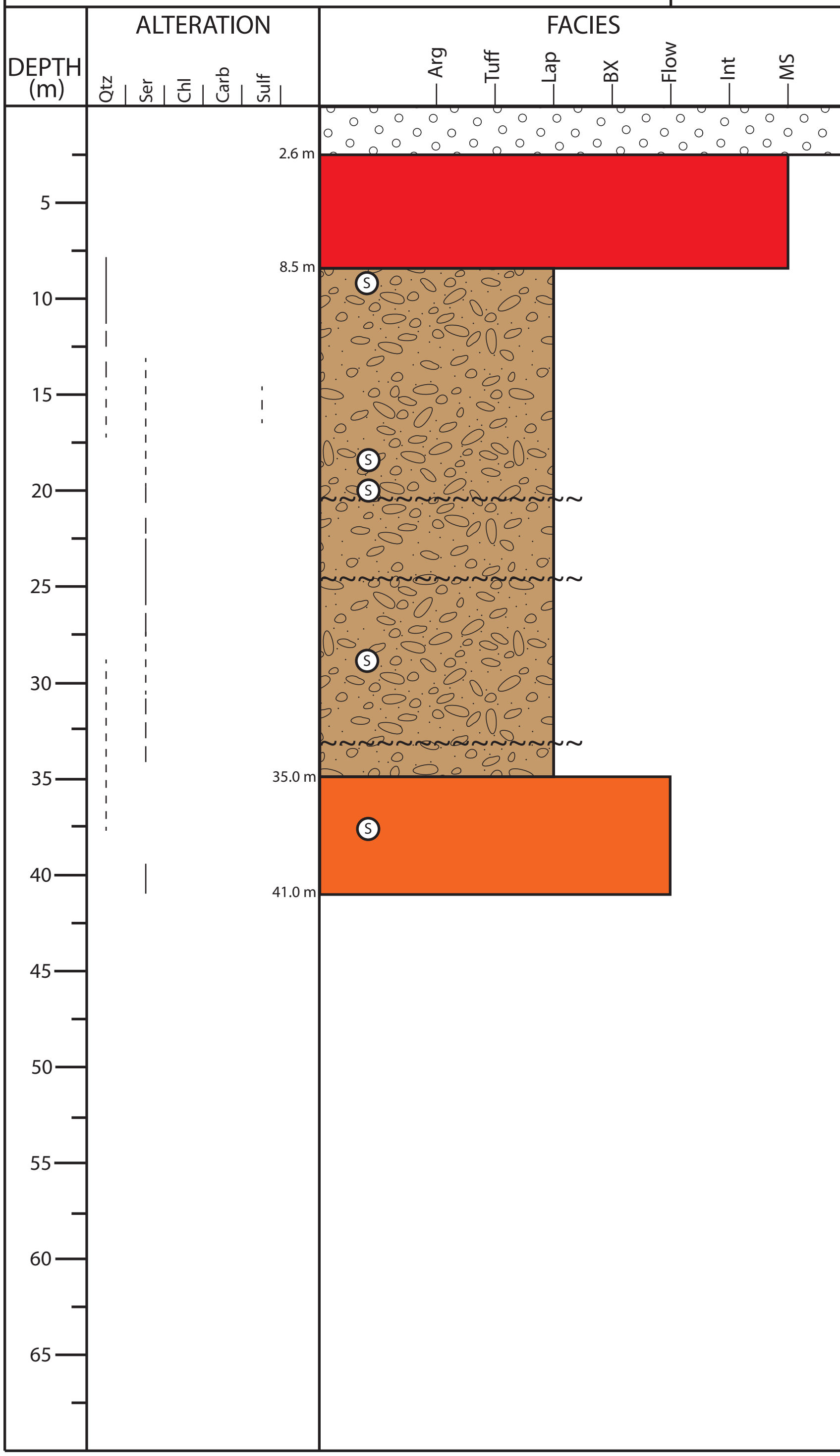

DESCRIPTION

Massive Ccp-Sph near top of MS then small 0.25-0.50 zones of replacement sulfides (ccp and py). Bottom of MS also Ccp and Sph rich.

Sample: H501286
Very pale (bleached white), difficult to make out clast boundaries. Could be tuff possibly?

LT unit greatly varies in alteration. Top of unit is white (silicified) and ~12m become easier to see clasts. Becomes matirix supported until ~20 m. Matrix consists of black either ser or chl? (geochem points towards chl). Some clasts are grey with bleached rims. Most clasts around 1 cm, fairly angular.

Sample: H501287
Sample: H501288
H501287 fits the LT description above. H501288 represents about a 4 meter wide zone of intense green/yellow sericite alteration that represents the Wagner Fault. Smaller, discrete int ser zones occur below as well.

Lower within the LT unit, clasts become darker in color (perhaps less silicified or altered in general?). Unit also becomes clast supported and bimodal clast size (~1 and 3 cm becomes apparent).
Sample: H501289

Lowest portion shows clast size increase-near breccia in size

Sample: H501290
Massive flow. Dark grey in color contains some Fe staining (Py?) otherwise litte to no sulfides visible. Small zone of int ser near bottom of hole.

Project: Boundary Diamond Drill Hole: BD10-028 Date: 8-16-2013	UTM 540558.80E 5389497.86N	Azimuth: 360 Dip: -90 Length: 35

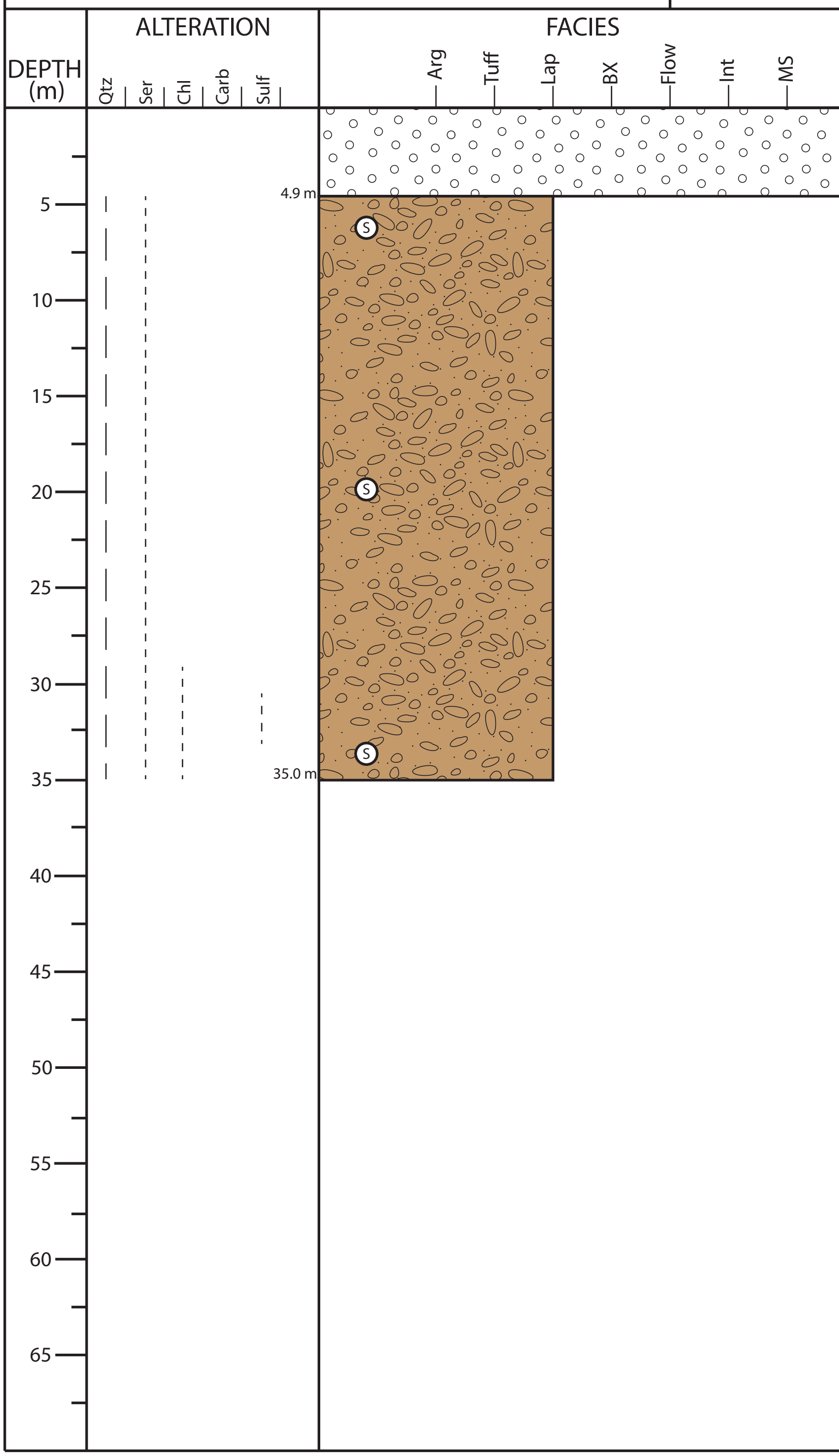

DESCRIPTION

Sample: H501247
Typical LT footwall all the way through with minor graded tuff beds (<10cm). LT clasts are bimodal in size (1cm and 3cm) and varying shades of gray. Near top of hole, LT is very much clast supported but become matrix supported further down in hole. Over the last five meters of the hole, the matrix contains black chl/ser, dis. Py, and minor Fe carbonate veins. Clasts over this stretch also have white rims with grey cores.

Sample: H501248

Sample: H501249

Project: Boundary Diamond Drill Hole: BD10-033 Date: 8-16-2013	UTM 540582.65E 5389514.34N	Azimuth: 360 Dip:-90 Length: 47 m

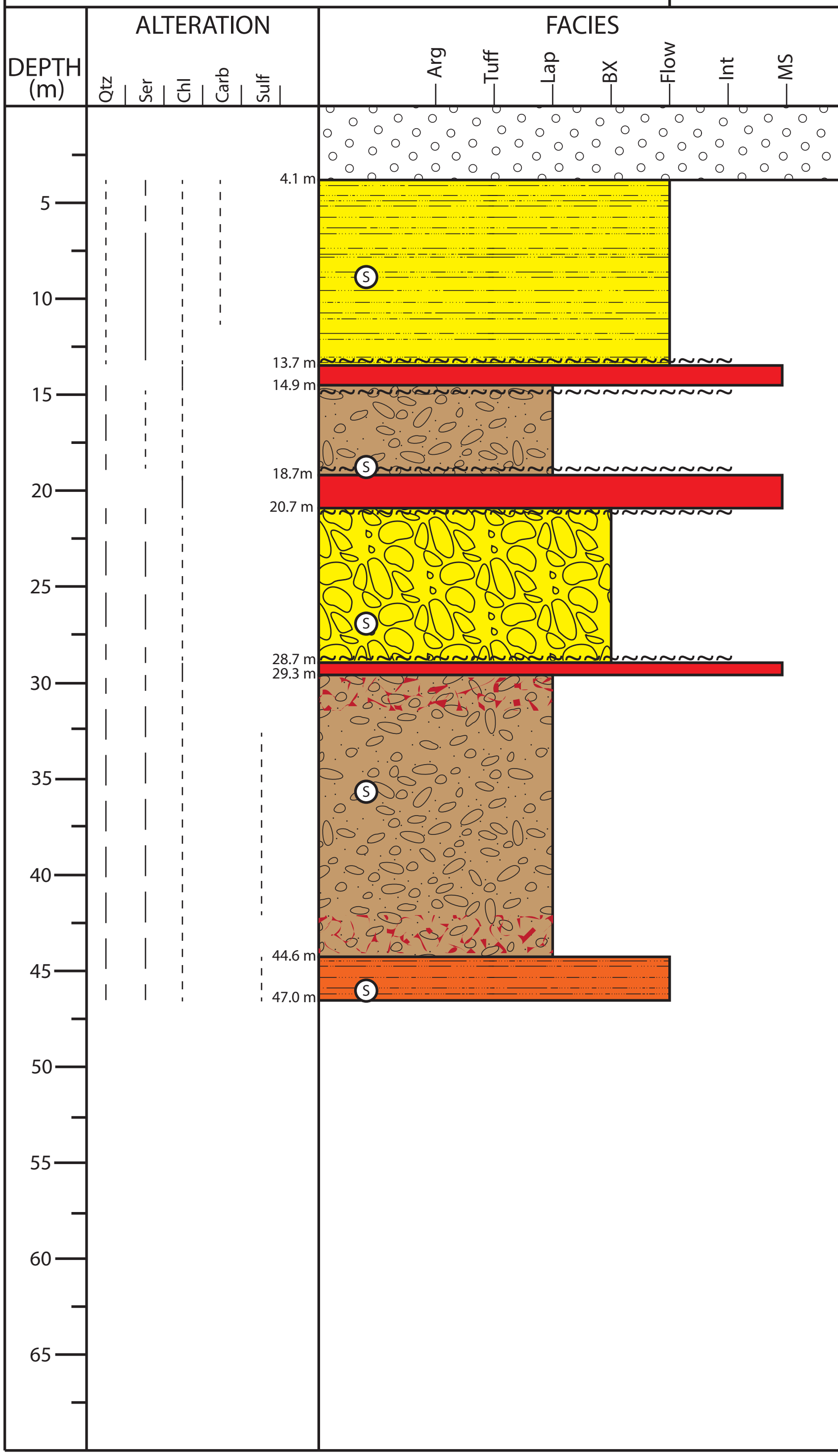

DESCRIPTION

HW flow is completely altered black. First logged as chl alt but geochem and petrology show sample is sericite altered. Flow bands barely visible unless outlined by brown carbonate weathering. High volume of qtz-phenos. Lower contact is a fault.

Sample: H501238

MS from 13.7-14.9 m is massive Sph-Py (minor lesser Ccp).

LT unit consists of dark gray clasts all 1cm and smaller. Very little matrix visible (black ser). Unit has high volume of beige carbonate spots.

Sample: H501239

MS is dominantly massive Sph-Py (minor Ccp). Thin layer of tuff (~10 cm) at 19.8 m.

BX is dark gray (same color as overylying tuff) and has a black (ser) matrix. Does contain qtz-phenos. Minor lighter gray tuff component visible in matrix. Contacts are both faulted.

Sample: H501240

Massive Sph-Ccp-Py. Unit contains minor LT similar to those in the MS above.

LT unit is dark gray-brown (weathering) and dominantly clast supported (~2 and <0.5 cm). Poorly sorted and angular clasts. Not nearly as many carbonate spots as higher in hole.

Sample: H501241

LT clasts gradualy increase in size but are still poorly sorted. See a wide range of angular clasts (1-4 cm) and very little to no tuff. Some larger clasts are flow banded. Sulfides are dominantly Py-Ccp.

Lower aphyric flow banded flow is dark gray-black. Fracture contain large amounts of Py.

Sample: H501242

Project: Boundary Diamond Drill Hole: BD10-034 Date:8-16-2013	UTM 540599.11E 5389500.27N	Azimuth: 360 Dip: -90 Length: 35 m

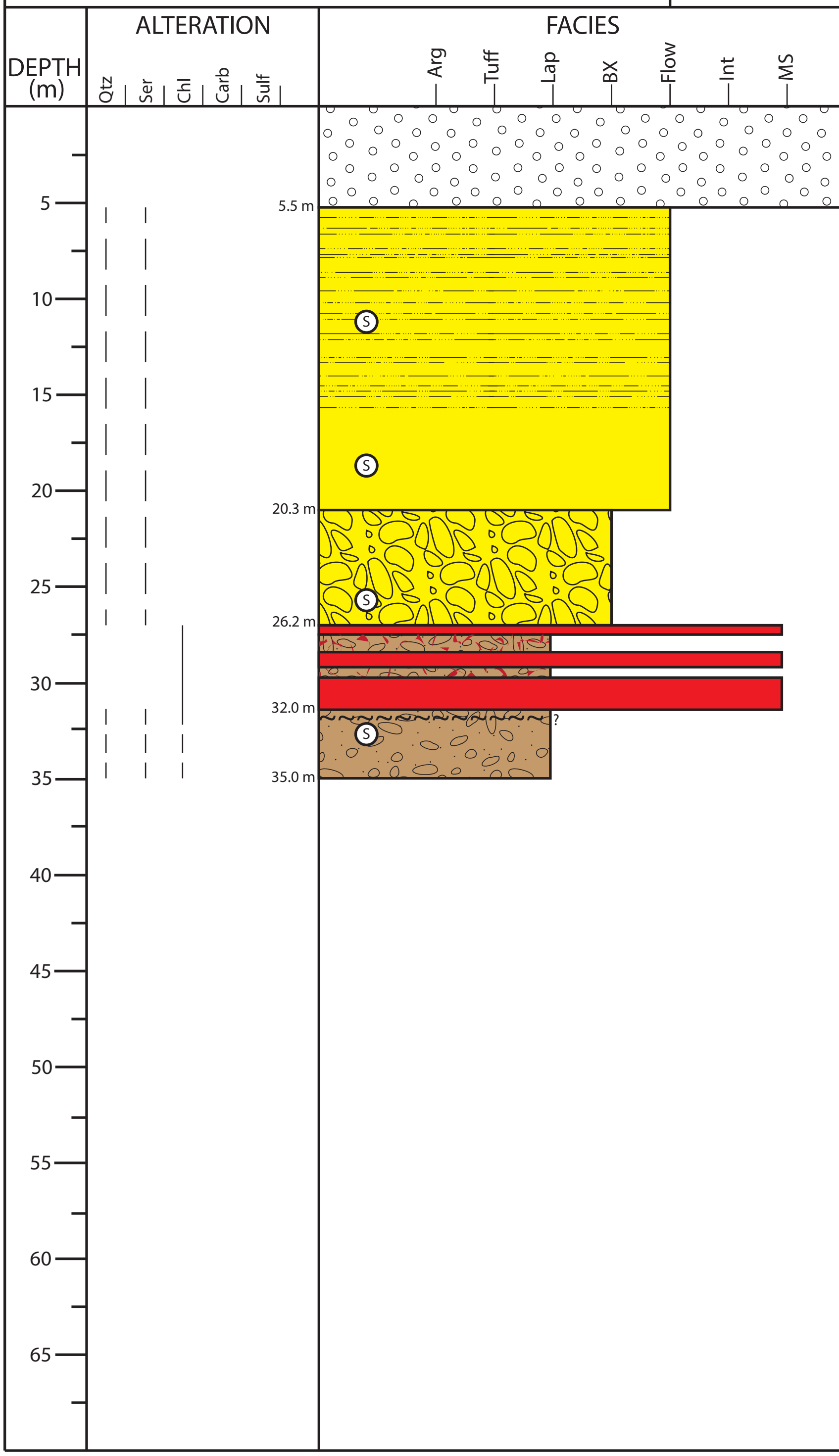

DESCRIPTION

Upper HW flow is qtz-phyric, dark gray-black, and both flow banded and massive. Minor fractures occur throughout and appear to be filled with dolomite. Qtz-ser alteration is consistent throughout. Very minor dis. Py found within fractures. Moderate carbonate spotting.

Sample: H501234

Sample: H501237

The BX is very similar to the overlying flow. It is qtz-phyric, gray-black, and contains moderate carbonate spots. The lower contact with the MS may be structual (fractured core, sharp contact).

Sample: H501235

The interval from 26.2-32.0 m consists of a series of thin massive sulfide (Py-Ccp), black chlorite, and LT with sulfides within matrix. Upper MS contains the most Sph and grades into Ccp-Py in lower lenses. Lenses are not separated by faults.

Sample: H501236

From 32-35.0 m, LT appears to be separated from overlying MS by a fault. The contact is sharp in terms of both alteration and mineralization. Additionally, there appears to be angular, flow banded fragments near the contact. The LT is matrix supported and contains large (>3 cm), gray clasts. Matrix consists of black sericite and no sulfides.

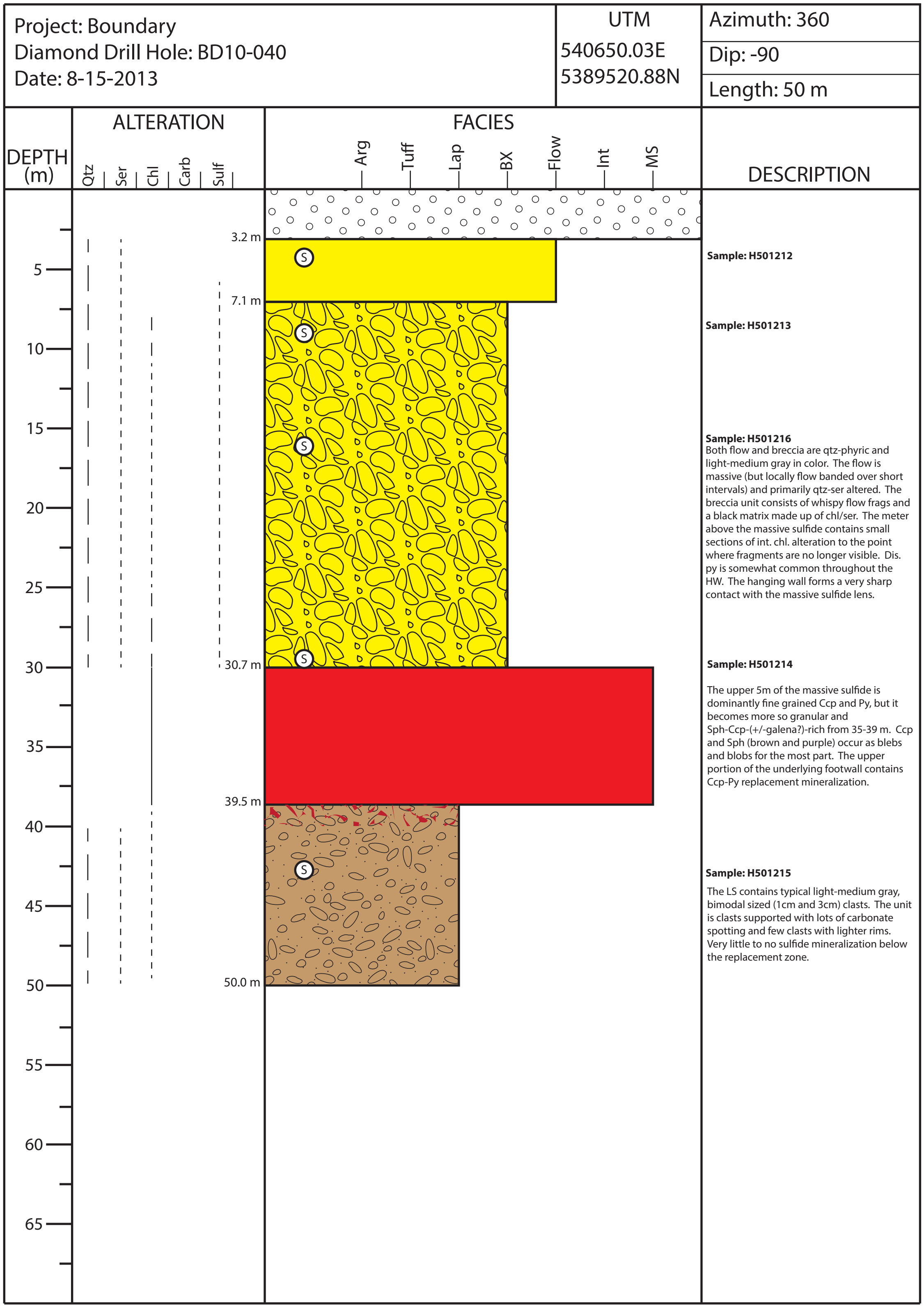

Project: Boundary
Diamond Drill Hole: BD10-040
Date: 8-15-2013
UTM
540650.03E
5389520.88N
Azimuth: 360
Dip: -90
Length: 50 m
DEPTH (m)
ALTERATION
Qtz
Ser
Chl
Carb
Sulf
FACIES
Arg
Tuff
Lap
BX
Flow
Int
MS
DESCRIPTION
5
10
15
20
25
30
35
40
45
50
55
60
65
3.2 m
7.1 m
30.7 m
39.5 m
50.0 m
S
Sample: H501212
Sample: H501213
Sample: H501216
Both flow and breccia are qtz-phyric and light-medium gray in color. The flow is massive (but locally flow banded over short intervals) and primarily qtz-ser altered. The breccia unit consists of whispy flow frags and a black matrix made up of chl/ser. The meter above the massive sulfide contains small sections of int. chl. alteration to the point where fragments are no longer visible. Dis. py is somewhat common throughout the HW. The hanging wall forms a very sharp contact with the massive sulfide lens.
Sample: H501214
The upper 5m of the massive sulfide is dominantly fine grained Ccp and Py, but it becomes more so granular and Sph-Ccp-(+/-galena?)-rich from 35-39 m. Ccp and Sph (brown and purple) occur as blebs and blobs for the most part. The upper portion of the underlying footwall contains Ccp-Py replacement mineralization.
Sample: H501215
The LS contains typical light-medium gray, bimodal sized (1cm and 3cm) clasts. The unit is clasts supported with lots of carbonate spotting and few clasts with lighter rims. Very little to no sulfide mineralization below the replacement zone.

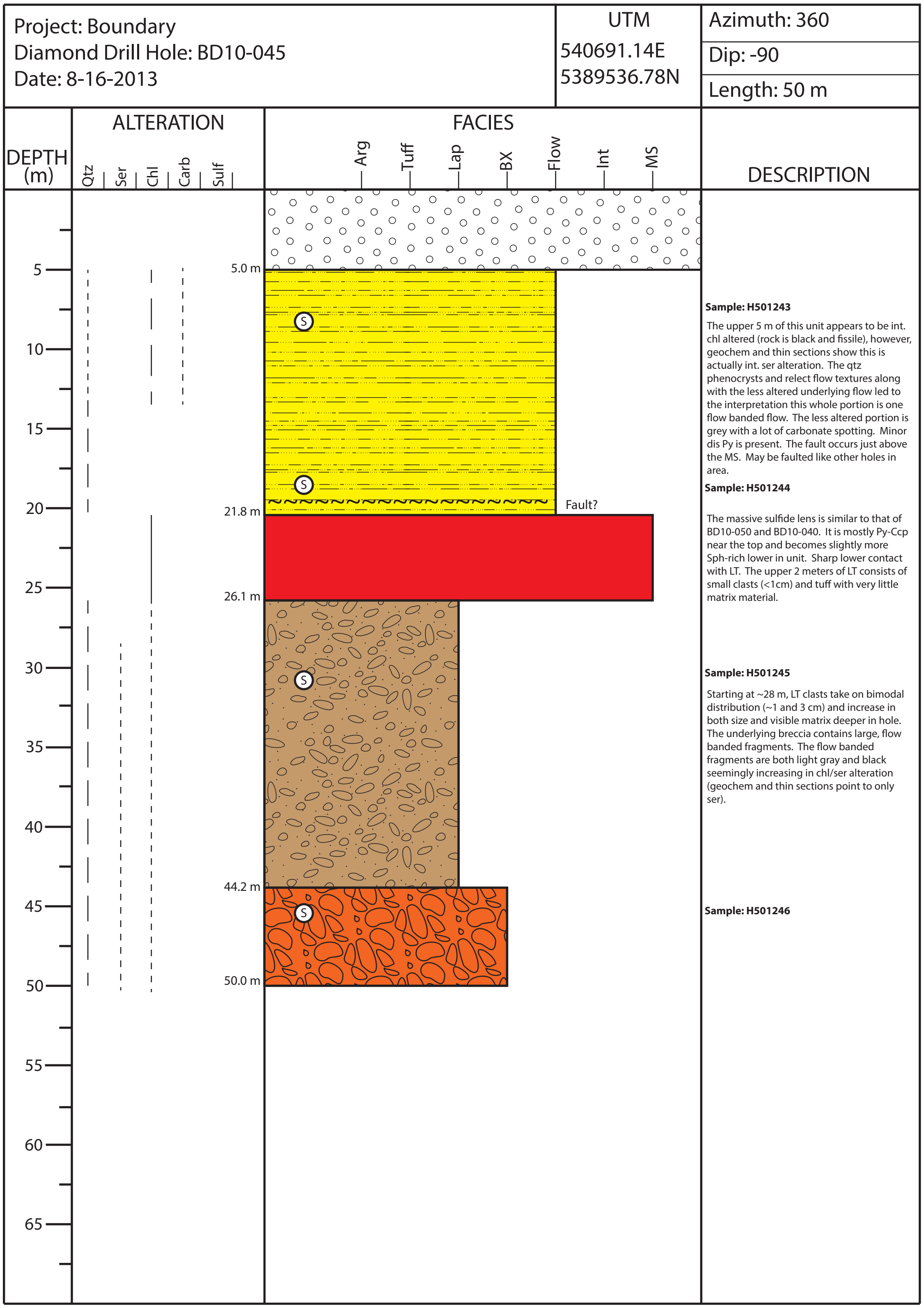
Project: Boundary
Diamond Drill Hole: BD10-045
Date: 8-16-2013
UTM
540691.14E
5389536.78N
Azimuth: 360
Dip: -90
Length: 50 m
DEPTH (m)
ALTERATION
Qtz
Ser
Chl
Carb
Sulf
FACIES
Arg
Tuff
Lap
BX
Flow
Int
MS
DESCRIPTION
5
10
15
20
25
30
35
40
45
50
55
60
65
5.0 m
21.8 m
26.1 m
44.2 m
50.0 m
Fault?
S
Sample: H501243
The upper 5 m of this unit appears to be int. chl altered (rock is black and fissile), however, geochem and thin sections show this is actually int. ser alteration. The qtz phenocrysts and relect flow textures along with the less altered underlying flow led to the interpretation this whole portion is one flow banded flow. The less altered portion is grey with a lot of carbonate spotting. Minor dis Py is present. The fault occurs just above the MS. May be faulted like other holes in area.
Sample: H501244
The massive sulfide lens is similar to that of BD10-050 and BD10-040. It is mostly Py-Ccp near the top and becomes slightly more Sph-rich lower in unit. Sharp lower contact with LT. The upper 2 meters of LT consists of small clasts (<1cm) and tuff with very little matrix material.
Sample: H501245
Starting at ~28 m, LT clasts take on bimodal distribution (~1 and 3 cm) and increase in both size and visible matrix deeper in hole. The underlying breccia contains large, flow banded fragments. The flow banded fragments are both light gray and black seemingly increasing in chl/ser alteration (geochem and thin sections point to only ser).
Sample: H501246

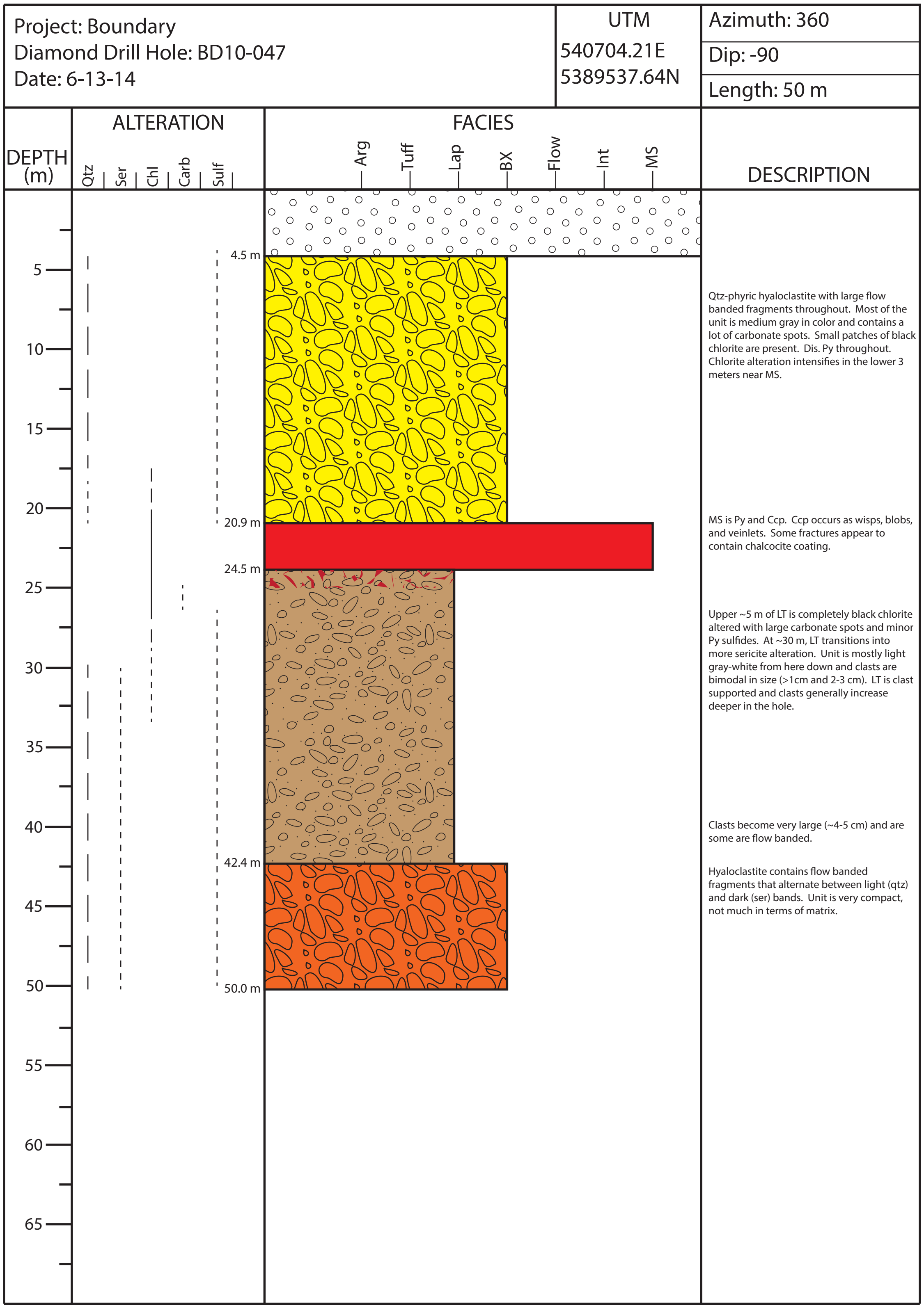
Project: Boundary
Diamond Drill Hole: BD10-047
Date: 6-13-14
UTM
540704.21E
5389537.64N
Azimuth: 360
Dip: -90
Length: 50 m
DEPTH (m)
ALTERATION
Qtz
Ser
Chl
Carb
Sulf
FACIES
Arg
Tuff
Lap
BX
Flow
Int
MS
DESCRIPTION
5
10
15
20
25
30
35
40
45
50
55
60
65
4.5 m
20.9 m
24.5 m
42.4 m
50.0 m
Qtz-phyric hyaloclastite with large flow banded fragments throughout. Most of the unit is medium gray in color and contains a lot of carbonate spots. Small patches of black chlorite are present. Dis. Py throughout. Chlorite alteration intensifies in the lower 3 meters near MS.
MS is Py and Ccp. Ccp occurs as wisps, blobs, and veinlets. Some fractures appear to contain chalcocite coating.
Upper ~5 m of LT is completely black chlorite altered with large carbonate spots and minor Py sulfides. At ~30 m, LT transitions into more sericite alteration. Unit is mostly light gray-white from here down and clasts are bimodal in size (>1cm and 2-3 cm). LT is clast supported and clasts generally increase deeper in the hole.
Clasts become very large (~4-5 cm) and are some are flow banded.
Hyaloclastite contains flow banded fragments that alternate between light (qtz) and dark (ser) bands. Unit is very compact, not much in terms of matrix.

Project: Boundary Diamond Drill Hole: BD10-049 Date: 8-16-2013	UTM 540712.41E 5389560.47N	Azimuth: 360 Dip: -90 Length: 35

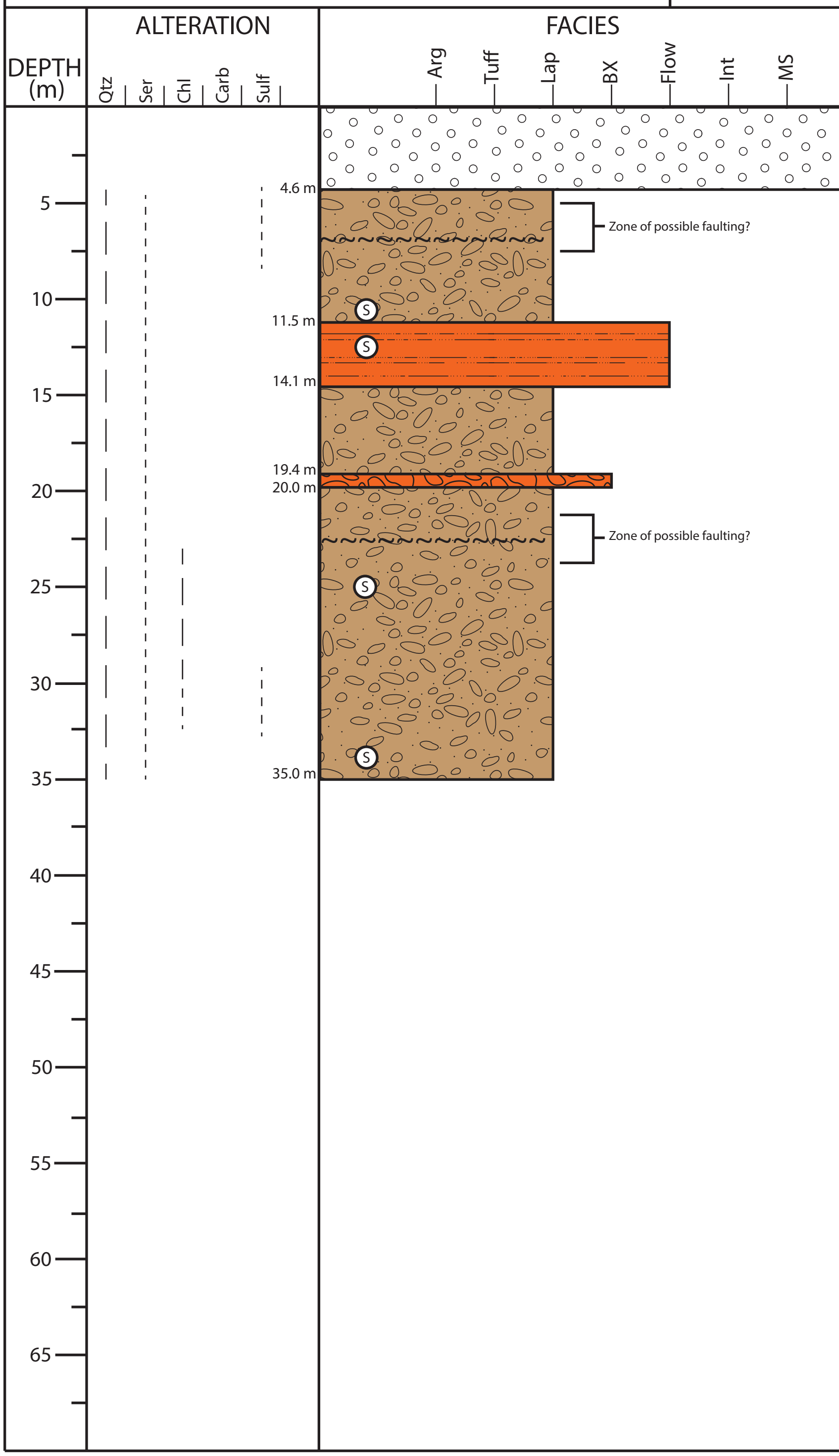

DESCRIPTION

Most of the LT clasts are light gray (mod. qtz) with somewhat large arg. fragments? Most of the LT clasts are ~1cm and very tightly packed. Core in general appears fairly fragmented (likely fault related).

Sample: H501230
Sample: H501231
Small flow banded flow with alternating light (qtz) and dark (ser) banding. Seemingly higher number of carbonate spots. Margins also appear to be hyaloclastites. Sharp contact with both overlying and underlying LT. Underlying LT appears to contain somewhat larger clasts (>2cm) but only qtz-ser altered. The breccia is very thin and may be the result of a fault. Contacts are very sharp and core is very "crumbly" at point of contact. Lower LT become matrix supported from ~22-30 m where chl-ser becomes prominent. Some clasts show light alt halos with dark cores. Lower section in hole is pretty much plain gray, clast supported LS with bimodal sized clasts (1cm and 3cm). Chl alteration dies out and clasts appear to just be qtz-ser altered.
Sample: H501232

Minor dis. Py and Ccp.

Sample: H501233

Project: Boundary Diamond Drill Hole: BD10-050 Date: 8-15-2013	UTM 540724.35E 5389549.97N	Azimuth: 360 Dip: -90 Length: 35 m

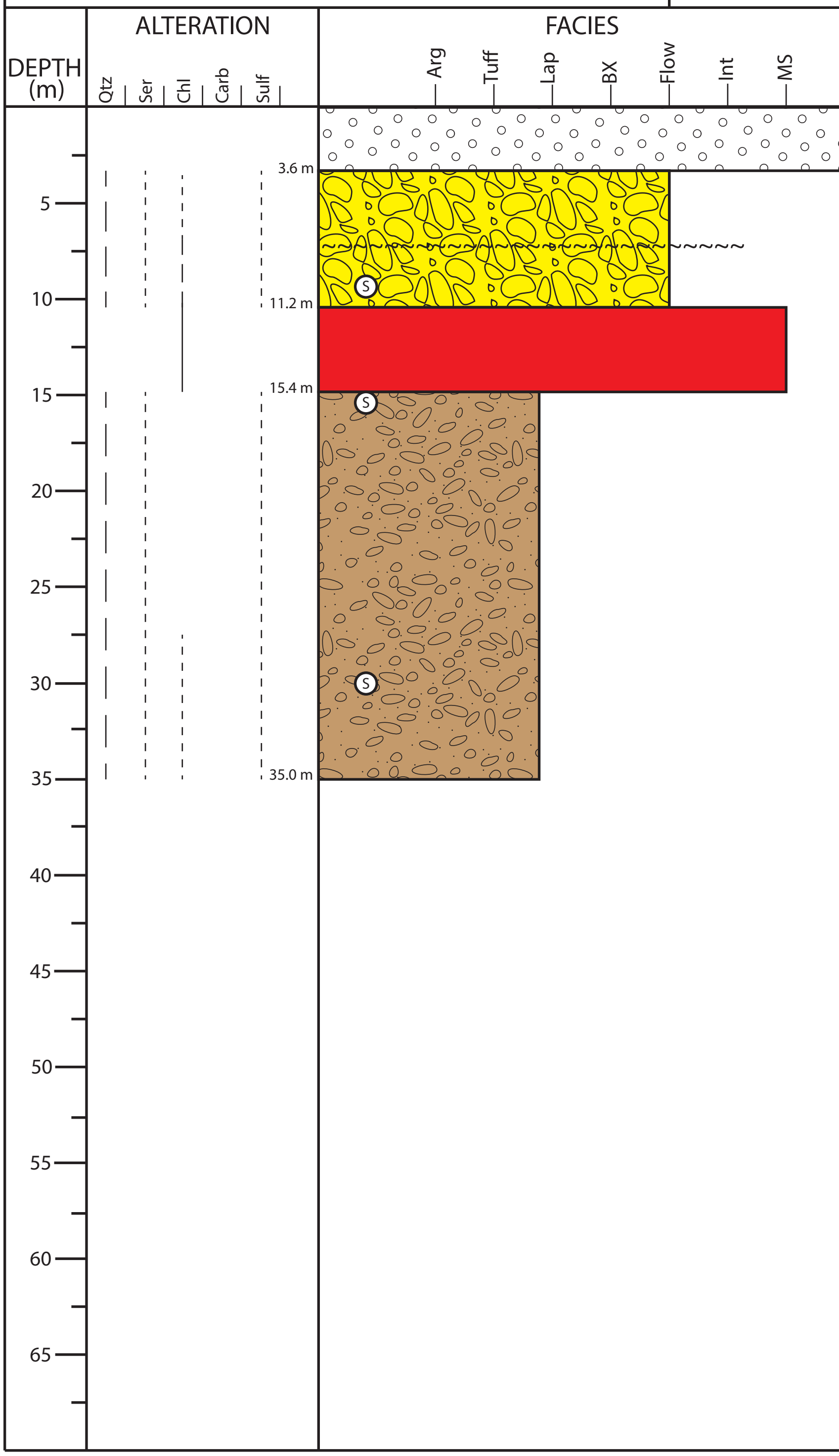

DESCRIPTION

The hanging wall has appears to have undergone faulting. The unit is generally grey to black. The matrix consists of chl/ser while the resiliant flow frags are dominantly qtz-ser. Minor dis. Py is found throughout the matrix.

Sample: H501222

Massive Py-Ccp-Sph. Ccp appears slightly more abundant within upper portions of the suflide lens. Lower contact is fairly sharp.

Sample: H501223

LT clasts are light-medium gray throughout. Clasts are generally ~1cm in diameter until 25 meters when clasts become bimodal in size. The LT also goes from clast supported to matrix (chl) supported deeper within hole.

Sample: H501224

Project: Boundary Diamond Drill Hole: BD10-051 Date: 6-13-14	UTM 540733.86E 5389535.91N	Azimuth: 360 Dip: -90 Length: 35 m

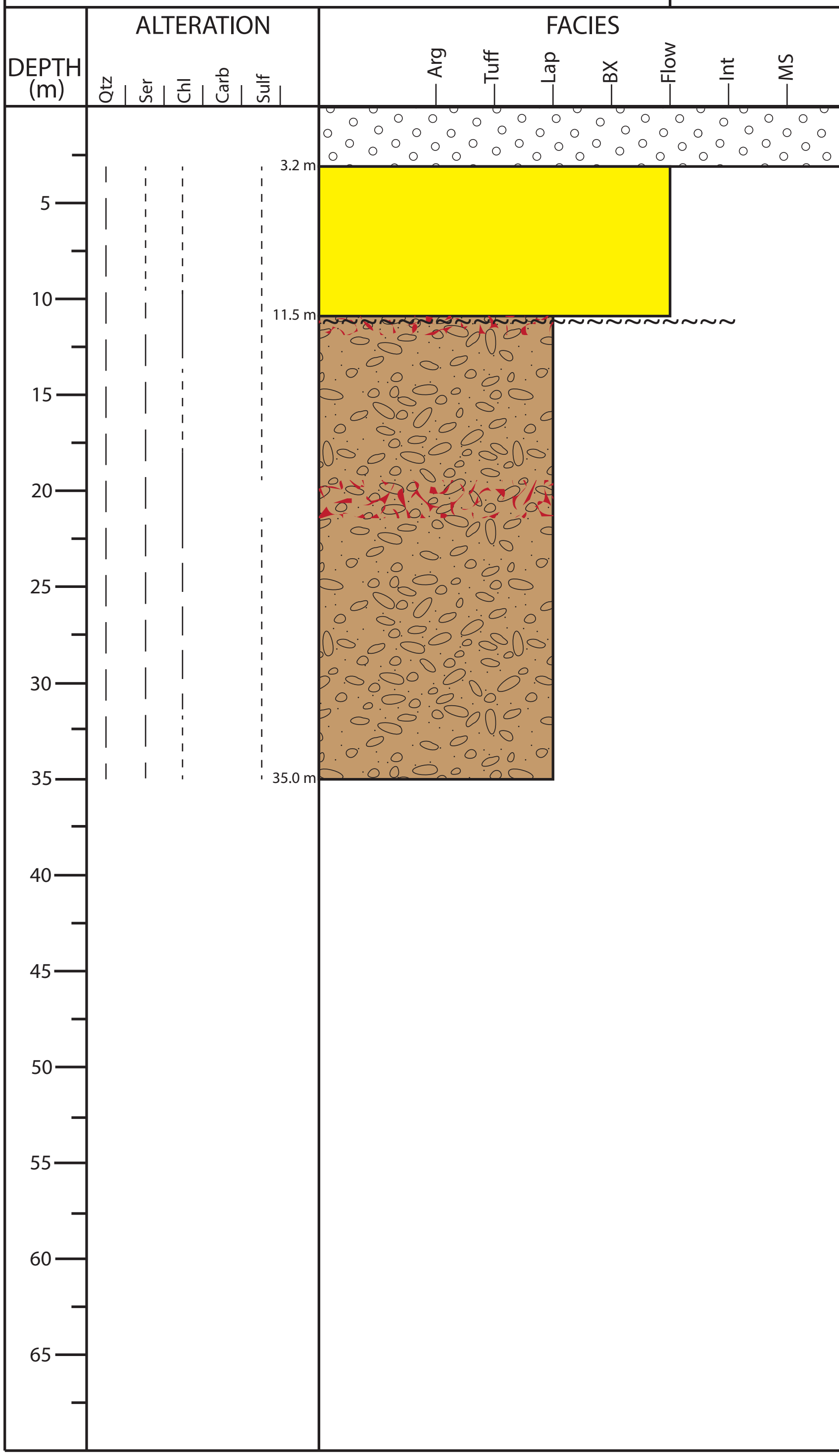

DESCRIPTION

Massive, dark gray, qtz-phyric flow. Moderate dis. Py throughout. Lower contact is faulted. At contact, core very fractured and contains some black chlorite alteration and fractured pieces of massive Py-Ccp. Unsure if this MS part of underlying LT or if transported during faulting.

Upper portion of LT may have hyaloclastite BX frags, but the core is too faulted to tell. The LT unit below fault contains small pockets of black chlorite alteration and Py mineralization. Clasts (1cm-tuff) are medium gray and clasts supported. LT becomes matrix supported ~20 m. After 21 m, clast size increases (~2-3 and <0.5 cm) and is more matrix suported near bottom of the hole. Dis. Py is found throughout. Mineralization at 20 m is Py-Ccp.

Project: Boundary Diamond Drill Hole: BD10-053 Date: 6-13-14	UTM 540743.57E 5389561.48N	Azimuth: 360 Dip: -90 Length: 35 m

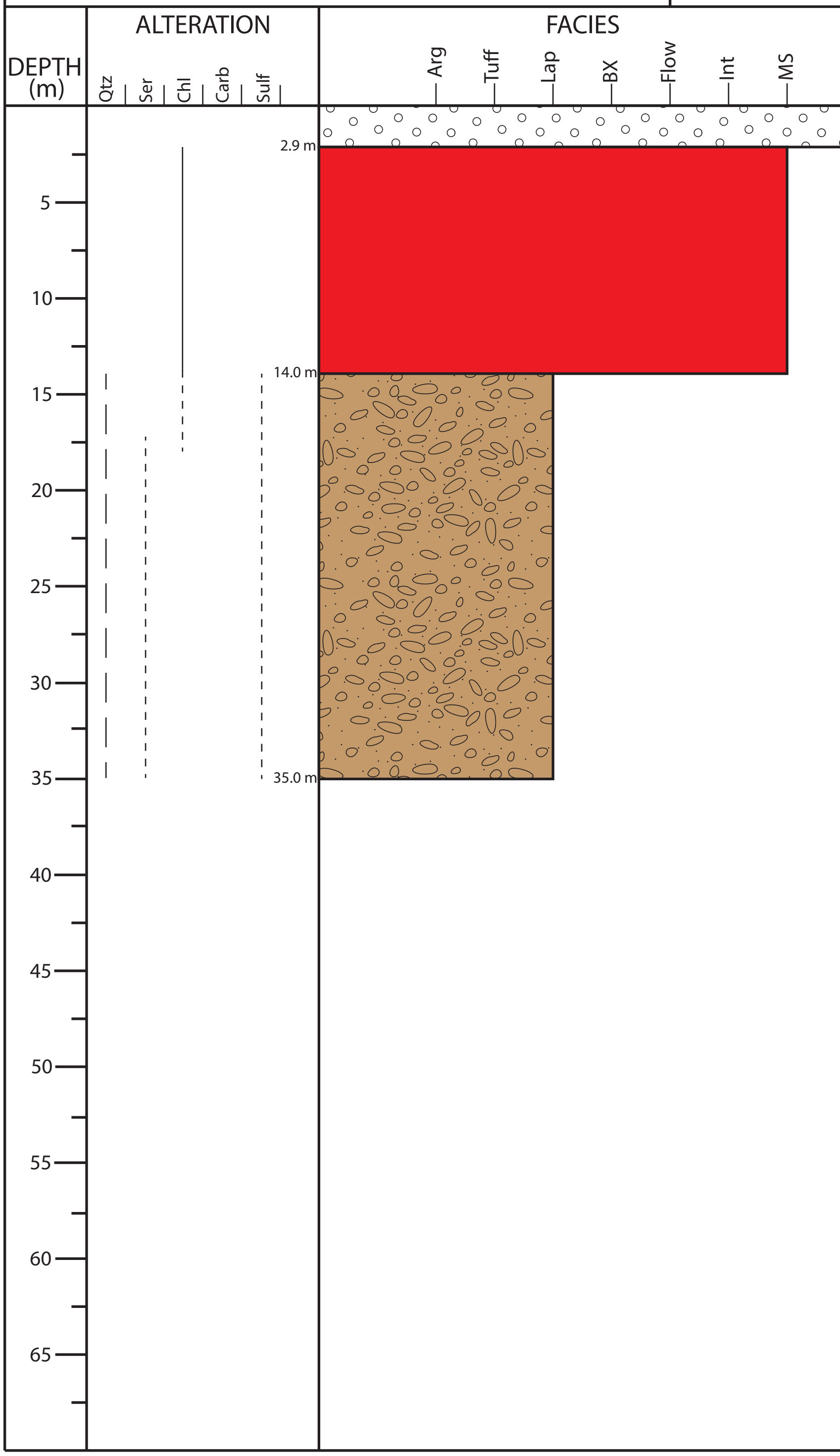

DESCRIPTION

Massive Py-Ccp-Sph. Ccp occurs as wisps and blobs. Sph ranges from brown to purple blobs throughout (may be due to oxidation). Upper five meters is Py-Ccp rich whereas the lower 6 meters Sph content increases and Ccp decreases.

Relatively sharp contact with overlying MS (<6cm of alteration). From 14-16.8 m, LT clasts are dark gray, >1cm, and rounded to subrounded. After 16.8 m, clasts become larger and bimodal (>1cm and 2-3 cm). Clast supported and visible matrix consists of black sericite. Carbonate spots and dis. Py occurs throughout the unit.

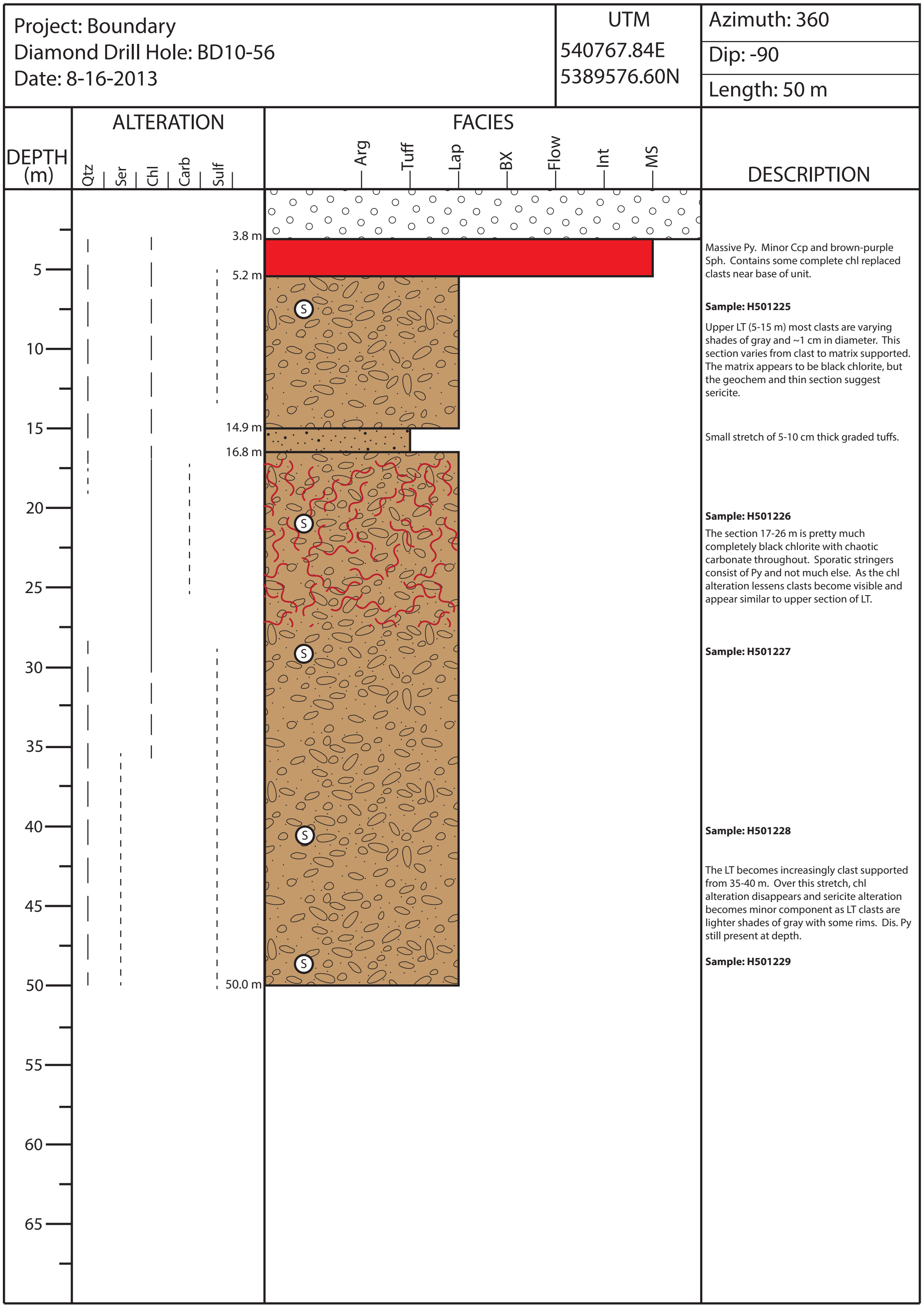
Project: Boundary
Diamond Drill Hole: BD10-56
Date: 8-16-2013
UTM
540767.84E
5389576.60N
Azimuth: 360
Dip: -90
Length: 50 m
DEPTH (m)
ALTERATION
Qtz
Ser
Chl
Carb
Sulf
FACIES
Arg
Tuff
Lap
BX
Flow
Int
MS
DESCRIPTION
5
10
15
20
25
30
35
40
45
50
55
60
65
3.8 m
5.2 m
14.9 m
16.8 m
50.0 m
S
Massive Py. Minor Ccp and brown-purple Sph. Contains some complete chl replaced clasts near base of unit.
Sample: H501225
Upper LT (5-15 m) most clasts are varying shades of gray and ~1 cm in diameter. This section varies from clast to matrix supported. The matrix appears to be black chlorite, but the geochem and thin section suggest sericite.
Small stretch of 5-10 cm thick graded tuffs.
Sample: H501226
The section 17-26 m is pretty much completely black chlorite with chaotic carbonate throughout. Sporatic stringers consist of Py and not much else. As the chl alteration lessens clasts become visible and appear similar to upper section of LT.
Sample: H501227
Sample: H501228
The LT becomes increasingly clast supported from 35-40 m. Over this stretch, chl alteration disappears and sericite alteration becomes minor component as LT clasts are lighter shades of gray with some rims. Dis. Py still present at depth.
Sample: H501229

Project: Boundary Diamond Drill Hole: BD10-058 Date: 8-15-2013	UTM 540801.31E 5389592.07N	Azimuth: 360 Dip: -90 Length: 60 m

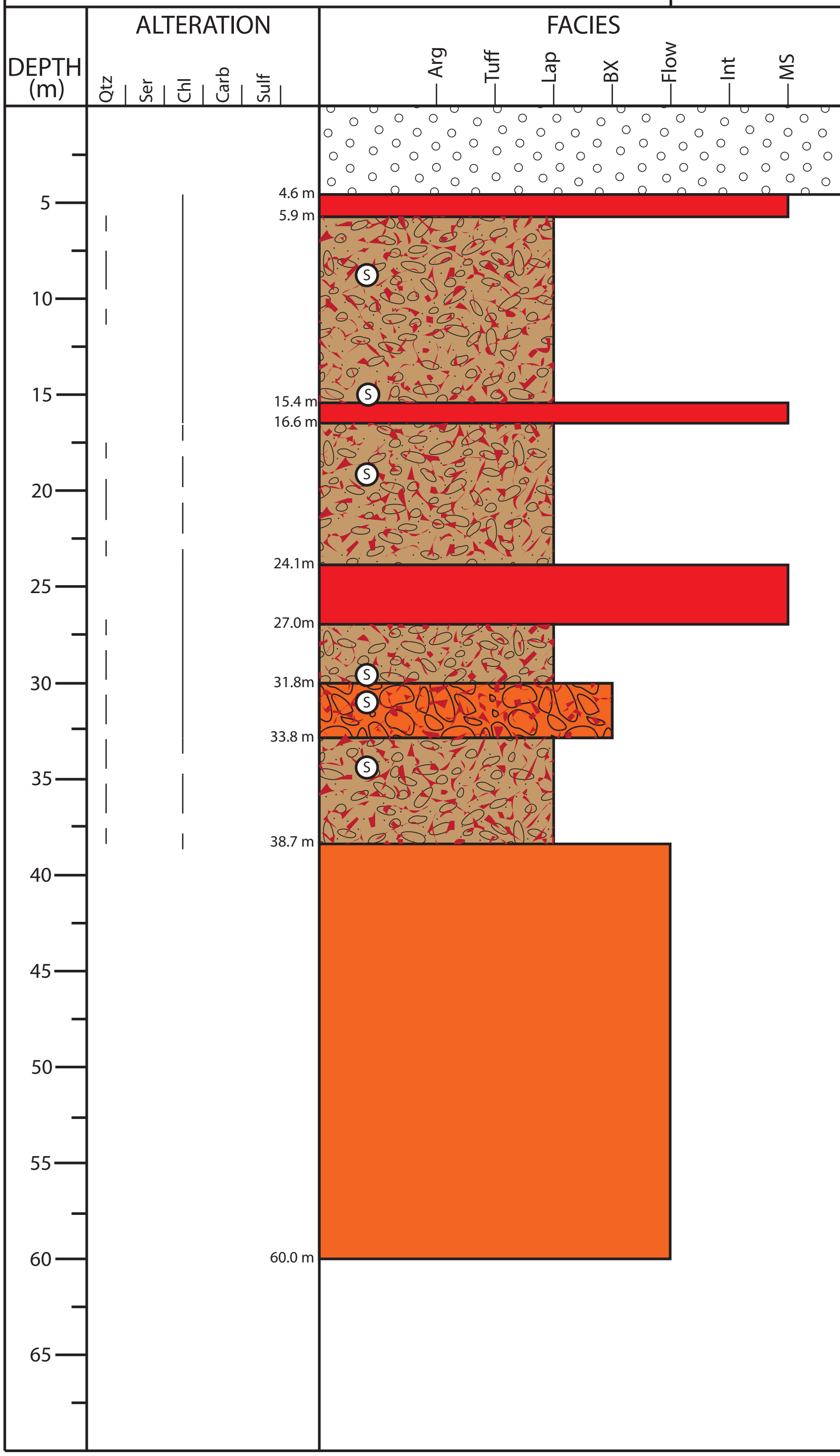

DESCRIPTION

Massive sulfide is Ccp-Py.

Sample: H501203
Upper LT is consists of clasts <1cm very tightly packed with replace Ccp inbetween. Many clasts show white rims with black cores. Lower within the LT, clasts become completely replaced by black chlorite.

Sample: H501204
Massive sulfide is Ccp-Py. Underlying LT consists of ~2 dark grey clasts with replacement Ccp and Py within matrix. Chl alteration lessens until next massive lens.
Sample: H501205

Massive suflide is mostly Py, where as the replacement sulfides below appear to be more Ccp rich. The LT below the lens contain zoned clasts (white to black) with ample replacement sulfide. The BX consists of large gray qtz frags with Py between frags.

Sample: H501206

Sample: H501207

Sample: H501208
Lower LT is mostly clast supported with larger (2-3 cm), dark gray clasts and replacement sulfides consist dominantly of Py with little to no Ccp.

Was not able to find this section of hole. Teck logs indicate unit is weakly qtz-sericite altered and occurs as both massive and flow banded throughout.

Project: Boundary Diamond Drill Hole: BD10-061 Date: 8-14-2013	UTM 540630.90E 5389572.74N	Azimuth: 360 Dip: -90 Length: 50 m

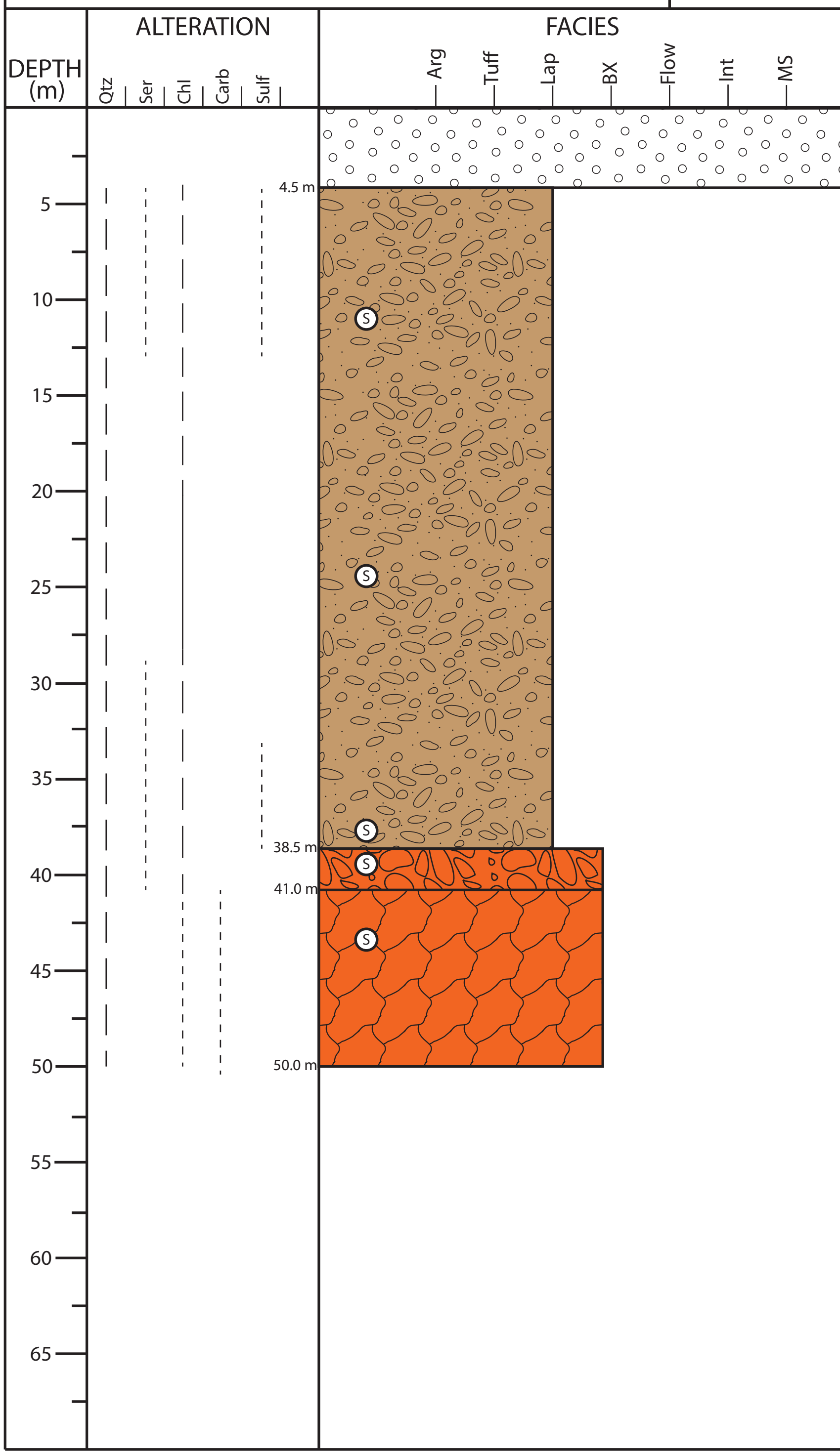

DESCRIPTION

LT is clast supported with most clasts ~1 cm. Clasts are light gray, with slightly darker cores. Disseminated Py occurs throughout within matrix.

Sample: H500698

LT is clasts are darker (dark gray-black). Matrix consists of black chlorite and ser? LT is slightly more matrix supported than upper portion.

Sample: H500699

Lower five meters of LT consist of dark gray-black clasts >1cm. The LT is clast supported (little-no matrix visible: chl altered). Dis. Py found throughout.

Sample: H500700

Sample: H501201

Sample: H501202

The BX from 38.5-41m is aphyric, dark gray, with heavily silicified fragments. Interfragment space is typically chl-ser altered and contains minor Ccp-Py. Some frags are flow banded. The lower jigsaw fit BX is lighter gray with mm-cm scale fractures commonly filled with milky carbonate (usually dolomite?).

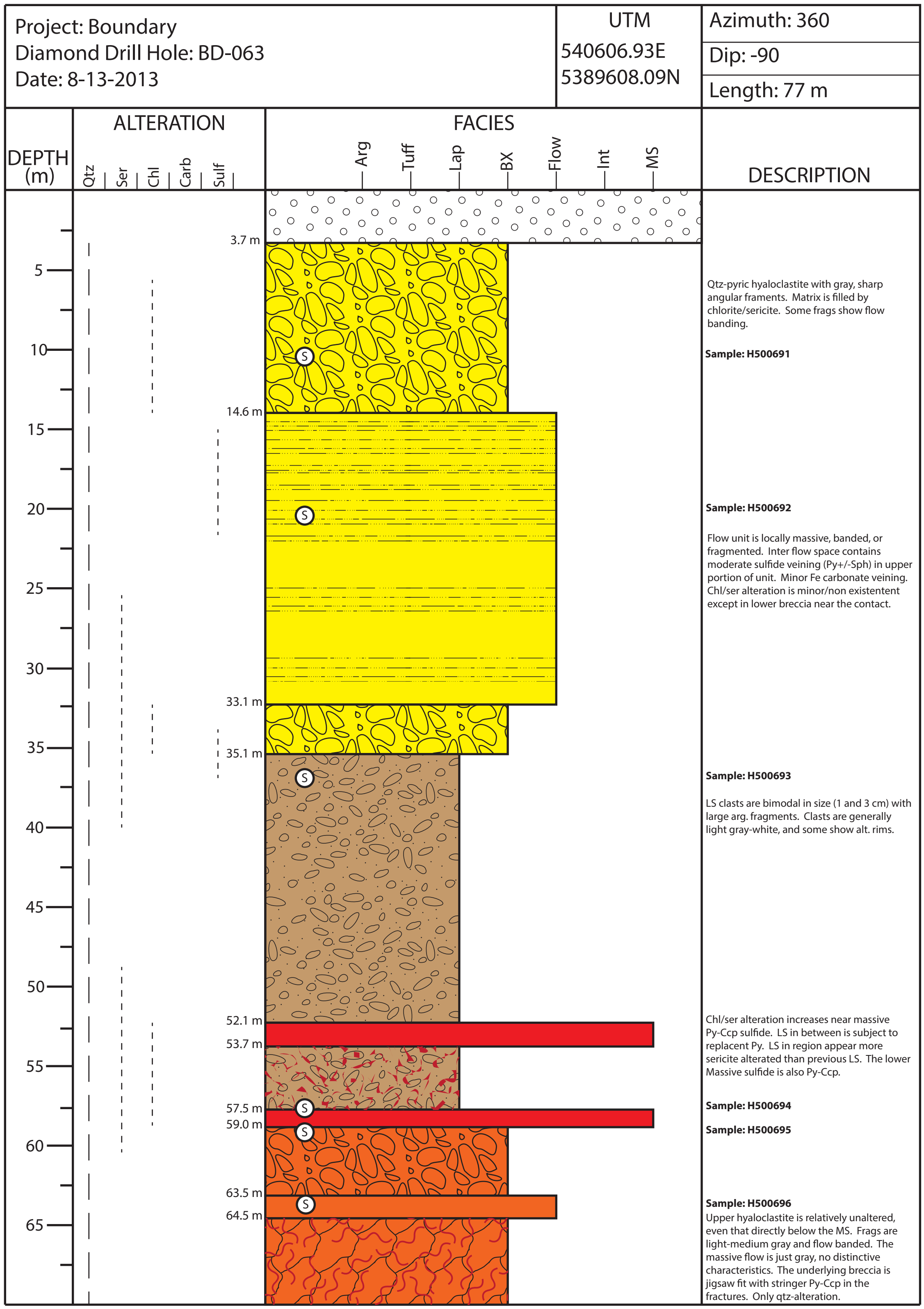

Project: Boundary
Diamond Drill Hole: BD-063
Date: 8-13-2013
UTM
540606.93E
5389608.09N
Azimuth: 360
Dip: -90
Length: 77 m
DEPTH (m)
ALTERATION
Qtz
Ser
Chl
Carb
Sulf
FACIES
Arg
Tuff
Lap
BX
Flow
Int
MS
DESCRIPTION
5
10
15
20
25
30
35
40
45
50
55
60
65
3.7 m
14.6 m
33.1 m
35.1 m
52.1 m
53.7 m
57.5 m
59.0 m
63.5 m
64.5 m
Qtz-pyric hyaloclastite with gray, sharp angular framents. Matrix is filled by chlorite/sericite. Some frags show flow banding.
Sample: H500691
Sample: H500692
Flow unit is locally massive, banded, or fragmented. Inter flow space contains moderate sulfide veining (Py+/-Sph) in upper portion of unit. Minor Fe carbonate veining. Chl/ser alteration is minor/non existentent except in lower breccia near the contact.
Sample: H500693
LS clasts are bimodal in size (1 and 3 cm) with large arg. fragments. Clasts are generally light gray-white, and some show alt. rims.
Chl/ser alteration increases near massive Py-Ccp sulfide. LS in between is subject to replacent Py. LS in region appear more sericite altered than previous LS. The lower Massive sulfide is also Py-Ccp.
Sample: H500694
Sample: H500695
Sample: H500696
Upper hyaloclastite is relatively unaltered, even that directly below the MS. Frags are light-medium gray and flow banded. The massive flow is just gray, no distinctive characteristics. The underlying breccia is jigsaw fit with stringer Py-Ccp in the fractures. Only qtz-alteration.

Project: Boundary Diamond Drill Hole: BD-063 Date: 8-13-2013	UTM 540606.93E 5389608.09N	Azimuth: 360 Dip: -90 Length: 77 m

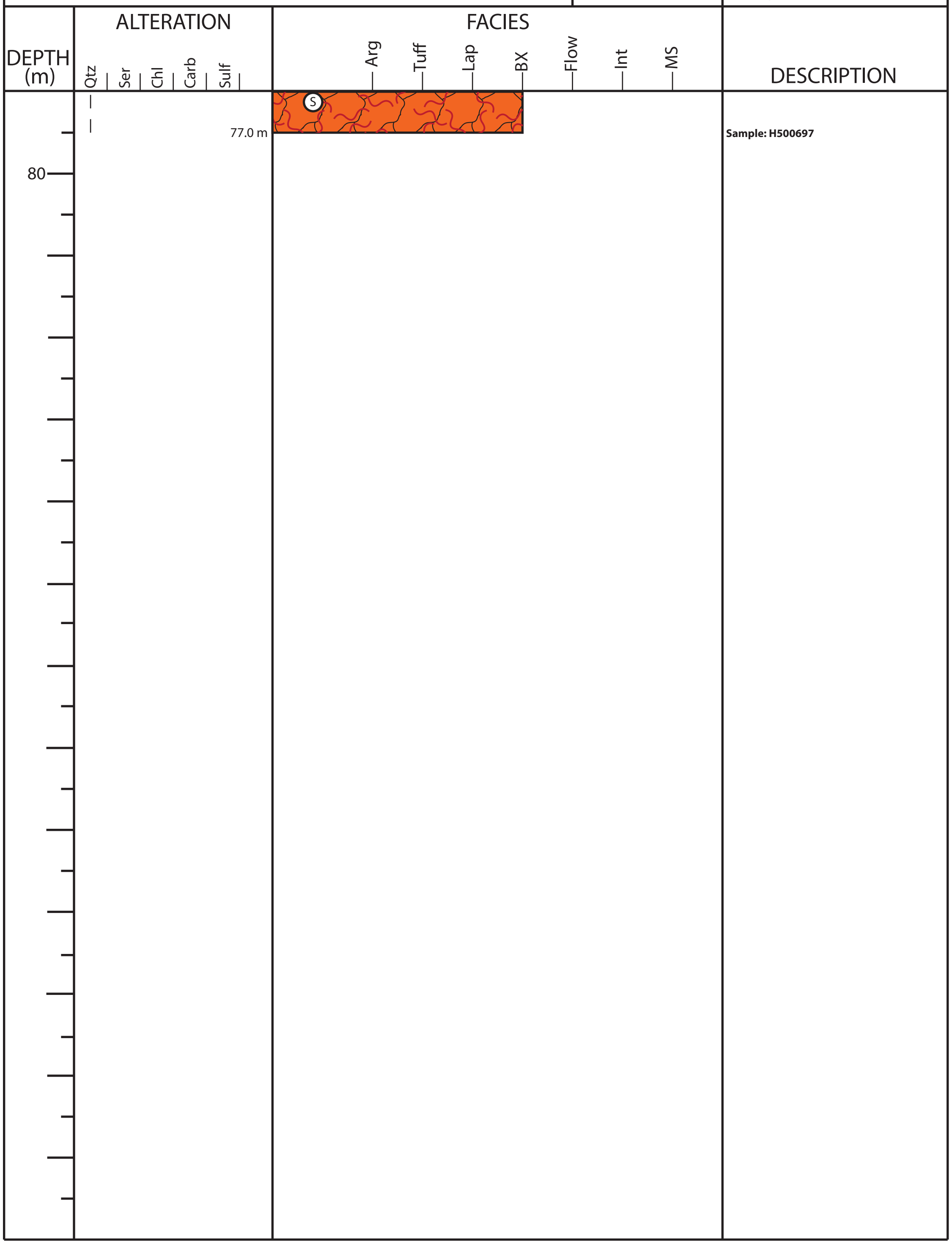

Project: Boundary Diamond Drill Hole: BD10-076 Date: 8-13-2013	UTM 540695.19E 5389603.35N	Azimuth: 360 Dip: -90 Length: 50 m

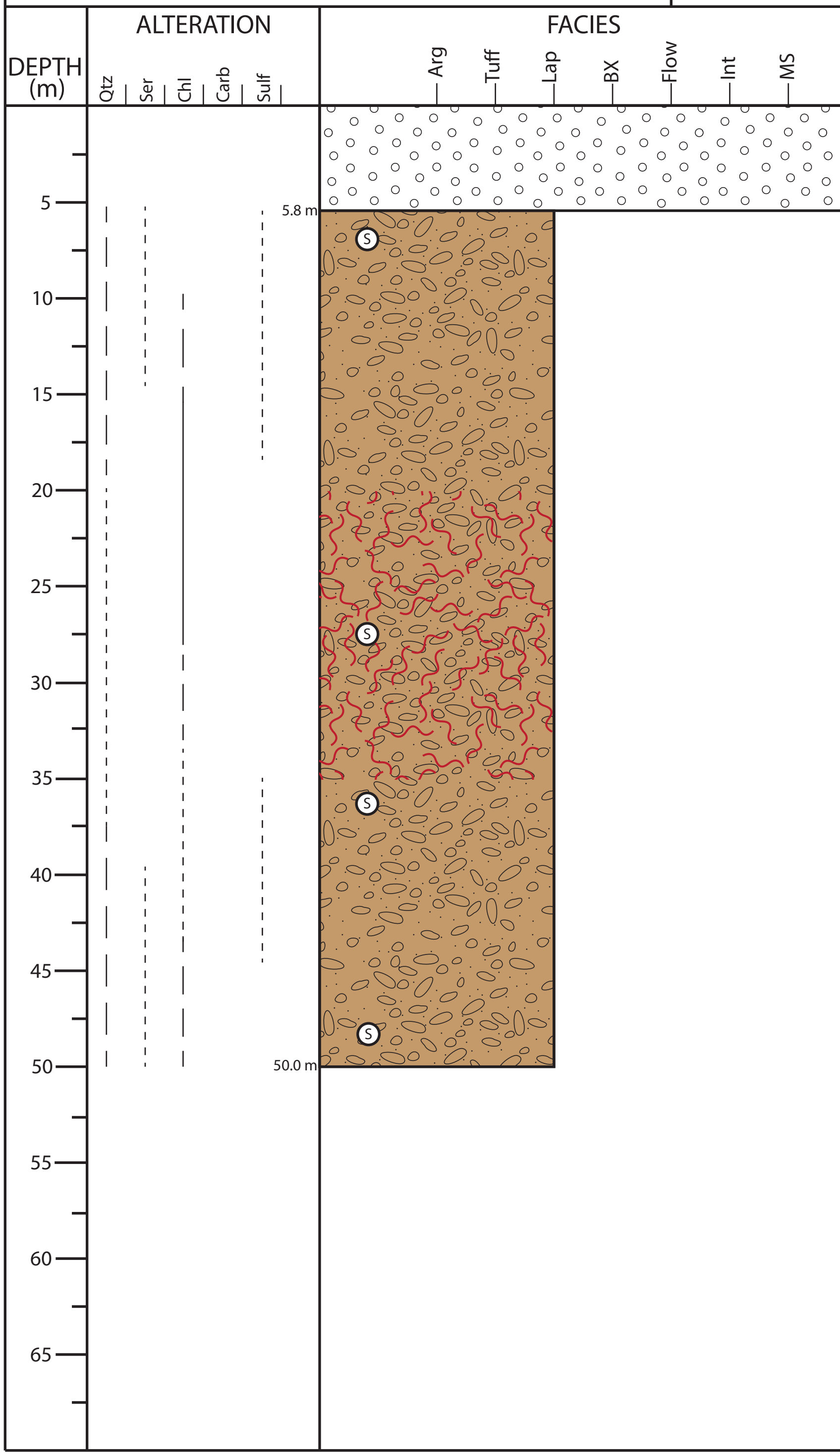

DESCRIPTION

Sample: H500690
LT is extremely clast supported. Subrounded clasts are varying shades of gray and all are ~1 cm in diameter. Most clasts are fairly hard (qtz alt) whereas darker ones are somewhat softer (ser). Deeper in unit (i. e. near 20 m), clasts become larger (up to 6 cm) and contain some flow banded frags. Matrix becomes more prevalent and is chl replaced.

Clasts (1-2 cm) are nearly completely altered by dark sericite or chlorite. Stringer Py occurs intermittently throughout over 20-35m stretch. This stretch is also more so matrix supported and contains seemingly high amount of carbonate spotting.

Sample: H500689

Sample: H500688

After stringer section, unit is much like upper portion (all ~1cm in diameter and little to no matrix). Dis. Py scattered throughout. Lowest section in hole doesn't look all that chl altered, but later geochem suggests it is actually significantly altered (CCPI=91).

Sample: H500687

Project: Boundary
Diamond Drill Hole: BD10-077
Date: 8-13-2013

UTM
540678.15E
5389625.82N

Azimuth: 360
Dip: -90
Length: 50m

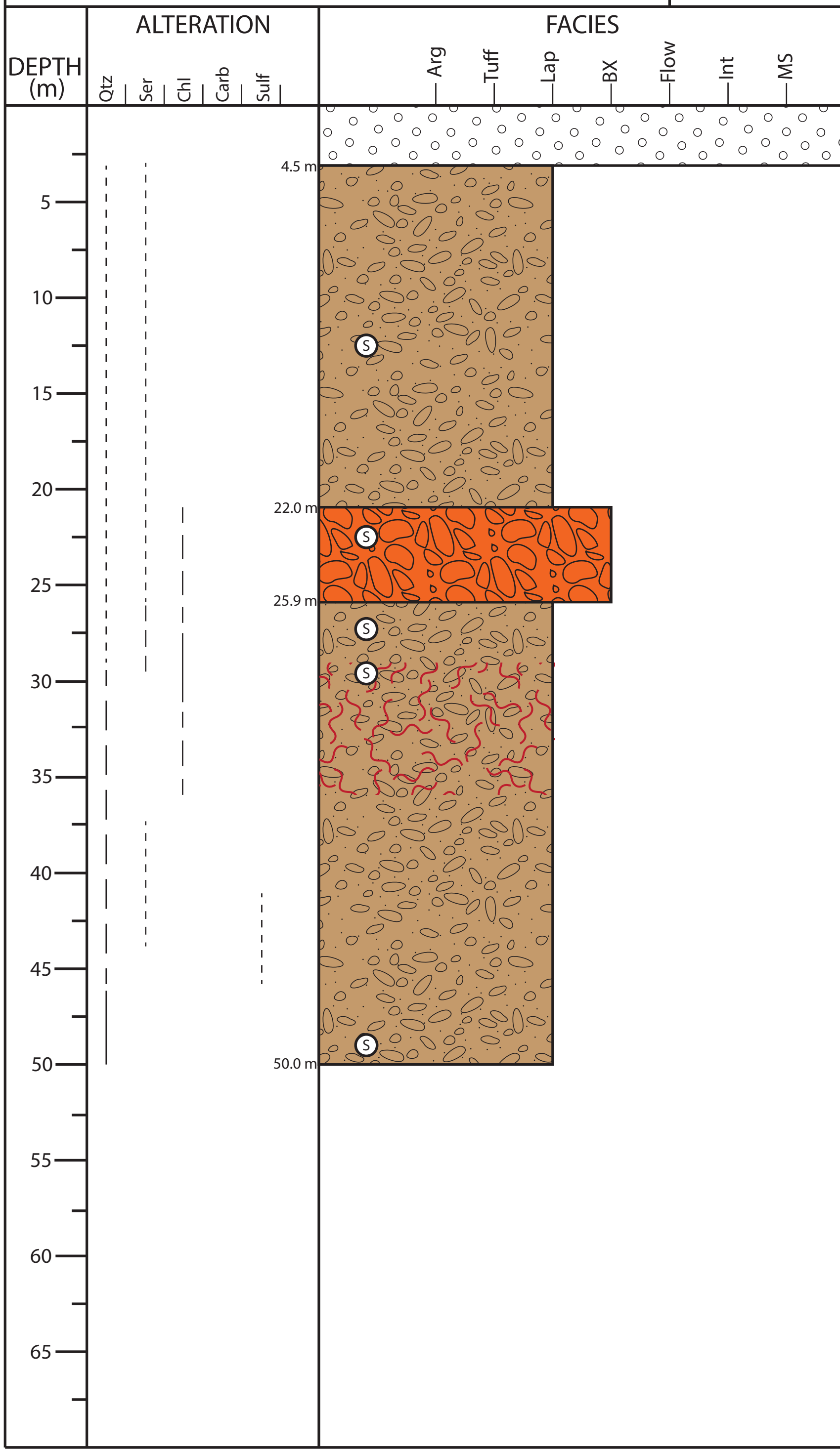

DESCRIPTION

The upper ~20 m of this unit is fairly consistent: dark grey clast supported, ~1cm clasts that are qtz-ser alt. Core appears to be somewhat fragmented (possible faulted).

Sample: H500682

Sample: H500683

This breccia unit might be fault related, but the chlorite alteration appears to be constrained to this unit and below. BX looks like it could have some qtz-altered, flow banded fr agments with black chl/ser intrafrag space.

Sample: H500684

Sample: H500685

Below BX, LT unit consists of clasts (~1cm) and varying alteration. From ~25-28, nearly all core (clasts included) are black. Geochem and thin sections point towards black sericite, not much chlorite at all. Chlorite content increases from 28-37, along with stringer Ccp and Py. The clasts over this period appear less altered (only qtz) while matrix is completely replaced. As stringers die out, unit becomes more clast supported and sulfides consist of just dis. Py. Near bottom of hole, LT appears to be greatly silicified.

Sample: H500686

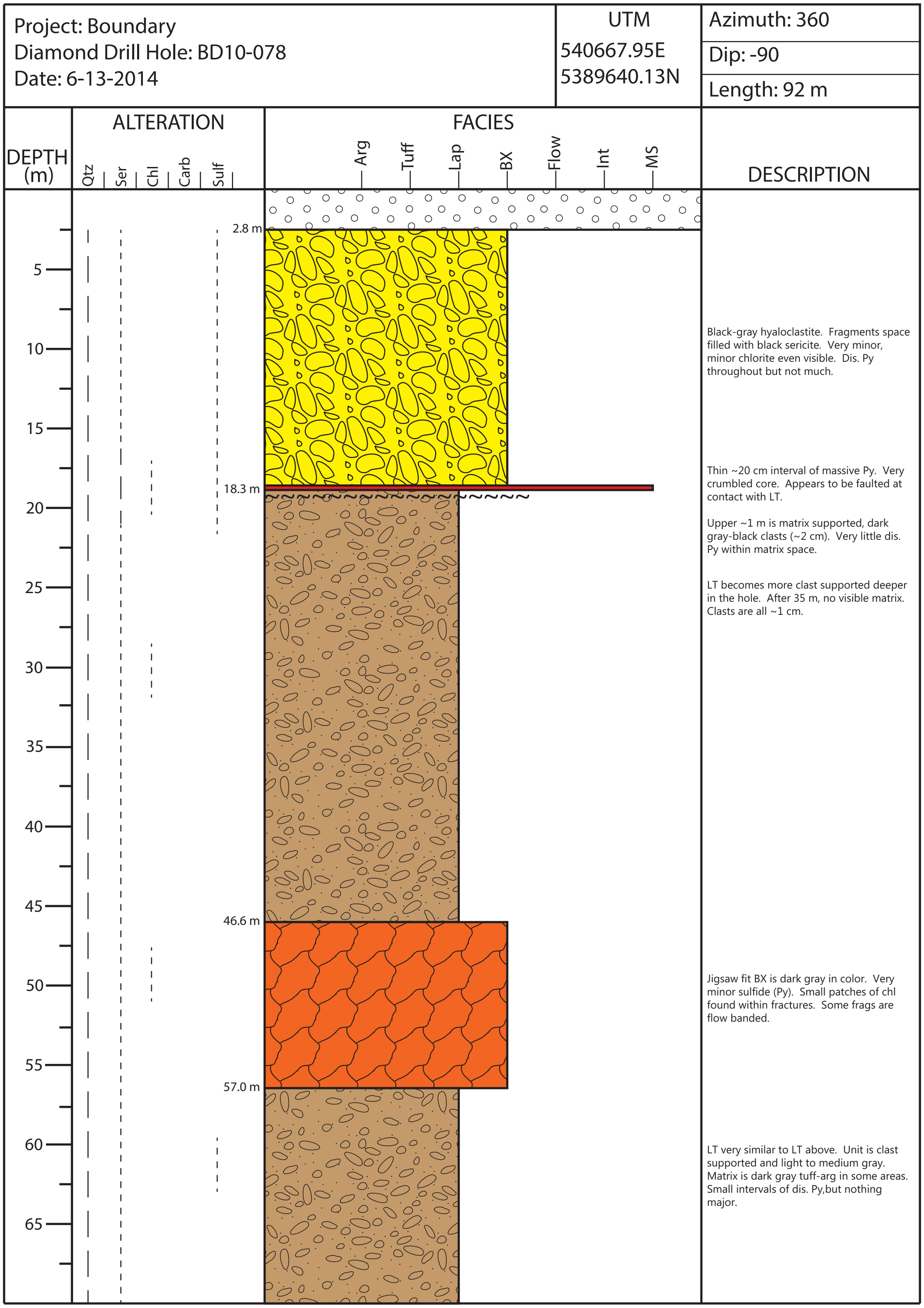
Project: Boundary
Diamond Drill Hole: BD10-078
Date: 6-13-2014
UTM
540667.95E
5389640.13N
Azimuth: 360
Dip: -90
Length: 92 m
DEPTH (m)
ALTERATION
Qtz
Ser
Chl
Carb
Sulf
FACIES
Arg
Tuff
Lap
BX
Flow
Int
MS
DESCRIPTION
5
10
15
20
25
30
35
40
45
50
55
60
65
2.8 m
18.3 m
46.6 m
57.0 m
Black-gray hyaloclastite. Fragments space filled with black sericite. Very minor, minor chlorite even visible. Dis. Py throughout but not much.
Thin ~20 cm interval of massive Py. Very crumbled core. Appears to be faulted at contact with LT.
Upper ~1 m is matrix supported, dark gray-black clasts (~2 cm). Very little dis. Py within matrix space.
LT becomes more clast supported deeper in the hole. After 35 m, no visible matrix. Clasts are all ~1 cm.
Jigsaw fit BX is dark gray in color. Very minor sulfide (Py). Small patches of chl found within fractures. Some frags are flow banded.
LT very similar to LT above. Unit is clast supported and light to medium gray. Matrix is dark gray tuff-arg in some areas. Small intervals of dis. Py,but nothing major.

Project: Boundary Diamond Drill Hole: BD10-078 Date: 6-13-2014	UTM 540667.95E 5389640.13N	Azimuth: 360 Dip: -90 Length: 92 m

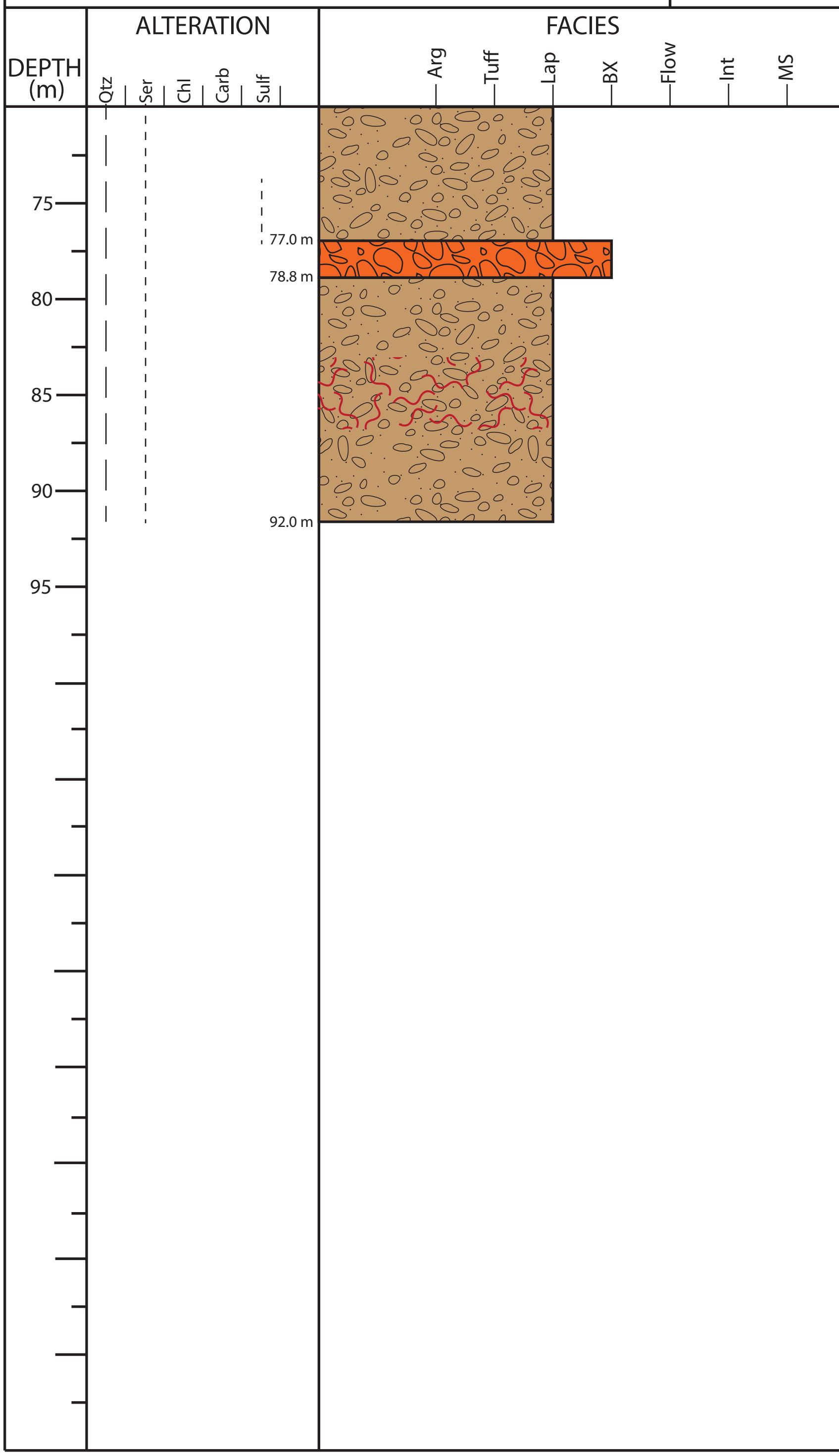

DESCRIPTION

Hyaloclastite is dark gray with black (ser) matrix. Some frags (~4-6 cm) are flow banded. Drill log mentions qtz-phenocrysts, but I did not note any. Lower LT is the same as the LT from 57-77 m. Small zone of stringer Py.

Project: Boundary Diamond Drill Hole: BD10-087 Date: 8-13-2013	UTM 540760.00E 5389605.50N	Azimuth: 360 Dip: -90 Length: 35 m

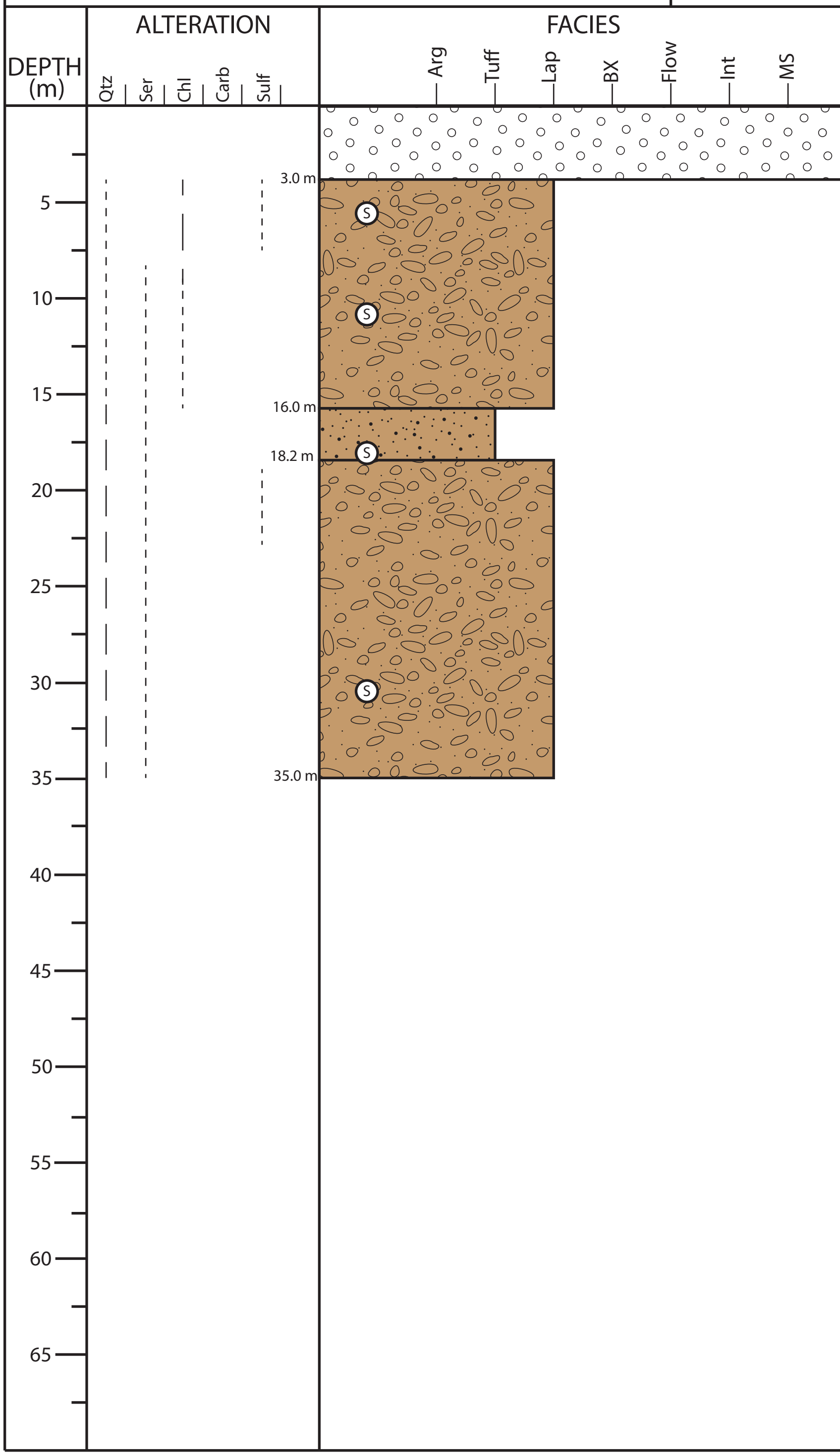

DESCRIPTION

Sample: H500678

Top 8 m of LT consists of matrix sup. LT with black chl/ser matrix. Clasts are uniformally dark gray and ~2cm in diameter. From 8-16 m, LT is matrix supported and clasts become bimodal in size and vary shades of gray. Entire section shows intense carbonate spotting.

Sample: H500679

Tuff unit consists of sevral semi-graded tuff layers. Tuff is light gray contains some small lapilli clasts (~1cm).

Sample: H500680

Lower LT section becomes more clast supported than the upper section. LT clasts vary in size from <1cm up to 5cm but most are ~1.5cm. Dis. Py is found throughout but appears somewhat concentrated from 18-22 m. Carbonate spotting is also less prevalent in the lower section.

Sample: H500681

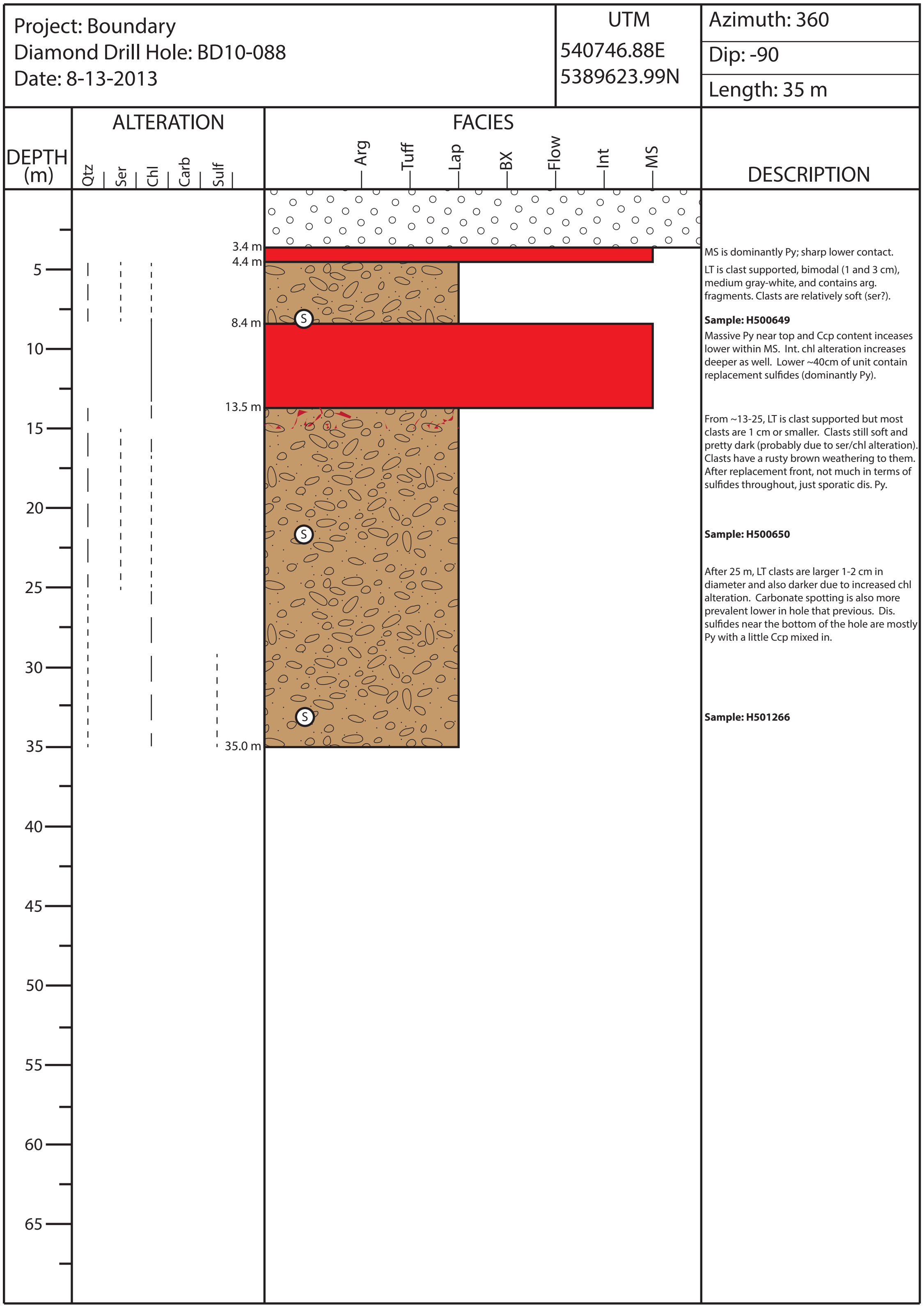
Project: Boundary
Diamond Drill Hole: BD10-088
Date: 8-13-2013
UTM
540746.88E
5389623.99N
Azimuth: 360
Dip: -90
Length: 35 m
DEPTH (m)
ALTERATION
Qtz
Ser
Chl
Carb
Sulf
FACIES
Arg
Tuff
Lap
BX
Flow
Int
MS
DESCRIPTION
3.4 m
4.4 m
8.4 m
13.5 m
35.0 m
5
10
15
20
25
30
35
40
45
50
55
60
65
S
MS is dominantly Py; sharp lower contact.
LT is clast supported, bimodal (1 and 3 cm), medium gray-white, and contains arg. fragments. Clasts are relatively soft (ser?).
Sample: H500649
Massive Py near top and Ccp content inceases lower within MS. Int. chl alteration increases deeper as well. Lower ~40cm of unit contain replacement sulfides (dominantly Py).
From ~13-25, LT is clast supported but most clasts are 1 cm or smaller. Clasts still soft and pretty dark (probably due to ser/chl alteration). Clasts have a rusty brown weathering to them. After replacement front, not much in terms of sulfides throughout, just sporatic dis. Py.
Sample: H500650
After 25 m, LT clasts are larger 1-2 cm in diameter and also darker due to increased chl alteration. Carbonate spotting is also more prevalent lower in hole that previous. Dis. sulfides near the bottom of the hole are mostly Py with a little Ccp mixed in.
Sample: H501266

Project: Boundary Diamond Drill Hole: BD10-098 Date: 8-15-2013	UTM 540642.34E 5389543.26N	Azimuth: 360 Dip: -90 Length: 52 m

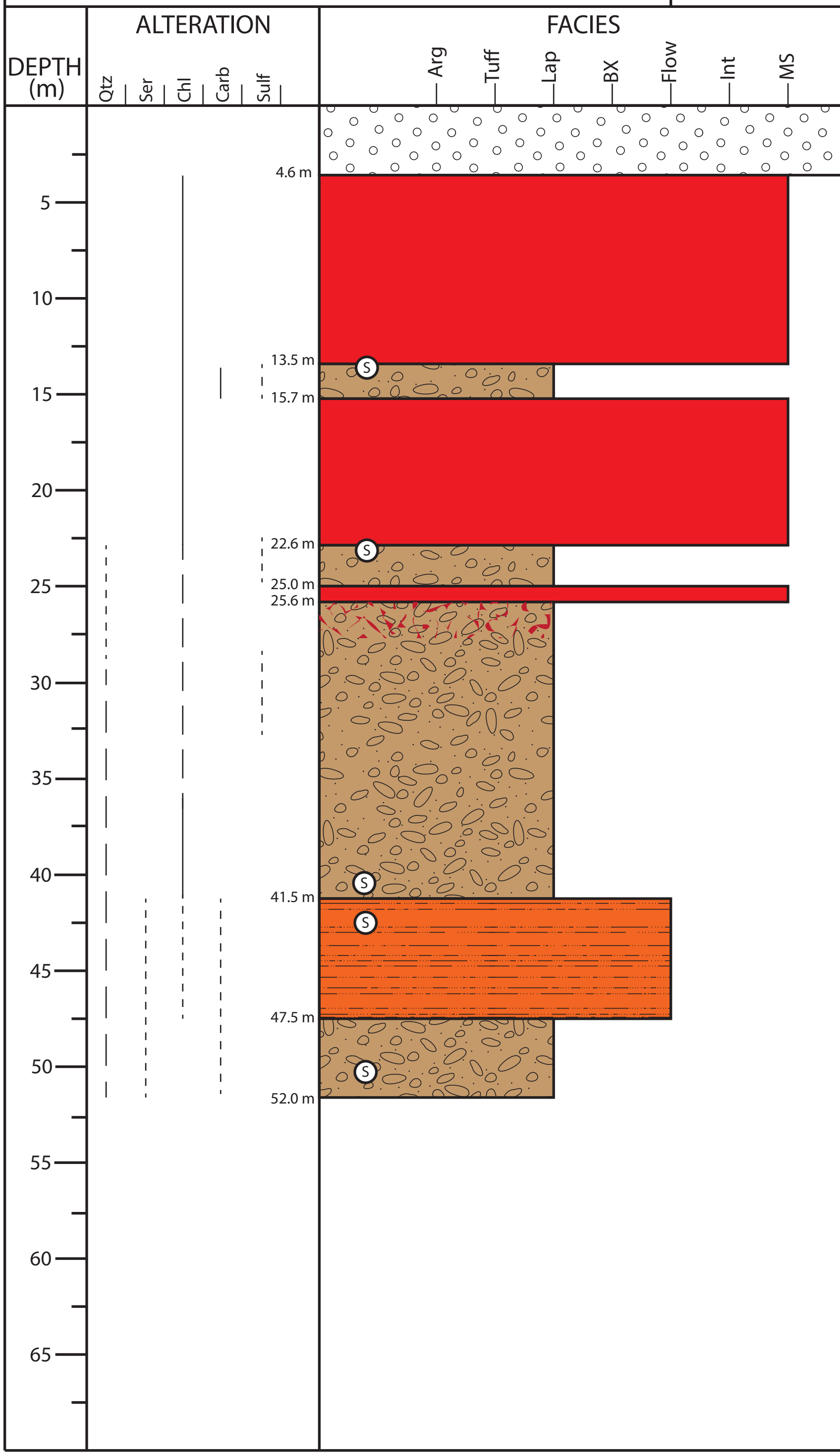

DESCRIPTION

Top of MS is Py-Po? Then grades into higher amounts of Ccp from ~6.5-9 m before Sph drastically increases in the rest of the MS. LT below completely black and chl altered. Cannot make out any individual clasts. Contains dark yellow-brown carbonate spotting.

Sample: H501217

Massive Py-Ccp except the last meter or so is Zn rich. Qtz veining in some areas contains Ccp and maybe bournite? The last meter also contains a fair amount of black chlorite alteration but clasts are not visible. The next LT interval consists of large (~3-4 cm) , dark gray clasts in a black chlorite matrix. Clasts are matrix supported

Sample: H501218

MS is massive Py-Ccp.

LT interval from 25.6-30 m contains replacement and dis. sulfides (primarily Py and Sph). Over this stretch, clasts are generally ~1 cm or smaller and matrix supported. Most contain lighter alteration rims and some graded bedding is present. After 30 meters, clasts become bimodal in size (<1 cm and ~2 cm) and range from light to dark gray. Mostly clast supported but may be matrix supported over small intervals. Small ash tuffs also occur near the flow contact.

Sample: H501219

Sample: H501220

Flow banded flow unit is dark gray (qtz) with black bands (ser). Unit appears to be folded, but not faulted (maybe implies folding is primary feature). Carbonate sports are rusty red color in this unit. Small, milky blebs of carbonate occur along band margins.

Sample: H501221

Lower LT unit is dark gray with clasts ~1 in diameter. Clasts are matrix supported. Matrix consists of gray tuff and dis. Py. Carbonate sposts are pale brown unlike those above in the flow banded unit.

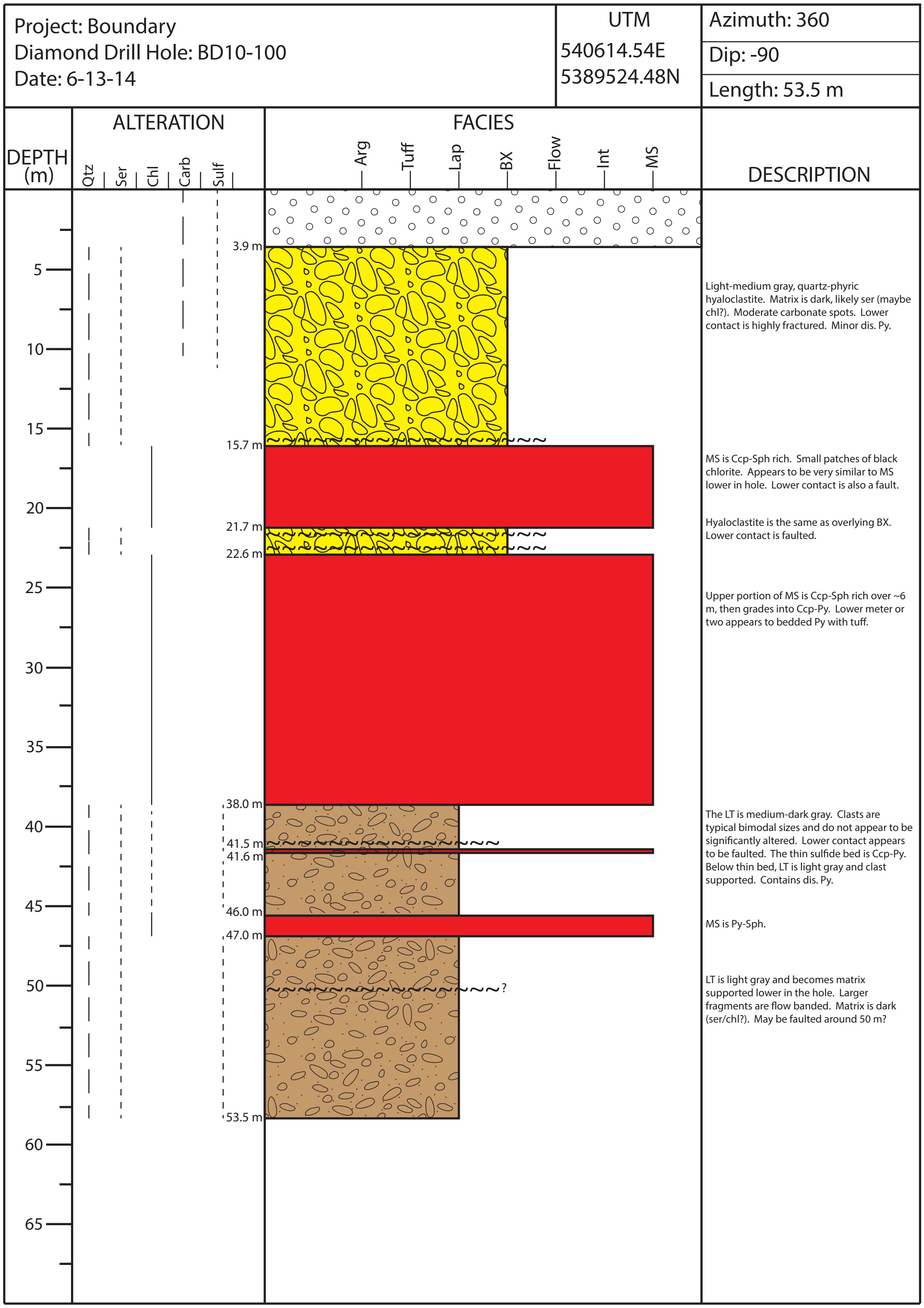
Project: Boundary
Diamond Drill Hole: BD10-100
Date: 6-13-14
UTM
540614.54E
5389524.48N
Azimuth: 360
Dip: -90
Length: 53.5 m
DEPTH (m)
ALTERATION
Qtz
Ser
Chl
Carb
Sulf
FACIES
Arg
Tuff
Lap
BX
Flow
Int
MS
DESCRIPTION
5
10
15
20
25
30
35
40
45
50
55
60
65
3.9 m
15.7 m
21.7 m
22.6 m
38.0 m
41.5 m
41.6 m
46.0 m
47.0 m
53.5 m
?
Light-medium gray, quartz-phyric hyaloclastite. Matrix is dark, likely ser (maybe chl?). Moderate carbonate spots. Lower contact is highly fractured. Minor dis. Py.
MS is Ccp-Sph rich. Small patches of black chlorite. Appears to be very similar to MS lower in hole. Lower contact is also a fault.
Hyaloclastite is the same as overlying BX. Lower contact is faulted.
Upper portion of MS is Ccp-Sph rich over ~6 m, then grades into Ccp-Py. Lower meter or two appears to bedded Py with tuff.
The LT is medium-dark gray. Clasts are typical bimodal sizes and do not appear to be significantly altered. Lower contact appears to be faulted. The thin sulfide bed is Ccp-Py. Below thin bed, LT is light gray and clast supported. Contains dis. Py.
MS is Py-Sph.
LT is light gray and becomes matrix supported lower in the hole. Larger fragments are flow banded. Matrix is dark (ser/chl?). May be faulted around 50 m?

Project: Boundary Diamond Drill Hole: BD10-102 Date: 8-15-2013	UTM 540734.00E 5389643.00N	Azimuth: 360 Dip: -90 Length: 47 m

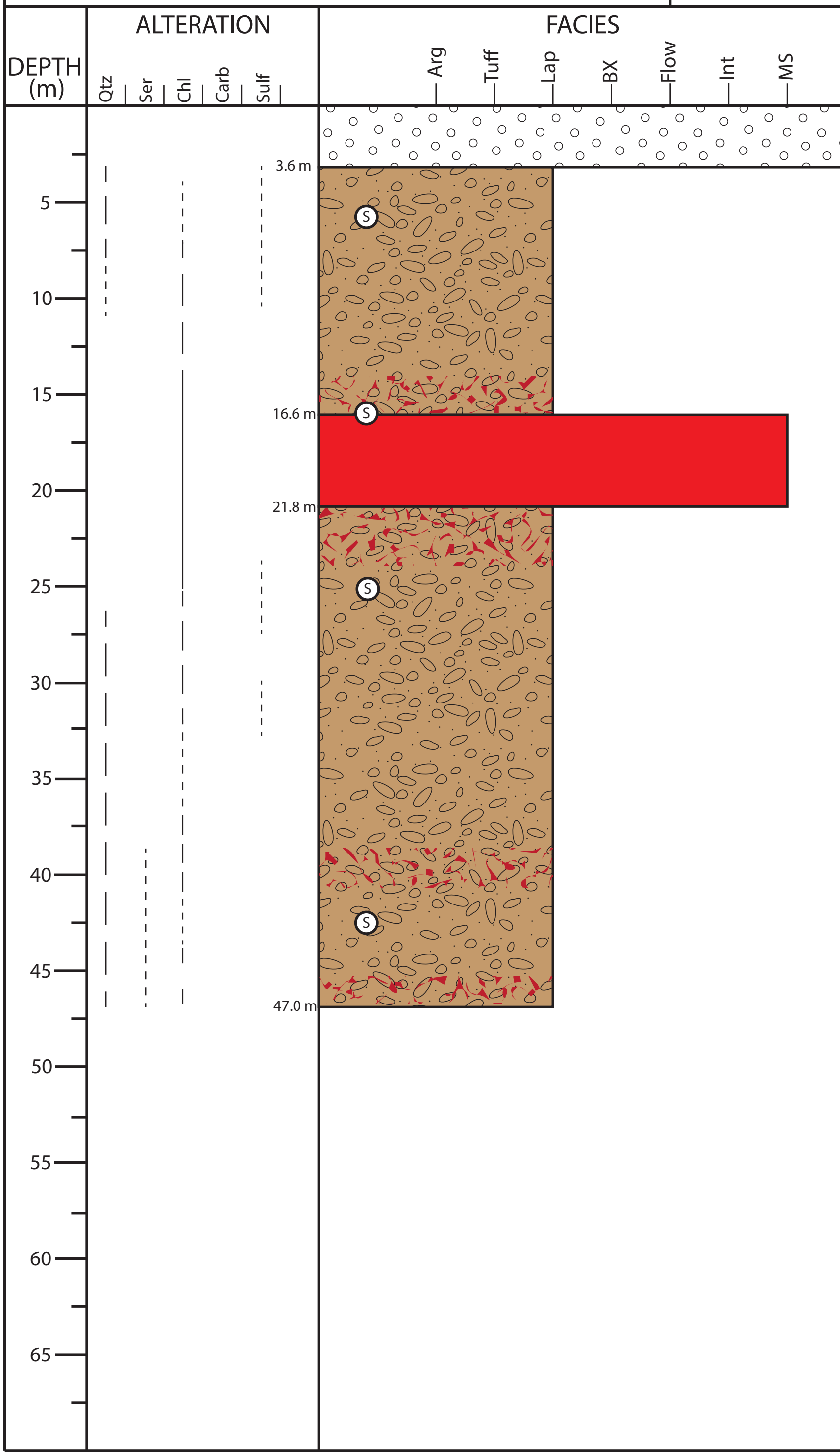

DESCRIPTION

Sample: H500661

Upper 10 meters of matrix supported LT unit consisting of gray-pink clasts. Clasts are bimodal in size (>2.5 cm and ~1 cm) and subangular. Matrix consists of chlorite or dis. Py. From 10-16.6 m, LT becomes more clast supported and heavily chl altered. Unit becomes completely chl altered with replacement Py (± Ccp) near the MS.

Sample: H500662

From upper meter of MS is dominantly massive Py that grades into massive Py-Ccp (not much Sph visible). From 20m-22m black chlorite content increases and sulfides occur within matrix space and clasts are visible.

LT is clast supported with clasts <0.5 cm and are varying shades of gray. Matrix contains either chl or Py.

Sample: H500663

LT clast size increases after 25m to about 1 cm. LT becomes even more clast supported with no visible matrix except where sulfides are present. Near end of hole, clasts are uniformly dark gray, rounded, and ~1 cm in diameter.

Ccp-Py sulfides.

Sample: H500664

Ccp-Py sulfides.

Project: Boundary Diamond Drill Hole: BD10-104 Date: 8-11-2013	UTM 540787.00E 5389648.00N	Azimuth: 360 Dip: -90 Length: 26.4

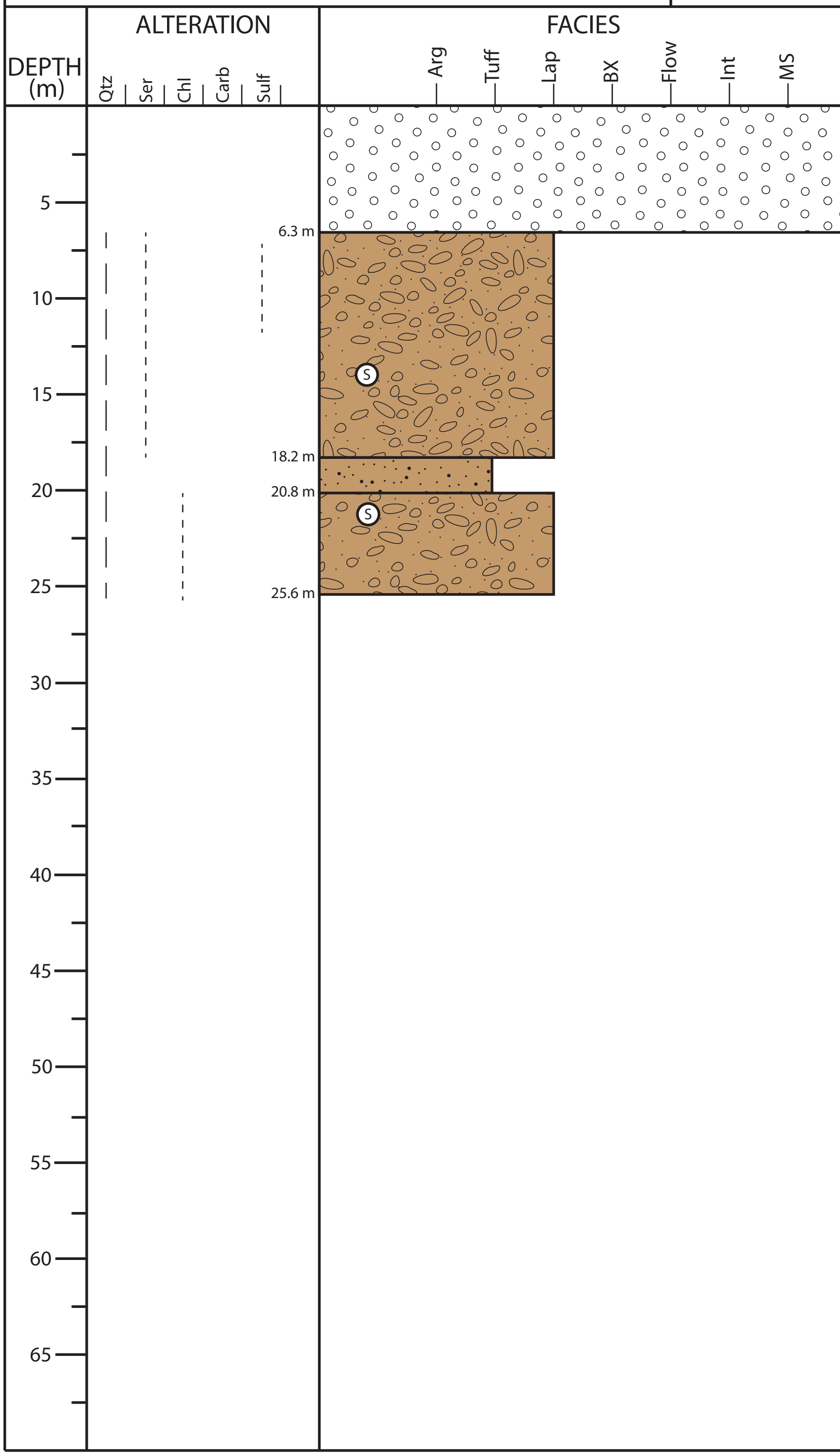

DESCRIPTION

LT is gray/green with zoned clasts. Clasts are bimodal in size (<1cm and ~2 cm). Generally clasts supported and clasts grade into tuff near 18 m. Minor dis. Py.

Sample: H500642

Sample: H500643

Lower LT unit is medium gray and clast supported. Contains moderate amount of arg. fragments. This section contains clasts that have a much wider range of clasts from <0.5 up to 4 cm with no size preference.

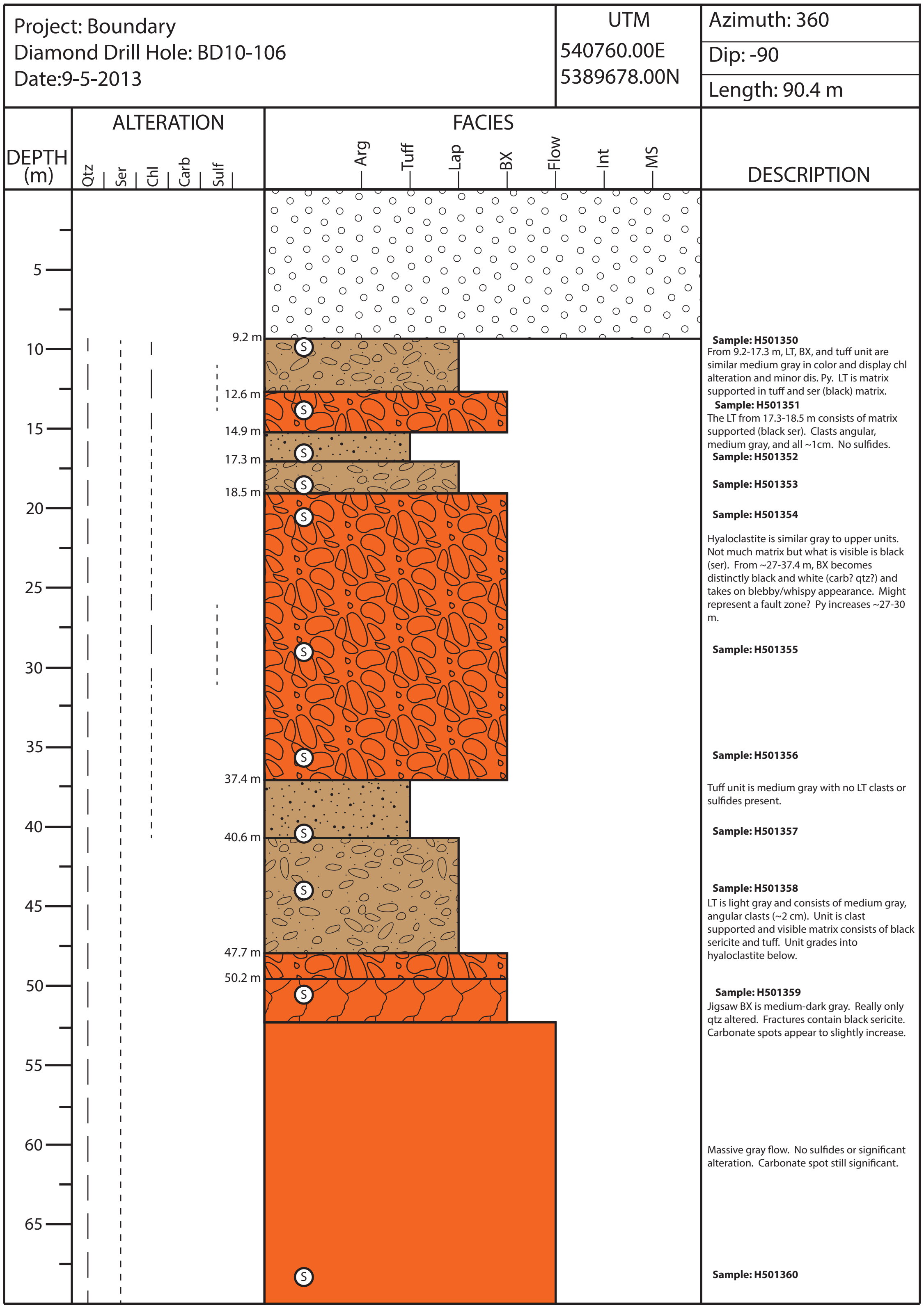

Project: Boundary
Diamond Drill Hole: BD10-106
Date:9-5-2013
UTM
540760.00E
5389678.00N
Azimuth: 360
Dip: -90
Length: 90.4 m
DEPTH (m)
ALTERATION
Qtz
Ser
Chl
Carb
Sulf
FACIES
Arg
Tuff
Lap
BX
Flow
Int
MS
DESCRIPTION
5
10
15
20
25
30
35
40
45
50
55
60
65
9.2 m
12.6 m
14.9 m
17.3 m
18.5 m
37.4 m
40.6 m
47.7 m
50.2 m
S
Sample: H501350
From 9.2-17.3 m, LT, BX, and tuff unit are similar medium gray in color and display chl alteration and minor dis. Py. LT is matrix supported in tuff and ser (black) matrix.
Sample: H501351
The LT from 17.3-18.5 m consists of matrix supported (black ser). Clasts angular, medium gray, and all ~1cm. No sulfides.
Sample: H501352
Sample: H501353
Sample: H501354
Hyaloclastite is similar gray to upper units. Not much matrix but what is visible is black (ser). From ~27-37.4 m, BX becomes distinctly black and white (carb? qtz?) and takes on blebby/whispy appearance. Might represent a fault zone? Py increases ~27-30 m.
Sample: H501355
Sample: H501356
Tuff unit is medium gray with no LT clasts or sulfides present.
Sample: H501357
Sample: H501358
LT is light gray and consists of medium gray, angular clasts (~2 cm). Unit is clast supported and visible matrix consists of black sericite and tuff. Unit grades into hyaloclastite below.
Sample: H501359
Jigsaw BX is medium-dark gray. Really only qtz altered. Fractures contain black sericite. Carbonate spots appear to slightly increase.
Massive gray flow. No sulfides or significant alteration. Carbonate spot still significant.
Sample: H501360

Project: Boundary Diamond Drill Hole: BD10-106 Date:9-5-2013	UTM 540760.00E 5389678.00N	Azimuth: 360 Dip: -90 Length: 90.4 m

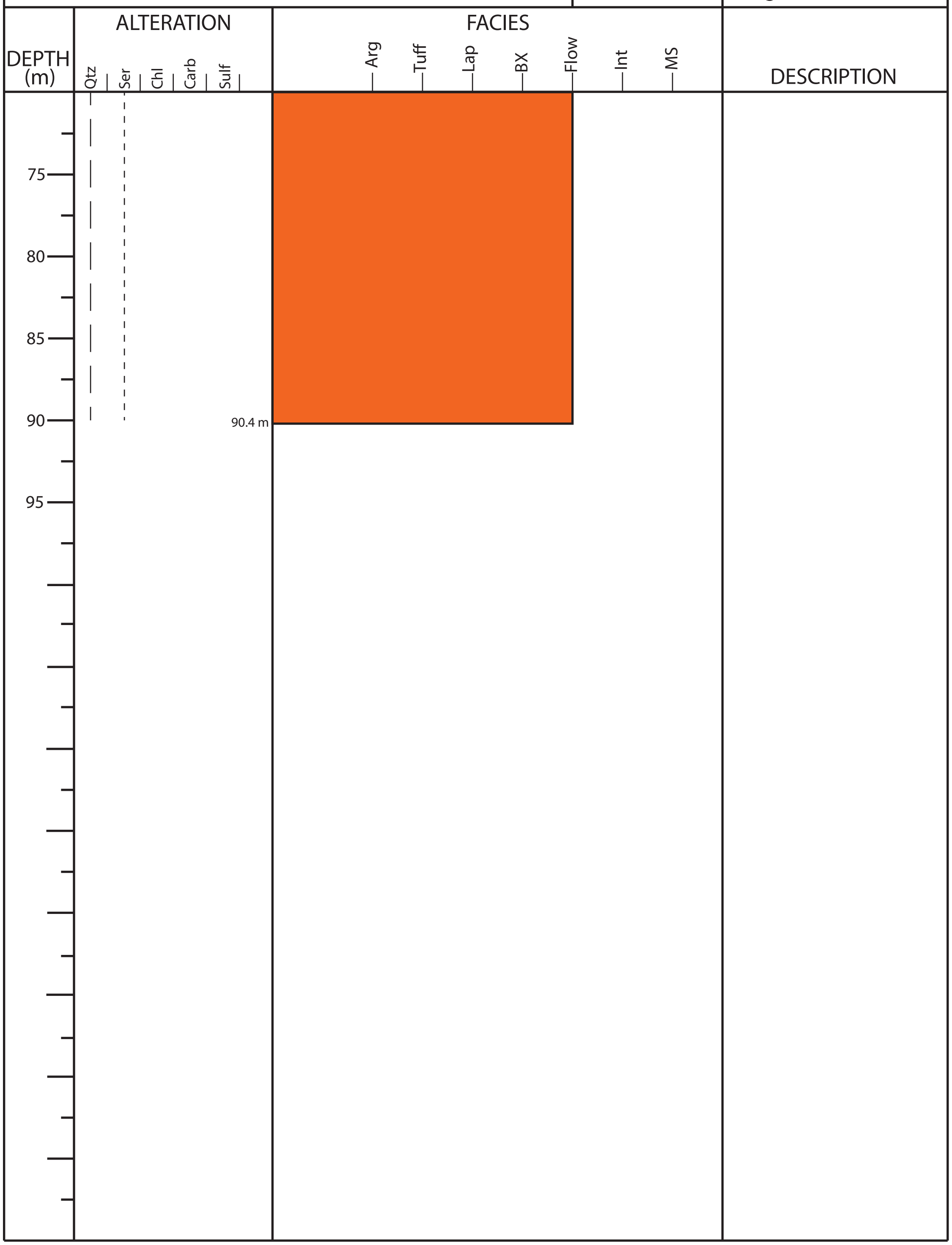

Project: Boundary Diamond Drill Hole: BD10-107 Date: 8-11-2013	UTM 540836.00E 5389592.00N	Azimuth: 360 Dip: -90 Length: 40 m

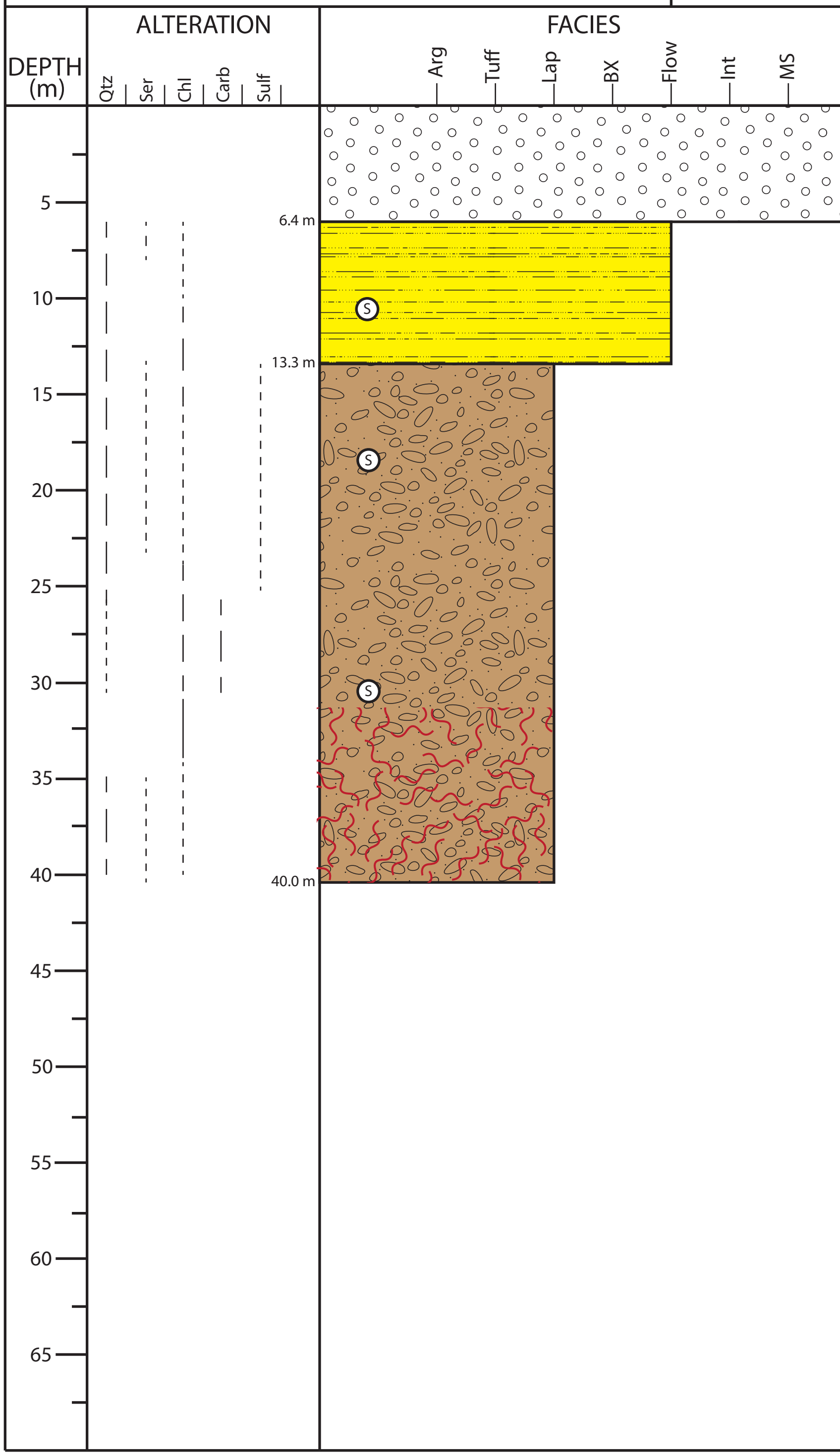

DESCRIPTION

Qtz-phyric, gray-black, hanging wall flow. Flow frags alternate between gray qtz altered frags and black chl/ser band (thin sections and chemistry show black alteration is sericite).

Sample: H500617

Upper 10 cm is tuff that grades into LT. Over the interval of 13.3-25 m, most of the clasts are <1.0 cm. Clasts are gray-white while matrix consists of black chl/ser. Well developed cubic Py throughout.

Sample: H500618

From 25-40 m, the LT clasts increase in size (up to 4 cm) and become more qtz altered. Stringer Py is prevalent in the int. chl altered regions. Moderate, large (~0.7 cm) carbonate spots within both clasts and matrix. LT is generally clast supported but locally can be matrix supported and may contain flow banded frags.

Sample: H500619

Project: Boundary Diamond Drill Hole: BD10-108 Date: 8-17-2013	UTM 540827.00E 5389600.00N	Azimuth: 360 Dip: -90 Length: 60 m

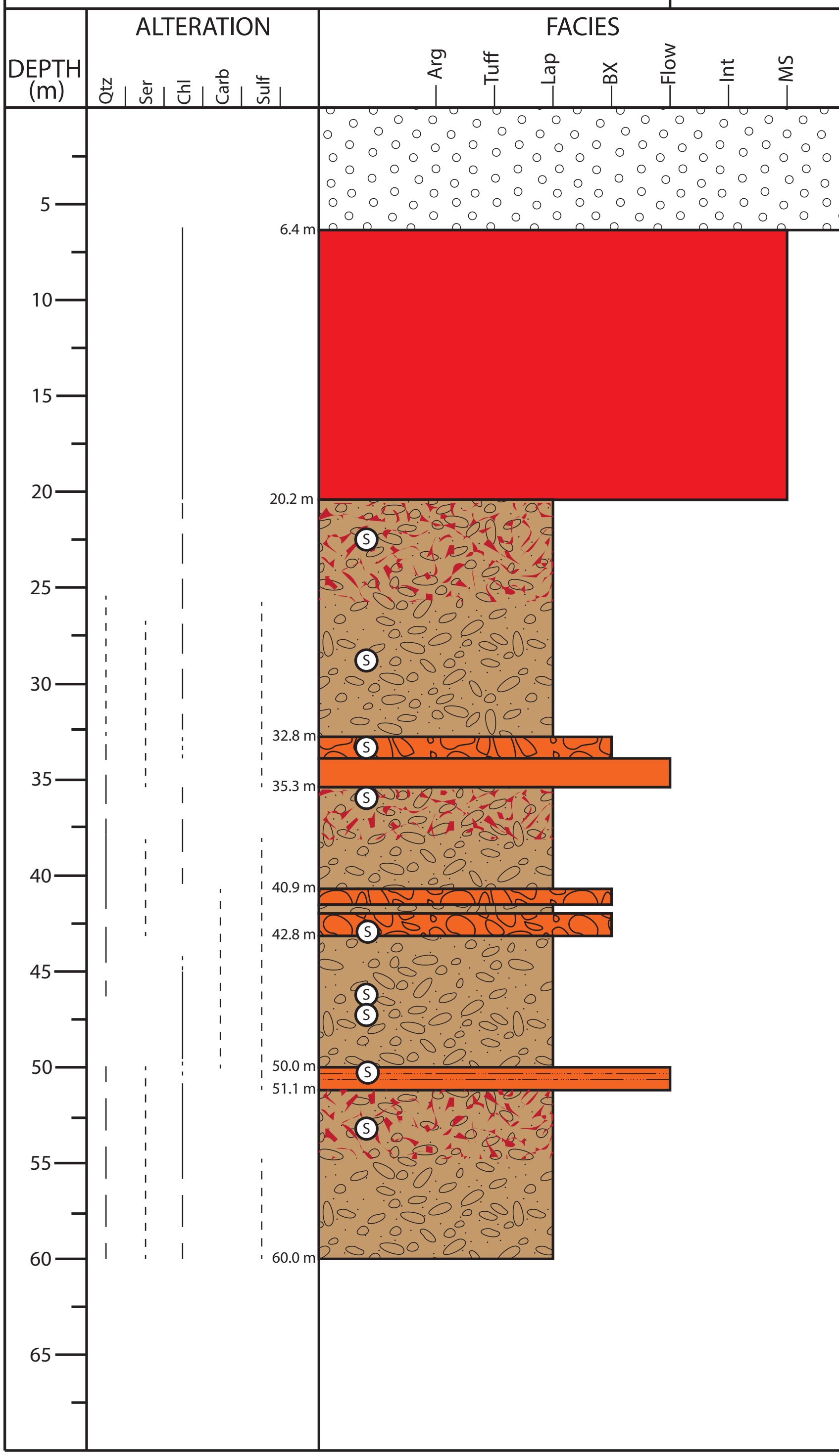

DESCRIPTION

MS is mostly Py with short intervals of increased Ccp (~7-8m and ~15-18 m). Small intervals of LT clasts within sulfides. Clasts content increases near base of massive sulfide.

Sample: H500621
Matrix sulfides are mostly Py with minor blebs of Ccp. LT clasts are matrix support (Py and black chl), dark gray, subangulalr, and most are <0.8 cm in diameter. Minor carbonate spotting. Sulfide matrix decreases after 25 m and is dominated by chl. Some clasts have white alteration rims.

Sample: H500622

Sample: H500623
Flow and BX are both dark gray with dark ser/chl filled fractures. Minor dis. Ccp.

Sample: H500624

LT is clast supported with dark gray clasts (~2-3 cm) in a Ccp-chl matrix. LT below sulfides are highly silicified.

BX very similar to BX/flow above.

Sample: H500625

Sample: H500626
Sample: H500627

Sample: H500628

Sample: H500628
LT (43.6-46.8 m): LT is matrix supported (chl). Clasts are generally medium to dark gray, sub angular, and between 1-3 cm in diameter. High volume of carbonate spotting/beige chaotic carbonate.

LT (46.8-50.2 m): LT becomes completely black with no recognizeable clasts. Py content increases and carbonate content decreases. White chaotic carbonate also present.

Flow (50.2-51.5 m): Flow is medium-dark gray and contains mionr amount of beige carbonate spots.

LT (51.5-60.0 m): LT similar to those from (43.6-46.8 m) though more clast supported and contain some Ccp in upper portion of unit.

Project: Boundary Diamond Drill Hole: BD10-112 Date: 8-13-2013	UTM 540848.00E 5389614.00N	Azimuth: 360 Dip: -90 Length: 60.6 m

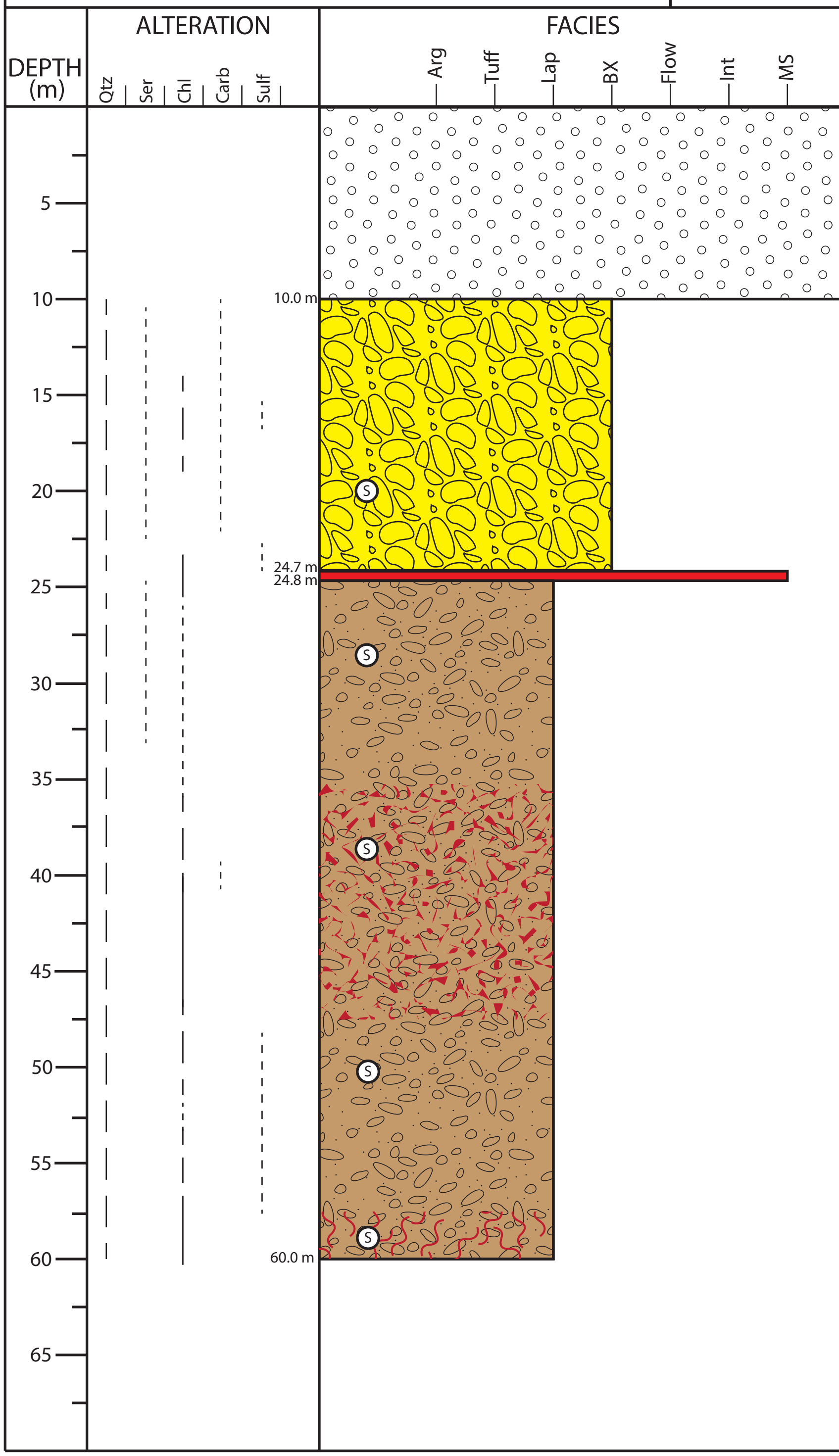

DESCRIPTION

Sample: H500606
Breccia appears to be most flow breccias with some smaller massive flows within. Unit is dark grey with inter flow fractures filled with black chlorite. Minor dis. Py throughout and small localized zones of intense chlorite. Carbonate appears to be fratcure filler-Not chaotic carbonate associated with the black chlorite alteration.

"Massive sulfide" is a thin lens consisting dominantly of Py and minor Ccp. Sulfide lens forms sharp contacts with black chlorite both above and below.

Sample: H500607
LT over the next 10 meters is fairly consistent in that most clasts are around 1cm and contains minor tuff layers. Clast supported with very minor visible matrix (black chl/ser). Some minor dis. Py but not much.

Sample: H500608
From ~38-43 m, LS becomes considerably more chl/ser altered. Matrix material is generally chl or Py replaced. Clasts are larger in size (~3-4 cm) and become considerably darker. Some clasts also show evidence of flow banding. Minor Ccp in a few localities.

Sample: H500609
LT alteration appears to be somewhat lesser than previous five meters but still contains chl and Py within matrix. Clasts are about the same size but appear lighter in color.

Sample: H500610
Could make case for last 3 meters to be hyaloclastite breccia. Fragmentsare large (~5 -7cm) and light-dark gray in color. Matrix area contains black chlorite and Py stringer along with minor Ccp. Likely marks the depth of transition to the lower footwall BX and flows.

Project: Boundary Diamond Drill Hole: BD10-113 Date: 8-22-13; 6-12-14	UTM 540854.00E 5389309.00N	Azimuth: 190 Dip: -70 Length: 251.5 m

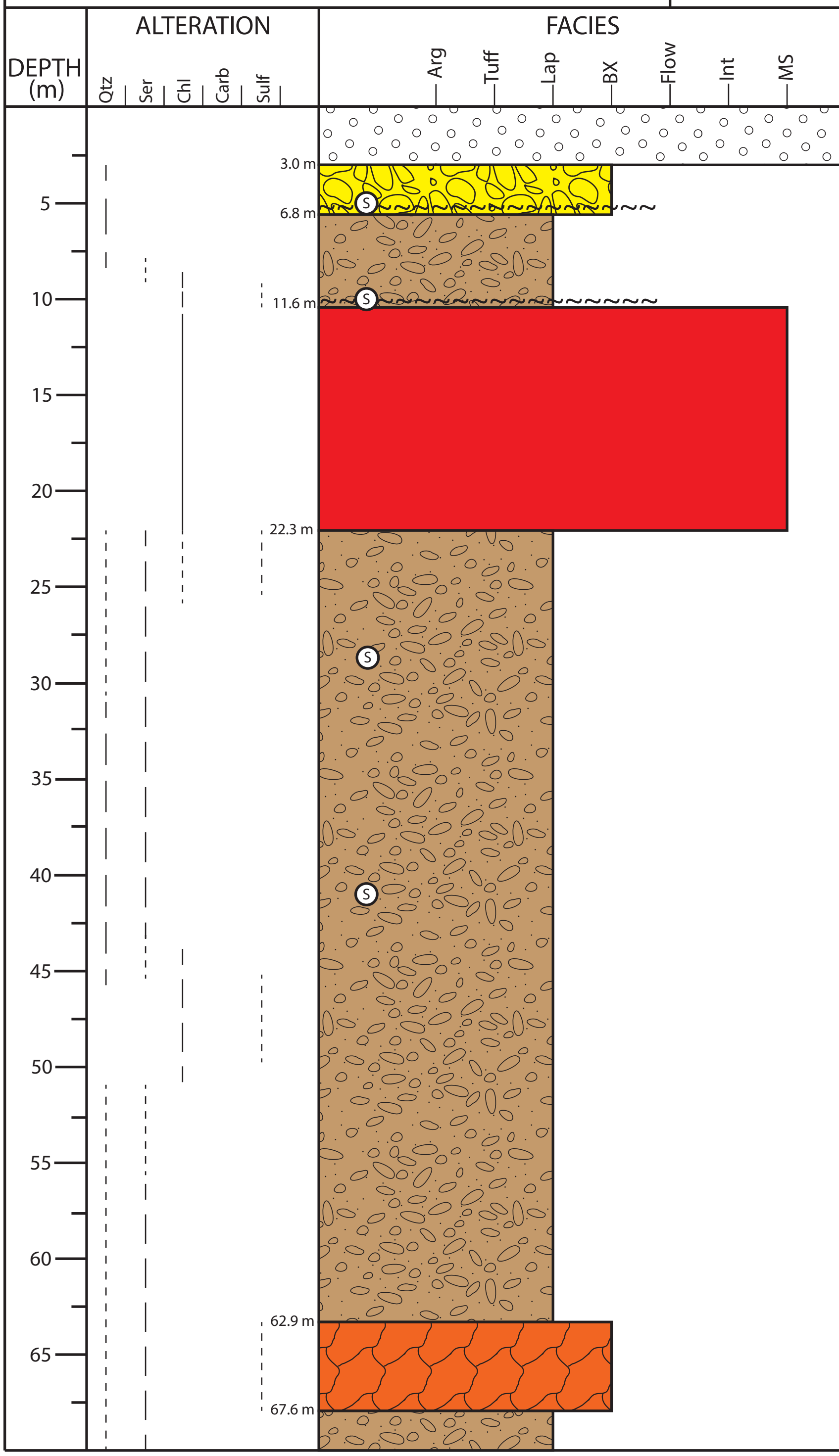

DESCRIPTION

Light gray, highly faulted and fragmented BX. Unit appears to be relatively unaltered. Fractures contain orange coating. Some large fragements care flow banded.

Sample: H501326

Clast supported, light gray LT. Clasts are typically around 1 cm. Lower meter is also highly faulted and contains large flow banded fragments. Near the contact, black chlorite is major matrix constituent with dis. Py.

Sample: H501327

MS is mostly Py with Ccp and Sph and trace Gal and chalcocite. MS is also fractured throughout. Top of MS is mostly Ccp and Py and becomes more Sph and Gal rich lower in hole. Lower contact also appears to be faulted? The lowest 20 cm is clast rich within sulfide matrix. Clasts are all <1cm.

Sample: H501328

LT clasts are large (~2-3 cm), gray-white, and contain lighter alteration rims. Core alters to dark brown color, though no major Fe-bearing phases visible (suflides or carbonates). Some fragments are flow banded.

Sample: H501329

LT becomes matrix supported from ~43-50 m. Clasts are larger and moderately ser altered and chl alteration also increases.

Clasts range from pink to white to green. Color change occurs over interval of increasing sericite alteration. Sulfides are not present.

Jigsaw fit BX. White to green in color. Fragments range in size from 10-15 cm in diameter. Very minor dis. Py. Lower contact is somewhat gradational.

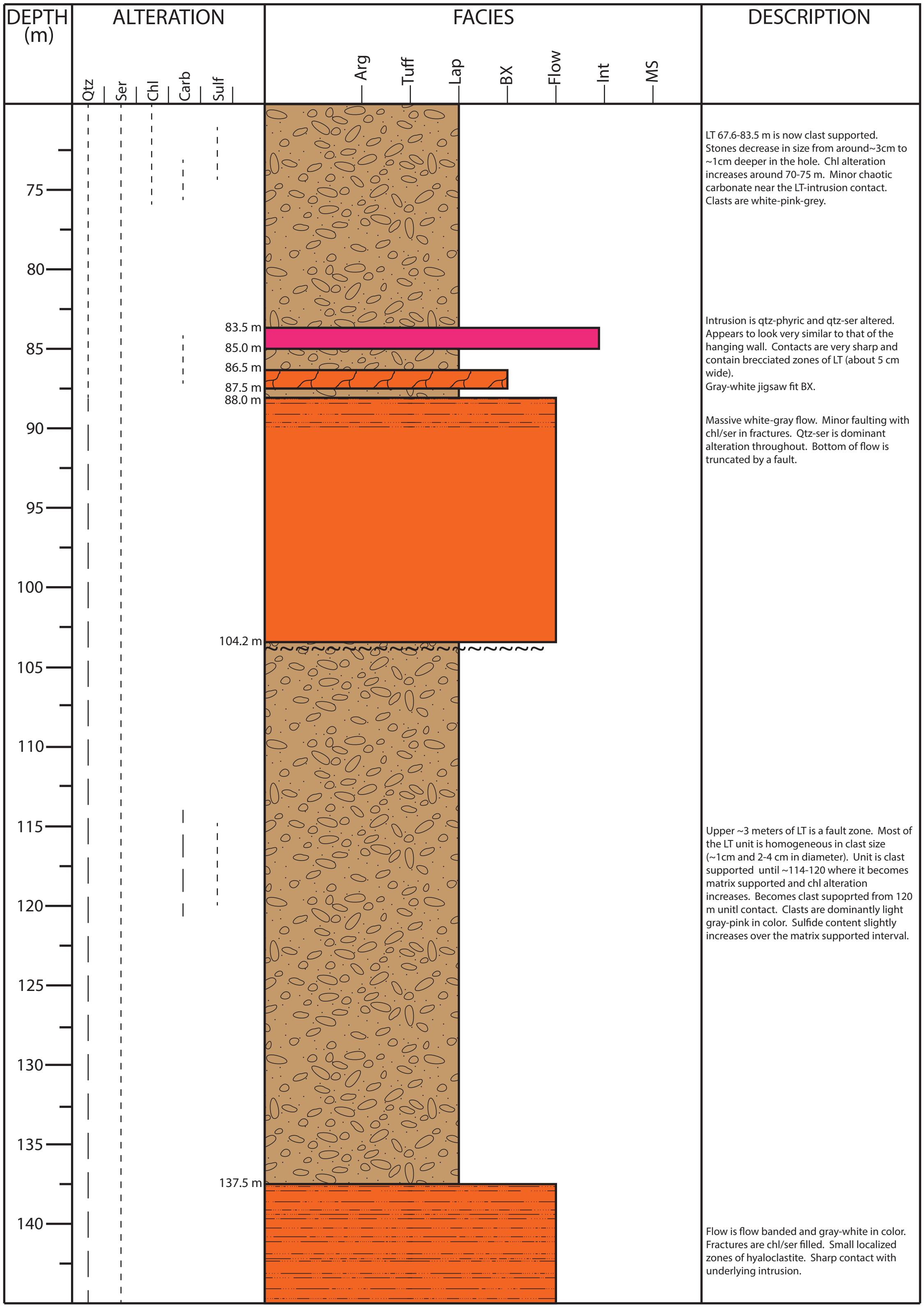
DEPTH (m)
ALTERATION
FACIES
DESCRIPTION
Qtz
Ser
Chl
Carb
Sulf
Arg
Tuff
Lap
BX
Flow
Int
MS
75
80
85
90
95
100
105
110
115
120
125
130
135
140
83.5 m
85.0 m
86.5 m
87.5 m
88.0 m
104.2 m
137.5 m
LT 67.6-83.5 m is now clast supported. Stones decrease in size from around~3cm to ~1cm deeper in the hole. Chl alteration increases around 70-75 m. Minor chaotic carbonate near the LT-intrusion contact. Clasts are white-pink-grey.
Intrusion is qtz-phyric and qtz-ser altered. Appears to look very similar to that of the hanging wall. Contacts are very sharp and contain brecciated zones of LT (about 5 cm wide).
Gray-white jigsaw fit BX.
Massive white-gray flow. Minor faulting with chl/ser in fractures. Qtz-ser is dominant alteration throughout. Bottom of flow is truncated by a fault.
Upper ~3 meters of LT is a fault zone. Most of the LT unit is homogeneous in clast size (~1cm and 2-4 cm in diameter). Unit is clast supported until ~114-120 where it becomes matrix supported and chl alteration increases. Becomes clast supoprted from 120 m unitl contact. Clasts are dominantly light gray-pink in color. Sulfide content slightly increases over the matrix supported interval.
Flow is flow banded and gray-white in color. Fractures are chl/ser filled. Small localized zones of hyaloclastite. Sharp contact with underlying intrusion.

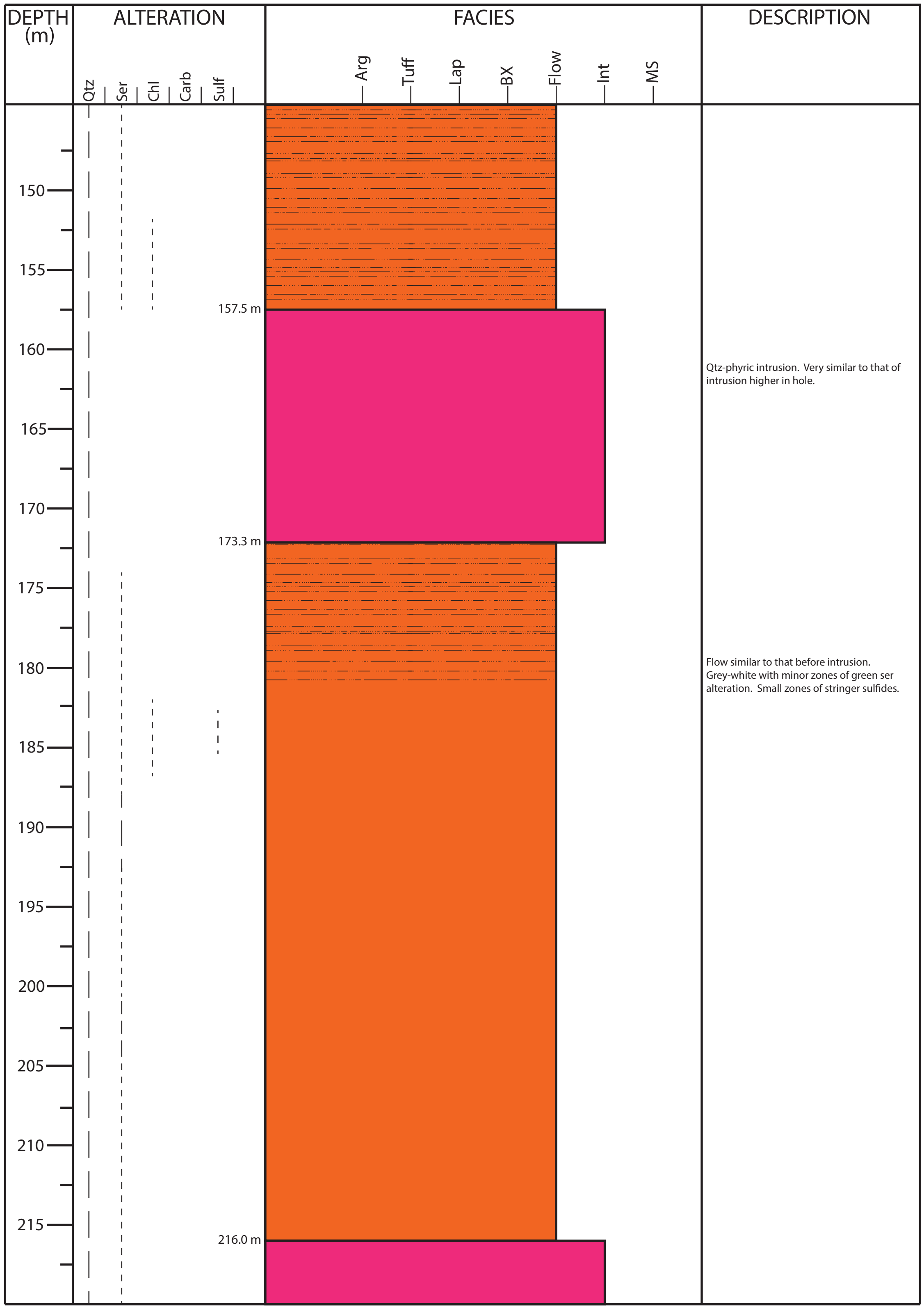
DEPTH (m)
ALTERATION
FACIES
DESCRIPTION
Qtz
Ser
Chl
Carb
Sulf
Arg
Tuff
Lap
BX
Flow
Int
MS
150
155
160
165
170
175
180
185
190
195
200
205
210
215
157.5 m
173.3 m
216.0 m
Qtz-phyric intrusion. Very similar to that of intrusion higher in hole.
Flow similar to that before intrusion. Grey-white with minor zones of green ser alteration. Small zones of stringer sulfides.

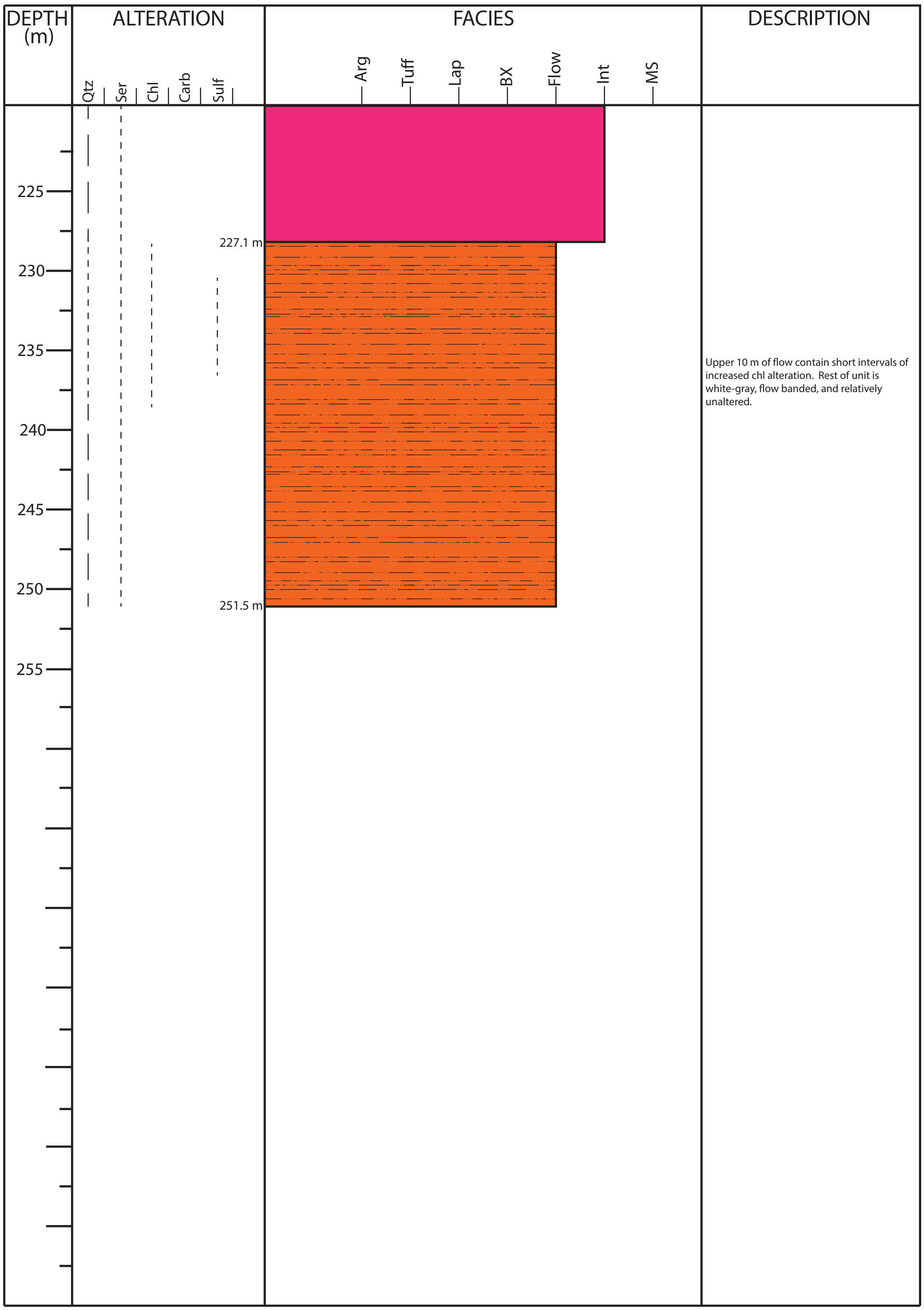
DEPTH (m)
ALTERATION
FACIES
DESCRIPTION
Qtz
Ser
Chl
Carb
Sulf
Arg
Tuff
Lap
BX
Flow
Int
MS
225
230
235
240
245
250
255
227.1 m
251.5 m
Upper 10 m of flow contain short intervals of increased chl alteration. Rest of unit is white-gray, flow banded, and relatively unaltered.

Project: Boundary Diamond Drill Hole: BD11-116 Date: 8-11-2013	UTM 540839.77E 5389619.84N	Azimuth: 360 Dip: -90 Length: 71

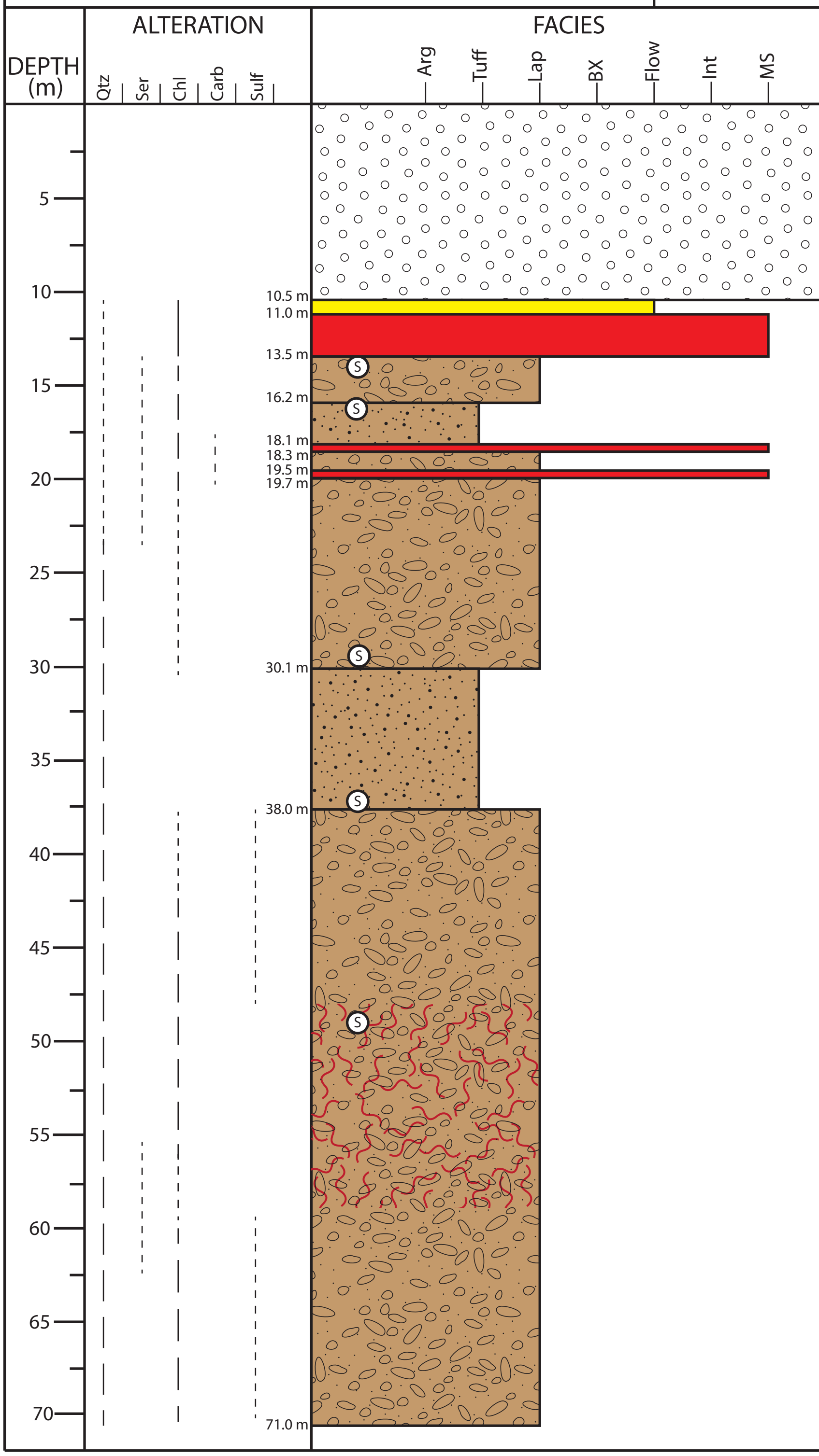

DESCRIPTION

Coarse grained, massive Py near the top. Near the LT contact, Ccp content slightly increases.

Sample: H501258

Sample: H501259

From 13.5-18.1 m, LT and tuff are dark grey to black with some white clasts. The LT is clast supoprted and grades into tuff. Clasts are angular. Lower sulfides are medium grained Py layers. They have sharp lower contacts with no sulfides below.

From ~20-30 m, the top of LT is fine grained clasts <0.5 cm that slowly grade into large clasts (>3 cm) by 25 m. LT is clasts supported and typically medium gray with some clasts having alteration rims.

Sample: H501260

The tuff unit is relatively unaltered. Most grains are <0.5 cm and range from white to dark gray in color. Show graded bedding. Where larger clasts are present, alteration slightly intensifies, but nothing significant.

Sample: H501261

At the top of the LT, clasts are distinctly bimodal (<1 cm and>2 cm). Clasts are generally medium gray, but become darker where chl alteration and dis. Py present. At 45 m clasts become larger (commonly 2-4 cm). Stringer sulfides (Py and Ccp) become prevalent from 47-57 m where LT becomes more matrix supported. Once LT becomes clast supported (57-71 m) sulfides phase out to dis. Py. Chlorite alteration still significant.

Sample: H501262

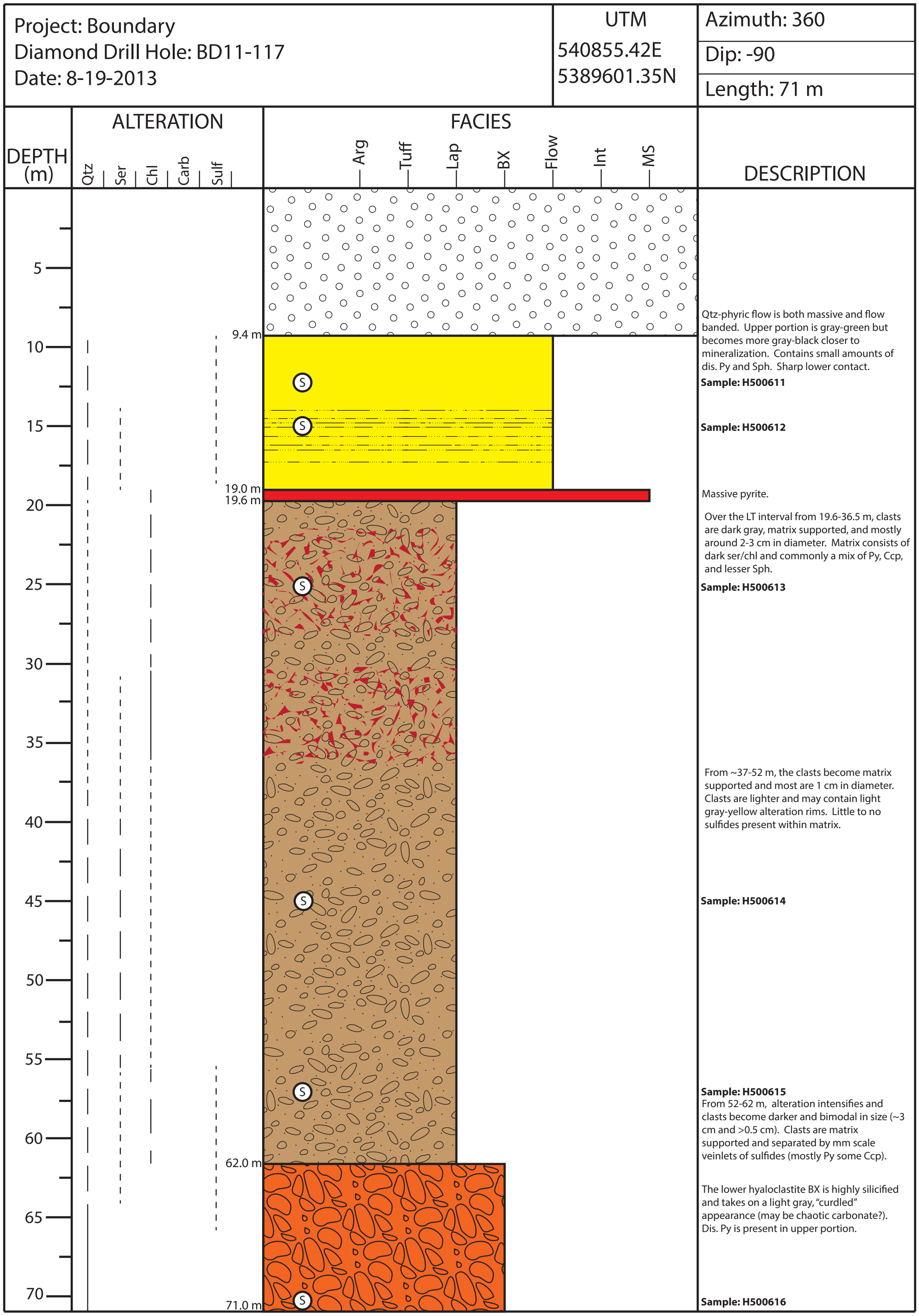
Project: Boundary
Diamond Drill Hole: BD11-117
Date: 8-19-2013
UTM
540855.42E
5389601.35N
Azimuth: 360
Dip: -90
Length: 71 m
DEPTH (m)
ALTERATION
Qtz
Ser
Chl
Carb
Sulf
FACIES
Arg
Tuff
Lap
BX
Flow
Int
MS
DESCRIPTION
5
10
15
20
25
30
35
40
45
50
55
60
65
70
9.4 m
19.0 m
19.6 m
62.0 m
71.0 m
S
Qtz-phyric flow is both massive and flow banded. Upper portion is gray-green but becomes more gray-black closer to mineralization. Contains small amounts of dis. Py and Sph. Sharp lower contact.
Sample: H500611
Sample: H500612
Massive pyrite.
Over the LT interval from 19.6-36.5 m, clasts are dark gray, matrix supported, and mostly around 2-3 cm in diameter. Matrix consists of dark ser/chl and commonly a mix of Py, Ccp, and lesser Sph.
Sample: H500613
From ~37-52 m, the clasts become matrix supported and most are 1 cm in diameter. Clasts are lighter and may contain light gray-yellow alteration rims. Little to no sulfides present within matrix.
Sample: H500614
Sample: H500615
From 52-62 m, alteration intensifies and clasts become darker and bimodal in size (~3 cm and >0.5 cm). Clasts are matrix supported and separated by mm scale veinlets of sulfides (mostly Py some Ccp).
The lower hyaloclastite BX is highly silicified and takes on a light gray, "curdled" appearance (may be chaotic carbonate?). Dis. Py is present in upper portion.
Sample: H500616

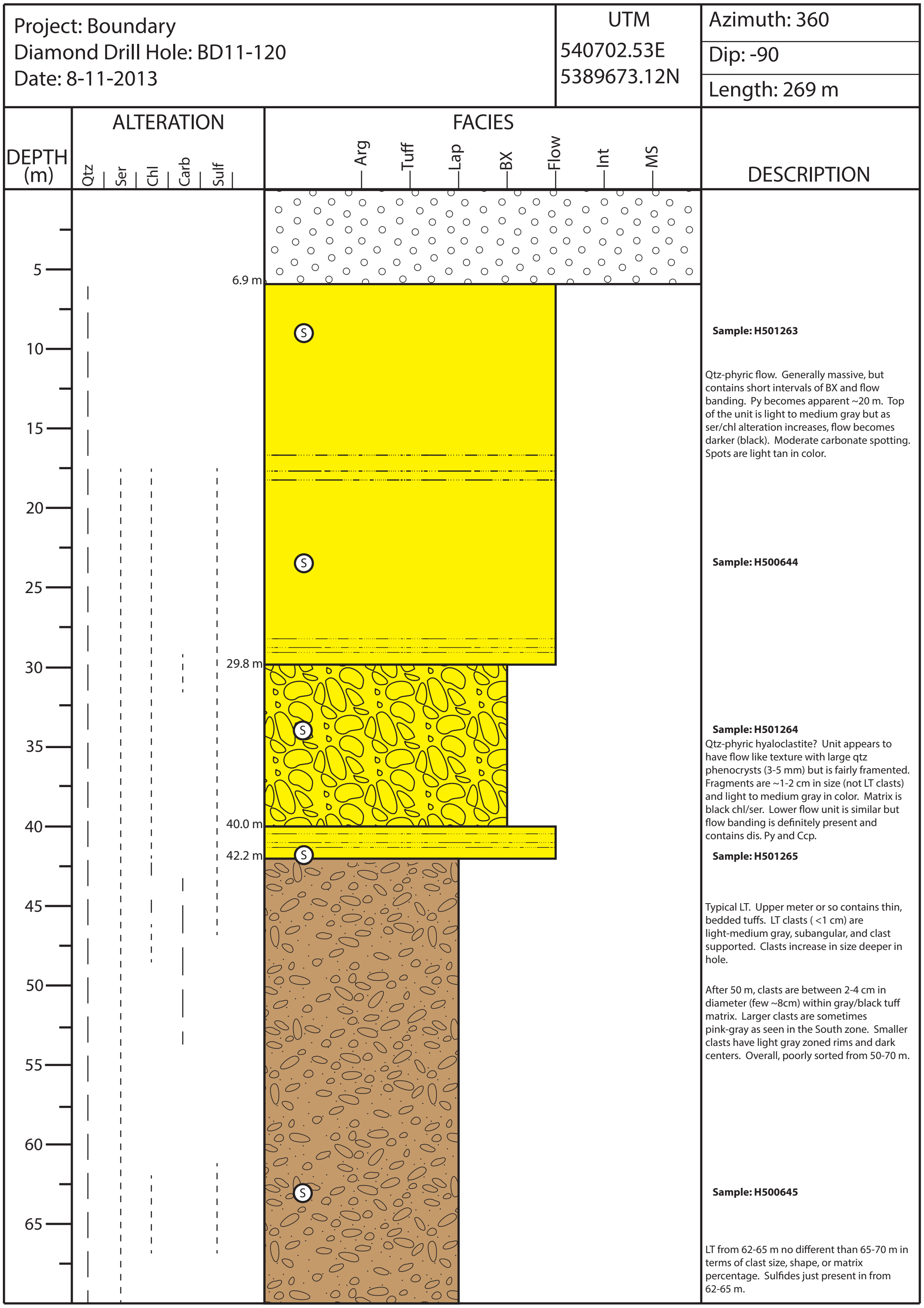

Project: Boundary
Diamond Drill Hole: BD11-120
Date: 8-11-2013
UTM
540702.53E
5389673.12N
Azimuth: 360
Dip: -90
Length: 269 m
DEPTH (m)
ALTERATION
Qtz
Ser
Chl
Carb
Sulf
FACIES
Arg
Tuff
Lap
BX
Flow
Int
MS
DESCRIPTION
5
10
15
20
25
30
35
40
45
50
55
60
65
6.9 m
29.8 m
40.0 m
42.2 m
S
Sample: H501263
Qtz-phyric flow. Generally massive, but contains short intervals of BX and flow banding. Py becomes apparent ~20 m. Top of the unit is light to medium gray but as ser/chl alteration increases, flow becomes darker (black). Moderate carbonate spotting. Spots are light tan in color.
Sample: H500644
Sample: H501264
Qtz-phyric hyaloclastite? Unit appears to have flow like texture with large qtz phenocrysts (3-5 mm) but is fairly framented. Fragments are ~1-2 cm in size (not LT clasts) and light to medium gray in color. Matrix is black chl/ser. Lower flow unit is similar but flow banding is definitely present and contains dis. Py and Ccp.
Sample: H501265
Typical LT. Upper meter or so contains thin, bedded tuffs. LT clasts (<1 cm) are light-medium gray, subangular, and clast supported. Clasts increase in size deeper in hole.
After 50 m, clasts are between 2-4 cm in diameter (few ~8cm) within gray/black tuff matrix. Larger clasts are sometimes pink-gray as seen in the South zone. Smaller clasts have light gray zoned rims and dark centers. Overall, poorly sorted from 50-70 m.
Sample: H500645
LT from 62-65 m no different than 65-70 m in terms of clast size, shape, or matrix percentage. Sulfides just present in from 62-65 m.

Project: Boundary Diamond Drill Hole: BD11-120 Date: 8-11-2013	UTM 540702.53E 5389673.12N	Azimuth: 360 Dip: -90 Length: 269 m

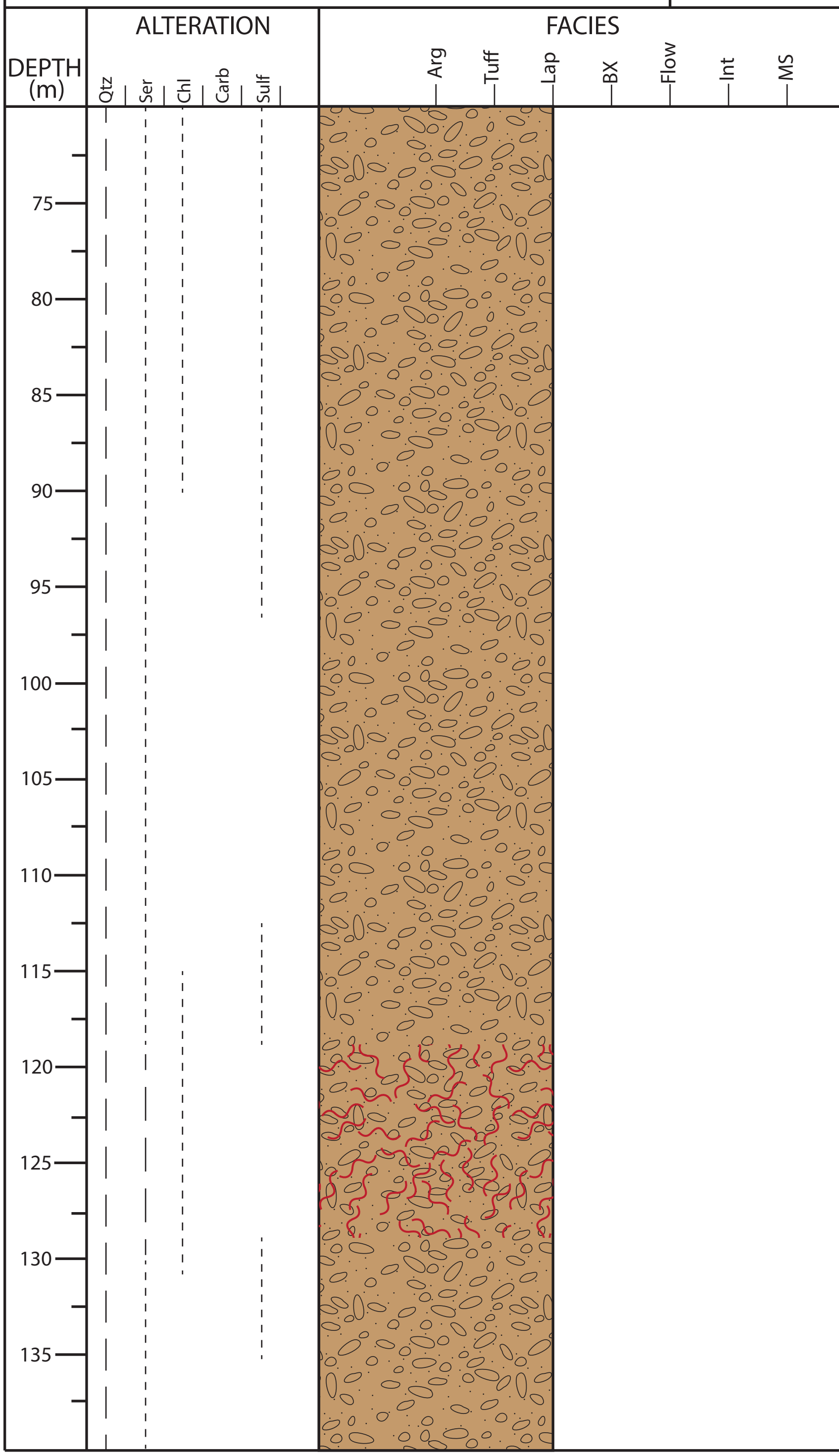

DESCRIPTION

LT clasts are mostly ~1-2 cm by 100 m. Clasts are varying shades of gray within a dark gray/black tuff-sericite matrix. Minor dis. Py throughout.

Interval of stringer Py-Ccp. LT clasts are softer (chl/ser alt.) and slightly darker. Clasts are still subangular, 1-2 cm in diameter, and clast supported.

Project: Boundary Diamond Drill Hole: BD11-120 Date: 8-11-2013	UTM 540702.53E 5389673.12N	Azimuth: 360 Dip: -90 Length: 269 m

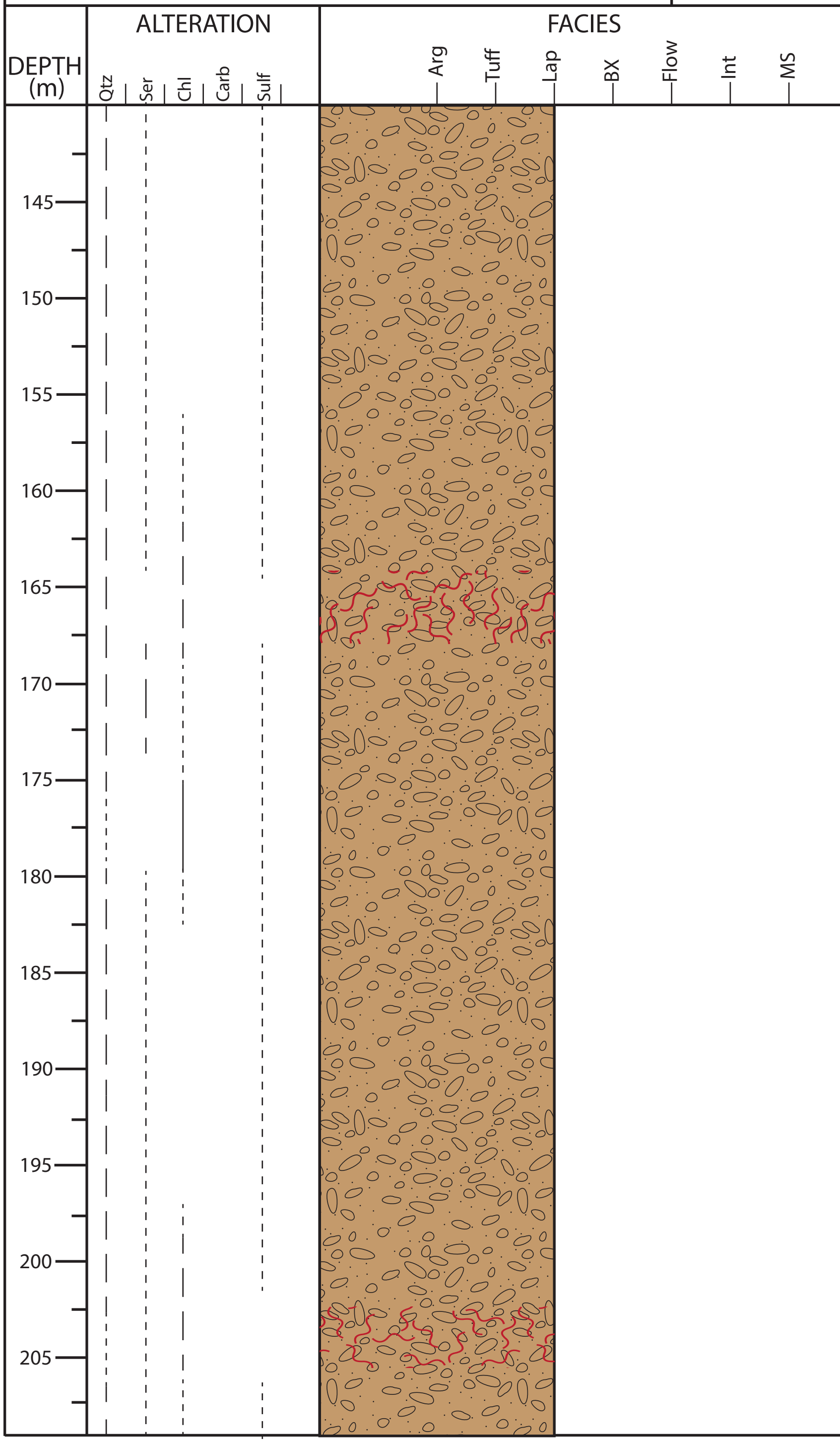

DESCRIPTION

LT clasts slowly increasing in size from ~135-155 m (from ~1 cm up to ~3-4 cm). Over this stretch chl alteration increases. Clasts become darker and dis. Py content increases.

From 167-169 m, interval is marked by several thin layers of strong stringer Py and lesser Ccp (near 50-70%). Percentages are near massive, but sulfides appear to be directional or wormlike (near vertical). Matrix is consists dominantly of black chl.

Few other small intervals of strong stringer Py marked by int. chl alteration, though mostly the rest of the unit is only qtz-ser altered. Clasts appear to be light-medium gray throughout and remain clast supported.

Slight increase in dis. Ccp from 200-210 m.

Project: Boundary Diamond Drill Hole: BD11-120 Date: 8-11-2013	UTM 540702.53E 5389673.12N	Azimuth: 360 Dip: -90 Length: 269 m

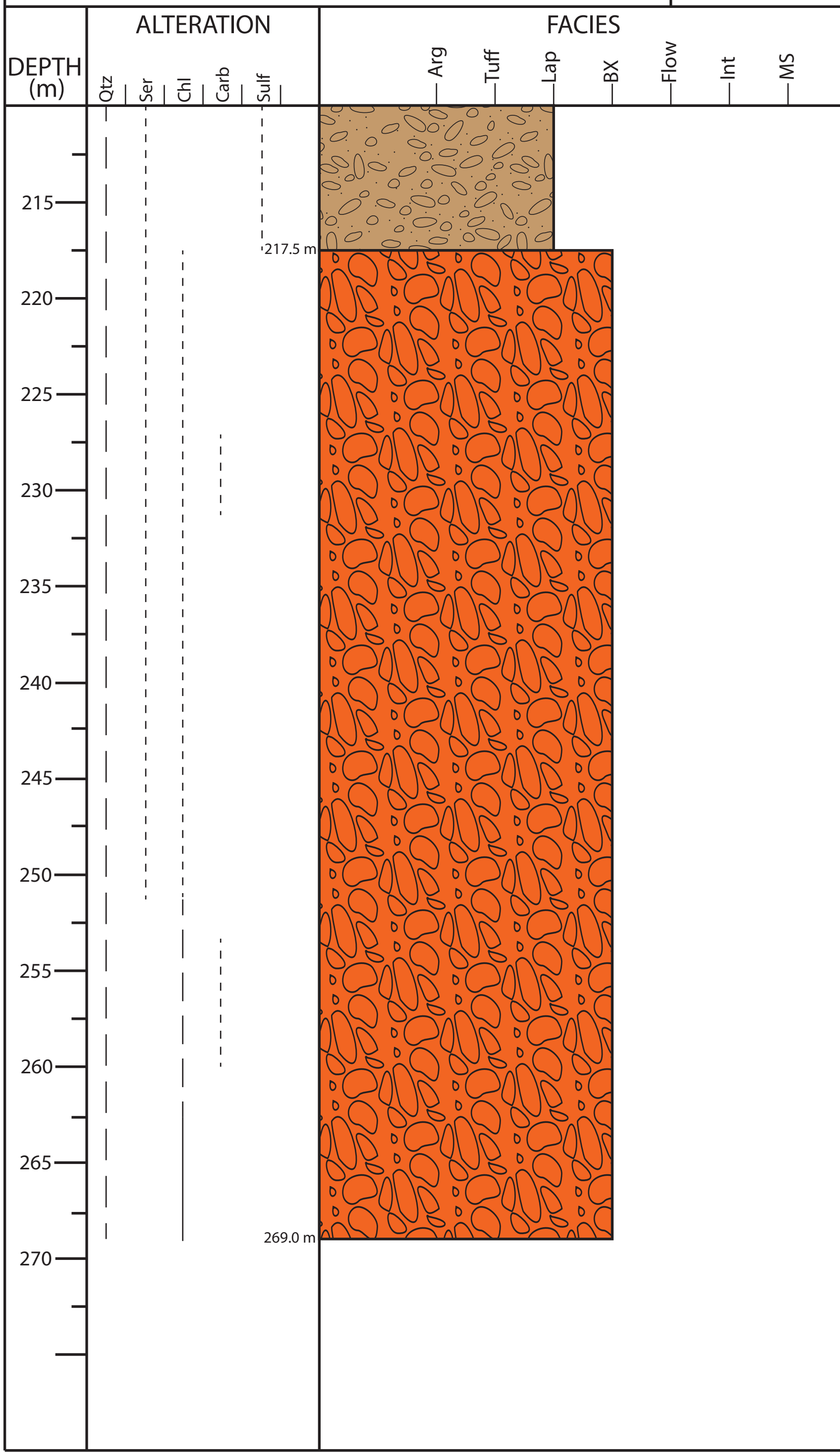

DESCRIPTION

Hyaloclastite is fairly consistent thoughout except for the final 10 m. The unit consists of medium gray fragments in darker gray (qtz-ser) matrix. About half the fragments are flow banded. Multiple meter scale intervals of massive flows throughout. Chlorite alteration and chaotic carbonate alteration increases ~250 m and becomes intense from 260 until the end of the hole.

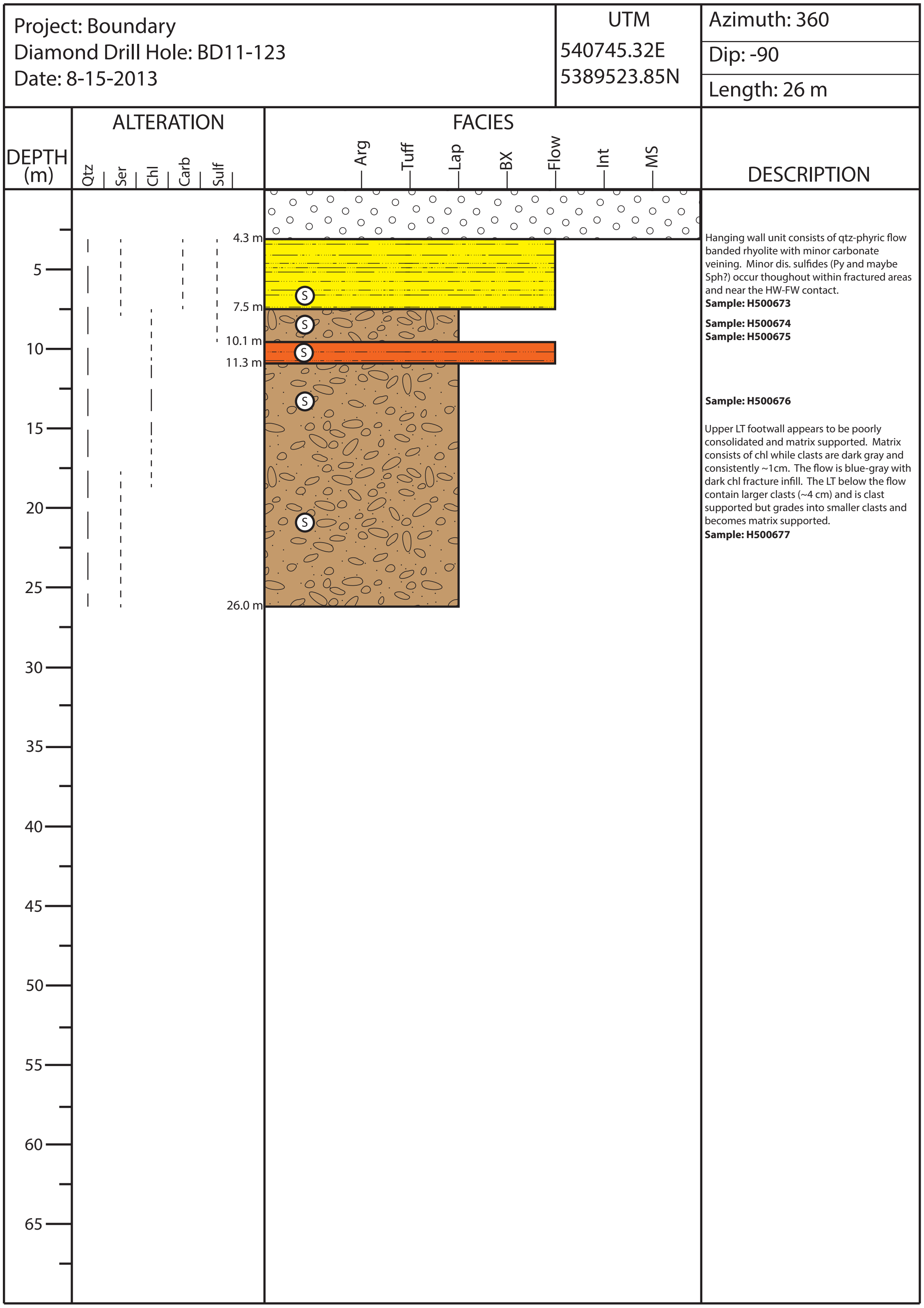
Project: Boundary
Diamond Drill Hole: BD11-123
Date: 8-15-2013
UTM
540745.32E
5389523.85N
Azimuth: 360
Dip: -90
Length: 26 m
DEPTH (m)
ALTERATION
Qtz
Ser
Chl
Carb
Sulf
FACIES
Arg
Tuff
Lap
BX
Flow
Int
MS
DESCRIPTION
5
10
15
20
25
30
35
40
45
50
55
60
65
4.3 m
7.5 m
10.1 m
11.3 m
26.0 m
S
Hanging wall unit consists of qtz-phyric flow banded rhyolite with minor carbonate veining. Minor dis. sulfides (Py and maybe Sph?) occur thoughout within fractured areas and near the HW-FW contact.
Sample: H500673
Sample: H500674
Sample: H500675
Sample: H500676
Upper LT footwall appears to be poorly consolidated and matrix supported. Matrix consists of chl while clasts are dark gray and consistently ~1cm. The flow is blue-gray with dark chl fracture infill. The LT below the flow contain larger clasts (~4 cm) and is clast supported but grades into smaller clasts and becomes matrix supported.
Sample: H500677

Project: Boundary
Diamond Drill Hole: BD11-127
Date: 8-19-2013

UTM
540687.89E
5389495.66N

Azimuth: 360
Dip: -90
Length: 50 m

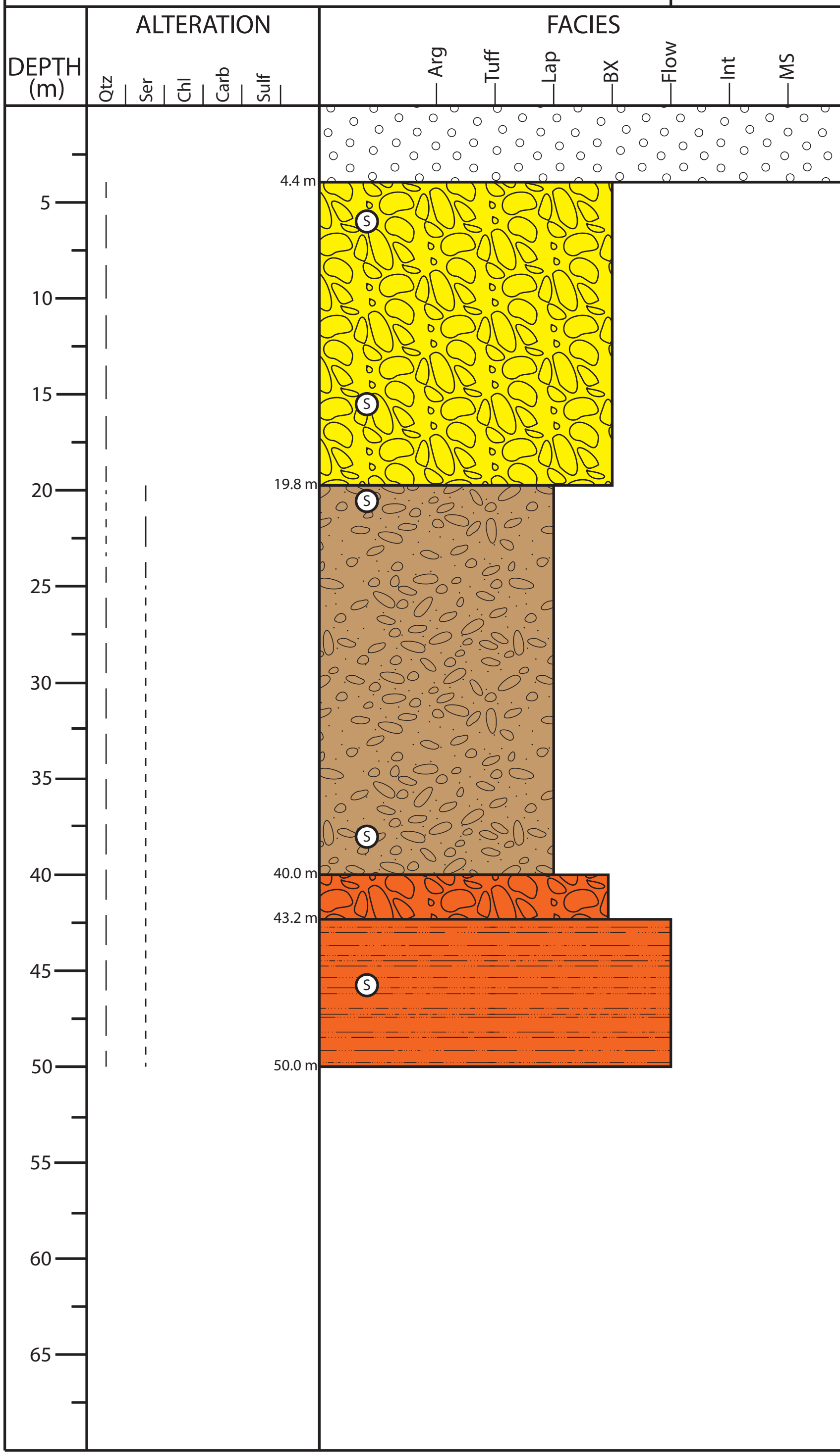

DESCRIPTION

Sample: H501250
Upper portion of BX is less brecciated and light gray in color. Contains large amount of carbonate spots. From ~10m and lower, BX becomes more fragmented. Fragments are wispy and light gray in color whereas matrix is black chl/ser. Minor brown carbonate and small intervals of dis. Py present.

Sample: H501251

Sample: H501252
Contact is sharp between HW and FW. FW LT is a mixture of poorly sorted, angular, yellow-gray clasts that range in size from >0.5 cm up to 4 cm. Larger clasts are sometimes flow banded. By 25 m, clasts are all ~1cm in diameter and do not contain significant ser alt. Clasts are light-medium gray and clast supported. Carbonate spotting is moderate-intense still.

Sample: H501253
Hyaloclastite fragments are light-moderate gray with dark ser alteration in the matrix. No sulfides present. Carbonate spotting still moderate. The underlying flow is flow-banded with alteranating dark ser altered bands and light qtz altered bands. Carbonate spotting is moderate. Minute Py and Ccp present.
Sample: H501254

Project: Boundary Diamond Drill Hole: BD11-128 Date: 8-19-2013	UTM 540602.40E 5389475.67N	Azimuth: 360 Dip: -90 Length: 32 m

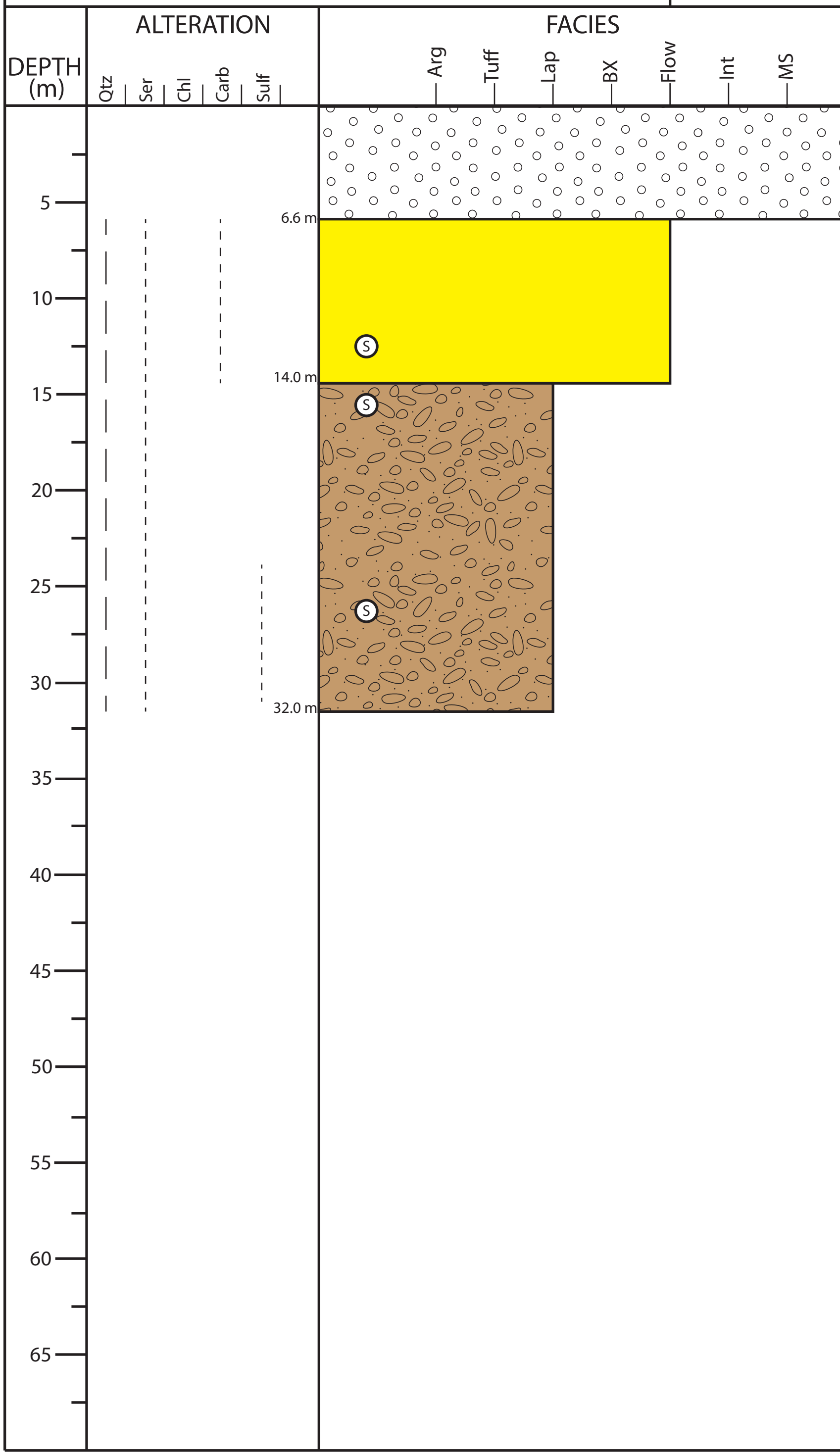

DESCRIPTION

HW: Qtz-phyric massive flow. Unit shows minor carbonate veining throughout but is fairly competent. The flow is dark gray and shows no significant alteration other than silicification.

Sample: H501255

Sample: H501256

The LT from ~15-23 are light grey clasts with no visible matrix. Clast sizes are generally bimodal (1 and 3 cm) and contain minor amounts of sericite along clast bounaries. From 23 m on, clasts become larger (3-4 cm) but but ~1cm clasts still present. Clasts consistent medium gray. Matrix slightly more visible and contains some dis. Py. May mark early transition to an underlying breccia.

Sample: H501257

Project: Boundary Diamond Drill Hole: BD11-129 Date: 8-12-13	UTM 540789.64E 5389563.49N	Azimuth: 360 Dip: -90 Length: 62 m

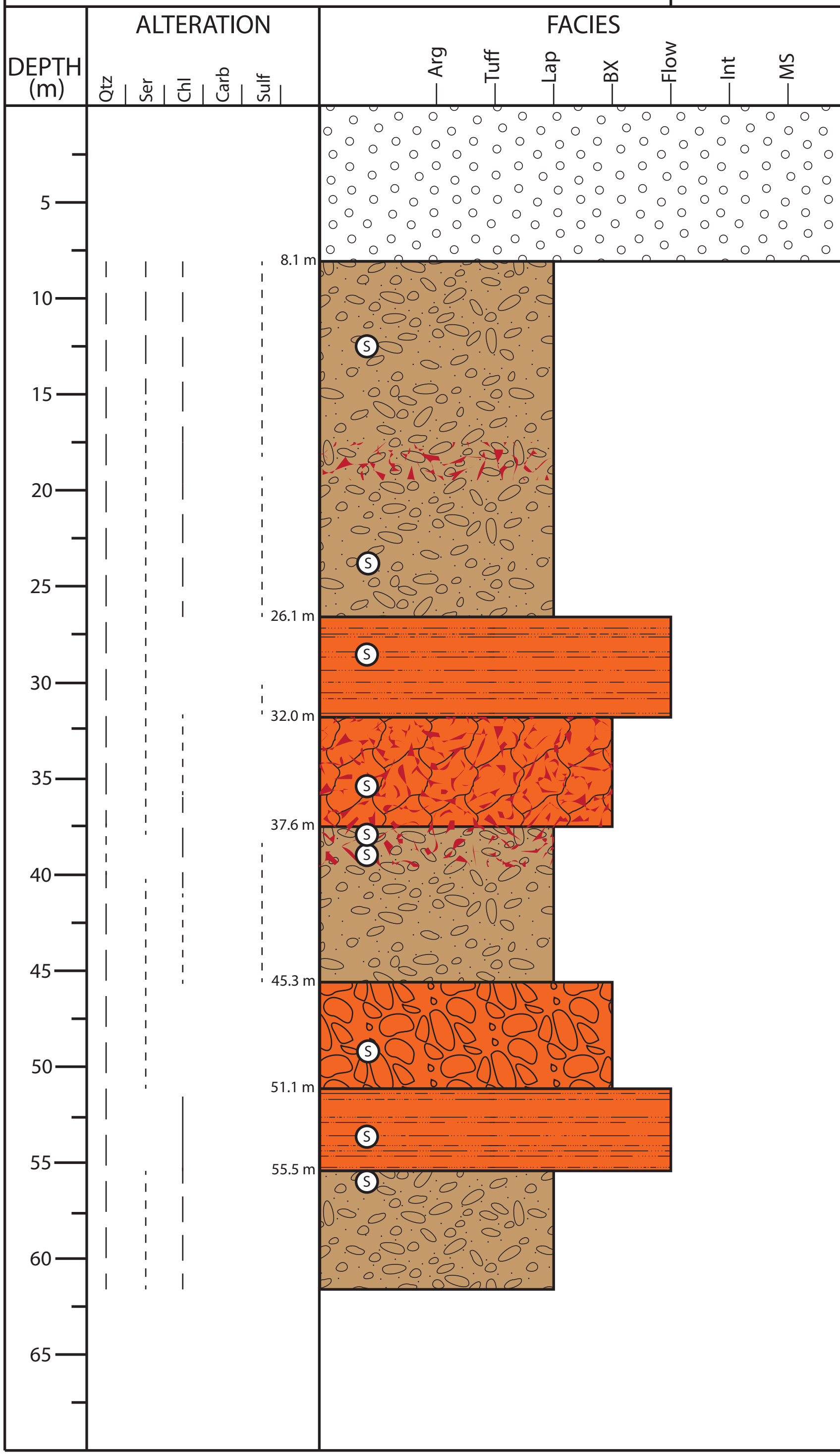

DESCRIPTION

Sample: H500665

Top of LT consists of distinct bimodal clast sizes (<0.5 cm and ~2 cm). Clasts are light to medium gray, angular, and matrix supported. Matrix is black ser/chl. Clasts even out in size (~1cm) and become more clast supported after ~15 m. Near the flow banded contact, As content seemingly increases. Minor dis. Py throughout. Localized zone of Ccpy and moderate-intense chl alteration.

Sample: H500666

Sample: H501361

Dark gray, flow banded, aphyric flow. Darker bands may be slighly chl altered but seem to dominantly be ser altered. Moderate dis. Py (lesser Ccp) located around margins and contact with underlying jigsaw BX. Jigsaw fit BX is dark gray with Py-Ccp filled fractures.

Sample: H500668

Sample: H500667

Sample: H500669

From 37.6-39.0 m, LT consists of large (~3 cm), black, angular clasts with Ccp-Py sulfides within matrix. Rest of LT is lighter gray in color and clasts are all ~1cm. Lesser sulfides within matrix.

Hyaloclastite from 45.3-51.1 m consists of light to medium gray fragments that range in size from 4-8 cm with minor tuff within matrix, though most matrix is black sericite.

Sample: H500670

Flow banded flow is intensely chl altered with lighter bands of quartz present. No sulfides just altered.

Sample: H500671

Sample: H500672

Lower LT unit is moderately chl altered but no sulfides. Unit is matrix (ser) supported with ~1 cm, grey-white, rounded clasts.

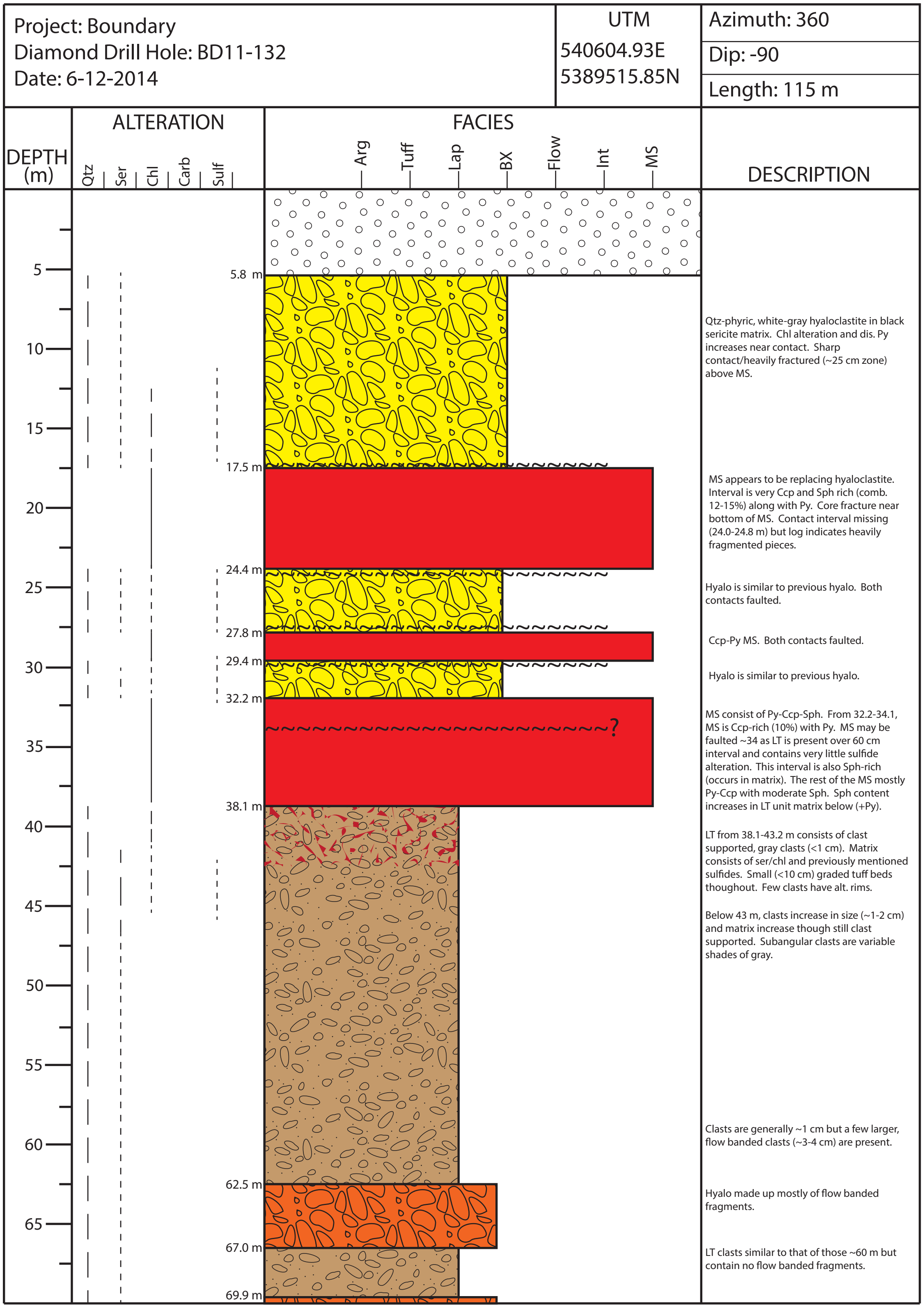

Project: Boundary
Diamond Drill Hole: BD11-132
Date: 6-12-2014
UTM
540604.93E
5389515.85N
Azimuth: 360
Dip: -90
Length: 115 m
DEPTH (m)
ALTERATION
Qtz
Ser
Chl
Carb
Sulf
FACIES
Arg
Tuff
Lap
BX
Flow
Int
MS
DESCRIPTION
5
10
15
20
25
30
35
40
45
50
55
60
65
5.8 m
17.5 m
24.4 m
27.8 m
29.4 m
32.2 m
38.1 m
62.5 m
67.0 m
69.9 m
?
Qtz-phyric, white-gray hyaloclastite in black sericite matrix. Chl alteration and dis. Py increases near contact. Sharp contact/heavily fractured (~25 cm zone) above MS.
MS appears to be replacing hyaloclastite. Interval is very Ccp and Sph rich (comb. 12-15%) along with Py. Core fracture near bottom of MS. Contact interval missing (24.0-24.8 m) but log indicates heavily fragmented pieces.
Hyalo is similar to previous hyalo. Both contacts faulted.
Ccp-Py MS. Both contacts faulted.
Hyalo is similar to previous hyalo.
MS consist of Py-Ccp-Sph. From 32.2-34.1, MS is Ccp-rich (10%) with Py. MS may be faulted ~34 as LT is present over 60 cm interval and contains very little sulfide alteration. This interval is also Sph-rich (occurs in matrix). The rest of the MS mostly Py-Ccp with moderate Sph. Sph content increases in LT unit matrix below (+Py).
LT from 38.1-43.2 m consists of clast supported, gray clasts (<1 cm). Matrix consists of ser/chl and previously mentioned sulfides. Small (<10 cm) graded tuff beds thoughout. Few clasts have alt. rims.
Below 43 m, clasts increase in size (~1-2 cm) and matrix increase though still clast supported. Subangular clasts are variable shades of gray.
Clasts are generally ~1 cm but a few larger, flow banded clasts (~3-4 cm) are present.
Hyalo made up mostly of flow banded fragments.
LT clasts similar to that of those ~60 m but contain no flow banded fragments.

Project: Boundary Diamond Drill Hole: BD11-132 Date: 6-12-2014	UTM 540604.93E 5389515.85N	Azimuth: 360 Dip: -90 Length: 110 m

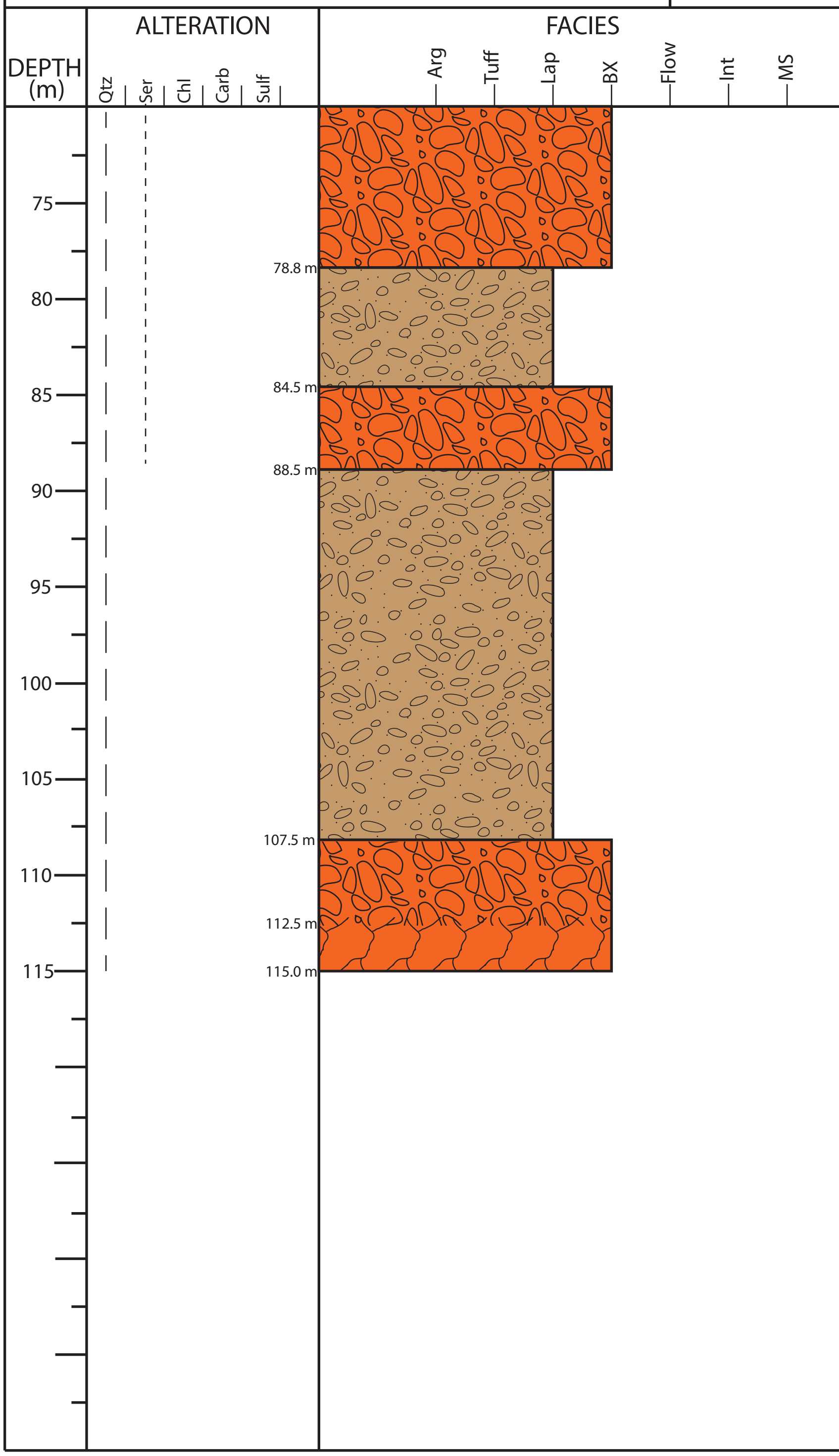

DESCRIPTION

Hyalo similar to previous.

LT clasts are bimodal in size (1-2 cm and <0.5 cm), light-medium gray, and clast supported within a light gray tuff matrix.

Hyalo similar to previous.

LT clasts are bimodal in size (1-2 cm and <0.5 cm), light-medium gray, and clast supported within a light gray tuff matrix. No apparent alteration other than qtz.

Hyaloclastite that grades into jigsaw fit breccia. Unit is light gray with slightly darker gray fractures. No sulifdes or discernable alt.

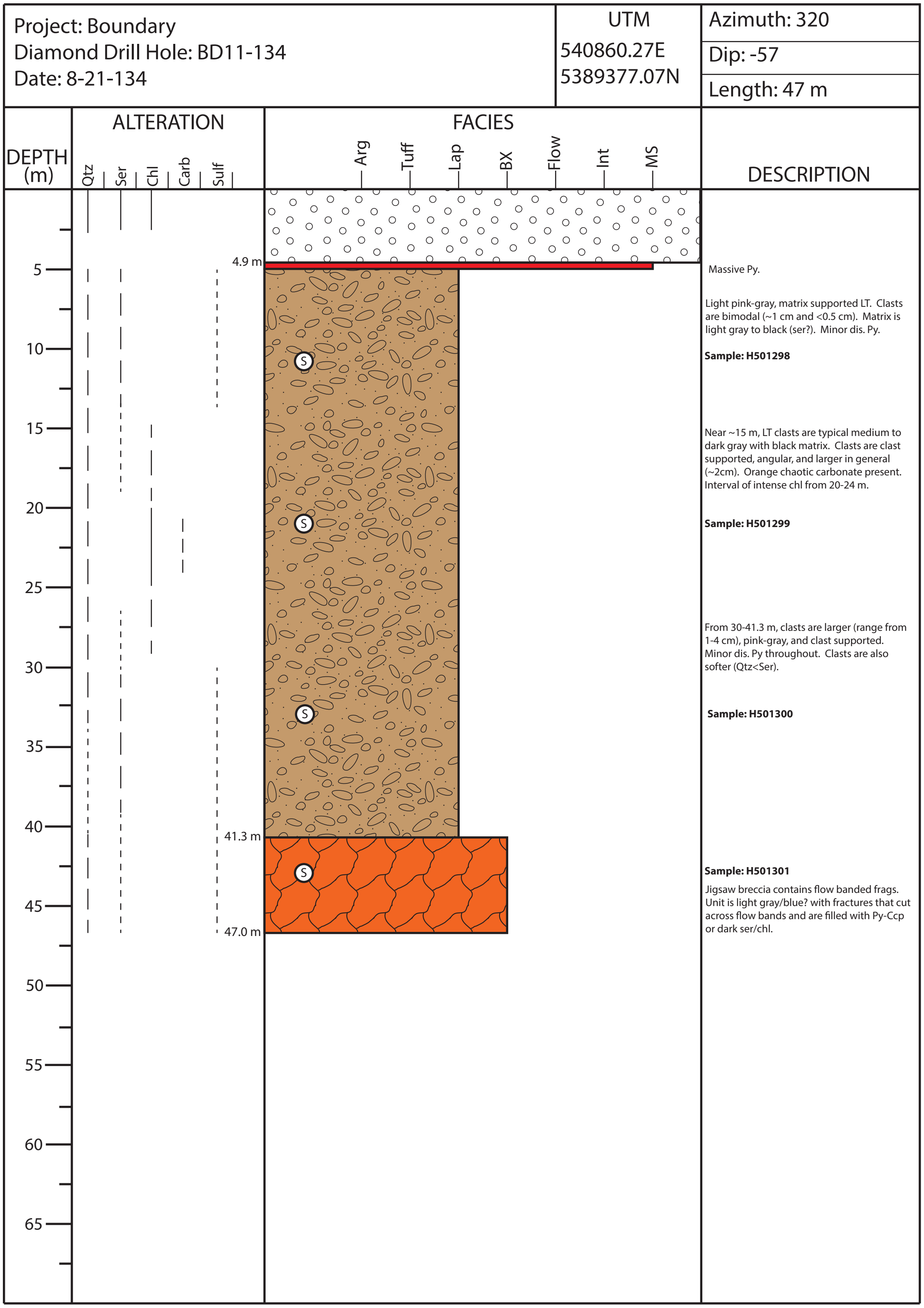

Project: Boundary
Diamond Drill Hole: BD11-134
Date: 8-21-134
UTM
540860.27E
5389377.07N
Azimuth: 320
Dip: -57
Length: 47 m
DEPTH (m)
ALTERATION
Qtz
Ser
Chl
Carb
Sulf
FACIES
Arg
Tuff
Lap
BX
Flow
Int
MS
DESCRIPTION
5
10
15
20
25
30
35
40
45
50
55
60
65
4.9 m
41.3 m
47.0 m
S
Massive Py.
Light pink-gray, matrix supported LT. Clasts are bimodal (~1 cm and <0.5 cm). Matrix is light gray to black (ser?). Minor dis. Py.
Sample: H501298
Near ~15 m, LT clasts are typical medium to dark gray with black matrix. Clasts are clast supported, angular, and larger in general (~2cm). Orange chaotic carbonate present. Interval of intense chl from 20-24 m.
Sample: H501299
From 30-41.3 m, clasts are larger (range from 1-4 cm), pink-gray, and clast supported. Minor dis. Py throughout. Clasts are also softer (Qtz<Ser).
Sample: H501300
Sample: H501301
Jigsaw breccia contains flow banded frags. Unit is light gray/blue? with fractures that cut across flow bands and are filled with Py-Ccp or dark ser/chl.

Project: Boundary Diamond Drill Hole: BD11-136 Date: 8-21-2013	UTM 540884.00E 5389400.00N	Azimuth: 360 Dip: -90 Length: 32 m

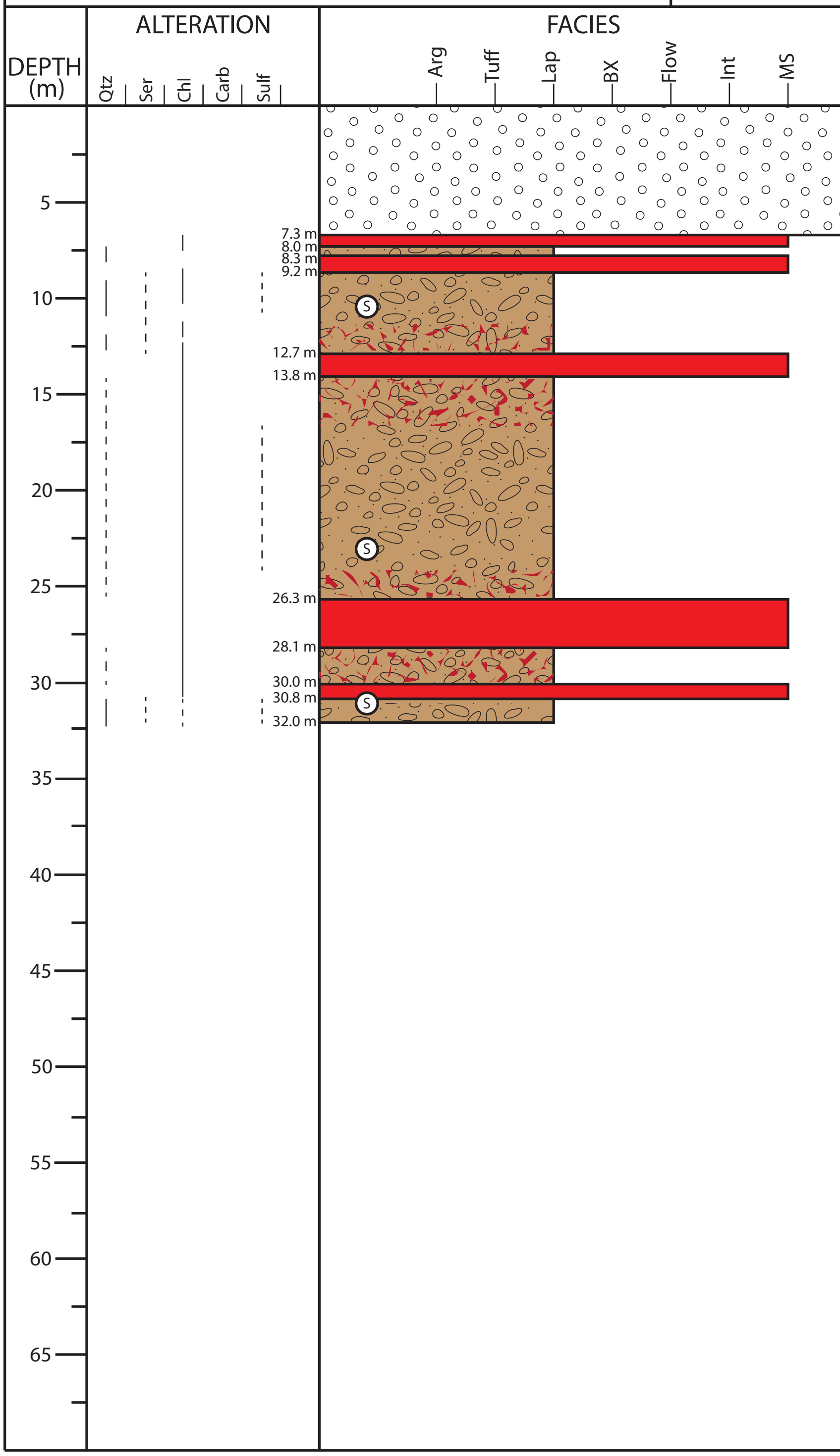

DESCRIPTION

Two MS units are Py-Ccp (very minor Sph). LT in between is mostly chl altered but clasts are visible. Clasts are dark gray, matrix supported, and ~1 cm in diameter.

Sample: H501309

LT from 9.2-12.7 m is matrix supported. Clasts are angular, light-dark gray (zoned rims), and all <1 cm in diameter. Matrix is dark gray and consists of Py and sericite.

MS (12.7-13.8 m) is Py-Ccp.

Most of the LT unit is black (int. chl) but some dark gray clasts visible. When visible, clasts are matrix supported, rounded, and ~1.5 cm in diameter. Matrix sulfides are dominantly Py.

Sample: H501310

MS is massive Py.

LT from 28.1-32.0 m is clast supported. Clasts are bimodal (~1.5 and <0.5 cm), pink-gray, and subangular. Matrix is dark gray and consists of PY or chlorite? MS is Py.

Sample: H501311

Project: Boundary Diamond Drill Hole: BD11-143 Date: 8-21-2013	UTM 540823.49E 5389263.81N	Azimuth: 360 Dip: -90 Length: 29 m

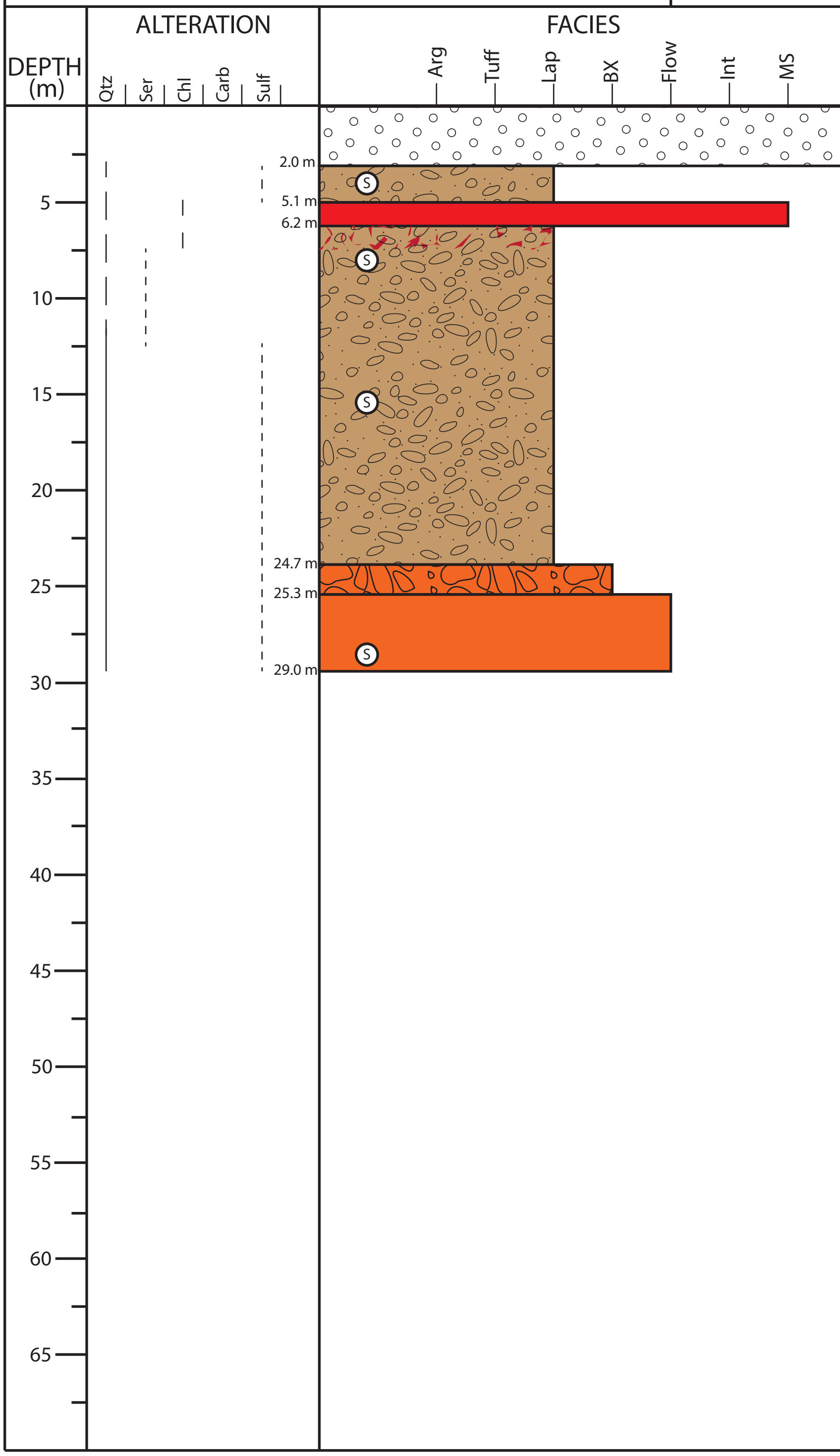

DESCRIPTION

Sample: H501294

Sample: H501295

The entire LT unit appears to be significantly qtz altered. The portion above the hole is clast supported (no matrix) and white in color with minor dis. Py. The massive sulfide is massive Py with replacement Py below. The clasts between 6-12 m appear to be moderately qtz-ser and are varying shades of white and pink. Minimal to no matrix.

Sample: H501296

Below 12 m, the LT becomes extremely silicified and light grey to white in color. Clast size and martix increase with depth but qtz alteration persists. Carbonate spots are more red in color. The lower breccia and flow are very similar in color and alteration to the LT. Both are bleached white with red carbonate spots.

Sample: H501297

Project: Boundary Diamond Drill Hole: BD11-146 Date:8-21-2013	UTM 540823.49E 5389263.81N	Azimuth: 360 Dip: -90 Length: 17 m

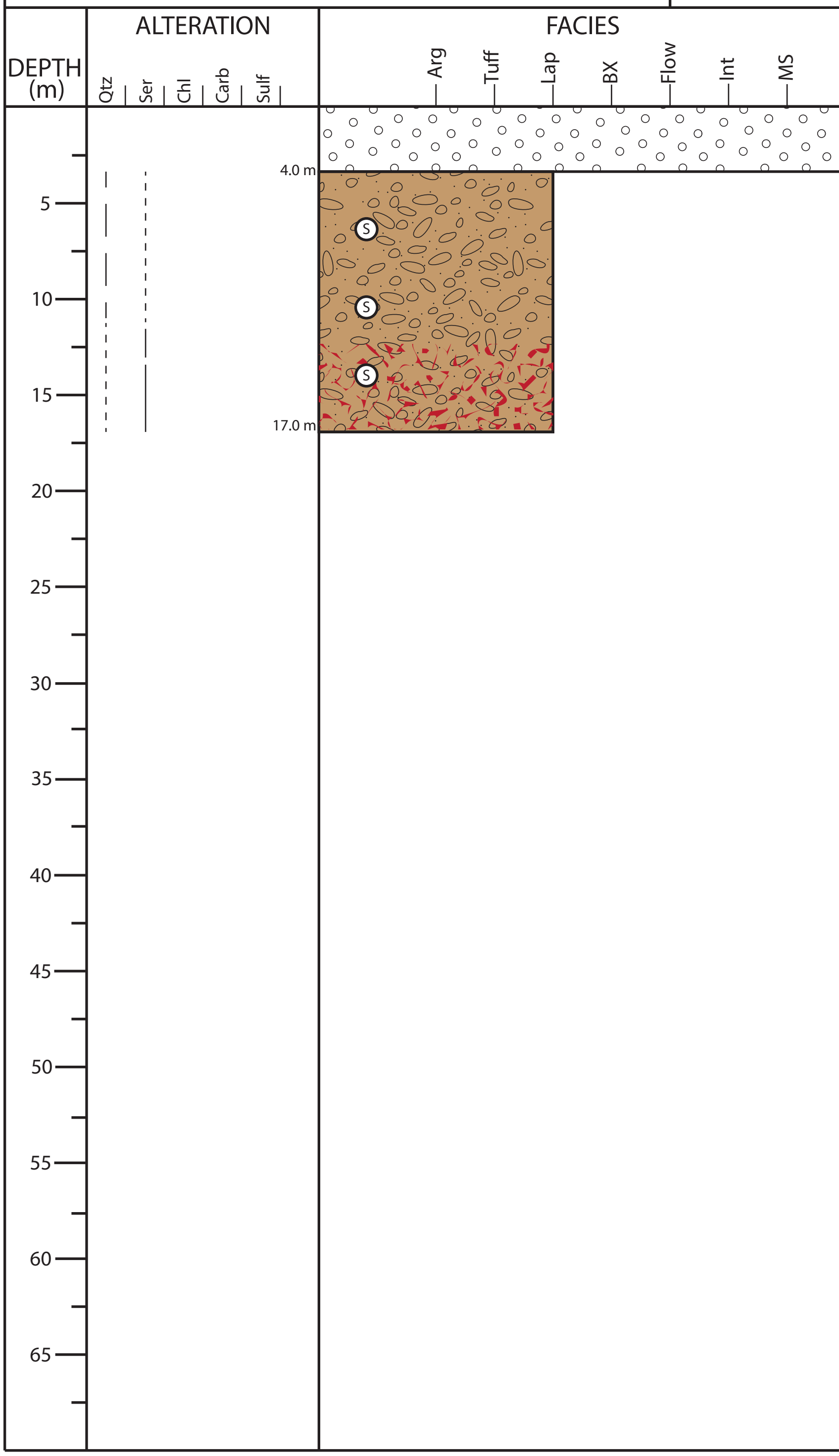

DESCRIPTION

Sample: H501291

Sample: H501292

Sample: H501293

Upper ten meters of LT is relatively unaltered. Most clasts are bimodal in size (~1cm and ~4cm). Clast supported. Clasts are generally gray with some rims. Sulfides not prevalent in upper portion. Below ten meters, LT dramatically changes. Only large clasts (>3cm) are left and everything else was subject to sulfide (Py) replacement. Matrix supported. Remainder clasts have 1-2 cm yellow/green rim with dark center. Rims are intense sericite altered.

Project: Boundary
Diamond Drill Hole: BD11-154
Date: 8-21-2013

UTM
54089.22E
5389415.15N

Azimuth: 360
Dip: -90
Length: 32 m

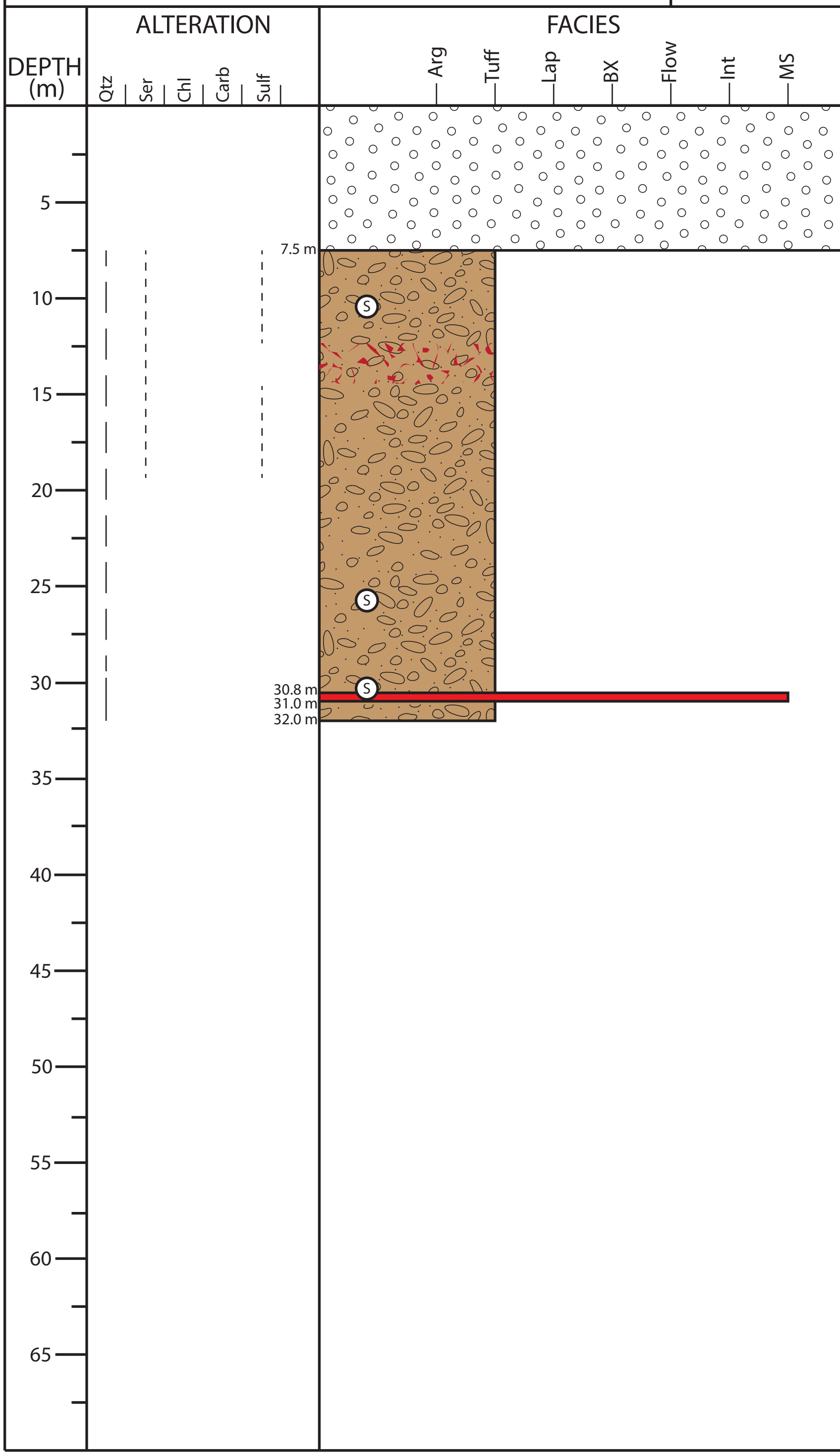

DESCRIPTION

Sample: H501302

Most of the LT unit is matrix supported and consists of large (>2 cm), angular clasts. Clasts vary in color. Near top, they are gray-yellow, the middle is gray-white, and lower portion is white and pink/purple. The LT is clast supported in the lower 5 m of the hole. The replacement sulfides are predominantly Py with minor Ccp. The clasts have white rims and dark cores. The lower sulfide layer (30.8 m) is a thin layer of massive Py bound by sharp contacts both above and below.

Sample: H501303

Sample: H501304

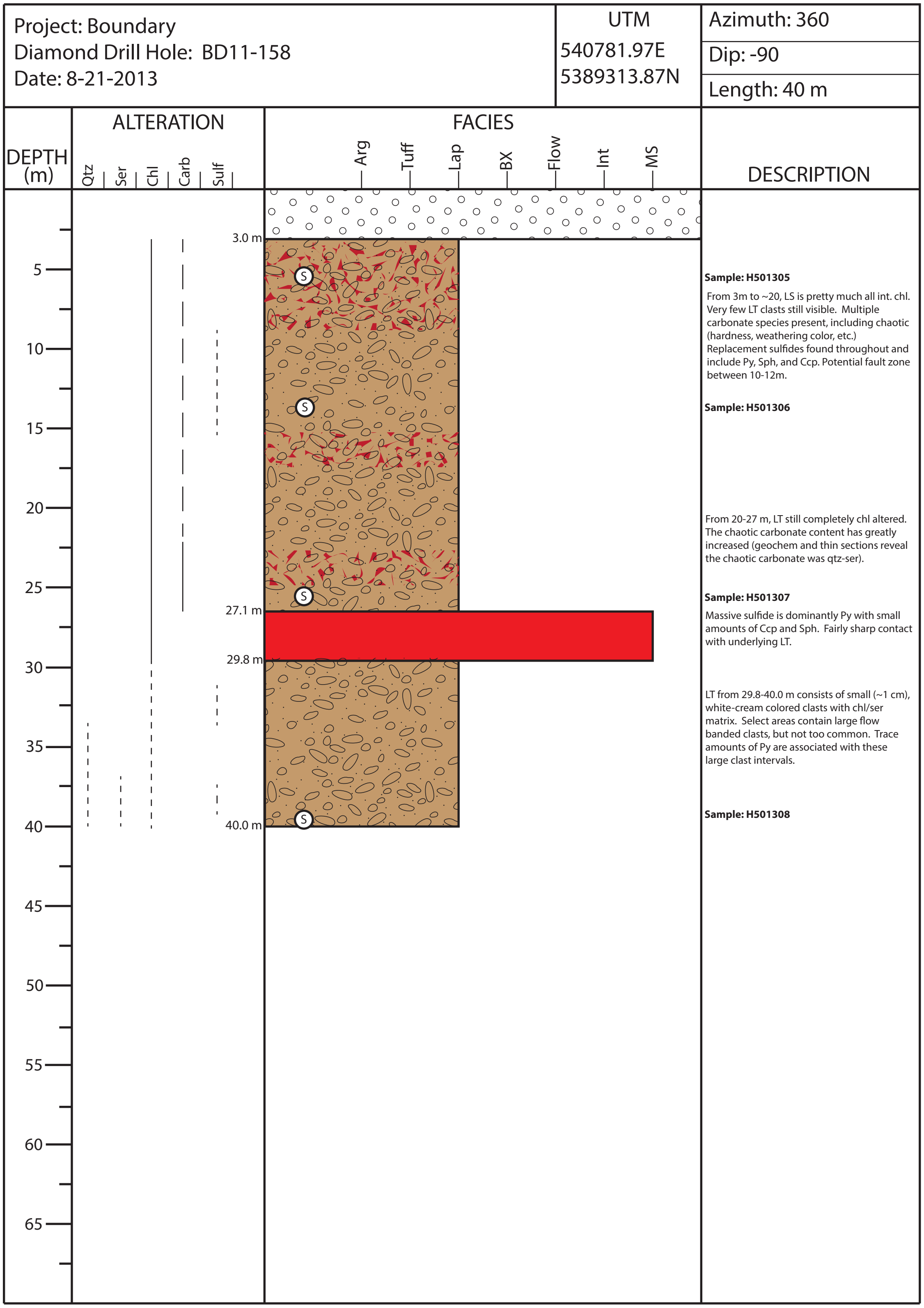
Project: Boundary
Diamond Drill Hole: BD11-158
Date: 8-21-2013
UTM
540781.97E
5389313.87N
Azimuth: 360
Dip: -90
Length: 40 m
DEPTH (m)
ALTERATION
Qtz
Ser
Chl
Carb
Sulf
FACIES
Arg
Tuff
Lap
BX
Flow
Int
MS
DESCRIPTION
5
10
15
20
25
30
35
40
45
50
55
60
65
3.0 m
27.1 m
29.8 m
40.0 m
S
Sample: H501305
From 3m to ~20, LS is pretty much all int. chl. Very few LT clasts still visible. Multiple carbonate species present, including chaotic (hardness, weathering color, etc.) Replacement sulfides found throughout and include Py, Sph, and Ccp. Potential fault zone between 10-12m.
Sample: H501306
From 20-27 m, LT still completely chl altered. The chaotic carbonate content has greatly increased (geochem and thin sections reveal the chaotic carbonate was qtz-ser).
Sample: H501307
Massive sulfide is dominantly Py with small amounts of Ccp and Sph. Fairly sharp contact with underlying LT.
LT from 29.8-40.0 m consists of small (~1 cm), white-cream colored clasts with chl/ser matrix. Select areas contain large flow banded clasts, but not too common. Trace amounts of Py are associated with these large clast intervals.
Sample: H501308

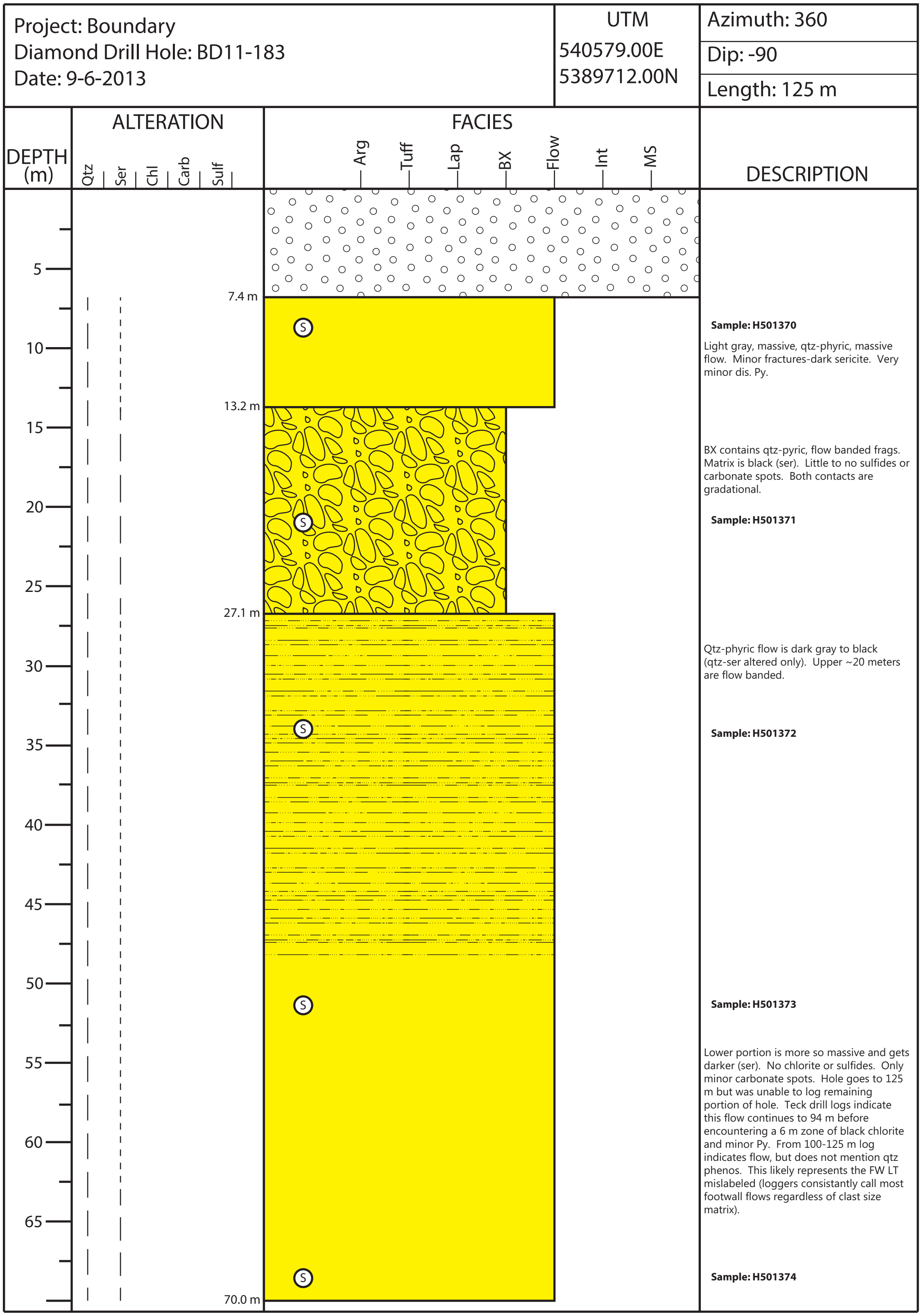
Project: Boundary
Diamond Drill Hole: BD11-183
Date: 9-6-2013
UTM
540579.00E
5389712.00N
Azimuth: 360
Dip: -90
Length: 125 m
DEPTH (m)
ALTERATION
Qtz
Ser
Chl
Carb
Sulf
FACIES
Arg
Tuff
Lap
BX
Flow
Int
MS
DESCRIPTION
5
10
15
20
25
30
35
40
45
50
55
60
65
7.4 m
13.2 m
27.1 m
70.0 m
S
Sample: H501370
Light gray, massive, qtz-phyric, massive flow. Minor fractures-dark sericite. Very minor dis. Py.
BX contains qtz-pyric, flow banded frags. Matrix is black (ser). Little to no sulfides or carbonate spots. Both contacts are gradational.
Sample: H501371
Qtz-phyric flow is dark gray to black (qtz-ser altered only). Upper ~20 meters are flow banded.
Sample: H501372
Sample: H501373
Lower portion is more so massive and gets darker (ser). No chlorite or sulfides. Only minor carbonate spots. Hole goes to 125 m but was unable to log remaining portion of hole. Teck drill logs indicate this flow continues to 94 m before encountering a 6 m zone of black chlorite and minor Py. From 100-125 m log indicates flow, but does not mention qtz phenos. This likely represents the FW LT mislabeled (loggers consistantly call most footwall flows regardless of clast size matrix).
Sample: H501374

Project: Boundary
Diamond Drill Hole: BD11-189
Date: 8-24-2013

UTM
540958.00E
5389452.00N

Azimuth: 360
Dip: -90
Length: 40 m

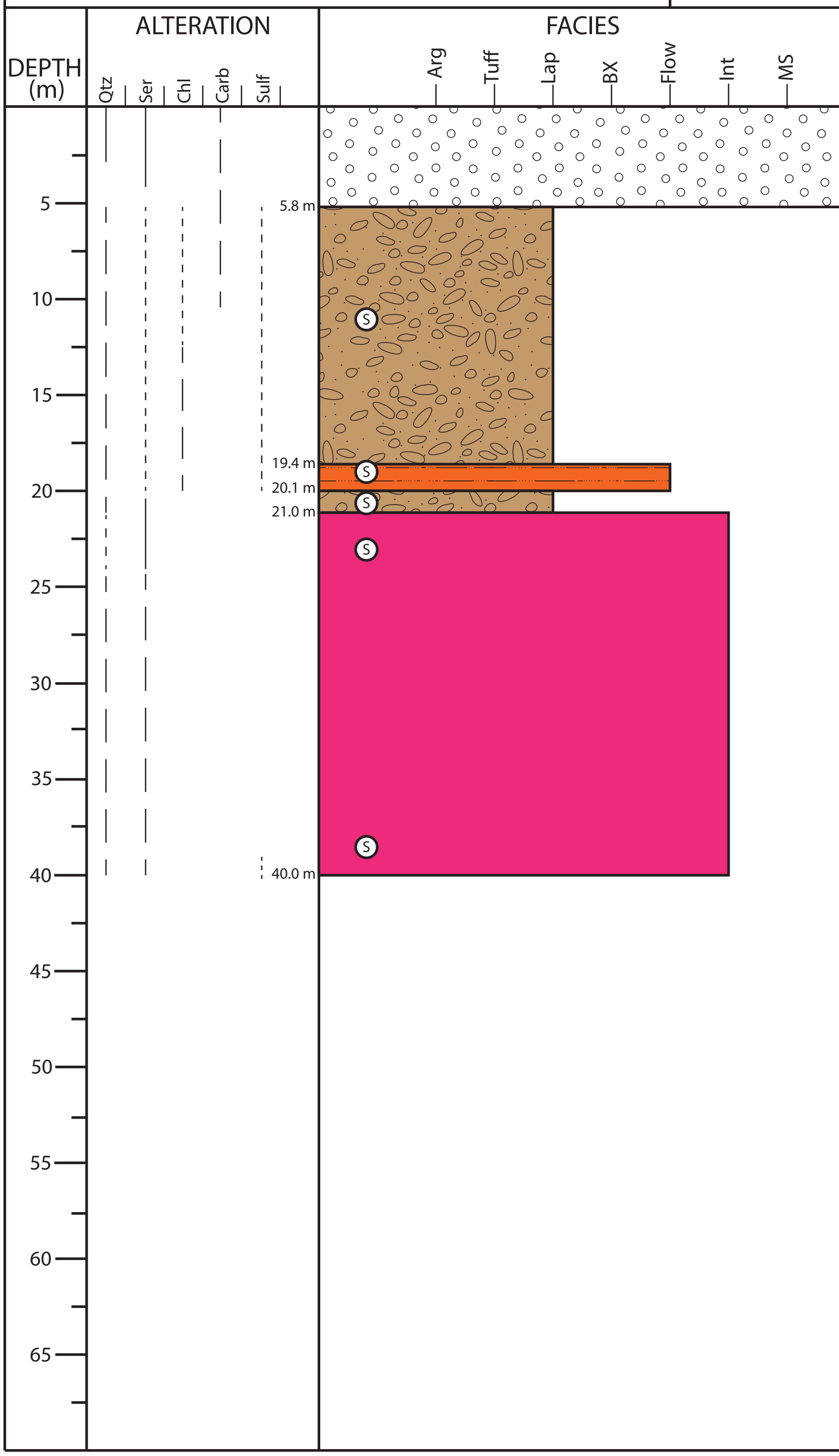

DESCRIPTION

Sample: H501345

From 5.8-19.4 m LT consists of large (3-4cm) brown-gray clasts with tuff/argillite? matrix. LT is clast supported and contains trace amoounts of dis. Py. Underlying flow banded unit contains moderate-intense chl alteration. Some bands appear to be replaced by either qtz or carbonate. The lower LT consists of gray, bimodal (<0.5 cm and 1cm) clasts. Matrix supported (black ser).

Sample: H501346

Sample: H501347

Sample: H501348

Unit is qtz-phyric. Irregular contact with LT but does not look faulted. Upper ~4 appears to be almost flow banded in appearance and is sigficantly sericite altered (dark green and black). After period of intense alteration, unit looks very similar to massive hanging wall flows seen elsewhere. The intrusion is gray in color, massive , and contains qtz phenocrysts, though in lower proportions than typical HW. Entire hole has typical beige-brown carbonate spots. Dis. Py near very end of hole.

Sample: H501349

Project: Boundary Diamond Drill Hole: BD11-190 Date: 8-23-2013	UTM 540919.78E 5389438.01N	Azimuth: 360 Dip: -90 Length: 40 m

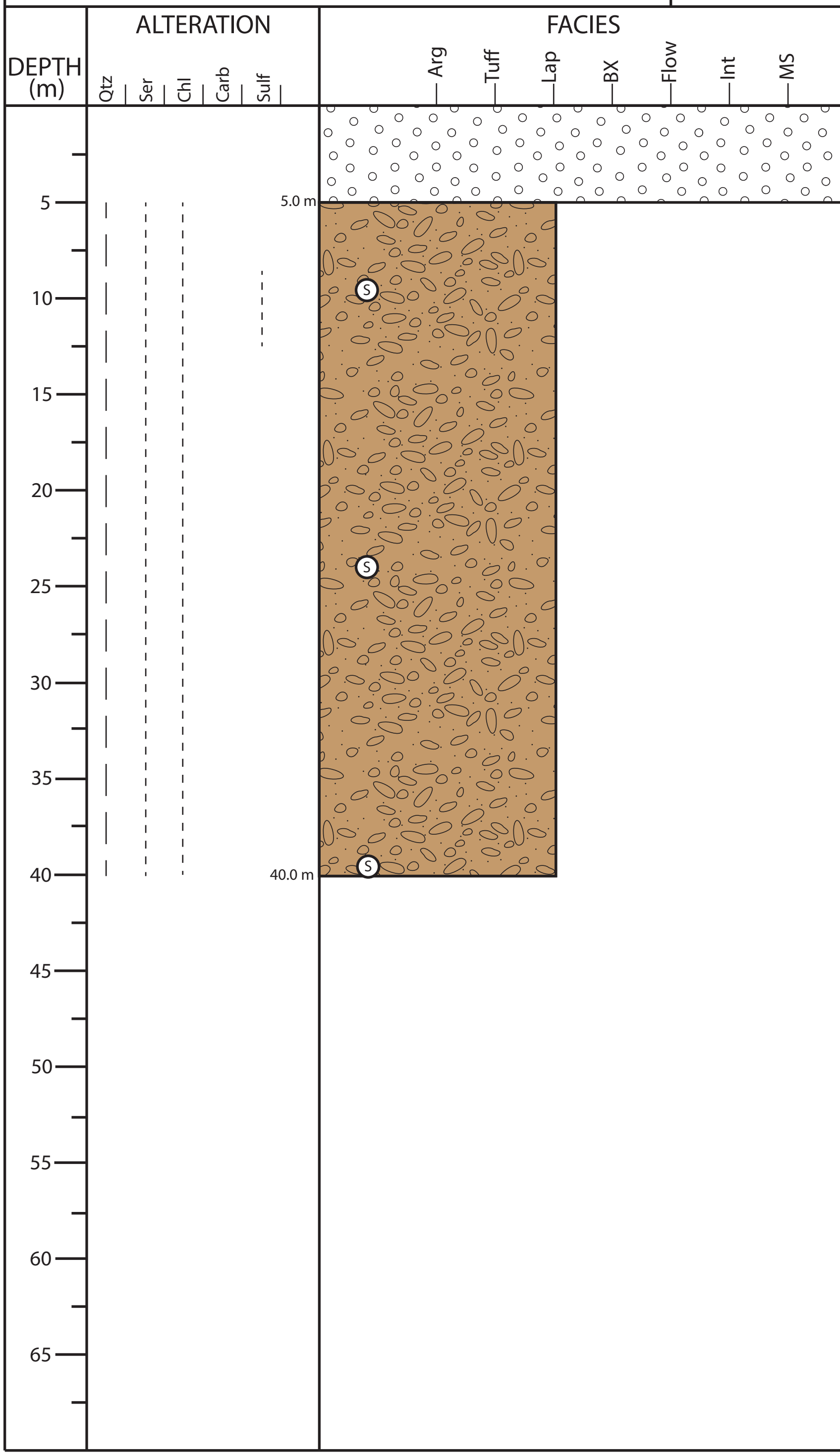

DESCRIPTION

Sample: H501342

LT unit is fairly homogeneous thoughout. Most of the unit is clast supported. Clasts follow general bimodal (1 cm and 3 cm in dia.). The matrix that is visible is soft and dark, likely ser/chl. Carbonate spotting (moderate) and dis. Py (minor) is consistent throughout.

Sample: H501343

Sample: H501344

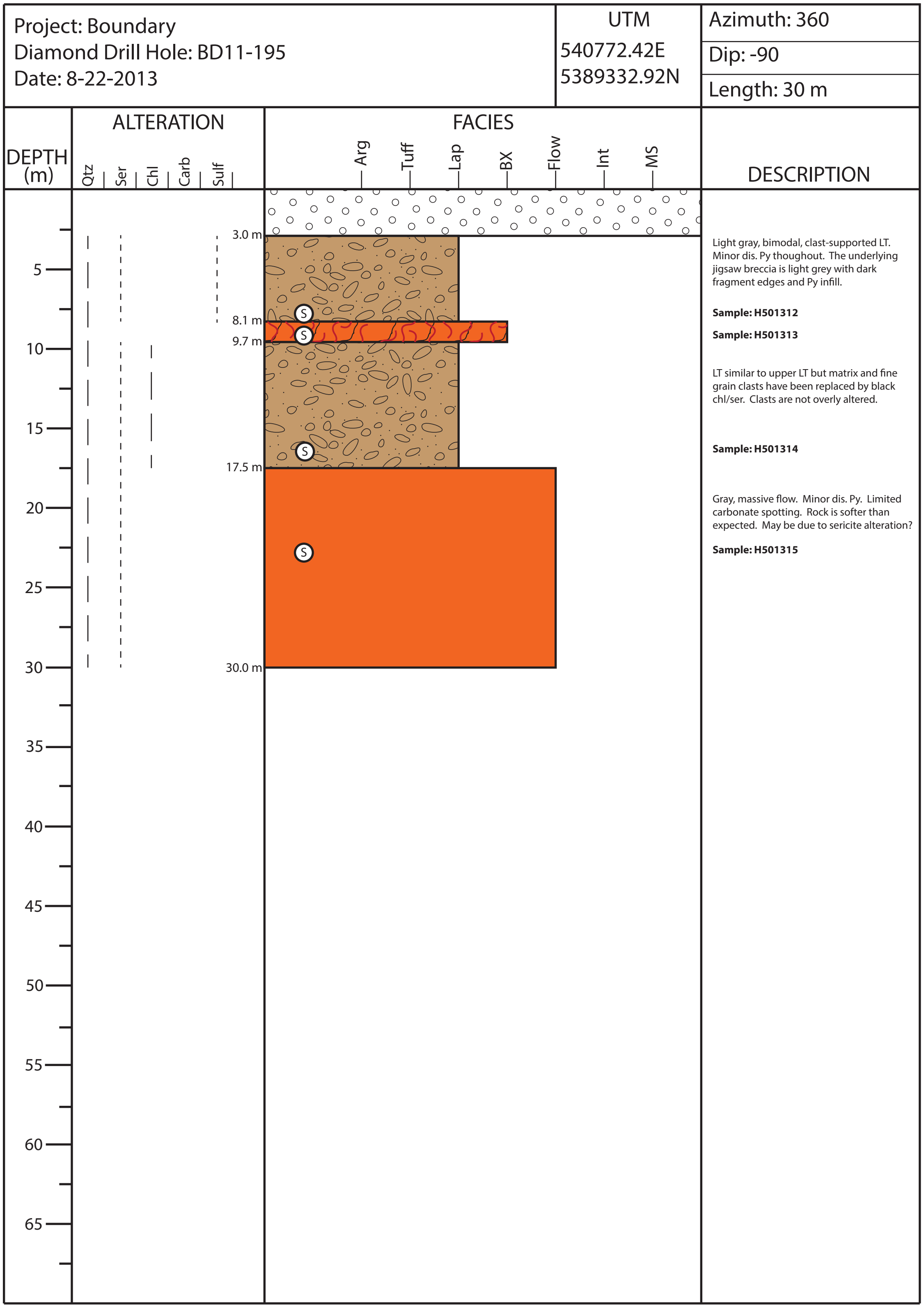
Project: Boundary
Diamond Drill Hole: BD11-195
Date: 8-22-2013
UTM
540772.42E
5389332.92N
Azimuth: 360
Dip: -90
Length: 30 m
DEPTH (m)
ALTERATION
Qtz
Ser
Chl
Carb
Sulf
FACIES
Arg
Tuff
Lap
BX
Flow
Int
MS
DESCRIPTION
5
10
15
20
25
30
35
40
45
50
55
60
65
3.0 m
8.1 m
9.7 m
17.5 m
30.0 m
S
Light gray, bimodal, clast-supported LT. Minor dis. Py thoughout. The underlying jigsaw breccia is light grey with dark fragment edges and Py infill.
Sample: H501312
Sample: H501313
LT similar to upper LT but matrix and fine grain clasts have been replaced by black chl/ser. Clasts are not overly altered.
Sample: H501314
Gray, massive flow. Minor dis. Py. Limited carbonate spotting. Rock is softer than expected. May be due to sericite alteration?
Sample: H501315

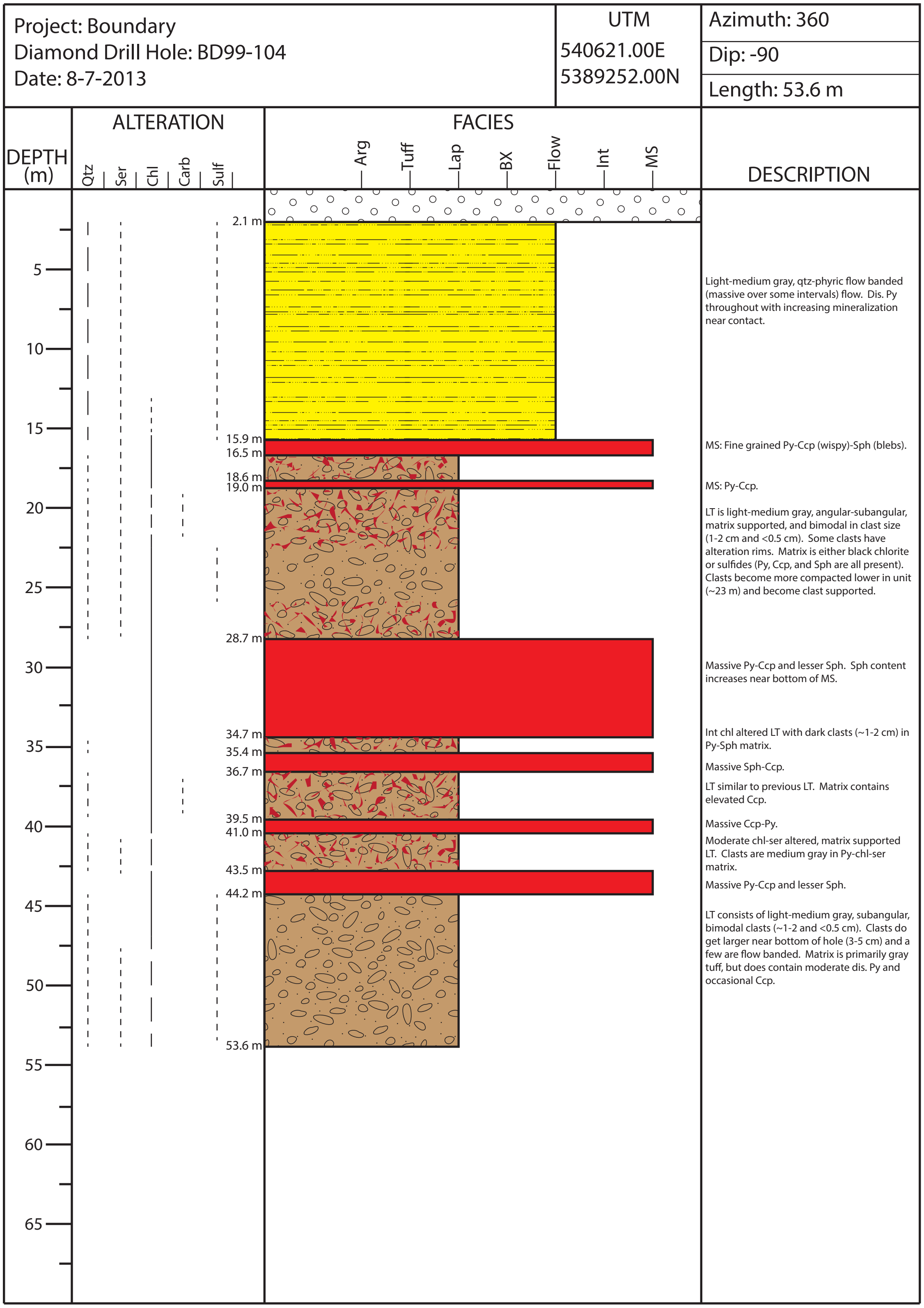
Project: Boundary
Diamond Drill Hole: BD99-104
Date: 8-7-2013
UTM
540621.00E
5389252.00N
Azimuth: 360
Dip: -90
Length: 53.6 m
DEPTH (m)
ALTERATION
Qtz
Ser
Chl
Carb
Sulf
FACIES
Arg
Tuff
Lap
BX
Flow
Int
MS
DESCRIPTION
5
10
15
20
25
30
35
40
45
50
55
60
65
2.1 m
15.9 m
16.5 m
18.6 m
19.0 m
28.7 m
34.7 m
35.4 m
36.7 m
39.5 m
41.0 m
43.5 m
44.2 m
53.6 m
Light-medium gray, qtz-phyric flow banded (massive over some intervals) flow. Dis. Py throughout with increasing mineralization near contact.
MS: Fine grained Py-Ccp (wispy)-Sph (blebs).
MS: Py-Ccp.
LT is light-medium gray, angular-subangular, matrix supported, and bimodal in clast size (1-2 cm and <0.5 cm). Some clasts have alteration rims. Matrix is either black chlorite or sulfides (Py, Ccp, and Sph are all present). Clasts become more compacted lower in unit (~23 m) and become clast supported.
Massive Py-Ccp and lesser Sph. Sph content increases near bottom of MS.
Int chl altered LT with dark clasts (~1-2 cm) in Py-Sph matrix.
Massive Sph-Ccp.
LT similar to previous LT. Matrix contains elevated Ccp.
Massive Ccp-Py.
Moderate chl-ser altered, matrix supported LT. Clasts are medium gray in Py-chl-ser matrix.
Massive Py-Ccp and lesser Sph.
LT consists of light-medium gray, subangular, bimodal clasts (~1-2 and <0.5 cm). Clasts do get larger near bottom of hole (3-5 cm) and a few are flow banded. Matrix is primarily gray tuff, but does contain moderate dis. Py and occasional Ccp.

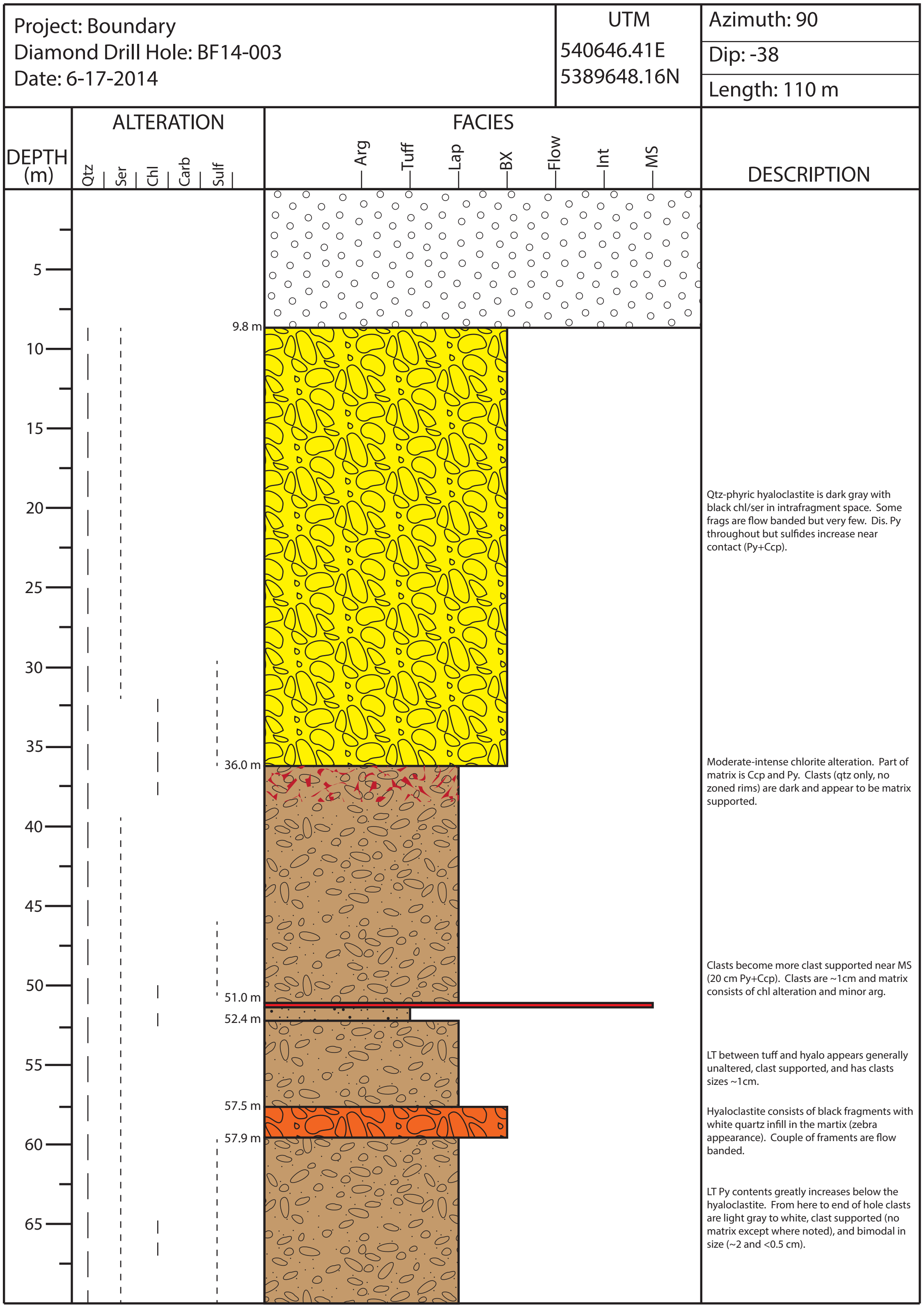

Project: Boundary
Diamond Drill Hole: BF14-003
Date: 6-17-2014
UTM
540646.41E
5389648.16N
Azimuth: 90
Dip: -38
Length: 110 m
DEPTH (m)
ALTERATION
Qtz
Ser
Chl
Carb
Sulf
FACIES
Arg
Tuff
Lap
BX
Flow
Int
MS
DESCRIPTION
5
10
15
20
25
30
35
40
45
50
55
60
65
9.8 m
36.0 m
51.0 m
52.4 m
57.5 m
57.9 m
Qtz-phyric hyaloclastite is dark gray with black chl/ser in intrafragment space. Some frags are flow banded but very few. Dis. Py throughout but sulfides increase near contact (Py+Ccp).
Moderate-intense chlorite alteration. Part of matrix is Ccp and Py. Clasts (qtz only, no zoned rims) are dark and appear to be matrix supported.
Clasts become more clast supported near MS (20 cm Py+Ccp). Clasts are ~1cm and matrix consists of chl alteration and minor arg.
LT between tuff and hyalo appears generally unaltered, clast supported, and has clasts sizes ~1cm.
Hyaloclastite consists of black fragments with white quartz infill in the martix (zebra appearance). Couple of framents are flow banded.
LT Py contents greatly increases below the hyaloclastite. From here to end of hole clasts are light gray to white, clast supported (no matrix except where noted), and bimodal in size (~2 and <0.5 cm).

Project: Boundary Diamond Drill Hole: BF14-003 Date:6-17-2014	UTM 540646.41E 5389648.16N	Azimuth: 90 Dip: -38 Length: 110 m

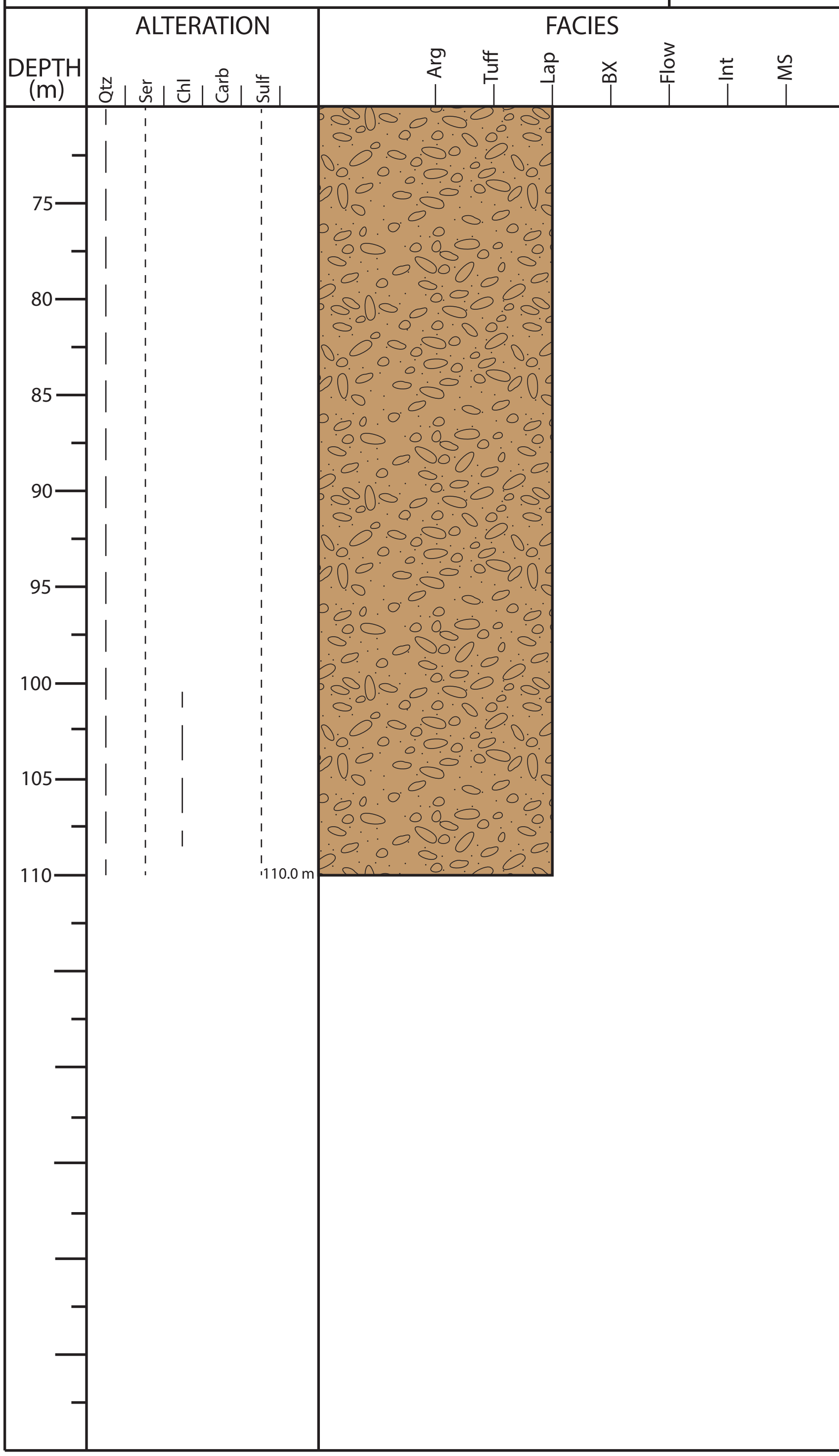

DESCRIPTION

Over the interval of 87-100 m, matrix volume slightly increases as do the amount of sulfides present (Py).

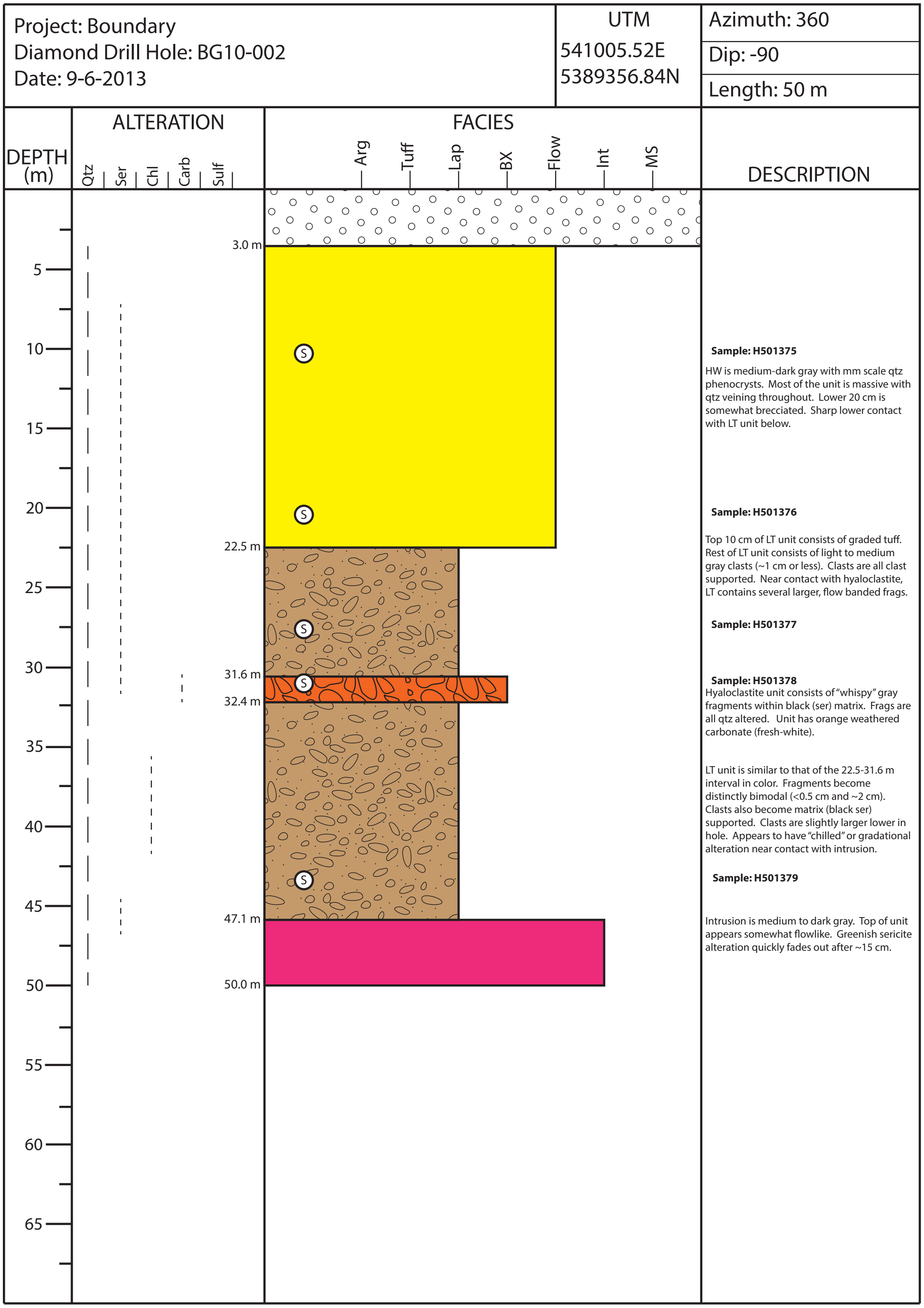
Project: Boundary
Diamond Drill Hole: BG10-002
Date: 9-6-2013
UTM
541005.52E
5389356.84N
Azimuth: 360
Dip: -90
Length: 50 m
DEPTH (m)
ALTERATION
Qtz
Ser
Chl
Carb
Sulf
FACIES
Arg
Tuff
Lap
BX
Flow
Int
MS
DESCRIPTION
5
10
15
20
25
30
35
40
45
50
55
60
65
3.0 m
22.5 m
31.6 m
32.4 m
47.1 m
50.0 m
Sample: H501375
HW is medium-dark gray with mm scale qtz phenocrysts. Most of the unit is massive with qtz veining throughout. Lower 20 cm is somewhat brecciated. Sharp lower contact with LT unit below.
Sample: H501376
Top 10 cm of LT unit consists of graded tuff. Rest of LT unit consists of light to medium gray clasts (~1 cm or less). Clasts are all clast supported. Near contact with hyaloclastite, LT contains several larger, flow banded frags.
Sample: H501377
Sample: H501378
Hyaloclastite unit consists of "whispy" gray fragments within black (ser) matrix. Frags are all qtz altered. Unit has orange weathered carbonate (fresh-white).
LT unit is similar to that of the 22.5-31.6 m interval in color. Fragments become distinctly bimodal (<0.5 cm and ~2 cm). Clasts also become matrix (black ser) supported. Clasts are slightly larger lower in hole. Appears to have "chilled" or gradational alteration near contact with intrusion.
Sample: H501379
Intrusion is medium to dark gray. Top of unit appears somewhat flowlike. Greenish sericite alteration quickly fades out after ~15 cm.

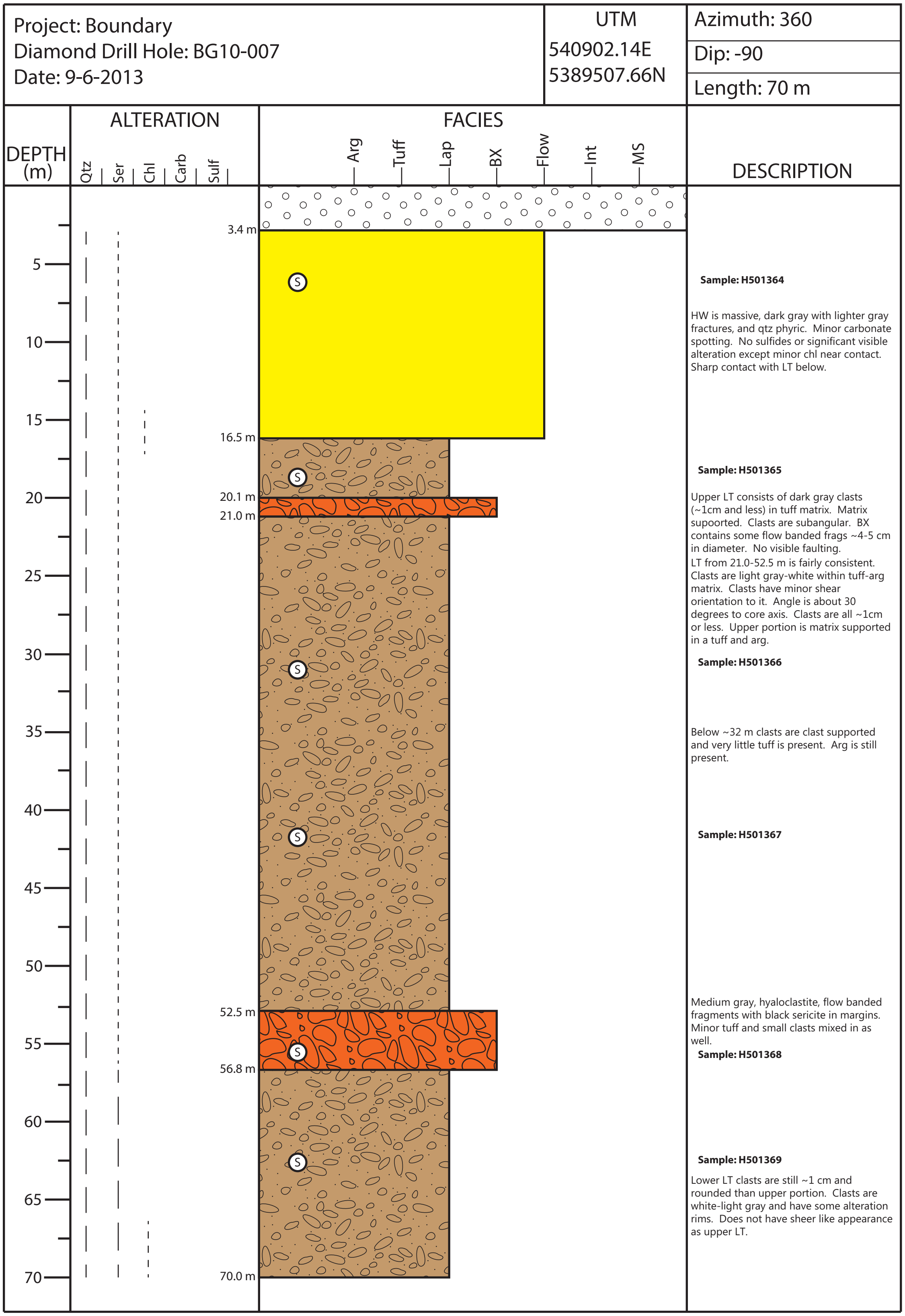

Project: Boundary
Diamond Drill Hole: BG10-007
Date: 9-6-2013
UTM
540902.14E
5389507.66N
Azimuth: 360
Dip: -90
Length: 70 m
DEPTH (m)
ALTERATION
Qtz
Ser
Chl
Carb
Sulf
FACIES
Arg
Tuff
Lap
BX
Flow
Int
MS
DESCRIPTION
5
10
15
20
25
30
35
40
45
50
55
60
65
70
3.4 m
16.5 m
20.1 m
21.0 m
52.5 m
56.8 m
70.0 m
S
Sample: H501364
HW is massive, dark gray with lighter gray fractures, and qtz phyric. Minor carbonate spotting. No sulfides or significant visible alteration except minor chl near contact. Sharp contact with LT below.
Sample: H501365
Upper LT consists of dark gray clasts (~1cm and less) in tuff matrix. Matrix supoorted. Clasts are subangular. BX contains some flow banded frags ~4-5 cm in diameter. No visible faulting.
LT from 21.0-52.5 m is fairly consistent. Clasts are light gray-white within tuff-arg matrix. Clasts have minor shear orientation to it. Angle is about 30 degrees to core axis. Clasts are all ~1cm or less. Upper portion is matrix supported in a tuff and arg.
Sample: H501366
Below ~32 m clasts are clast supported and very little tuff is present. Arg is still present.
Sample: H501367
Medium gray, hyaloclastite, flow banded fragments with black sericite in margins. Minor tuff and small clasts mixed in as well.
Sample: H501368
Sample: H501369
Lower LT clasts are still ~1 cm and rounded than upper portion. Clasts are white-light gray and have some alteration rims. Does not have sheer like appearance as upper LT.

Appendix B: Table B1.1 Whole-rock Geochemistry and Terraspec™ Data

Sample ID			**H500606**	**H500607**	**H500608**	**H500609**	**H500610**	**H500611**	**H500612**
Hole ID			BD10-112	BD10-112	BD10-112	BD10-112	BD10-112	BD11-117	BD11-117
Depth (m)			20.1	28.8	39.8	50.9	58.2	12.6	15.2
Lithology			HBX	FLT	FLT	FLT	FLT	HFL	HFL
Alteration			Qtz-Ser	Qtz-Ser	Qtz-Ser	Qtz-Ser	Chl-Ser	Qtz-Ser	Qtz-Ser
SiO_2	%	FUS-ICP	76	71.25	68.23	67.25	63.33	72.98	70.63
Al_2O_3	%	FUS-ICP	9.68	11.19	10.84	8.11	9.74	12.62	11.89
Fe_2O_3(T)	%	FUS-ICP	4.79	5.63	10.11	12.64	10.91	4.68	5.12
MnO	%	FUS-ICP	0.219	0.041	0.019	0.009	0.061	0.089	0.123
MgO	%	FUS-ICP	3.21	2.16	0.63	0.37	4.82	2.46	3.87
CaO	%	FUS-ICP	0.27	0.1	0.09	0.05	0.07	0.07	0.08
Na_2O	%	FUS-ICP	0.14	0.18	0.21	0.15	0.1	0.2	0.15
K_2O	%	FUS-ICP	2.01	2.65	3	2.27	1.46	2.84	2.37
TiO_2	%	FUS-ICP	0.12	0.161	0.154	0.116	0.142	0.156	0.144
P_2O_5	%	FUS-ICP	0.01	< 0.01	0.01	< 0.01	0.02	0.01	0.01
LOI	%	FUS-ICP	4.49	4.73	6.79	7.94	7.59	4.21	4.7
Total	%	FUS-ICP	100.9	98.1	100.1	98.9	98.24	100.3	99.08
Ba	ppm	FUS-ICP	1279	1653	1571	1139	726	2516	1761
Sr	ppm	FUS-ICP	7	9	10	6	6	9	7
Y	ppm	FUS-ICP	29	33	38	23	38	41	40
Sc	ppm	FUS-ICP	9	13	13	8	10	11	10
Zr	ppm	FUS-ICP	132	151	157	113	136	159	145
Be	ppm	FUS-ICP	< 1	< 1	< 1	< 1	< 1	1	< 1
V	ppm	FUS-ICP	< 5	12	< 5	< 5	< 5	< 5	5
Hg	ppb	FIMS	< 5	6	46	51	10	< 5	6
Cr	ppm	HF/HNO3	9.59	13.17	<8.9	<8.9	9.28	<8.9	<8.9
Co	ppm	HF/HNO3	1.19	1.59	<0.9	24.48	29.46	<0.9	2.59
Ni	ppm	HF/HNO3	<10	<10	<10	<10	<10	<10	<10
Cu	ppm	HF/HNO3	344.01	78.89	2271.38	635.39	2428.34	639.85	95.41
Zn	ppm	HF/HNO3	187.11	143.24	50.92	74.64	124.52	165.12	202.06
As	ppm	HF/HNO3	<1.6	6.58	35.62	61.22	17.62	1.90	4.99
Se	ppm	HF/HNO3	<26.7	<26.7	<26.7	<26.7	<26.7	<26.7	<26.7
Br	ppm	HF/HNO3	145.73	157.96	171.52	167.48	157.66	177.37	170.50
Mo	ppm	HF/HNO3	1.98	23.53	9.41	22.00	13.17	2.73	2.39
Ag	ppm	HF/HNO3	<1	<1	1.30	4.87	<1	<1	<1
Cd	ppm	HF/HNO3	<0.9	<0.9	<0.9	<0.9	<0.9	1.70	<0.9
Sn	ppm	HF/HNO3	6.24	6.21	7.81	6.09	5.55	8.60	6.90
Sb	ppm	HF/HNO3	1.06	3.37	5.98	4.99	1.89	1.22	7.28
Te	ppm	HF/HNO3	<4.3	<4.3	<4.3	10.93	5.26	<4.3	<4.3
I	ppm	HF/HNO3	<37	<37	<37	<37	<37	<37	<37
W	ppm	HF/HNO3	1.70	3.09	4.10	4.67	2.13	1.56	1.72
Pb	ppm	HF/HNO3	<25.3	<25.3	26.50	32.67	<25.3	<25.3	<25.3
Bi	ppm	HF/HNO3	0.25	0.97	0.23	19.30	7.10	0.44	0.55
Nb	ppm	Na_2O_2 Sinter	5.14	6.33	6.01	4.53	5.96	6.75	6.21
La	ppm	Na_2O_2 Sinter	15.51	19.76	17.87	11.81	18.76	19.25	17.82
Ce	ppm	Na_2O_2 Sinter	32.87	42.76	37.71	25.75	38.97	41.75	38.08
Pr	ppm	Na_2O_2 Sinter	4.13	5.46	4.74	3.24	4.99	5.29	4.81
Nd	ppm	Na_2O_2 Sinter	17.70	23.28	19.86	13.63	21.28	22.80	20.89
Sm	ppm	Na_2O_2 Sinter	4.39	5.61	4.99	3.33	5.09	5.54	5.07
Eu	ppm	Na_2O_2 Sinter	0.78	1.34	1.27	0.91	1.18	0.83	1.15
Tb	ppm	Na_2O_2 Sinter	0.79	0.95	0.97	0.62	1.00	1.04	0.96
Dy	ppm	Na_2O_2 Sinter	5.24	6.27	6.42	4.18	6.48	6.93	6.34
Ho	ppm	Na_2O_2 Sinter	1.14	1.34	1.38	0.92	1.36	1.47	1.37
Er	ppm	Na_2O_2 Sinter	3.62	4.10	4.11	2.81	4.17	4.57	4.25
Tm	ppm	Na_2O_2 Sinter	0.55	0.61	0.62	0.43	0.62	0.70	0.66
Yb	ppm	Na_2O_2 Sinter	3.76	4.08	4.15	2.95	4.15	4.92	4.64
Lu	ppm	Na_2O_2 Sinter	0.59	0.62	0.63	0.45	0.65	0.77	0.72
Hf	ppm	Na_2O_2 Sinter	3.34	4.11	3.83	3.07	3.43	4.55	4.16
Ta	ppm	Na_2O_2 Sinter	0.25	0.29	0.25	0.21	0.24	0.28	0.26
Th	ppm	Na_2O_2 Sinter	4.33	5.00	4.61	3.66	4.36	5.57	4.99
AlOH WL	nm	Terraspec	2,204	2,202	2,203	2,204	2,199	2,202	2,202
AlOH Depth	%	Terraspec	5.99%	6.26%	3.89%	10.76%	1.66%	9.90%	5.83%
FeOH WL	nm	Terraspec	2,253	2,253	#DIV/0!	#DIV/0!	2,252	2,253	2,253
FeOH Depth	%	Terraspec	2.79%	1.93%	#DIV/0!	#DIV/0!	3.06%	2.80%	1.91%
AlOH depth/FeOH depth		Terraspec	2.15	3.24	#DIV/0!	#DIV/0!	0.54	3.54	3.06

Abbreviations:	**Units**		**Alteration**	**Other**
	HFL= Hanging wall flow	FT= Footwall tuff	Qtz-Ser= Quartz-sericite	WL= Wavelength
	HBX= Hanging wall breccia	FBX= Footwall breccia	Chl-Ser= Chlorite-sericite	
	FLT= Footwall lapilli tuff	FFL= Footwall flow	Chl=Chlorite	
		INT= Intrusion		

Appendix B: Table B1.1 Whole-rock Geochemistry and Terraspec™ Data

Sample ID			**H500613**	**H500614**	**H500615**	**H500616**	**H500617**	**H500618**	**H500619**	**H500621**
Hole ID			BD11-117	BD11-117	BD11-117	BD11-117	BD10-107	BD10-107	BD10-107	BD10-108
Depth (m)			25.5	45.1	57.7	70.4	10.8	18.3	31.2	22.5
Lithology			FLT	FLT	FLT	FBX	FBX	FLT	FLT	FLT
Alteration			Chl-Ser	Qtz-Ser	Qtz-Ser	Qtz-Ser	Qtz-Ser	Qtz-Ser	Chl-Ser	Chl-Ser
SiO_2	%	FUS-ICP	60.72	58.05	63.78	73.95	72.99	71	46.74	55.03
Al_2O_3	%	FUS-ICP	9.29	13.79	8.84	11.57	12.62	11.66	18.87	8.85
Fe_2O_3(T)	%	FUS-ICP	14.59	10.85	13.65	4.08	3.99	4.6	14.28	18.7
MnO	%	FUS-ICP	0.049	0.066	0.015	0.035	0.047	0.092	0.088	0.189
MgO	%	FUS-ICP	2.33	2.87	0.56	1.97	2.21	4.2	8.39	2.71
CaO	%	FUS-ICP	0.07	0.06	0.09	0.11	0.24	0.14	0.26	0.21
Na_2O	%	FUS-ICP	0.13	0.22	0.16	0.18	0.21	0.2	0.2	0.15
K_2O	%	FUS-ICP	2.08	3.4	2.43	2.87	3.07	2.33	2.33	1.87
TiO_2	%	FUS-ICP	0.122	0.19	0.123	0.158	0.157	0.18	0.263	0.128
P_2O_5	%	FUS-ICP	< 0.01	0.03	< 0.01	< 0.01	0.03	0.01	0.05	0.01
LOI	%	FUS-ICP	9.67	8.62	8.9	3.95	4	4.91	8.11	11.37
Total	%	FUS-ICP	99.06	98.14	98.56	98.88	99.57	99.31	99.6	99.22
Ba	ppm	FUS-ICP	1419	1837	1196	1676	2911	1341	1207	931
Sr	ppm	FUS-ICP	7	10	7	9	10	10	11	7
Y	ppm	FUS-ICP	25	43	31	42	47	40	60	30
Sc	ppm	FUS-ICP	7	14	8	12	10	11	16	11
Zr	ppm	FUS-ICP	116	174	111	147	146	144	209	105
Be	ppm	FUS-ICP	< 1	< 1	< 1	< 1	1	< 1	< 1	< 1
V	ppm	FUS-ICP	5	< 5	< 5	< 5	< 5	15	< 5	21
Hg	ppb	FIMS	458	263	37	< 5	5	< 5	7	10
Cr	ppm	HF/HNO3	10.80	<8.9	<8.9	15.21	<8.9	<8.9	<8.9	21.34
Co	ppm	HF/HNO3	1.89	1.71	35.76	0.93	<0.9	2.22	6.21	4.11
Ni	ppm	HF/HNO3	<10	<10	<10	<10	<10	14.61	<10	<10
Cu	ppm	HF/HNO3	117.56	816.42	512.75	940.60	646.06	<19	312.02	25.39
Zn	ppm	HF/HNO3	123.86	113.78	36.54	113.27	70.34	112.58	187.70	53.61
As	ppm	HF/HNO3	78.03	47.76	28.56	3.89	5.24	2.01	<1.6	135.59
Se	ppm	HF/HNO3	<26.7	<26.7	<26.7	<26.7	<26.7	<26.7	<26.7	<26.7
Br	ppm	HF/HNO3	164.68	170.70	164.06	173.52	198.44	182.29	220.37	236.73
Mo	ppm	HF/HNO3	19.39	21.94	20.53	7.51	1.76	5.00	19.28	11.54
Ag	ppm	HF/HNO3	1.37	<1	<1	<1	<1	<1	<1	<1
Cd	ppm	HF/HNO3	<0.9	<0.9	<0.9	<0.9	<0.9	<0.9	<0.9	<0.9
Sn	ppm	HF/HNO3	6.76	7.88	5.98	6.78	4.96	3.46	5.47	5.44
Sb	ppm	HF/HNO3	25.53	18.63	2.18	1.78	1.27	0.71	1.33	1.21
Te	ppm	HF/HNO3	<4.3	<4.3	10.95	<4.3	<4.3	<4.3	20.10	10.70
I	ppm	HF/HNO3	<37	<37	<37	<37	<37	<37	<37	<37
W	ppm	HF/HNO3	2.73	2.45	1.58	2.10	2.29	3.64	6.10	7.49
Pb	ppm	HF/HNO3	96.62	<25.3	<25.3	<25.3	<25.3	<25.3	<25.3	<25.3
Bi	ppm	HF/HNO3	4.33	6.24	11.82	1.45	0.36	0.52	19.97	10.08
Nb	ppm	Na_2O_2 Sinter	4.44	7.22	4.52	6.35	8.27	8.78	12.81	5.40
La	ppm	Na_2O_2 Sinter	15.94	18.28	17.24	18.28	21.45	22.52	32.20	16.61
Ce	ppm	Na_2O_2 Sinter	33.59	39.49	36.10	38.66	45.20	47.62	69.18	33.98
Pr	ppm	Na_2O_2 Sinter	4.24	5.05	4.50	4.85	5.76	6.01	8.77	4.15
Nd	ppm	Na_2O_2 Sinter	18.07	21.22	19.34	21.01	23.95	25.76	38.20	17.08
Sm	ppm	Na_2O_2 Sinter	4.28	5.24	4.56	5.04	5.75	6.23	9.04	4.11
Eu	ppm	Na_2O_2 Sinter	1.14	1.28	0.94	1.02	0.81	1.48	2.18	1.20
Tb	ppm	Na_2O_2 Sinter	0.64	1.03	0.83	1.06	1.16	1.15	1.71	0.84
Dy	ppm	Na_2O_2 Sinter	4.14	6.97	5.41	7.19	7.98	7.73	11.62	5.42
Ho	ppm	Na_2O_2 Sinter	0.88	1.49	1.12	1.53	1.71	1.60	2.43	1.14
Er	ppm	Na_2O_2 Sinter	2.66	4.51	3.38	4.74	5.21	4.93	7.48	3.48
Tm	ppm	Na_2O_2 Sinter	0.39	0.70	0.50	0.72	0.80	0.77	1.13	0.52
Yb	ppm	Na_2O_2 Sinter	2.72	4.71	3.39	4.92	5.36	5.11	7.50	3.72
Lu	ppm	Na_2O_2 Sinter	0.42	0.74	0.52	0.76	0.85	0.79	1.19	0.60
Hf	ppm	Na_2O_2 Sinter	2.89	4.78	2.97	4.02	5.89	5.95	9.12	4.05
Ta	ppm	Na_2O_2 Sinter	0.16	0.27	0.19	0.27	0.34	0.36	0.49	0.20
Th	ppm	Na_2O_2 Sinter	3.63	5.40	3.72	5.09	7.35	7.42	10.68	4.19
AlOH WL	nm	Terraspec	2,204	2,203	2,204	2,205	2,205	2,201	2,195	2,197
AlOH Depth	%	Terraspec	3.09%	6.64%	6.14%	11.38%	3.88%	8.73%	2.83%	4.14%
FeOH WL	nm	Terraspec	2,250	2,252	#DIV/0!	2,253	2,253	2,252	2,252	2,253
FeOH Depth	%	Terraspec	1.21%	1.11%	#DIV/0!	1.20%	1.21%	1.98%	5.56%	2.88%
AlOH depth/FeOH depth		Terraspec	2.57	5.98	#DIV/0!	9.51	3.21	4.42	0.51	1.44

Abbreviations:

Units
HFL= Hanging wall flow
HBX= Hanging wall breccia
FLT= Footwall lapilli tuff
FT= Footwall tuff
FBX= Footwall breccia
FFL= Footwall flow
INT= Intrusion

Alteration
Qtz-Ser= Quartz-sericite
Chl-Ser= Chlorite-sericite
Chl=Chlorite

Other
WL= Wavelength

Appendix B: Table B1.1 Whole-rock Geochemistry and Terraspec™ Data

Sample ID			**H500622**	**H500623**	**H500624**	**H500625**	**H500626**	**H500627**	**H500628**
Hole ID			BD10-108	BD10-108	BD10-108	BD10-108	BD10-108	BD10-108	BD10-108
Depth (m)			28.3	34	36.6	43.5	46.4	47.4	50.6
Lithology			FLT	FBX	FLT	FBX	FLT	FLT	FFL
Alteration			Chl-Ser	Qtz-Ser	Chl-Ser	Qtz-Ser	Chl	Chl	Qtz-Ser
SiO_2	%	FUS-ICP	55.07	64.4	55.94	80.91	51.87	39.09	67.96
Al_2O_3	%	FUS-ICP	14.42	12.38	9.29	7.01	10.68	14.09	14.33
Fe_2O_3(T)	%	FUS-ICP	12.8	10.12	19.03	4.74	18.37	21.68	5.49
MnO	%	FUS-ICP	0.065	0.021	0.016	0.043	0.172	0.108	0.025
MgO	%	FUS-ICP	4.12	0.79	0.73	1.13	8.27	9.05	2.37
CaO	%	FUS-ICP	0.16	0.05	0.06	0.07	0.11	0.1	0.04
Na_2O	%	FUS-ICP	0.24	0.22	0.18	0.13	0.06	0.11	0.25
K_2O	%	FUS-ICP	3.2	3.32	2.38	1.66	0.39	1.24	3.23
TiO_2	%	FUS-ICP	0.417	0.21	0.129	0.103	0.231	0.199	0.197
P_2O_5	%	FUS-ICP	0.06	0.02	< 0.01	< 0.01	0.04	0.04	0.02
LOI	%	FUS-ICP	9.34	7.32	10.91	3.3	9.84	12.46	4.28
Total	%	FUS-ICP	99.89	98.86	98.68	99.1	100	98.17	98.19
Ba	ppm	FUS-ICP	1498	2181	1123	998	165	622	1560
Sr	ppm	FUS-ICP	13	11	7	6	3	6	10
Y	ppm	FUS-ICP	37	46	28	27	44	50	41
Sc	ppm	FUS-ICP	21	17	9	8	13	14	16
Zr	ppm	FUS-ICP	123	142	118	94	130	189	186
Be	ppm	FUS-ICP	< 1	< 1	< 1	< 1	< 1	< 1	< 1
V	ppm	FUS-ICP	98	23	6	6	26	5	8
Hg	ppb	FIMS	44	171	93	24	14	16	7
Cr	ppm	HF/HNO3	45.51	20.65	19.25	<8.9	12.59	10.43	<8.9
Co	ppm	HF/HNO3	17.03	8.79	12.82	6.26	29.92	29.07	3.86
Ni	ppm	HF/HNO3	23.55	11.39	<10	<10	<10	<10	<10
Cu	ppm	HF/HNO3	112.95	458.08	2522.04	727.91	1129.33	451.65	1205.19
Zn	ppm	HF/HNO3	103.93	526.75	49.30	93.12	132.26	176.51	38.46
As	ppm	HF/HNO3	25.84	41.76	218.58	7.88	16.35	144.47	8.01
Se	ppm	HF/HNO3	<26.7	<26.7	40.56	<26.7	<26.7	<26.7	<26.7
Br	ppm	HF/HNO3	254.58	262.97	269.21	238.24	240.28	253.41	211.83
Mo	ppm	HF/HNO3	3.42	6.84	6.20	8.16	12.85	10.77	6.44
Ag	ppm	HF/HNO3	1.30	1.19	1.03	<1	<1	<1	<1
Cd	ppm	HF/HNO3	<0.9	1.56	<0.9	<0.9	<0.9	<0.9	<0.9
Sn	ppm	HF/HNO3	4.71	5.32	5.70	4.07	3.43	4.14	4.15
Sb	ppm	HF/HNO3	5.40	6.84	9.76	1.51	1.12	1.82	1.39
Te	ppm	HF/HNO3	<4.3	<4.3	<4.3	5.39	11.04	8.22	5.05
I	ppm	HF/HNO3	<37	<37	<37	<37	<37	<37	<37
W	ppm	HF/HNO3	14.21	9.52	4.11	3.23	6.49	2.78	6.88
Pb	ppm	HF/HNO3	<25.3	31.65	<25.3	<25.3	<25.3	<25.3	<25.3
Bi	ppm	HF/HNO3	4.34	7.73	13.26	4.07	10.56	9.84	7.26
Nb	ppm	Na_2O_2 Sinter	7.46	7.79	6.46	5.31	8.46	10.72	10.90
La	ppm	Na_2O_2 Sinter	15.75	19.26	16.14	14.54	16.38	25.16	25.23
Ce	ppm	Na_2O_2 Sinter	33.26	40.06	34.33	30.37	34.62	53.21	53.28
Pr	ppm	Na_2O_2 Sinter	4.22	5.08	4.35	3.73	4.35	6.69	6.59
Nd	ppm	Na_2O_2 Sinter	18.51	21.29	18.25	15.82	18.64	28.38	27.23
Sm	ppm	Na_2O_2 Sinter	4.75	5.24	4.43	3.73	4.92	6.78	6.46
Eu	ppm	Na_2O_2 Sinter	1.31	2.19	0.93	0.85	1.07	1.46	1.37
Tb	ppm	Na_2O_2 Sinter	0.98	1.16	0.79	0.70	1.19	1.33	1.12
Dy	ppm	Na_2O_2 Sinter	6.79	7.82	5.29	4.46	8.17	9.05	7.47
Ho	ppm	Na_2O_2 Sinter	1.46	1.69	1.11	0.98	1.70	1.97	1.58
Er	ppm	Na_2O_2 Sinter	4.43	5.03	3.31	2.97	5.16	5.93	4.90
Tm	ppm	Na_2O_2 Sinter	0.67	0.76	0.52	0.46	0.81	0.92	0.74
Yb	ppm	Na_2O_2 Sinter	4.71	5.30	3.73	3.06	5.27	6.28	5.14
Lu	ppm	Na_2O_2 Sinter	0.69	0.77	0.55	0.46	0.78	0.95	0.78
Hf	ppm	Na_2O_2 Sinter	4.79	4.77	4.10	3.00	4.33	6.86	5.48
Ta	ppm	Na_2O_2 Sinter	0.25	0.25	0.24	0.21	0.30	0.37	0.40
Th	ppm	Na_2O_2 Sinter	4.65	5.40	4.60	3.77	4.94	7.30	7.30
AlOH WL	nm	Terraspec	2,201	2,203	2,203	2,200	2,195	2,196	2,200
AlOH Depth	%	Terraspec	7.31%	3.51%	4.06%	8.28%	1.82%	5.73%	13.68%
FeOH WL	nm	Terraspec	2,252	#DIV/0!	#DIV/0!	2,253	2,253	2,252	2,254
FeOH Depth	%	Terraspec	1.89%	#DIV/0!	#DIV/0!	5.23%	5.24%	7.46%	3.47%
AlOH depth/FeOH depth		Terraspec	3.87	#DIV/0!	#DIV/0!	1.58	0.35	0.77	3.95

Abbreviations:	**Units**		**Alteration**	**Other**
	HFL= Hanging wall flow	FT= Footwall tuff	Qtz-Ser= Quartz-sericite	WL= Wavelength
	HBX= Hanging wall breccia	FBX= Footwall breccia	Chl-Ser= Chlorite-sericite	
	FLT= Footwall lapilli tuff	FFL= Footwall flow	Chl=Chlorite	
		INT= Intrusion		

Appendix B: Table B1.1 Whole-rock Geochemistry and Terraspec[TM] Data

Sample ID			H500629	H500642	H500643	H500644	H500645	H500649	H500650	H500661
Hole ID			BD10-108	BD10-104	BD10-104	BD11-120	BD11-120	BD10-88	BD10-88	BD10-102
Depth (m)			53.2	14.3	21.6	22.8	63.3	8.2	22.1	6.2
Lithology			FLT	FLT	FLT	HFL	FLT	FLT	FLT	FLT
Alteration			Chl	Qtz-Ser	Qtz-Ser	Qtz-Ser	Qtz-Ser	Chl-Ser	Chl-Ser	Qtz-Ser
SiO_2	%	FUS-ICP	55.23	73.5	73.56	78.78	75.98	73.06	73.2	55.23
Al_2O_3	%	FUS-ICP	9.43	11.72	9.18	9.21	6.94	9.41	9.95	8.63
Fe_2O_3(T)	%	FUS-ICP	16.51	3.54	5.79	3.54	8.29	6.79	6.72	20.71
MnO	%	FUS-ICP	0.173	0.067	0.041	0.102	0.023	0.042	0.087	0.015
MgO	%	FUS-ICP	6.81	1.7	3.02	1.49	2.45	3.83	4.15	0.35
CaO	%	FUS-ICP	0.04	0.13	0.1	0.32	0.06	0.05	0.05	0.08
Na_2O	%	FUS-ICP	0.04	0.24	0.16	0.15	0.13	0.12	0.15	0.17
K_2O	%	FUS-ICP	0.22	3	1.82	2.35	1.2	1.51	1.42	2.31
TiO_2	%	FUS-ICP	0.14	0.164	0.148	0.115	0.137	0.156	0.18	0.157
P_2O_5	%	FUS-ICP	< 0.01	0.02	0.02	0.02	< 0.01	< 0.01	< 0.01	< 0.01
LOI	%	FUS-ICP	8.41	3.97	4.36	3.71	5.41	4.84	4.62	11.27
Total	%	FUS-ICP	97	98.06	98.2	99.79	100.6	99.81	100.5	98.93
Ba	ppm	FUS-ICP	106	1380	764	1082	405	778	579	1258
Sr	ppm	FUS-ICP	< 2	13	8	9	7	6	9	13
Y	ppm	FUS-ICP	32	30	30	26	24	27	31	30
Sc	ppm	FUS-ICP	10	12	9	7	7	13	13	9
Zr	ppm	FUS-ICP	121	132	95	110	112	111	117	104
Be	ppm	FUS-ICP	< 1	1	< 1	< 1	< 1	< 1	< 1	< 1
V	ppm	FUS-ICP	5	7	16	< 5	11	18	21	12
Hg	ppb	FIMS	34	< 5	< 5	7	< 5	30	< 5	19
Cr	ppm	HF/HNO3	<8.9	<8.9	9.08	<8.9	12.69	13.18	19.99	12.77
Co	ppm	HF/HNO3	19.90	1.77	2.65	<0.9	17.84	8.04	12.53	25.47
Ni	ppm	HF/HNO3	<10	<10	<10	<10	<10	<10	<10	<10
Cu	ppm	HF/HNO3	16782.95	<19	290.37	93.11	<19	197.34	71.07	8312.24
Zn	ppm	HF/HNO3	200.77	176.25	96.23	66.14	26.31	112.58	167.27	322.51
As	ppm	HF/HNO3	15.47	<1.6	7.12	6.95	5.11	<1.6	12.85	23.15
Se	ppm	HF/HNO3	<26.7	<26.7	<26.7	<26.7	<26.7	<26.7	<26.7	<26.7
Br	ppm	HF/HNO3	242.58	232.87	180.67	174.04	256.87	152.15	158.47	174.28
Mo	ppm	HF/HNO3	19.41	41.77	7.75	3.79	13.99	3.72	2.90	32.17
Ag	ppm	HF/HNO3	<1	<1	<1	<1	<1	<1	<1	1.60
Cd	ppm	HF/HNO3	<0.9	<0.9	<0.9	<0.9	<0.9	<0.9	<0.9	<0.9
Sn	ppm	HF/HNO3	4.33	6.79	5.26	5.90	3.43	5.54	4.79	8.55
Sb	ppm	HF/HNO3	2.43	1.04	0.98	1.56	0.76	0.39	0.74	1.66
Te	ppm	HF/HNO3	6.12	<4.3	4.66	<4.3	<4.3	<4.3	<4.3	<4.3
I	ppm	HF/HNO3	<37	<37	<37	<37	<37	<37	<37	<37
W	ppm	HF/HNO3	6.40	5.00	4.62	1.97	5.71	6.75	5.83	3.80
Pb	ppm	HF/HNO3	28.91	<25.3	<25.3	<25.3	<25.3	<25.3	<25.3	<25.3
Bi	ppm	HF/HNO3	7.86	1.17	3.98	2.80	1.49	0.58	0.50	4.39
Nb	ppm	Na_2O_2 Sinter	7.50	7.02	5.36	4.11	4.16	4.16	4.41	4.41
La	ppm	Na_2O_2 Sinter	15.12	2.97	12.67	14.00	8.75	15.47	14.92	16.22
Ce	ppm	Na_2O_2 Sinter	31.48	6.35	26.79	29.76	17.39	28.10	30.33	33.24
Pr	ppm	Na_2O_2 Sinter	3.97	0.83	3.33	3.71	2.15	3.30	3.77	4.08
Nd	ppm	Na_2O_2 Sinter	16.85	3.84	14.36	16.04	8.56	14.03	15.85	17.40
Sm	ppm	Na_2O_2 Sinter	4.22	1.33	3.48	3.62	2.12	3.21	3.74	4.09
Eu	ppm	Na_2O_2 Sinter	0.79	0.35	0.62	0.67	0.41	0.65	0.58	0.86
Tb	ppm	Na_2O_2 Sinter	0.94	0.58	0.73	0.64	0.49	0.63	0.75	0.76
Dy	ppm	Na_2O_2 Sinter	6.12	4.44	5.06	4.21	3.40	3.96	5.11	5.08
Ho	ppm	Na_2O_2 Sinter	1.32	1.07	1.18	0.89	0.81	0.88	1.08	1.05
Er	ppm	Na_2O_2 Sinter	3.94	3.39	3.54	2.70	2.51	2.84	3.43	3.22
Tm	ppm	Na_2O_2 Sinter	0.60	0.55	0.55	0.42	0.37	0.43	0.52	0.47
Yb	ppm	Na_2O_2 Sinter	4.07	3.97	3.76	2.98	2.72	3.03	3.56	3.24
Lu	ppm	Na_2O_2 Sinter	0.61	0.61	0.56	0.47	0.42	0.48	0.56	0.51
Hf	ppm	Na_2O_2 Sinter	4.74	4.94	4.05	2.88	2.29	2.50	2.80	2.89
Ta	ppm	Na_2O_2 Sinter	0.24	0.31	0.23	0.19	0.16	0.18	0.20	0.13
Th	ppm	Na_2O_2 Sinter	4.66	5.98	4.92	3.80	3.14	3.59	3.99	3.47
AlOH WL	nm	Terraspec	2,197	2,202	2,201	2,205	2,198	2,200	2,198	2,203
AlOH Depth	%	Terraspec	4.55%	13.45%	9.71%	5.95%	10.41%	13.60%	9.75%	10.87%
FeOH WL	nm	Terraspec	2,253	2,254	2,252	#DIV/0!	2,253	2,253	2,254	#DIV/0!
FeOH Depth	%	Terraspec	6.50%	1.42%	3.18%	#DIV/0!	2.96%	7.78%	5.15%	#DIV/0!
AlOH depth/FeOH depth		Terraspec	0.70	9.51	3.06	#DIV/0!	3.52	1.75	1.89	#DIV/0!

Abbreviations:

Units
HFL= Hanging wall flow
HBX= Hanging wall breccia
FLT= Footwall lapilli tuff
FT= Footwall tuff
FBX= Footwall breccia
FFL= Footwall flow
INT= Intrusion

Alteration
Qtz-Ser= Quartz-sericite
Chl-Ser= Chlorite-sericite
Chl=Chlorite

Other
WL= Wavelength

Appendix B: Table B1.1 Whole-rock Geochemistry and Terraspec™ Data

Sample ID			**H500662**	**H500663**	**H500664**	**H500665**	**H500666**	**H500667**	**H500668**	**H500669**
Hole ID			BD10-102	BD10-102	BD10-102	BD11-129	BD11-129	BD11-129	BD11-129	BD11-129
Depth (m)			16.6	25.1	43.7	12.8	24.8	38.1	35.4	38.4
Lithology			FLT	FLT	FLT	FLT	FLT	FLT	FFL	FLT
Alteration			Chl	Chl	Qtz-Ser	Qtz-Ser	Qtz-Ser	Qtz-Ser	Qtz-Ser	Chl-Ser
SiO_2	%	FUS-ICP	19.65	52.08	74.39	70.17	64.64	60.05	77.19	62.75
Al_2O_3	%	FUS-ICP	15.81	6.05	9.66	13.78	8.64	6.94	8.48	8.47
Fe_2O_3(T)	%	FUS-ICP	27.58	21.35	6.89	3.37	14.33	13.72	5.76	11.67
MnO	%	FUS-ICP	0.142	0.073	0.058	0.061	0.007	0.025	0.008	0.01
MgO	%	FUS-ICP	16.1	5.47	2.98	4.45	0.3	0.45	0.38	0.34
CaO	%	FUS-ICP	0.07	0.06	0.06	0.07	0.04	0.08	0.03	0.06
Na_2O	%	FUS-ICP	0.02	0.03	0.16	0.24	0.2	0.16	0.18	0.2
K_2O	%	FUS-ICP	0.05	0.12	1.65	3.02	2.32	1.87	2.27	2.32
TiO_2	%	FUS-ICP	0.251	0.095	0.183	0.186	0.137	0.107	0.116	0.124
P_2O_5	%	FUS-ICP	0.02	0.01	0.02	0.03	< 0.01	< 0.01	< 0.01	< 0.01
LOI	%	FUS-ICP	15.65	11.66	4.18	4.77	8.81	9.87	4.04	9.2
Total	%	FUS-ICP	95.33	97	100.2	100.1	99.43	93.28	98.47	95.13
Ba	ppm	FUS-ICP	22	46	641	2096	1154	951	1098	1099
Sr	ppm	FUS-ICP	3	4	9	14	8	8	6	8
Y	ppm	FUS-ICP	59	23	31	38	30	22	28	33
Sc	ppm	FUS-ICP	16	7	11	14	9	7	8	8
Zr	ppm	FUS-ICP	219	86	118	178	104	95	107	108
Be	ppm	FUS-ICP	< 1	< 1	< 1	1	< 1	< 1	< 1	< 1
V	ppm	FUS-ICP	17	6	25	22	16	14	7	16
Hg	ppb	FIMS	108	100	11	37	62	237	49	134
Cr	ppm	HF/HNO3	<8.9	14.01	15.31	<8.9	<8.9	<8.9	17.99	<8.9
Co	ppm	HF/HNO3	107.92	133.23	4.84	<0.9	13.44	44.93	11.01	9.61
Ni	ppm	HF/HNO3	<10	<10	<10	<10	<10	<10	<10	<10
Cu	ppm	HF/HNO3	27636.08	16898.55	271.56	138.77	215.86	14253.16	993.30	<19
Zn	ppm	HF/HNO3	246.54	167.78	73.02	168.01	47.86	62.94	38.88	74.06
As	ppm	HF/HNO3	34.05	31.47	3.75	3.80	47.26	37.57	9.16	23.86
Se	ppm	HF/HNO3	34.65	61.22	<26.7	<26.7	<26.7	38.76	<26.7	<26.7
Br	ppm	HF/HNO3	180.37	162.60	151.22	238.10	219.01	225.14	226.02	257.14
Mo	ppm	HF/HNO3	61.23	27.15	2.30	6.36	6.86	16.68	4.77	3.69
Ag	ppm	HF/HNO3	3.01	2.13	<1	<1	1.02	3.03	<1	<1
Cd	ppm	HF/HNO3	<0.9	<0.9	<0.9	<0.9	<0.9	<0.9	<0.9	<0.9
Sn	ppm	HF/HNO3	7.49	4.25	5.71	3.92	4.10	4.90	3.61	3.52
Sb	ppm	HF/HNO3	3.40	2.33	0.65	8.05	6.53	8.00	1.56	1.67
Te	ppm	HF/HNO3	59.31	45.98	<4.3	<4.3	7.05	16.30	<4.3	<4.3
I	ppm	HF/HNO3	<37	<37	<37	<37	<37	<37	<37	<37
W	ppm	HF/HNO3	26.54	15.59	9.54	4.05	3.67	2.62	3.85	3.95
Pb	ppm	HF/HNO3	<25.3	<25.3	<25.3	<25.3	<25.3	33.81	<25.3	<25.3
Bi	ppm	HF/HNO3	83.73	44.03	1.76	0.32	24.32	27.08	5.10	1.89
Nb	ppm	Na_2O_2 Sinter	8.17	3.00	5.68	10.77	5.86	5.47	5.79	6.07
La	ppm	Na_2O_2 Sinter	33.76	9.32	10.41	25.38	15.66	13.02	15.54	15.94
Ce	ppm	Na_2O_2 Sinter	65.11	19.28	22.45	53.38	32.56	26.88	32.42	33.18
Pr	ppm	Na_2O_2 Sinter	8.13	2.41	2.93	6.86	4.13	3.38	4.15	4.13
Nd	ppm	Na_2O_2 Sinter	34.95	10.36	12.70	29.59	18.18	14.08	17.38	17.58
Sm	ppm	Na_2O_2 Sinter	8.76	2.36	3.28	6.87	4.44	3.47	4.01	4.24
Eu	ppm	Na_2O_2 Sinter	1.03	0.25	0.61	1.66	1.00	0.82	0.71	0.94
Tb	ppm	Na_2O_2 Sinter	1.59	0.55	0.75	1.14	0.84	0.63	0.76	0.83
Dy	ppm	Na_2O_2 Sinter	10.19	3.75	5.28	7.09	5.52	4.06	5.14	5.44
Ho	ppm	Na_2O_2 Sinter	2.09	0.83	1.18	1.55	1.22	0.87	1.08	1.20
Er	ppm	Na_2O_2 Sinter	6.26	2.53	3.63	4.67	3.91	2.69	3.42	3.68
Tm	ppm	Na_2O_2 Sinter	0.96	0.38	0.56	0.74	0.58	0.40	0.54	0.56
Yb	ppm	Na_2O_2 Sinter	6.75	2.65	3.85	4.84	3.78	2.90	3.60	3.86
Lu	ppm	Na_2O_2 Sinter	1.01	0.40	0.59	0.76	0.59	0.45	0.55	0.60
Hf	ppm	Na_2O_2 Sinter	5.25	2.03	3.25	6.15	3.86	3.21	3.17	3.65
Ta	ppm	Na_2O_2 Sinter	0.34	0.13	0.21	0.37	0.22	0.17	0.21	0.18
Th	ppm	Na_2O_2 Sinter	7.59	2.68	4.44	6.98	4.38	3.57	4.28	4.11
AlOH WL	nm	Terraspec	#DIV/0!	#DIV/0!	2,199	2,202	2,202	2,208	2,202	2,202
AlOH Depth	%	Terraspec	#DIV/0!	#DIV/0!	2.81%	11.62%	4.19%	1.74%	4.64%	6.71%
FeOH WL	nm	Terraspec	2,251	2,251	2,253	2,252	#DIV/0!	#DIV/0!	#DIV/0!	#DIV/0!
FeOH Depth	%	Terraspec	2.28%	2.45%	2.02%	1.60%	#DIV/0!	#DIV/0!	#DIV/0!	#DIV/0!
AlOH depth/FeOH depth		Terraspec	#DIV/0!	#DIV/0!	1.39	7.25	#DIV/0!	#DIV/0!	#DIV/0!	#DIV/0!

Abbreviations:	**Units**		**Alteration**	**Other**
	HFL= Hanging wall flow	FT= Footwall tuff	Qtz-Ser= Quartz-sericite	WL= Wavelength
	HBX= Hanging wall breccia	FBX= Footwall breccia	Chl-Ser= Chlorite-sericite	
	FLT= Footwall lapilli tuff	FFL= Footwall flow	Chl=Chlorite	
		INT= Intrusion		

Appendix B: Table B1.1 Whole-rock Geochemistry and Terraspec™ Data

Sample ID			**H500670**	**H500671**	**H500672**	**H500673**	**H500674**	**H500675**	**H500676**	**H500677**
Hole ID			BD11-129	BD11-129	BD11-129	BD11-123	BD11-123	BD11-123	BD11-123	BD11-123
Depth (m)			49.4	53.8	56.4	7.4	9	10.8	14.8	22.3
Lithology			FBX	FFL	FLT	HFL	FLT	FFL	FLT	FLT
Alteration			Qtz-Ser	Chl-Ser	Chl-Ser	Qtz-Ser	Qtz-Ser	Qtz-Ser	Qtz-Ser	Qtz-Ser
SiO_2	%	FUS-ICP	70.86	66.7	63.16	75.93	66.95	73.3	68.59	63.93
Al_2O_3	%	FUS-ICP	11.31	11.2	14.32	11.19	13.78	11.38	11.63	15.22
Fe_2O_3(T)	%	FUS-ICP	6.97	9.1	7.06	3.5	5.82	4.31	5.7	6.9
MnO	%	FUS-ICP	0.024	0.061	0.089	0.108	0.137	0.236	0.195	0.118
MgO	%	FUS-ICP	1.93	5.96	5.64	2.41	3.16	2.9	3.67	2.41
CaO	%	FUS-ICP	0.03	0.03	0.07	0.07	0.12	0.07	0.07	0.1
Na_2O	%	FUS-ICP	0.21	0.11	0.2	0.28	0.31	0.2	0.21	0.33
K_2O	%	FUS-ICP	2.68	1.2	2.42	2.71	3.37	2.89	2.77	3.98
TiO_2	%	FUS-ICP	0.155	0.151	0.208	0.14	0.193	0.153	0.164	0.224
P_2O_5	%	FUS-ICP	< 0.01	< 0.01	0.03	0.02	0.03	< 0.01	0.03	0.03
LOI	%	FUS-ICP	5.15	5.58	5.87	4.38	6.2	5.2	6.31	6.89
Total	%	FUS-ICP	99.33	100.1	99.07	100.7	100.1	100.6	99.35	100.1
Ba	ppm	FUS-ICP	1310	579	1206	1843	2082	1595	1394	3118
Sr	ppm	FUS-ICP	8	4	8	12	13	8	9	16
Y	ppm	FUS-ICP	40	46	61	38	47	37	45	55
Sc	ppm	FUS-ICP	13	11	16	10	14	13	12	16
Zr	ppm	FUS-ICP	147	146	183	170	191	152	162	194
Be	ppm	FUS-ICP	< 1	< 1	< 1	1	1	1	< 1	1
V	ppm	FUS-ICP	< 5	8	9	< 5	7	< 5	< 5	8
Hg	ppb	FIMS	25	12	< 5	30	37	16	17	61
Cr	ppm	HF/HNO3	<8.9	<8.9	<8.9	9.12	10.11	<8.9	<8.9	9.33
Co	ppm	HF/HNO3	26.51	15.11	9.73	2.67	3.93	<0.9	<0.9	2.13
Ni	ppm	HF/HNO3	<10	<10	<10	<10	<10	<10	<10	10.61
Cu	ppm	HF/HNO3	40.63	<19	<19	43.20	881.23	991.96	1033.22	32.03
Zn	ppm	HF/HNO3	29.14	47.49	111.19	148.80	130.67	105.96	130.59	222.72
As	ppm	HF/HNO3	78.27	8.05	2.59	5.78	3.43	3.49	2.15	22.39
Se	ppm	HF/HNO3	<26.7	<26.7	<26.7	<26.7	<26.7	<26.7	<26.7	<26.7
Br	ppm	HF/HNO3	240.36	246.27	239.64	258.72	272.84	279.42	263.40	284.94
Mo	ppm	HF/HNO3	15.10	11.26	7.83	22.08	13.67	7.12	5.16	8.12
Ag	ppm	HF/HNO3	<1	<1	<1	<1	<1	<1	<1	<1
Cd	ppm	HF/HNO3	<0.9	<0.9	<0.9	<0.9	1.96	<0.9	<0.9	<0.9
Sn	ppm	HF/HNO3	4.52	3.20	3.87	4.03	4.65	4.40	4.06	4.85
Sb	ppm	HF/HNO3	1.80	0.68	1.20	1.30	1.85	1.55	1.17	10.33
Te	ppm	HF/HNO3	12.11	<4.3	<4.3	<4.3	<4.3	<4.3	<4.3	<4.3
I	ppm	HF/HNO3	<37	<37	<37	<37	<37	<37	<37	<37
W	ppm	HF/HNO3	3.48	3.39	5.58	1.84	3.67	10.96	3.11	5.41
Pb	ppm	HF/HNO3	<25.3	<25.3	<25.3	<25.3	28.66	<25.3	<25.3	<25.3
Bi	ppm	HF/HNO3	14.68	2.37	7.01	0.36	1.61	0.30	0.34	2.36
Nb	ppm	Na_2O_2 Sinter	8.50	8.11	11.00	6.20	7.74	6.83	7.02	9.18
La	ppm	Na_2O_2 Sinter	18.16	21.70	23.82	17.33	21.24	17.82	20.00	27.70
Ce	ppm	Na_2O_2 Sinter	37.74	45.79	50.50	36.61	45.24	37.40	41.65	58.40
Pr	ppm	Na_2O_2 Sinter	4.76	5.70	6.41	4.61	5.56	4.72	5.31	7.35
Nd	ppm	Na_2O_2 Sinter	20.54	24.05	27.26	19.78	23.84	19.90	22.24	31.16
Sm	ppm	Na_2O_2 Sinter	4.93	6.36	6.97	4.94	6.00	4.92	5.75	7.91
Eu	ppm	Na_2O_2 Sinter	1.63	1.26	1.48	1.10	1.42	0.82	1.11	2.76
Tb	ppm	Na_2O_2 Sinter	1.04	1.28	1.48	0.94	1.13	0.98	1.11	1.39
Dy	ppm	Na_2O_2 Sinter	7.07	8.56	10.07	6.38	7.79	6.67	7.64	9.39
Ho	ppm	Na_2O_2 Sinter	1.53	1.68	2.06	1.46	1.71	1.43	1.67	2.07
Er	ppm	Na_2O_2 Sinter	4.69	5.10	6.72	4.48	5.33	4.45	5.11	6.29
Tm	ppm	Na_2O_2 Sinter	0.70	0.74	1.00	0.70	0.80	0.66	0.73	0.95
Yb	ppm	Na_2O_2 Sinter	4.88	5.25	7.08	4.67	5.39	4.48	5.07	6.65
Lu	ppm	Na_2O_2 Sinter	0.74	0.81	1.12	0.70	0.81	0.72	0.80	1.00
Hf	ppm	Na_2O_2 Sinter	5.55	5.27	5.38	4.05	4.27	3.75	3.59	4.98
Ta	ppm	Na_2O_2 Sinter	0.32	0.31	0.38	0.24	0.30	0.26	0.26	0.35
Th	ppm	Na_2O_2 Sinter	5.81	5.62	6.94	5.15	6.41	5.19	5.51	7.17
AlOH WL	nm	Terraspec	2,200	2,199	2,200	2,201	2,200	2,205	2,203	2,204
AlOH Depth	%	Terraspec	9.23%	9.50%	10.98%	9.85%	6.90%	16.13%	12.83%	11.10%
FeOH WL	nm	Terraspec	2,254	2,253	2,253	2,251	2,253	2,252	2,252	#DIV/0!
FeOH Depth	%	Terraspec	2.43%	6.15%	4.05%	1.19%	1.16%	2.87%	2.33%	#DIV/0!
AlOH depth/FeOH depth		Terraspec	3.80	1.54	2.71	8.25	5.93	5.61	5.51	#DIV/0!

Abbreviations:	**Units**		**Alteration**	**Other**
	HFL= Hanging wall flow	FT= Footwall tuff	Qtz-Ser= Quartz-sericite	WL= Wavelength
	HBX= Hanging wall breccia	FBX= Footwall breccia	Chl-Ser= Chlorite-sericite	
	FLT= Footwall lapilli tuff	FFL= Footwall flow	Chl=Chlorite	
		INT= Intrusion		

Appendix B: Table B1.1 Whole-rock Geochemistry and Terraspec^{TM} Data

Sample ID			H500678	H500679	H500680	H500681	H500682	H500683	H500684	H500685
Hole ID			BD10-87	BD10-87	BD10-87	BD10-87	BD10-77	BD10-77	BD10-77	BD10-77
Depth (m)			6.3	11	17.9	30.5	12.4	22.3	26	29.5
Lithology			FLT	FLT	FT	FLT	FLT	FBX	FLT	FLT
Alteration			Chl	Chl-Ser	Qtz-Ser	Qtz-Ser	Qtz-Ser	Qtz-Ser	Qtz-Ser	Chl-Ser
SiO_2	%	FUS-ICP	46.6	62.04	70.79	72.73	71.37	50.47	70.96	48.35
Al_2O_3	%	FUS-ICP	12.42	8.33	11.14	11.09	10.73	18.12	11.8	8.97
Fe_2O_3(T)	%	FUS-ICP	19.04	13.07	8.06	6.15	6.31	12.09	4.35	18.36
MnO	%	FUS-ICP	0.217	0.103	0.045	0.032	0.091	0.051	0.056	0.123
MgO	%	FUS-ICP	9.14	6.21	3	1.78	2.78	1.67	3.61	5.92
CaO	%	FUS-ICP	0.06	0.04	0.05	0.04	0.14	0.14	0.09	0.06
Na_2O	%	FUS-ICP	0.08	0.05	0.2	0.22	0.19	0.33	0.2	0.1
K_2O	%	FUS-ICP	0.69	0.38	2.06	2.62	2.77	5.11	2.67	1.18
TiO_2	%	FUS-ICP	0.218	0.149	0.169	0.163	0.169	0.296	0.169	0.118
P_2O_5	%	FUS-ICP	< 0.01	< 0.01	< 0.01	< 0.01	< 0.01	0.04	0.03	0.02
LOI	%	FUS-ICP	11.71	8.12	5.42	4.69	6.18	9.42	5.07	11.47
Total	%	FUS-ICP	100.2	98.49	100.9	99.51	100.7	97.75	99	94.67
Ba	ppm	FUS-ICP	289	163	811	1054	1692	2785	1329	445
Sr	ppm	FUS-ICP	6	4	11	11	11	14	11	7
Y	ppm	FUS-ICP	24	44	43	42	40	60	35	18
Sc	ppm	FUS-ICP	11	8	10	11	11	17	12	7
Zr	ppm	FUS-ICP	175	123	126	138	154	230	137	116
Be	ppm	FUS-ICP	< 1	< 1	< 1	< 1	< 1	1	< 1	< 1
V	ppm	FUS-ICP	7	6	8	9	9	6	5	< 5
Hg	ppb	FIMS	16	16	11	< 5	15	70	< 5	38
Cr	ppm	HF/HNO3	<8.9	9.22	<8.9	<8.9	<8.9	<8.9	<8.9	<8.9
Co	ppm	HF/HNO3	9.11	14.78	15.34	45.48	1.07	1.88	<0.9	11.87
Ni	ppm	HF/HNO3	<10	<10	<10	<10	<10	<10	<10	<10
Cu	ppm	HF/HNO3	37.86	<19	<19	132.74	549.00	52.78	<19	31841.13
Zn	ppm	HF/HNO3	159.94	130.42	58.08	52.98	123.00	104.45	110.70	456.28
As	ppm	HF/HNO3	15.80	3.11	1.96	19.60	12.72	24.24	<1.6	8.96
Se	ppm	HF/HNO3	<26.7	<26.7	<26.7	<26.7	<26.7	<26.7	<26.7	35.91
Br	ppm	HF/HNO3	278.84	254.22	247.70	171.07	220.64	192.71	196.51	184.84
Mo	ppm	HF/HNO3	11.78	11.48	18.77	2.65	11.39	39.96	3.65	8.01
Ag	ppm	HF/HNO3	<1	<1	<1	<1	<1	<1	<1	2.55
Cd	ppm	HF/HNO3	<0.9	<0.9	<0.9	<0.9	<0.9	<0.9	<0.9	<0.9
Sn	ppm	HF/HNO3	4.12	3.31	4.11	7.79	5.65	6.57	3.90	8.00
Sb	ppm	HF/HNO3	1.74	0.70	0.64	0.92	2.24	8.43	0.98	2.68
Te	ppm	HF/HNO3	4.98	<4.3	<4.3	<4.3	<4.3	6.88	<4.3	<4.3
I	ppm	HF/HNO3	<37	<37	<37	<37	<37	<37	<37	<37
W	ppm	HF/HNO3	13.30	7.71	6.89	5.63	5.23	9.37	7.16	3.14
Pb	ppm	HF/HNO3	<25.3	<25.3	<25.3	<25.3	<25.3	31.60	<25.3	<25.3
Bi	ppm	HF/HNO3	5.14	5.23	2.09	3.59	7.01	10.73	1.59	4.52
Nb	ppm	Na_2O_2 Sinter	8.77	5.88	6.03	5.42	7.92	13.40	7.03	5.59
La	ppm	Na_2O_2 Sinter	4.38	22.54	33.51	12.97	21.44	28.92	12.54	6.28
Ce	ppm	Na_2O_2 Sinter	9.11	48.50	71.84	28.10	44.59	62.15	26.56	12.71
Pr	ppm	Na_2O_2 Sinter	1.15	6.21	9.16	3.59	5.67	7.76	3.36	1.64
Nd	ppm	Na_2O_2 Sinter	4.86	25.54	40.38	15.91	24.49	32.85	14.65	7.10
Sm	ppm	Na_2O_2 Sinter	1.33	6.30	9.22	4.06	5.83	8.12	3.72	1.83
Eu	ppm	Na_2O_2 Sinter	0.32	0.82	1.10	0.47	1.32	2.09	0.91	0.34
Tb	ppm	Na_2O_2 Sinter	0.43	1.08	1.29	0.88	1.11	1.46	0.75	0.44
Dy	ppm	Na_2O_2 Sinter	3.55	7.50	8.20	6.14	7.25	9.99	5.33	3.18
Ho	ppm	Na_2O_2 Sinter	0.90	1.61	1.69	1.34	1.69	2.26	1.25	0.74
Er	ppm	Na_2O_2 Sinter	3.22	4.73	4.87	4.12	5.02	6.95	3.88	2.50
Tm	ppm	Na_2O_2 Sinter	0.56	0.69	0.70	0.62	0.79	1.07	0.59	0.42
Yb	ppm	Na_2O_2 Sinter	4.22	4.61	4.49	4.18	5.41	7.30	4.28	3.15
Lu	ppm	Na_2O_2 Sinter	0.68	0.68	0.65	0.64	0.79	1.14	0.67	0.48
Hf	ppm	Na_2O_2 Sinter	4.89	3.53	3.04	3.48	4.87	7.14	4.08	3.85
Ta	ppm	Na_2O_2 Sinter	0.31	0.22	0.22	0.22	0.30	0.46	0.28	0.21
Th	ppm	Na_2O_2 Sinter	6.09	4.36	4.62	4.38	6.84	9.86	5.93	4.64
AlOH WL	nm	Terraspec	2,196	#DIV/0!	2,198	2,200	2,204	2,204	2,201	2,198
AlOH Depth	%	Terraspec	2.26%	#DIV/0!	13.28%	15.10%	8.93%	11.10%	6.75%	2.89%
FeOH WL	nm	Terraspec	2,252	2,253	2,254	2,254	#DIV/0!	#DIV/0!	2,252	2,252
FeOH Depth	%	Terraspec	7.94%	9.73%	6.02%	1.95%	#DIV/0!	#DIV/0!	2.00%	2.82%
AlOH depth/FeOH depth		Terraspec	0.28	#DIV/0!	2.21	7.76	#DIV/0!	#DIV/0!	3.38	1.02

Abbreviations:	**Units**		**Alteration**	**Other**
	HFL= Hanging wall flow	FT= Footwall tuff	Qtz-Ser= Quartz-sericite	WL= Wavelength
	HBX= Hanging wall breccia	FBX= Footwall breccia	Chl-Ser= Chlorite-sericite	
	FLT= Footwall lapilli tuff	FFL= Footwall flow	Chl=Chlorite	
		INT= Intrusion		

Appendix B: Table B1.1 Whole-rock Geochemistry and Terraspec™ Data

Sample ID			**H500686**	**H500687**	**H500688**	**H500689**	**H500690**	**H500691**	**H500692**	**H500693**
Hole ID			BD10-77	BD10-76	BD10-76	BD10-76	BD10-76	BD10-63	BD10-63	BD10-63
Depth (m)			49.1	48.2	36	27.2	7.7	11.4	21.3	37.5
Lithology			FLT	FLT	FLT	FLT	FLT	HBX	HFL	FLT
Alteration			Qtz-Ser	Chl-Ser	Qtz-Ser	Chl	Qtz-Ser	Qtz-Ser	Qtz-Ser	Qtz-Ser
SiO_2	%	FUS-ICP	80.12	69.63	77.39	35.35	76.08	75.18	69.35	67.18
Al_2O_3	%	FUS-ICP	10.49	8.46	9.65	12.86	7.96	9.55	9.13	13.06
Fe_2O_3(T)	%	FUS-ICP	2.75	10.3	4.29	22.93	7.56	2.5	7.65	5.71
MnO	%	FUS-ICP	0.012	0.071	0.023	0.154	0.025	0.225	0.043	0.158
MgO	%	FUS-ICP	0.88	3.91	0.77	12.64	1.09	2.48	0.59	2.92
CaO	%	FUS-ICP	0.06	0.05	0.07	0.06	0.04	0.16	0.05	0.08
Na_2O	%	FUS-ICP	0.2	0.13	0.22	0.04	0.15	0.12	0.12	0.18
K_2O	%	FUS-ICP	2.75	1.18	2.57	0.38	2.07	2.7	2.71	3.37
TiO_2	%	FUS-ICP	0.152	0.128	0.145	0.178	0.112	0.127	0.105	0.212
P_2O_5	%	FUS-ICP	0.02	0.01	0.02	< 0.01	< 0.01	0.02	< 0.01	0.03
LOI	%	FUS-ICP	2.79	6.26	3.66	14.75	5.29	4.22	5.51	5.69
Total	%	FUS-ICP	100.2	100.1	98.82	99.35	100.4	97.31	95.25	98.59
Ba	ppm	FUS-ICP	949	431	945	156	918	1611	1999	2138
Sr	ppm	FUS-ICP	9	6	10	3	7	7	6	7
Y	ppm	FUS-ICP	35	33	35	47	28	35	29	40
Sc	ppm	FUS-ICP	11	11	11	16	8	9	7	13
Zr	ppm	FUS-ICP	124	110	118	150	106	110	128	142
Be	ppm	FUS-ICP	< 1	< 1	< 1	< 1	< 1	1	< 1	< 1
V	ppm	FUS-ICP	5	< 5	< 5	< 5	7	5	6	10
Hg	ppb	FIMS	< 5	< 5	< 5	6	6	393	3170	102
Cr	ppm	HF/HNO3	<8.9	<8.9	<8.9	<8.9	<8.9	12.24	<8.9	<8.9
Co	ppm	HF/HNO3	19.43	52.74	16.26	83.18	14.74	<0.9	<0.9	1.37
Ni	ppm	HF/HNO3	<10	<10	<10	<10	<10	<10	<10	<10
Cu	ppm	HF/HNO3	301.78	73.83	52.16	35.83	576.22	140.39	2416.34	788.50
Zn	ppm	HF/HNO3	33.87	39.48	27.71	201.16	99.93	4684.56	29897.05	453.44
As	ppm	HF/HNO3	2.22	15.03	3.11	13.47	8.30	4.80	126.17	15.04
Se	ppm	HF/HNO3	<26.7	<26.7	<26.7	35.33	<26.7	<26.7	<26.7	<26.7
Br	ppm	HF/HNO3	200.28	206.82	187.45	205.52	253.93	181.51	177.63	164.87
Mo	ppm	HF/HNO3	12.04	2.18	10.43	50.37	7.46	6.07	5.39	4.30
Ag	ppm	HF/HNO3	<1	<1	<1	<1	<1	<1	4.18	<1
Cd	ppm	HF/HNO3	<0.9	<0.9	<0.9	<0.9	<0.9	14.33	95.10	1.35
Sn	ppm	HF/HNO3	3.47	3.67	4.23	3.51	3.77	3.24	8.26	3.58
Sb	ppm	HF/HNO3	0.94	1.80	0.80	0.91	0.99	3.96	12.11	6.39
Te	ppm	HF/HNO3	<4.3	6.93	4.74	8.18	<4.3	<4.3	<4.3	<4.3
I	ppm	HF/HNO3	<37	<37	<37	<37	<37	<37	<37	<37
W	ppm	HF/HNO3	3.78	5.69	3.70	8.62	3.38	3.06	6.17	3.36
Pb	ppm	HF/HNO3	<25.3	<25.3	<25.3	<25.3	<25.3	501.85	3494.63	59.91
Bi	ppm	HF/HNO3	2.29	8.37	7.69	12.87	1.86	<0.1	4.34	1.65
Nb	ppm	Na_2O_2 Sinter	5.23	5.29	5.41	8.86	4.59	5.75	5.12	7.61
La	ppm	Na_2O_2 Sinter	21.45	16.63	16.81	20.37	12.04	14.30	14.18	20.02
Ce	ppm	Na_2O_2 Sinter	46.55	35.48	34.37	42.72	26.05	31.03	30.79	42.45
Pr	ppm	Na_2O_2 Sinter	6.05	4.58	4.35	5.32	3.31	3.92	3.90	5.35
Nd	ppm	Na_2O_2 Sinter	25.42	19.76	18.76	23.09	13.66	16.97	16.48	22.98
Sm	ppm	Na_2O_2 Sinter	5.77	4.74	4.29	5.83	3.61	4.09	4.08	5.41
Eu	ppm	Na_2O_2 Sinter	0.90	0.55	0.70	1.13	0.39	0.78	1.23	1.12
Tb	ppm	Na_2O_2 Sinter	0.92	0.83	0.83	1.20	0.67	0.88	0.79	1.03
Dy	ppm	Na_2O_2 Sinter	5.87	5.58	5.46	8.48	4.45	5.90	5.41	6.91
Ho	ppm	Na_2O_2 Sinter	1.28	1.21	1.19	1.84	0.87	1.31	1.16	1.50
Er	ppm	Na_2O_2 Sinter	3.86	3.69	3.62	5.49	2.74	4.00	3.48	4.53
Tm	ppm	Na_2O_2 Sinter	0.58	0.55	0.58	0.84	0.38	0.62	0.53	0.69
Yb	ppm	Na_2O_2 Sinter	4.17	3.64	3.88	5.41	2.67	4.17	3.86	4.74
Lu	ppm	Na_2O_2 Sinter	0.62	0.58	0.58	0.86	0.45	0.65	0.59	0.73
Hf	ppm	Na_2O_2 Sinter	4.14	3.64	4.07	4.70	3.14	3.67	3.91	4.59
Ta	ppm	Na_2O_2 Sinter	0.23	0.22	0.22	0.31	0.19	0.21	0.21	0.27
Th	ppm	Na_2O_2 Sinter	5.35	4.57	5.01	6.27	3.49	4.89	4.84	5.78
AlOH WL	nm	Terraspec	2,202	2,199	2,203	#DIV/0!	2,202	2,208	2,207	2,205
AlOH Depth	%	Terraspec	12.75%	7.86%	10.58%	#DIV/0!	5.73%	13.20%	6.97%	9.01%
FeOH WL	nm	Terraspec	2,256	2,253	#DIV/0!	2,251	#DIV/0!	2,252	#DIV/0!	2,254
FeOH Depth	%	Terraspec	1.04%	7.08%	#DIV/0!	6.24%	#DIV/0!	1.31%	#DIV/0!	1.66%
AlOH depth/FeOH depth		Terraspec	12.26	1.11	#DIV/0!	#DIV/0!	#DIV/0!	10.11	#DIV/0!	5.44

Abbreviations:	**Units**		**Alteration**	**Other**
	HFL= Hanging wall flow	FT= Footwall tuff	Qtz-Ser= Quartz-sericite	WL= Wavelength
	HBX= Hanging wall breccia	FBX= Footwall breccia	Chl-Ser= Chlorite-sericite	
	FLT= Footwall lapilli tuff	FFL= Footwall flow	Chl=Chlorite	
		INT= Intrusion		

Appendix B: Table B1.1 Whole-rock Geochemistry and Terraspec^{TM} Data

Sample ID			**H500694**	**H500695**	**H500696**	**H500697**	**H500698**	**H500699**	**H500700**	**H501201**
Hole ID			BD10-63	BD10-63	BD10-63	BD10-63	BD10-61	BD10-61	BD10-61	BD10-61
Depth (m)			57.3	59.1	64.1	75.4	11.1	24.9	37.9	39.5
Lithology			FLT	FBX	FFL	FBX	FLT	FLT	FLT	FBX
Alteration			Chl	Qtz-Ser	Qtz-Ser	Qtz-Ser	Chl-Ser	Chl	Chl-Ser	Chl-Ser
SiO_2	%	FUS-ICP	48.39	75.63	76.1	74.08	66.13	55.32	67.31	70.52
Al_2O_3	%	FUS-ICP	6.36	10.83	10.88	10.17	7.18	12.26	8.27	8.18
Fe_2O_3(T)	%	FUS-ICP	23	4.32	3.78	5.89	14.65	7.5	11.4	9.1
MnO	%	FUS-ICP	0.099	0.056	0.048	0.044	0.012	0.204	0.068	0.061
MgO	%	FUS-ICP	4.35	2.41	2.53	1.95	0.29	12.97	5.37	4.94
CaO	%	FUS-ICP	0.05	0.13	0.08	0.08	0.04	0.88	0.04	0.05
Na_2O	%	FUS-ICP	0.06	0.18	0.18	0.17	0.13	0.06	0.06	0.07
K_2O	%	FUS-ICP	0.5	2.7	2.73	2.51	2.05	0.52	0.48	0.68
TiO_2	%	FUS-ICP	0.084	0.177	0.173	0.166	0.107	0.387	0.167	0.141
P_2O_5	%	FUS-ICP	< 0.01	0.03	0.03	0.02	0.02	0.08	< 0.01	0.02
LOI	%	FUS-ICP	12.54	3.99	4.17	4.94	8.38	8.92	6.01	5
Total	%	FUS-ICP	95.44	100.4	100.7	100	98.98	99.11	99.18	98.75
Ba	ppm	FUS-ICP	215	1156	1103	1059	1592	312	208	308
Sr	ppm	FUS-ICP	4	8	7	8	4	12	2	3
Y	ppm	FUS-ICP	16	36	40	29	24	32	31	30
Sc	ppm	FUS-ICP	5	9	11	10	7	16	9	8
Zr	ppm	FUS-ICP	79	134	133	126	89	119	102	105
Be	ppm	FUS-ICP	< 1	< 1	< 1	< 1	< 1	< 1	< 1	< 1
V	ppm	FUS-ICP	< 5	8	< 5	< 5	< 5	77	11	5
Hg	ppb	FIMS	42	10	< 5	< 5	52	13	11	12
Cr	ppm	HF/HNO3	<8.9	<8.9	<8.9	<8.9	28.66	58.80	10.50	<8.9
Co	ppm	HF/HNO3	30.32	1.09	<0.9	1.73	9.53	5.01	43.73	27.87
Ni	ppm	HF/HNO3	<10	<10	<10	<10	20.12	18.11	<10	<10
Cu	ppm	HF/HNO3	26390.83	504.50	145.31	62.86	1270.79	25.55	529.14	402.61
Zn	ppm	HF/HNO3	222.84	86.13	71.48	202.89	290.41	365.36	81.92	72.94
As	ppm	HF/HNO3	30.49	3.09	5.05	13.04	72.59	<1.6	21.25	3.76
Se	ppm	HF/HNO3	43.17	<26.7	<26.7	<26.7	<26.7	<26.7	<26.7	<26.7
Br	ppm	HF/HNO3	173.88	167.92	185.64	189.40	162.49	197.07	185.95	217.70
Mo	ppm	HF/HNO3	10.47	15.41	2.47	4.36	12.37	1.99	14.91	8.62
Ag	ppm	HF/HNO3	2.80	<1	<1	<1	1.02	<1	<1	<1
Cd	ppm	HF/HNO3	<0.9	<0.9	<0.9	<0.9	<0.9	<0.9	<0.9	<0.9
Sn	ppm	HF/HNO3	3.11	4.15	3.27	3.30	3.57	3.39	2.79	2.83
Sb	ppm	HF/HNO3	2.60	1.74	1.22	1.85	3.54	0.72	0.62	0.84
Te	ppm	HF/HNO3	10.94	<4.3	<4.3	<4.3	6.58	<4.3	6.73	<4.3
I	ppm	HF/HNO3	<37	<37	<37	<37	<37	<37	<37	<37
W	ppm	HF/HNO3	4.92	1.51	1.99	1.56	2.44	2.53	8.62	2.26
Pb	ppm	HF/HNO3	27.75	<25.3	<25.3	<25.3	132.00	67.27	<25.3	<25.3
Bi	ppm	HF/HNO3	17.94	1.73	0.68	1.36	6.06	0.78	6.90	3.13
Nb	ppm	Na_2O_2 Sinter	4.22	7.25	6.45	5.48	4.14	6.90	5.08	4.79
La	ppm	Na_2O_2 Sinter	8.95	19.08	16.50	16.11	12.25	12.62	10.67	11.13
Ce	ppm	Na_2O_2 Sinter	17.98	41.02	34.55	33.92	25.58	28.17	22.20	22.95
Pr	ppm	Na_2O_2 Sinter	2.26	5.05	4.35	4.24	3.15	3.58	2.75	2.95
Nd	ppm	Na_2O_2 Sinter	9.52	21.09	18.33	18.03	13.52	14.83	11.71	12.20
Sm	ppm	Na_2O_2 Sinter	2.35	5.07	4.51	4.32	3.46	3.81	3.11	3.06
Eu	ppm	Na_2O_2 Sinter	0.50	0.98	0.91	0.75	0.87	1.05	0.52	0.55
Tb	ppm	Na_2O_2 Sinter	0.49	0.90	0.92	0.79	0.64	0.78	0.75	0.72
Dy	ppm	Na_2O_2 Sinter	3.51	5.91	6.35	5.18	4.35	5.54	5.12	4.75
Ho	ppm	Na_2O_2 Sinter	0.77	1.28	1.30	1.06	0.93	1.20	1.02	0.98
Er	ppm	Na_2O_2 Sinter	2.27	3.87	4.04	3.16	2.74	3.69	3.20	2.89
Tm	ppm	Na_2O_2 Sinter	0.36	0.59	0.60	0.48	0.42	0.58	0.48	0.45
Yb	ppm	Na_2O_2 Sinter	2.47	4.00	4.09	3.32	2.83	3.87	3.32	2.96
Lu	ppm	Na_2O_2 Sinter	0.39	0.61	0.65	0.51	0.45	0.61	0.51	0.45
Hf	ppm	Na_2O_2 Sinter	2.35	4.07	4.29	3.60	2.95	4.18	2.92	2.85
Ta	ppm	Na_2O_2 Sinter	0.15	0.26	0.26	0.22	0.17	0.25	0.19	0.19
Th	ppm	Na_2O_2 Sinter	3.19	5.60	5.19	4.85	3.65	4.53	3.81	3.92
AlOH WL	nm	Terraspec	2,197	2,205	2,204	2,202	2,206	#DIV/0!	2,198	2,202
AlOH Depth	%	Terraspec	1.68%	9.43%	17.00%	13.63%	6.12%	#DIV/0!	2.74%	8.61%
FeOH WL	nm	Terraspec	2,251	2,251	2,252	2,255	#DIV/0!	2,250	2,253	2,253
FeOH Depth	%	Terraspec	4.00%	1.12%	2.64%	1.16%	#DIV/0!	3.44%	6.41%	7.46%
AlOH depth/FeOH depth		Terraspec	0.42	8.44	6.45	11.75	#DIV/0!	#DIV/0!	0.43	1.15

Abbreviations:	**Units**		**Alteration**	**Other**
	HFL= Hanging wall flow	FT= Footwall tuff	Qtz-Ser= Quartz-sericite	WL= Wavelength
	HBX= Hanging wall breccia	FBX= Footwall breccia	Chl-Ser= Chlorite-sericite	
	FLT= Footwall lapilli tuff	FFL= Footwall flow	Chl=Chlorite	
		INT= Intrusion		

Appendix B: Table B1.1 Whole-rock Geochemistry and Terraspec^{TM} Data

Sample ID			**H501202**	**H501203**	**H501204**	**H501205**	**H501206**	**H501207**	**H501208**	**H501212**
Hole ID			BD10-61	BD10-58	BD10-58	BD10-58	BD10-58	BD10-58	BD10-58	BD10-40
Depth (m)			44.4	8.2	15	18.2	29.5	32.3	34.9	4
Lithology			FBX	FLT	FLT	FLT	FLT	FBX	FLT	HFL
Alteration			Chl-Ser	Chl-Ser	Chl	Chl-Ser	Chl-Ser	Chl-Ser	Chl-Ser	Qtz-Ser
SiO_2	%	FUS-ICP	68.61	59.01	15.62	65.17	47.86	57.12	67.85	74.58
Al_2O_3	%	FUS-ICP	8.9	6.46	13.37	7.92	7.41	4.37	7.63	10.69
Fe_2O_3(T)	%	FUS-ICP	6.54	18.33	41.47	15.57	23.44	21.52	11.82	5.99
MnO	%	FUS-ICP	0.261	0.046	0.176	0.035	0.096	0.037	0.049	0.078
MgO	%	FUS-ICP	4.44	3.31	9.62	0.79	3.12	0.8	1.36	1.29
CaO	%	FUS-ICP	1.73	0.05	0.05	0.06	0.05	0.04	0.05	0.05
Na_2O	%	FUS-ICP	0.11	0.08	0.05	0.19	0.1	0.08	0.15	0.22
K_2O	%	FUS-ICP	1.46	0.64	0.33	2.02	0.8	0.86	1.43	2.8
TiO_2	%	FUS-ICP	0.148	0.107	0.208	0.118	0.081	0.052	0.092	0.134
P_2O_5	%	FUS-ICP	0.01	< 0.01	0.01	< 0.01	< 0.01	< 0.01	< 0.01	0.02
LOI	%	FUS-ICP	5.99	9.87	19.31	8.4	14.26	11.16	7.3	4.75
Total	%	FUS-ICP	98.19	97.9	100.2	100.3	97.2	96.04	97.73	100.6
Ba	ppm	FUS-ICP	638	375	167	966	372	380	625	1320
Sr	ppm	FUS-ICP	28	3	3	10	5	5	7	8
Y	ppm	FUS-ICP	31	15	27	19	17	10	25	55
Sc	ppm	FUS-ICP	10	7	12	9	7	4	10	10
Zr	ppm	FUS-ICP	105	69	169	103	76	54	88	140
Be	ppm	FUS-ICP	< 1	< 1	< 1	< 1	< 1	< 1	< 1	< 1
V	ppm	FUS-ICP	< 5	12	27	16	10	< 5	6	7
Hg	ppb	FIMS	6	143	115	111	61	344	33	16
Cr	ppm	HF/HNO3	25.64	15.55	<8.9	9.25	9.49	15.08	<8.9	<8.9
Co	ppm	HF/HNO3	12.77	83.27	43.54	26.24	85.57	5.38	14.42	39.97
Ni	ppm	HF/HNO3	22.32	<10	11.46	<10	<10	<10	<10	<10
Cu	ppm	HF/HNO3	660.81	1354.59	6775.19	7902.28	16384.09	16923.74	3928.48	3118.32
Zn	ppm	HF/HNO3	65.25	66.97	295.22	79.35	130.89	182.75	69.21	49.23
As	ppm	HF/HNO3	3.37	37.57	303.63	40.52	80.96	236.23	16.71	30.08
Se	ppm	HF/HNO3	<26.7	67.46	73.96	43.53	75.58	<26.7	<26.7	<26.7
Br	ppm	HF/HNO3	175.61	187.03	150.81	165.52	154.26	166.20	179.81	255.44
Mo	ppm	HF/HNO3	12.16	49.06	59.84	26.72	56.11	13.99	14.84	11.06
Ag	ppm	HF/HNO3	<1	<1	1.31	<1	2.20	3.65	<1	<1
Cd	ppm	HF/HNO3	<0.9	<0.9	<0.9	<0.9	<0.9	<0.9	<0.9	<0.9
Sn	ppm	HF/HNO3	2.83	3.14	4.51	4.55	4.18	5.36	5.05	4.13
Sb	ppm	HF/HNO3	0.91	1.33	4.39	2.55	4.94	36.48	1.18	4.75
Te	ppm	HF/HNO3	<4.3	9.85	45.12	11.85	248.50	10.17	6.24	11.08
I	ppm	HF/HNO3	<37	<37	<37	<37	<37	<37	<37	<37
W	ppm	HF/HNO3	2.07	8.44	15.84	4.40	6.50	3.46	2.49	3.57
Pb	ppm	HF/HNO3	<25.3	<25.3	50.63	<25.3	26.37	50.08	<25.3	<25.3
Bi	ppm	HF/HNO3	2.16	9.34	65.44	19.66	374.70	19.50	9.36	15.66
Nb	ppm	Na2O2 Sinter	6.12	3.03	8.03	4.09	3.37	2.72	4.63	7.65
La	ppm	Na2O2 Sinter	18.58	8.39	21.00	10.45	9.14	6.49	8.81	20.30
Ce	ppm	Na2O2 Sinter	38.35	16.83	42.87	22.48	19.15	13.76	18.65	42.90
Pr	ppm	Na2O2 Sinter	4.86	2.08	5.26	2.87	2.44	1.74	2.39	5.41
Nd	ppm	Na2O2 Sinter	20.43	8.53	22.15	12.41	10.28	7.25	9.94	22.38
Sm	ppm	Na2O2 Sinter	4.83	1.84	4.96	3.01	2.70	1.77	2.63	5.87
Eu	ppm	Na2O2 Sinter	0.61	0.27	0.89	0.77	0.40	0.53	0.76	0.74
Tb	ppm	Na2O2 Sinter	0.86	0.36	0.82	0.52	0.52	0.28	0.66	1.26
Dy	ppm	Na2O2 Sinter	5.70	2.31	5.81	3.54	3.57	2.05	4.38	8.67
Ho	ppm	Na2O2 Sinter	1.23	0.52	1.27	0.78	0.77	0.42	1.02	1.84
Er	ppm	Na_2O_2 Sinter	3.59	1.64	4.14	2.36	2.45	1.33	3.22	5.81
Tm	ppm	Na2O2 Sinter	0.54	0.26	0.65	0.38	0.37	0.20	0.51	0.88
Yb	ppm	Na2O2 Sinter	3.81	1.83	4.72	2.64	2.56	1.49	3.52	6.02
Lu	ppm	Na2O2 Sinter	0.55	0.30	0.73	0.39	0.42	0.25	0.58	0.96
Hf	ppm	Na2O2 Sinter	3.88	2.45	4.83	3.34	3.36	2.02	3.51	4.49
Ta	ppm	Na2O2 Sinter	0.23	0.10	0.29	0.16	0.14	0.11	0.20	0.28
Th	ppm	Na2O2 Sinter	4.88	2.43	6.59	3.64	3.25	2.23	3.74	5.04
AlOH WL	nm	Terraspec	2,202	2,202	#DIV/0!	2,201	2,204	2,202	2,200	2,203
AlOH Depth	%	Terraspec	7.13%	1.56%	#DIV/0!	3.87%	1.91%	3.22%	2.24%	13.80%
FeOH WL	nm	Terraspec	2,253	2,253	2,253	#DIV/0!	2,255	#DIV/0!	2,257	#DIV/0!
FeOH Depth	%	Terraspec	4.50%	2.26%	2.06%	#DIV/0!	1.37%	#DIV/0!	1.57%	#DIV/0!
AlOH depth/FeOH depth		Terraspec	1.58	0.69	#DIV/0!	#DIV/0!	1.39	#DIV/0!	1.43	#DIV/0!

Abbreviations:	**Units**		**Alteration**	**Other**
	HFL= Hanging wall flow	FT= Footwall tuff	Qtz-Ser= Quartz-sericite	WL= Wavelength
	HBX= Hanging wall breccia	FBX= Footwall breccia	Chl-Ser= Chlorite-sericite	
	FLT= Footwall lapilli tuff	FFL= Footwall flow	Chl=Chlorite	
		INT= Intrusion		

Appendix B: Table B1.1 Whole-rock Geochemistry and Terraspec™ Data

Sample ID			**H501213**	**H501214**	**H501215**	**H501216**	**H501217**	**H501218**	**H501219**	**H501220**
Hole ID			BD10-40	BD10-40	BD10-40	BD10-40	BD10-98	BD10-98	BD10-98	BD10-98
Depth (m)			9.5	30.5	43.7	16.4	13.7	23	40.4	42.8
Lithology			HBX	HBX	FLT	HBX	FLT	FLT	FLT	FFL
Alteration			Qtz-Ser	Qtz-Ser	Qtz-Ser	Qtz-Ser	Chl	Chl-Ser	Chl	Qtz-Ser
SiO_2	%	FUS-ICP	65.39	67.62	69.79	76.73	21.26	60.94	62.32	72.7
Al_2O_3	%	FUS-ICP	12.23	13.34	10.26	11.11	18.1	14.73	10.43	13
Fe_2O_3(T)	%	FUS-ICP	7.94	4.88	7.21	2.79	24.73	6.29	9.78	4.15
MnO	%	FUS-ICP	0.185	0.145	0.071	0.132	0.233	0.102	0.128	0.065
MgO	%	FUS-ICP	2.41	2.99	1.97	1.79	16.23	7.97	9.63	2.44
CaO	%	FUS-ICP	0.07	0.14	0.06	0.28	0.09	0.31	0.06	0.06
Na_2O	%	FUS-ICP	0.28	0.47	0.39	0.24	0.61	0.27	0.06	0.23
K_2O	%	FUS-ICP	3.01	3.44	2.63	2.97	0.71	2.19	0.5	3.28
TiO_2	%	FUS-ICP	0.156	0.168	0.149	0.14	0.242	0.243	0.167	0.182
P_2O_5	%	FUS-ICP	0.02	0.02	0.01	0.03	0.01	0.03	0.02	0.03
LOI	%	FUS-ICP	6.85	6.76	6.91	3.86	17.88	6.96	7.63	4.41
Total	%	FUS-ICP	98.54	99.97	99.47	100.1	100.1	100	100.7	100.5
Ba	ppm	FUS-ICP	1367	1377	832	1295	391	2759	202	1444
Sr	ppm	FUS-ICP	12	25	17	12	34	27	5	9
Y	ppm	FUS-ICP	45	52	35	41	70	46	38	50
Sc	ppm	FUS-ICP	11	12	9	11	17	20	10	14
Zr	ppm	FUS-ICP	153	180	132	152	250	168	145	175
Be	ppm	FUS-ICP	1	1	< 1	1	< 1	< 1	< 1	1
V	ppm	FUS-ICP	7	6	10	7	11	42	13	7
Hg	ppb	FIMS	9	19	23	9	68	20	6	8
Cr	ppm	HF/HNO3	32.25	<8.9	<8.9	13.63	<8.9	<8.9	9.09	<8.9
Co	ppm	HF/HNO3	3.11	2.47	9.56	<0.9	16.42	0.94	8.00	3.11
Ni	ppm	HF/HNO3	<10	<10	<10	<10	<10	<10	<10	<10
Cu	ppm	HF/HNO3	55.96	50.21	275.50	21.99	198.95	<19	38.83	233.80
Zn	ppm	HF/HNO3	287.07	231.26	128.79	130.56	1109.40	238.01	202.13	65.67
As	ppm	HF/HNO3	9.96	6.56	18.05	12.47	79.21	<1.6	2.69	10.90
Se	ppm	HF/HNO3	<26.7	<26.7	<26.7	<26.7	<26.7	<26.7	<26.7	<26.7
Br	ppm	HF/HNO3	257.37	244.01	235.41	246.97	240.93	218.08	252.34	236.83
Mo	ppm	HF/HNO3	8.96	3.11	6.62	5.93	3.10	4.80	4.88	3.98
Ag	ppm	HF/HNO3	<1	<1	<1	<1	<1	<1	<1	<1
Cd	ppm	HF/HNO3	<0.9	<0.9	<0.9	<0.9	3.14	<0.9	<0.9	<0.9
Sn	ppm	HF/HNO3	3.92	5.47	5.35	3.22	3.46	5.79	3.21	4.62
Sb	ppm	HF/HNO3	1.39	1.79	1.37	1.14	1.29	0.69	0.93	1.68
Te	ppm	HF/HNO3	<4.3	<4.3	5.93	<4.3	<4.3	<4.3	<4.3	<4.3
I	ppm	HF/HNO3	<37	<37	<37	<37	<37	<37	<37	<37
W	ppm	HF/HNO3	3.41	4.74	9.59	5.55	6.01	6.54	1.91	4.00
Pb	ppm	HF/HNO3	<25.3	<25.3	33.28	<25.3	<25.3	<25.3	<25.3	28.18
Bi	ppm	HF/HNO3	1.34	0.62	8.32	0.59	4.02	0.47	1.58	1.01
Nb	ppm	Na2O2 Sinter	7.58	9.54	8.43	9.83	15.55	10.72	9.17	10.96
La	ppm	Na2O2 Sinter	21.14	19.82	15.73	19.78	27.67	19.41	18.78	22.56
Ce	ppm	Na2O2 Sinter	43.82	41.90	32.77	41.52	55.42	40.30	39.77	48.20
Pr	ppm	Na2O2 Sinter	5.50	5.32	4.06	5.22	6.86	5.12	5.05	6.08
Nd	ppm	Na2O2 Sinter	23.26	22.23	17.80	22.24	29.77	21.79	22.04	25.50
Sm	ppm	Na2O2 Sinter	5.97	5.51	4.16	5.41	7.36	5.40	5.48	6.15
Eu	ppm	Na2O2 Sinter	1.15	0.96	0.57	0.94	1.19	1.98	0.83	1.08
Tb	ppm	Na2O2 Sinter	1.22	1.19	0.83	0.99	1.73	1.13	1.00	1.28
Dy	ppm	Na2O2 Sinter	8.12	8.21	5.77	6.70	11.70	7.74	6.53	8.51
Ho	ppm	Na2O2 Sinter	1.69	1.68	1.19	1.43	2.45	1.60	1.42	1.78
Er	ppm	Na_2O_2 Sinter	5.20	5.17	3.67	4.33	7.50	5.10	4.18	5.52
Tm	ppm	Na2O2 Sinter	0.75	0.79	0.57	0.68	1.13	0.77	0.64	0.81
Yb	ppm	Na2O2 Sinter	5.29	5.50	3.92	4.69	7.87	5.10	4.44	5.65
Lu	ppm	Na2O2 Sinter	0.80	0.87	0.57	0.70	1.20	0.77	0.67	0.87
Hf	ppm	Na2O2 Sinter	5.15	4.82	4.50	6.64	7.09	6.41	4.75	6.15
Ta	ppm	Na2O2 Sinter	0.32	0.35	0.30	0.36	0.58	0.40	0.32	0.40
Th	ppm	Na2O2 Sinter	5.87	6.16	7.88	7.77	12.23	8.16	7.64	8.09
AlOH WL	nm	Terraspec	2,202	2,203	2,201	2,204	2,190	2,200	2,195	2,203
AlOH Depth	%	Terraspec	7.52%	9.53%	17.75%	13.10%	3.08%	2.70%	3.02%	12.55%
FeOH WL	nm	Terraspec	#DIV/0!	#DIV/0!	#DIV/0!	2,254	2,252	2,251	2,251	2,253
FeOH Depth	%	Terraspec	#DIV/0!	#DIV/0!	#DIV/0!	1.49%	4.24%	2.09%	9.66%	2.45%
AlOH depth/FeOH depth		Terraspec	#DIV/0!	#DIV/0!	#DIV/0!	8.81	0.73	1.29	0.31	5.12

Abbreviations:

Units
HFL= Hanging wall flow
HBX= Hanging wall breccia
FLT= Footwall lapilli tuff
FT= Footwall tuff
FBX= Footwall breccia
FFL= Footwall flow
INT= Intrusion

Alteration
Qtz-Ser= Quartz-sericite
Chl-Ser= Chlorite-sericite
Chl=Chlorite

Other
WL= Wavelength

Appendix B: Table B1.1 Whole-rock Geochemistry and Terraspec™ Data

Sample ID			**H501221**	**H501222**	**H501223**	**H501224**	**H501225**	**H501226**	**H501227**	**H501228**
Hole ID			BD10-98	BD10-50	BD10-50	BD10-50	BD10-56	BD10-56	BD10-56	BD10-56
Depth (m)			50.8	9	15.6	30.6	7.4	21.2	29.9	41.4
Lithology			FLT	HFL	FLT	FLT	FLT	FLT	FLT	FLT
Alteration			Qtz-Ser	Chl-Ser	Qtz-Ser	Qtz-Ser	Qtz-Ser	Chl	Chl	Chl-Ser
SiO_2	%	FUS-ICP	74.1	54.83	74.15	70.79	72.28	32.36	37.01	67.44
Al_2O_3	%	FUS-ICP	10.86	13.1	10.56	12.06	13.9	17.04	9.97	8.67
Fe_2O_3(T)	%	FUS-ICP	4.48	13.69	7.04	4.86	2.63	8.69	24.22	10.11
MnO	%	FUS-ICP	0.095	0.07	0.019	0.086	0.044	0.318	0.114	0.048
MgO	%	FUS-ICP	2.3	4.75	0.32	2.68	2.98	24.79	11.18	1.4
CaO	%	FUS-ICP	0.04	0.05	0.08	0.07	0.07	1.33	0.17	0.05
Na_2O	%	FUS-ICP	0.19	0.22	0.23	0.23	0.29	0.02	0.03	0.19
K_2O	%	FUS-ICP	2.72	2.41	2.76	2.79	3.22	0.03	0.13	2.08
TiO_2	%	FUS-ICP	0.154	0.162	0.161	0.177	0.182	0.243	0.15	0.132
P_2O_5	%	FUS-ICP	< 0.01	0.01	0.02	0.03	0.02	0.1	0.02	0.01
LOI	%	FUS-ICP	4.45	9.44	4.75	4.56	4.27	14.96	16.08	7.54
Total	%	FUS-ICP	99.39	98.73	100.1	98.33	99.89	99.89	99.09	97.67
Ba	ppm	FUS-ICP	1217	1441	1193	1035	2370	30	69	971
Sr	ppm	FUS-ICP	7	12	16	11	21	38	4	8
Y	ppm	FUS-ICP	37	46	38	42	42	78	36	33
Sc	ppm	FUS-ICP	11	13	11	12	14	16	10	9
Zr	ppm	FUS-ICP	130	158	142	141	156	205	125	104
Be	ppm	FUS-ICP	1	< 1	< 1	1	1	< 1	< 1	< 1
V	ppm	FUS-ICP	8	< 5	17	6	16	12	< 5	< 5
Hg	ppb	FIMS	< 5	333	23	< 5	22	16	85	104
Cr	ppm	HF/HNO3	<8.9	<8.9	11.54	<8.9	<8.9	<8.9	<8.9	<8.9
Co	ppm	HF/HNO3	4.41	6.04	1.99	3.61	<0.9	1.28	47.23	1.12
Ni	ppm	HF/HNO3	<10	<10	<10	<10	<10	<10	<10	<10
Cu	ppm	HF/HNO3	398.02	108.98	1167.01	33.62	22.82	42.54	541.56	3173.38
Zn	ppm	HF/HNO3	58.19	151.30	70.33	84.13	107.68	474.89	127.19	150.08
As	ppm	HF/HNO3	3.58	17.89	10.62	9.48	4.35	1.96	46.02	47.86
Se	ppm	HF/HNO3	<26.7	<26.7	<26.7	<26.7	<26.7	<26.7	50.19	<26.7
Br	ppm	HF/HNO3	228.50	142.76	142.58	146.94	157.50	141.61	151.63	132.76
Mo	ppm	HF/HNO3	3.58	7.57	3.15	5.47	1.01	4.04	30.74	4.81
Ag	ppm	HF/HNO3	<1	<1	<1	<1	<1	<1	<1	<1
Cd	ppm	HF/HNO3	<0.9	<0.9	<0.9	<0.9	<0.9	<0.9	<0.9	<0.9
Sn	ppm	HF/HNO3	4.30	4.47	4.66	4.25	6.02	3.77	4.94	4.52
Sb	ppm	HF/HNO3	2.18	7.16	1.58	1.69	1.10	9.29	9.05	5.27
Te	ppm	HF/HNO3	<4.3	<4.3	<4.3	<4.3	<4.3	<4.3	4.59	<4.3
I	ppm	HF/HNO3	<37	<37	<37	<37	<37	<37	<37	<37
W	ppm	HF/HNO3	3.70	1.71	10.87	1.74	3.77	1.17	3.32	4.30
Pb	ppm	HF/HNO3	<25.3	<25.3	<25.3	<25.3	<25.3	<25.3	<25.3	<25.3
Bi	ppm	HF/HNO3	0.42	5.33	3.74	0.80	0.22	0.42	14.65	8.27
Nb	ppm	Na2O2 Sinter	7.80	8.10	6.52	7.50	8.51	11.47	12.56	5.98
La	ppm	Na2O2 Sinter	18.94	19.53	18.55	20.65	23.76	32.82	20.65	12.24
Ce	ppm	Na2O2 Sinter	38.54	40.85	37.15	42.75	48.50	67.33	43.03	25.33
Pr	ppm	Na2O2 Sinter	4.80	5.35	4.73	5.44	6.19	8.43	5.45	3.19
Nd	ppm	Na2O2 Sinter	19.59	22.78	20.25	22.93	26.69	36.34	23.78	13.42
Sm	ppm	Na2O2 Sinter	4.43	5.62	4.88	5.79	6.64	8.81	5.80	3.88
Eu	ppm	Na2O2 Sinter	1.04	1.12	0.69	1.13	1.53	2.29	0.95	0.93
Tb	ppm	Na2O2 Sinter	0.92	1.20	0.93	1.13	1.15	1.97	1.11	0.87
Dy	ppm	Na2O2 Sinter	5.79	8.00	6.08	7.52	7.48	13.19	7.51	5.89
Ho	ppm	Na2O2 Sinter	1.22	1.61	1.24	1.57	1.57	2.85	1.59	1.16
Er	ppm	Na_2O_2 Sinter	3.78	5.05	3.88	4.74	4.91	8.49	3.70	3.41
Tm	ppm	Na2O2 Sinter	0.60	0.74	0.60	0.73	0.75	1.23	0.75	0.56
Yb	ppm	Na2O2 Sinter	4.02	4.91	4.10	4.82	5.10	8.25	5.22	3.76
Lu	ppm	Na2O2 Sinter	0.61	0.79	0.64	0.75	0.82	1.29	0.81	0.67
Hf	ppm	Na2O2 Sinter	4.83	6.26	4.34	5.30	5.91	6.46	6.46	3.83
Ta	ppm	Na2O2 Sinter	0.30	0.31	0.25	0.31	0.33	0.43	0.43	0.23
Th	ppm	Na2O2 Sinter	6.09	6.37	5.13	5.81	6.45	9.14	8.16	4.24
AlOH WL	nm	Terraspec	2,204	2,196	2,201	2,201	2,200	#DIV/0!	#DIV/0!	2,203
AlOH Depth	%	Terraspec	13.20%	2.16%	8.14%	10.63%	13.53%	#DIV/0!	#DIV/0!	5.49%
FeOH WL	nm	Terraspec	2,252	2,252	#DIV/0!	2,254	2,252	2,250	2,251	#DIV/0!
FeOH Depth	%	Terraspec	1.84%	2.94%	#DIV/0!	2.00%	2.41%	1.92%	3.47%	#DIV/0!
AlOH depth/FeOH depth		Terraspec	7.17	0.73	#DIV/0!	5.30	5.61	#DIV/0!	#DIV/0!	#DIV/0!

Abbreviations:	**Units**		**Alteration**	**Other**
	HFL= Hanging wall flow	FT= Footwall tuff	Qtz-Ser= Quartz-sericite	WL= Wavelength
	HBX= Hanging wall breccia	FBX= Footwall breccia	Chl-Ser= Chlorite-sericite	
	FLT= Footwall lapilli tuff	FFL= Footwall flow	Chl=Chlorite	
		INT= Intrusion		

Appendix B: Table B1.1 Whole-rock Geochemistry and Terraspec^{TM} Data

Sample ID			**H501229**	**H501230**	**H501231**	**H501232**	**H501233**	**H501234**	**H501235**	**H501236**
Hole ID			BD10-56	BD10-49	BD10-49	BD10-49	BD10-49	BD10-34	BD10-34	BD10-34
Depth (m)			49.2	10.9	11.8	25	34.6	11.5	26	33.6
Lithology			FLT	FLT	FFL	FLT	FLT	HFL	HBX	FLT
Alteration			Chl-Ser	Qtz-Ser	Qtz-Ser	Qtz-Ser	Qtz-Ser	Qtz-Ser	Qtz-Ser	Qtz-Ser
SiO_2	%	FUS-ICP	66.73	73.42	77.61	69.72	65.45	65.88	75.32	76.8
Al_2O_3	%	FUS-ICP	9.04	10.52	11.28	12.09	11.9	13.36	12.74	10.39
Fe_2O_3(T)	%	FUS-ICP	12.87	6.1	3.57	5.8	8.94	7.18	2.08	3.06
MnO	%	FUS-ICP	0.017	0.032	0.036	0.145	0.081	0.117	0.069	0.089
MgO	%	FUS-ICP	0.56	0.77	1.37	3.66	2.14	1.87	1.74	1.6
CaO	%	FUS-ICP	0.06	0.06	0.06	0.13	0.12	0.08	0.08	0.39
Na_2O	%	FUS-ICP	0.2	0.22	0.21	0.2	0.23	0.21	0.22	0.18
K_2O	%	FUS-ICP	2.46	2.84	2.87	2.64	2.86	3.55	3.48	2.89
TiO_2	%	FUS-ICP	0.14	0.159	0.148	0.327	0.174	0.168	0.156	0.158
P_2O_5	%	FUS-ICP	0.01	0.01	< 0.01	0.06	0.09	0.02	0.02	0.02
LOI	%	FUS-ICP	7.97	4.83	3.42	5.47	6.98	6.17	3.44	4.04
Total	%	FUS-ICP	100.1	98.97	100.6	100.2	98.97	98.6	99.34	99.62
Ba	ppm	FUS-ICP	970	1292	1242	943	1280	1249	1211	782
Sr	ppm	FUS-ICP	7	10	10	11	11	7	12	13
Y	ppm	FUS-ICP	33	40	36	36	40	48	46	37
Sc	ppm	FUS-ICP	9	11	11	17	12	11	10	11
Zr	ppm	FUS-ICP	114	137	141	118	149	167	158	135
Be	ppm	FUS-ICP	< 1	< 1	< 1	< 1	< 1	1	1	1
V	ppm	FUS-ICP	< 5	6	< 5	71	6	< 5	7	7
Hg	ppb	FIMS	29	17	< 5	11	22	870	22	116
Cr	ppm	HF/HNO3	<8.9	12.94	<8.9	25.90	12.07	9.73	11.13	<8.9
Co	ppm	HF/HNO3	2.23	7.28	3.58	9.39	4.63	<0.9	<0.9	1.46
Ni	ppm	HF/HNO3	<10	<10	<10	20.41	<10	<10	<10	<10
Cu	ppm	HF/HNO3	2450.53	4906.70	249.57	184.23	389.14	472.52	<19	1503.49
Zn	ppm	HF/HNO3	84.62	104.43	78.53	94.79	115.93	10031.59	165.98	1111.95
As	ppm	HF/HNO3	32.41	5.39	5.03	20.08	27.71	37.91	22.32	8.19
Se	ppm	HF/HNO3	<26.7	<26.7	<26.7	<26.7	<26.7	<26.7	<26.7	<26.7
Br	ppm	HF/HNO3	133.78	162.94	163.63	158.49	159.93	262.27	274.49	151.87
Mo	ppm	HF/HNO3	5.61	8.77	6.41	6.07	8.35	3.89	8.97	1.18
Ag	ppm	HF/HNO3	<1	1.41	<1	<1	<1	<1	<1	1.48
Cd	ppm	HF/HNO3	<0.9	<0.9	<0.9	<0.9	<0.9	36.60	1.16	3.86
Sn	ppm	HF/HNO3	4.93	6.51	6.06	7.12	8.93	6.04	4.67	6.04
Sb	ppm	HF/HNO3	1.53	0.77	0.45	3.10	6.31	3.26	19.38	2.03
Te	ppm	HF/HNO3	<4.3	4.51	<4.3	4.91	6.73	<4.3	<4.3	<4.3
I	ppm	HF/HNO3	<37	<37	<37	<37	<37	<37	<37	<37
W	ppm	HF/HNO3	3.67	4.23	3.48	6.33	3.45	2.69	2.42	6.22
Pb	ppm	HF/HNO3	<25.3	<25.3	<25.3	<25.3	61.37	69.83	<25.3	340.65
Bi	ppm	HF/HNO3	4.86	10.50	3.65	3.69	8.37	1.01	0.20	1.58
Nb	ppm	Na2O2 Sinter	4.99	5.04	4.86	5.00	5.24	6.16	7.94	7.02
La	ppm	Na2O2 Sinter	14.09	13.37	13.10	17.15	14.29	18.86	19.83	18.69
Ce	ppm	Na2O2 Sinter	29.50	28.68	27.20	36.03	29.32	39.77	41.37	40.04
Pr	ppm	Na2O2 Sinter	3.71	3.61	3.49	4.61	3.72	5.12	5.17	5.09
Nd	ppm	Na2O2 Sinter	16.08	15.29	14.49	19.08	15.82	21.38	21.93	22.48
Sm	ppm	Na2O2 Sinter	4.49	4.19	3.64	4.77	4.04	5.34	5.54	5.42
Eu	ppm	Na2O2 Sinter	1.06	0.77	0.44	0.45	1.35	0.87	1.17	1.08
Tb	ppm	Na2O2 Sinter	0.88	0.78	0.73	0.82	0.83	1.01	1.15	1.05
Dy	ppm	Na2O2 Sinter	5.75	5.23	4.86	5.37	5.58	6.82	8.07	7.24
Ho	ppm	Na2O2 Sinter	1.09	0.99	1.04	1.14	1.19	1.47	1.78	1.63
Er	ppm	Na_2O_2 Sinter	3.05	3.17	3.68	3.72	4.51	5.47	5.15	3.91
Tm	ppm	Na2O2 Sinter	0.52	0.45	0.49	0.56	0.56	0.69	0.82	0.81
Yb	ppm	Na2O2 Sinter	3.53	3.19	3.40	3.86	3.84	4.76	5.68	5.30
Lu	ppm	Na2O2 Sinter	0.61	0.55	0.52	0.62	0.59	0.71	0.82	0.80
Hf	ppm	Na2O2 Sinter	3.80	3.74	2.68	3.16	2.73	4.23	4.19	4.47
Ta	ppm	Na2O2 Sinter	0.21	0.20	0.19	0.21	0.19	0.23	0.30	0.29
Th	ppm	Na2O2 Sinter	3.88	3.84	3.71	4.44	3.80	5.16	6.13	5.77
AlOH WL	nm	Terraspec	2,202	2,203	2,203	2,202	2,201	2,203	2,206	2,206
AlOH Depth	%	Terraspec	6.51%	12.88%	10.54%	11.15%	6.41%	9.57%	5.61%	4.96%
FeOH WL	nm	Terraspec	#DIV/0!	#DIV/0!	2,253	2,252	2,255	2,255	#DIV/0!	#DIV/0!
FeOH Depth	%	Terraspec	#DIV/0!	#DIV/0!	1.03%	1.43%	1.38%	1.18%	#DIV/0!	#DIV/0!
AlOH depth/FeOH depth		Terraspec	#DIV/0!	#DIV/0!	10.24	7.82	4.64	8.11	#DIV/0!	#DIV/0!

Abbreviations:	**Units**		**Alteration**	**Other**
	HFL= Hanging wall flow	FT= Footwall tuff	Qtz-Ser= Quartz-sericite	WL= Wavelength
	HBX= Hanging wall breccia	FBX= Footwall breccia	Chl-Ser= Chlorite-sericite	
	FLT= Footwall lapilli tuff	FFL= Footwall flow	Chl=Chlorite	
		INT= Intrusion		

Appendix B: Table B1.1 Whole-rock Geochemistry and Terraspec™ Data

Sample ID			**H501237**	**H501238**	**H501239**	**H501240**	**H501241**	**H501242**	**H501243**	**H501244**
Hole ID			BD10-34	BD10-33	BD10-33	BD10-33	BD10-33	BD10-33	BD10-45	BD10-45
Depth (m)			18.6	9.5	18.3	27.1	36.3	46.2	8.1	18.4
Lithology			HFL	HFL	FLT	HBX	FLT	FFL	HFL	HFL
Alteration			Qtz-Ser	Chl-Ser	Qtz-Ser	Qtz-Ser	Qtz-Ser	Qtz-Ser	Qtz-Ser	Qtz-Ser
SiO_2	%	FUS-ICP	72.35	60.66	74.96	72.76	64.89	76.19	58.85	76
Al_2O_3	%	FUS-ICP	11.04	15.82	11.62	13.19	12.98	9.72	18.41	10.78
Fe_2O_3(T)	%	FUS-ICP	4.19	4.76	3.3	3.67	7.02	4.78	6.53	5.21
MnO	%	FUS-ICP	0.177	0.329	0.084	0.136	0.106	0.089	0.201	0.067
MgO	%	FUS-ICP	3.14	5.42	1.89	2.52	1.89	2.47	4.04	1.45
CaO	%	FUS-ICP	0.07	0.17	0.07	0.17	0.47	0.06	0.1	0.07
Na_2O	%	FUS-ICP	0.19	0.18	0.16	0.18	0.23	0.16	0.37	0.24
K_2O	%	FUS-ICP	2.71	3.98	3	3.57	3.31	2.33	4.35	2.53
TiO_2	%	FUS-ICP	0.135	0.194	0.19	0.164	0.309	0.133	0.217	0.131
P_2O_5	%	FUS-ICP	< 0.01	0.03	0.02	0.03	0.06	0.02	0.03	0.03
LOI	%	FUS-ICP	5.27	6.84	3.71	4.54	6.55	4.32	7.24	4.4
Total	%	FUS-ICP	99.27	98.37	99.02	100.9	97.81	100.3	100.3	100.9
Ba	ppm	FUS-ICP	811	1135	1385	1409	2988	721	2472	3586
Sr	ppm	FUS-ICP	9	8	8	10	18	7	20	13
Y	ppm	FUS-ICP	38	59	37	80	41	35	52	26
Sc	ppm	FUS-ICP	9	14	12	13	16	10	15	9
Zr	ppm	FUS-ICP	135	189	134	178	129	119	216	128
Be	ppm	FUS-ICP	1	1	1	1	1	< 1	1	1
V	ppm	FUS-ICP	< 5	< 5	16	< 5	61	< 5	< 5	< 5
Hg	ppb	FIMS	143	10	115	19	22	56	8	5
Cr	ppm	HF/HNO3	9.63	<8.9	<8.9	<8.9	27.63	<8.9	<8.9	<8.9
Co	ppm	HF/HNO3	<0.9	<0.9	<0.9	<0.9	6.23	1.66	<0.9	1.43
Ni	ppm	HF/HNO3	<10	<10	<10	<10	10.17	<10	<10	<10
Cu	ppm	HF/HNO3	113.06	31.00	180.75	20.47	1346.30	359.61	<19	<19
Zn	ppm	HF/HNO3	1475.50	134.13	2193.91	285.67	121.86	496.65	165.88	86.99
As	ppm	HF/HNO3	3.16	2.87	6.29	3.31	21.22	11.44	1.94	3.29
Se	ppm	HF/HNO3	<26.7	<26.7	<26.7	<26.7	<26.7	<26.7	<26.7	<26.7
Br	ppm	HF/HNO3	256.49	149.18	143.95	120.25	128.58	142.30	139.08	134.06
Mo	ppm	HF/HNO3	1.90	1.73	<1	5.06	3.10	1.88	3.27	2.03
Ag	ppm	HF/HNO3	<1	<1	2.70	<1	1.91	<1	<1	<1
Cd	ppm	HF/HNO3	4.51	<0.9	6.23	1.16	0.97	1.74	<0.9	<0.9
Sn	ppm	HF/HNO3	4.68	4.73	10.08	4.63	5.79	4.07	5.08	5.12
Sb	ppm	HF/HNO3	1.46	1.47	7.85	1.31	2.07	3.44	1.23	0.98
Te	ppm	HF/HNO3	<4.3	<4.3	4.38	<4.3	<4.3	<4.3	<4.3	<4.3
I	ppm	HF/HNO3	<37	<37	<37	<37	<37	<37	<37	<37
W	ppm	HF/HNO3	2.12	2.11	4.19	3.00	7.66	1.82	1.13	1.80
Pb	ppm	HF/HNO3	<25.3	<25.3	2402.52	<25.3	62.93	155.94	<25.3	<25.3
Bi	ppm	HF/HNO3	0.17	0.26	0.42	0.53	1.87	1.11	0.29	1.01
Nb	ppm	Na2O2 Sinter	5.40	6.08	9.50	7.45	8.08	6.92	6.18	10.26
La	ppm	Na2O2 Sinter	16.59	17.13	21.11	18.30	21.03	16.77	18.39	23.19
Ce	ppm	Na2O2 Sinter	35.30	35.05	44.44	37.94	44.20	35.94	37.89	48.85
Pr	ppm	Na2O2 Sinter	4.50	4.44	5.56	4.82	5.62	4.56	4.78	6.19
Nd	ppm	Na2O2 Sinter	18.89	19.53	23.25	20.93	24.42	19.63	20.35	26.73
Sm	ppm	Na2O2 Sinter	4.84	4.76	7.10	4.91	6.15	4.77	4.84	6.36
Eu	ppm	Na2O2 Sinter	0.98	0.93	1.67	1.16	1.17	0.90	0.91	0.91
Tb	ppm	Na2O2 Sinter	0.91	0.97	1.53	0.96	1.42	0.98	0.88	1.29
Dy	ppm	Na2O2 Sinter	5.99	6.43	10.23	6.39	9.87	6.78	5.85	8.77
Ho	ppm	Na2O2 Sinter	1.28	1.44	1.98	1.42	2.39	1.57	1.30	1.93
Er	ppm	Na_2O_2 Sinter	4.30	6.08	4.40	7.92	4.62	3.99	6.13	3.64
Tm	ppm	Na2O2 Sinter	0.59	0.66	0.94	0.68	1.22	0.71	0.63	0.95
Yb	ppm	Na2O2 Sinter	4.01	4.53	6.48	4.45	8.43	4.74	4.05	6.58
Lu	ppm	Na2O2 Sinter	0.62	0.66	1.10	0.68	1.31	0.71	0.63	0.97
Hf	ppm	Na2O2 Sinter	3.59	3.98	5.97	4.88	5.46	4.06	3.18	5.73
Ta	ppm	Na2O2 Sinter	0.22	0.26	0.42	0.30	0.31	0.25	0.24	0.43
Th	ppm	Na2O2 Sinter	4.61	5.05	6.68	5.25	6.19	5.12	4.77	8.03
AlOH WL	nm	Terraspec	2,201	2,203	2,205	2,206	2,202	2,205	2,203	2,200
AlOH Depth	%	Terraspec	4.62%	12.05%	6.92%	8.94%	12.38%	3.57%	7.89%	9.93%
FeOH WL	nm	Terraspec	2,254	2,251	#DIV/0!	#DIV/0!	2,257	2,252	#DIV/0!	#DIV/0!
FeOH Depth	%	Terraspec	1.32%	2.94%	#DIV/0!	#DIV/0!	1.27%	1.08%	#DIV/0!	#DIV/0!
AlOH depth/FeOH depth		Terraspec	3.50	4.11	#DIV/0!	#DIV/0!	9.74	3.31	#DIV/0!	#DIV/0!

Abbreviations:	**Units**		**Alteration**	**Other**
	HFL= Hanging wall flow	FT= Footwall tuff	Qtz-Ser= Quartz-sericite	WL= Wavelength
	HBX= Hanging wall breccia	FBX= Footwall breccia	Chl-Ser= Chlorite-sericite	
	FLT= Footwall lapilli tuff	FFL= Footwall flow	Chl=Chlorite	
		INT= Intrusion		

Appendix B: Table B1.1 Whole-rock Geochemistry and Terraspec^{TM} Data

Sample ID			**H501245**	**H501246**	**H501247**	**H501248**	**H501249**	**H501250**	**H501251**	**H501252**
Hole ID			BD10-45	BD10-45	BD10-28	BD10-28	BD10-28	BD11-127	BD11-127	BD11-127
Depth (m)			31.4	46.7	6	20.4	34.3	6.7	16.4	21.1
Lithology			FLT	FBX	FLT	FLT	FLT	HBX	HBX	FLT
Alteration			Qtz-Ser	Qtz-Ser	Qtz-Ser	Qtz-Ser	Chl-Ser	Qtz-Ser	Qtz-Ser	Qtz-Ser
SiO_2	%	FUS-ICP	69.73	70.61	74.05	71.3	69.5	75.85	71.33	74.86
Al_2O_3	%	FUS-ICP	11.61	12.64	9.76	13.39	10.11	10.8	12.43	10.99
Fe_2O_3(T)	%	FUS-ICP	6.39	4.28	4.61	2.99	5.72	2.74	5.24	4.56
MnO	%	FUS-ICP	0.07	0.11	0.189	0.135	0.288	0.128	0.118	0.112
MgO	%	FUS-ICP	1.38	2.67	3.85	1.39	3.99	2.48	2.38	1.92
CaO	%	FUS-ICP	0.1	0.06	0.06	1.37	0.96	0.18	0.07	0.06
Na_2O	%	FUS-ICP	0.26	0.22	0.07	0.14	0.1	0.26	0.32	0.28
K_2O	%	FUS-ICP	3.15	3.02	2.3	4.15	2.39	2.9	3.25	2.96
TiO_2	%	FUS-ICP	0.172	0.173	0.135	0.189	0.228	0.132	0.153	0.165
P_2O_5	%	FUS-ICP	0.03	0.03	< 0.01	0.01	0.03	0.01	0.01	0.01
LOI	%	FUS-ICP	5.77	4.3	5.09	5.07	6.44	4.58	5.65	4.99
Total	%	FUS-ICP	98.66	98.12	100.1	100.1	99.76	100.1	101	100.9
Ba	ppm	FUS-ICP	1140	970	318	602	413	863	919	861
Sr	ppm	FUS-ICP	14	8	4	15	13	11	14	12
Y	ppm	FUS-ICP	37	45	37	48	28	36	45	33
Sc	ppm	FUS-ICP	12	13	9	14	14	9	11	11
Zr	ppm	FUS-ICP	138	154	121	170	108	130	155	137
Be	ppm	FUS-ICP	1	1	1	1	< 1	1	1	1
V	ppm	FUS-ICP	7	< 5	< 5	< 5	56	< 5	< 5	11
Hg	ppb	FIMS	17	< 5	14	11	37	89	83	16
Cr	ppm	HF/HNO3	<8.9	<8.9	<8.9	<8.9	18.39	<8.9	12.41	10.14
Co	ppm	HF/HNO3	2.61	<0.9	<0.9	<0.9	7.84	<0.9	1.20	3.85
Ni	ppm	HF/HNO3	<10	<10	<10	<10	13.23	<10	<10	<10
Cu	ppm	HF/HNO3	1440.83	348.74	<19	<19	<19	97.50	435.41	117.09
Zn	ppm	HF/HNO3	65.80	68.54	131.26	96.97	203.60	352.67	708.98	119.76
As	ppm	HF/HNO3	7.39	4.89	4.33	9.59	9.68	4.81	8.04	10.39
Se	ppm	HF/HNO3	<26.7	<26.7	<26.7	<26.7	<26.7	<26.7	<26.7	<26.7
Br	ppm	HF/HNO3	141.44	154.99	256.10	261.95	239.05	228.56	267.04	245.28
Mo	ppm	HF/HNO3	6.72	4.12	12.79	4.90	6.55	3.80	7.92	2.42
Ag	ppm	HF/HNO3	<1	<1	<1	<1	<1	<1	<1	<1
Cd	ppm	HF/HNO3	<0.9	<0.9	<0.9	<0.9	<0.9	1.28	1.47	<0.9
Sn	ppm	HF/HNO3	6.32	3.63	3.49	4.25	3.41	2.92	4.79	4.02
Sb	ppm	HF/HNO3	1.38	1.61	1.52	1.42	1.37	50.51	2.35	2.69
Te	ppm	HF/HNO3	<4.3	<4.3	<4.3	<4.3	<4.3	<4.3	<4.3	<4.3
I	ppm	HF/HNO3	<37	<37	<37	<37	<37	<37	<37	<37
W	ppm	HF/HNO3	2.64	3.90	1.15	2.26	1.91	1.77	2.76	3.01
Pb	ppm	HF/HNO3	<25.3	<25.3	<25.3	<25.3	<25.3	<25.3	31.93	<25.3
Bi	ppm	HF/HNO3	4.01	0.44	1.64	0.90	1.63	0.61	0.62	2.19
Nb	ppm	Na2O2 Sinter	6.43	8.16	7.41	5.62	7.90	4.42	5.96	6.75
La	ppm	Na2O2 Sinter	18.19	22.35	19.65	17.13	22.17	14.37	16.67	19.18
Ce	ppm	Na2O2 Sinter	37.29	46.61	41.06	35.02	47.30	30.31	35.34	39.40
Pr	ppm	Na2O2 Sinter	4.72	5.86	4.98	4.43	5.94	3.87	4.56	5.00
Nd	ppm	Na2O2 Sinter	20.24	25.14	21.33	18.69	25.29	16.60	19.40	21.41
Sm	ppm	Na2O2 Sinter	4.71	5.74	4.67	4.45	6.02	3.90	4.63	5.03
Eu	ppm	Na2O2 Sinter	0.39	0.75	1.02	1.36	1.55	1.18	0.49	0.96
Tb	ppm	Na2O2 Sinter	0.80	1.02	1.13	0.96	1.16	0.71	0.94	1.15
Dy	ppm	Na2O2 Sinter	5.36	6.65	7.64	6.34	8.09	4.93	6.25	7.87
Ho	ppm	Na2O2 Sinter	1.15	1.49	1.56	1.40	1.70	1.03	1.23	1.61
Er	ppm	Na_2O_2 Sinter	4.53	4.71	4.14	5.43	3.28	3.77	4.99	3.83
Tm	ppm	Na2O2 Sinter	0.54	0.72	0.73	0.62	0.83	0.52	0.60	0.73
Yb	ppm	Na2O2 Sinter	3.79	4.62	5.05	4.10	5.82	3.43	4.12	5.04
Lu	ppm	Na2O2 Sinter	0.56	0.71	0.69	0.60	0.87	0.54	0.61	0.80
Hf	ppm	Na2O2 Sinter	4.17	4.06	4.00	2.33	4.34	2.95	3.53	4.13
Ta	ppm	Na2O2 Sinter	0.26	0.30	0.26	0.22	0.29	0.18	0.24	0.26
Th	ppm	Na2O2 Sinter	5.01	5.96	5.72	4.42	6.18	3.93	5.05	5.50
AlOH WL	nm	Terraspec	2,203	2,205	2,208	2,208	2,205	2,205	2,205	2,204
AlOH Depth	%	Terraspec	11.48%	13.10%	5.75%	10.99%	9.49%	13.86%	10.20%	7.34%
FeOH WL	nm	Terraspec	#DIV/0!	2,253	2,251	#DIV/0!	2,254	#DIV/0!	#DIV/0!	#DIV/0!
FeOH Depth	%	Terraspec	#DIV/0!	1.53%	1.58%	#DIV/0!	1.45%	#DIV/0!	#DIV/0!	#DIV/0!
AlOH depth/FeOH depth		Terraspec	#DIV/0!	8.54	3.64	#DIV/0!	6.56	#DIV/0!	#DIV/0!	#DIV/0!

Abbreviations:

Units
HFL= Hanging wall flow
HBX= Hanging wall breccia
FLT= Footwall lapilli tuff
FT= Footwall tuff
FBX= Footwall breccia
FFL= Footwall flow
INT= Intrusion

Alteration
Qtz-Ser= Quartz-sericite
Chl-Ser= Chlorite-sericite
Chl=Chlorite

Other
WL= Wavelength

Appendix B: Table B1.1 Whole-rock Geochemistry and Terraspec™ Data

Sample ID			**H501253**	**H501254**	**H501255**	**H501256**	**H501257**	**H501258**	**H501259**	**H501260**
Hole ID			BD11-127	BD11-127	BD11-128	BD11-128	BD11-128	BD11-116	BD11-116	BD11-116
Depth (m)			37.9	46.5	12.6	15.5	26.5	13.6	16.8	29.2
Lithology			FLT	FFL	HFL	FLT	FLT	FLT	FT	FLT
Alteration			Qtz-Ser	Qtz-Ser	Qtz-Ser	Qtz-Ser	Qtz-Ser	Qtz-Ser	Qtz-Ser	Chl-Ser
SiO_2	%	FUS-ICP	70.47	75.83	73.78	73.34	78.17	68.54	75.19	68.97
Al_2O_3	%	FUS-ICP	11.69	11.3	12.23	10.69	10.27	14.63	10.67	9.6
Fe_2O_3(T)	%	FUS-ICP	4.69	3.17	2.77	3.88	4.01	5.25	4.56	10.67
MnO	%	FUS-ICP	0.184	0.109	0.078	0.166	0.045	0.082	0.071	0.052
MgO	%	FUS-ICP	3.87	1.86	1.37	3.05	1.01	2.1	2.54	2.34
CaO	%	FUS-ICP	0.08	0.11	0.32	0.49	0.07	0.05	0.06	0.06
Na_2O	%	FUS-ICP	0.38	0.36	0.22	0.2	0.19	0.26	0.17	0.15
K_2O	%	FUS-ICP	2.72	3.1	3.5	2.83	2.92	3.76	2.38	2.09
TiO_2	%	FUS-ICP	0.178	0.157	0.147	0.181	0.147	0.228	0.127	0.131
P_2O_5	%	FUS-ICP	0.02	0.02	0.05	0.04	0.03	0.01	0.02	0.01
LOI	%	FUS-ICP	6.58	4.6	3.98	5.6	3.76	5.31	3.71	6.57
Total	%	FUS-ICP	100.9	100.6	98.45	100.5	100.6	100.2	99.49	100.6
Ba	ppm	FUS-ICP	701	924	673	543	596	2579	1797	1239
Sr	ppm	FUS-ICP	17	15	13	17	9	12	8	6
Y	ppm	FUS-ICP	44	40	42	37	33	42	36	24
Sc	ppm	FUS-ICP	13	11	10	13	10	15	9	8
Zr	ppm	FUS-ICP	143	148	158	137	134	177	127	124
Be	ppm	FUS-ICP	1	1	1	1	1	1	< 1	< 1
V	ppm	FUS-ICP	8	< 5	< 5	18	< 5	15	< 5	< 5
Hg	ppb	FIMS	17	11	< 5	10	208	113	25	16
Cr	ppm	HF/HNO3	<8.9	9.46	<8.9	9.69	26.17	8.99	15.72	<8.9
Co	ppm	HF/HNO3	1.69	<0.9	1.09	2.42	1.78	1.96	<0.9	1.81
Ni	ppm	HF/HNO3	<10	<10	<10	<10	17.59	<10	<10	<10
Cu	ppm	HF/HNO3	<19	447.77	73.79	<19	21.63	66.42	109.15	182.71
Zn	ppm	HF/HNO3	163.13	45.31	50.04	89.79	1322.82	110.38	126.51	61.06
As	ppm	HF/HNO3	4.48	4.11	8.72	6.40	9.75	27.05	5.55	14.79
Se	ppm	HF/HNO3	<26.7	<26.7	<26.7	<26.7	<26.7	<26.7	<26.7	<26.7
Br	ppm	HF/HNO3	239.92	271.78	126.95	112.29	179.92	235.32	264.42	263.65
Mo	ppm	HF/HNO3	4.08	4.82	2.35	2.98	10.90	10.11	4.33	21.81
Ag	ppm	HF/HNO3	<1	<1	<1	<1	<1	<1	<1	<1
Cd	ppm	HF/HNO3	<0.9	<0.9	<0.9	<0.9	4.58	<0.9	<0.9	<0.9
Sn	ppm	HF/HNO3	4.15	3.78	3.50	3.74	3.16	5.82	5.45	4.42
Sb	ppm	HF/HNO3	1.42	3.80	1.56	1.42	1.50	13.27	2.08	1.77
Te	ppm	HF/HNO3	<4.3	<4.3	<4.3	<4.3	<4.3	<4.3	<4.3	<4.3
I	ppm	HF/HNO3	<37	<37	<37	<37	<37	<37	<37	<37
W	ppm	HF/HNO3	2.61	8.05	2.72	2.10	2.13	4.86	1.62	2.05
Pb	ppm	HF/HNO3	<25.3	<25.3	<25.3	<25.3	<25.3	<25.3	42.97	<25.3
Bi	ppm	HF/HNO3	0.59	0.26	0.55	0.54	1.32	2.91	0.41	2.46
Nb	ppm	Na2O2 Sinter	5.58	6.46	11.85	7.24	6.40	6.00	13.39	10.23
La	ppm	Na2O2 Sinter	17.48	18.15	15.60	20.95	15.33	15.37	21.88	16.45
Ce	ppm	Na2O2 Sinter	37.24	37.46	34.15	43.39	32.08	32.14	46.48	34.87
Pr	ppm	Na2O2 Sinter	4.73	4.85	4.40	5.34	4.04	4.02	5.89	4.45
Nd	ppm	Na2O2 Sinter	19.68	20.68	17.72	22.42	17.52	17.25	24.45	18.74
Sm	ppm	Na2O2 Sinter	4.79	5.24	4.70	4.43	3.98	3.79	5.77	4.48
Eu	ppm	Na2O2 Sinter	0.81	0.95	0.92	0.76	0.85	0.87	1.19	0.97
Tb	ppm	Na2O2 Sinter	0.94	1.17	0.89	1.01	0.91	0.79	1.01	0.85
Dy	ppm	Na2O2 Sinter	6.16	7.70	6.06	6.90	6.01	5.28	6.96	5.70
Ho	ppm	Na2O2 Sinter	1.21	1.55	1.36	1.39	1.24	1.08	1.46	1.20
Er	ppm	Na_2O_2 Sinter	4.56	4.35	4.45	3.87	3.42	4.57	3.73	2.87
Tm	ppm	Na2O2 Sinter	0.57	0.73	0.65	0.67	0.59	0.55	0.73	0.60
Yb	ppm	Na2O2 Sinter	3.87	4.90	4.33	4.55	4.01	3.67	4.81	4.06
Lu	ppm	Na2O2 Sinter	0.59	0.73	0.66	0.66	0.56	0.51	0.73	0.63
Hf	ppm	Na2O2 Sinter	3.49	3.94	4.14	4.01	3.13	3.53	5.88	4.65
Ta	ppm	Na2O2 Sinter	0.22	0.25	0.34	0.27	0.23	0.22	0.41	0.30
Th	ppm	Na2O2 Sinter	4.89	5.04	7.55	5.56	4.56	4.31	9.02	6.73
AlOH WL	nm	Terraspec	2,200	2,205	2,205	2,203	2,204	2,204	2,202	2,202
AlOH Depth	%	Terraspec	11.90%	8.57%	9.53%	10.26%	8.14%	4.57%	7.16%	8.50%
FeOH WL	nm	Terraspec	2,252	#DIV/0!	#DIV/0!	2,250	#DIV/0!	#DIV/0!	2,252	2,256
FeOH Depth	%	Terraspec	1.40%	#DIV/0!	#DIV/0!	1.16%	#DIV/0!	#DIV/0!	1.92%	1.47%
AlOH depth/FeOH depth		Terraspec	8.52	#DIV/0!	#DIV/0!	8.85	#DIV/0!	#DIV/0!	3.72	5.80

Abbreviations:	**Units**		**Alteration**	**Other**
	HFL= Hanging wall flow	FT= Footwall tuff	Qtz-Ser= Quartz-sericite	WL= Wavelength
	HBX= Hanging wall breccia	FBX= Footwall breccia	Chl-Ser= Chlorite-sericite	
	FLT= Footwall lapilli tuff	FFL= Footwall flow	Chl=Chlorite	
		INT= Intrusion		

Appendix B: Table B1.1 Whole-rock Geochemistry and Terraspec^{TM} Data

Sample ID			**H501261**	**H501262**	**H501263**	**H501264**	**H501265**	**H501266**	**H501267**	**H501268**
Hole ID			BD11-116	BD11-116	BD11-120	BD11-120	BD11-120	BD10-88	BD10-7	BD10-7
Depth (m)			38.1	49.7	9.4	34.7	42.2	33.5	11.2	17.7
Lithology			FT	FLT	HFL	HBX	HFL	FLT	FLT	FLT
Alteration			Qtz-Ser	Qtz-Ser	Qtz-Ser	Qtz-Ser	Chl-Ser	Chl	Qtz-Ser	Chl
SiO_2	%	FUS-ICP	63.36	50.52	83.04	72.57	65.98	40.75	69.7	34.12
Al_2O_3	%	FUS-ICP	15.4	8.22	8.06	10.02	12.94	14.95	12.94	8.59
Fe_2O_3(T)	%	FUS-ICP	7.04	23.38	3.17	5.38	6.4	17.95	6.03	28.8
MnO	%	FUS-ICP	0.058	0.036	0.051	0.11	0.169	0.178	0.01	0.307
MgO	%	FUS-ICP	2.19	0.41	0.92	1.92	3.42	11.34	1.03	10.02
CaO	%	FUS-ICP	0.09	0.03	0.1	0.21	0.76	0.1	0.03	0.2
Na_2O	%	FUS-ICP	0.26	0.16	0.14	0.18	0.24	0.3	0.16	0.01
K_2O	%	FUS-ICP	4.04	2.26	2.15	2.58	3.13	1.22	3.64	0.04
TiO_2	%	FUS-ICP	0.316	0.114	0.1	0.165	0.216	0.254	0.176	0.111
P_2O_5	%	FUS-ICP	0.04	< 0.01	< 0.01	0.01	0.03	0.03	0.02	0.1
LOI	%	FUS-ICP	6.08	13.6	2.7	5.08	6.95	13.51	4.68	15.96
Total	%	FUS-ICP	98.89	98.74	100.5	98.24	100.2	100.6	98.42	98.25
Ba	ppm	FUS-ICP	2181	1167	813	1094	1208	332	1749	14
Sr	ppm	FUS-ICP	11	6	7	10	19	31	8	2
Y	ppm	FUS-ICP	48	25	30	38	42	42	51	25
Sc	ppm	FUS-ICP	18	9	7	11	13	13	13	9
Zr	ppm	FUS-ICP	162	106	98	132	166	184	170	92
Be	ppm	FUS-ICP	1	< 1	< 1	< 1	< 1	< 1	< 1	< 1
V	ppm	FUS-ICP	57	< 5	< 5	12	7	14	< 5	< 5
Hg	ppb	FIMS	92	785	31	18	22	9	785	36
Cr	ppm	HF/HNO3	47.76	<8.9	13.41	<8.9	12.84	14.35	35.14	32.01
Co	ppm	HF/HNO3	10.15	12.59	<0.9	1.73	4.98	16.38	1.55	343.86
Ni	ppm	HF/HNO3	20.88	<10	<10	13.82	<10	<10	21.27	19.59
Cu	ppm	HF/HNO3	937.63	127.77	839.61	729.77	438.07	<19	154.46	18284.15
Zn	ppm	HF/HNO3	96.85	30.40	99.01	78.62	122.61	194.48	6300.16	4096.77
As	ppm	HF/HNO3	50.33	159.18	26.50	102.87	8.90	11.86	18.66	81.83
Se	ppm	HF/HNO3	<26.7	<26.7	<26.7	<26.7	<26.7	<26.7	30.13	55.28
Br	ppm	HF/HNO3	255.24	242.90	283.43	152.74	266.53	228.98	236.81	198.56
Mo	ppm	HF/HNO3	6.99	32.86	7.71	36.71	8.96	18.63	9.35	6.95
Ag	ppm	HF/HNO3	1.80	6.20	<1	<1	<1	<1	<1	2.47
Cd	ppm	HF/HNO3	0.96	<0.9	<0.9	<0.9	<0.9	<0.9	27.28	<0.9
Sn	ppm	HF/HNO3	5.02	4.71	4.17	4.93	4.48	3.49	15.80	7.32
Sb	ppm	HF/HNO3	11.79	196.01	11.19	4.08	2.32	0.86	5.02	1.49
Te	ppm	HF/HNO3	<4.3	19.07	<4.3	<4.3	<4.3	<4.3	<4.3	16.21
I	ppm	HF/HNO3	<37	<37	<37	<37	<37	<37	<37	<37
W	ppm	HF/HNO3	8.19	2.96	3.61	4.64	5.73	13.61	5.05	7.10
Pb	ppm	HF/HNO3	33.29	44.77	<25.3	<25.3	<25.3	<25.3	57.98	<25.3
Bi	ppm	HF/HNO3	0.97	42.21	1.93	9.84	3.27	4.61	19.96	16.60
Nb	ppm	Na2O2 Sinter	7.86	10.71	6.90	7.03	5.71	9.93	6.55	4.45
La	ppm	Na2O2 Sinter	17.10	21.98	13.22	12.09	16.88	21.41	20.79	15.73
Ce	ppm	Na2O2 Sinter	36.02	46.92	27.65	26.05	35.32	43.69	43.95	33.82
Pr	ppm	Na2O2 Sinter	4.54	5.93	3.43	3.23	4.51	5.38	5.52	4.39
Nd	ppm	Na2O2 Sinter	18.31	25.17	13.99	13.78	19.50	22.22	24.34	19.00
Sm	ppm	Na2O2 Sinter	4.36	6.41	3.43	3.46	4.64	5.41	5.28	4.54
Eu	ppm	Na2O2 Sinter	0.96	1.52	0.90	0.75	1.07	0.97	1.03	0.71
Tb	ppm	Na2O2 Sinter	0.71	1.28	0.70	0.69	0.89	1.05	1.25	0.91
Dy	ppm	Na2O2 Sinter	4.50	8.59	4.73	4.77	6.01	7.24	8.00	5.67
Ho	ppm	Na2O2 Sinter	0.94	1.77	0.97	1.01	1.27	1.52	1.67	1.06
Er	ppm	Na_2O_2 Sinter	5.58	3.01	3.11	3.89	4.92	4.88	5.19	3.16
Tm	ppm	Na2O2 Sinter	0.42	0.87	0.46	0.48	0.61	0.74	0.78	0.47
Yb	ppm	Na2O2 Sinter	2.93	5.82	3.22	3.24	4.21	5.12	5.19	3.08
Lu	ppm	Na2O2 Sinter	0.44	0.92	0.49	0.51	0.60	0.78	0.74	0.45
Hf	ppm	Na2O2 Sinter	3.93	6.09	3.79	3.10	3.30	5.26	3.95	2.32
Ta	ppm	Na2O2 Sinter	0.22	0.37	0.19	0.24	0.21	0.33	0.23	0.16
Th	ppm	Na2O2 Sinter	6.15	7.10	3.85	4.38	4.25	7.12	5.56	3.26
AlOH WL	nm	Terraspec	2,203	2,204	2,203	2,205	2,203	2,192	2,205	#DIV/0!
AlOH Depth	%	Terraspec	5.22%	4.02%	7.54%	9.52%	3.32%	4.00%	18.50%	#DIV/0!
FeOH WL	nm	Terraspec	2,252	#DIV/0!	2,252	2,255	#DIV/0!	2,252	#DIV/0!	2,250
FeOH Depth	%	Terraspec	2.70%	#DIV/0!	1.14%	1.50%	#DIV/0!	5.17%	#DIV/0!	4.65%
AlOH depth/FeOH depth		Terraspec	1.93	#DIV/0!	6.62	6.35	#DIV/0!	0.77	#DIV/0!	#DIV/0!

Abbreviations:	**Units**	FT= Footwall tuff	**Alteration**	**Other**
	HFL= Hanging wall flow	FBX= Footwall breccia	Qtz-Ser= Quartz-sericite	WL= Wavelength
	HBX= Hanging wall breccia	FFL= Footwall flow	Chl-Ser= Chlorite-sericite	
	FLT= Footwall lapilli tuff	INT= Intrusion	Chl=Chlorite	

Appendix B: Table B1.1 Whole-rock Geochemistry and Terraspec^{TM} Data

Sample ID			**H501269**	**H501270**	**H501271**	**H501272**	**H501273**	**H501274**	**H501275**	**H501276**
Hole ID			BD10-7	BD10-22	BD10-22	BD10-22	BD10-22	BD10-9	BD10-9	BD10-9
Depth (m)			27.8	4.6	13.9	17.9	23.1	4.1	13.5	20.4
Lithology			FLT	HBX	FLT	FFL	FLT	HBX	FLT	FBX
Alteration			Chl	Chl-Ser	Qtz-Ser	Qtz-Ser	Qtz-Ser	Chl-Ser	Qtz-Ser	Qtz-Ser
SiO_2	%	FUS-ICP	22.81	63.05	71.11	72.07	72.17	64.31	78.03	72.4
Al_2O_3	%	FUS-ICP	17.24	13.04	12.48	13.25	11.84	12.54	11.88	12.93
Fe_2O_3(T)	%	FUS-ICP	22.88	5.76	4.24	3.15	4.46	5.61	2.22	3.04
MnO	%	FUS-ICP	0.161	0.195	0.11	0.251	0.075	0.215	0.019	0.145
MgO	%	FUS-ICP	20.67	8.06	1.79	2.95	1.23	7.65	1.05	1.88
CaO	%	FUS-ICP	0.06	0.06	0.06	0.06	0.15	0.06	0.05	0.17
Na_2O	%	FUS-ICP	< 0.01	0.08	0.14	0.17	2.11	0.07	0.1	0.12
K_2O	%	FUS-ICP	< 0.01	2.04	3.49	3.55	2.49	2.23	3.49	3.99
TiO_2	%	FUS-ICP	0.248	0.186	0.184	0.203	0.159	0.178	0.165	0.182
P_2O_5	%	FUS-ICP	0.03	0.03	0.03	0.01	0.01	0.02	0.02	0.02
LOI	%	FUS-ICP	15.67	5.84	4.24	4.43	4.01	5.88	2.65	3.97
Total	%	FUS-ICP	99.78	98.33	97.89	100.1	98.73	98.77	99.67	98.85
Ba	ppm	FUS-ICP	8	1962	2922	2110	1312	1554	1819	1852
Sr	ppm	FUS-ICP	< 2	4	8	11	26	5	8	10
Y	ppm	FUS-ICP	66	45	39	48	38	48	39	51
Sc	ppm	FUS-ICP	21	12	13	14	12	11	12	13
Zr	ppm	FUS-ICP	235	162	162	168	141	150	150	167
Be	ppm	FUS-ICP	< 1	1	1	1	1	1	1	1
V	ppm	FUS-ICP	< 5	7	22	7	7	6	25	9
Hg	ppb	FIMS	19	29	1360	95	1390	72	289	1070
Cr	ppm	HF/HNO3	29.66	9.98	<8.9	<8.9	<8.9	11.39	<8.9	<8.9
Co	ppm	HF/HNO3	41.05	10.59	2.07	<0.9	3.70	12.93	<0.9	1.02
Ni	ppm	HF/HNO3	19.46	<10	<10	<10	<10	<10	<10	<10
Cu	ppm	HF/HNO3	295.60	301.01	2858.49	183.18	777.63	177.05	386.27	672.49
Zn	ppm	HF/HNO3	406.50	301.32	8466.09	628.35	6724.56	607.21	1295.26	3357.90
As	ppm	HF/HNO3	9.15	7.94	14.81	<1.6	45.93	6.81	17.83	7.63
Se	ppm	HF/HNO3	<26.7	<26.7	<26.7	<26.7	<26.7	<26.7	<26.7	<26.7
Br	ppm	HF/HNO3	212.21	241.52	233.82	254.93	300.71	157.39	157.06	158.46
Mo	ppm	HF/HNO3	23.34	5.98	3.00	3.34	6.92	12.02	1.91	3.11
Ag	ppm	HF/HNO3	1.03	1.04	8.16	<1	<1	2.38	<1	<1
Cd	ppm	HF/HNO3	<0.9	<0.9	31.16	1.27	22.51	<0.9	4.93	12.83
Sn	ppm	HF/HNO3	2.04	6.56	16.28	4.96	17.44	5.27	15.52	36.40
Sb	ppm	HF/HNO3	1.43	4.20	13.11	1.94	10.46	2.64	7.05	4.21
Te	ppm	HF/HNO3	32.13	12.41	<4.3	<4.3	<4.3	<4.3	<4.3	<4.3
I	ppm	HF/HNO3	<37	<37	<37	<37	<37	<37	<37	<37
W	ppm	HF/HNO3	9.53	7.87	3.28	2.28	1.51	6.12	3.55	1.64
Pb	ppm	HF/HNO3	<25.3	28.44	771.81	<25.3	1110.64	462.41	28.25	<25.3
Bi	ppm	HF/HNO3	35.85	14.71	13.65	0.23	2.07	5.32	0.90	0.90
Nb	ppm	Na2O2 Sinter	11.49	12.50	11.17	12.10	7.87	7.82	6.23	7.20
La	ppm	Na2O2 Sinter	38.22	23.19	22.22	23.45	18.48	21.90	20.56	24.34
Ce	ppm	Na2O2 Sinter	77.26	48.76	47.01	49.75	38.73	45.61	42.96	50.94
Pr	ppm	Na2O2 Sinter	9.60	5.99	5.81	6.18	4.90	5.76	5.42	6.33
Nd	ppm	Na2O2 Sinter	41.53	25.08	24.08	25.84	21.14	24.75	23.62	27.21
Sm	ppm	Na2O2 Sinter	8.86	6.03	5.91	6.18	5.54	5.70	5.53	6.36
Eu	ppm	Na2O2 Sinter	0.98	1.14	2.01	1.58	1.30	0.96	1.48	1.51
Tb	ppm	Na2O2 Sinter	1.77	1.20	0.99	1.17	0.93	1.20	0.99	1.38
Dy	ppm	Na2O2 Sinter	11.39	7.98	6.56	7.96	6.33	8.20	6.55	9.26
Ho	ppm	Na2O2 Sinter	2.31	1.69	1.41	1.65	1.29	1.74	1.42	1.94
Er	ppm	Na_2O_2 Sinter	7.14	5.15	4.47	5.17	4.11	5.27	4.33	5.88
Tm	ppm	Na2O2 Sinter	1.06	0.79	0.68	0.78	0.63	0.80	0.68	0.88
Yb	ppm	Na2O2 Sinter	7.36	5.47	4.66	5.38	4.33	5.25	4.68	6.04
Lu	ppm	Na2O2 Sinter	1.04	0.85	0.72	0.86	0.66	0.79	0.68	0.89
Hf	ppm	Na2O2 Sinter	5.95	5.70	5.10	5.70	4.96	4.90	4.48	5.06
Ta	ppm	Na2O2 Sinter	0.34	0.37	0.34	0.35	0.29	0.27	0.25	0.28
Th	ppm	Na2O2 Sinter	8.05	7.59	6.99	7.17	5.91	5.70	5.51	6.34
AlOH WL	nm	Terraspec	#DIV/0!	2,205	2,210	2,208	2,210	2,210	2,210	2,213
AlOH Depth	%	Terraspec	#DIV/0!	11.08%	13.83%	31.00%	8.27%	10.67%	20.38%	30.28%
FeOH WL	nm	Terraspec	2,250	2,251	2,254	2,253	#DIV/0!	2,251	#DIV/0!	#DIV/0!
FeOH Depth	%	Terraspec	8.90%	8.41%	1.12%	1.71%	#DIV/0!	6.00%	#DIV/0!	#DIV/0!
AlOH depth/FeOH depth		Terraspec	#DIV/0!	1.32	12.35	18.18	#DIV/0!	1.78	#DIV/0!	#DIV/0!

Abbreviations:	**Units**		**Alteration**	**Other**
	HFL= Hanging wall flow	FT= Footwall tuff	Qtz-Ser= Quartz-sericite	WL= Wavelength
	HBX= Hanging wall breccia	FBX= Footwall breccia	Chl-Ser= Chlorite-sericite	
	FLT= Footwall lapilli tuff	FFL= Footwall flow	Chl=Chlorite	
		INT= Intrusion		

Appendix B: Table B1.1 Whole-rock Geochemistry and Terraspec™ Data

Sample ID			H501277	H501278*	H501279	H501280	H501281	H501282	H501283	H501284
Hole ID			BD10-9	BD10-11	BD10-11	BD10-11	BD10-11	BD10-21	BD10-21	BD10-21
Depth (m)			30.1	4	9.8	17.1	28.2	2.4	15.9	30.1
Lithology			FBX	HFL	HFL	FLT	FBX	HFL	FLT	FBX
Alteration			Qtz-Ser	Qtz-Ser	Qtz-Ser	Qtz-Ser	Qtz-Ser	Qtz-Ser	Chl-Ser	Qtz-Ser
SiO_2	%	FUS-ICP	75.06	73.94	70.41	80.77	72.22	66.63	43.91	79.58
Al_2O_3	%	FUS-ICP	11.98	11.79	13.66	8.65	13.92	18.73	7.93	8.23
Fe_2O_3(T)	%	FUS-ICP	2.55	2.34	3.31	2.45	1.69	2.82	18.49	1.69
MnO	%	FUS-ICP	0.142	0.095	0.148	0.177	0.112	0.015	0.153	0.24
MgO	%	FUS-ICP	2.49	2.46	3.02	1.23	2.76	2.05	3.87	2.24
CaO	%	FUS-ICP	0.06	0.16	0.04	0.05	0.09	0.64	0.09	1.31
Na_2O	%	FUS-ICP	0.26	1.97	0.1	0.08	0.13	3.19	0.09	0.75
K_2O	%	FUS-ICP	3.28	2.29	3.68	2.66	3.99	3.43	1.33	1.86
TiO_2	%	FUS-ICP	0.162	0.144	0.169	0.12	0.181	0.253	0.13	0.109
P_2O_5	%	FUS-ICP	0.01	0.01	0.02	0.01	0.01	0.05	0.01	0.02
LOI	%	FUS-ICP	3.58	2.93	3.67	3.02	3.85	2.79	11.62	3.68
Total	%	FUS-ICP	99.59	98.15	98.23	99.21	98.95	100.6	87.63	99.71
Ba	ppm	FUS-ICP	1060	1408	1982	1642	1410	764	945	682
Sr	ppm	FUS-ICP	8	22	6	5	10	138	5	35
Y	ppm	FUS-ICP	43	39	47	29	42	73	28	30
Sc	ppm	FUS-ICP	12	10	12	8	13	19	8	8
Zr	ppm	FUS-ICP	155	145	174	111	162	245	103	103
Be	ppm	FUS-ICP	1	1	1	< 1	2	2	< 1	< 1
V	ppm	FUS-ICP	< 5	< 5	< 5	< 5	13	7	21	< 5
Hg	ppb	FIMS	606	12	96	641	222	16	4050	250
Cr	ppm	HF/HNO3	<8.9	<8.9	<8.9	15.90	<8.9	<8.9	<8.9	36.47
Co	ppm	HF/HNO3	<0.9	1.11	2.84	<0.9	<0.9	<0.9	80.92	1.74
Ni	ppm	HF/HNO3	<10	<10	<10	<10	<10	<10	<10	18.66
Cu	ppm	HF/HNO3	156.95	83.36	142.11	399.44	96.69	<19	18118.48	84.41
Zn	ppm	HF/HNO3	1636.20	150.64	576.76	2115.76	604.56	121.17	32065.80	859.15
As	ppm	HF/HNO3	3.12	2.12	17.17	45.27	7.31	<1.6	102.23	<1.6
Se	ppm	HF/HNO3	<26.7	<26.7	<26.7	<26.7	<26.7	<26.7	36.86	<26.7
Br	ppm	HF/HNO3	164.94	176.10	227.26	228.59	242.65	214.24	208.28	202.61
Mo	ppm	HF/HNO3	2.70	<1	2.61	3.08	3.87	<1	11.05	7.87
Ag	ppm	HF/HNO3	<1	<1	1.42	<1	<1	<1	30.34	<1
Cd	ppm	HF/HNO3	6.21	<0.9	1.63	8.82	1.98	<0.9	112.27	2.09
Sn	ppm	HF/HNO3	6.20	5.61	11.47	28.25	11.76	4.15	28.20	3.34
Sb	ppm	HF/HNO3	1.51	0.82	2.83	4.22	1.25	0.41	44.07	1.75
Te	ppm	HF/HNO3	<4.3	<4.3	<4.3	<4.3	<4.3	<4.3	7.43	<4.3
I	ppm	HF/HNO3	<37	<37	<37	<37	<37	<37	<37	<37
W	ppm	HF/HNO3	1.87	1.32	3.50	2.08	3.71	2.19	2.37	2.03
Pb	ppm	HF/HNO3	<25.3	<25.3	345.54	78.81	<25.3	<25.3	6050.88	<25.3
Bi	ppm	HF/HNO3	0.85	0.30	2.05	0.69	1.65	0.21	41.66	0.74
Nb	ppm	Na2O2 Sinter	6.43	6.07	7.08	4.32	6.86	14.37	6.23	4.57
La	ppm	Na2O2 Sinter	21.20	20.65	21.64	15.37	14.68	28.08	14.47	13.57
Ce	ppm	Na2O2 Sinter	44.41	43.88	45.65	32.40	30.79	60.54	29.72	28.71
Pr	ppm	Na2O2 Sinter	5.54	5.49	5.79	4.10	3.94	7.71	3.71	3.67
Nd	ppm	Na2O2 Sinter	24.00	23.07	24.53	17.02	16.50	32.43	15.50	15.98
Sm	ppm	Na2O2 Sinter	5.76	5.55	5.88	4.15	4.15	8.05	3.81	3.93
Eu	ppm	Na2O2 Sinter	1.27	1.19	1.36	0.84	1.22	2.04	1.21	0.85
Tb	ppm	Na2O2 Sinter	1.15	1.04	1.18	0.74	0.99	1.81	0.74	0.77
Dy	ppm	Na2O2 Sinter	7.48	6.72	7.72	4.97	6.95	12.21	4.86	5.17
Ho	ppm	Na2O2 Sinter	1.58	1.48	1.65	1.07	1.52	2.55	1.05	1.12
Er	ppm	Na_2O_2 Sinter	4.68	4.53	5.23	3.28	4.68	8.09	3.26	3.34
Tm	ppm	Na2O2 Sinter	0.72	0.68	0.79	0.53	0.71	1.24	0.49	0.51
Yb	ppm	Na2O2 Sinter	4.95	4.80	5.47	3.56	5.01	8.52	3.26	3.59
Lu	ppm	Na2O2 Sinter	0.73	0.74	0.84	0.55	0.73	1.27	0.52	0.57
Hf	ppm	Na2O2 Sinter	4.80	4.70	4.71	3.20	4.72	8.96	4.11	3.70
Ta	ppm	Na2O2 Sinter	0.28	0.25	0.28	0.18	0.26	0.53	0.19	0.20
Th	ppm	Na2O2 Sinter	5.67	5.59	6.11	4.14	5.44	9.84	5.28	3.81
AlOH WL	nm	Terraspec	2,210	2,213	2,211	2,212	2,210	2,205	#DIV/0!	2,206
AlOH Depth	%	Terraspec	29.25%	14.85%	12.28%	12.34%	25.58%	30.53%	#DIV/0!	23.90%
FeOH WL	nm	Terraspec	2,252	2,252	2,256	2,253	2,251	2,255	2,251	2,251
FeOH Depth	%	Terraspec	2.98%	2.42%	1.64%	1.95%	1.44%	5.53%	1.60%	1.37%
AlOH depth/FeOH depth		Terraspec	9.81	6.14	7.51	6.35	17.76	5.52	#DIV/0!	17.48

Abbreviations:

Units
HFL= Hanging wall flow
HBX= Hanging wall breccia
FLT= Footwall lapilli tuff
FT= Footwall tuff
FBX= Footwall breccia
FFL= Footwall flow
INT= Intrusion

Alteration
Qtz-Ser= Quartz-sericite
Chl-Ser= Chlorite-sericite
Chl=Chlorite

Other
WL= Wavelength
* Indicates least altered

Appendix B: Table B1.1 Whole-rock Geochemistry and Terraspec^{TM} Data

Sample ID			H501285	H501286	H501287	H501288	H501289	H501290	H501291	H501292
Hole ID			BD10-21	BD10-26	BD10-26	BD10-26	BD10-26	BD10-26	BD11-146	BD11-146
Depth (m)			31.1	9.2	18.5	20.6	29.1	37	6.2	11.8
Lithology			FBX	FLT	FLT	FLT	FLT	FFL	FLT	FLT
Alteration			Chl-Ser	Qtz-Ser	Qtz-Ser	Qtz-Ser	Qtz-Ser	Qtz-Ser	Qtz-Ser	Qtz-Ser
SiO_2	%	FUS-ICP	67.49	81.44	70.94	67.29	69.08	75.62	77.68	75.31
Al_2O_3	%	FUS-ICP	15.24	9.57	16.29	21.34	11.18	12.33	10.62	11.99
Fe_2O_3(T)	%	FUS-ICP	2.98	2.49	2.43	0.42	9.31	3.86	2.53	3.11
MnO	%	FUS-ICP	0.155	0.012	0.023	0.023	0.029	0.027	0.024	0.08
MgO	%	FUS-ICP	4.55	0.86	1.7	0.9	0.43	2.01	1.37	1.43
CaO	%	FUS-ICP	0.59	0.03	0.05	0.04	0.04	0.05	0.03	0.04
Na_2O	%	FUS-ICP	0.42	0.1	0.16	0.23	0.12	0.12	0.08	0.1
K_2O	%	FUS-ICP	3.74	2.93	4.79	6.4	3.24	3.16	3.05	3.56
TiO_2	%	FUS-ICP	0.206	0.15	0.217	0.301	0.15	0.166	0.147	0.176
P_2O_5	%	FUS-ICP	0.03	0.02	0.03	< 0.01	0.02	0.03	0.01	< 0.01
LOI	%	FUS-ICP	5.44	2.64	3.64	3.15	6.36	3.34	3.14	3.67
Total	%	FUS-ICP	100.8	100.2	100.3	100.1	99.95	100.7	98.69	99.48
Ba	ppm	FUS-ICP	1443	1447	1999	2603	1475	1092	1327	1473
Sr	ppm	FUS-ICP	25	6	7	12	5	6	5	5
Y	ppm	FUS-ICP	57	28	68	18	103	45	32	38
Sc	ppm	FUS-ICP	16	10	19	12	13	12	10	12
Zr	ppm	FUS-ICP	202	147	203	276	149	163	134	155
Be	ppm	FUS-ICP	1	< 1	1	1	< 1	< 1	1	1
V	ppm	FUS-ICP	< 5	27	7	7	7	< 5	28	6
Hg	ppb	FIMS	98	214	903	45	132	7	522	342
Cr	ppm	HF/HNO3	34.22	27.96	32.87	26.92	15.42	28.18	<8.9	<8.9
Co	ppm	HF/HNO3	1.08	0.96	0.96	<0.9	6.05	1.28	<0.9	<0.9
Ni	ppm	HF/HNO3	20.10	18.25	20.89	16.59	<10	18.43	<10	<10
Cu	ppm	HF/HNO3	32.39	296.53	49.29	<19	654.56	21.31	557.08	92.69
Zn	ppm	HF/HNO3	466.29	935.20	4146.84	133.86	326.72	131.58	1745.07	948.30
As	ppm	HF/HNO3	14.91	4.62	15.04	<1.6	53.96	72.20	51.37	91.97
Se	ppm	HF/HNO3	<26.7	<26.7	<26.7	<26.7	<26.7	<26.7	<26.7	<26.7
Br	ppm	HF/HNO3	230.24	197.87	219.23	195.34	230.99	192.30	222.12	215.74
Mo	ppm	HF/HNO3	10.08	6.59	11.00	9.89	4.10	7.75	4.31	3.96
Ag	ppm	HF/HNO3	<1	<1	1.50	1.01	1.94	<1	<1	1.06
Cd	ppm	HF/HNO3	<0.9	3.16	13.49	<0.9	1.17	<0.9	7.36	2.84
Sn	ppm	HF/HNO3	5.06	5.39	120.76	10.30	9.68	16.31	10.28	12.32
Sb	ppm	HF/HNO3	2.20	3.29	10.42	0.95	13.31	5.17	6.20	6.52
Te	ppm	HF/HNO3	<4.3	<4.3	<4.3	<4.3	<4.3	<4.3	<4.3	<4.3
I	ppm	HF/HNO3	<37	<37	<37	<37	<37	<37	<37	<37
W	ppm	HF/HNO3	3.45	3.99	3.46	6.69	6.62	3.76	3.65	4.76
Pb	ppm	HF/HNO3	<25.3	264.73	1353.53	<25.3	83.87	<25.3	375.03	554.99
Bi	ppm	HF/HNO3	0.27	3.50	2.35	0.24	0.77	4.65	2.35	0.21
Nb	ppm	Na2O2 Sinter	8.22	5.92	7.86	8.91	8.28	6.52	5.42	6.09
La	ppm	Na2O2 Sinter	21.38	20.35	29.34	1.72	26.23	19.53	19.98	22.49
Ce	ppm	Na2O2 Sinter	45.49	41.62	62.91	3.12	51.99	41.13	40.79	47.48
Pr	ppm	Na2O2 Sinter	5.67	5.19	7.98	0.35	6.38	5.11	5.10	5.92
Nd	ppm	Na2O2 Sinter	24.90	22.55	33.99	1.39	26.86	21.99	21.67	24.74
Sm	ppm	Na2O2 Sinter	6.09	5.01	8.25	0.48	6.87	5.48	5.01	5.68
Eu	ppm	Na2O2 Sinter	1.59	1.47	1.36	0.07	2.17	0.97	1.50	1.45
Tb	ppm	Na2O2 Sinter	1.38	0.72	1.56	0.23	1.76	1.02	0.87	0.99
Dy	ppm	Na2O2 Sinter	9.15	4.62	10.28	2.01	13.44	6.90	5.52	6.70
Ho	ppm	Na2O2 Sinter	2.03	1.02	2.25	0.54	3.04	1.50	1.16	1.49
Er	ppm	Na_2O_2 Sinter	6.17	3.18	6.83	2.03	10.04	4.63	3.53	4.82
Tm	ppm	Na2O2 Sinter	0.93	0.53	1.05	0.36	1.61	0.70	0.55	0.78
Yb	ppm	Na2O2 Sinter	6.26	3.84	6.81	2.83	11.68	4.72	3.76	5.70
Lu	ppm	Na2O2 Sinter	0.96	0.59	1.07	0.45	1.88	0.72	0.56	0.90
Hf	ppm	Na2O2 Sinter	5.30	3.82	4.91	8.82	11.98	3.89	3.98	4.47
Ta	ppm	Na2O2 Sinter	0.34	0.24	0.33	0.39	0.28	0.28	0.22	0.25
Th	ppm	Na2O2 Sinter	6.90	4.94	6.50	8.75	6.22	5.48	5.00	5.85
AlOH WL	nm	Terraspec	2,208	2,212	2,210	2,204	2,205	2,205	2,211	2,211
AlOH Depth	%	Terraspec	12.68%	19.88%	16.78%	47.73%	4.64%	12.93%	10.53%	11.79%
FeOH WL	nm	Terraspec	#DIV/0!	#DIV/0!	#DIV/0!	#DIV/0!	#DIV/0!	2,254	#DIV/0!	#DIV/0!
FeOH Depth	%	Terraspec	#DIV/0!	#DIV/0!	#DIV/0!	#DIV/0!	#DIV/0!	2.77%	#DIV/0!	#DIV/0!
AlOH depth/FeOH depth		Terraspec	#DIV/0!	#DIV/0!	#DIV/0!	#DIV/0!	#DIV/0!	4.67	#DIV/0!	#DIV/0!

Abbreviations:

Units
HFL= Hanging wall flow
HBX= Hanging wall breccia
FLT= Footwall lapilli tuff
FT= Footwall tuff
FBX= Footwall breccia
FFL= Footwall flow
INT= Intrusion

Alteration
Qtz-Ser= Quartz-sericite
Chl-Ser= Chlorite-sericite
Chl=Chlorite

Other
WL= Wavelength

Appendix B: Table B1.1 Whole-rock Geochemistry and Terraspec™ Data

Sample ID			**H501293**	**H501294**	**H501295**	**H501296**	**H501297**	**H501298**	**H501299**	**H501300**
Hole ID			BD11-146	BD11-143	BD11-143	BD11-143	BD11-143	BD11-134	BD11-134	BD11-134
Depth (m)			14.9	4.3	7.9	16.7	28.1	10.9	21.5	33.1
Lithology			FLT	FLT	FLT	FLT	FFL	FLT	FLT	FLT
Alteration			Qtz-Ser	Qtz-Ser	Qtz-Ser	Qtz-Ser	Qtz-Ser	Qtz-Ser	Chl	Qtz-Ser
SiO_2	%	FUS-ICP	55.61	75.69	78.11	79.36	80.81	62.43	53.49	74.01
Al_2O_3	%	FUS-ICP	8.65	7.7	7.89	7.94	10.22	10.21	11.38	9.35
Fe_2O_3(T)	%	FUS-ICP	18.16	7.86	6.11	4.83	1.8	13.91	11.46	8.32
MnO	%	FUS-ICP	0.065	0.007	0.027	0.017	0.014	0.023	0.193	0.007
MgO	%	FUS-ICP	1.44	0.38	2.3	1.7	1.29	1.48	12.37	0.38
CaO	%	FUS-ICP	0.02	0.03	0.02	0.03	0.03	0.03	1.43	0.03
Na_2O	%	FUS-ICP	0.07	0.11	0.08	0.09	0.12	0.13	0.02	0.14
K_2O	%	FUS-ICP	2.51	2.14	1.61	1.86	2.74	2.71	0.15	2.69
TiO_2	%	FUS-ICP	0.122	0.118	0.103	0.116	0.147	0.146	0.179	0.137
P_2O_5	%	FUS-ICP	< 0.01	< 0.01	0.01	< 0.01	0.02	< 0.01	0.02	< 0.01
LOI	%	FUS-ICP	11.49	5.47	3.98	3.22	2.2	8.77	9.65	5.26
Total	%	FUS-ICP	98.14	99.5	100.2	99.18	99.4	99.84	100.3	100.3
Ba	ppm	FUS-ICP	1060	698	520	603	871	1099	56	763
Sr	ppm	FUS-ICP	4	5	4	4	6	8	33	7
Y	ppm	FUS-ICP	16	27	29	33	36	36	46	34
Sc	ppm	FUS-ICP	12	8	8	9	11	11	13	10
Zr	ppm	FUS-ICP	120	105	103	111	136	130	152	121
Be	ppm	FUS-ICP	< 1	< 1	< 1	< 1	< 1	< 1	< 1	< 1
V	ppm	FUS-ICP	19	< 5	< 5	< 5	< 5	< 5	6	< 5
Hg	ppb	FIMS	1410	12	11	9	< 5	30	16	18
Cr	ppm	HF/HNO3	<8.9	29.63	<8.9	34.09	30.72	9.09	<8.9	<8.9
Co	ppm	HF/HNO3	<0.9	19.63	12.46	14.29	2.49	8.06	4.15	10.26
Ni	ppm	HF/HNO3	<10	16.30	<10	19.58	19.84	<10	<10	<10
Cu	ppm	HF/HNO3	177.31	3026.08	963.65	1147.85	47.36	702.85	139.90	22.90
Zn	ppm	HF/HNO3	1794.40	84.39	82.09	88.66	68.46	114.18	348.40	26.90
As	ppm	HF/HNO3	481.71	18.34	16.13	33.61	1.97	65.73	6.24	34.43
Se	ppm	HF/HNO3	<26.7	<26.7	<26.7	<26.7	<26.7	<26.7	<26.7	<26.7
Br	ppm	HF/HNO3	249.22	185.88	216.22	233.90	211.15	265.11	251.45	264.97
Mo	ppm	HF/HNO3	2.89	9.20	3.81	13.69	9.92	4.49	5.29	4.41
Ag	ppm	HF/HNO3	<1	<1	<1	<1	<1	<1	<1	<1
Cd	ppm	HF/HNO3	5.71	<0.9	<0.9	<0.9	<0.9	<0.9	<0.9	<0.9
Sn	ppm	HF/HNO3	10.03	4.17	3.81	4.10	4.18	6.04	3.15	3.94
Sb	ppm	HF/HNO3	26.83	1.66	1.27	1.38	0.82	1.96	1.67	2.11
Te	ppm	HF/HNO3	<4.3	7.92	4.32	<4.3	<4.3	12.05	<4.3	<4.3
I	ppm	HF/HNO3	<37	<37	<37	<37	<37	<37	<37	<37
W	ppm	HF/HNO3	3.12	7.07	5.96	5.07	6.55	6.45	7.71	4.00
Pb	ppm	HF/HNO3	58.38	<25.3	<25.3	<25.3	<25.3	73.04	46.15	<25.3
Bi	ppm	HF/HNO3	0.19	9.91	5.23	4.13	1.82	17.73	1.71	4.07
Nb	ppm	Na2O2 Sinter	4.60	4.70	5.54	5.26	5.82	7.42	10.09	5.94
La	ppm	Na2O2 Sinter	12.41	10.38	13.01	13.24	16.30	13.66	20.32	15.11
Ce	ppm	Na2O2 Sinter	25.64	21.78	28.69	27.67	32.67	29.51	43.41	32.13
Pr	ppm	Na2O2 Sinter	3.13	2.69	3.65	3.47	4.08	3.76	5.49	4.09
Nd	ppm	Na2O2 Sinter	13.18	11.00	15.40	14.54	18.17	16.06	22.96	17.16
Sm	ppm	Na2O2 Sinter	2.79	2.64	3.68	3.63	4.73	4.17	6.02	4.32
Eu	ppm	Na2O2 Sinter	0.66	0.73	0.98	0.88	1.02	1.01	1.48	0.84
Tb	ppm	Na2O2 Sinter	0.41	0.60	0.71	0.82	0.94	0.87	1.20	0.77
Dy	ppm	Na2O2 Sinter	2.73	4.34	4.48	5.60	5.95	6.03	7.59	5.19
Ho	ppm	Na2O2 Sinter	0.60	0.99	0.96	1.20	1.28	1.22	1.64	1.06
Er	ppm	Na_2O_2 Sinter	1.95	3.04	2.87	3.65	4.04	3.91	5.01	3.16
Tm	ppm	Na2O2 Sinter	0.32	0.45	0.44	0.56	0.60	0.61	0.75	0.50
Yb	ppm	Na2O2 Sinter	2.20	3.17	3.00	3.65	4.23	4.08	5.24	3.41
Lu	ppm	Na2O2 Sinter	0.33	0.49	0.46	0.54	0.69	0.67	0.83	0.52
Hf	ppm	Na2O2 Sinter	3.45	3.16	4.07	2.80	4.46	4.98	6.20	3.84
Ta	ppm	Na2O2 Sinter	0.17	0.17	0.22	0.19	0.24	0.22	0.30	0.21
Th	ppm	Na2O2 Sinter	3.63	3.83	4.59	3.93	4.85	5.28	6.28	4.35
AlOH WL	nm	Terraspec	2,211	2,204	2,201	2,202	2,204	2,205	#DIV/0!	2,205
AlOH Depth	%	Terraspec	13.52%	20.60%	16.25%	17.58%	33.75%	14.50%	#DIV/0!	21.43%
FeOH WL	nm	Terraspec	#DIV/0!	#DIV/0!	2,253	2,253	2,254	2,253	2,250	#DIV/0!
FeOH Depth	%	Terraspec	#DIV/0!	#DIV/0!	6.28%	4.56%	2.03%	1.28%	17.43%	#DIV/0!
AlOH depth/FeOH depth		Terraspec	#DIV/0!	#DIV/0!	2.59	3.85	16.65	11.33	#DIV/0!	#DIV/0!

Abbreviations:	**Units**		**Alteration**	**Other**
	HFL= Hanging wall flow	FT= Footwall tuff	Qtz-Ser= Quartz-sericite	WL= Wavelength
	HBX= Hanging wall breccia	FBX= Footwall breccia	Chl-Ser= Chlorite-sericite	
	FLT= Footwall lapilli tuff	FFL= Footwall flow	Chl=Chlorite	
		INT= Intrusion		

Appendix B: Table B1.1 Whole-rock Geochemistry and Terraspec^{TM} Data

Sample ID			**H501301**	**H501302**	**H501303**	**H501304**	**H501305**	**H501306**	**H501307**	**H501308**
Hole ID			BD11-134	BD11-154	BD11-154	BD11-154	BD11-158	BD11-158	BD11-158	BD11-158
Depth (m)			43	10.9	26.1	30.5	5.8	14	25.4	39.8
Lithology			FBX	FLT	FLT	FLT	FLT	FLT	FLT	FLT
Alteration			Qtz-Ser	Qtz-Ser	Qtz-Ser	Qtz-Ser	Chl	Chl	Chl-Ser	Qtz-Ser
SiO_2	%	FUS-ICP	70.04	75.55	76.35	76.39	22.68	44.36	75.98	72.15
Al_2O_3	%	FUS-ICP	9.54	12.77	10.4	12.91	15.85	8.25	10.21	11.75
Fe_2O_3(T)	%	FUS-ICP	10.29	4.29	5.45	3.24	17.59	8.53	3.4	4.34
MnO	%	FUS-ICP	0.031	0.007	0.013	0.012	0.1	0.204	0.036	0.047
MgO	%	FUS-ICP	1.5	0.46	0.48	0.61	22.54	15.7	5.27	3.85
CaO	%	FUS-ICP	0.12	0.03	0.05	0.04	0.21	6.53	0.08	0.06
Na_2O	%	FUS-ICP	0.12	0.2	0.18	0.2	0.03	0.01	0.06	0.08
K_2O	%	FUS-ICP	2.49	3.72	2.96	3.76	0.03	0.02	1.85	2.6
TiO_2	%	FUS-ICP	0.144	0.185	0.156	0.18	0.23	0.19	0.143	0.171
P_2O_5	%	FUS-ICP	< 0.01	< 0.01	< 0.01	< 0.01	0.01	0.08	0.01	0.02
LOI	%	FUS-ICP	6.41	3.74	4.07	3.38	14.93	14.36	3.85	4.01
Total	%	FUS-ICP	100.7	101	100.1	100.7	94.2	98.22	100.9	99.07
Ba	ppm	FUS-ICP	728	1611	1022	1395	19	15	624	657
Sr	ppm	FUS-ICP	9	12	10	13	4	120	4	5
Y	ppm	FUS-ICP	35	16	19	27	23	54	36	43
Sc	ppm	FUS-ICP	10	8	8	13	14	11	10	13
Zr	ppm	FUS-ICP	125	160	139	156	200	198	123	152
Be	ppm	FUS-ICP	< 1	< 1	< 1	< 1	< 1	< 1	< 1	< 1
V	ppm	FUS-ICP	< 5	< 5	6	7	< 5	< 5	6	5
Hg	ppb	FIMS	30	9	11	9	2530	74	14	7
Cr	ppm	HF/HNO3	17.42	12.67	12.02	17.01	<8.9	<8.9	<8.9	<8.9
Co	ppm	HF/HNO3	2.79	2.14	6.77	8.44	80.15	18.63	1.50	1.09
Ni	ppm	HF/HNO3	<10	<10	<10	<10	<10	<10	<10	<10
Cu	ppm	HF/HNO3	731.55	<19	<19	<19	23776.05	310.99	145.74	131.84
Zn	ppm	HF/HNO3	52.37	32.65	33.15	32.02	9964.99	686.97	176.31	238.35
As	ppm	HF/HNO3	175.59	17.96	30.15	6.84	106.22	25.32	6.53	46.66
Se	ppm	HF/HNO3	<26.7	<26.7	<26.7	<26.7	<26.7	<26.7	<26.7	<26.7
Br	ppm	HF/HNO3	251.86	248.03	238.46	230.34	295.54	236.62	315.08	259.59
Mo	ppm	HF/HNO3	2.74	6.26	4.58	9.30	<1	8.16	3.30	3.67
Ag	ppm	HF/HNO3	<1	1.12	<1	<1	5.76	<1	<1	<1
Cd	ppm	HF/HNO3	<0.9	<0.9	<0.9	<0.9	36.17	1.45	<0.9	<0.9
Sn	ppm	HF/HNO3	4.57	5.19	4.76	6.76	14.22	8.09	14.92	9.14
Sb	ppm	HF/HNO3	11.04	1.29	1.19	1.64	1.76	<0.3	1.19	2.30
Te	ppm	HF/HNO3	<4.3	<4.3	<4.3	<4.3	11.47	<4.3	<4.3	<4.3
I	ppm	HF/HNO3	<37	<37	<37	<37	<37	<37	<37	<37
W	ppm	HF/HNO3	2.15	4.62	4.27	3.28	3.23	1.92	6.74	3.14
Pb	ppm	HF/HNO3	32.09	29.18	<25.3	<25.3	<25.3	<25.3	<25.3	<25.3
Bi	ppm	HF/HNO3	7.28	3.95	3.33	1.67	7.56	0.83	1.05	2.03
Nb	ppm	Na2O2 Sinter	6.52	8.37	7.48	8.06	8.30	6.75	5.00	6.11
La	ppm	Na2O2 Sinter	15.19	7.82	3.75	19.40	3.01	46.75	17.17	19.75
Ce	ppm	Na2O2 Sinter	32.12	12.93	7.42	36.56	6.18	98.67	35.73	41.61
Pr	ppm	Na2O2 Sinter	4.01	1.40	0.89	4.20	0.80	12.27	4.45	5.28
Nd	ppm	Na2O2 Sinter	16.79	5.35	3.59	16.58	3.60	51.98	18.80	22.47
Sm	ppm	Na2O2 Sinter	4.30	1.04	0.92	3.26	1.09	11.61	4.49	5.35
Eu	ppm	Na2O2 Sinter	1.23	0.34	0.29	0.69	0.18	1.20	1.32	1.41
Tb	ppm	Na2O2 Sinter	0.83	0.30	0.33	0.66	0.37	1.69	0.86	1.05
Dy	ppm	Na2O2 Sinter	5.65	2.37	2.65	4.39	2.98	9.91	5.71	6.93
Ho	ppm	Na2O2 Sinter	1.19	0.59	0.64	0.95	0.74	1.97	1.26	1.51
Er	ppm	Na_2O_2 Sinter	3.52	2.22	2.28	3.16	2.57	5.81	3.81	4.55
Tm	ppm	Na2O2 Sinter	0.55	0.40	0.39	0.50	0.42	0.87	0.58	0.70
Yb	ppm	Na2O2 Sinter	3.65	3.27	2.97	3.79	3.31	5.78	4.04	4.80
Lu	ppm	Na2O2 Sinter	0.58	0.48	0.46	0.59	0.55	0.90	0.62	0.73
Hf	ppm	Na2O2 Sinter	4.39	4.34	4.41	4.94	6.16	5.25	3.58	3.66
Ta	ppm	Na2O2 Sinter	0.24	0.32	0.28	0.31	0.31	0.28	0.21	0.26
Th	ppm	Na2O2 Sinter	4.72	5.99	5.34	6.37	6.22	6.52	4.63	5.52
AlOH WL	nm	Terraspec	2,204	2,204	2,204	2,205	#DIV/0!	#DIV/0!	2,207	2,207
AlOH Depth	%	Terraspec	11.60%	22.75%	25.58%	30.14%	#DIV/0!	#DIV/0!	14.30%	10.06%
FeOH WL	nm	Terraspec	2,253	#DIV/0!	#DIV/0!	#DIV/0!	2,249	2,248	2,251	2,252
FeOH Depth	%	Terraspec	1.21%	#DIV/0!	#DIV/0!	#DIV/0!	4.22%	1.71%	6.83%	3.86%
AlOH depth/FeOH depth		Terraspec	9.59	#DIV/0!	#DIV/0!	#DIV/0!	#DIV/0!	#DIV/0!	2.09	2.61

Abbreviations:	**Units**	FT= Footwall tuff	**Alteration**	**Other**
	HFL= Hanging wall flow	FBX= Footwall breccia	Qtz-Ser= Quartz-sericite	WL= Wavelength
	HBX= Hanging wall breccia	FFL= Footwall flow	Chl-Ser= Chlorite-sericite	
	FLT= Footwall lapilli tuff	INT= Intrusion	Chl=Chlorite	

Appendix B: Table B1.1 Whole-rock Geochemistry and Terraspec™ Data

Sample ID			**H501309**	**H501310**	**H501311**	**H501312**	**H501313**	**H501314**	**H501315**	**H501316**
Hole ID			BD11-136	BD11-136	BD11-136	BD11-195	BD11-195	BD11-195	BD11-195	BD10-6
Depth (m)			10.7	23.4	31.9	7.9	9.5	16.8	23.8	4.6
Lithology			FLT	FLT	FLT	FLT	FFL	FLT	FFL	HFL
Alteration			Qtz-Ser	Chl	Qtz-Ser	Qtz-Ser	Chl-Ser	Qtz-Ser	Qtz-Ser	Qtz-Ser
SiO_2	%	FUS-ICP	73.45	25.79	72.61	73.61	68.86	75.05	72.89	76.59
Al_2O_3	%	FUS-ICP	7.25	20.66	10.28	10.08	11.99	10.82	12.03	10.21
Fe_2O_3(T)	%	FUS-ICP	8.61	15.94	6.84	6.95	6.77	5.02	4.25	2.24
MnO	%	FUS-ICP	0.014	0.136	0.007	0.014	0.071	0.019	0.049	0.1
MgO	%	FUS-ICP	0.68	22.87	0.77	0.56	4.4	1.52	3.54	3.29
CaO	%	FUS-ICP	0.03	0.04	0.04	0.04	0.06	0.04	0.05	0.05
Na_2O	%	FUS-ICP	0.1	< 0.01	0.13	0.11	0.09	0.1	0.09	0.08
K_2O	%	FUS-ICP	2	< 0.01	2.89	3.02	2.51	2.91	2.92	2.5
TiO_2	%	FUS-ICP	0.105	0.317	0.148	0.144	0.191	0.144	0.167	0.126
P_2O_5	%	FUS-ICP	< 0.01	0.01	0.01	0.01	0.03	< 0.01	0.02	0.01
LOI	%	FUS-ICP	6.05	12.8	5.27	4.98	5.78	4.06	4.19	3.11
Total	%	FUS-ICP	98.28	98.58	99.01	99.52	100.8	99.7	100.2	98.32
Ba	ppm	FUS-ICP	1429	13	1082	955	779	937	820	2076
Sr	ppm	FUS-ICP	7	< 2	8	5	5	6	6	5
Y	ppm	FUS-ICP	46	49	41	36	45	36	44	39
Sc	ppm	FUS-ICP	10	17	11	10	12	11	13	9
Zr	ppm	FUS-ICP	94	274	130	128	154	127	157	127
Be	ppm	FUS-ICP	< 1	< 1	< 1	< 1	< 1	< 1	< 1	1
V	ppm	FUS-ICP	< 5	6	< 5	< 5	< 5	< 5	< 5	< 5
Hg	ppb	FIMS	117	< 5	13	45	19	34	28	11
Cr	ppm	HF/HNO3	14.86	<8.9	<8.9	13.19	<8.9	<8.9	<8.9	<8.9
Co	ppm	HF/HNO3	2.84	34.35	5.34	<0.9	<0.9	<0.9	<0.9	1.06
Ni	ppm	HF/HNO3	<10	<10	<10	<10	<10	<10	<10	<10
Cu	ppm	HF/HNO3	1782.60	101.31	92.00	2618.66	103.67	200.60	<19	70.07
Zn	ppm	HF/HNO3	306.96	511.51	76.65	178.41	174.03	72.41	97.77	180.71
As	ppm	HF/HNO3	203.53	48.49	10.07	70.64	9.15	6.39	4.26	2.00
Se	ppm	HF/HNO3	<26.7	<26.7	<26.7	<26.7	<26.7	<26.7	<26.7	<26.7
Br	ppm	HF/HNO3	278.55	317.36	271.89	225.88	240.39	241.35	227.99	255.04
Mo	ppm	HF/HNO3	7.23	5.18	3.06	5.76	3.58	3.64	4.05	<1
Ag	ppm	HF/HNO3	1.01	1.06	<1	<1	<1	<1	<1	1.30
Cd	ppm	HF/HNO3	<0.9	<0.9	<0.9	<0.9	<0.9	<0.9	<0.9	<0.9
Sn	ppm	HF/HNO3	21.43	13.46	13.33	4.40	3.78	4.54	3.24	12.94
Sb	ppm	HF/HNO3	12.71	1.08	0.99	4.16	3.74	3.86	2.40	1.96
Te	ppm	HF/HNO3	<4.3	<4.3	<4.3	<4.3	<4.3	<4.3	<4.3	<4.3
I	ppm	HF/HNO3	<37	<37	<37	<37	<37	<37	<37	<37
W	ppm	HF/HNO3	2.05	17.26	2.97	3.79	2.94	3.84	2.67	1.85
Pb	ppm	HF/HNO3	31.13	<25.3	<25.3	26.39	<25.3	<25.3	<25.3	128.82
Bi	ppm	HF/HNO3	18.59	1.78	2.58	2.19	1.52	1.79	0.40	1.94
Nb	ppm	Na2O2 Sinter	3.42	13.79	5.13	7.40	9.71	6.34	7.70	5.09
La	ppm	Na2O2 Sinter	25.54	24.68	21.50	16.14	19.80	18.77	20.06	18.06
Ce	ppm	Na2O2 Sinter	57.09	49.26	45.44	33.83	41.15	37.87	42.33	37.11
Pr	ppm	Na2O2 Sinter	7.58	5.89	5.87	4.32	5.16	4.74	5.34	4.75
Nd	ppm	Na2O2 Sinter	32.96	24.56	25.53	18.29	22.34	20.29	22.63	19.98
Sm	ppm	Na2O2 Sinter	7.98	5.38	6.27	4.17	5.26	4.77	5.47	4.90
Eu	ppm	Na2O2 Sinter	1.70	1.10	1.07	1.22	1.35	1.14	1.56	1.18
Tb	ppm	Na2O2 Sinter	1.28	1.14	1.05	0.91	1.22	0.86	1.13	0.94
Dy	ppm	Na2O2 Sinter	7.70	8.17	6.60	6.07	8.20	5.70	7.50	6.41
Ho	ppm	Na2O2 Sinter	1.54	1.94	1.33	1.28	1.73	1.24	1.66	1.36
Er	ppm	Na_2O_2 Sinter	4.46	6.47	4.06	4.02	5.06	3.92	5.03	4.29
Tm	ppm	Na2O2 Sinter	0.64	1.08	0.60	0.63	0.80	0.59	0.78	0.66
Yb	ppm	Na2O2 Sinter	4.28	7.70	3.95	4.10	5.33	4.02	5.38	4.40
Lu	ppm	Na2O2 Sinter	0.63	1.23	0.62	0.62	0.80	0.62	0.77	0.71
Hf	ppm	Na2O2 Sinter	2.52	9.60	3.68	4.02	3.92	4.49	5.27	4.31
Ta	ppm	Na2O2 Sinter	0.14	0.52	0.21	0.26	0.35	0.24	0.30	0.23
Th	ppm	Na2O2 Sinter	3.02	11.75	4.48	5.26	6.42	5.24	6.43	4.64
AlOH WL	nm	Terraspec	2,206	#DIV/0!	2,206	2,208	2,207	2,205	2,207	2,213
AlOH Depth	%	Terraspec	10.24%	#DIV/0!	19.40%	13.70%	15.90%	9.60%	12.40%	19.93%
FeOH WL	nm	Terraspec	#DIV/0!	2,250	#DIV/0!	#DIV/0!	2,253	2,252	2,251	2,252
FeOH Depth	%	Terraspec	#DIV/0!	12.39%	#DIV/0!	#DIV/0!	1.46%	2.95%	3.64%	2.16%
AlOH depth/FeOH depth		Terraspec	#DIV/0!	#DIV/0!	#DIV/0!	#DIV/0!	10.87	3.25	3.41	9.24

Abbreviations:

Units
HFL= Hanging wall flow
HBX= Hanging wall breccia
FLT= Footwall lapilli tuff
FT= Footwall tuff
FBX= Footwall breccia
FFL= Footwall flow
INT= Intrusion

Alteration
Qtz-Ser= Quartz-sericite
Chl-Ser= Chlorite-sericite
Chl=Chlorite

Other
WL= Wavelength

Appendix B: Table B1.1 Whole-rock Geochemistry and Terraspec^{TM} Data

Sample ID			H501317	H501318	H501319	H501320	H501326	H501327	H501328	H501329
Hole ID			BD10-6	BD10-6	BD10-6	BD10-6	BD10-113	BD10-113	BD10-113	BD10-113
Depth (m)			7.3	13.7	17.9	32.1	5	10	28.3	40.8
Lithology			FLT	FLT	FBX	FBX	HFL	FLT	FLT	FLT
Alteration			Chl-Ser	Qtz-Ser	Qtz-Ser	Qtz-Ser	Qtz-Ser	Chl	Qtz-Ser	Qtz-Ser
SiO_2	%	FUS-ICP	65.02	72.29	76.48	75.46	78.95	53.65	72.47	76.4
Al_2O_3	%	FUS-ICP	11.35	12.49	11.31	12.51	11.22	11.33	13.27	10.32
Fe_2O_3(T)	%	FUS-ICP	8.49	3.9	3.01	2.34	1.6	11.18	2.4	1.9
MnO	%	FUS-ICP	0.164	0.158	0.136	0.089	0.024	0.269	0.183	0.27
MgO	%	FUS-ICP	3.11	1.95	1.55	2.24	2.38	11.35	2.83	2.25
CaO	%	FUS-ICP	0.04	0.06	0.23	0.14	0.03	0.04	0.35	0.34
Na_2O	%	FUS-ICP	0.08	0.12	0.67	0.22	0.09	0.03	0.66	0.11
K_2O	%	FUS-ICP	2.56	3.54	3.1	3.55	3	0.48	3.3	2.98
TiO_2	%	FUS-ICP	0.14	0.178	0.156	0.159	0.129	0.162	0.182	0.16
P_2O_5	%	FUS-ICP	0.01	0.02	0.02	0.02	0.03	0.02	0.03	0.05
LOI	%	FUS-ICP	6.14	4.23	3.62	3.61	2.61	9.51	4.23	3.81
Total	%	FUS-ICP	97.1	98.94	100.3	100.3	100.1	98.02	99.9	98.59
Ba	ppm	FUS-ICP	1776	1881	1737	1175	2481	344	1437	1206
Sr	ppm	FUS-ICP	5	7	15	9	5	< 2	18	17
Y	ppm	FUS-ICP	36	41	33	28	37	37	39	39
Sc	ppm	FUS-ICP	11	13	10	11	10	10	13	11
Zr	ppm	FUS-ICP	120	154	138	151	130	136	161	147
Be	ppm	FUS-ICP	1	1	1	1	1	< 1	1	1
V	ppm	FUS-ICP	22	13	< 5	7	< 5	14	15	< 5
Hg	ppb	FIMS	1580	357	313	546	30	113	397	193
Cr	ppm	HF/HNO3	12.73	<8.9	<8.9	11.20	<8.9	<8.9	<8.9	<8.9
Co	ppm	HF/HNO3	18.74	1.20	<0.9	<0.9	<0.9	30.03	2.73	0.92
Ni	ppm	HF/HNO3	<10	<10	<10	<10	<10	<10	<10	<10
Cu	ppm	HF/HNO3	2252.77	223.85	363.20	626.73	231.49	2080.79	226.52	128.03
Zn	ppm	HF/HNO3	5509.07	1355.64	1355.19	1698.80	298.16	796.81	1897.05	609.64
As	ppm	HF/HNO3	183.87	55.90	24.80	14.20	4.10	109.44	35.94	21.95
Se	ppm	HF/HNO3	<26.7	<26.7	<26.7	<26.7	<26.7	<26.7	<26.7	<26.7
Br	ppm	HF/HNO3	267.29	296.89	269.17	258.91	263.76	259.46	284.07	270.59
Mo	ppm	HF/HNO3	18.90	5.69	2.66	4.15	2.04	8.04	2.97	2.38
Ag	ppm	HF/HNO3	9.78	1.28	<1	<1	<1	4.40	<1	<1
Cd	ppm	HF/HNO3	15.47	4.57	4.75	5.91	<0.9	5.33	5.65	1.44
Sn	ppm	HF/HNO3	13.47	20.74	17.99	9.59	10.68	16.99	21.59	9.62
Sb	ppm	HF/HNO3	25.57	13.13	4.24	1.57	3.95	10.63	3.42	2.20
Te	ppm	HF/HNO3	<4.3	<4.3	<4.3	<4.3	<4.3	4.61	<4.3	<4.3
I	ppm	HF/HNO3	<37	<37	<37	<37	<37	<37	<37	<37
W	ppm	HF/HNO3	3.32	2.95	2.75	3.64	2.39	3.48	1.70	1.20
Pb	ppm	HF/HNO3	1331.20	49.99	84.52	<25.3	88.35	195.20	145.10	<25.3
Bi	ppm	HF/HNO3	9.38	1.74	1.67	0.56	0.60	14.69	0.66	0.16
Nb	ppm	Na2O2 Sinter	5.04	6.46	5.83	6.03	5.03	6.51	7.26	6.09
La	ppm	Na2O2 Sinter	16.75	21.49	16.93	19.75	18.87	21.93	24.68	19.45
Ce	ppm	Na2O2 Sinter	34.47	45.15	35.95	41.70	39.06	45.22	52.15	40.95
Pr	ppm	Na2O2 Sinter	4.35	5.70	4.51	5.29	5.01	5.73	6.58	5.18
Nd	ppm	Na2O2 Sinter	18.36	23.98	19.04	22.05	21.52	23.91	28.06	21.96
Sm	ppm	Na2O2 Sinter	4.48	5.69	4.61	5.03	5.15	5.57	6.44	5.31
Eu	ppm	Na2O2 Sinter	1.41	1.47	1.05	1.00	1.11	1.49	1.72	1.32
Tb	ppm	Na2O2 Sinter	0.87	1.06	0.84	0.79	0.95	1.02	1.12	1.07
Dy	ppm	Na2O2 Sinter	5.80	7.16	5.72	5.11	6.34	6.83	7.24	7.15
Ho	ppm	Na2O2 Sinter	1.25	1.53	1.21	1.07	1.39	1.46	1.54	1.56
Er	ppm	Na_2O_2 Sinter	3.92	4.73	3.71	3.45	4.33	4.48	4.85	4.70
Tm	ppm	Na2O2 Sinter	0.58	0.74	0.57	0.54	0.65	0.68	0.76	0.72
Yb	ppm	Na2O2 Sinter	4.04	5.00	4.00	3.79	4.47	4.62	5.25	4.87
Lu	ppm	Na2O2 Sinter	0.62	0.78	0.63	0.62	0.67	0.70	0.81	0.71
Hf	ppm	Na2O2 Sinter	3.77	4.19	4.03	3.95	3.94	3.84	5.32	4.41
Ta	ppm	Na2O2 Sinter	0.21	0.27	0.24	0.25	0.21	0.25	0.29	0.23
Th	ppm	Na2O2 Sinter	4.18	5.38	4.78	5.01	4.88	5.43	6.32	5.23
AlOH WL	nm	Terraspec	2,209	2,210	2,213	2,211	2,210	2,204	2,209	2,209
AlOH Depth	%	Terraspec	10.41%	13.83%	21.15%	18.60%	18.50%	5.14%	14.95%	19.70%
FeOH WL	nm	Terraspec	2,253	#DIV/0!	#DIV/0!	#DIV/0!	2,252	2,250	#DIV/0!	2,250
FeOH Depth	%	Terraspec	3.39%	#DIV/0!	#DIV/0!	#DIV/0!	2.16%	4.88%	#DIV/0!	1.09%
AlOH depth/FeOH depth		Terraspec	3.07	#DIV/0!	#DIV/0!	#DIV/0!	8.56	1.05	#DIV/0!	18.07

Abbreviations:	**Units**		**Alteration**	**Other**
	HFL= Hanging wall flow	FT= Footwall tuff	Qtz-Ser= Quartz-sericite	WL= Wavelength
	HBX= Hanging wall breccia	FBX= Footwall breccia	Chl-Ser= Chlorite-sericite	
	FLT= Footwall lapilli tuff	FFL= Footwall flow	Chl=Chlorite	
		INT= Intrusion		

Appendix B: Table B1.1 Whole-rock Geochemistry and Terraspec^{TM} Data

Sample ID			**H501332**	**H501333**	**H501334**	**H501335**	**H501336**	**H501337**	**H501338**	**H501339**
Hole ID			BD10-3	BD10-3	BD10-3	BD10-3	BD10-3	BD10-18	BD10-18	BD10-18
Depth (m)			6.6	8.2	16.3	30.7	37.9	4.3	9.9	19.7
Lithology			HFL	FLT	FLT	FLT	FLT	FLT	FFL	FBX
Alteration			Qtz-Ser	Qtz-Ser	Qtz-Ser	Qtz-Ser	Chl	Chl-Ser	Qtz-Ser	Qtz-Ser
SiO_2	%	FUS-ICP	74.87	70.98	70.38	55.23	29.41	61.73	76.76	77.83
Al_2O_3	%	FUS-ICP	12.33	9.95	13.14	14.36	15.55	9.09	10.26	10.35
Fe_2O_3(T)	%	FUS-ICP	2.46	7.34	5.35	13.34	14.64	13.5	5.03	4.55
MnO	%	FUS-ICP	0.041	0.024	0.025	0.091	1.166	0.058	0.016	0.007
MgO	%	FUS-ICP	1.19	0.69	0.79	1.95	20.18	2.02	0.94	0.49
CaO	%	FUS-ICP	0.03	0.03	0.03	0.04	1.94	0.05	0.12	0.03
Na_2O	%	FUS-ICP	0.16	0.12	0.16	0.18	< 0.01	0.07	0.09	0.09
K_2O	%	FUS-ICP	3.6	2.95	3.95	4.13	0.04	2.44	3.08	3.14
TiO_2	%	FUS-ICP	0.171	0.156	0.186	0.195	0.191	0.131	0.138	0.148
P_2O_5	%	FUS-ICP	< 0.01	< 0.01	< 0.01	< 0.01	0.02	0.02	0.02	0.01
LOI	%	FUS-ICP	3.16	5.49	4.61	9.33	14.92	8.86	4.18	3.76
Total	%	FUS-ICP	98.01	97.73	98.62	98.86	98.07	97.97	100.6	100.4
Ba	ppm	FUS-ICP	2778	2538	2461	1664	15	858	1037	933
Sr	ppm	FUS-ICP	8	6	8	10	21	3	5	5
Y	ppm	FUS-ICP	44	29	47	49	56	36	28	43
Sc	ppm	FUS-ICP	13	10	13	16	23	10	10	11
Zr	ppm	FUS-ICP	154	117	166	174	173	120	130	132
Be	ppm	FUS-ICP	1	< 1	1	1	< 1	< 1	< 1	< 1
V	ppm	FUS-ICP	< 5	6	5	< 5	11	5	< 5	< 5
Hg	ppb	FIMS	481	1460	1110	551	60	31	18	9
Cr	ppm	HF/HNO3	<8.9	8.94	<8.9	<8.9	<8.9	<8.9	11.06	<8.9
Co	ppm	HF/HNO3	<0.9	<0.9	<0.9	0.99	24.01	<0.9	1.78	<0.9
Ni	ppm	HF/HNO3	<10	13.76	<10	<10	<10	<10	<10	<10
Cu	ppm	HF/HNO3	269.22	69.57	120.75	137.50	154.03	3709.45	553.25	640.67
Zn	ppm	HF/HNO3	3140.30	8869.23	5706.97	1376.58	11001.81	302.94	129.46	321.15
As	ppm	HF/HNO3	11.44	106.90	16.89	117.04	2.59	116.32	59.65	53.73
Se	ppm	HF/HNO3	<26.7	<26.7	<26.7	<26.7	<26.7	<26.7	<26.7	<26.7
Br	ppm	HF/HNO3	233.63	237.31	228.89	201.31	214.99	254.75	275.79	229.06
Mo	ppm	HF/HNO3	2.44	3.22	3.17	6.69	5.15	39.47	4.15	2.59
Ag	ppm	HF/HNO3	2.95	1.62	<1	1.02	<1	<1	<1	1.44
Cd	ppm	HF/HNO3	11.26	31.42	23.58	5.14	9.55	<0.9	<0.9	<0.9
Sn	ppm	HF/HNO3	12.68	5.73	5.60	50.67	5.62	9.98	10.48	8.93
Sb	ppm	HF/HNO3	6.55	8.06	6.74	28.65	94.47	2.63	2.45	1.54
Te	ppm	HF/HNO3	<4.3	<4.3	<4.3	<4.3	<4.3	<4.3	<4.3	18.88
I	ppm	HF/HNO3	<37	<37	<37	<37	<37	<37	<37	<37
W	ppm	HF/HNO3	3.85	4.81	5.78	2.26	14.36	3.93	3.53	5.23
Pb	ppm	HF/HNO3	3140.32	303.07	34.61	109.40	165.01	47.75	37.17	<25.3
Bi	ppm	HF/HNO3	0.21	1.44	0.33	19.98	2.26	11.78	4.98	26.09
Nb	ppm	Na2O2 Sinter	7.92	8.09	9.38	10.46	9.48	5.06	4.96	5.44
La	ppm	Na2O2 Sinter	18.38	17.52	21.02	21.10	30.44	22.70	15.88	16.63
Ce	ppm	Na2O2 Sinter	38.12	35.94	43.92	44.84	65.07	47.94	33.46	35.41
Pr	ppm	Na2O2 Sinter	4.78	4.62	5.51	5.64	8.25	6.12	4.27	4.48
Nd	ppm	Na2O2 Sinter	20.36	19.95	23.83	24.77	36.12	26.68	18.14	19.25
Sm	ppm	Na2O2 Sinter	4.84	4.55	5.72	5.92	8.69	6.24	4.37	5.08
Eu	ppm	Na2O2 Sinter	1.32	1.08	1.38	1.13	1.20	1.30	0.85	0.95
Tb	ppm	Na2O2 Sinter	0.99	0.79	1.19	1.19	1.63	1.02	0.74	1.11
Dy	ppm	Na2O2 Sinter	6.75	5.19	7.90	8.08	10.73	6.48	4.94	7.33
Ho	ppm	Na2O2 Sinter	1.56	1.15	1.74	1.82	2.26	1.38	1.08	1.58
Er	ppm	Na_2O_2 Sinter	4.82	3.57	5.31	5.81	6.65	4.10	3.27	4.75
Tm	ppm	Na2O2 Sinter	0.76	0.56	0.85	0.90	0.99	0.63	0.52	0.71
Yb	ppm	Na2O2 Sinter	5.21	3.77	5.62	6.10	6.48	4.18	3.68	4.70
Lu	ppm	Na2O2 Sinter	0.80	0.57	0.87	0.96	1.03	0.63	0.59	0.72
Hf	ppm	Na2O2 Sinter	5.75	3.82	5.03	5.54	6.51	3.65	3.27	3.27
Ta	ppm	Na2O2 Sinter	0.32	0.24	0.30	0.35	0.33	0.20	0.21	0.22
Th	ppm	Na2O2 Sinter	6.31	4.99	6.63	6.87	7.35	4.22	4.43	5.47
AlOH WL	nm	Terraspec	2,210	2,210	2,209	2,209	#DIV/0!	2,210	2,210	2,208
AlOH Depth	%	Terraspec	9.74%	7.17%	10.30%	10.94%	#DIV/0!	10.91%	12.65%	17.90%
FeOH WL	nm	Terraspec	#DIV/0!	#DIV/0!	#DIV/0!	#DIV/0!	2,250	2,252	#DIV/0!	#DIV/0!
FeOH Depth	%	Terraspec	#DIV/0!	#DIV/0!	#DIV/0!	#DIV/0!	8.54%	2.22%	#DIV/0!	#DIV/0!
AlOH depth/FeOH depth		Terraspec	#DIV/0!	#DIV/0!	#DIV/0!	#DIV/0!	#DIV/0!	4.91	#DIV/0!	#DIV/0!

Abbreviations:	**Units**		**Alteration**	**Other**
	HFL= Hanging wall flow	FT= Footwall tuff	Qtz-Ser= Quartz-sericite	WL= Wavelength
	HBX= Hanging wall breccia	FBX= Footwall breccia	Chl-Ser= Chlorite-sericite	
	FLT= Footwall lapilli tuff	FFL= Footwall flow	Chl=Chlorite	
		INT= Intrusion		

Appendix B: Table B1.1 Whole-rock Geochemistry and Terraspec™ Data

Sample ID			H501340	H501341	H501342	H501343	H501344	H501345	H501346	H501347
Hole ID			BD10-18	BD10-18	BD11-190	BD11-190	BD11-190	BD11-189	BD11-189	BD11-189
Depth (m)			27.2	31.3	9.8	24.9	39.3	11.3	19.5	20.7
Lithology			FFL	FBX	FLT	FLT	FLT	FLT	FFL	FLT
Alteration			Qtz-Ser	Chl	Qtz-Ser	Qtz-Ser	Qtz-Ser	Qtz-Ser	Chl-Ser	Qtz-Ser
SiO_2	%	FUS-ICP	75.27	63.27	76.25	69.47	72.57	71.97	61.57	64.03
Al_2O_3	%	FUS-ICP	9.95	11.09	11.95	10.94	11.24	11.4	10.92	18.11
Fe_2O_3(T)	%	FUS-ICP	5.48	7.97	3.63	7.9	4.77	6.75	10.99	4.46
MnO	%	FUS-ICP	0.026	0.254	0.039	0.051	0.113	0.105	0.339	0.092
MgO	%	FUS-ICP	1.02	9.13	1.54	1.13	2.7	2.34	3.98	2.22
CaO	%	FUS-ICP	0.04	0.07	0.05	0.04	0.07	0.05	0.1	0.08
Na_2O	%	FUS-ICP	0.09	0.03	0.16	0.17	0.16	0.17	0.18	0.31
K_2O	%	FUS-ICP	2.82	0.9	3	2.87	2.51	2.61	2.24	4.86
TiO_2	%	FUS-ICP	0.146	0.158	0.17	0.155	0.179	0.168	0.226	0.256
P_2O_5	%	FUS-ICP	< 0.01	0.04	0.02	< 0.01	0.03	0.03	0.02	0.04
LOI	%	FUS-ICP	4.27	6.8	3.45	5.9	4.05	4.65	8.4	5.26
Total	%	FUS-ICP	99.12	99.71	100.3	98.64	98.39	100.2	98.96	99.73
Ba	ppm	FUS-ICP	793	270	1262	1009	992	1119	917	2046
Sr	ppm	FUS-ICP	6	2	9	9	9	7	10	16
Y	ppm	FUS-ICP	34	41	43	40	37	41	37	60
Sc	ppm	FUS-ICP	10	10	12	11	11	12	12	19
Zr	ppm	FUS-ICP	129	148	144	141	141	147	175	240
Be	ppm	FUS-ICP	< 1	< 1	< 1	< 1	< 1	< 1	< 1	1
V	ppm	FUS-ICP	< 5	5	6	< 5	9	< 5	6	< 5
Hg	ppb	FIMS	11	24	< 5	12	8	< 5	115	8
Cr	ppm	HF/HNO3	9.69	<8.9	<8.9	15.30	15.70	34.71	36.99	26.36
Co	ppm	HF/HNO3	<0.9	<0.9	1.24	4.87	1.05	6.21	20.61	1.71
Ni	ppm	HF/HNO3	<10	13.17	<10	<10	<10	27.63	20.04	15.20
Cu	ppm	HF/HNO3	234.51	287.67	963.89	784.11	381.03	20.48	1279.01	<19
Zn	ppm	HF/HNO3	120.82	416.08	86.39	167.04	77.22	136.43	172.84	97.96
As	ppm	HF/HNO3	96.88	30.38	23.31	14.48	2.80	16.77	21.19	3.83
Se	ppm	HF/HNO3	<26.7	<26.7	<26.7	<26.7	<26.7	<26.7	<26.7	<26.7
Br	ppm	HF/HNO3	262.65	252.70	249.99	195.49	222.96	215.16	203.30	213.63
Mo	ppm	HF/HNO3	2.98	4.46	3.41	5.98	5.52	11.33	16.27	9.31
Ag	ppm	HF/HNO3	<1	<1	<1	<1	<1	<1	<1	<1
Cd	ppm	HF/HNO3	<0.9	<0.9	<0.9	<0.9	<0.9	<0.9	<0.9	<0.9
Sn	ppm	HF/HNO3	9.78	7.87	11.41	5.26	4.30	5.17	4.18	4.36
Sb	ppm	HF/HNO3	2.69	4.57	1.25	3.83	1.27	1.34	6.14	1.70
Te	ppm	HF/HNO3	<4.3	<4.3	<4.3	<4.3	<4.3	<4.3	<4.3	<4.3
I	ppm	HF/HNO3	<37	<37	<37	<37	<37	<37	<37	<37
W	ppm	HF/HNO3	6.13	2.34	3.66	6.66	3.90	3.70	14.07	6.17
Pb	ppm	HF/HNO3	31.06	<25.3	<25.3	<25.3	<25.3	<25.3	28.66	<25.3
Bi	ppm	HF/HNO3	6.89	1.90	1.39	7.70	0.82	1.05	7.25	0.31
Nb	ppm	Na2O2 Sinter	4.92	6.59	5.77	7.46	8.33	6.53	9.03	9.86
La	ppm	Na2O2 Sinter	17.26	17.74	19.23	16.86	17.26	18.14	16.49	31.65
Ce	ppm	Na2O2 Sinter	36.49	37.20	39.95	35.55	35.88	37.77	31.42	64.64
Pr	ppm	Na2O2 Sinter	4.67	4.72	5.10	4.51	4.54	4.69	3.82	8.00
Nd	ppm	Na2O2 Sinter	19.47	20.42	22.03	19.27	19.11	20.53	16.01	35.59
Sm	ppm	Na2O2 Sinter	4.66	5.03	5.37	4.75	4.73	5.24	4.29	9.23
Eu	ppm	Na2O2 Sinter	0.90	1.41	0.89	0.91	0.77	1.03	0.73	1.65
Tb	ppm	Na2O2 Sinter	0.82	1.08	1.06	1.00	0.93	1.00	0.89	1.52
Dy	ppm	Na2O2 Sinter	5.45	7.30	7.17	6.76	6.34	6.78	6.20	9.71
Ho	ppm	Na2O2 Sinter	1.21	1.60	1.55	1.42	1.33	1.42	1.36	2.03
Er	ppm	Na_2O_2 Sinter	3.66	4.87	4.77	4.28	4.16	4.35	4.16	6.07
Tm	ppm	Na2O2 Sinter	0.57	0.74	0.73	0.66	0.60	0.67	0.66	0.95
Yb	ppm	Na2O2 Sinter	3.95	4.97	4.84	4.36	4.13	4.37	4.84	6.71
Lu	ppm	Na2O2 Sinter	0.62	0.77	0.76	0.68	0.67	0.75	0.82	1.08
Hf	ppm	Na2O2 Sinter	2.76	4.36	4.22	3.53	4.59	4.08	5.49	6.36
Ta	ppm	Na2O2 Sinter	0.21	0.25	0.25	0.25	0.28	0.28	0.30	0.38
Th	ppm	Na2O2 Sinter	4.41	5.27	5.12	5.00	5.19	4.93	6.07	8.03
AlOH WL	nm	Terraspec	2,207	2,204	2,203	2,203	2,201	2,202	2,198	2,202
AlOH Depth	%	Terraspec	24.18%	5.25%	16.55%	14.80%	18.78%	14.13%	2.96%	12.65%
FeOH WL	nm	Terraspec	#DIV/0!	2,251	2,255	#DIV/0!	2,254	2,255	2,256	2,254
FeOH Depth	%	Terraspec	#DIV/0!	10.31%	3.09%	#DIV/0!	4.11%	3.37%	1.19%	1.55%
AlOH depth/FeOH depth		Terraspec	#DIV/0!	0.51	5.36	#DIV/0!	4.57	4.19	2.49	8.15

Abbreviations:	**Units**		**Alteration**	**Other**
	HFL= Hanging wall flow	FT= Footwall tuff	Qtz-Ser= Quartz-sericite	WL= Wavelength
	HBX= Hanging wall breccia	FBX= Footwall breccia	Chl-Ser= Chlorite-sericite	
	FLT= Footwall lapilli tuff	FFL= Footwall flow	Chl=Chlorite	
		INT= Intrusion		

Appendix B: Table B1.1 Whole-rock Geochemistry and Terraspec^{TM} Data

Sample ID			H501348	H501349	H501350	H501351	H501352	H501353	H501354	H501355
Hole ID			BD11-189	BD11-189	BD10-106	BD10-106	BD10-106	BD10-106	BD10-106	BD10-106
Depth (m)			23.7	38.2	9.6	13.9	17.1	18.4	21.8	29.4
Lithology			INT	INT	FLT	FBX	FT	FLT	FBX	FLT
Alteration			Qtz-Ser	Qtz-Ser	Qtz-Ser	Chl-Ser	Qtz-Ser	Qtz-Ser	Qtz-Ser	Chl-Ser
SiO_2	%	FUS-ICP	71.29	77.44	73.49	70.53	71.62	72.04	72.58	67.6
Al_2O_3	%	FUS-ICP	10.66	10.55	10.26	11.22	12	11.29	11.96	12.4
Fe_2O_3(T)	%	FUS-ICP	6.48	3.44	4.13	3.18	4.86	4.54	4.38	5.89
MnO	%	FUS-ICP	0.171	0.049	0.136	0.167	0.06	0.118	0.064	0.195
MgO	%	FUS-ICP	2.87	1.37	4.76	6.93	2.09	2.88	1.95	4.91
CaO	%	FUS-ICP	0.06	0.04	0.1	0.43	0.06	0.14	0.05	0.07
Na_2O	%	FUS-ICP	0.15	0.17	0.16	0.14	0.23	0.19	0.22	0.23
K_2O	%	FUS-ICP	2.24	2.64	2.04	1.78	3.08	2.61	3.02	2.64
TiO_2	%	FUS-ICP	0.154	0.143	0.183	0.167	0.187	0.18	0.197	0.208
P_2O_5	%	FUS-ICP	0.02	0.01	0.05	0.03	0.03	0.03	0.04	0.02
LOI	%	FUS-ICP	4.68	2.67	4.92	5.28	4.72	4.54	4.34	6.59
Total	%	FUS-ICP	98.79	98.55	100.2	99.85	98.95	98.55	98.8	100.7
Ba	ppm	FUS-ICP	913	1309	846	778	1176	1183	1113	939
Sr	ppm	FUS-ICP	8	7	8	16	10	9	10	13
Y	ppm	FUS-ICP	43	34	29	42	40	43	45	42
Sc	ppm	FUS-ICP	12	11	11	12	12	11	12	13
Zr	ppm	FUS-ICP	152	133	121	151	145	147	156	167
Be	ppm	FUS-ICP	< 1	< 1	< 1	< 1	< 1	< 1	< 1	< 1
V	ppm	FUS-ICP	< 5	< 5	21	7	10	9	9	12
Hg	ppb	FIMS	5	< 5	7	7	15	9	7	< 5
Cr	ppm	HF/HNO3	27.13	26.49	33.89	29.16	<8.9	30.93	<8.9	<8.9
Co	ppm	HF/HNO3	5.28	1.81	1.67	1.54	1.30	<0.9	1.58	<0.9
Ni	ppm	HF/HNO3	15.12	15.47	21.41	20.92	<10	<10	<10	<10
Cu	ppm	HF/HNO3	28.38	<19	304.66	38.79	324.78	1860.28	54.62	<19
Zn	ppm	HF/HNO3	107.49	100.86	143.78	167.31	80.55	75.42	56.43	110.06
As	ppm	HF/HNO3	4.70	<1.6	2.09	1.83	12.62	4.69	14.45	5.08
Se	ppm	HF/HNO3	<26.7	<26.7	<26.7	<26.7	<26.7	<26.7	<26.7	<26.7
Br	ppm	HF/HNO3	204.08	215.01	207.01	214.03	224.70	242.41	252.56	217.40
Mo	ppm	HF/HNO3	7.96	7.48	11.47	7.94	4.70	8.78	5.86	4.01
Ag	ppm	HF/HNO3	<1	<1	<1	<1	<1	<1	<1	<1
Cd	ppm	HF/HNO3	<0.9	<0.9	<0.9	<0.9	<0.9	<0.9	<0.9	<0.9
Sn	ppm	HF/HNO3	3.78	6.48	2.86	2.53	3.79	3.69	3.35	3.64
Sb	ppm	HF/HNO3	1.63	0.74	1.06	0.78	2.50	1.23	1.61	0.88
Te	ppm	HF/HNO3	<4.3	<4.3	<4.3	<4.3	<4.3	<4.3	<4.3	<4.3
I	ppm	HF/HNO3	<37	<37	<37	<37	<37	<37	<37	<37
W	ppm	HF/HNO3	4.78	4.60	6.87	6.48	2.82	3.63	3.36	2.21
Pb	ppm	HF/HNO3	<25.3	<25.3	<25.3	<25.3	<25.3	<25.3	<25.3	<25.3
Bi	ppm	HF/HNO3	0.82	0.77	0.92	0.33	3.06	4.06	2.64	0.51
Nb	ppm	Na2O2 Sinter	6.61	5.94	5.14	6.86	8.48	9.26	8.48	10.08
La	ppm	Na2O2 Sinter	16.20	15.96	16.47	19.17	17.78	15.99	21.26	20.55
Ce	ppm	Na2O2 Sinter	33.31	33.10	33.04	40.23	38.41	35.32	42.70	43.31
Pr	ppm	Na2O2 Sinter	4.17	4.20	4.00	4.95	4.71	4.45	5.06	5.36
Nd	ppm	Na2O2 Sinter	18.38	17.95	17.44	21.31	20.01	18.92	20.50	23.26
Sm	ppm	Na2O2 Sinter	4.91	4.46	4.40	5.15	4.64	4.59	4.77	5.49
Eu	ppm	Na2O2 Sinter	0.76	0.68	0.78	0.93	0.90	0.82	0.87	1.00
Tb	ppm	Na2O2 Sinter	1.02	0.84	0.81	1.01	0.91	1.04	1.04	1.05
Dy	ppm	Na2O2 Sinter	6.95	5.72	5.26	6.68	6.14	7.27	7.16	7.04
Ho	ppm	Na2O2 Sinter	1.48	1.21	1.09	1.47	1.29	1.54	1.55	1.57
Er	ppm	Na_2O_2 Sinter	4.47	3.65	3.32	4.53	4.13	4.56	4.66	4.90
Tm	ppm	Na2O2 Sinter	0.67	0.57	0.51	0.70	0.62	0.70	0.70	0.74
Yb	ppm	Na2O2 Sinter	4.62	3.71	3.54	4.66	4.01	4.67	4.73	5.05
Lu	ppm	Na2O2 Sinter	0.76	0.65	0.59	0.73	0.64	0.73	0.71	0.77
Hf	ppm	Na2O2 Sinter	4.26	4.15	3.83	4.99	4.08	5.10	4.66	5.66
Ta	ppm	Na2O2 Sinter	0.26	0.25	0.21	0.26	0.31	0.35	0.32	0.36
Th	ppm	Na2O2 Sinter	4.90	4.62	3.97	5.22	6.20	6.28	6.12	7.08
AlOH WL	nm	Terraspec	2,200	2,202	2,203	2,201	2,205	2,204	2,204	2,200
AlOH Depth	%	Terraspec	10.83%	21.80%	12.78%	11.52%	13.30%	10.68%	15.98%	12.73%
FeOH WL	nm	Terraspec	2,254	2,256	2,252	2,251	2,252	2,252	2,254	2,253
FeOH Depth	%	Terraspec	4.24%	3.56%	4.80%	6.31%	1.48%	2.20%	1.16%	3.90%
AlOH depth/FeOH depth		Terraspec	2.55	6.12	2.66	1.83	8.99	4.85	13.73	3.26

Abbreviations:	**Units**		**Alteration**	**Other**
	HFL= Hanging wall flow	FT= Footwall tuff	Qtz-Ser= Quartz-sericite	WL= Wavelength
	HBX= Hanging wall breccia	FBX= Footwall breccia	Chl-Ser= Chlorite-sericite	
	FLT= Footwall lapilli tuff	FFL= Footwall flow	Chl=Chlorite	
		INT= Intrusion		

Appendix B: Table B1.1 Whole-rock Geochemistry and Terraspec™ Data

Sample ID			**H501356**	**H501357**	**H501358**	**H501359**	**H501360**	**H501361**	**H501363**	**H501364**
Hole ID			BD10-106	BD10-106	BD10-106	BD10-106	BD10-106	BD11-129	BD10-9	BG10-7
Depth (m)			36.9	40.5	44.3	51.2	68.5	28.3	10.1	6.5
Lithology			FLT	FT	FLT	FBX	FFL	FFL	HBX	HFL
Alteration			Qtz-Ser	Qtz-Ser	Qtz-Ser	Qtz-Ser	Qtz-Ser	Qtz-Ser	Qtz-Ser	Qtz-Ser
SiO_2	%	FUS-ICP	71.34	68.77	75.54	77.33	77.81	74.77	67.44	80.41
Al_2O_3	%	FUS-ICP	12.45	12.74	11.59	10.91	11.16	8.54	14.24	8.8
Fe_2O_3(T)	%	FUS-ICP	3.58	4.68	3.8	1.49	2.6	6.9	4.94	2.53
MnO	%	FUS-ICP	0.134	0.121	0.068	0.095	0.108	0.006	0.197	0.017
MgO	%	FUS-ICP	2.96	4.26	2.19	2.21	1.59	0.27	3.22	1.29
CaO	%	FUS-ICP	0.07	0.09	0.05	0.05	0.06	0.02	0.04	0.03
Na_2O	%	FUS-ICP	0.24	0.24	0.21	0.19	0.21	0.18	0.11	0.12
K_2O	%	FUS-ICP	3.08	2.89	2.88	2.76	3.14	2.33	3.43	2.24
TiO_2	%	FUS-ICP	0.204	0.294	0.196	0.17	0.182	0.114	0.191	0.118
P_2O_5	%	FUS-ICP	0.03	0.05	0.03	0.03	0.03	< 0.01	0.03	0.02
LOI	%	FUS-ICP	4.37	5.59	4.16	3.25	3.87	5.02	4.19	2.61
Total	%	FUS-ICP	98.48	99.72	100.7	98.49	100.7	98.16	98.04	98.19
Ba	ppm	FUS-ICP	1138	1023	1084	1085	1045	1151	1927	1343
Sr	ppm	FUS-ICP	11	12	11	9	10	7	6	5
Y	ppm	FUS-ICP	44	43	41	34	40	30	49	28
Sc	ppm	FUS-ICP	13	16	13	12	12	9	15	8
Zr	ppm	FUS-ICP	166	134	142	137	146	104	184	110
Be	ppm	FUS-ICP	< 1	1	1	1	1	< 1	2	< 1
V	ppm	FUS-ICP	< 5	55	18	16	6	6	7	7
Hg	ppb	FIMS	< 5	10	< 5	< 5	11	56	198	8
Cr	ppm	HF/HNO3	34.20	61.58	20.42	<8.9	<8.9	18.56	<8.9	13.60
Co	ppm	HF/HNO3	<0.9	3.78	1.31	<0.9	1.85	9.48	<0.9	1.91
Ni	ppm	HF/HNO3	17.32	29.54	<10	<10	<10	<10	<10	<10
Cu	ppm	HF/HNO3	777.56	21.84	<19	29.14	55.10	735.36	<19	<19
Zn	ppm	HF/HNO3	156.15	152.11	88.06	70.38	55.24	34.30	900.28	51.81
As	ppm	HF/HNO3	2.24	5.05	2.37	<1.6	2.92	12.74	1.88	2.61
Se	ppm	HF/HNO3	<26.7	<26.7	<26.7	<26.7	<26.7	<26.7	<26.7	<26.7
Br	ppm	HF/HNO3	238.58	189.06	237.68	238.81	239.32	224.09	216.37	284.03
Mo	ppm	HF/HNO3	9.55	9.32	3.46	3.52	12.12	7.85	2.28	3.90
Ag	ppm	HF/HNO3	<1	<1	<1	<1	<1	<1	<1	<1
Cd	ppm	HF/HNO3	<0.9	<0.9	<0.9	<0.9	<0.9	<0.9	2.46	<0.9
Sn	ppm	HF/HNO3	3.81	3.02	5.20	4.12	2.98	3.41	6.70	3.51
Sb	ppm	HF/HNO3	0.85	2.00	1.35	1.33	1.04	1.87	2.01	1.84
Te	ppm	HF/HNO3	<4.3	<4.3	<4.3	<4.3	<4.3	<4.3	<4.3	<4.3
I	ppm	HF/HNO3	<37	<37	<37	<37	<37	<37	<37	<37
W	ppm	HF/HNO3	4.59	8.08	7.37	6.16	4.20	3.12	4.09	1.68
Pb	ppm	HF/HNO3	<25.3	<25.3	<25.3	<25.3	<25.3	<25.3	493.51	<25.3
Bi	ppm	HF/HNO3	0.75	1.05	0.43	<0.1	2.41	8.06	0.41	1.78
Nb	ppm	Na2O2 Sinter	7.68	5.94	8.21	8.30	7.84	4.90	10.92	6.30
La	ppm	Na2O2 Sinter	19.28	18.37	16.09	19.57	18.52	13.07	22.99	14.68
Ce	ppm	Na2O2 Sinter	40.92	39.37	34.96	41.57	38.70	26.79	48.42	30.97
Pr	ppm	Na2O2 Sinter	5.11	5.16	4.44	5.17	4.93	3.38	6.14	3.91
Nd	ppm	Na2O2 Sinter	22.54	22.72	18.74	21.25	20.92	14.36	26.15	16.97
Sm	ppm	Na2O2 Sinter	5.68	5.82	4.53	5.05	4.88	3.51	6.24	4.13
Eu	ppm	Na2O2 Sinter	0.93	0.88	0.85	0.82	0.75	0.84	1.97	0.78
Tb	ppm	Na2O2 Sinter	1.05	1.02	0.96	0.82	0.97	0.68	1.27	0.73
Dy	ppm	Na2O2 Sinter	7.15	6.82	6.37	5.15	6.61	4.49	8.34	5.05
Ho	ppm	Na2O2 Sinter	1.59	1.47	1.39	1.12	1.36	0.97	1.78	1.08
Er	ppm	Na_2O_2 Sinter	5.06	4.57	4.13	3.59	4.11	2.76	5.49	3.21
Tm	ppm	Na2O2 Sinter	0.75	0.68	0.62	0.56	0.62	0.43	0.81	0.47
Yb	ppm	Na2O2 Sinter	5.22	4.43	4.28	4.04	4.29	2.92	5.61	3.38
Lu	ppm	Na2O2 Sinter	0.82	0.69	0.60	0.65	0.66	0.45	0.94	0.50
Hf	ppm	Na2O2 Sinter	5.22	4.03	4.60	5.63	5.69	3.66	6.36	3.44
Ta	ppm	Na2O2 Sinter	0.29	0.24	0.31	0.33	0.34	0.20	0.41	0.25
Th	ppm	Na2O2 Sinter	5.76	4.69	5.53	5.71	6.46	4.80	8.39	5.02
AlOH WL	nm	Terraspec	2,204	2,201	2,202	2,204	2,205	2,203	2,207	2,205
AlOH Depth	%	Terraspec	9.87%	11.04%	12.50%	13.58%	9.90%	4.12%	7.55%	11.05%
FeOH WL	nm	Terraspec	2,252	2,252	2,252	2,253	#DIV/0!	#DIV/0!	2,254	2,251
FeOH Depth	%	Terraspec	1.31%	3.45%	1.87%	1.33%	#DIV/0!	#DIV/0!	2.83%	2.04%
AlOH depth/FeOH depth		Terraspec	7.53	3.20	6.68	10.25	#DIV/0!	#DIV/0!	2.66	5.43

Abbreviations:

Units
HFL= Hanging wall flow
HBX= Hanging wall breccia
FLT= Footwall lapilli tuff
FT= Footwall tuff
FBX= Footwall breccia
FFL= Footwall flow
INT= Intrusion

Alteration
Qtz-Ser= Quartz-sericite
Chl-Ser= Chlorite-sericite
Chl=Chlorite

Other
WL= Wavelength

Appendix B: Table B1.1 Whole-rock Geochemistry and Terraspec^{TM} Data

Sample ID			**H501365**	**H501366**	**H501367**	**H501368**	**H501369**	**H501370**	**H501371**	**H501372**
Hole ID			BG10-7	BG10-7	BG10-7	BG10-7	BG10-7	BD11-183	BD11-183	BD11-183
Depth (m)			18.7	31.9	47.2	55.2	63	8.2	21.1	34.3
Lithology			FLT	FLT	FLT	FBX	FLT	HFL	HBX	HFL
Alteration			Qtz-Ser	Chl-Ser	Qtz-Ser	Qtz-Ser	Chl-Ser	Qtz-Ser	Qtz-Ser	Qtz-Ser
SiO_2	%	FUS-ICP	70.74	63.81	74.74	68.63	62.27	77.92	61.63	74.63
Al_2O_3	%	FUS-ICP	14.24	11.45	11.31	12.99	13.76	7	15.55	11.19
Fe_2O_3(T)	%	FUS-ICP	3.46	9.88	5.69	4.91	7.24	7.13	8.43	4.56
MnO	%	FUS-ICP	0.026	0.041	0.02	0.148	0.263	0.018	0.08	0.059
MgO	%	FUS-ICP	1.65	2.29	0.94	3.38	4.73	0.37	2.05	1.47
CaO	%	FUS-ICP	0.04	0.05	0.04	0.07	0.07	0.02	0.07	0.05
Na_2O	%	FUS-ICP	0.2	0.15	0.16	0.16	0.15	0.11	0.23	0.16
K_2O	%	FUS-ICP	3.75	2.75	3.2	3.11	2.98	1.99	4.1	2.93
TiO_2	%	FUS-ICP	0.209	0.179	0.153	0.195	0.21	0.088	0.234	0.135
P_2O_5	%	FUS-ICP	0.03	0.02	0.02	0.03	0.05	0.01	0.04	0.01
LOI	%	FUS-ICP	3.92	7.22	4.51	4.84	6.71	4.64	6.22	3.89
Total	%	FUS-ICP	98.27	97.83	100.8	98.48	98.42	99.29	98.65	99.09
Ba	ppm	FUS-ICP	1940	1226	1137	1044	957	1341	1904	1202
Sr	ppm	FUS-ICP	10	7	8	8	8	4	9	6
Y	ppm	FUS-ICP	48	40	37	46	52	33	54	40
Sc	ppm	FUS-ICP	15	13	11	13	14	5	15	9
Zr	ppm	FUS-ICP	177	134	137	167	165	88	196	146
Be	ppm	FUS-ICP	1	< 1	< 1	1	1	< 1	1	< 1
V	ppm	FUS-ICP	9	15	6	< 5	< 5	6	5	8
Hg	ppb	FIMS	13	100	12	< 5	14	6	10	< 5
Cr	ppm	HF/HNO3	<8.9	<8.9	16.74	26.36	<8.9	<8.9	35.80	<8.9
Co	ppm	HF/HNO3	<0.9	8.35	<0.9	<0.9	1.09	17.03	14.61	3.71
Ni	ppm	HF/HNO3	<10	<10	<10	15.24	<10	<10	17.82	<10
Cu	ppm	HF/HNO3	<19	45.67	<19	923.75	595.75	<19	22.51	<19
Zn	ppm	HF/HNO3	42.44	49.03	25.94	147.75	337.96	32.16	144.77	53.97
As	ppm	HF/HNO3	8.33	120.65	13.84	17.12	68.63	25.65	15.59	5.49
Se	ppm	HF/HNO3	<26.7	<26.7	<26.7	<26.7	<26.7	<26.7	<26.7	<26.7
Br	ppm	HF/HNO3	235.74	228.26	230.56	201.20	245.48	216.07	216.01	221.52
Mo	ppm	HF/HNO3	3.80	5.71	6.59	7.61	3.44	8.07	60.91	9.19
Ag	ppm	HF/HNO3	<1	<1	<1	<1	<1	<1	<1	<1
Cd	ppm	HF/HNO3	<0.9	<0.9	<0.9	<0.9	<0.9	<0.9	<0.9	<0.9
Sn	ppm	HF/HNO3	3.84	3.68	3.83	4.09	8.81	4.50	4.69	4.22
Sb	ppm	HF/HNO3	3.16	6.98	2.45	1.35	17.11	1.84	2.65	1.51
Te	ppm	HF/HNO3	4.28	5.05	<4.3	<4.3	<4.3	<4.3	<4.3	<4.3
I	ppm	HF/HNO3	<37	<37	<37	<37	<37	<37	<37	<37
W	ppm	HF/HNO3	5.54	3.70	4.35	2.81	1.86	1.57	12.96	3.76
Pb	ppm	HF/HNO3	<25.3	<25.3	<25.3	<25.3	<25.3	<25.3	<25.3	<25.3
Bi	ppm	HF/HNO3	4.69	7.93	2.82	3.51	2.54	2.97	2.69	1.14
Nb	ppm	Na2O2 Sinter	9.38	8.70	7.38	7.16	7.03	4.84	9.33	7.62
La	ppm	Na2O2 Sinter	22.36	18.41	15.99	17.86	19.37	9.66	21.96	17.68
Ce	ppm	Na2O2 Sinter	46.68	38.52	32.96	37.08	40.90	20.22	45.92	36.75
Pr	ppm	Na2O2 Sinter	5.90	4.94	4.17	4.62	5.15	2.59	5.85	4.64
Nd	ppm	Na2O2 Sinter	25.86	20.98	17.85	19.60	22.50	11.48	24.65	19.92
Sm	ppm	Na2O2 Sinter	6.12	5.15	4.34	5.14	5.49	3.19	6.14	4.86
Eu	ppm	Na2O2 Sinter	1.64	1.23	1.80	1.08	1.17	0.53	0.97	0.73
Tb	ppm	Na2O2 Sinter	1.23	1.00	0.88	1.06	1.25	0.83	1.24	0.96
Dy	ppm	Na2O2 Sinter	8.11	6.62	5.93	7.10	8.57	5.42	8.49	6.25
Ho	ppm	Na2O2 Sinter	1.78	1.45	1.29	1.59	1.84	1.13	1.89	1.35
Er	ppm	Na_2O_2 Sinter	5.30	4.45	4.08	4.85	5.69	3.35	5.71	4.23
Tm	ppm	Na2O2 Sinter	0.81	0.66	0.59	0.74	0.86	0.49	0.84	0.63
Yb	ppm	Na2O2 Sinter	5.28	4.57	4.23	4.92	5.91	3.26	5.80	4.32
Lu	ppm	Na2O2 Sinter	0.83	0.69	0.63	0.84	0.91	0.50	0.90	0.68
Hf	ppm	Na2O2 Sinter	5.37	4.69	3.63	4.21	4.36	2.99	5.53	4.58
Ta	ppm	Na2O2 Sinter	0.35	0.29	0.29	0.27	0.27	0.17	0.32	0.32
Th	ppm	Na2O2 Sinter	7.71	6.41	5.63	5.50	5.64	4.08	6.54	6.13
AlOH WL	nm	Terraspec	2,203	2,203	2,205	2,204	2,203	2,205	2,203	2,203
AlOH Depth	%	Terraspec	11.83%	10.64%	14.08%	12.30%	13.08%	17.50%	6.48%	19.83%
FeOH WL	nm	Terraspec	2,253	2,254	#DIV/0!	2,254	2,252	#DIV/0!	2,255	2,254
FeOH Depth	%	Terraspec	1.10%	1.20%	#DIV/0!	1.71%	2.34%	#DIV/0!	1.34%	2.55%
AlOH depth/FeOH depth		Terraspec	10.75	8.88	#DIV/0!	7.19	5.59	#DIV/0!	4.85	7.78

Abbreviations:	**Units**		**Alteration**	**Other**
	HFL= Hanging wall flow	FT= Footwall tuff	Qtz-Ser= Quartz-sericite	WL= Wavelength
	HBX= Hanging wall breccia	FBX= Footwall breccia	Chl-Ser= Chlorite-sericite	
	FLT= Footwall lapilli tuff	FFL= Footwall flow	Chl=Chlorite	
		INT= Intrusion		

Appendix B: Table B1.1 Whole-rock Geochemistry and Terraspec™ Data

Sample ID			H501373	H501374	H501375	H501376	H501377	H501378	H501379
Hole ID			BD11-183	BD11-183	BG10-2	BG10-2	BG10-2	BG10-2	BG10-2
Depth (m)			52	68	10.1	20.4	27.6	31.9	44.3
Lithology			HFL	HFL	HFL	HFL	FLT	FBX	FLT
Alteration			Qtz-Ser	Qtz-Ser	Qtz-Ser	Qtz-Ser	Qtz-Ser	Qtz-Ser	Qtz-Ser
SiO_2	%	FUS-ICP	78.91	58.3	77.05	75.8	68.11	76.29	71.48
Al_2O_3	%	FUS-ICP	9.37	22.62	11.14	11.88	11.55	10.56	12.39
Fe_2O_3(T)	%	FUS-ICP	4.16	3.62	3.88	3.24	7	3.08	4.49
MnO	%	FUS-ICP	0.033	0.082	0.091	0.074	0.206	0.151	0.115
MgO	%	FUS-ICP	0.75	2.88	2.06	1.51	2.74	2.12	2.44
CaO	%	FUS-ICP	0.07	0.13	0.04	0.06	1.22	1.08	0.06
Na_2O	%	FUS-ICP	0.15	0.31	0.14	0.17	0.14	0.13	0.18
K_2O	%	FUS-ICP	2.58	6.11	2.69	3.23	2.87	2.79	2.84
TiO_2	%	FUS-ICP	0.145	0.363	0.137	0.15	0.186	0.149	0.171
P_2O_5	%	FUS-ICP	< 0.01	0.04	0.02	0.03	0.03	0.02	0.02
LOI	%	FUS-ICP	3.39	5.72	3.19	3.03	6.51	4.2	3.81
Total	%	FUS-ICP	99.56	100.2	100.4	99.17	100.6	100.6	97.99
Ba	ppm	FUS-ICP	1115	2666	951	1120	925	831	1000
Sr	ppm	FUS-ICP	9	13	5	7	24	26	11
Y	ppm	FUS-ICP	30	61	43	42	42	34	46
Sc	ppm	FUS-ICP	10	23	10	11	13	11	13
Zr	ppm	FUS-ICP	117	291	138	147	143	140	164
Be	ppm	FUS-ICP	1	2	< 1	1	< 1	1	1
V	ppm	FUS-ICP	20	18	6	< 5	13	7	8
Hg	ppb	FIMS	6	72	65	9	11	< 5	< 5
Cr	ppm	HF/HNO3	28.93	<8.9	<8.9	27.42	<8.9	11.64	<8.9
Co	ppm	HF/HNO3	3.42	<0.9	3.75	3.03	12.63	1.46	5.80
Ni	ppm	HF/HNO3	<10	<10	<10	15.87	<10	<10	<10
Cu	ppm	HF/HNO3	<19	<19	280.10	85.66	86.05	<19	<19
Zn	ppm	HF/HNO3	39.04	71.33	430.29	148.83	108.64	114.32	272.57
As	ppm	HF/HNO3	8.52	19.99	2.17	4.85	44.66	3.91	1.95
Se	ppm	HF/HNO3	<26.7	<26.7	<26.7	<26.7	<26.7	<26.7	<26.7
Br	ppm	HF/HNO3	240.46	211.77	229.02	194.50	263.31	190.16	218.00
Mo	ppm	HF/HNO3	8.23	11.69	1.97	11.55	6.24	4.19	3.44
Ag	ppm	HF/HNO3	<1	<1	<1	<1	<1	<1	<1
Cd	ppm	HF/HNO3	<0.9	<0.9	2.01	<0.9	<0.9	<0.9	<0.9
Sn	ppm	HF/HNO3	3.39	4.27	3.50	3.32	12.28	4.16	5.01
Sb	ppm	HF/HNO3	3.66	12.17	2.06	1.57	2.66	1.76	1.28
Te	ppm	HF/HNO3	<4.3	<4.3	<4.3	<4.3	<4.3	<4.3	<4.3
I	ppm	HF/HNO3	<37	<37	<37	<37	<37	<37	<37
W	ppm	HF/HNO3	6.73	6.58	4.80	3.62	1.64	1.64	2.48
Pb	ppm	HF/HNO3	<25.3	<25.3	<25.3	<25.3	<25.3	<25.3	<25.3
Bi	ppm	HF/HNO3	2.05	2.00	0.42	0.38	3.40	0.65	<0.1
Nb	ppm	Na2O2 Sinter	6.19	15.02	7.37	6.42	6.05	8.03	9.05
La	ppm	Na2O2 Sinter	10.36	31.18	17.10	18.63	22.70	16.29	20.50
Ce	ppm	Na2O2 Sinter	21.71	67.10	35.88	38.19	47.78	33.97	42.80
Pr	ppm	Na2O2 Sinter	2.66	8.47	4.49	4.74	6.07	4.22	5.28
Nd	ppm	Na2O2 Sinter	10.98	36.72	18.92	20.70	25.83	17.96	23.01
Sm	ppm	Na2O2 Sinter	2.71	8.70	4.65	5.13	6.53	4.23	5.53
Eu	ppm	Na2O2 Sinter	0.45	2.23	0.88	0.92	1.55	0.98	1.15
Tb	ppm	Na2O2 Sinter	0.61	1.58	0.90	0.95	1.25	0.80	1.11
Dy	ppm	Na2O2 Sinter	4.55	10.40	6.10	6.46	8.11	5.46	7.46
Ho	ppm	Na2O2 Sinter	1.03	2.30	1.39	1.43	1.69	1.25	1.70
Er	ppm	Na_2O_2 Sinter	3.22	6.98	4.39	4.54	4.97	3.93	5.17
Tm	ppm	Na2O2 Sinter	0.49	1.11	0.65	0.69	0.77	0.60	0.79
Yb	ppm	Na2O2 Sinter	3.42	7.34	4.45	4.88	5.11	4.15	5.29
Lu	ppm	Na2O2 Sinter	0.52	1.12	0.66	0.77	0.79	0.65	0.86
Hf	ppm	Na2O2 Sinter	4.47	11.05	4.27	4.36	4.95	6.20	5.12
Ta	ppm	Na2O2 Sinter	0.26	0.56	0.30	0.24	0.26	0.33	0.36
Th	ppm	Na2O2 Sinter	4.95	11.44	5.78	5.15	5.32	5.81	6.66
AlOH WL	nm	Terraspec	2,205	2,205	2,206	2,205	2,206	2,207	2,202
AlOH Depth	%	Terraspec	21.80%	12.10%	5.85%	27.03%	8.55%	15.72%	20.00%
FeOH WL	nm	Terraspec	2,254	#DIV/0!	2,255	2,256	2,253	2,254	2,255
FeOH Depth	%	Terraspec	1.50%	#DIV/0!	2.17%	2.46%	1.36%	2.98%	5.34%
AlOH depth/FeOH depth		Terraspec	14.58	#DIV/0!	2.69	11.00	6.31	5.28	3.75

Abbreviations:	**Units**		**Alteration**	**Other**
	HFL= Hanging wall flow	FT= Footwall tuff	Qtz-Ser= Quartz-sericite	WL= Wavelength
	HBX= Hanging wall breccia	FBX= Footwall breccia	Chl-Ser= Chlorite-sericite	
	FLT= Footwall lapilli tuff	FFL= Footwall flow	Chl=Chlorite	
		INT= Intrusion		

Table C.1.1 Correlation Coefficients

	Al_2O_3	TiO_2	Y	Zr	La	Ce	Pr	Nd	Sm	Eu	Tb	Dy	Ho	Tm	Yb	Lu	Nb	Hf	Ta	Th
Al_2O_3	1																			
TiO_2	0.78	1																		
Y	0.66	0.46	1																	
Zr	0.93	0.67	0.67	1																
La	0.5	0.38	0.71	0.55	1															
Ce	0.49	0.37	0.71	0.54	1	1														
Pr	0.48	0.37	0.7	0.53	0.99	1	1													
Nd	0.49	0.37	0.71	0.53	0.99	1	1	1												
Sm	0.49	0.38	0.73	0.53	0.97	0.98	0.98	0.99	1											
Eu	0.44	0.32	0.58	0.42	0.66	0.67	0.67	0.67	0.69	1										
Tb	0.56	0.42	0.84	0.58	0.88	0.89	0.89	0.89	0.92	0.69	1									
Dy	0.58	0.44	0.85	0.59	0.84	0.85	0.85	0.85	0.88	0.69	0.99	1								
Ho	0.61	0.47	0.86	0.62	0.82	0.82	0.82	0.82	0.86	0.69	0.97	0.99	1							
Tm	0.64	0.5	0.84	0.65	0.77	0.77	0.77	0.77	0.8	0.67	0.93	0.96	0.98	1						
Yb	0.64	0.5	0.82	0.66	0.75	0.74	0.74	0.74	0.77	0.65	0.91	0.94	0.97	0.99	1					
Lu	0.63	0.49	0.81	0.65	0.72	0.72	0.71	0.71	0.75	0.64	0.89	0.92	0.95	0.98	0.99	1				
Nb	0.68	0.54	0.54	0.7	0.53	0.53	0.52	0.51	0.52	0.47	0.62	0.64	0.66	0.7	0.7	0.69	1			
Hf	0.67	0.51	0.57	0.69	0.5	0.49	0.48	0.48	0.5	0.49	0.59	0.63	0.67	0.73	0.75	0.77	0.8	1		
Ta	0.74	0.55	0.55	0.76	0.55	0.55	0.53	0.53	0.55	0.47	0.64	0.67	0.69	0.73	0.73	0.73	0.94	0.84	1	
Th	0.76	0.56	0.56	0.78	0.59	0.58	0.57	0.57	0.57	0.48	0.64	0.67	0.69	0.73	0.74	0.73	0.93	0.84	0.95	1

Appendix C: Table C.1.2 Mass changes for samples at the Boundary deposit

Sample ID	**H500606**	**H500607**	**H500608**	**H500609**	**H500610**	**H500611**	**H500612**	**H500613**	**H500614**	**H500615**
Hole ID	BD10-112	BD10-112	BD10-112	BD10-112	BD10-112	BD11-117	BD11-117	BD11-117	BD11-117	BD11-117
Depth (m)	20.1	28.8	39.8	50.9	58.2	12.6	15.2	25.5	45.1	57.7
Lithology	HBX	FLT	FLT	FLT	FLT	HFL	HFL	FLT	FLT	FLT
Alteration	Qtz-Ser	Qtz-Ser	Qtz-Ser	Qtz-Ser	Chl-Ser	Qtz-Ser	Qtz-Ser	Chl-Ser	Qtz-Ser	Qtz-Ser
SiO_2	19.19	1.16	0.28	24.54	2.80	-5.93	-4.02	3.21	-25.04	11.46
Al_2O_3	0.00	0.00	0.00	0.00	0.00	0.00	0.00	0.00	0.00	0.00
FeO	3.24	3.33	8.02	14.86	10.07	1.88	2.54	14.99	6.43	14.70
MnO	0.17	-0.06	-0.08	-0.09	-0.03	-0.02	0.02	-0.04	-0.04	-0.08
MgO	1.49	-0.19	-1.83	-1.98	3.48	-0.17	1.42	0.51	-0.01	-1.76
CaO	0.17	-0.06	-0.06	-0.09	-0.08	-0.10	-0.08	-0.07	-0.11	-0.04
Na_2O	-1.85	-1.83	-1.79	-1.80	-1.90	-1.84	-1.88	-1.86	-1.84	-1.81
K_2O	0.16	0.52	1.00	1.04	-0.54	0.37	0.06	0.36	0.64	0.98
TiO_2	0.01	0.03	0.02	0.04	0.03	0.01	0.00	0.01	0.02	0.02
P_2O_5	0.00	0.00	0.00	0.00	0.01	0.00	0.00	0.00	0.02	0.00
Net Oxide Change	22.58	2.89	5.56	36.51	13.84	-5.79	-1.95	17.11	-19.94	23.46
Ba	201.25	347.85	376.29	316.08	-508.43	1009.81	363.38	466.48	180.80	244.42
Sr	-13.19	-12.44	-10.64	-12.92	-14.57	-13.35	-14.96	-12.75	-13.35	-12.33
Y	-2.51	-3.95	4.16	-4.19	8.09	0.40	1.24	-5.98	-1.81	3.83
Sc	1.32	3.81	4.76	2.11	2.39	0.57	0.06	-0.75	2.11	1.05
Zr	21.08	15.40	33.32	26.05	23.51	7.80	0.85	8.23	5.49	8.36
Be	-0.37	-0.47	-0.43	-0.24	-0.38	-0.04	-0.50	-0.34	-0.57	-0.31
V	0.65	10.25	0.34	1.28	0.60	-0.10	2.53	4.10	-0.34	0.95
Hg	-8.85	-5.63	40.25	65.20	0.39	-9.60	-5.96	593.01	215.46	39.12
Cr 52	7.62	9.54	0.60	2.29	7.05	-0.17	0.03	9.82	-0.60	1.70
Co	0.39	0.58	-0.60	35.94	35.39	-0.68	1.50	1.39	0.37	48.30
Ni	1.29	0.31	0.68	2.57	1.20	-0.20	0.03	1.60	-0.68	1.91
Cu	349.48	0.44	2496.39	878.41	2925.55	531.52	12.61	71.93	622.75	625.07
Zn	84.78	1.51	-92.81	-37.66	3.65	8.04	52.61	12.98	-52.23	-100.16
As	-1.11	4.87	38.34	90.55	19.71	-0.29	2.90	100.96	39.19	37.34
Se 78	3.45	0.83	1.81	6.86	3.19	-0.52	0.08	4.29	-1.80	5.09
Br 79	7.26	-8.31	18.71	77.41	19.25	-5.65	-4.60	41.44	-28.46	50.57
Mo	1.99	24.49	10.19	32.80	15.82	2.12	1.90	25.11	18.48	27.86
Ag 107	0.13	0.03	0.98	6.87	0.12	-0.02	0.00	1.31	-0.07	0.19
Cd	0.12	0.03	0.06	0.23	0.11	1.18	0.00	0.14	-0.06	0.17
Sn	2.24	0.99	3.26	3.61	1.27	2.65	1.33	3.32	1.21	2.65
Sb	0.51	2.76	5.97	6.73	1.52	0.35	6.50	32.90	15.29	2.19
Te	0.56	0.13	0.29	14.39	4.37	-0.08	0.01	0.69	-0.29	12.98
I	4.78	1.15	2.51	9.50	4.42	-0.72	0.11	5.94	-2.50	7.06
W	0.82	1.96	3.34	5.75	1.32	0.18	0.41	2.29	0.80	0.86
Pb	3.27	0.79	17.44	36.79	3.03	-0.49	0.07	114.97	-1.71	4.83
Bi	0.01	0.73	-0.04	28.91	8.50	0.12	0.25	5.42	5.10	16.03
Nb	0.40	0.65	0.76	0.79	1.31	0.42	0.18	-0.20	0.17	0.17
La	-1.14	0.34	-0.35	-2.77	2.60	-2.15	-2.73	0.41	-4.84	3.17
Ce	-2.52	1.54	-1.05	-4.90	4.41	-3.76	-5.58	0.49	-9.73	6.00
Pr	-0.29	0.31	-0.11	-0.59	0.69	-0.41	-0.65	0.11	-1.12	0.73
Nd	-0.80	1.66	-0.51	-2.44	3.30	-1.16	-2.06	0.80	-4.72	3.65
Sm	-0.03	0.41	0.12	-0.51	0.76	-0.23	-0.45	0.10	-1.02	0.75
Eu	-0.21	0.23	0.25	0.19	0.27	-0.39	-0.03	0.32	-0.08	0.11
Tb	-0.05	-0.03	0.06	-0.10	0.20	-0.04	-0.07	-0.19	-0.15	0.11
Dy	-0.13	-0.06	0.57	-0.39	1.31	-0.06	-0.34	-1.25	-0.69	0.75
Ho	-0.05	-0.06	0.09	-0.09	0.21	-0.07	-0.10	-0.32	-0.19	0.07
Er	0.02	-0.17	0.14	-0.28	0.64	-0.14	-0.25	-1.02	-0.63	0.14
Tm	0.01	-0.03	0.02	-0.03	0.09	-0.01	-0.02	-0.16	-0.07	0.01
Yb	-0.07	-0.47	-0.09	-0.33	0.34	-0.07	-0.13	-1.21	-0.73	-0.12
Lu	0.00	-0.08	-0.02	-0.06	0.07	0.00	-0.02	-0.19	-0.10	-0.02
Hf	-0.50	-0.33	-0.35	-0.05	-0.45	-0.33	-0.52	-0.88	-0.57	-0.60
Ta	0.06	0.06	0.03	0.07	0.05	0.02	0.01	-0.04	-0.02	0.01
Th	-0.14	-0.28	-0.35	-0.05	-0.19	-0.24	-0.57	-0.79	-0.92	-0.45

Abbreviations:

Units

HFL= Hanging wall flow
HBX= Hanging wall breccia
FLT= Footwall lapilli tuff
FT= Footwall tuff
FBX= Footwall breccia
FFL= Footwall flow
INT= Intrusion

Alteration

Qtz-Ser= Quartz-sericite
Chl-Ser= Chlorite-sericite
Chl= Chlorite

Appendix C: Table C.1.2 Mass changes for samples at the Boundary deposit

Sample ID	**H500616**	**H500617**	**H500618**	**H500619**	**H500621**	**H500622**	**H500623**	**H500624**	**H500625**	**H500626**
Hole ID	BD11-117	BD10-107	BD10-107	BD10-107	BD10-108	BD10-108	BD10-108	BD10-108	BD10-108	BD10-108
Depth (m)	70.4	10.8	18.3	31.2	22.5	28.3	34	36.6	43.5	46.4
Lithology	FBX	FBX	FLT	FLT	FLT	FLT	FBX	FLT	FBX	FLT
Alteration	Qtz-Ser	Qtz-Ser	Qtz-Ser	Chl-Ser	Chl-Ser	Chl-Ser	Qtz-Ser	Chl-Ser	Qtz-Ser	Chl
SiO_2	1.46	-5.92	-2.21	-46.09	-0.65	-29.79	-12.99	-3.04	64.02	-17.18
Al_2O_3	0.00	0.00	0.00	0.00	0.00	0.00	0.00	0.00	0.00	0.00
FeO	1.68	1.29	2.14	6.10	20.91	7.53	6.76	20.21	5.22	16.62
MnO	-0.06	-0.05	-0.01	-0.05	0.16	-0.04	-0.08	-0.08	-0.03	0.09
MgO	-0.47	-0.41	1.84	2.87	1.19	0.94	-1.76	-1.58	-0.58	6.87
CaO	-0.05	0.07	-0.02	0.00	0.12	-0.03	-0.12	-0.09	-0.04	-0.04
Na_2O	-1.84	-1.83	-1.82	-1.90	-1.82	-1.83	-1.81	-1.79	-1.80	-1.96
K_2O	0.65	0.60	0.07	-0.86	0.21	0.34	0.90	0.75	0.52	-1.92
TiO_2	0.02	0.01	0.04	0.02	0.03	0.21	0.06	0.03	0.03	0.12
P_2O_5	-0.01	0.02	0.00	0.02	0.00	0.04	0.01	0.00	0.00	0.04
Net Oxide Change	1.40	-6.24	0.03	-39.88	20.15	-22.64	-9.03	14.41	67.32	2.63
Ba	319.65	1358.83	-37.87	-608.76	-94.69	-136.36	723.48	103.74	313.95	-1211.23
Sr	-12.72	-12.50	-11.78	-14.72	-12.13	-10.96	-11.25	-12.58	-11.65	-18.42
Y	4.29	5.67	1.87	0.73	3.32	-7.59	5.96	-1.31	7.59	13.47
Sc	2.37	-0.50	1.24	0.59	5.52	7.83	6.61	2.12	3.80	5.50
Zr	6.53	-6.23	2.13	-6.61	3.12	-40.59	-6.22	13.85	17.19	10.03
Be	-0.48	-0.05	-0.49	-0.67	-0.29	-0.58	-0.51	-0.33	-0.14	-0.40
V	0.08	-0.12	12.83	-0.84	27.12	80.69	19.98	5.58	7.85	28.51
Hg	-9.42	-7.25	-9.45	-7.36	2.11	25.35	155.12	113.19	29.41	4.70
Cr 52	11.23	-0.22	0.10	-1.50	25.65	34.18	15.73	21.46	3.23	10.56
Co	-0.15	-0.68	1.16	3.00	4.69	13.35	7.48	16.15	9.69	34.57
Ni	0.15	-0.25	9.93	-1.69	2.05	14.99	6.13	1.73	3.63	0.96
Cu	886.23	530.70	-73.81	123.25	-47.54	12.52	364.32	3311.71	1172.58	1263.42
Zn	-33.88	-83.78	-35.61	-26.35	-75.02	-62.41	364.15	-84.27	10.03	7.09
As	1.89	2.86	-0.07	-1.59	189.15	19.82	38.69	292.12	11.48	17.38
Se 78	0.41	-0.66	0.29	-4.51	5.48	-2.02	-0.30	41.25	9.68	2.57
Br 79	2.77	12.51	10.15	-30.18	157.84	40.01	80.90	186.30	234.96	110.44
Mo	7.24	1.17	4.61	12.27	15.78	2.40	6.18	7.85	13.58	14.82
Ag 107	0.02	-0.02	0.01	-0.17	0.21	0.60	0.66	0.89	0.36	0.10
Cd	0.01	-0.02	0.01	-0.15	0.18	-0.07	1.07	0.16	0.33	0.09
Sn	1.38	-0.90	-2.07	-1.99	2.06	-1.61	-0.41	2.06	1.41	-1.52
Sb	1.01	0.39	-0.09	0.06	0.89	3.76	5.86	12.32	1.79	0.52
Te	0.07	-0.11	0.05	11.16	12.94	-0.32	-0.05	0.74	7.15	11.02
I	0.57	-0.92	0.40	-6.25	7.60	-2.80	-0.42	6.40	13.42	3.56
W	0.84	0.86	2.40	2.72	9.25	10.74	7.98	4.21	4.25	6.42
Pb	0.39	-0.63	0.27	-4.28	5.20	-1.91	18.27	4.38	9.18	2.44
Bi	1.19	0.04	0.23	12.92	13.92	3.38	7.25	17.55	6.72	12.29
Nb	0.48	1.79	2.90	2.41	1.55	0.26	1.54	2.63	3.09	4.02
La	-1.81	-0.26	2.36	0.67	2.78	-7.28	-1.83	1.08	4.44	-1.12
Ce	-4.03	-0.92	4.77	1.93	4.05	-15.65	-4.73	2.33	8.52	-2.59
Pr	-0.49	-0.02	0.65	0.32	0.36	-1.91	-0.53	0.37	0.95	-0.30
Nd	-1.41	-0.31	3.25	2.22	1.02	-7.36	-2.26	1.50	4.23	-0.84
Sm	-0.35	-0.08	0.82	0.44	0.25	-1.52	-0.43	0.41	0.89	0.32
Eu	-0.14	-0.42	0.32	0.25	0.50	-0.08	0.95	0.06	0.28	0.09
Tb	0.05	0.06	0.13	0.09	0.14	-0.21	0.09	0.02	0.17	0.38
Dy	0.69	0.86	1.18	0.97	0.93	-0.96	0.92	0.40	0.98	3.02
Ho	0.10	0.15	0.15	0.13	0.13	-0.24	0.17	0.01	0.21	0.55
Er	0.36	0.42	0.51	0.42	0.38	-0.77	0.39	-0.07	0.59	1.62
Tm	0.06	0.08	0.11	0.07	0.05	-0.11	0.06	0.02	0.11	0.29
Yb	0.27	0.29	0.42	0.17	0.45	-0.80	0.38	0.22	0.48	1.48
Lu	0.04	0.07	0.07	0.05	0.11	-0.15	0.01	0.00	0.05	0.19
Hf	-0.56	0.90	1.38	1.34	1.01	-0.63	-0.04	0.82	0.48	0.46
Ta	0.03	0.07	0.12	0.07	0.03	-0.04	-0.01	0.07	0.11	0.11
Th	-0.34	1.40	1.99	1.48	0.32	-1.64	-0.31	0.60	0.91	0.30

Abbreviations:

Units

HFL= Hanging wall flow
HBX= Hanging wall breccia
FLT= Footwall lapilli tuff
FT= Footwall tuff
FBX= Footwall breccia
FFL= Footwall flow
INT= Intrusion

Alteration

Qtz-Ser= Quartz-sericite
Chl-Ser= Chlorite-sericite
Chl= Chlorite

Appendix C: Table C.1.2 Mass changes for samples at the Boundary deposit

Sample ID	H500627	H500628	H500629	H500642	H500643	H500644	H500645	H500649	H500650
Hole ID	BD10-108	BD10-108	BD10-108	BD10-104	BD10-104	BD11-120	BD11-120	BD10-88	BD10-88
Depth (m)	47.4	50.6	53.2	14.3	21.6	22.8	63.3	8.2	22.1
Lithology	FLT	FFL	FLT	FLT	FLT	HFL	FLT	FLT	FLT
Alteration	Chl	Qtz-Ser	Chl	Qtz-Ser	Qtz-Ser	Qtz-Ser	Qtz-Ser	Chl-Ser	Chl-Ser
SiO_2	-42.48	-18.57	-5.04	0.00	21.15	27.72	56.80	18.13	13.18
$A_{l2}O_3$	0.00	0.00	0.00	0.00	0.00	0.00	0.00	0.00	0.00
FeO	14.64	2.02	16.96	1.13	4.72	2.03	10.88	5.71	5.21
MnO	-0.01	-0.08	0.12	-0.03	-0.05	0.03	-0.07	-0.05	0.01
MgO	5.27	-0.53	6.24	-0.77	1.46	-0.57	1.75	2.41	2.53
CaO	-0.08	-0.13	-0.11	-0.03	-0.03	0.26	-0.06	-0.10	-0.10
Na_2O	-1.93	-1.82	-1.98	-1.78	-1.82	-1.83	-1.80	-1.87	-1.85
K_2O	-1.29	0.38	-2.08	0.75	0.05	0.74	-0.26	-0.41	-0.63
TiO_2	0.03	0.03	0.04	0.02	0.05	0.01	0.10	0.06	0.08
P_2O_5	0.02	0.01	0.00	0.01	0.02	0.02	0.00	0.00	0.00
Net Oxide Change	-25.83	-18.69	14.14	-0.70	25.56	28.41	67.35	23.88	18.43
Ba	-855.60	-108.17	-1269.04	-22.07	-412.68	3.33	-686.18	-399.80	-692.15
Sr	-16.67	-13.67	-20.69	-8.94	-11.58	-10.26	-9.52	-14.22	-10.87
Y	5.40	-4.84	2.95	-8.87	0.08	-5.09	3.77	-4.01	-0.67
Sc	2.43	3.33	3.11	2.05	1.72	-0.87	2.48	6.85	6.07
Zr	22.85	9.98	13.62	-12.43	-21.24	-1.52	54.61	-1.16	-0.35
Be	-0.56	-0.58	-0.34	0.00	-0.35	-0.35	-0.11	-0.35	-0.38
V	1.94	4.17	4.05	4.53	18.34	0.76	17.10	20.83	23.46
Hg	2.21	-6.17	32.57	-9.49	-8.74	-2.87	-7.54	26.88	-8.91
Cr 52	4.81	-0.74	1.38	0.02	7.38	1.35	18.17	12.63	20.26
Co	24.71	2.11	24.98	0.67	2.34	-0.52	30.69	9.31	14.38
Ni	-0.56	-0.83	1.55	0.02	1.51	1.52	3.91	1.48	1.18
Cu	317.75	920.83	21918.18	-73.97	294.93	38.09	-66.70	172.37	4.51
Zn	6.12	-118.59	112.56	26.37	-25.27	-64.37	-103.75	-4.75	56.16
As	126.18	4.55	18.16	-1.32	7.16	6.95	6.99	-1.08	13.77
Se 78	-1.49	-2.23	4.15	0.06	4.04	4.06	10.44	3.95	3.16
Br 79	48.95	0.40	141.91	57.77	59.27	50.91	281.71	21.07	19.82
Mo	9.06	4.87	24.95	41.45	9.60	4.44	24.43	4.32	3.09
Ag 107	-0.06	-0.08	0.16	0.00	0.15	0.15	0.39	0.15	0.12
Cd	-0.05	-0.08	0.14	0.00	0.14	0.14	0.35	0.13	0.11
Sn	-1.93	-2.15	0.07	1.21	1.24	2.09	0.50	1.57	0.31
Sb	0.80	0.34	2.37	0.22	0.46	1.21	0.53	-0.31	0.09
Te	5.15	2.06	5.87	0.01	3.92	0.65	1.68	0.64	0.51
I	-2.07	-3.09	5.75	0.08	5.60	5.63	14.47	5.47	4.37
W	1.15	4.41	7.07	3.70	4.70	1.25	8.86	7.43	5.89
Pb	-1.42	-2.11	25.24	0.05	3.83	3.85	9.90	3.75	2.99
Bi	8.44	5.75	10.00	0.88	4.89	3.35	2.36	0.45	0.32
Nb	3.45	3.01	3.76	0.98	0.91	-0.71	1.34	-0.68	-0.62
La	1.69	0.37	-0.83	-17.67	-4.14	-2.39	-5.06	-0.60	-2.20
Ce	3.38	0.51	-2.61	-37.50	-8.98	-5.06	-12.89	-7.47	-6.38
Pr	0.45	0.00	-0.29	-4.66	-1.15	-0.65	-1.66	-1.21	-0.83
Nd	2.13	-0.38	-0.98	-19.21	-4.36	-2.15	-7.81	-4.89	-3.47
Sm	0.47	-0.17	-0.02	-4.21	-1.02	-0.83	-1.77	-1.39	-0.93
Eu	0.11	-0.05	-0.15	-0.84	-0.38	-0.32	-0.46	-0.35	-0.47
Tb	0.14	-0.11	0.19	-0.46	-0.09	-0.21	-0.17	-0.22	-0.11
Dy	1.32	-0.50	1.30	-2.26	-0.13	-1.23	-0.66	-1.59	-0.40
Ho	0.27	-0.16	0.25	-0.41	0.06	-0.32	-0.04	-0.34	-0.14
Er	0.74	-0.45	0.64	-1.13	0.08	-1.01	-0.06	-0.85	-0.29
Tm	0.14	-0.06	0.11	-0.13	0.04	-0.13	-0.02	-0.12	-0.04
Yb	0.78	-0.52	0.54	-0.81	0.10	-0.91	0.05	-0.87	-0.40
Lu	0.10	-0.09	0.06	-0.13	-0.01	-0.13	0.01	-0.12	-0.05
Hf	1.39	-0.13	1.51	0.26	0.58	-0.94	-0.62	-1.46	-1.24
Ta	0.08	0.08	0.06	0.06	0.05	0.00	0.04	-0.02	0.00
Th	0.89	0.49	0.52	0.42	0.82	-0.63	0.01	-0.94	-0.66

Abbreviations:

Units

HFL= Hanging wall flow
HBX= Hanging wall breccia
FLT= Footwall lapilli tuff
FT= Footwall tuff
FBX= Footwall breccia
FFL= Footwall flow
INT= Intrusion

Alteration

Qtz-Ser= Quartz-sericite
Chl-Ser= Chlorite-sericite
Chl= Chlorite

Appendix C: Table C.1.2 Mass changes for samples at the Boundary deposit

Sample ID	**H500661**	**H500662**	**H500663**	**H500664**	**H500665**	**H500666**	**H500667**	**H500668**	**H500669**	**H500670**
Hole ID	BD10-102	BD10-102	BD10-102	BD10-102	BD11-129	BD11-129	BD11-129	BD11-129	BD11-129	BD11-129
Depth (m)	6.2	16.6	25.1	43.7	12.8	24.8	38.1	35.4	38.4	49.4
Lithology	FLT	FLT	FLT	FLT	FLT	FLT	FLT	FFL	FLT	FBX
Alteration	Qtz-Ser	Chl	Chl	Qtz-Ser	Qtz-Ser	Qtz-Ser	Qtz-Ser	Qtz-Ser	Chl-Ser	Qtz-Ser
SiO_2	1.56	-61.08	28.38	17.36	-14.32	14.70	28.92	34.39	13.81	-0.07
$A_{l2}O_3$	0.00	0.00	0.00	0.00	0.00	0.00	0.00	0.00	0.00	0.00
FeO	24.04	16.89	36.38	5.62	0.50	15.95	19.43	5.25	12.88	4.56
MnO	-0.07	0.00	0.04	-0.03	-0.05	-0.09	-0.05	-0.09	-0.09	-0.08
MgO	-2.04	9.83	8.45	1.21	1.39	-2.11	-1.75	-1.99	-2.05	-0.46
CaO	-0.05	-0.11	-0.04	-0.09	-0.10	-0.11	-0.02	-0.12	-0.08	-0.13
Na_2O	-1.79	-2.01	-1.97	-1.83	-1.82	-1.75	-1.75	-1.77	-1.74	-1.80
K_2O	0.89	-2.32	-2.12	-0.28	0.30	0.90	0.91	0.89	0.97	0.52
TiO_2	0.08	0.05	0.06	0.08	0.02	0.05	0.05	0.03	0.03	0.03
P_2O_5	0.00	0.01	0.01	0.01	0.02	0.00	0.00	0.00	0.00	0.00
Net Oxide Change	22.61	-38.74	69.18	22.06	-14.06	27.54	45.74	36.58	23.73	2.55
Ba	436.97	-1390.81	-1313.44	-589.53	403.83	247.85	162.72	149.35	93.35	-4.81
Sr	-2.93	-19.66	-13.78	-10.51	-9.90	-10.52	-8.79	-13.49	-11.07	-13.43
Y	5.00	7.10	8.28	0.58	-6.15	4.05	-2.66	0.71	6.08	3.85
Sc	3.20	2.50	4.39	4.05	2.10	2.91	1.56	1.35	0.93	3.92
Zr	7.53	26.13	31.78	5.67	8.87	4.23	11.91	6.76	2.54	12.46
Be	-0.27	-0.61	0.03	-0.36	-0.14	-0.28	-0.17	-0.29	-0.32	-0.46
V	15.10	10.78	9.83	29.42	16.52	20.46	20.62	7.43	19.36	0.18
Hg	15.87	72.39	193.56	2.05	19.98	76.96	379.44	57.50	171.06	14.78
Cr 52	14.28	-0.97	24.35	15.10	-0.60	1.94	2.90	21.07	1.63	0.32
Co	36.24	83.22	272.76	5.07	-0.72	18.17	73.10	14.51	12.02	27.29
Ni	2.33	-1.09	5.28	1.38	-0.68	2.17	3.26	2.09	1.83	0.36
Cu	12107.27	21512.26	34653.18	263.39	36.60	226.37	23457.83	1325.49	-70.59	-39.84
Zn	322.35	42.01	194.25	-57.40	-5.41	-81.97	-46.69	-95.49	-49.47	-119.43
As	31.83	24.49	62.57	2.67	1.16	65.69	59.93	10.87	30.48	81.72
Se 78	6.23	13.73	112.49	3.70	-1.81	5.81	50.67	5.58	4.89	0.95
Br 79	79.50	-35.15	158.14	16.99	29.72	138.15	195.75	144.48	175.18	81.36
Mo	46.68	47.35	55.31	2.44	5.00	9.34	27.05	6.27	4.54	15.67
Ag 107	1.85	1.85	3.88	0.14	-0.07	0.96	4.50	0.21	0.18	0.04
Cd	0.21	-0.10	0.48	0.12	-0.06	0.20	0.29	0.19	0.16	0.03
Sn	6.93	0.24	3.13	1.68	-2.22	0.27	2.48	-0.49	-0.80	-0.77
Sb	1.61	1.84	3.97	0.01	6.14	8.55	12.39	1.39	1.46	1.11
Te	1.00	44.20	92.37	0.60	-0.29	7.97	24.77	0.90	0.79	10.82
I	8.63	-4.04	19.53	5.12	-2.51	8.05	12.06	7.74	6.77	1.32
W	4.25	19.42	30.73	10.86	2.18	3.95	3.01	4.14	4.08	2.41
Pb	5.91	-2.77	13.36	3.51	-1.72	5.51	43.18	5.30	4.63	0.90
Bi	6.14	65.13	90.21	1.95	-0.02	34.60	44.43	6.93	2.28	15.42
Nb	0.40	0.31	0.10	1.18	3.24	2.34	2.96	2.14	2.22	3.03
La	3.14	5.73	-1.49	-7.36	1.29	1.82	0.85	1.39	1.13	-1.20
Ce	4.87	7.00	-4.25	-15.21	2.26	2.84	0.52	2.10	1.45	-3.46
Pr	0.49	0.86	-0.54	-1.75	0.44	0.44	0.09	0.40	0.15	-0.39
Nd	2.45	4.24	-1.77	-6.85	2.51	3.02	0.19	1.58	0.95	-1.07
Sm	0.45	1.30	-0.70	-1.36	0.39	0.82	0.18	0.14	0.24	-0.27
Eu	0.07	-0.39	-0.68	-0.41	0.24	0.24	0.16	-0.18	0.09	0.56
Tb	0.07	0.20	0.09	-0.08	-0.05	0.17	0.00	0.04	0.09	0.07
Dy	0.73	1.24	0.99	0.02	-0.59	1.20	-0.01	0.57	0.71	0.85
Ho	0.06	0.15	0.23	0.03	-0.14	0.27	-0.04	0.05	0.16	0.16
Er	0.19	0.36	0.67	0.11	-0.49	1.08	-0.09	0.32	0.50	0.49
Tm	0.01	0.07	0.10	0.04	-0.04	0.15	-0.02	0.09	0.09	0.07
Yb	-0.05	0.47	0.65	0.12	-0.62	0.62	-0.01	0.31	0.47	0.43
Lu	0.01	0.05	0.08	0.01	-0.08	0.11	0.00	0.04	0.08	0.05
Hf	-0.46	-0.60	-0.53	-0.55	0.62	0.84	0.60	-0.20	0.29	1.24
Ta	-0.06	0.02	0.02	0.02	0.07	0.07	0.03	0.05	0.00	0.09
Th	-0.50	0.34	-0.08	0.08	0.44	0.69	0.31	0.48	0.02	0.63

Abbreviations:

Units

HFL= Hanging wall flow
HBX= Hanging wall breccia
FLT= Footwall lapilli tuff
FT= Footwall tuff
FBX= Footwall breccia
FFL= Footwall flow
INT= Intrusion

Alteration

Qtz-Ser= Quartz-sericite
Chl-Ser= Chlorite-sericite
Chl= Chlorite

Appendix C: Table C.1.2 Mass changes for samples at the Boundary deposit

Sample ID	**H500671**	**H500672**	**H500673**	**H500674**	**H500675**	**H500676**	**H500677**	**H500678**	**H500679**	**H500680**
Hole ID	BD11-129	BD11-129	BD11-123	BD11-123	BD11-123	BD11-123	BD11-123	BD10-87	BD10-87	BD10-87
Depth (m)	53.8	56.4	7.4	9	10.8	14.8	22.3	6.3	11	17.9
Lithology	FFL	FLT	HFL	FLT	FFL	FLT	FLT	FLT	FLT	FT
Alteration	Chl-Ser	Chl-Ser	Qtz-Ser	Qtz-Ser	Qtz-Ser	Qtz-Ser	Qtz-Ser	Chl	Chl-Ser	Qtz-Ser
SiO_2	-3.84	-22.60	6.24	-17.16	2.06	-4.54	-25.15	-30.60	14.29	1.01
Al_2O_3	0.00	0.00	0.00	0.00	0.00	0.00	0.00	0.00	0.00	0.00
FeO	6.71	3.22	1.25	2.45	1.97	3.19	2.78	14.58	14.97	5.74
MnO	-0.04	-0.03	0.02	0.02	0.15	0.11	-0.01	0.11	0.04	-0.05
MgO	3.93	2.25	0.08	0.25	0.56	1.30	-0.61	6.40	6.52	0.74
CaO	-0.13	-0.11	-0.09	-0.06	-0.09	-0.09	-0.09	-0.11	-0.11	-0.11
Na_2O	-1.91	-1.86	-1.73	-1.76	-1.82	-1.81	-1.77	-1.95	-1.96	-1.81
K_2O	-1.06	-0.31	0.58	0.61	0.73	0.53	0.82	-1.68	-1.81	-0.11
TiO_2	0.02	0.03	0.01	0.02	0.02	0.02	0.03	0.07	0.07	0.04
P_2O_5	0.00	0.02	0.01	0.02	0.00	0.02	0.01	-0.01	0.00	0.00
Net Oxide Change	3.67	-19.38	6.38	-15.61	3.57	-1.27	-23.98	-13.18	32.03	5.43
Ba	-768.90	-396.97	575.56	399.93	275.42	12.65	1049.17	-1114.97	-1168.40	-506.41
Sr	-17.58	-15.29	-9.08	-10.71	-13.56	-12.83	-9.39	-15.92	-16.12	-9.77
Y	11.77	12.14	1.90	1.81	0.05	6.86	4.34	-14.67	25.68	8.80
Sc	2.14	3.41	0.76	2.16	3.72	2.23	2.61	1.15	1.76	1.12
Zr	16.15	8.41	37.97	20.86	15.43	20.10	7.88	32.44	35.80	-4.93
Be	-0.45	-0.58	0.08	-0.13	0.06	-0.49	-0.21	-0.49	-0.27	-0.44
V	6.33	5.04	0.19	3.58	0.14	0.05	3.80	4.60	6.32	6.39
Hg	1.25	-9.90	20.29	20.13	4.89	5.33	36.07	4.22	11.52	0.23
Cr 52	0.46	-0.72	5.37	4.33	0.25	0.09	2.90	0.06	9.10	0.50
Co	15.57	7.05	1.76	2.30	-0.64	-0.65	0.57	8.13	20.62	15.94
Ni	0.52	-0.81	0.38	-0.66	0.28	0.10	3.36	0.07	2.35	0.56
Cu	-73.04	-75.52	-36.87	681.87	963.59	969.61	-58.12	-44.97	-69.62	-72.97
Zn	-98.22	-57.43	9.51	-37.17	-38.81	-17.55	24.88	11.53	41.07	-86.07
As	6.77	0.05	4.10	0.86	1.56	0.07	15.52	13.90	2.45	0.06
Se 78	1.39	-2.16	1.02	-1.76	0.74	0.26	-2.83	0.19	6.27	1.49
Br 79	95.73	24.80	102.35	60.82	118.81	92.34	48.45	106.63	197.59	99.27
Mo	11.93	6.06	23.26	11.37	7.01	4.76	5.90	11.44	16.38	20.37
Ag 107	0.05	-0.08	0.04	-0.07	0.03	0.01	-0.11	0.01	0.23	0.06
Cd	0.05	-0.07	0.03	1.25	0.02	0.01	-0.10	0.01	0.21	0.05
Sn	-2.08	-2.37	-1.27	-1.57	-0.97	-1.47	-1.79	-1.43	-0.74	-1.04
Sb	-0.07	0.19	0.58	0.79	0.82	0.37	7.32	0.94	0.21	-0.11
Te	0.22	-0.35	0.16	-0.28	0.12	0.04	-0.46	2.90	1.01	0.24
I	1.92	-2.99	1.41	-2.44	1.03	0.35	-3.92	0.26	8.69	2.07
W	2.42	3.36	0.66	1.87	10.25	1.85	2.94	12.17	10.01	6.34
Pb	1.31	-2.05	0.97	12.23	0.70	0.24	-2.68	0.18	5.95	1.41
Bi	2.32	5.58	0.09	1.10	0.02	0.05	1.56	4.91	7.39	2.02
Nb	2.88	3.15	0.60	0.65	1.14	1.08	1.16	2.82	2.57	0.63
La	3.30	-0.68	-2.00	-2.21	-1.84	-0.27	1.18	-16.21	12.48	16.60
Ce	6.66	-1.54	-4.48	-4.60	-4.41	-1.43	2.14	-34.64	27.41	35.98
Pr	0.80	-0.12	-0.53	-0.66	-0.51	-0.08	0.30	-4.32	3.64	4.69
Nd	3.48	-0.22	-1.78	-2.37	-2.07	-0.40	1.49	-18.14	14.47	21.82
Sm	1.47	0.29	-0.23	-0.34	-0.36	0.31	0.68	-4.20	3.71	4.70
Eu	0.20	0.05	-0.01	0.04	-0.32	-0.06	0.99	-0.87	0.02	0.03
Tb	0.37	0.20	-0.03	-0.06	-0.01	0.09	0.06	-0.60	0.55	0.39
Dy	2.73	1.72	0.15	0.04	0.32	1.07	0.68	-3.12	4.30	2.40
Ho	0.37	0.25	0.09	0.00	0.03	0.22	0.15	-0.57	0.89	0.40
Er	1.10	1.10	0.29	0.10	0.17	0.68	0.43	-1.27	2.42	0.88
Tm	0.14	0.16	0.07	0.01	0.02	0.06	0.07	-0.11	0.33	0.10
Yb	0.99	1.14	0.23	-0.12	-0.07	0.37	0.44	-0.52	1.98	0.19
Lu	0.15	0.20	0.01	-0.04	0.02	0.08	0.05	-0.05	0.26	-0.02
Hf	1.12	-0.19	-0.34	-0.99	-0.74	-1.04	-0.78	0.26	0.49	-1.32
Ta	0.09	0.07	0.01	0.01	0.02	0.01	0.03	0.06	0.07	-0.01
Th	0.61	0.23	-0.05	-0.02	-0.11	0.03	0.06	0.58	0.82	-0.45

Abbreviations:

Units

HFL= Hanging wall flow
HBX= Hanging wall breccia
FLT= Footwall lapilli tuff
FT= Footwall tuff
FBX= Footwall breccia
FFL= Footwall flow
INT= Intrusion

Alteration

Qtz-Ser= Quartz-sericite
Chl-Ser= Chlorite-sericite
Chl= Chlorite

Appendix C: Table C.1.2 Mass changes for samples at the Boundary deposit

Sample ID	**H500681**	**H500682**	**H500683**	**H500684**	**H500685**	**H500686**	**H500687**	**H500688**	**H500689**	**H500690**
Hole ID	BD10-87	BD10-77	BD10-77	BD10-77	BD10-77	BD10-77	BD10-76	BD10-76	BD10-76	BD10-76
Depth (m)	30.5	12.4	22.3	26	29.5	49.1	48.2	36	27.2	7.7
Lithology	FLT	FLT	FBX	FLT	FLT	FLT	FLT	FLT	FLT	FLT
Alteration	Qtz-Ser	Qtz-Ser	Qtz-Ser	Qtz-Ser	Chl-Ser	Qtz-Ser	Chl-Ser	Qtz-Ser	Chl	Qtz-Ser
SiO_2	3.48	4.62	-42.34	-3.13	-10.70	16.60	23.80	21.23	-42.79	39.92
Al_2O_3	0.00	0.00	0.00	0.00	0.00	0.00	0.00	0.00	0.00	0.00
FeO	3.89	4.26	5.12	1.86	20.19	0.70	11.13	2.69	17.31	8.21
MnO	-0.07	0.00	-0.07	-0.04	0.06	-0.09	0.00	-0.08	0.04	-0.06
MgO	-0.58	0.61	-1.41	1.18	5.48	-1.52	3.08	-1.57	9.40	-0.87
CaO	-0.12	-0.01	-0.07	-0.07	-0.08	-0.10	-0.09	-0.08	-0.11	-0.10
Na_2O	-1.79	-1.81	-1.81	-1.82	-1.89	-1.80	-1.84	-1.75	-1.99	-1.80
K_2O	0.51	0.78	1.07	0.39	-0.76	0.82	-0.67	0.88	-2.00	0.80
TiO_2	0.03	0.05	0.06	0.03	0.02	0.03	0.04	0.04	0.03	0.02
P_2O_5	0.00	0.00	0.02	0.02	0.02	0.01	0.00	0.01	-0.01	0.00
Net Oxide Change	5.34	8.48	-39.45	-1.59	12.32	14.66	35.45	21.39	-20.11	46.11
Ba	-256.68	499.52	421.01	-75.40	-818.32	-313.29	-776.25	-235.51	-1256.38	8.62
Sr	-9.98	-9.60	-12.81	-10.97	-12.72	-11.62	-13.21	-9.59	-19.08	-11.20
Y	6.88	6.10	0.40	-3.91	-15.15	1.37	9.37	4.43	6.68	4.21
Sc	2.02	2.40	1.16	2.03	-0.72	2.69	6.12	3.65	5.55	2.35
Zr	5.74	28.62	6.05	-7.63	8.71	-1.96	16.24	1.41	0.79	18.58
Be	-0.45	-0.44	-0.34	-0.50	-0.34	-0.42	-0.27	-0.38	-0.51	-0.23
V	7.33	7.65	1.44	2.51	0.81	3.27	1.16	0.60	-0.07	8.30
Hg	-9.27	4.91	33.97	-9.49	38.35	-9.12	-8.34	-8.90	-6.17	-2.74
Cr 52	0.41	0.57	-1.53	0.01	1.45	0.68	2.07	1.07	-0.12	2.42
Co	48.57	0.10	0.12	-0.66	14.62	21.30	76.20	19.06	79.74	21.64
Ni	0.46	0.64	-1.72	0.01	1.63	0.77	2.33	1.20	-0.14	2.72
Cu	61.64	535.57	-48.70	-73.98	42110.18	264.76	24.86	-18.64	-48.54	805.84
Zn	-92.77	-11.97	-82.04	-39.64	453.99	-111.57	-92.77	-116.26	44.87	3.57
As	19.29	12.22	13.80	-1.32	9.75	0.44	19.91	1.74	10.97	10.69
Se 78	1.23	1.70	-4.58	0.04	34.24	2.05	6.22	3.21	20.99	7.25
Br 79	10.77	72.64	-49.54	20.94	68.84	54.93	127.05	56.48	23.65	215.76
Mo	2.39	12.34	25.74	3.16	10.11	13.39	2.70	12.44	48.46	11.01
Ag 107	0.05	0.06	-0.17	0.00	2.88	0.08	0.23	0.12	-0.01	0.27
Cd	0.04	0.06	-0.15	0.00	0.15	0.07	0.21	0.11	-0.01	0.24
Sn	2.90	0.76	-1.30	-1.70	4.99	-1.61	-0.23	-0.36	-2.20	0.21
Sb	0.18	1.71	4.72	0.16	2.73	0.26	1.82	0.17	0.06	0.71
Te	0.20	0.27	2.37	0.01	0.70	0.33	8.01	3.73	5.80	1.17
I	1.71	2.36	-6.35	0.05	6.01	2.84	8.62	4.45	-0.52	10.05
W	4.83	4.58	4.83	5.86	2.84	3.04	7.02	3.27	7.06	3.90
Pb	1.17	1.61	8.09	0.03	4.12	1.94	5.90	3.05	-0.36	6.88
Bi	3.62	7.60	6.75	1.29	5.69	2.34	11.97	9.24	12.21	2.57
Nb	-0.15	2.86	2.73	0.98	1.34	-0.04	1.68	0.64	2.54	1.01
La	-6.48	3.52	-1.66	-8.08	-12.33	4.09	3.73	0.21	-0.85	-2.07
Ce	-13.19	6.39	-3.06	-17.25	-27.04	9.82	8.13	-1.24	-2.36	-3.68
Pr	-1.57	0.90	-0.39	-2.12	-3.32	1.49	1.22	-0.09	-0.32	-0.38
Nd	-5.69	4.54	-1.50	-8.38	-13.66	6.25	5.89	0.21	-0.63	-1.99
Sm	-1.12	1.02	-0.22	-1.82	-3.13	1.11	1.40	-0.23	0.12	0.02
Eu	-0.68	0.30	0.18	-0.28	-0.74	-0.15	-0.38	-0.32	-0.09	-0.59
Tb	-0.08	0.21	-0.08	-0.29	-0.46	0.02	0.18	-0.01	0.13	-0.01
Dy	-0.01	1.45	-0.16	-1.38	-2.51	0.05	1.46	0.05	1.52	0.15
Ho	-0.02	0.43	0.00	-0.23	-0.50	0.00	0.29	0.00	0.31	-0.14
Er	-0.03	1.13	0.03	-0.64	-1.22	-0.08	0.88	-0.04	0.81	-0.30
Tm	0.00	0.21	0.02	-0.09	-0.12	-0.01	0.13	0.04	0.14	-0.09
Yb	-0.23	1.30	-0.01	-0.51	-0.63	0.01	0.54	0.01	0.46	-0.68
Lu	-0.04	0.15	0.01	-0.07	-0.10	-0.02	0.11	-0.02	0.10	-0.05
Hf	-0.90	0.79	-0.01	-0.61	0.40	0.08	0.64	0.35	-0.13	0.15
Ta	-0.01	0.09	0.05	0.03	0.03	0.02	0.07	0.02	0.05	0.04
Th	-0.81	2.12	0.89	0.36	0.56	0.58	1.11	0.63	0.50	-0.20

Abbreviations:

Units

HFL= Hanging wall flow
HBX= Hanging wall breccia
FLT= Footwall lapilli tuff
FT= Footwall tuff
FBX= Footwall breccia
FFL= Footwall flow
INT= Intrusion

Alteration

Qtz-Ser= Quartz-sericite
Chl-Ser= Chlorite-sericite
Chl= Chlorite

Appendix C: Table C.1.2 Mass changes for samples at the Boundary deposit

Sample ID	H500691	H500692	H500693	H500694	H500695	H500696	H500697	H500698	H500699	H500700
Hole ID	BD10-63	BD10-63	BD10-63	BD10-63	BD10-63	BD10-63	BD10-63	BD10-61	BD10-61	BD10-61
Depth (m)	11.4	21.3	37.5	57.3	59.1	64.1	75.4	11.1	24.9	37.9
Lithology	HBX	HFL	FLT	FLT	FBX	FFL	FBX	FLT	FLT	FLT
Alteration	Qtz-Ser	Qtz-Ser	Qtz-Ser	Chl	Qtz-Ser	Qtz-Ser	Qtz-Ser	Chl-Ser	Chl	Chl-Ser
SiO_2	19.44	16.09	-13.69	16.24	8.65	8.78	12.30	35.70	-21.37	22.68
$A_{l2}O_3$	0.00	0.00	0.00	0.00	0.00	0.00	0.00	0.00	0.00	0.00
FeO	0.69	6.98	2.61	37.33	2.19	1.63	4.16	20.12	4.51	12.89
MnO	0.19	-0.05	0.05	0.09	-0.04	-0.05	-0.06	-0.09	0.10	0.00
MgO	0.62	-1.75	0.18	5.77	0.17	0.29	-0.21	-2.04	10.32	5.35
CaO	0.04	-0.10	-0.09	-0.07	-0.02	-0.08	-0.07	-0.10	0.71	-0.11
Na_2O	-1.88	-1.87	-1.86	-1.91	-1.83	-1.83	-1.83	-1.81	-1.97	-1.94
K_2O	1.07	1.25	0.78	-1.40	0.67	0.69	0.64	1.11	-1.84	-1.65
TiO_2	0.02	0.00	0.05	0.01	0.06	0.05	0.06	0.04	0.24	0.11
P_2O_5	0.02	0.00	0.02	0.00	0.02	0.02	0.01	0.02	0.07	0.00
Net Oxide Change	20.22	20.55	-11.97	56.05	9.87	9.51	15.01	52.95	-9.24	37.33
Ba	539.84	1141.37	529.87	-992.22	-112.56	-182.21	-145.97	1347.30	-1110.74	-1095.55
Sr	-13.54	-14.35	-15.66	-14.26	-13.04	-14.22	-12.47	-15.08	-10.57	-19.00
Y	3.32	-2.02	-2.74	-8.06	1.34	5.45	-4.44	2.54	-8.51	7.57
Sc	0.88	-1.07	1.78	-0.33	0.09	2.22	1.92	2.12	5.24	3.52
Zr	-12.00	18.24	-16.29	7.78	5.16	2.81	5.16	9.03	-31.62	8.22
Be	0.21	-0.36	-0.55	-0.03	-0.44	-0.44	-0.40	-0.13	-0.52	-0.25
V	3.55	5.15	6.56	2.33	6.46	0.28	0.48	1.83	70.86	14.02
Hg	463.17	4030.78	80.45	69.22	-0.79	-9.22	-9.02	78.00	0.39	4.52
Cr 52	10.35	1.23	-0.42	4.16	0.54	0.50	0.85	45.15	51.57	11.32
Co	-0.57	-0.54	0.13	57.52	0.11	-0.61	0.95	15.38	3.66	64.58
Ni	1.05	1.38	-0.47	4.67	0.60	0.56	0.96	29.82	12.25	2.51
Cu	86.38	2998.26	631.33	50953.08	481.99	78.13	-8.45	2116.02	-59.02	711.49
Zn	5513.41	37977.79	260.36	280.30	-54.12	-71.20	91.15	351.98	197.46	-27.58
As	3.68	158.79	11.51	56.84	1.34	3.49	13.42	123.51	-1.36	29.80
Se 78	2.79	3.68	-1.25	70.14	1.61	1.49	2.56	9.76	-0.63	6.70
Br 79	43.36	50.44	-26.66	160.16	12.07	30.21	49.61	105.12	11.66	103.23
Mo	6.84	6.37	3.40	19.75	16.77	2.24	4.70	20.91	1.40	21.90
Ag 107	0.10	4.83	-0.05	4.91	0.06	0.06	0.10	1.27	-0.02	0.25
Cd	16.88	120.83	0.77	0.42	0.05	0.05	0.09	1.18	-0.02	0.23
Sn	-1.69	4.92	-2.37	0.40	-0.96	-1.98	-1.68	0.57	-2.38	-1.42
Sb	3.97	14.62	4.97	4.21	1.13	0.54	1.38	5.31	-0.13	0.11
Te	0.45	0.59	-0.20	19.01	0.26	0.24	0.41	9.24	-0.10	7.96
I	3.87	5.09	-1.73	17.28	2.23	2.06	3.55	13.52	-0.87	9.29
W	2.38	6.55	1.73	8.19	0.37	0.89	0.54	2.90	1.09	11.63
Pb	594.12	4444.13	41.64	41.00	1.53	1.41	2.43	215.79	51.43	6.36
Bi	0.30	5.23	1.20	34.39	1.64	0.46	1.32	10.19	0.44	10.06
Nb	0.88	0.46	0.83	2.09	2.05	1.10	0.46	1.10	0.50	1.56
La	-3.36	-2.57	-2.50	-3.34	0.73	-2.31	-1.45	0.55	-8.63	-4.62
Ce	-6.36	-4.61	-5.40	-9.11	2.09	-5.48	-3.46	0.39	-17.04	-10.53
Pr	-0.75	-0.52	-0.64	-1.12	0.17	-0.66	-0.44	-0.04	-2.08	-1.36
Nd	-2.55	-2.05	-2.24	-4.66	0.56	-2.70	-1.58	0.33	-8.94	-5.48
Sm	-0.60	-0.35	-0.65	-1.01	0.13	-0.54	-0.40	0.44	-1.92	-0.88
Eu	-0.25	0.38	-0.17	-0.22	-0.09	-0.18	-0.30	0.32	-0.19	-0.41
Tb	0.02	-0.03	-0.11	-0.09	-0.03	-0.02	-0.10	0.07	-0.30	0.09
Dy	0.41	0.18	-0.46	0.07	-0.10	0.34	-0.55	0.81	-1.44	0.97
Ho	0.10	0.00	-0.12	0.01	-0.05	-0.04	-0.22	0.13	-0.34	0.05
Er	0.31	-0.09	-0.42	-0.14	-0.19	-0.04	-0.76	0.21	-1.01	0.28
Tm	0.07	0.00	-0.05	0.02	-0.02	-0.01	-0.11	0.05	-0.13	0.04
Yb	0.24	0.12	-0.50	-0.02	-0.32	-0.25	-0.84	0.10	-1.11	0.19
Lu	0.05	0.01	-0.08	0.01	-0.06	-0.02	-0.13	0.04	-0.16	0.03
Hf	-0.26	0.29	-0.54	-0.16	-0.14	0.07	-0.41	0.41	-0.72	-0.31
Ta	0.00	0.02	-0.01	0.04	0.04	0.04	0.01	0.04	-0.01	0.04
Th	0.32	0.58	-0.35	0.58	0.69	0.18	0.19	0.73	-1.27	0.13

Abbreviations:

Units

HFL= Hanging wall flow
HBX= Hanging wall breccia
FLT= Footwall lapilli tuff
FT= Footwall tuff
FBX= Footwall breccia
FFL= Footwall flow
INT= Intrusion

Alteration

Qtz-Ser= Quartz-sericite
Chl-Ser= Chlorite-sericite
Chl= Chlorite

Appendix C: Table C.1.2 Mass changes for samples at the Boundary deposit

Sample ID	**H501201**	**H501202**	**H501203**	**H501204**	**H501205**	**H501206**	**H501207**	**H501208**	**H501212**	**H501213**
Hole ID	BD10-61	BD10-61	BD10-58	BD10-58	BD10-58	BD10-58	BD10-58	BD10-58	BD10-40	BD10-40
Depth (m)	39.5	44.4	8.2	15	18.2	29.5	32.3	34.9	4	9.5
Lithology	FBX	FBX	FLT	FLT	FLT	FLT	FBX	FLT	HFL	HBX
Alteration	Chl-Ser	Chl-Ser	Chl-Ser	Chl	Chl-Ser	Chl-Ser	Chl-Ser	Chl-Ser	Qtz-Ser	Qtz-Ser
SiO_2	28.54	17.46	34.78	-61.98	23.77	2.28	82.59	31.84	8.57	-11.23
Al_2O_3	0.00	0.00	0.00	0.00	0.00	0.00	0.00	0.00	0.00	0.00
FeO	9.98	5.86	28.83	31.71	19.31	32.38	51.62	14.75	3.95	4.92
MnO	-0.01	0.25	-0.01	0.06	-0.04	0.06	0.01	-0.02	-0.01	0.09
MgO	4.80	3.53	3.69	6.21	-1.32	2.58	-0.31	-0.37	-1.07	-0.14
CaO	-0.09	2.20	-0.07	-0.12	-0.07	-0.08	-0.05	-0.09	-0.11	-0.10
Na_2O	-1.93	-1.88	-1.88	-1.98	-1.74	-1.87	-1.81	-1.79	-1.78	-1.75
K_2O	-1.35	-0.37	-1.16	-2.06	0.74	-1.05	0.03	-0.08	0.82	0.63
TiO_2	0.06	0.06	0.06	0.05	0.04	-0.01	-0.01	0.00	0.00	0.01
P_2O_5	0.02	0.00	0.00	0.00	0.00	0.00	0.00	0.00	0.01	0.01
Net Oxide Change	40.03	27.11	64.24	-28.12	40.68	34.29	132.08	44.23	10.39	-7.56
Ba	-945.97	-559.66	-684.01	-1235.01	137.43	-787.97	-329.95	-414.32	101.29	-76.98
Sr	-17.50	15.23	-16.21	-18.89	-6.00	-13.67	-7.82	-10.87	-12.85	-10.32
Y	6.00	2.22	-10.04	-11.03	-8.60	-10.67	-10.63	0.75	23.89	4.82
Sc	2.00	3.30	3.51	2.43	4.40	1.67	1.35	5.90	1.43	0.71
Zr	12.51	-5.38	-11.79	30.07	19.78	-18.33	8.20	-5.09	15.08	3.97
Be	-0.25	-0.34	-0.03	-0.48	-0.20	-0.17	0.42	-0.21	-0.43	-0.03
V	5.00	0.82	20.67	25.47	23.10	14.17	4.59	7.04	5.50	4.32
Hg	6.00	-4.02	264.08	107.13	165.58	89.67	963.92	40.47	6.29	-3.24
Cr 52	2.23	29.64	25.57	0.16	10.35	11.37	38.33	2.62	0.64	26.95
Co	40.70	15.87	159.65	43.99	40.87	141.51	14.15	21.82	44.59	1.92
Ni	2.50	24.68	4.65	6.87	3.00	3.33	9.18	2.95	0.72	-0.13
Cu	520.59	795.31	2531.87	6935.00	12558.94	27224.77	47928.80	6162.45	3482.14	-28.87
Zn	-41.22	-63.88	-21.34	155.18	-23.69	67.52	367.82	-40.60	-94.35	128.87
As	3.52	2.36	70.41	312.41	62.71	132.82	668.06	24.45	32.27	7.58
Se 78	6.68	4.40	116.89	63.26	56.29	112.62	45.40	7.87	1.91	-0.35
Br 79	150.47	57.41	184.99	-19.88	88.70	81.01	295.40	109.78	115.97	74.50
Mo	12.43	15.67	94.22	61.49	42.25	93.02	39.19	23.09	12.15	8.22
Ag 107	0.25	0.16	0.47	0.86	0.30	3.17	9.85	0.29	0.07	-0.01
Cd	0.23	0.15	0.42	0.02	0.27	0.30	1.51	0.27	0.06	-0.01
Sn	-1.36	-1.85	0.45	-0.94	1.67	1.36	9.60	2.42	-0.89	-1.79
Sb	0.44	0.39	1.75	3.73	3.26	7.41	102.67	1.06	4.61	0.53
Te	1.08	0.71	16.87	44.59	16.81	412.04	26.70	7.77	10.52	-0.06
I	9.25	6.10	17.22	0.66	11.10	12.33	33.98	10.91	2.65	-0.49
W	2.07	1.43	14.97	15.09	5.72	9.51	8.50	2.64	2.76	2.00
Pb	6.33	4.17	11.78	39.79	19.67	31.29	129.42	7.47	1.82	-0.33
Bi	4.40	2.57	17.73	67.49	31.15	624.23	55.02	14.58	17.61	1.00
Nb	1.12	2.07	-0.22	2.25	0.47	-0.45	1.65	1.29	2.68	1.31
La	-3.95	4.06	-4.45	1.10	-3.93	-5.42	-2.24	-6.64	2.56	-0.07
Ce	-9.45	7.11	-11.39	0.53	-7.92	-11.96	-4.84	-14.23	5.17	-1.21
Pr	-1.06	0.97	-1.47	-0.04	-0.90	-1.42	-0.55	-1.69	0.70	-0.13
Nd	-4.77	4.10	-6.60	-0.12	-3.22	-5.94	-2.50	-7.27	2.52	-0.42
Sm	-0.96	0.87	-2.00	-0.41	-0.73	-1.05	-0.53	-1.37	1.16	0.26
Eu	-0.36	-0.38	-0.67	-0.27	0.04	-0.52	0.31	0.02	-0.34	-0.07
Tb	0.04	0.10	-0.34	-0.19	-0.21	-0.17	-0.25	0.01	0.40	0.15
Dy	0.41	0.86	-2.26	-0.70	-1.06	-0.77	-0.90	0.24	3.19	1.19
Ho	-0.01	0.16	-0.48	-0.16	-0.23	-0.20	-0.29	0.14	0.62	0.17
Er	-0.19	0.24	-1.36	-0.24	-0.75	-0.45	-0.76	0.59	2.11	0.53
Tm	0.00	0.04	-0.18	-0.01	-0.07	-0.06	-0.11	0.13	0.33	0.05
Yb	-0.36	0.27	-1.27	0.09	-0.58	-0.53	-0.57	0.80	2.08	0.35
Lu	-0.06	-0.01	-0.16	0.02	-0.12	-0.04	-0.03	0.18	0.36	0.04
Hf	-0.42	0.46	0.03	0.30	0.64	0.90	1.03	0.88	0.43	0.31
Ta	0.04	0.06	-0.06	0.05	0.01	-0.02	0.06	0.07	0.07	0.06
Th	0.29	0.90	-0.90	1.24	0.23	-0.17	0.74	0.36	0.17	0.13

Abbreviations:

Units

HFL= Hanging wall flow
HBX= Hanging wall breccia
FLT= Footwall lapilli tuff
FT= Footwall tuff
FBX= Footwall breccia
FFL= Footwall flow
INT= Intrusion

Alteration

Qtz-Ser= Quartz-sericite
Chl-Ser= Chlorite-sericite
Chl= Chlorite

Appendix C: Table C.1.2 Mass changes for samples at the Boundary deposit

Sample ID	H501214	H501215	H501216	H501217	H501218	H501219	H501220	H501221	H501222	H501223
Hole ID	BD10-40	BD10-40	BD10-40	BD10-98	BD10-98	BD10-98	BD10-98	BD10-98	BD10-50	BD10-50
Depth (m)	30.5	43.7	16.4	13.7	23	40.4	42.8	50.8	9	15.6
Lithology	HBX	FLT	HBX	FLT	FLT	FLT	FFL	FLT	HFL	FLT
Alteration	Qtz-Ser	Qtz-Ser	Qtz-Ser	Chl	Chl-Ser	Chl	Qtz-Ser	Qtz-Ser	Chl-Ser	Qtz-Ser
SiO_2	-14.61	6.45	7.71	-61.91	-25.92	-3.60	-8.25	6.70	-25.34	9.11
Al_2O_3	0.00	0.00	0.00	0.00	0.00	0.00	0.00	0.00	0.00	0.00
FeO	1.83	5.51	0.58	12.76	2.50	8.07	1.32	2.34	9.25	5.11
MnO	0.03	-0.02	0.04	0.05	-0.02	0.05	-0.04	0.01	-0.04	-0.08
MgO	0.19	-0.20	-0.58	8.36	4.04	8.68	-0.25	0.04	1.87	-2.17
CaO	-0.04	-0.09	0.14	-0.10	0.09	-0.09	-0.11	-0.12	-0.12	-0.07
Na_2O	-1.60	-1.57	-1.77	-1.62	-1.81	-1.96	-1.81	-1.82	-1.83	-1.76
K_2O	0.77	0.75	0.89	-1.88	-0.55	-1.78	0.71	0.68	-0.12	0.82
TiO_2	0.01	0.03	0.01	0.02	0.05	0.05	0.02	0.02	0.00	0.04
P_2O_5	0.01	0.00	0.02	0.00	0.01	0.01	0.02	0.00	0.00	0.01
Net Oxide Change	-13.40	10.86	7.04	-44.34	-21.61	9.44	-8.40	7.85	-16.32	11.01
Ba	-190.39	-439.82	-14.35	-1140.48	823.63	-1170.62	-66.22	-66.99	-68.96	-22.62
Sr	0.11	-2.22	-9.09	1.26	-0.16	-16.12	-13.64	-14.29	-10.85	-3.42
Y	6.98	1.73	5.12	8.89	-1.79	5.65	7.46	1.77	3.75	5.13
Sc	0.61	0.47	1.84	1.63	6.18	1.75	3.01	2.12	2.08	2.77
Zr	14.16	8.60	18.58	26.05	-9.11	25.39	17.61	-1.75	1.82	19.90
Be	-0.12	-0.42	0.08	-0.66	-0.60	-0.41	-0.07	0.10	-0.54	-0.42
V	2.81	9.14	5.03	5.03	31.47	12.78	4.00	6.32	-0.18	17.24
Hg	4.80	14.76	-2.31	34.53	4.18	-4.95	-4.57	-9.25	297.44	14.71
Cr 52	-0.52	0.73	10.22	-1.41	-0.85	6.23	-0.32	0.45	-0.31	8.95
Co	1.07	10.01	-0.63	10.12	-0.35	8.29	1.78	3.75	4.50	1.20
Ni	-0.58	0.82	0.38	-1.58	-0.96	0.88	-0.35	0.51	-0.35	0.81
Cu	-38.96	237.23	-59.69	52.76	-75.80	-37.73	133.89	355.22	17.91	1271.84
Zn	53.85	-0.77	-10.13	608.41	41.88	86.89	-89.62	-86.52	-10.05	-68.97
As	3.68	18.88	11.30	52.08	-1.47	1.04	8.01	1.82	14.50	10.21
Se 78	-1.55	2.19	1.02	-4.22	-2.55	2.34	-0.95	1.36	-0.94	2.15
Br 79	39.67	97.84	89.68	-11.26	0.30	120.43	43.96	75.68	-43.40	-10.50
Mo	2.25	7.20	5.88	1.62	3.38	5.23	3.20	3.44	6.53	3.16
Ag 107	-0.06	0.08	0.04	-0.16	-0.10	0.09	-0.04	0.05	-0.04	0.08
Cd	-0.05	0.07	0.03	1.70	-0.09	0.08	-0.03	0.05	-0.03	0.07
Sn	-0.77	0.62	-2.14	-3.24	-0.93	-1.84	-1.32	-0.87	-1.46	-0.20
Sb	0.76	0.77	0.41	0.06	-0.26	0.27	0.74	1.58	5.83	1.01
Te	-0.25	4.75	0.16	-0.68	-0.41	0.38	-0.15	0.22	-0.15	0.35
I	-2.14	3.03	1.41	-5.84	-3.54	3.24	-1.31	1.89	-1.31	2.98
W	2.87	9.84	4.65	2.79	3.97	0.92	2.40	2.76	0.27	11.31
Pb	-1.47	26.07	0.96	-4.00	-2.42	2.22	13.53	1.29	-0.90	2.04
Bi	0.25	9.38	0.33	2.45	0.08	1.56	0.64	0.16	4.65	4.05
Nb	2.37	3.74	4.51	4.57	2.60	4.71	4.11	2.52	1.46	1.50
La	-3.12	-2.35	0.64	-1.72	-4.95	1.42	0.31	0.22	-2.50	0.89
Ce	-6.83	-5.75	0.80	-5.96	-11.28	2.85	0.91	-1.41	-5.92	-0.74
Pr	-0.79	-0.77	0.13	-0.80	-1.35	0.44	0.16	-0.20	-0.52	0.00
Nd	-3.41	-2.36	0.86	-2.70	-5.45	2.83	0.62	-1.48	-1.90	0.45
Sm	-0.68	-0.71	0.27	-0.51	-1.18	0.89	0.16	-0.67	-0.33	0.12
Eu	-0.34	-0.53	-0.18	-0.38	0.41	-0.21	-0.19	-0.04	-0.15	-0.39
Tb	0.01	-0.07	0.03	0.14	-0.13	0.14	0.15	-0.03	0.08	0.04
Dy	0.54	-0.01	0.49	1.29	-0.46	0.95	1.19	-0.34	0.71	0.34
Ho	0.01	-0.10	0.06	0.20	-0.19	0.19	0.17	-0.14	0.02	-0.04
Er	0.04	-0.26	0.13	0.60	-0.40	0.38	0.60	-0.36	0.16	-0.02
Tm	0.02	-0.02	0.05	0.09	-0.06	0.07	0.07	-0.02	0.01	0.02
Yb	0.06	-0.24	0.25	0.58	-0.67	0.42	0.45	-0.37	-0.24	-0.04
Lu	0.03	-0.08	0.01	0.08	-0.12	0.05	0.07	-0.07	-0.01	0.00
Hf	-0.44	0.54	2.45	0.15	0.48	0.88	1.01	0.62	1.12	0.34
Ta	0.06	0.10	0.14	0.15	0.07	0.13	0.12	0.08	0.04	0.04
Th	-0.14	3.58	2.77	2.78	1.01	3.39	1.93	1.12	0.33	0.37

Abbreviations:

Units

HFL= Hanging wall flow
HBX= Hanging wall breccia
FLT= Footwall lapilli tuff
FT= Footwall tuff
FBX= Footwall breccia
FFL= Footwall flow
INT= Intrusion

Alteration

Qtz-Ser= Quartz-sericite
Chl-Ser= Chlorite-sericite
Chl= Chlorite

Appendix C: Table C.1.2 Mass changes for samples at the Boundary deposit

Sample ID	H501224	H501225	H501226	H501227	H501228	H501229	H501230	H501231	H501232	H501233
Hole ID	BD10-50	BD10-56	BD10-56	BD10-56	BD10-56	BD10-56	BD10-49	BD10-49	BD10-49	BD10-49
Depth (m)	30.6	7.4	21.2	29.9	41.4	49.2	10.9	11.8	25	34.6
Lithology	FLT	FLT	FLT	FLT	FLT	FLT	FLT	FFL	FLT	FLT
Alteration	Qtz-Ser	Qtz-Ser	Chl	Chl	Chl-Ser	Chl-Ser	Qtz-Ser	Qtz-Ser	Qtz-Ser	Qtz-Ser
SiO_2	-4.88	-13.01	-53.11	-31.09	18.31	13.48	8.60	7.40	-6.13	-9.37
$A_{l2}O_3$	0.00	0.00	0.00	0.00	0.00	0.00	0.00	0.00	0.00	0.00
FeO	2.23	-0.10	3.40	24.37	10.57	13.38	4.17	1.29	3.07	6.04
MnO	-0.01	-0.07	0.13	0.03	-0.03	-0.08	-0.07	-0.06	0.05	-0.02
MgO	0.16	0.07	15.14	11.09	-0.57	-1.78	-1.65	-1.06	1.14	-0.35
CaO	-0.09	-0.10	0.78	0.04	-0.09	-0.08	-0.10	-0.10	-0.03	-0.04
Na_2O	-1.80	-1.78	-2.02	-1.99	-1.76	-1.76	-1.78	-1.80	-1.83	-1.79
K_2O	0.45	0.45	-2.34	-2.20	0.55	0.95	0.92	0.73	0.29	0.56
TiO_2	0.04	0.01	0.03	0.04	0.04	0.04	0.04	0.02	0.19	0.03
P_2O_5	0.02	0.01	0.06	0.01	0.00	0.00	0.00	0.00	0.05	0.08
Net Oxide Change	-3.88	-14.52	-37.93	0.30	27.01	24.16	10.14	6.41	-3.20	-4.87
Ba	-390.00	615.52	-1388.36	-1321.98	-72.13	-73.86	68.80	-70.43	-466.20	-113.04
Sr	-11.18	-4.07	2.88	-17.01	-10.99	-12.37	-10.57	-11.23	-11.01	-10.87
Y	2.31	-3.14	12.07	5.88	6.40	6.39	6.72	-0.23	-3.05	1.47
Sc	1.80	1.95	0.48	2.47	2.38	2.38	2.57	1.85	6.98	2.14
Zr	-6.32	-11.81	-10.77	10.83	-1.92	11.80	11.60	6.85	-27.15	5.74
Be	-0.02	-0.15	-0.67	-0.38	-0.31	-0.31	-0.43	-0.46	-0.50	-0.49
V	3.40	11.16	5.36	0.62	0.94	0.94	4.36	0.19	68.41	3.57
Hg	-9.54	6.78	-1.52	93.97	131.08	27.89	7.43	-9.31	-1.01	10.26
Cr 52	-0.07	-0.65	-1.54	1.10	1.67	1.67	10.34	0.34	21.42	7.76
Co	2.44	-0.73	-0.27	57.77	0.43	1.96	7.21	2.75	8.27	3.57
Ni	-0.08	-0.73	-1.73	1.23	1.88	1.88	0.72	0.38	15.38	0.06
Cu	-50.29	-63.88	-55.51	591.79	4282.46	3287.11	5525.18	185.41	100.64	310.33
Zn	-67.89	-58.70	160.30	7.92	55.82	-34.25	-31.27	-66.07	-55.97	-33.36
As	7.20	1.59	-0.83	55.25	63.72	42.46	4.04	3.30	17.93	25.91
Se 78	-0.22	-1.95	-4.61	49.23	5.02	5.01	1.91	1.03	-0.02	0.16
Br 79	-31.61	-41.63	-83.38	12.90	6.60	7.93	10.15	0.12	-17.81	-14.30
Mo	4.88	0.36	2.15	37.82	6.12	7.22	9.52	6.40	5.56	7.95
Ag 107	-0.01	-0.07	-0.17	0.12	0.19	0.19	1.11	0.04	0.00	0.01
Cd	-0.01	-0.07	-0.16	0.11	0.17	0.17	0.06	0.03	0.00	0.01
Sn	-1.43	-0.47	-3.14	0.55	0.61	1.17	1.83	0.92	1.50	3.42
Sb	0.84	0.12	5.26	10.46	6.43	1.28	0.06	-0.34	2.28	5.56
Te	-0.04	-0.31	-0.74	5.69	4.12	0.81	3.01	0.17	2.75	4.66
I	-0.30	-2.70	-6.39	4.56	6.95	6.94	2.65	1.42	-0.02	0.22
W	0.39	1.90	-0.55	2.82	4.60	3.73	3.52	2.43	5.00	2.17
Pb	-0.21	-1.85	-4.37	3.12	4.76	4.75	1.81	0.97	-0.02	49.43
Bi	0.49	-0.11	-0.02	17.96	11.08	6.38	11.70	3.63	3.39	8.17
Nb	1.31	1.20	1.44	9.59	2.16	0.79	-0.31	-0.84	-1.08	-0.77
La	-0.34	-0.36	0.84	5.09	-3.81	-1.27	-5.37	-6.54	-3.52	-6.19
Ce	-1.83	-2.47	0.21	9.76	-9.03	-3.31	-11.10	-14.59	-7.90	-14.22
Pr	-0.14	-0.20	0.03	1.30	-1.10	-0.39	-1.36	-1.73	-0.89	-1.73
Nd	-0.52	-0.28	0.72	6.58	-4.61	-0.95	-5.59	-7.47	-4.01	-7.07
Sm	0.14	0.12	0.22	1.68	-0.21	0.63	-0.76	-1.63	-0.79	-1.46
Eu	-0.08	0.12	0.31	-0.01	0.09	0.27	-0.31	-0.72	-0.74	0.18
Tb	0.07	-0.06	0.25	0.34	0.16	0.17	-0.15	-0.25	-0.22	-0.20
Dy	0.68	-0.33	1.92	2.64	1.38	1.19	-0.74	-1.49	-1.36	-1.07
Ho	0.06	-0.14	0.39	0.50	0.12	0.02	-0.35	-0.36	-0.34	-0.28
Er	0.13	-0.34	1.03	0.08	0.16	-0.34	-0.91	-0.57	-0.81	0.03
Tm	0.04	-0.04	0.13	0.26	0.09	0.04	-0.17	-0.15	-0.12	-0.11
Yb	-0.06	-0.45	0.60	1.71	0.37	0.06	-1.15	-1.14	-0.94	-0.92
Lu	0.00	-0.04	0.10	0.27	0.18	0.10	-0.11	-0.18	-0.12	-0.14
Hf	0.51	0.35	-0.47	3.35	0.57	0.53	-0.43	-1.81	-1.54	-1.94
Ta	0.05	0.03	0.03	0.29	0.07	0.04	-0.02	-0.05	-0.04	-0.06
Th	0.12	-0.08	0.39	4.58	0.24	-0.25	-1.20	-1.59	-1.16	-1.75

Abbreviations:

Units

HFL= Hanging wall flow
HBX= Hanging wall breccia
FLT= Footwall lapilli tuff
FT= Footwall tuff
FBX= Footwall breccia
FFL= Footwall flow
INT= Intrusion

Alteration

Qtz-Ser= Quartz-sericite
Chl-Ser= Chlorite-sericite
Chl= Chlorite

Appendix C: Table C.1.2 Mass changes for samples at the Boundary deposit

Sample ID	**H501234**	**H501235**	**H501236**	**H501237**	**H501238**	**H501239**	**H501240**	**H501241**	**H501242**	**H501243**
Hole ID	BD10-34	BD10-34	BD10-34	BD10-34	BD10-33	BD10-33	BD10-33	BD10-33	BD10-33	BD10-45
Depth (m)	11.5	26	33.6	18.6	9.5	18.3	27.1	36.3	46.2	8.1
Lithology	HFL	HBX	FLT	HFL	HFL	FLT	HBX	FLT	FFL	HFL
Alteration	Qtz-Ser	Qtz-Ser	Qtz-Ser	Qtz-Ser	Chl-Ser	Qtz-Ser	Qtz-Ser	Qtz-Ser	Qtz-Ser	Qtz-Ser
SiO_2	-16.28	-4.36	13.61	3.43	-29.60	2.18	-9.17	-15.45	19.03	-37.35
Al_2O_3	0.00	0.00	0.00	0.00	0.00	0.00	0.00	0.00	0.00	0.00
FeO	3.70	-0.38	1.05	1.98	1.12	0.93	0.87	3.74	3.20	1.71
MnO	0.01	-0.04	0.00	0.10	0.15	-0.02	0.03	0.00	0.01	0.03
MgO	-0.83	-0.88	-0.66	0.92	1.63	-0.56	-0.21	-0.77	0.55	0.13
CaO	-0.09	-0.09	0.29	-0.09	-0.03	-0.09	-0.01	0.27	-0.09	-0.10
Na_2O	-1.84	-1.82	-1.82	-1.82	-1.89	-1.86	-1.86	-1.81	-1.83	-1.79
K_2O	0.87	0.96	1.02	0.62	0.70	0.78	0.93	0.74	0.55	0.51
TiO_2	0.01	0.01	0.04	0.01	0.00	0.05	0.00	0.15	0.02	0.00
P_2O_5	0.01	0.01	0.01	0.00	0.01	0.01	0.02	0.05	0.01	0.01
Net Oxide Change	-14.45	-6.59	13.54	5.14	-27.92	1.42	-9.41	-13.09	21.46	-36.84
Ba	-293.23	-281.50	-511.90	-539.30	-577.18	9.66	-119.33	1300.68	-509.14	195.42
Sr	-15.75	-10.84	-7.10	-12.36	-16.14	-13.81	-12.85	-5.68	-13.27	-9.03
Y	3.84	3.79	3.40	1.70	4.19	-1.13	34.17	-1.83	4.63	-5.27
Sc	-0.18	-0.70	2.60	-0.36	0.25	2.28	1.89	4.50	2.47	-0.27
Zr	4.05	1.97	9.70	-0.39	-6.65	-7.84	17.80	-28.06	3.36	-4.90
Be	-0.11	-0.07	0.15	0.07	-0.27	0.02	-0.09	-0.09	-0.38	-0.35
V	-0.27	4.01	5.52	0.18	-0.67	13.88	-0.21	52.80	0.62	-0.88
Hg	764.50	8.46	120.93	141.17	-4.68	105.71	5.38	7.94	57.81	-6.81
Cr 52	4.23	5.90	0.65	5.87	-1.19	0.10	-0.38	20.60	1.10	-1.56
Co	-0.71	-0.69	0.56	-0.63	-0.78	-0.65	-0.70	4.54	-0.55	-0.82
Ni	-0.54	-0.35	0.73	0.36	-1.34	0.12	-0.43	4.22	1.23	-1.76
Cu	338.38	-74.66	1639.50	37.74	-60.67	101.65	-64.64	1137.09	364.96	-77.30
Zn	8802.89	3.76	1123.55	1429.84	-52.46	2095.01	110.63	-40.17	468.53	-43.04
As	31.72	18.64	7.26	1.26	-0.02	4.32	0.91	17.12	12.14	-0.86
Se 78	-1.43	-0.93	1.95	0.95	-3.58	0.31	-1.14	-1.25	3.29	-4.69
Br 79	57.98	79.24	-2.07	98.64	-66.89	-28.70	-66.17	-59.52	1.30	-85.87
Mo	2.97	7.84	0.85	1.54	0.77	0.01	4.13	2.31	1.84	1.62
Ag 107	-0.05	-0.03	1.20	0.04	-0.13	2.26	-0.04	1.23	0.12	-0.18
Cd	32.22	0.63	3.97	4.38	-0.12	5.93	0.61	0.43	1.72	-0.16
Sn	-0.22	-1.27	1.31	-0.60	-2.15	4.71	-1.38	-0.36	-0.54	-2.31
Sb	2.09	17.21	1.51	0.74	0.26	7.22	0.38	1.06	3.47	-0.02
Te	-0.23	-0.15	0.31	0.15	-0.58	2.33	-0.18	-0.20	0.53	-0.76
I	-1.99	-1.29	2.70	1.32	-4.96	0.44	-1.58	-1.73	4.56	-6.50
W	1.08	0.93	5.81	0.95	0.22	2.97	1.42	5.62	0.95	-0.59
Pb	49.67	-0.88	377.69	0.90	-3.39	2446.52	-1.08	44.39	181.75	-4.45
Bi	0.60	-0.11	1.51	-0.12	-0.11	0.13	0.18	1.40	1.08	-0.11
Nb	-0.57	1.32	1.97	-0.29	-1.62	3.65	0.74	1.25	2.56	-2.06
La	-3.82	-2.20	0.77	-2.88	-8.11	0.96	-3.91	-1.59	0.26	-8.72
Ce	-8.38	-5.40	2.00	-6.07	-18.22	1.61	-9.18	-3.81	0.93	-19.30
Pr	-0.92	-0.68	0.34	-0.67	-2.24	0.20	-1.08	-0.40	0.19	-2.39
Nd	-3.99	-2.67	2.69	-2.84	-8.77	0.73	-3.93	-0.93	1.40	-9.87
Sm	-0.78	-0.40	0.66	-0.37	-2.07	1.72	-1.06	0.03	0.40	-2.41
Eu	-0.41	-0.10	0.05	-0.14	-0.51	0.52	-0.13	-0.13	-0.07	-0.60
Tb	-0.14	0.03	0.16	-0.07	-0.33	0.53	-0.16	0.25	0.18	-0.47
Dy	-0.63	0.79	1.58	-0.30	-2.01	3.75	-0.88	2.23	1.73	-2.93
Ho	-0.17	0.18	0.39	-0.11	-0.43	0.55	-0.18	0.69	0.48	-0.64
Er	0.35	0.26	-0.05	0.08	-0.08	-0.03	2.71	-0.34	0.44	-0.55
Tm	-0.06	0.08	0.25	-0.05	-0.20	0.28	-0.06	0.43	0.21	-0.27
Yb	-0.55	0.48	1.27	-0.50	-1.48	1.83	-0.73	2.84	1.11	-2.17
Lu	-0.11	0.02	0.18	-0.08	-0.26	0.39	-0.12	0.45	0.15	-0.33
Hf	-0.92	-0.80	0.42	-0.85	-1.79	1.41	-0.24	0.25	0.36	-2.64
Ta	-0.04	0.03	0.08	-0.01	-0.06	0.18	0.02	0.03	0.06	-0.09
Th	-0.98	0.11	1.02	-0.65	-1.89	1.25	-0.79	0.02	0.79	-2.50

Abbreviations:

Units

HFL= Hanging wall flow
HBX= Hanging wall breccia
FLT= Footwall lapilli tuff
FT= Footwall tuff
FBX= Footwall breccia
FFL= Footwall flow
INT= Intrusion

Alteration

Qtz-Ser= Quartz-sericite
Chl-Ser= Chlorite-sericite
Chl= Chlorite

Appendix C: Table C.1.2 Mass changes for samples at the Boundary deposit

Sample ID	**H501244**	**H501245**	**H501246**	**H501247**	**H501248**	**H501249**	**H501250**	**H501251**	**H501252**	**H501253**
Hole ID	BD10-45	BD10-45	BD10-45	BD10-28	BD10-28	BD10-28	BD11-127	BD11-127	BD11-127	BD11-127
Depth (m)	18.4	31.4	46.7	6	20.4	34.3	6.7	16.4	21.1	37.9
Lithology	HFL	FLT	FBX	FLT	FLT	FLT	HBX	HBX	FLT	FLT
Alteration	Qtz-Ser	Qtz-Ser	Qtz-Ser	Qtz-Ser	Qtz-Ser	Chl-Ser	Qtz-Ser	Qtz-Ser	Qtz-Ser	Qtz-Ser
SiO_2	9.46	-3.22	-8.32	15.98	-11.50	7.32	9.13	-6.47	6.56	-2.95
Al_2O_3	0.00	0.00	0.00	0.00	0.00	0.00	0.00	0.00	0.00	0.00
FeO	3.11	3.84	1.53	2.99	0.27	4.01	0.60	2.44	2.36	2.21
MnO	-0.02	-0.03	0.00	0.13	0.02	0.25	0.04	0.01	0.02	0.08
MgO	-0.90	-1.09	0.03	2.26	-1.27	2.26	0.25	-0.21	-0.41	1.49
CaO	-0.09	-0.06	-0.11	-0.09	1.08	0.99	0.04	-0.10	-0.10	-0.08
Na_2O	-1.76	-1.76	-1.82	-1.94	-1.90	-1.91	-1.74	-1.72	-1.72	-1.63
K_2O	0.49	0.94	0.54	0.50	1.41	0.51	0.90	0.82	0.91	0.47
TiO_2	0.00	0.03	0.02	0.03	0.03	0.13	0.00	0.00	0.04	0.04
P_2O_5	0.02	0.02	0.02	0.00	0.00	0.03	0.00	0.00	0.00	0.01
Net Oxide Change	10.32	-1.33	-8.10	19.86	-11.87	13.59	9.24	-5.22	7.67	-0.36
Ba	2659.51	-239.30	-501.74	-1017.34	-875.81	-922.31	-460.07	-514.62	-460.60	-694.04
Sr	-7.25	-7.65	-14.53	-17.09	-8.74	-6.71	-9.92	-8.39	-8.80	-4.69
Y	-9.51	-1.07	3.04	6.45	3.43	-6.07	0.54	4.75	-2.69	5.81
Sc	0.21	2.30	2.15	1.06	2.38	6.46	-0.11	0.69	2.10	3.24
Zr	0.19	-3.53	-1.12	3.65	5.29	-17.99	-2.21	5.68	5.75	0.64
Be	0.13	0.03	-0.07	0.23	-0.12	-0.41	0.10	-0.03	0.10	0.02
V	0.34	4.68	-0.16	0.57	-0.29	63.36	0.25	-0.07	9.60	5.65
Hg	-6.33	5.43	-9.66	5.20	-2.28	31.51	85.76	68.69	5.61	5.31
Cr 52	0.60	0.11	-0.29	1.02	-0.52	17.18	0.44	7.61	6.71	0.08
Co	0.51	1.57	-0.69	-0.56	-0.71	8.11	-0.62	0.06	3.13	0.61
Ni	0.67	0.13	-0.33	1.14	-0.58	10.56	0.49	-0.14	0.50	0.09
Cu	-72.75	1393.74	242.46	-71.87	-75.09	-72.36	23.73	339.91	45.48	-73.84
Zn	-51.97	-83.17	-86.60	10.61	-64.91	88.80	236.74	538.57	-18.86	15.51
As	1.61	5.46	2.45	3.20	6.36	9.26	3.16	5.70	9.31	2.44
Se 78	1.79	0.34	-0.88	3.05	-1.55	2.35	1.31	-0.37	1.34	0.25
Br 79	-23.99	-31.14	-31.29	138.52	55.47	105.03	74.95	83.49	93.79	68.26
Mo	1.80	6.39	3.35	15.21	3.83	7.20	3.67	7.20	2.16	3.66
Ag 107	0.07	0.01	-0.03	0.11	-0.06	0.09	0.05	-0.01	0.05	0.01
Cd	0.06	0.01	-0.03	0.10	-0.05	0.08	0.96	0.98	0.05	0.01
Sn	0.20	0.87	-2.22	-1.32	-1.85	-1.60	-2.40	-0.95	-1.19	-1.38
Sb	0.29	0.59	0.68	1.05	0.44	0.79	54.66	1.46	2.14	0.63
Te	0.29	0.05	-0.14	0.49	-0.25	0.38	0.21	-0.06	0.22	0.04
I	2.48	0.47	-1.22	4.23	-2.15	3.26	1.82	-0.52	1.86	0.34
W	0.72	1.39	2.32	0.09	0.68	0.93	0.62	1.36	1.99	1.34
Pb	1.70	12.27	-0.83	2.89	-1.47	2.23	1.25	18.38	1.27	0.23
Bi	0.85	3.81	0.11	1.71	0.50	1.62	0.37	0.30	2.11	0.30
Nb	5.57	0.52	1.55	3.03	-1.10	3.22	-1.22	-0.28	1.36	-0.39
La	5.65	-2.00	0.23	3.49	-5.51	5.42	-4.87	-4.44	0.45	-2.85
Ce	11.53	-5.65	-0.33	6.56	-12.92	11.75	-10.59	-9.53	-0.53	-5.95
Pr	1.53	-0.65	-0.02	0.63	-1.57	1.50	-1.24	-1.06	0.01	-0.67
Nd	7.25	-2.32	0.42	3.13	-6.55	6.67	-4.84	-4.21	0.49	-3.03
Sm	1.66	-0.72	-0.19	0.19	-1.62	1.53	-1.27	-1.05	-0.02	-0.67
Eu	-0.16	-0.79	-0.49	0.06	0.01	0.63	0.11	-0.71	-0.13	-0.37
Tb	0.42	-0.22	-0.09	0.35	-0.19	0.32	-0.26	-0.13	0.23	-0.08
Dy	3.23	-1.23	-0.51	2.67	-1.12	2.79	-1.30	-0.64	1.94	-0.45
Ho	0.71	-0.30	-0.09	0.44	-0.24	0.52	-0.35	-0.28	0.29	-0.25
Er	-0.40	0.11	-0.13	0.56	0.27	-0.67	-0.39	0.32	-0.32	0.11
Tm	0.40	-0.13	-0.01	0.22	-0.13	0.30	-0.11	-0.10	0.12	-0.10
Yb	2.66	-0.91	-0.48	1.40	-1.18	2.04	-1.03	-0.79	0.75	-0.86
Lu	0.36	-0.17	-0.08	0.11	-0.21	0.28	-0.15	-0.15	0.14	-0.14
Hf	1.80	-0.43	-0.91	0.21	-2.64	0.40	-1.46	-1.27	-0.16	-1.15
Ta	0.24	0.02	0.03	0.07	-0.06	0.09	-0.05	-0.02	0.04	-0.03
Th	3.52	-0.45	-0.02	1.44	-1.68	1.68	-1.27	-0.68	0.46	-0.61

Abbreviations:

Units

HFL= Hanging wall flow
HBX= Hanging wall breccia
FLT= Footwall lapilli tuff
FT= Footwall tuff
FBX= Footwall breccia
FFL= Footwall flow
INT= Intrusion

Alteration

Qtz-Ser= Quartz-sericite
Chl-Ser= Chlorite-sericite
Chl= Chlorite

Appendix C: Table C.1.2 Mass changes for samples at the Boundary deposit

Sample ID	**H501254**	**H501255**	**H501256**	**H501257**	**H501258**	**H501259**	**H501260**	**H501261**	**H501262**	**H501263**
Hole ID	BD11-127	BD11-128	BD11-128	BD11-128	BD11-116	BD11-116	BD11-116	BD11-116	BD11-116	BD11-120
Depth (m)	46.5	12.6	15.5	26.5	13.6	16.8	29.2	38.1	49.7	9.4
Lithology	FFL	HFL	FLT	FLT	FLT	FT	FLT	FT	FLT	HFL
Alteration	Qtz-Ser	Qtz-Ser	Qtz-Ser	Qtz-Ser	Qtz-Ser	Qtz-Ser	Chl-Ser	Qtz-Ser	Qtz-Ser	Qtz-Ser
SiO_2	5.33	-2.90	7.16	16.28	-19.27	9.42	11.09	-26.20	-1.52	48.96
$A_{l2}O_3$	0.00	0.00	0.00	0.00	0.00	0.00	0.00	0.00	0.00	0.00
FeO	0.90	0.31	1.80	2.10	1.75	2.50	9.97	2.83	28.90	2.13
MnO	0.02	-0.02	0.09	-0.04	-0.04	-0.02	-0.04	-0.06	-0.04	-0.03
MgO	-0.54	-1.17	0.93	-1.34	-0.79	0.36	0.43	-0.81	-1.93	-1.15
CaO	-0.05	0.15	0.39	-0.08	-0.12	-0.10	-0.09	-0.09	-0.12	-0.01
Na_2O	-1.64	-1.81	-1.80	-1.80	-1.81	-1.84	-1.84	-1.82	-1.79	-1.82
K_2O	0.97	1.12	0.86	1.09	0.76	0.35	0.29	0.83	0.98	0.88
TiO_2	0.03	0.00	0.06	0.03	0.05	0.00	0.02	0.11	0.02	0.01
P_2O_5	0.01	0.04	0.04	0.03	0.00	0.01	0.00	0.02	0.00	0.00
Net Oxide Change	5.03	-4.29	9.52	16.26	-19.48	10.69	19.83	-25.20	24.49	48.97
Ba	-429.21	-761.80	-803.57	-702.62	713.91	625.96	200.21	285.02	382.02	-179.58
Sr	-6.11	-9.52	-3.08	-11.35	-12.13	-12.95	-14.21	-13.46	-12.80	-11.42
Y	3.37	1.33	2.19	0.06	-4.44	1.75	-7.85	-1.74	-0.65	6.33
Sc	1.65	-0.40	4.47	1.84	2.34	0.19	0.38	3.97	3.80	0.58
Zr	11.78	6.71	7.50	13.59	0.63	-1.25	15.95	-19.25	17.59	3.07
Be	0.06	-0.04	0.11	0.18	-0.18	-0.43	-0.35	-0.22	-0.23	-0.24
V	0.15	-0.10	17.54	0.46	9.84	0.33	0.74	41.75	1.33	1.28
Hg	-0.35	-9.60	-0.87	234.17	80.97	16.30	8.77	59.42	1192.08	34.84
Cr 52	5.57	-0.18	6.34	26.52	2.95	13.34	1.33	32.62	2.38	15.81
Co	-0.63	-0.06	1.58	1.00	0.50	-0.60	1.24	6.77	18.20	-0.43
Ni	0.30	-0.20	0.57	15.82	-0.89	0.66	1.49	11.21	2.67	2.55
Cu	390.96	-12.51	-72.95	-57.76	-28.71	40.18	153.80	644.48	112.62	1185.26
Zn	-102.64	-102.58	-50.69	1414.95	-59.82	-7.45	-71.38	-75.46	-104.01	-1.04
As	2.23	6.25	5.00	9.42	20.14	4.16	17.08	36.95	242.04	37.92
Se 78	0.79	-0.53	1.51	2.45	-2.37	1.76	3.98	-2.99	7.13	6.82
Br 79	111.80	-54.16	-51.10	36.84	17.51	123.19	166.12	22.03	196.48	252.15
Mo	4.61	1.76	2.82	12.40	7.82	4.40	27.81	4.93	49.90	11.15
Ag 107	0.03	-0.02	0.06	0.09	-0.09	0.07	0.15	0.90	9.01	0.26
Cd	0.03	-0.02	0.05	4.97	-0.08	0.06	0.13	0.30	0.24	0.23
Sn	-1.61	-2.25	-1.45	-1.87	-0.82	0.56	0.13	-1.71	1.61	0.69
Sb	3.21	0.68	0.76	0.96	10.10	1.53	1.48	8.33	299.83	16.09
Te	0.13	-0.09	0.24	0.39	-0.38	0.28	0.64	-0.48	27.10	1.10
I	1.10	-0.74	2.09	3.40	-3.28	2.44	5.51	-4.14	9.88	9.45
W	7.21	1.29	1.02	1.20	2.68	0.51	1.34	5.04	3.22	4.13
Pb	0.75	-0.50	1.43	2.32	-2.24	35.98	3.77	13.18	56.01	6.47
Bi	-0.02	0.23	0.30	1.26	2.09	0.16	2.89	0.45	64.44	2.62
Nb	0.77	5.31	1.99	1.50	-1.13	9.09	7.21	0.03	10.36	4.36
La	-1.42	-5.67	2.67	-2.51	-8.00	4.12	0.70	-7.38	13.06	-0.67
Ce	-4.20	-11.09	4.42	-5.91	-17.44	8.73	1.38	-15.92	28.09	-2.10
Pr	-0.35	-1.27	0.45	-0.71	-2.18	1.18	0.29	-1.97	3.61	-0.31
Nd	-1.16	-6.06	1.89	-2.33	-8.88	4.60	1.25	-8.86	15.54	-1.93
Sm	0.00	-1.04	-0.62	-0.84	-2.43	0.98	0.27	-2.17	4.28	-0.37
Eu	-0.18	-0.31	-0.34	-0.18	-0.47	0.16	0.07	-0.44	1.14	0.17
Tb	0.20	-0.19	0.08	0.04	-0.39	0.10	0.06	-0.49	0.92	0.02
Dy	1.44	-0.90	0.96	0.39	-2.38	1.16	0.68	-3.23	6.46	0.43
Ho	0.16	-0.17	0.07	-0.01	-0.59	0.17	0.08	-0.75	1.23	-0.01
Er	0.08	-0.26	-0.22	-0.48	-0.77	-0.31	-0.80	-0.20	0.09	0.17
Tm	0.09	-0.06	0.07	0.02	-0.23	0.15	0.10	-0.35	0.65	0.02
Yb	0.39	-0.64	0.26	-0.05	-1.78	0.64	0.47	-2.53	4.13	0.07
Lu	0.03	-0.11	-0.01	-0.08	-0.32	0.09	0.08	-0.40	0.67	0.00
Hf	-0.53	-0.72	-0.24	-1.00	-1.80	1.96	1.34	-1.65	4.64	1.03
Ta	0.01	0.08	0.05	0.02	-0.07	0.21	0.14	-0.08	0.32	0.04
Th	-0.25	1.66	0.60	-0.19	-2.04	4.62	3.15	-0.82	5.30	0.23

Abbreviations:

Units

HFL= Hanging wall flow
HBX= Hanging wall breccia
FLT= Footwall lapilli tuff
FT= Footwall tuff
FBX= Footwall breccia
FFL= Footwall flow
INT= Intrusion

Alteration

Qtz-Ser= Quartz-sericite
Chl-Ser= Chlorite-sericite
Chl= Chlorite

Appendix C: Table C.1.2 Mass changes for samples at the Boundary deposit

Sample ID	H501264	H501265	H501266	H501267	H501268	H501269	H501270	H501271	H501272	H501273
Hole ID	BD11-120	BD11-120	BD10-88	BD10-7	BD10-7	BD10-7	BD10-22	BD10-22	BD10-22	BD10-22
Depth (m)	34.7	42.2	33.5	11.2	17.7	27.8	4.6	13.9	17.9	23.1
Lithology	HBX	HFL	FLT	FLT	FLT	FLT	HBX	FLT	FFL	FLT
Alteration	Qtz-Ser	Chl-Ser	Chl	Qtz-Ser	Chl	Chl	Chl-Ser	Qtz-Ser	Qtz-Ser	Qtz-Ser
SiO_2	11.79	-14.24	-43.07	-10.75	-27.93	-60.10	-17.45	-6.97	-10.11	-2.14
Al_2O_3	0.00	0.00	0.00	0.00	0.00	0.00	0.00	0.00	0.00	0.00
FeO	3.70	3.23	10.95	2.92	34.45	12.33	2.66	1.54	0.43	1.95
MnO	0.03	0.06	0.04	-0.09	0.34	0.01	0.08	0.00	0.13	-0.02
MgO	-0.21	0.68	6.68	-1.57	11.63	12.03	4.97	-0.79	0.17	-1.27
CaO	0.09	0.55	-0.08	-0.14	0.12	-0.12	-0.11	-0.11	-0.11	-0.01
Na_2O	-1.81	-1.80	-1.79	-1.88	-2.02	-2.03	-1.95	-1.89	-1.87	0.14
K_2O	0.77	0.58	-1.37	1.06	-2.30	-2.36	-0.46	1.04	0.90	0.20
TiO_2	0.06	0.06	0.06	0.02	0.01	0.03	0.03	0.03	0.04	0.02
P_2O_5	0.00	0.02	0.01	0.01	0.13	0.01	0.02	0.02	0.00	0.00
Net Oxide Change	14.43	-10.87	-28.56	-10.41	14.44	-40.20	-12.20	-7.12	-10.43	-1.15
Ba	-115.74	-292.25	-1134.48	209.97	-1387.16	-1402.23	366.68	1350.95	490.91	-85.48
Sr	-10.19	-4.45	3.54	-14.60	-19.02	-21.28	-18.38	-14.45	-12.10	4.21
Y	5.89	-0.21	-4.40	8.18	-1.78	8.61	1.70	-2.18	4.20	-0.70
Sc	2.99	2.01	0.71	2.03	3.40	5.15	0.85	2.27	2.60	2.10
Zr	10.92	8.32	6.59	12.26	-8.02	24.51	1.53	7.96	6.19	-2.87
Be	-0.41	-0.54	-0.59	-0.54	-0.26	-0.64	-0.10	-0.06	-0.10	0.01
V	11.67	3.97	9.03	-0.19	1.22	-0.70	3.83	18.27	3.80	4.56
Hg	9.26	8.32	-4.59	714.19	41.60	1.70	14.23	1272.11	73.50	1389.14
Cr 52	0.81	7.41	7.37	28.06	43.21	16.94	4.58	-0.25	-0.45	0.04
Co	0.93	3.49	12.38	0.32	510.87	28.50	8.47	0.84	-0.71	2.62
Ni	11.32	-0.38	-0.88	14.68	24.17	9.04	-0.48	-0.28	-0.50	0.04
Cu	778.66	321.26	-75.66	59.53	27140.09	129.86	188.91	2615.62	81.49	700.50
Zn	-57.77	-37.39	9.58	5677.54	5949.08	142.57	121.91	7843.03	414.85	6627.82
As	119.39	6.10	7.65	15.14	119.72	4.48	5.06	11.86	-1.40	44.18
Se 78	2.42	-1.02	-2.35	14.52	68.96	-3.72	-1.27	-0.74	-1.34	0.11
Br 79	4.32	70.08	12.55	42.97	119.54	-23.03	42.36	44.67	53.33	127.02
Mo	42.86	7.78	14.85	8.15	9.85	16.34	4.91	2.33	2.51	6.48
Ag 107	0.09	-0.04	-0.09	-0.04	3.18	0.24	0.44	7.20	-0.05	0.00
Cd	0.08	-0.03	-0.08	24.79	0.22	-0.13	-0.04	28.97	0.69	22.24
Sn	0.21	-1.47	-2.73	9.01	5.29	-4.14	0.32	9.76	-1.15	11.97
Sb	4.00	1.32	-0.11	3.82	1.40	0.21	2.98	11.56	0.93	9.72
Te	0.39	-0.16	-0.38	-0.16	21.99	21.03	9.08	-0.12	-0.22	0.02
I	3.35	-1.41	-3.26	-1.39	9.04	-5.16	-1.77	-1.03	-1.85	0.15
W	4.16	3.97	9.89	3.35	9.25	5.55	5.80	1.78	0.73	0.20
Pb	2.29	-0.97	-2.23	40.98	6.19	-3.53	13.06	716.08	-1.27	1106.88
Bi	11.32	2.72	3.50	18.16	24.42	25.56	13.01	12.59	-0.09	1.79
Nb	2.23	-0.80	2.11	-0.01	0.56	2.22	5.24	4.48	4.82	1.86
La	-6.37	-5.06	-3.01	-1.42	2.77	6.92	0.33	0.33	0.45	-2.02
Ce	-13.11	-11.26	-7.89	-3.22	6.47	11.85	0.22	0.51	0.89	-4.84
Pr	-1.67	-1.32	-1.06	-0.38	1.05	1.43	-0.07	0.00	0.07	-0.55
Nd	-6.79	-5.06	-4.76	-0.55	5.22	6.89	-0.38	-0.33	0.18	-1.76
Sm	-1.46	-1.26	-1.09	-0.67	1.21	0.84	-0.10	0.03	0.01	0.03
Eu	-0.30	-0.20	-0.39	-0.24	-0.13	-0.48	-0.16	0.71	0.23	0.12
Tb	-0.22	-0.22	-0.17	0.12	0.31	0.24	0.05	-0.11	0.01	-0.10
Dy	-1.09	-1.17	-0.76	0.68	1.72	1.50	0.50	-0.53	0.44	-0.34
Ho	-0.29	-0.31	-0.23	0.06	0.10	0.19	0.05	-0.15	0.00	-0.18
Er	0.06	0.01	-0.51	0.27	0.17	0.62	0.13	-0.31	0.12	-0.39
Tm	-0.11	-0.12	-0.07	0.04	0.02	0.08	0.03	-0.04	0.02	-0.04
Yb	-0.97	-0.91	-0.58	0.00	-0.21	0.51	0.15	-0.40	0.04	-0.44
Lu	-0.14	-0.19	-0.10	-0.06	-0.07	0.01	0.03	-0.06	0.03	-0.07
Hf	-1.04	-1.65	-0.37	-1.05	-1.25	-0.41	0.46	0.12	0.43	0.30
Ta	0.03	-0.06	0.02	-0.04	-0.01	0.00	0.08	0.07	0.06	0.04
Th	-0.42	-1.66	0.28	-0.45	-0.74	0.22	1.28	1.01	0.86	0.37

Abbreviations:

Units

HFL= Hanging wall flow
HBX= Hanging wall breccia
FLT= Footwall lapilli tuff
FT= Footwall tuff
FBX= Footwall breccia
FFL= Footwall flow
INT= Intrusion

Alteration

Qtz-Ser= Quartz-sericite
Chl-Ser= Chlorite-sericite
Chl= Chlorite

Appendix C: Table C.1.2 Mass changes for samples at the Boundary deposit

Sample ID	**H501274**	**H501275**	**H501276**	**H501277**	**H501278***	**H501279**	**H501280**	**H501281**	**H501282**	**H501283**
Hole ID	BD10-9	BD10-9	BD10-9	BD10-9	BD10-11	BD10-11	BD10-11	BD10-11	BD10-21	BD10-21
Depth (m)	4.1	13.5	20.4	30.1	4	9.8	17.1	28.2	2.4	15.9
Lithology	HBX	FLT	FBX	FBX	HFL	HFL	FLT	FBX	HFL	FLT
Alteration	Chl-Ser	Qtz-Ser	Qtz-Ser	Qtz-Ser	Qtz-Ser	Qtz-Ser	Qtz-Ser	Qtz-Ser	Qtz-Ser	Chl-Ser
SiO_2	-13.88	3.60	-8.16	-0.07	0.00	-13.57	37.24	-13.16	-32.96	-8.92
Al_2O_3	0.00	0.00	0.00	0.00	0.00	0.00	0.00	0.00	0.00	0.00
FeO	2.72	-0.13	0.40	0.16	0.00	0.48	0.93	-0.84	-0.52	23.30
MnO	0.11	-0.08	0.04	0.04	0.00	0.03	0.15	-0.01	-0.09	0.13
MgO	4.88	-1.46	-0.77	-0.01	0.00	0.15	-0.81	-0.13	-1.20	3.39
CaO	-0.11	-0.11	-0.01	-0.10	0.00	-0.13	-0.09	-0.09	0.25	-0.03
Na_2O	-1.96	-1.93	-1.92	-1.77	0.00	-1.94	-1.92	-1.92	0.04	-1.89
K_2O	-0.20	1.21	1.39	0.97	0.00	0.91	1.38	1.12	-0.13	-0.32
TiO_2	0.03	0.03	0.02	0.02	0.00	0.01	0.02	0.01	0.02	0.05
P_2O_5	0.01	0.01	0.01	0.00	0.00	0.01	0.00	0.00	0.02	0.01
Net Oxide Change	-8.41	1.14	-8.99	-0.77	0.00	-14.05	36.90	-15.00	-34.59	15.72
Ba	57.59	429.47	284.87	-354.52	0.00	305.04	855.14	-221.37	-912.25	-94.24
Sr	-17.28	-13.92	-12.86	-14.05	0.00	-16.81	-15.11	-13.58	67.55	-15.05
Y	6.27	0.40	7.62	3.74	0.00	1.62	0.97	-3.65	8.37	-0.07
Sc	0.37	2.12	1.88	1.93	0.00	0.37	1.03	0.94	2.33	1.12
Zr	-3.53	6.52	7.65	9.05	0.00	5.39	7.99	-8.66	13.98	-1.81
Be	-0.06	0.01	-0.09	-0.01	0.00	-0.14	-0.31	0.68	0.30	-0.30
V	3.16	22.75	5.73	-0.02	0.00	-0.34	0.95	8.44	2.04	26.69
Hg	55.90	279.93	966.06	590.27	0.00	70.97	871.48	174.83	-1.62	5618.41
Cr 52	6.29	0.05	-0.38	-0.03	0.00	-0.60	17.46	-0.70	-1.56	1.74
Co	11.08	-0.66	-0.18	-0.66	0.00	1.34	-0.49	-0.73	-0.82	111.39
Ni	-0.28	0.05	-0.43	-0.03	0.00	-0.68	1.89	-0.79	-1.76	1.95
Cu	83.62	306.83	531.35	72.62	0.00	39.47	467.18	-1.99	-77.29	25105.40
Zn	422.03	1157.77	2918.74	1475.50	0.00	347.85	2765.47	358.15	-72.01	44428.03
As	4.30	15.89	4.85	0.98	0.00	12.72	60.27	4.03	-1.60	140.00
Se 78	-0.76	0.14	-1.15	-0.08	0.00	-1.81	5.05	-2.11	-4.69	37.89
Br 79	-27.66	-17.45	-31.26	-12.17	0.00	20.32	138.96	28.11	-37.08	113.46
Mo	10.84	1.43	2.34	2.18	0.00	1.76	3.75	2.76	-0.18	14.86
Ag 107	1.74	0.01	-0.04	0.00	0.00	0.73	0.19	-0.08	-0.18	41.68
Cd	-0.03	4.53	11.28	5.72	0.00	0.96	11.71	1.22	-0.16	155.63
Sn	-0.64	10.07	27.66	0.55	0.00	4.30	33.33	4.29	-2.92	33.59
Sb	1.67	6.30	3.03	0.68	0.00	1.63	5.00	0.23	-0.55	60.45
Te	-0.12	0.02	-0.18	-0.01	0.00	-0.29	0.81	-0.34	-0.75	8.18
I	-1.05	0.19	-1.59	-0.11	0.00	-2.51	7.00	-2.93	-6.50	7.22
W	4.45	2.27	0.18	0.54	0.00	1.71	1.55	1.80	0.10	1.97
Pb	423.44	15.88	-1.09	-0.08	0.00	285.99	95.96	-2.01	-4.45	8399.42
Bi	4.72	0.61	0.52	0.54	0.00	1.47	0.65	1.09	-0.16	57.62
Nb	1.31	0.22	0.51	0.32	0.00	0.05	-0.12	-0.30	3.25	2.59
La	0.00	0.12	1.60	0.42	0.00	-1.95	0.53	-8.30	-2.43	-0.53
Ce	-0.86	-0.48	2.68	0.26	0.00	-4.42	0.78	-17.97	-4.60	-2.56
Pr	-0.06	-0.01	0.30	0.02	0.00	-0.49	0.16	-2.17	-0.49	-0.33
Nd	0.27	0.79	1.80	0.78	0.00	-1.87	0.39	-9.18	-2.03	-1.52
Sm	-0.17	0.04	0.26	0.17	0.00	-0.47	0.17	-2.06	-0.33	-0.25
Eu	-0.28	0.31	0.19	0.07	0.00	-0.01	-0.03	-0.16	0.13	0.49
Tb	0.09	-0.04	0.22	0.10	0.00	-0.02	-0.02	-0.21	0.13	-0.01
Dy	1.01	-0.10	1.74	0.71	0.00	-0.05	0.13	-0.87	1.20	0.04
Ho	0.16	-0.05	0.29	0.09	0.00	-0.05	-0.01	-0.20	0.17	-0.02
Er	0.44	-0.16	0.84	0.12	0.00	-0.01	-0.01	-0.59	0.72	0.00
Tm	0.07	0.01	0.12	0.04	0.00	0.00	0.05	-0.08	0.12	0.00
Yb	0.15	-0.07	0.72	0.12	0.00	-0.07	0.11	-0.58	0.73	-0.27
Lu	0.01	-0.05	0.07	-0.01	0.00	-0.01	0.02	-0.13	0.08	-0.02
Hf	-0.08	-0.17	-0.07	0.07	0.00	-0.63	-0.29	-0.73	1.11	1.01
Ta	0.00	0.00	0.01	0.03	0.00	-0.01	0.00	-0.03	0.09	0.01
Th	-0.21	-0.02	0.21	0.05	0.00	-0.31	0.12	-1.01	0.80	1.75

Abbreviations:

Units

HFL= Hanging wall flow
HBX= Hanging wall breccia
FLT= Footwall lapilli tuff
FT= Footwall tuff
FBX= Footwall breccia
FFL= Footwall flow
INT= Intrusion

Alteration

Qtz-Ser= Quartz-sericite
Chl-Ser= Chlorite-sericite
Chl= Chlorite

* Inicates least altered sample

Appendix C: Table C.1.2 Mass changes for samples at the Boundary deposit

Sample ID	H501284	H501285	H501286	H501287	H501288	H501289	H501290	H501291	H501292	H501293
Hole ID	BD10-21	BD10-21	BD10-26	BD10-26	BD10-26	BD10-26	BD10-26	BD11-146	BD11-146	BD11-146
Depth (m)	30.1	31.1	9.2	18.5	20.6	29.1	37	6.2	11.8	14.9
Lithology	FBX	FBX	FLT	FLT	FLT	FLT	FFL	FLT	FLT	FLT
Alteration	Qtz-Ser	Chl-Ser	Qtz-Ser	Qtz-Ser	Qtz-Ser	Qtz-Ser	Qtz-Ser	Qtz-Ser	Qtz-Ser	Qtz-Ser
SiO_2	41.27	-22.38	27.19	-23.28	-37.87	-1.12	-1.68	12.67	0.12	1.91
$A_{l2}O_3$	0.00	0.00	0.00	0.00	0.00	0.00	0.00	0.00	0.00	0.00
FeO	0.08	-0.03	0.67	-0.54	-1.95	6.93	1.25	0.43	0.67	20.76
MnO	0.25	0.02	-0.09	-0.09	-0.09	-0.07	-0.07	-0.08	-0.02	0.00
MgO	0.77	1.09	-1.44	-1.27	-2.02	-2.07	-0.55	-0.97	-1.09	-0.51
CaO	1.77	0.31	-0.13	-0.13	-0.14	-0.12	-0.12	-0.13	-0.12	-0.14
Na_2O	-0.92	-1.69	-1.90	-1.91	-1.90	-1.90	-1.91	-1.94	-1.93	-1.93
K_2O	0.39	0.62	1.36	1.21	1.28	1.16	0.75	1.13	1.25	1.17
TiO_2	0.02	0.02	0.05	0.02	0.03	0.02	0.02	0.03	0.04	0.02
P_2O_5	0.02	0.01	0.02	0.01	-0.01	0.01	0.02	0.00	-0.01	0.00
Net Oxide Change	43.64	-22.03	25.72	-25.97	-42.68	2.84	-2.29	11.15	-1.10	21.28
Ba	-427.86	-283.37	420.94	61.18	33.25	211.04	-327.32	72.66	58.63	97.65
Sr	28.30	-2.52	-14.42	-16.86	-15.36	-16.51	-16.06	-16.42	-17.02	-16.32
Y	4.11	5.42	-3.61	10.98	-29.03	74.06	5.53	-3.29	-1.16	-16.27
Sc	1.50	2.47	2.64	3.96	-3.36	4.27	1.88	1.16	1.95	7.05
Zr	3.03	12.43	40.80	4.20	7.82	18.55	16.31	4.52	9.33	25.45
Be	-0.28	-0.22	-0.37	-0.27	-0.45	-0.45	-0.51	0.12	0.00	-0.29
V	1.09	-0.55	31.63	2.64	1.38	5.18	-0.03	28.74	3.47	24.49
Hg	347.29	64.38	258.49	651.66	12.92	132.89	-5.07	570.44	328.52	1990.79
Cr 52	47.96	22.22	30.89	19.71	10.46	12.48	23.44	0.52	-0.02	1.87
Co	1.39	-0.27	0.10	-0.40	-0.86	5.53	0.16	-0.61	-0.66	-0.47
Ni	21.82	10.67	18.07	10.35	4.19	0.49	13.24	0.58	-0.02	2.10
Cu	37.95	-58.12	291.44	-47.13	-78.18	635.12	-62.27	538.23	8.93	168.49
Zn	1084.09	212.77	1031.41	2897.10	-76.52	207.98	-20.42	1796.50	793.56	2398.16
As	-0.97	9.50	3.72	8.93	-1.68	57.11	69.33	55.20	89.45	682.11
Se 78	5.84	-2.95	3.52	-3.54	-5.96	1.30	-0.14	1.55	-0.06	5.61
Br 79	115.08	3.34	74.00	-14.98	-67.94	77.45	14.21	71.74	38.71	177.90
Mo	10.81	7.36	7.83	7.58	4.98	4.00	7.17	4.31	3.44	3.61
Ag 107	0.22	-0.11	0.13	0.60	0.06	1.63	-0.01	0.06	0.56	0.21
Cd	2.55	0.28	3.54	9.46	-0.20	0.83	0.00	7.76	2.38	7.66
Sn	-0.81	-1.67	1.20	83.14	0.09	5.02	10.53	5.86	6.66	8.64
Sb	1.70	0.89	3.34	6.84	-0.29	13.79	4.30	6.10	5.67	37.29
Te	0.94	-0.47	0.57	-0.57	-0.96	0.21	-0.02	0.25	-0.01	0.90
I	8.09	-4.08	4.88	-4.90	-8.26	1.81	-0.19	2.14	-0.08	7.78
W	1.60	1.37	3.72	1.22	2.38	5.95	2.40	2.75	3.42	3.11
Pb	5.53	-2.79	321.95	982.12	-5.65	79.40	-0.13	405.80	539.93	70.26
Bi	0.76	-0.09	4.12	1.43	-0.17	0.55	4.30	2.32	-0.09	-0.03
Nb	0.50	0.34	1.41	-0.29	-1.14	3.02	0.38	-0.02	-0.01	0.46
La	-1.15	-3.99	5.07	0.91	-19.70	8.14	-1.32	1.64	1.74	-3.02
Ce	-2.62	-8.43	8.73	2.36	-42.15	13.19	-3.18	1.63	3.39	-7.46
Pr	-0.22	-1.07	1.07	0.37	-5.30	1.51	-0.43	0.20	0.40	-1.04
Nd	-0.10	-3.66	5.43	1.91	-22.30	6.41	-1.31	1.11	1.56	-4.35
Sm	0.10	-0.80	0.78	0.51	-5.28	1.99	-0.13	0.04	0.11	-1.59
Eu	0.03	0.05	0.67	-0.19	-1.15	1.19	-0.23	0.48	0.25	-0.25
Tb	0.07	0.04	-0.13	0.11	-0.91	0.89	-0.03	-0.07	-0.05	-0.46
Dy	0.71	0.41	-0.88	0.84	-5.61	8.03	0.11	-0.56	-0.05	-2.84
Ho	0.13	0.10	-0.19	0.17	-1.18	1.86	0.00	-0.19	0.00	-0.63
Er	0.27	0.28	-0.51	0.49	-3.41	6.49	0.05	-0.59	0.27	-1.76
Tm	0.05	0.04	-0.01	0.09	-0.48	1.09	0.01	-0.07	0.10	-0.23
Yb	0.36	0.08	0.05	0.21	-3.23	8.02	-0.13	-0.60	0.88	-1.68
Lu	0.08	0.01	0.01	0.05	-0.49	1.32	-0.03	-0.12	0.16	-0.27
Hf	0.62	-0.57	0.13	-1.09	0.18	8.45	-0.85	-0.26	-0.25	0.20
Ta	0.04	0.01	0.05	-0.01	-0.03	0.06	0.03	0.00	0.00	-0.01
Th	-0.11	-0.21	0.65	-0.81	-0.75	1.24	-0.17	-0.01	0.23	-0.43

Abbreviations:

Units

HFL= Hanging wall flow
HBX= Hanging wall breccia
FLT= Footwall lapilli tuff
FT= Footwall tuff
FBX= Footwall breccia
FFL= Footwall flow
INT= Intrusion

Alteration

Qtz-Ser= Quartz-sericite
Chl-Ser= Chlorite-sericite
Chl= Chlorite

Appendix C: Table C.1.2 Mass changes for samples at the Boundary deposit

Sample ID	H501294	H501295	H501296	H501297	H501298	H501299	H501300	H501301	H501302	H501303
Hole ID	BD11-143	BD11-143	BD11-143	BD11-143	BD11-134	BD11-134	BD11-134	BD11-134	BD11-154	BD11-154
Depth (m)	4.3	7.9	16.7	28.1	10.9	21.5	33.1	43	10.9	26.1
Lithology	FLT	FLT	FLT	FFL	FLT	FLT	FLT	FBX	FLT	FLT
Alteration	Qtz-Ser	Qtz-Ser	Qtz-Ser	Qtz-Ser	Qtz-Ser	Chl	Qtz-Ser	Qtz-Ser	Qtz-Ser	Qtz-Ser
SiO_2	43.22	44.07	45.23	19.87	-1.90	-19.08	19.97	13.00	-4.31	13.00
Al_2O_3	0.00	0.00	0.00	0.00	0.00	0.00	0.00	0.00	0.00	0.00
FeO	8.98	6.29	4.48	-0.24	12.71	8.83	7.55	9.61	1.50	3.56
MnO	-0.09	-0.06	-0.07	-0.09	-0.08	0.10	-0.09	-0.06	-0.09	-0.09
MgO	-1.93	1.01	0.07	-1.00	-0.77	10.67	-2.04	-0.62	-2.10	-1.97
CaO	-0.12	-0.13	-0.12	-0.13	-0.13	1.36	-0.13	-0.01	-0.14	-0.11
Na_2O	-1.86	-1.91	-1.89	-1.89	-1.87	-2.01	-1.85	-1.88	-1.84	-1.82
K_2O	1.02	0.12	0.49	0.90	0.86	-2.20	1.14	0.81	1.18	1.10
TiO_2	0.05	0.01	0.04	0.03	0.03	0.05	0.04	0.03	0.04	0.04
P_2O_5	0.00	0.01	0.00	0.01	0.00	0.01	0.00	0.00	-0.01	0.00
Net Oxide Change	49.27	49.41	48.21	17.46	8.85	-2.27	24.59	20.88	-5.77	13.70
Ba	-303.42	-598.38	-487.31	-387.06	-72.06	-1348.32	-399.79	-458.03	134.26	-209.68
Sr	-14.09	-15.77	-15.89	-14.97	-12.28	13.17	-12.75	-10.26	-10.51	-10.27
Y	3.73	6.15	11.39	3.20	4.76	10.02	5.93	6.67	-23.68	-16.72
Sc	2.66	2.46	3.74	2.89	3.37	3.85	3.21	3.05	-2.34	-0.62
Zr	21.16	15.37	24.48	14.41	13.03	16.98	14.89	18.11	8.17	17.98
Be	-0.21	-0.22	-0.24	-0.41	-0.39	-0.47	-0.34	-0.35	-0.52	-0.41
V	1.46	1.39	1.32	0.43	0.54	3.89	0.80	0.76	-0.11	4.54
Hg	6.99	5.13	1.74	-9.07	24.47	5.05	11.78	27.15	-3.38	0.90
Cr 52	42.44	2.48	47.60	31.56	6.60	0.29	1.43	18.28	7.68	9.64
Co	29.95	18.29	20.71	1.81	8.69	3.31	12.45	2.53	0.94	6.83
Ni	20.79	2.78	24.90	18.26	1.08	0.33	1.61	1.52	-0.21	0.86
Cu	4705.37	1417.01	1669.24	-27.85	771.02	65.72	-53.10	871.24	-74.41	-72.40
Zn	-17.09	-22.83	-15.27	-70.39	-11.84	220.62	-115.09	-82.30	-119.38	-111.77
As	26.90	22.99	49.20	0.19	77.78	4.53	43.37	227.01	15.07	33.23
Se 78	7.78	7.44	7.03	2.30	2.88	0.88	4.29	4.07	-0.57	2.30
Br 79	118.05	160.55	181.03	71.40	146.17	91.85	174.03	152.55	61.35	103.50
Mo	14.06	5.43	20.40	11.13	4.96	5.14	5.33	3.08	5.49	4.87
Ag 107	0.29	0.28	0.26	0.09	0.11	0.03	0.16	0.15	0.57	0.09
Cd	0.26	0.25	0.24	0.08	0.10	0.03	0.14	0.14	-0.02	0.08
Sn	0.99	0.32	0.65	-0.71	1.73	-2.25	-0.40	0.35	-0.64	-0.03
Sb	1.81	1.16	1.29	0.14	1.56	0.96	1.97	13.59	0.41	0.58
Te	10.38	4.58	1.13	0.37	12.50	0.14	0.69	0.66	-0.09	0.37
I	10.78	10.30	9.75	3.18	3.99	1.21	5.95	5.64	-0.79	3.19
W	9.87	7.96	6.42	6.36	6.52	6.90	3.97	1.49	3.10	3.69
Pb	7.37	7.05	6.67	2.18	76.13	36.52	4.07	29.21	15.27	2.18
Bi	15.38	7.84	6.01	1.83	21.25	1.52	5.08	9.20	3.48	3.60
Nb	1.37	2.56	1.96	0.75	2.95	4.68	1.78	2.44	1.94	2.70
La	-4.22	-0.39	-0.43	-1.54	-4.04	1.00	-0.68	-0.83	-13.16	-16.25
Ce	-9.41	0.79	-1.63	-5.59	-8.01	2.38	-1.42	-1.97	-31.50	-35.18
Pr	-1.23	0.19	-0.19	-0.71	-0.92	0.36	-0.09	-0.26	-4.15	-4.45
Nd	-5.66	0.91	-0.87	-1.77	-3.55	1.40	-0.40	-1.16	-17.95	-18.86
Sm	-1.37	0.18	-0.01	-0.01	-0.48	0.87	0.16	0.06	-4.55	-4.47
Eu	-0.03	0.34	0.15	0.01	0.04	0.39	-0.08	0.42	-0.86	-0.85
Tb	-0.09	0.07	0.21	0.06	0.02	0.24	-0.02	0.04	-0.75	-0.65
Dy	0.15	0.26	1.83	0.25	0.61	1.37	0.14	0.65	-4.45	-3.61
Ho	0.09	0.01	0.35	0.02	0.00	0.27	-0.08	0.07	-0.92	-0.73
Er	0.28	-0.06	1.04	0.21	0.22	0.81	-0.35	0.06	-2.40	-1.86
Tm	0.03	0.01	0.18	0.02	0.06	0.12	-0.02	0.04	-0.30	-0.22
Yb	0.22	-0.13	0.77	0.16	0.16	0.78	-0.29	-0.04	-1.67	-1.32
Lu	0.04	-0.02	0.08	0.07	0.07	0.14	-0.05	0.02	-0.28	-0.20
Hf	0.30	1.64	-0.42	0.53	1.35	1.91	0.37	1.03	-0.55	0.47
Ta	0.02	0.09	0.04	0.03	0.02	0.07	0.03	0.06	0.06	0.08
Th	0.47	1.56	0.41	0.09	0.83	1.10	0.16	0.57	0.14	0.67

Abbreviations:

Units

HFL= Hanging wall flow
HBX= Hanging wall breccia
FLT= Footwall lapilli tuff
FT= Footwall tuff
FBX= Footwall breccia
FFL= Footwall flow
INT= Intrusion

Alteration

Qtz-Ser= Quartz-sericite
Chl-Ser= Chlorite-sericite
Chl= Chlorite

Appendix C: Table C.1.2 Mass changes for samples at the Boundary deposit

Sample ID	**H501304**	**H501305**	**H501306**	**H501307**	**H501308**	**H501309**	**H501310**	**H501311**	**H501312**	**H501313**
Hole ID	BD11-154	BD11-158	BD11-158	BD11-158	BD11-158	BD11-136	BD11-136	BD11-136	BD11-195	BD11-195
Depth (m)	30.5	5.8	14	25.4	39.8	10.7	23.4	31.9	7.9	9.5
Lithology	FLT	FLT	FLT	FLT	FLT	FLT	FLT	FLT	FLT	FFL
Alteration	Qtz-Ser	Chl	Chl	Chl-Ser	Qtz-Ser	Qtz-Ser	Chl	Qtz-Ser	Qtz-Ser	Chl-Ser
SiO_2	-4.30	-58.79	-10.86	14.21	-1.59	46.88	-61.01	9.62	12.52	-6.42
Al_2O_3	0.00	0.00	0.00	0.00	0.00	0.00	0.00	0.00	0.00	0.00
FeO	0.57	9.95	9.13	1.47	1.87	10.80	6.26	5.10	5.36	4.00
MnO	-0.09	-0.03	0.19	-0.06	-0.05	-0.09	-0.02	-0.09	-0.09	-0.03
MgO	-1.96	14.74	20.58	3.74	1.45	-1.40	10.91	-1.62	-1.86	1.92
CaO	-0.13	0.00	9.45	-0.07	-0.10	-0.11	-0.14	-0.12	-0.12	-0.10
Na_2O	-1.84	-2.01	-2.01	-1.96	-1.95	-1.86	-2.03	-1.88	-1.90	-1.94
K_2O	1.18	-2.34	-2.33	-0.16	0.33	0.99	-2.36	1.06	1.28	0.18
TiO_2	0.03	0.03	0.14	0.02	0.03	0.04	0.04	0.03	0.02	0.05
P_2O_5	-0.01	0.00	0.11	0.00	0.01	0.00	0.00	0.00	0.00	0.02
Net Oxide Change	-6.55	-38.44	24.38	17.20	-0.01	55.25	-48.35	12.10	15.23	-2.32
Ba	-96.44	-1394.41	-1387.97	-667.49	-738.80	964.98	-1400.47	-139.92	-256.34	-615.89
Sr	-9.78	-19.14	138.21	-17.25	-16.91	-10.38	-21.42	-12.62	-15.97	-16.92
Y	-13.61	-22.55	33.09	3.72	4.80	37.39	-10.62	9.05	4.41	6.76
Sc	2.22	0.01	4.69	1.87	3.24	6.61	-0.15	2.89	2.06	2.20
Zr	1.67	-1.98	119.34	0.97	9.82	11.10	13.68	7.36	9.36	11.59
Be	-0.53	-0.64	-0.33	-0.41	-0.49	-0.17	-0.71	-0.41	-0.40	-0.49
V	4.08	-0.71	0.84	4.62	2.59	1.65	0.97	0.43	0.51	0.04
Hg	-3.54	1797.21	86.79	4.61	-4.87	182.29	-10.55	3.24	42.27	7.32
Cr 52	11.54	-1.27	1.49	0.83	0.08	20.23	-1.87	0.77	11.46	0.07
Co	6.83	56.21	23.76	0.67	0.00	3.61	18.78	5.15	-0.57	-0.65
Ni	-0.30	-1.42	1.68	0.93	0.09	3.30	-2.10	0.86	1.03	0.08
Cu	-74.57	16918.93	331.83	89.59	50.93	2876.80	-24.69	24.46	3074.56	22.05
Zn	-120.54	6975.34	766.51	58.59	92.14	359.09	145.60	-60.81	64.51	26.32
As	4.31	73.84	31.68	5.63	45.41	335.86	25.96	9.68	83.07	7.18
Se 78	-0.80	-3.80	4.47	2.49	0.25	8.82	-5.62	2.30	2.75	0.22
Br 79	40.46	35.24	139.80	197.81	88.31	286.46	7.70	142.55	96.30	68.34
Mo	8.24	-0.14	10.39	3.42	3.24	11.51	2.50	3.09	6.45	3.14
Ag 107	-0.03	3.62	0.17	0.09	0.01	1.18	0.11	0.09	0.10	0.01
Cd	-0.03	25.42	1.49	0.08	0.01	0.30	-0.19	0.08	0.09	0.01
Sn	0.75	4.56	5.19	12.10	3.70	29.98	2.19	10.01	-0.30	-1.77
Sb	0.72	0.44	-0.62	0.59	1.52	20.29	-0.19	0.34	4.20	2.98
Te	-0.13	6.05	0.72	0.40	0.04	1.42	-0.90	0.37	0.44	0.04
I	-1.11	-5.27	6.20	3.45	0.34	12.22	-7.79	3.18	3.81	0.31
W	1.76	0.99	1.24	6.68	1.88	2.08	8.68	2.16	3.25	1.67
Pb	-0.76	-3.61	4.24	2.36	0.24	39.03	-5.33	2.18	19.16	0.21
Bi	1.27	5.11	0.81	0.95	1.77	30.57	0.73	2.72	2.34	1.25
Nb	1.51	-0.13	2.94	-0.14	0.15	-0.39	1.92	-0.06	2.85	3.80
La	-2.41	-18.50	41.76	-0.27	-0.53	21.76	-6.36	4.55	-1.19	-0.52
Ce	-9.51	-39.46	87.85	-1.48	-1.50	50.92	-15.35	9.37	-3.08	-2.04
Pr	-1.54	-4.92	10.89	-0.21	-0.11	7.10	-2.08	1.39	-0.28	-0.24
Nd	-7.48	-20.50	46.33	-0.76	-0.18	31.66	-8.85	6.85	-1.01	-0.35
Sm	-2.48	-4.77	9.95	-0.22	-0.10	7.70	-2.43	1.80	-0.52	-0.20
Eu	-0.54	-1.06	0.41	0.38	0.25	1.63	-0.55	0.06	0.28	0.18
Tb	-0.42	-0.78	1.22	-0.02	0.03	1.09	-0.38	0.19	0.06	0.20
Dy	-2.59	-4.59	6.51	0.06	0.34	6.07	-1.99	1.02	0.60	1.62
Ho	-0.59	-0.95	1.15	0.02	0.06	1.08	-0.36	0.08	0.06	0.28
Er	-1.56	-2.69	3.23	-0.01	0.10	2.88	-0.78	0.23	0.32	0.62
Tm	-0.21	-0.38	0.48	0.01	0.03	0.38	-0.05	0.02	0.08	0.13
Yb	-1.24	-2.43	2.92	-0.01	0.09	2.31	-0.34	-0.17	0.14	0.62
Lu	-0.19	-0.35	0.46	0.00	0.00	0.31	-0.03	-0.01	0.01	0.07
Hf	-0.06	-0.29	2.31	-0.45	-0.97	-0.52	0.86	-0.39	0.15	-0.71
Ta	0.04	-0.03	0.12	0.00	0.01	-0.02	0.05	0.00	0.06	0.11
Th	0.40	-1.14	3.11	-0.10	0.03	-0.58	1.21	-0.34	0.75	0.94

Abbreviations:

Units

HFL= Hanging wall flow
HBX= Hanging wall breccia
FLT= Footwall lapilli tuff
FT= Footwall tuff
FBX= Footwall breccia
FFL= Footwall flow
INT= Intrusion

Alteration

Qtz-Ser= Quartz-sericite
Chl-Ser= Chlorite-sericite
Chl= Chlorite

Appendix C: Table C.1.2 Mass changes for samples at the Boundary deposit

Sample ID	**H501314**	**H501315**	**H501316**	**H501317**	**H501318**	**H501319**	**H501320**	**H501326**	**H501327**	**H501328**
Hole ID	BD11-195	BD11-195	BD10-6	BD10-6	BD10-6	BD10-6	BD10-6	BD10-113	BD10-113	BD10-113
Depth (m)	16.8	23.8	4.6	7.3	13.7	17.9	32.1	5	10	28.3
Lithology	FLT	FFL	HFL	FLT	FLT	FBX	FBX	HFL	FLT	FLT
Alteration	Qtz-Ser	Qtz-Ser	Qtz-Ser	Chl-Ser	Qtz-Ser	Qtz-Ser	Qtz-Ser	Qtz-Ser	Chl	Qtz-Ser
SiO_2	8.07	-2.58	14.94	-6.59	-5.87	5.96	-2.91	9.29	-18.66	-9.84
$A_{l2}O_3$	0.00	0.00	0.00	0.00	0.00	0.00	0.00	0.00	0.00	0.00
FeO	2.90	1.69	0.23	6.00	1.24	0.74	-0.12	-0.61	8.61	-0.19
MnO	-0.08	-0.05	0.02	0.07	0.05	0.05	-0.02	-0.08	0.19	0.06
MgO	-0.83	1.04	1.38	0.79	-0.64	-0.87	-0.36	0.04	9.63	0.06
CaO	-0.12	-0.11	-0.11	-0.12	-0.11	0.08	-0.03	-0.13	-0.12	0.16
Na_2O	-1.92	-1.94	-1.93	-1.94	-1.91	-1.31	-1.82	-1.93	-2.00	-1.43
K_2O	0.91	0.59	0.61	0.38	1.08	0.97	1.09	0.89	-1.84	0.66
TiO_2	0.01	0.03	0.01	0.01	0.03	0.03	0.01	0.00	0.03	0.02
P_2O_5	0.00	0.01	0.00	0.00	0.01	0.01	0.01	0.02	0.01	0.02
Net Oxide Change	8.94	-1.33	15.15	-1.41	-6.11	5.66	-4.15	7.49	-4.15	-10.49
Ba	-360.02	-585.02	987.29	449.61	381.41	440.12	-283.17	1243.60	-1048.67	-124.46
Sr	-15.29	-15.98	-16.23	-16.77	-15.34	-6.04	-13.38	-16.66	-20.96	-5.92
Y	1.26	5.16	6.00	-1.35	0.00	-3.89	-12.20	0.54	-0.35	-4.16
Sc	2.30	3.05	0.38	1.51	2.37	0.64	0.53	0.69	0.45	1.61
Zr	-2.96	12.57	1.53	-19.49	1.50	1.83	-0.45	-6.06	-2.94	-1.19
Be	-0.44	-0.50	0.15	0.05	-0.05	0.06	-0.04	0.07	-0.48	-0.11
V	0.30	0.01	0.38	20.51	9.87	0.16	4.20	0.17	12.12	10.90
Hg	26.03	16.10	0.69	1640.60	327.62	321.02	510.69	20.06	106.04	342.60
Cr 52	0.53	0.02	0.68	8.86	-0.22	0.28	6.27	0.31	0.20	-0.48
Co	-0.61	-0.66	0.11	18.49	0.03	-0.63	-0.68	-0.63	30.26	1.33
Ni	0.59	0.02	0.77	0.23	-0.24	0.32	-0.21	0.34	0.22	-0.53
Cu	141.00	-73.98	-2.51	2272.93	129.59	303.08	516.61	164.05	2090.16	118.97
Zn	-69.65	-52.52	57.86	5611.58	1138.99	1291.25	1475.62	168.02	681.68	1543.83
As	5.03	2.16	0.19	190.20	51.06	24.27	11.47	2.26	112.20	29.98
Se 78	1.58	0.05	2.05	0.61	-0.65	0.85	-0.57	0.92	0.59	-1.43
Br 79	93.84	52.72	118.17	103.47	106.33	110.29	71.75	105.80	94.92	77.63
Mo	3.57	3.56	0.08	19.27	4.91	2.33	3.47	1.68	7.90	2.15
Ag 107	0.06	0.00	1.00	9.73	0.72	0.03	-0.02	0.03	4.10	-0.05
Cd	0.05	0.00	0.07	15.73	3.90	4.60	5.21	0.03	5.12	4.60
Sn	-0.53	-2.36	9.32	8.48	14.12	13.53	3.57	5.80	12.14	13.67
Sb	3.50	1.59	1.44	25.92	11.67	3.69	0.68	3.40	10.28	2.23
Te	0.25	0.01	0.33	0.10	-0.10	0.14	-0.09	0.15	2.67	-0.23
I	2.19	0.07	2.85	0.85	-0.90	1.18	-0.79	1.27	0.82	-1.98
W	2.97	1.36	0.81	2.15	1.49	1.61	2.16	1.23	2.32	0.20
Pb	1.50	0.05	135.97	1379.71	34.90	77.27	-0.54	81.77	191.24	116.94
Bi	1.70	0.10	1.94	9.51	1.36	1.48	0.24	0.34	15.04	0.29
Nb	1.02	1.66	-0.20	-0.80	0.08	0.13	-0.30	-0.69	0.73	0.41
La	0.34	-0.52	0.19	-3.13	-0.21	-2.64	-1.74	-0.48	2.26	1.39
Ce	-1.52	-1.40	-1.06	-7.83	-0.93	-5.63	-3.96	-2.13	3.36	2.70
Pr	-0.19	-0.13	-0.01	-0.94	-0.07	-0.69	-0.43	-0.14	0.50	0.39
Nd	-0.38	-0.36	-0.02	-3.87	-0.26	-2.81	-1.96	-0.07	1.91	1.99
Sm	-0.22	-0.06	0.10	-0.86	-0.14	-0.65	-0.73	-0.05	0.27	0.20
Eu	0.09	0.38	0.17	0.28	0.21	-0.07	-0.23	0.00	0.37	0.35
Tb	-0.08	0.09	0.04	-0.13	-0.03	-0.15	-0.28	-0.02	0.03	-0.04
Dy	-0.34	0.81	0.68	-0.65	0.09	-0.63	-1.83	0.06	0.41	-0.25
Ho	-0.09	0.19	0.09	-0.17	-0.02	-0.19	-0.46	0.01	0.05	-0.10
Er	-0.15	0.52	0.42	-0.43	-0.03	-0.58	-1.23	0.10	0.15	-0.20
Tm	-0.02	0.10	0.08	-0.07	0.02	-0.07	-0.16	0.01	0.03	0.00
Yb	-0.30	0.60	0.28	-0.57	-0.04	-0.54	-1.17	-0.02	0.03	-0.11
Lu	-0.05	0.03	0.08	-0.09	0.00	-0.07	-0.15	-0.02	-0.01	-0.02
Hf	0.32	0.59	0.27	-0.76	-0.71	-0.41	-0.92	-0.49	-0.69	0.05
Ta	0.02	0.05	0.02	-0.03	0.01	0.01	-0.01	-0.03	0.01	0.01
Th	0.27	0.86	-0.24	-1.22	-0.47	-0.50	-0.79	-0.37	0.08	0.06

Abbreviations:

Units

HFL= Hanging wall flow
HBX= Hanging wall breccia
FLT= Footwall lapilli tuff
FT= Footwall tuff
FBX= Footwall breccia
FFL= Footwall flow
INT= Intrusion

Alteration

Qtz-Ser= Quartz-sericite
Chl-Ser= Chlorite-sericite
Chl= Chlorite

Appendix C: Table C.1.2 Mass changes for samples at the Boundary deposit

Sample ID	H501329	H501332	H501333	H501334	H501335	H501336	H501337	H501338	H501339	H501340
Hole ID	BD10-113	BD10-3	BD10-3	BD10-3	BD10-3	BD10-3	BD10-18	BD10-18	BD10-18	BD10-18
Depth (m)	40.8	6.6	8.2	16.3	30.7	37.9	4.3	9.9	19.7	27.2
Lithology	FLT	HFL	FLT	FLT	FLT	FLT	FLT	FFL	FBX	FFL
Alteration	Qtz-Ser	Qtz-Ser	Qtz-Ser	Qtz-Ser	Qtz-Ser	Chl	Chl-Ser	Qtz-Ser	Qtz-Ser	Qtz-Ser
SiO_2	13.75	-2.42	10.47	-11.12	-29.46	-53.20	6.31	14.70	15.16	15.71
$A_{l2}O_3$	0.00	0.00	0.00	0.00	0.00	0.00	0.00	0.00	0.00	0.00
FeO	-0.16	0.01	5.89	2.28	7.98	8.12	14.05	3.19	2.63	3.85
MnO	0.21	-0.06	-0.08	-0.08	-0.03	0.81	-0.02	-0.08	-0.09	-0.07
MgO	0.11	-1.36	-1.69	-1.80	-0.88	13.23	0.16	-1.42	-1.96	-1.29
CaO	0.24	-0.14	-0.13	-0.14	-0.13	1.35	-0.10	-0.02	-0.13	-0.12
Na_2O	-1.90	-1.87	-1.88	-1.88	-1.88	-2.03	-1.94	-1.92	-1.92	-1.92
K_2O	1.15	1.19	1.24	1.29	1.13	-2.33	0.90	1.29	1.33	1.08
TiO_2	0.04	0.02	0.05	0.03	0.02	0.00	0.03	0.02	0.03	0.04
P_2O_5	0.05	-0.01	0.00	-0.01	-0.01	0.01	0.02	0.01	0.00	0.00
Net Oxide Change	13.49	-4.64	13.87	-11.42	-23.25	-34.04	19.42	15.76	15.05	17.28
Ba	-41.16	1241.52	1631.50	828.11	1.96	-1396.89	-262.79	-174.52	-309.99	-447.42
Sr	-2.73	-14.37	-14.81	-14.73	-13.53	-6.44	-18.00	-16.05	-16.12	-14.73
Y	5.20	2.96	-4.27	3.71	2.52	2.48	9.05	-5.69	11.60	2.19
Sc	2.47	2.40	1.98	1.81	3.56	7.04	3.35	1.89	2.95	2.11
Zr	21.60	1.88	-4.88	5.83	2.44	-16.85	15.17	9.63	10.35	11.26
Be	0.13	-0.05	-0.40	-0.09	-0.15	-0.63	-0.33	-0.41	-0.41	-0.39
V	0.33	-0.12	4.69	2.04	-0.38	5.65	4.17	0.47	0.44	0.53
Hg	206.74	446.75	1736.49	996.57	454.88	32.45	29.38	9.41	-1.41	1.32
Cr 52	0.59	-0.21	6.26	-0.41	-0.68	-1.15	1.49	8.71	0.79	7.29
Co	-0.07	-0.68	-0.57	-0.70	-0.27	16.68	-0.51	1.01	-0.58	-0.56
Ni	0.67	-0.23	11.48	-0.46	-0.76	-1.30	1.67	0.95	0.88	1.06
Cu	61.74	173.41	-0.04	26.36	33.15	30.74	4867.80	574.71	670.62	200.71
Zn	540.30	2844.42	10471.11	5034.82	1015.78	7999.10	253.71	3.35	227.31	-4.29
As	22.76	8.79	125.90	13.23	97.05	-0.20	153.14	68.83	61.11	115.23
Se 78	1.78	-0.62	2.64	-1.22	-2.04	-3.46	4.47	2.53	2.36	2.82
Br 79	130.58	46.72	108.10	31.87	-5.52	-16.84	163.93	151.94	93.47	142.05
Mo	2.20	1.83	3.36	2.38	5.17	3.31	52.18	4.44	2.55	3.11
Ag 107	0.07	2.31	1.44	-0.05	0.36	-0.13	0.17	0.09	1.19	0.11
Cd	1.18	10.29	37.18	20.98	3.91	6.62	0.15	0.09	0.08	0.10
Sn	5.29	6.48	1.25	-0.52	37.32	-1.45	7.71	6.86	4.90	6.24
Sb	1.67	5.43	8.83	5.30	23.46	69.16	2.69	2.09	0.99	2.44
Te	0.29	-0.10	0.42	-0.20	-0.33	-0.56	0.72	0.41	20.07	0.45
I	2.47	-0.86	3.66	-1.69	-2.82	-4.80	6.19	3.51	3.27	3.91
W	0.04	2.35	4.44	3.93	0.59	9.32	3.93	2.88	4.83	6.11
Pb	1.69	2982.42	350.30	18.79	80.04	109.57	51.07	31.55	2.24	24.96
Bi	-0.12	-0.10	1.42	0.00	16.63	1.37	15.42	5.62	30.40	8.05
Nb	0.83	1.48	3.62	2.45	2.79	0.95	0.68	-0.17	0.33	-0.11
La	1.39	-3.12	0.33	-1.55	-2.77	1.90	9.65	-1.76	-1.08	0.26
Ce	2.53	-7.52	-0.84	-3.97	-5.89	4.32	20.11	-4.08	-2.21	0.32
Pr	0.38	-0.93	0.04	-0.48	-0.71	0.62	2.68	-0.41	-0.22	0.17
Nd	1.82	-3.65	0.82	-1.42	-2.08	3.69	12.54	-1.49	-0.42	0.51
Sm	0.47	-0.93	-0.10	-0.35	-0.53	0.89	2.78	-0.35	0.43	0.09
Eu	0.31	0.07	0.10	0.06	-0.23	-0.30	0.55	-0.18	-0.07	-0.10
Tb	0.17	-0.10	-0.09	0.04	-0.03	0.17	0.32	-0.16	0.27	-0.05
Dy	1.38	-0.28	-0.50	0.46	0.13	1.23	1.93	-0.84	1.91	-0.12
Ho	0.29	0.01	-0.10	0.10	0.06	0.19	0.36	-0.20	0.38	-0.01
Er	0.80	0.07	-0.25	0.29	0.39	0.40	0.94	-0.64	1.06	-0.10
Tm	0.14	0.04	-0.01	0.09	0.08	0.05	0.16	-0.06	0.16	0.01
Yb	0.72	0.17	-0.29	0.31	0.37	0.00	0.78	-0.42	0.73	-0.02
Lu	0.06	0.02	-0.06	0.05	0.07	0.02	0.10	-0.04	0.11	0.01
Hf	0.30	0.78	-0.13	-0.13	-0.01	0.12	0.17	-0.81	-0.85	-1.36
Ta	0.01	0.06	0.04	0.02	0.05	-0.01	0.02	0.00	0.01	0.00
Th	0.34	0.43	0.39	0.43	0.23	-0.15	0.04	-0.32	0.85	-0.25

Abbreviations:

Units

HFL= Hanging wall flow
HBX= Hanging wall breccia
FLT= Footwall lapilli tuff
FT= Footwall tuff
FBX= Footwall breccia
FFL= Footwall flow
INT= Intrusion

Alteration

Qtz-Ser= Quartz-sericite
Chl-Ser= Chlorite-sericite
Chl= Chlorite

Appendix C: Table C.1.2 Mass changes for samples at the Boundary deposit

Sample ID	H501341	H501342	H501343	H501344	H501345	H501346	H501347	H501348	H501349	H501350
Hole ID	BD10-18	BD11-190	BD11-190	BD11-190	BD11-189	BD11-189	BD11-189	BD11-189	BD11-189	BD10-106
Depth (m)	31.3	9.8	24.9	39.3	11.3	19.5	20.7	23.7	38.2	9.6
Lithology	FBX	FLT	FLT	FLT	FLT	FFL	FLT	INT	INT	FLT
Alteration	Chl	Qtz-Ser	Qtz-Ser	Qtz-Ser	Qtz-Ser	Chl-Ser	Qtz-Ser	Qtz-Ser	Qtz-Ser	Qtz-Ser
SiO_2	-6.88	1.33	0.96	2.25	0.51	-7.69	-33.23	5.06	12.98	10.83
Al_2O_3	0.00	0.00	0.00	0.00	0.00	0.00	0.00	0.00	0.00	0.00
FeO	5.68	1.15	5.72	2.47	4.30	8.83	0.52	4.47	1.39	2.23
MnO	0.17	-0.06	-0.05	0.02	0.01	0.28	-0.04	0.09	-0.05	0.06
MgO	7.47	-0.97	-1.28	0.38	-0.04	1.89	-1.05	0.74	-0.96	3.10
CaO	-0.09	-0.11	-0.12	-0.09	-0.11	-0.05	-0.11	-0.10	-0.12	-0.05
Na_2O	-2.00	-1.87	-1.84	-1.86	-1.85	-1.83	-1.82	-1.86	-1.83	-1.84
K_2O	-1.37	0.69	0.83	0.35	0.42	0.13	0.90	0.19	0.68	0.06
TiO_2	0.03	0.03	0.03	0.05	0.04	0.11	0.03	0.03	0.02	0.07
P_2O_5	0.03	0.01	0.00	0.02	0.02	0.01	0.02	0.01	0.00	0.05
Net Oxide Change	3.05	0.19	4.24	3.59	3.30	1.68	-34.78	8.63	12.12	14.51
Ba	-1114.43	-129.03	-298.48	-355.88	-203.96	-394.71	-62.93	-375.37	77.89	-420.42
Sr	-19.83	-12.88	-12.10	-12.45	-14.47	-10.95	-11.48	-12.95	-14.05	-12.66
Y	5.58	4.58	4.99	0.24	5.12	1.89	0.44	9.63	-0.41	-5.15
Sc	0.87	2.16	2.10	1.67	2.91	3.26	2.49	3.57	2.49	2.84
Zr	15.92	0.94	10.05	4.55	13.17	48.38	12.78	26.92	5.97	-3.75
Be	-0.46	-0.49	-0.45	-0.47	-0.46	-0.45	-0.34	-0.43	-0.43	-0.42
V	2.94	3.58	0.25	7.05	0.19	4.13	-0.86	0.33	0.34	22.01
Hg	14.09	-9.47	1.20	-3.52	-9.31	115.08	-6.74	-6.34	-9.16	-3.83
Cr 52	0.39	0.06	12.37	12.20	32.90	36.42	12.88	26.23	25.62	35.11
Co	-0.62	0.15	4.25	0.00	5.57	21.66	0.01	4.86	0.94	0.84
Ni	9.32	0.07	0.50	0.30	24.73	17.14	4.99	12.10	12.56	19.99
Cu	229.42	893.49	778.87	320.76	-61.32	1329.95	-77.21	-51.26	-72.75	272.28
Zn	301.76	-63.09	33.04	-68.74	-3.84	40.35	-86.24	-29.07	-36.15	17.20
As	30.91	21.50	13.80	0.85	15.92	21.30	0.40	3.20	-1.21	0.32
Se 78	1.17	0.18	1.33	0.81	1.01	1.40	-4.57	1.75	1.80	2.23
Br 79	98.66	77.25	38.87	60.37	55.41	48.55	-35.66	54.72	67.96	65.55
Mo	4.35	2.96	6.08	5.35	11.69	17.48	5.62	8.50	7.99	12.89
Ag 107	0.04	0.01	0.05	0.03	0.04	0.05	-0.17	0.07	0.07	0.08
Cd	0.04	0.01	0.04	0.03	0.03	0.05	-0.15	0.06	0.06	0.08
Sn	2.95	5.95	0.17	-1.05	-0.05	-0.99	-2.74	-1.33	1.75	-2.27
Sb	4.15	0.45	3.39	0.53	0.62	5.96	0.30	1.02	0.02	0.42
Te	0.19	0.03	0.21	0.13	0.16	0.23	-0.74	0.28	0.29	0.36
I	1.61	0.25	1.84	1.12	1.41	1.94	-6.34	2.42	2.50	3.10
W	1.22	2.39	6.00	2.82	2.66	14.23	2.74	4.09	3.90	6.70
Pb	1.10	0.17	1.26	0.77	0.96	19.01	-4.34	1.66	1.71	2.12
Bi	1.77	1.11	8.17	0.57	0.83	7.71	-0.10	0.63	0.57	0.77
Nb	1.10	-0.22	2.13	2.76	0.96	3.91	0.41	1.41	0.67	-0.07
La	-1.36	-1.16	-2.11	-2.34	-1.13	-2.43	0.16	-2.33	-2.53	-1.42
Ce	-3.43	-3.39	-4.79	-5.83	-3.24	-9.16	-1.38	-6.21	-6.31	-5.31
Pr	-0.36	-0.32	-0.53	-0.67	-0.44	-1.27	-0.23	-0.77	-0.72	-0.82
Nd	-0.87	-0.74	-1.88	-2.80	-0.98	-5.38	0.33	-2.28	-2.69	-2.71
Sm	-0.08	-0.11	-0.33	-0.53	0.09	-0.81	0.52	0.00	-0.49	-0.41
Eu	0.34	-0.29	-0.19	-0.37	-0.08	-0.38	-0.11	-0.33	-0.42	-0.28
Tb	0.13	0.03	0.06	-0.05	0.04	-0.06	-0.04	0.11	-0.09	-0.09
Dy	1.22	0.55	0.71	0.00	0.58	0.13	-0.34	1.14	-0.23	-0.58
Ho	0.26	0.09	0.08	-0.07	0.05	0.02	-0.15	0.19	-0.11	-0.21
Er	0.77	0.30	0.18	-0.12	0.15	0.07	-0.54	0.53	-0.39	-0.65
Tm	0.12	0.06	0.05	-0.04	0.04	0.05	-0.06	0.08	-0.03	-0.08
Yb	0.60	0.11	-0.01	-0.42	-0.10	0.55	-0.39	0.43	-0.59	-0.67
Lu	0.10	0.03	0.01	-0.03	0.07	0.17	-0.03	0.12	0.00	-0.05
Hf	0.04	-0.42	-0.82	0.17	-0.31	1.37	-0.52	0.12	0.01	-0.23
Ta	0.02	0.00	0.02	0.05	0.05	0.08	0.00	0.04	0.03	0.00
Th	0.14	-0.40	-0.09	-0.09	-0.29	1.12	-0.31	-0.05	-0.35	-0.96

Abbreviations:

Units

HFL= Hanging wall flow
HBX= Hanging wall breccia
FLT= Footwall lapilli tuff
FT= Footwall tuff
FBX= Footwall breccia
FFL= Footwall flow
INT= Intrusion

Alteration

Qtz-Ser= Quartz-sericite
Chl-Ser= Chlorite-sericite
Chl= Chlorite

Appendix C: Table C.1.2 Mass changes for samples at the Boundary deposit

Sample ID	**H501351**	**H501352**	**H501353**	**H501354**	**H501355**	**H501356**	**H501357**	**H501358**	**H501359**	**H501360**
Hole ID	BD10-106	BD10-106	BD10-106	BD10-106	BD10-106	BD10-106	BD10-106	BD10-106	BD10-106	BD10-106
Depth (m)	13.9	17.1	18.4	21.8	29.4	36.9	40.5	44.3	51.2	68.5
Lithology	FBX	FT	FLT	FBX	FLT	FLT	FT	FLT	FBX	FFL
Alteration	Chl-Ser	Qtz-Ser	Qtz-Ser	Qtz-Ser	Chl-Ser	Qtz-Ser	Qtz-Ser	Qtz-Ser	Qtz-Ser	Qtz-Ser
SiO_2	0.18	-3.68	1.33	-2.46	-9.96	-6.57	-10.61	2.99	9.92	8.51
$A_{l2}O_3$	0.00	0.00	0.00	0.00	0.00	0.00	0.00	0.00	0.00	0.00
FeO	0.93	2.26	2.22	1.83	3.02	0.97	1.84	1.41	-0.68	0.38
MnO	0.08	-0.04	0.03	-0.04	0.09	0.02	0.01	-0.03	0.01	0.02
MgO	4.97	-0.42	0.56	-0.55	2.28	0.35	1.53	-0.24	-0.07	-0.80
CaO	0.30	-0.10	-0.01	-0.11	-0.10	-0.10	-0.08	-0.11	-0.11	-0.10
Na_2O	-1.88	-1.80	-1.83	-1.81	-1.80	-1.80	-1.80	-1.81	-1.82	-1.80
K_2O	-0.43	0.76	0.45	0.71	0.23	0.65	0.40	0.66	0.71	1.06
TiO_2	0.04	0.05	0.05	0.06	0.06	0.05	0.13	0.07	0.05	0.05
P_2O_5	0.02	0.02	0.02	0.03	0.01	0.02	0.04	0.02	0.02	0.02
Net Oxide Change	4.21	-2.96	2.82	-2.35	-6.17	-6.40	-8.54	2.96	8.03	7.33
Ba	-590.05	-240.29	-165.27	-300.77	-498.59	-331.77	-453.49	-276.60	-243.20	-282.43
Sr	-5.18	-12.07	-12.55	-12.05	-9.41	-11.60	-10.80	-10.52	-12.34	-11.23
Y	5.16	0.72	6.17	5.77	1.68	2.61	1.12	3.79	-2.50	4.08
Sc	2.62	1.92	1.56	1.94	2.59	2.29	4.93	3.57	2.88	2.93
Zr	13.75	-1.02	9.42	10.19	16.74	11.99	-19.97	3.21	2.08	12.26
Be	-0.47	-0.50	-0.47	-0.50	-0.52	-0.53	-0.07	0.04	0.07	0.08
V	4.86	7.43	6.95	6.45	9.12	-0.14	48.82	16.29	14.68	3.96
Hg	-4.64	2.89	-2.55	-5.04	-9.58	-9.64	-2.67	-9.39	-9.32	-0.15
Cr 52	26.21	-0.03	28.04	-0.02	-0.14	27.89	53.01	16.86	0.33	0.34
Co	0.51	0.18	-0.64	0.46	-0.67	-0.68	2.42	0.26	-0.63	0.88
Ni	16.99	-0.04	0.25	-0.03	-0.16	11.38	22.56	0.22	0.37	0.39
Cu	-42.58	239.13	1870.85	-29.02	-74.30	652.00	-62.98	-73.60	-52.08	-24.01
Zn	25.26	-70.66	-71.41	-94.50	-44.05	-2.97	-8.71	-58.73	-75.08	-91.14
As	-0.20	10.41	2.81	12.26	2.80	0.00	2.59	0.35	-1.26	1.03
Se 78	0.69	-0.09	0.67	-0.07	-0.42	-0.72	-0.89	0.58	0.98	1.03
Br 79	48.92	47.02	78.55	75.15	34.45	49.53	0.30	71.97	80.27	81.67
Mo	7.85	4.17	8.72	5.33	3.38	8.53	8.20	3.11	3.28	12.55
Ag 107	0.03	0.00	0.03	0.00	-0.02	-0.03	-0.03	0.02	0.04	0.04
Cd	0.02	0.00	0.02	0.00	-0.01	-0.02	-0.03	0.02	0.03	0.03
Sn	-2.95	-1.85	-1.73	-2.28	-2.08	-2.01	-2.79	-0.18	-1.19	-2.40
Sb	0.00	1.66	0.47	0.78	0.03	-0.02	1.05	0.59	0.61	0.30
Te	0.11	-0.02	0.11	-0.01	-0.07	-0.12	-0.14	0.09	0.16	0.17
I	0.95	-0.13	0.93	-0.10	-0.58	-1.00	-1.24	0.81	1.36	1.43
W	5.49	1.48	2.49	2.02	0.82	3.02	6.22	6.37	5.29	3.20
Pb	0.65	-0.09	0.64	-0.07	-0.40	-0.69	-0.85	0.55	0.93	0.98
Bi	0.05	2.74	3.97	2.33	0.19	0.41	0.68	0.15	0.24	2.30
Nb	1.14	2.35	3.66	2.37	3.69	1.19	-0.53	2.50	2.84	2.37
La	-0.50	-3.00	-3.85	0.50	-0.75	-2.42	-3.51	-3.86	0.36	-0.70
Ce	-1.58	-5.74	-6.78	-1.40	-1.93	-5.18	-7.15	-7.39	0.75	-2.20
Pr	-0.29	-0.81	-0.82	-0.46	-0.30	-0.66	-0.68	-0.86	0.06	-0.18
Nd	-0.67	-3.20	-3.19	-2.68	-0.54	-1.75	-1.87	-3.51	-0.26	-0.54
Sm	-0.14	-0.94	-0.73	-0.80	-0.23	-0.18	-0.12	-0.82	-0.13	-0.29
Eu	-0.21	-0.30	-0.33	-0.32	-0.22	-0.31	-0.37	-0.30	-0.31	-0.38
Tb	0.02	-0.14	0.05	-0.01	-0.02	-0.05	-0.09	-0.04	-0.16	0.00
Dy	0.30	-0.62	0.92	0.40	0.10	0.04	-0.36	-0.07	-1.19	0.40
Ho	0.07	-0.20	0.14	0.06	0.04	0.02	-0.11	-0.03	-0.28	-0.02
Er	0.23	-0.43	0.26	0.11	0.22	0.26	-0.27	-0.22	-0.68	-0.10
Tm	0.06	-0.06	0.06	0.02	0.04	0.03	-0.05	-0.03	-0.08	-0.01
Yb	0.10	-0.82	0.11	-0.09	0.09	0.14	-0.67	-0.33	-0.46	-0.18
Lu	0.03	-0.10	0.03	-0.03	0.01	0.04	-0.10	-0.11	-0.04	-0.03
Hf	0.55	-0.65	0.66	-0.06	0.78	0.24	-0.94	0.10	1.34	1.43
Ta	0.02	0.06	0.12	0.07	0.10	0.02	-0.03	0.07	0.10	0.12
Th	-0.10	0.57	1.01	0.50	1.27	-0.14	-1.21	0.18	0.54	1.37

Abbreviations:

Units

HFL= Hanging wall flow
HBX= Hanging wall breccia
FLT= Footwall lapilli tuff
FT= Footwall tuff
FBX= Footwall breccia
FFL= Footwall flow
INT= Intrusion

Alteration

Qtz-Ser= Quartz-sericite
Chl-Ser= Chlorite-sericite
Chl= Chlorite

Appendix C: Table C.1.2 Mass changes for samples at the Boundary deposit

Sample ID	**H501361**	**H501363**	**H501364**	**H501365**	**H501366**	**H501367**	**H501368**	**H501369**	**H501370**	**H501371**
Hole ID	BD11-129	BD10-9	BG10-7	BG10-7	BG10-7	BG10-7	BG10-7	BG10-7	BD11-183	BD11-183
Depth (m)	28.3	10.1	6.5	18.7	31.9	47.2	55.2	63	8.2	21.1
Lithology	FFL	HBX	HFL	FLT	FLT	FLT	FBX	FLT	HFL	HBX
Alteration	Qtz-Ser	Qtz-Ser	Qtz-Ser	Qtz-Ser	Chl-Ser	Qtz-Ser	Qtz-Ser	Chl-Ser	Qtz-Ser	Qtz-Ser
SiO_2	30.17	-18.65	34.81	-15.84	-8.48	4.09	-12.00	-21.21	59.03	-28.03
Al_2O_3	0.00	0.00	0.00	0.00	0.00	0.00	0.00	0.00	0.00	0.00
FeO	6.66	1.62	0.97	0.49	7.26	3.33	1.96	3.58	8.96	3.75
MnO	-0.09	0.07	-0.08	-0.08	-0.06	-0.08	0.04	0.13	-0.07	-0.04
MgO	-2.15	0.21	-0.75	-1.13	-0.11	-1.52	0.63	1.64	-1.89	-0.93
CaO	-0.14	-0.13	-0.12	-0.13	-0.11	-0.12	-0.10	-0.10	-0.13	-0.11
Na_2O	-1.77	-1.94	-1.86	-1.86	-1.87	-1.86	-1.88	-1.90	-1.84	-1.85
K_2O	0.95	0.57	0.73	0.84	0.56	1.08	0.55	0.27	1.09	0.84
TiO_2	0.01	0.02	0.02	0.03	0.05	0.02	0.04	0.04	0.01	0.04
P_2O_5	0.00	0.02	0.02	0.02	0.01	0.01	0.02	0.03	0.01	0.02
Net Oxide Change	33.64	-18.22	33.74	-17.65	-2.76	4.94	-10.75	-17.51	65.17	-26.31
Ba	206.84	199.23	401.17	198.96	-126.85	-177.01	-455.73	-584.35	927.07	66.45
Sr	-12.18	-17.00	-15.26	-13.72	-14.69	-13.34	-14.70	-15.11	-15.03	-15.03
Y	3.09	1.87	-1.28	0.76	2.80	1.06	2.96	5.75	18.46	2.82
Sc	2.63	2.51	0.78	2.42	3.58	1.91	1.86	2.05	-1.29	1.62
Zr	0.91	8.47	3.18	1.61	-4.97	3.32	7.33	-2.99	8.23	6.78
Be	-0.30	0.67	-0.33	-0.17	-0.48	-0.46	-0.09	-0.14	-0.13	-0.23
V	5.92	3.34	6.93	4.95	13.17	4.00	-0.22	-0.35	7.95	1.37
Hg	66.57	153.14	-1.22	-1.23	92.50	0.99	-9.72	0.05	-1.55	-4.26
Cr 52	21.59	-0.74	13.87	-0.76	0.20	13.67	19.59	-0.62	3.30	23.27
Co	12.19	-0.73	1.46	-0.74	7.62	-0.62	-0.70	-0.17	28.54	10.20
Ni	2.01	-0.83	1.74	-0.86	0.22	0.41	8.90	-0.70	3.71	8.80
Cu	948.34	-75.56	-70.76	-75.62	-35.64	-73.24	759.22	429.38	-67.08	-65.93
Zn	-102.52	600.25	-80.85	-115.49	-99.40	-122.56	-15.87	140.23	-94.64	-38.53
As	15.75	-0.55	1.40	4.78	123.96	12.86	13.50	56.95	42.54	9.95
Se 78	5.38	-2.22	4.63	-2.29	0.60	1.10	-1.17	-1.86	9.90	-3.01
Br 79	138.30	4.37	206.52	19.17	62.43	73.52	7.42	35.17	200.14	-8.82
Mo	10.51	1.40	4.75	2.65	5.47	6.63	6.44	2.46	13.55	46.67
Ag 107	0.20	-0.08	0.17	-0.09	0.02	0.04	-0.04	-0.07	0.37	-0.11
Cd	0.18	1.60	0.16	-0.08	0.02	0.04	-0.04	-0.06	0.33	-0.10
Sn	-0.83	-0.02	-0.88	-2.43	-1.76	-1.46	-1.88	1.97	2.23	-1.98
Sb	1.80	0.86	1.66	1.80	6.47	1.83	0.41	13.91	2.38	1.23
Te	0.87	-0.36	0.75	-0.37	3.13	0.18	-0.19	-0.30	1.59	-0.49
I	7.46	-3.07	6.42	-3.18	0.83	1.53	-1.63	-2.58	13.71	-4.17
W	3.06	2.09	0.94	3.27	2.55	3.39	1.24	0.28	1.41	8.72
Pb	5.10	398.96	4.39	-2.17	0.57	1.05	-1.11	-1.76	9.38	-2.86
Bi	11.01	0.04	2.10	3.58	7.99	2.75	2.90	1.89	4.87	1.78
Nb	0.80	3.04	2.42	1.70	3.02	1.92	0.46	-0.02	2.36	1.16
La	-2.31	-1.47	-0.87	-2.13	-1.41	-3.34	-4.36	-3.98	-3.83	-3.64
Ce	-6.29	-3.49	-2.16	-5.21	-3.63	-8.20	-10.06	-8.68	-8.67	-8.32
Pr	-0.75	-0.37	-0.22	-0.60	-0.33	-0.98	-1.28	-1.06	-0.98	-0.96
Nd	-2.92	-1.26	-0.21	-1.65	-1.15	-3.74	-5.19	-3.71	-3.08	-3.98
Sm	-0.63	-0.35	0.01	-0.48	-0.17	-0.85	-0.86	-0.83	0.00	-0.80
Eu	-0.01	0.45	-0.14	0.17	0.10	0.76	-0.20	-0.18	-0.27	-0.44
Tb	-0.09	0.02	-0.06	-0.02	0.00	-0.09	-0.07	0.04	0.41	-0.08
Dy	-0.42	0.24	0.08	0.00	0.20	-0.30	-0.24	0.66	2.72	-0.15
Ho	-0.12	0.00	-0.03	-0.01	0.04	-0.08	-0.03	0.10	0.49	-0.02
Er	-0.66	0.05	-0.21	-0.14	0.12	-0.11	-0.11	0.37	1.30	-0.11
Tm	-0.08	0.00	-0.05	-0.01	0.01	-0.04	-0.01	0.06	0.17	-0.03
Yb	-0.70	-0.12	-0.25	-0.43	-0.02	-0.22	-0.31	0.29	0.88	-0.31
Lu	-0.11	0.04	-0.07	-0.05	-0.02	-0.06	0.03	0.04	0.13	-0.04
Hf	0.43	0.60	-0.07	-0.25	0.20	-0.77	-0.86	-0.95	0.51	-0.42
Ta	0.03	0.09	0.09	0.04	0.05	0.06	0.00	-0.02	0.05	0.00
Th	1.14	1.41	1.17	0.80	1.11	0.51	-0.57	-0.74	1.51	-0.53

Abbreviations:

Units

HFL= Hanging wall flow
HBX= Hanging wall breccia
FLT= Footwall lapilli tuff
FT= Footwall tuff
FBX= Footwall breccia
FFL= Footwall flow
INT= Intrusion

Alteration

Qtz-Ser= Quartz-sericite
Chl-Ser= Chlorite-sericite
Chl= Chlorite

Appendix C: Table C.1.2 Mass changes for samples at the Boundary deposit

Sample ID	H501372	H501373	H501374	H501375	H501376	H501377	H501378	H501379
Hole ID	BD11-183	BD11-183	BD11-183	BG10-2	BG10-2	BG10-2	BG10-2	BG10-2
Depth (m)	34.3	52	68	10.1	20.4	27.6	31.9	44.3
Lithology	HFL	HFL	HFL	HFL	HFL	FLT	FBX	FLT
Alteration	Qtz-Ser	Qtz-Ser	Qtz-Ser	Qtz-Ser	Qtz-Ser	Qtz-Ser	Qtz-Ser	Qtz-Ser
SiO_2	4.83	26.12	-44.87	7.84	1.32	-4.55	11.58	-6.10
$A_{l2}O_3$	0.00	0.00	0.00	0.00	0.00	0.00	0.00	0.00
FeO	2.28	2.68	-0.42	1.64	0.81	4.45	1.02	1.79
MnO	-0.04	-0.06	-0.06	0.00	-0.03	0.12	0.07	0.01
MgO	-0.94	-1.56	-0.99	-0.29	-0.99	0.35	-0.10	-0.14
CaO	-0.11	-0.07	-0.10	-0.12	-0.10	1.12	1.08	-0.11
Na_2O	-1.86	-1.84	-1.86	-1.88	-1.86	-1.88	-1.88	-1.85
K_2O	0.82	0.99	0.92	0.57	0.94	0.66	0.85	0.42
TiO_2	0.01	0.05	0.05	0.01	0.01	0.06	0.03	0.02
P_2O_5	0.00	0.00	0.01	0.01	0.02	0.02	0.01	0.01
Net Oxide Change	5.00	26.29	-47.31	7.77	0.13	0.34	12.66	-5.94
Ba	-118.42	30.07	-14.53	-367.50	-277.49	-438.67	-463.38	-449.50
Sr	-15.56	-10.39	-15.21	-16.53	-14.93	3.15	7.56	-11.46
Y	3.91	-0.31	-7.12	8.05	3.39	5.01	-0.35	5.09
Sc	-0.34	2.90	2.02	0.94	1.10	3.62	2.50	2.46
Zr	11.64	5.90	7.10	5.99	3.38	4.85	14.14	12.19
Be	-0.46	0.29	0.05	-0.45	0.01	-0.48	0.14	-0.04
V	6.08	23.30	6.91	4.06	0.02	11.12	5.46	5.17
Hg	-9.32	-4.26	25.63	59.12	-2.92	-0.47	-9.16	-9.60
Cr 52	0.32	32.86	-2.12	0.42	23.23	0.21	8.78	-0.18
Co	2.87	3.30	-0.87	2.99	1.95	12.13	0.55	4.45
Ni	0.36	1.45	-2.39	0.47	11.02	0.24	0.68	-0.21
Cu	-73.33	-71.30	-78.47	223.10	3.10	6.81	-72.73	-74.40
Zn	-92.74	-100.29	-113.36	320.14	-0.41	-36.79	-20.69	110.62
As	3.77	8.87	8.33	0.25	2.78	44.68	2.32	-0.25
Se 78	0.97	3.87	-6.37	1.26	0.13	0.64	1.83	-0.55
Br 79	61.56	134.03	-65.41	74.47	20.23	99.83	40.06	32.85
Mo	9.36	10.11	5.61	1.66	11.16	6.04	4.26	2.80
Ag 107	0.04	0.14	-0.24	0.05	0.00	0.02	0.07	-0.02
Cd	0.03	0.13	-0.21	1.75	0.00	0.02	0.06	-0.02
Sn	-1.08	-1.24	-3.38	-1.78	-2.26	7.26	-0.88	-0.81
Sb	0.80	3.90	5.54	1.43	0.76	1.97	1.18	0.41
Te	0.16	0.62	-1.03	0.20	0.02	0.10	0.29	-0.09
I	1.35	5.36	-8.83	1.74	0.17	0.89	2.53	-0.77
W	2.71	7.36	2.12	3.93	2.33	0.40	0.54	1.06
Pb	0.92	3.67	-6.04	1.19	0.12	0.61	1.73	-0.53
Bi	0.92	2.34	0.75	0.16	0.08	3.26	0.44	-0.30
Nb	2.11	1.91	1.78	1.99	0.41	0.27	3.06	2.60
La	-1.68	-7.29	-4.35	-1.94	-1.85	3.14	-2.13	-1.00
Ce	-4.45	-15.88	-8.81	-4.62	-5.33	6.19	-5.27	-2.86
Pr	-0.51	-2.06	-1.06	-0.58	-0.71	0.87	-0.69	-0.43
Nd	-1.70	-8.91	-3.88	-2.37	-2.18	4.00	-2.65	-1.01
Sm	-0.34	-2.05	-1.00	-0.46	-0.37	1.29	-0.74	-0.25
Eu	-0.41	-0.61	-0.02	-0.23	-0.26	0.43	-0.08	-0.09
Tb	-0.01	-0.25	-0.21	-0.06	-0.08	0.27	-0.13	0.02
Dy	-0.01	-0.85	-1.28	-0.05	-0.20	1.78	-0.51	0.43
Ho	-0.03	-0.15	-0.28	0.04	-0.04	0.29	-0.06	0.15
Er	0.01	-0.38	-0.88	0.27	0.05	0.68	-0.06	0.43
Tm	0.00	-0.05	-0.10	0.03	0.02	0.13	0.00	0.08
Yb	-0.17	-0.39	-0.96	0.07	0.13	0.55	-0.08	0.27
Lu	-0.01	-0.07	-0.15	-0.02	0.04	0.09	0.00	0.08
Hf	0.21	1.07	1.08	-0.03	-0.30	0.49	2.35	0.21
Ta	0.09	0.09	0.04	0.08	-0.01	0.02	0.13	0.10
Th	0.99	0.79	0.39	0.73	-0.39	-0.02	1.01	0.79

Abbreviations:

Units

HFL= Hanging wall flow
HBX= Hanging wall breccia
FLT= Footwall lapilli tuff
FT= Footwall tuff
FBX= Footwall breccia
FFL= Footwall flow
INT= Intrusion

Alteration

Qtz-Ser= Quartz-sericite
Chl-Ser= Chlorite-sericite
Chl= Chlorite

Appendix C.2: Mass Changes by Alteration Assemblage and Lithology

HFL= Hanging Wall Flow
HBX= Hanging Wall Breccia
FLT= Footwall Lapilli Tuff
FT= Footwall Tuff
FBX= Footwall Breccia
INT= Intrusion

Quartz-Sericite Alteration
Chlorite-Sericite Alteration
Intense Chlorite Alteration

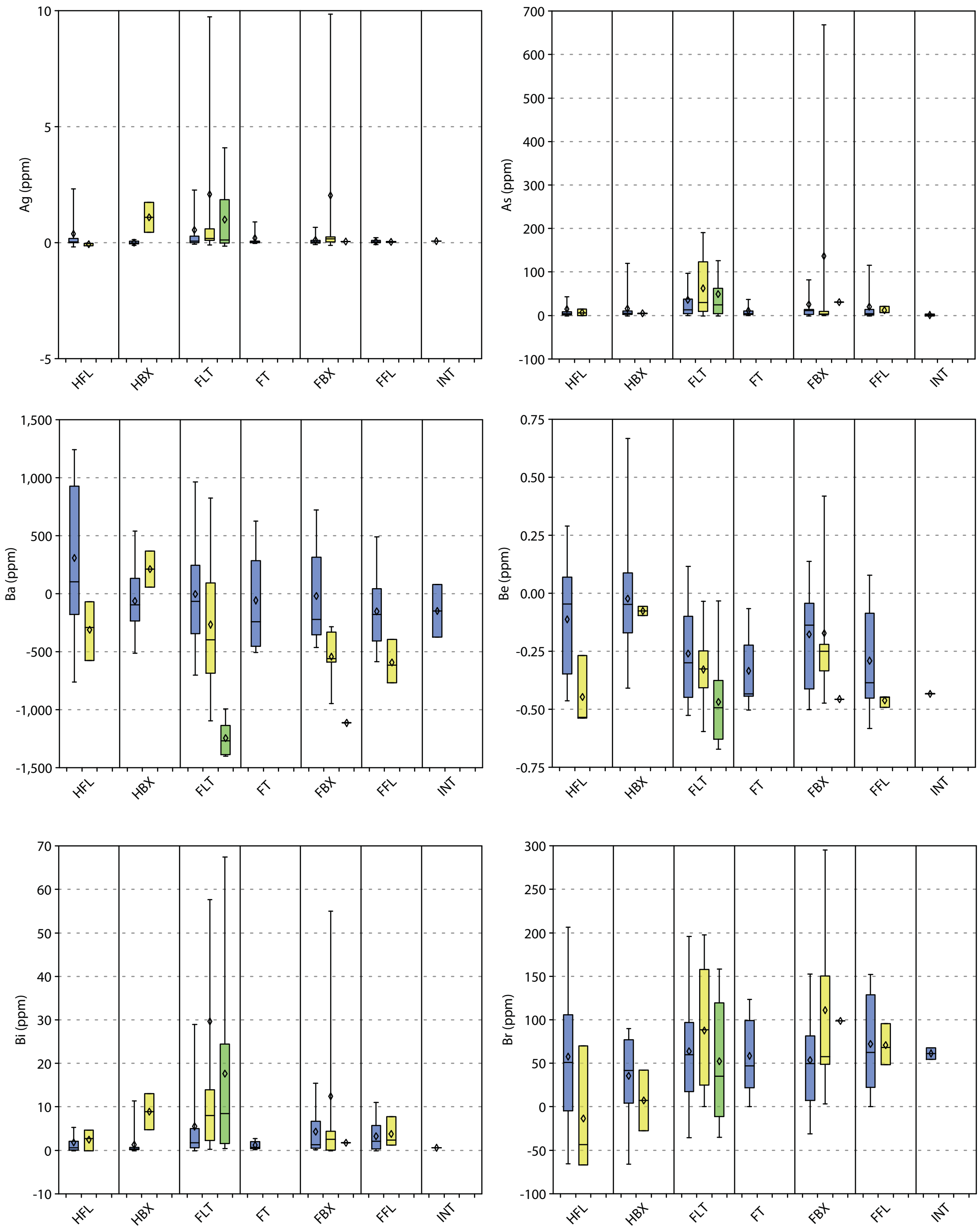

*Whiskers extend to 5th and 95th percentile; diamonds represent the mean.

Appendix C.2: Mass Changes by Alteration Assemblage and Lithology

HFL= Hanging Wall Flow
HBX= Hanging Wall Breccia
FLT= Footwall Lapilli Tuff
FT= Footwall Tuff
FBX= Footwall Breccia
INT= Intrusion

Quartz-Sericite Alteration
Chlorite-Sericite Alteration
Intense Chlorite Alteration

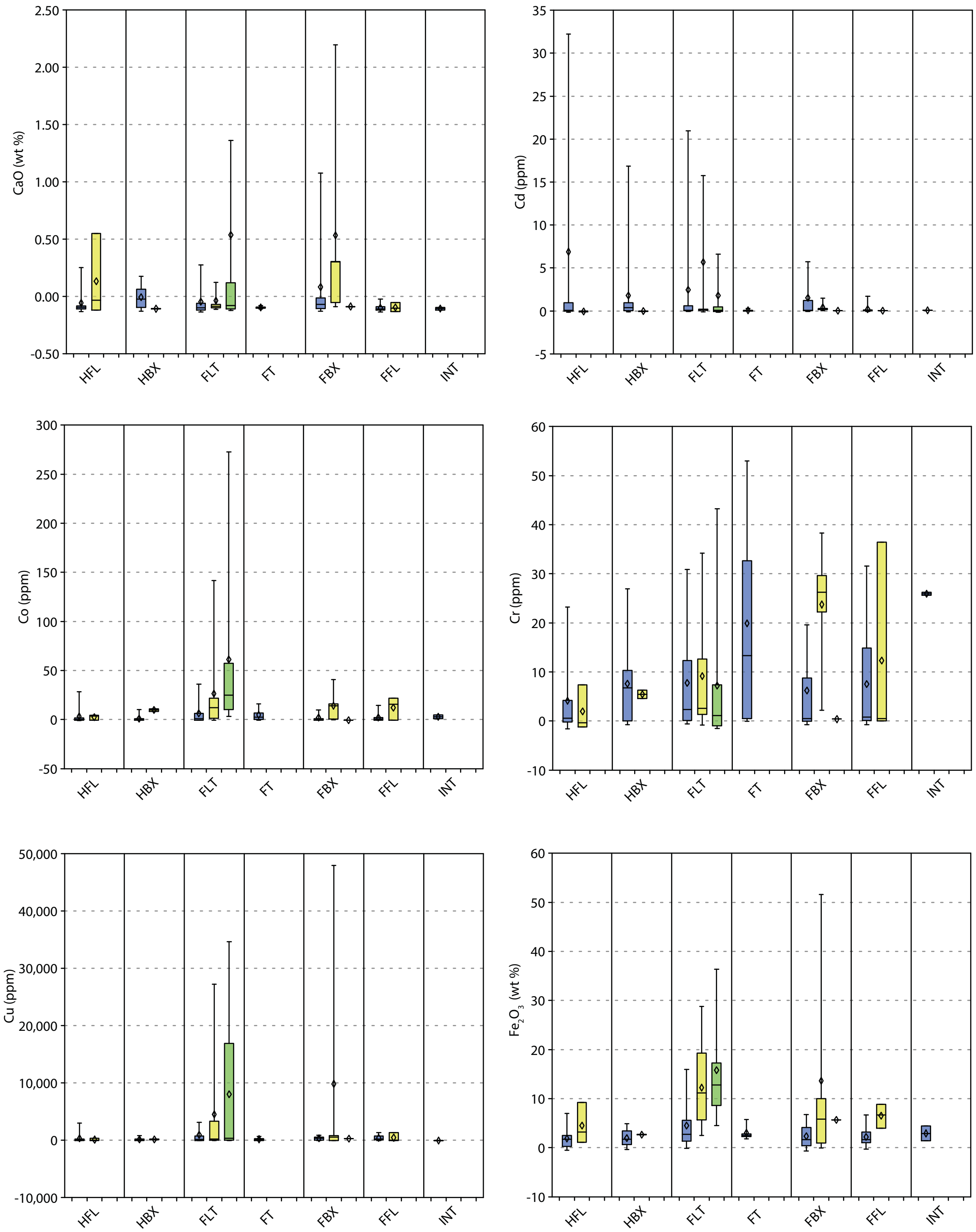

*Whiskers extend to 5th and 95th percentile; diamonds represent the mean.

Appendix C.2: Mass Changes by Alteration Assemblage and Lithology

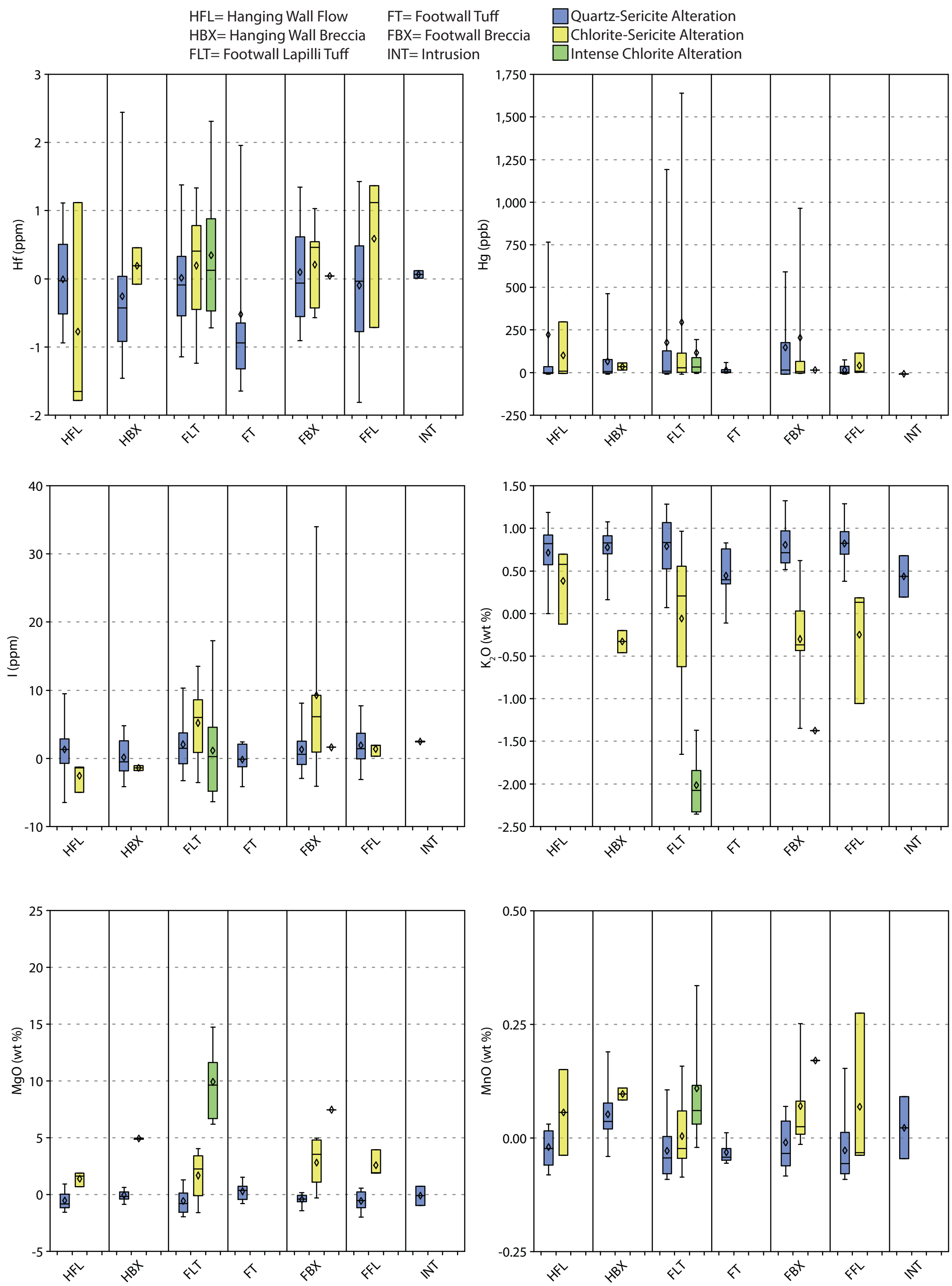

*Whiskers extend to 5th and 95th percentile; diamonds represent the mean.

Appendix C.2: Mass Changes by Alteration Assemblage and Lithology

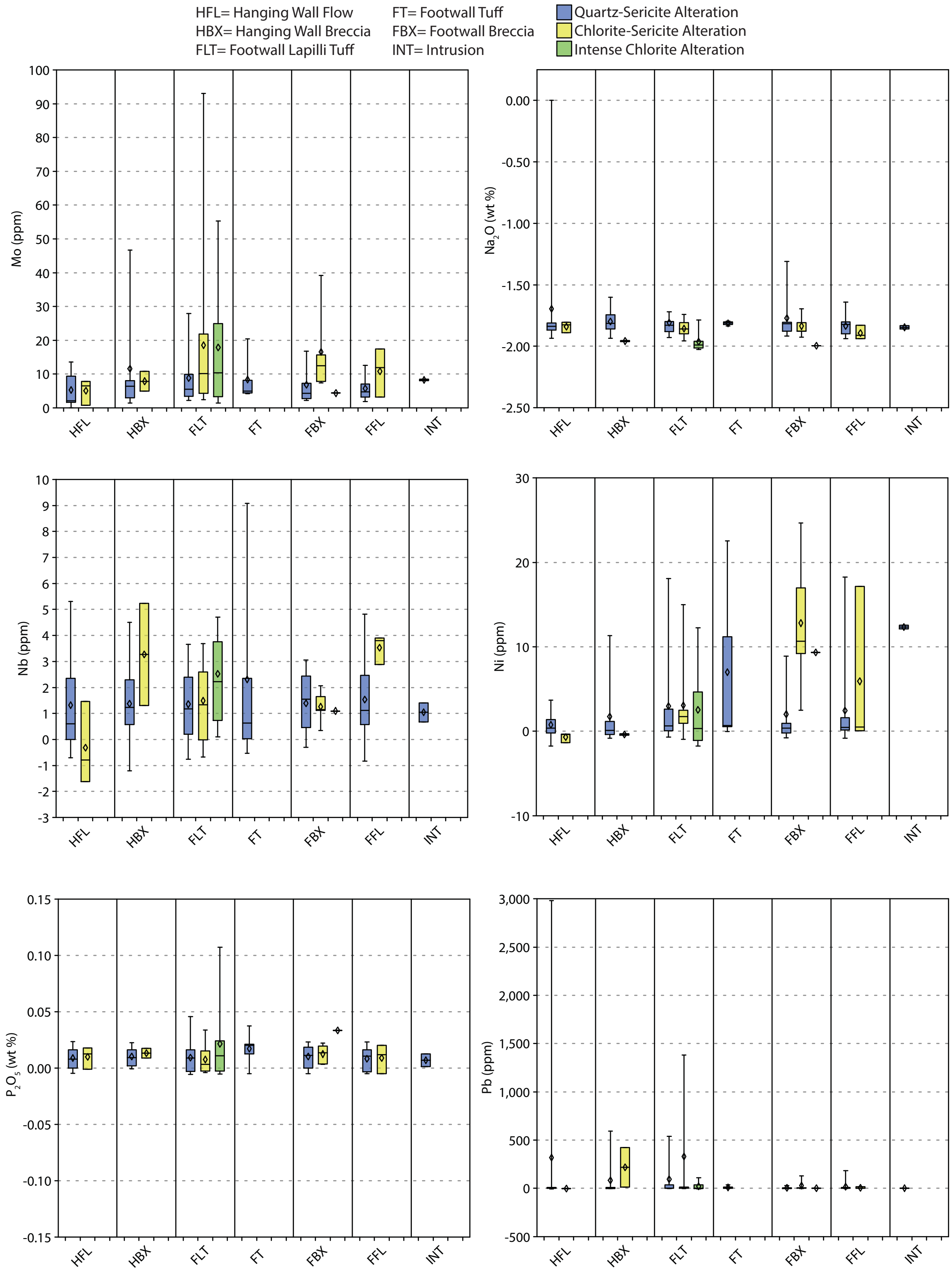

*Whiskers extend to 5th and 95th percentile; diamonds represent the mean.

Appendix C.2: Mass Changes by Alteration Assemblage and Lithology

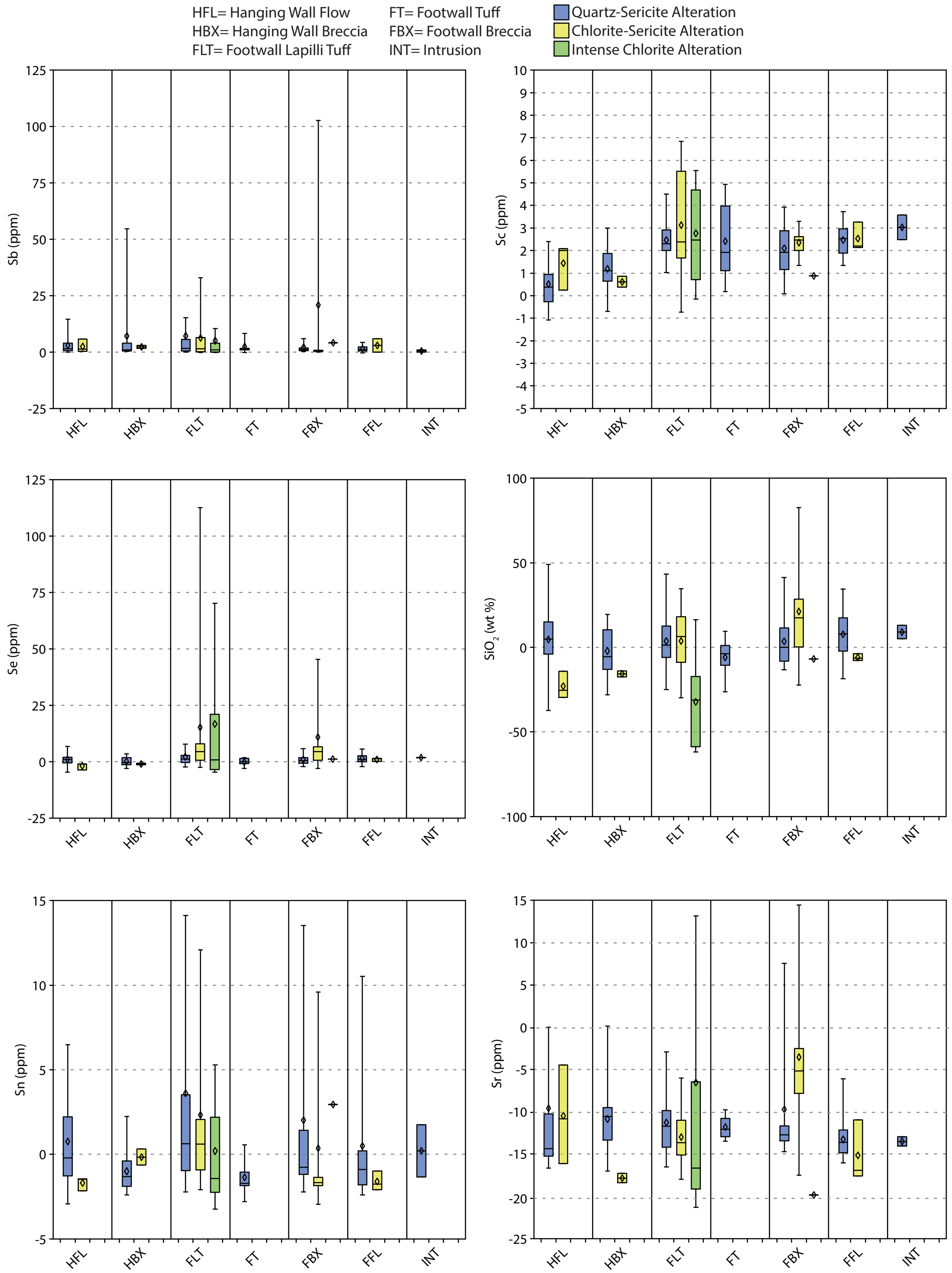

*Whiskers extend to 5th and 95th percentile; diamonds represent the mean.

Appendix C.2: Mass Changes by Alteration Assemblage and Lithology

HFL= Hanging Wall Flow
HBX= Hanging Wall Breccia
FLT= Footwall Lapilli Tuff
FT= Footwall Tuff
FBX= Footwall Breccia
INT= Intrusion

Quartz-Sericite Alteration
Chlorite-Sericite Alteration
Intense Chlorite Alteration

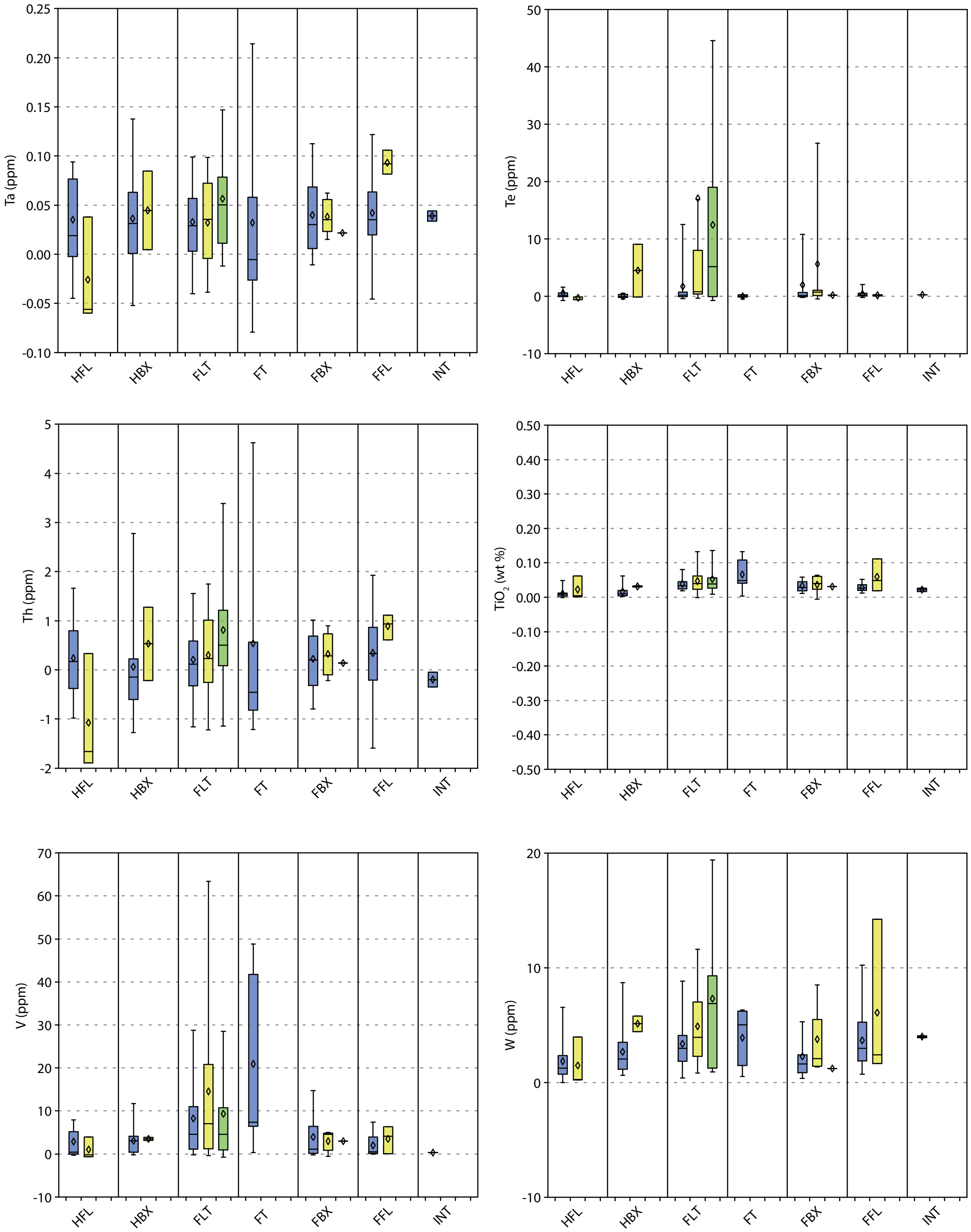

*Whiskers extend to 5th and 95th percentile; diamonds represent the mean.

Appendix C.2: Mass Changes by Alteration Assemblage and Lithology

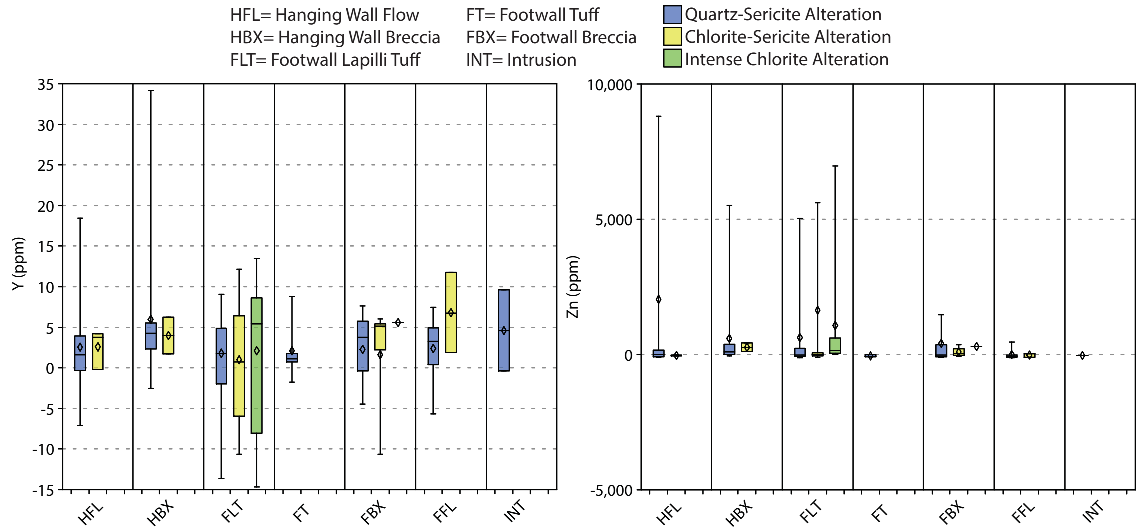

*Whiskers extend to 5th and 95th percentile; diamonds represent the mean.

Appendix D: Principal Component Analysis

D.1-Supplementary Principal Component Analysis Methods

A principal component analysis (PCA) was carried out on the geochemical dataset presented in Appendix B. A PCA is useful in determining geochemical trends in large data sets by grouping elements that exhibit similar behavior together. Prior to running the analysis, data had to be pretreated. Any element that contained more than 10% of values below the limit of detection had to be removed. Once these elements were removed the data underwent a pair of statistical tests known as the Kaiser-Meyer-Olkin (KMO) and Bartlett's tests. These tests are used to determine if the data require further treatment (e.g., log center transformation). The results of these tests indicated that the data do not require further treatment. One final round of data reduction was performed prior the analysis: a correlation matrix was created using the remaining elements and any elements that had low correlation coefficients (<0.5) with all other elements were removed. The elements that remained after reduction and that were used in the analysis are as follows: SiO_2, Al_2O_3, FeO, MnO, MgO, CaO, Na_2O, K_2O, TiO_2, P_2O_5, LOI, Ba, Sr, Y, Sc, V, Hg, Cr, Co, Cu, Zn, As, Br, Mo, Sn, Sb, W, Pb, Bi, and Lu. Previous PCA attempts included all rare earth elements and high field strength elements; however, these elements are essentially immobile and the results were heavily skewed towards these group of elements. In order to focus the analysis on the mobile elements, only one high field strength (Y) and one rare earth element (Lu) was included.

The actual analysis was performed using the IBM SPSS Statistics™ software. The conditions for the principal component analysis are as follows: the analysis used a correlation coefficient matrix, KMO and Bartlett's test of sphericity, utilized the varimax rotation option, and suppressed any coefficients below 0.3.

The results of the analysis are found in Table D.1.1. For a complete explanation of principal component analyses please refer to "Statistics and Data Analysis in Geology" by J.C. Davis and "Statistical Data Analysis Explained: Applied Environmental Statistics with R" by C. Reimann, P. Filzmoser, R. Garrett, and R. Dutter.

Table D1.1 KMO and Bartlett's Test

Kaiser-Meyer-Olkin Measure of Sampling Adequacy.		0.394
Bartlett's Test of Sphericity	Approx. Chi-Square	9149.84
	df	435
	Sig.	0.00

Table D1.2 Total Variance Explained

Component	Initial Eigenvalues			Extraction Sums of Squared Loadings			Rotation Sums of Squared Loadings		
	Total	% of Variance	Cumulative %	Total	% of Variance	Cumulative %	Total	% of Variance	Cumulative %
1	5.947	19.824	19.824	5.947	19.824	19.824	5.222	17.408	17.408
2	5.264	17.547	37.372	5.264	17.547	37.372	4.569	15.230	32.638
3	3.094	10.315	47.687	3.094	10.315	47.687	2.952	9.839	42.477
4	2.185	7.283	54.970	2.185	7.283	54.970	2.718	9.059	51.536
5	1.766	5.887	60.857	1.766	5.887	60.857	2.082	6.939	58.475
6	1.458	4.859	65.716	1.458	4.859	65.716	1.800	6.001	64.476
7	1.284	4.281	69.997	1.284	4.281	69.997	1.541	5.136	69.612
8	1.088	3.628	73.625	1.088	3.628	73.625	1.204	4.013	73.625
9	.944	3.148	76.773						
10	.877	2.923	79.697						
11	.739	2.465	82.162						
12	.716	2.386	84.548						
13	.662	2.207	86.754						
14	.621	2.069	88.823						
15	.526	1.753	90.576						
16	.455	1.518	92.094						
17	.438	1.461	93.555						
18	.367	1.222	94.777						
19	.352	1.174	95.952						
20	.281	.935	96.887						
21	.246	.821	97.708						
22	.198	.661	98.368						
23	.158	.528	98.896						
24	.113	.377	99.273						
25	.082	.274	99.547						
26	.055	.183	99.729						
27	.052	.174	99.903						
28	.025	.083	99.986						
29	.004	.014	100.000						
30	.000	.000	100.000						

Table D1.3 Rotated Component Matrix

	Component							
	1	2	3	4	5	6	7	8
FeO	.895							
SiO2	-.840			-.307				
LOI	.831			.347				
Co	.693							
Mo	.669							
Cu	.669							
K2O	-.608	.369		-.541				
W	.578				.306			
Bi	.567							.314
Al2O3		.911						
Sc		.864			.321			
Lu		.836						
Y		.834						
TiO2		.718			.592			
P2O5		.411		.401	.402			
Zn			.930					
Hg			.917					
Pb			.876					
Sn			.455					
MnO				.698				
CaO				.683		.465		
MgO	.483	.371		.682				
Ba	-.450	.348		-.495				
V					.857			
Cr					.741			
Sr				.303		.884		
Na2O						.808		
Sb							.770	
As	.331						.660	
Br								-.825

Extraction Method: Principal Component Analysis.

a. Rotation converged in 12 iterations.

Rotation Method: Varimax with Kaiser Normalization.

Appendix E: Scanning Electron Microscope Analysis

E.1-Supplementary Scanning Electron Microscope Analysis Methods

Scanning electron microscope (SEM) analyses were used to document finer scale textures, trace minerals, and semi-quantitative chemical information of the sulfide phases and textural relationships. SEM analyses were undertaken at Memorial University's CREAIT-Micro-Analysis Facility, Inco Innovation Centre (MAF-IIC) using the FEI MLA 650F SEM. Analyses took place on polished thin section (25x45 mm) at a constant 25 kV and variable working distance (14.0-15.5 mm). Characteristic mineral phases and textures were identified using backscatter electron imaging, whereas semi-quantitative data were collected using point analyses and element maps. The SEM analyses were critical in identifying all the mineral phases present within the Boundary deposit. The following set of images represents typical mineral phases from each alteration assemblage.

E.1.2 SEM Image Compilation: H500615

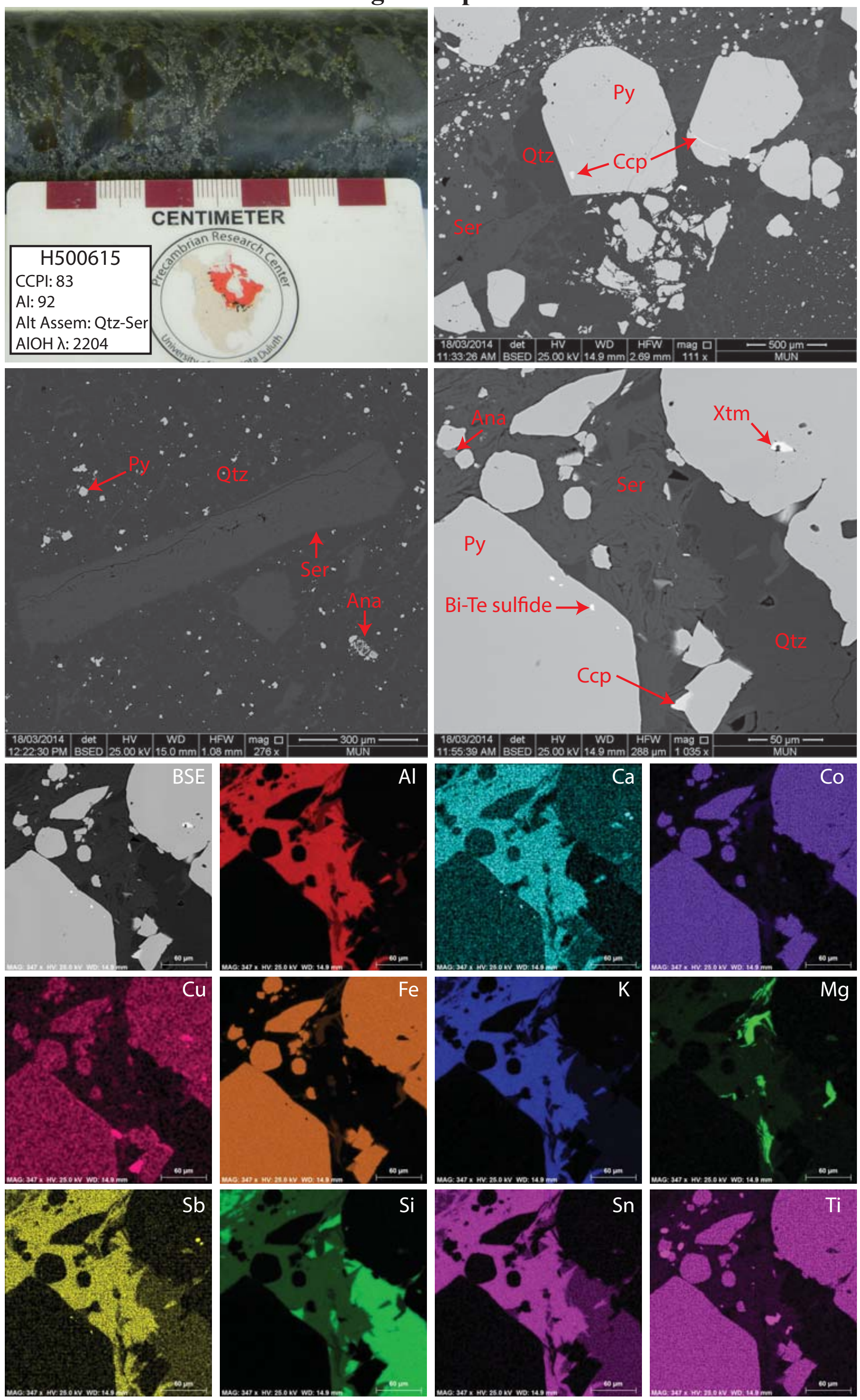

E.1.2 SEM Image Compilation: H500684

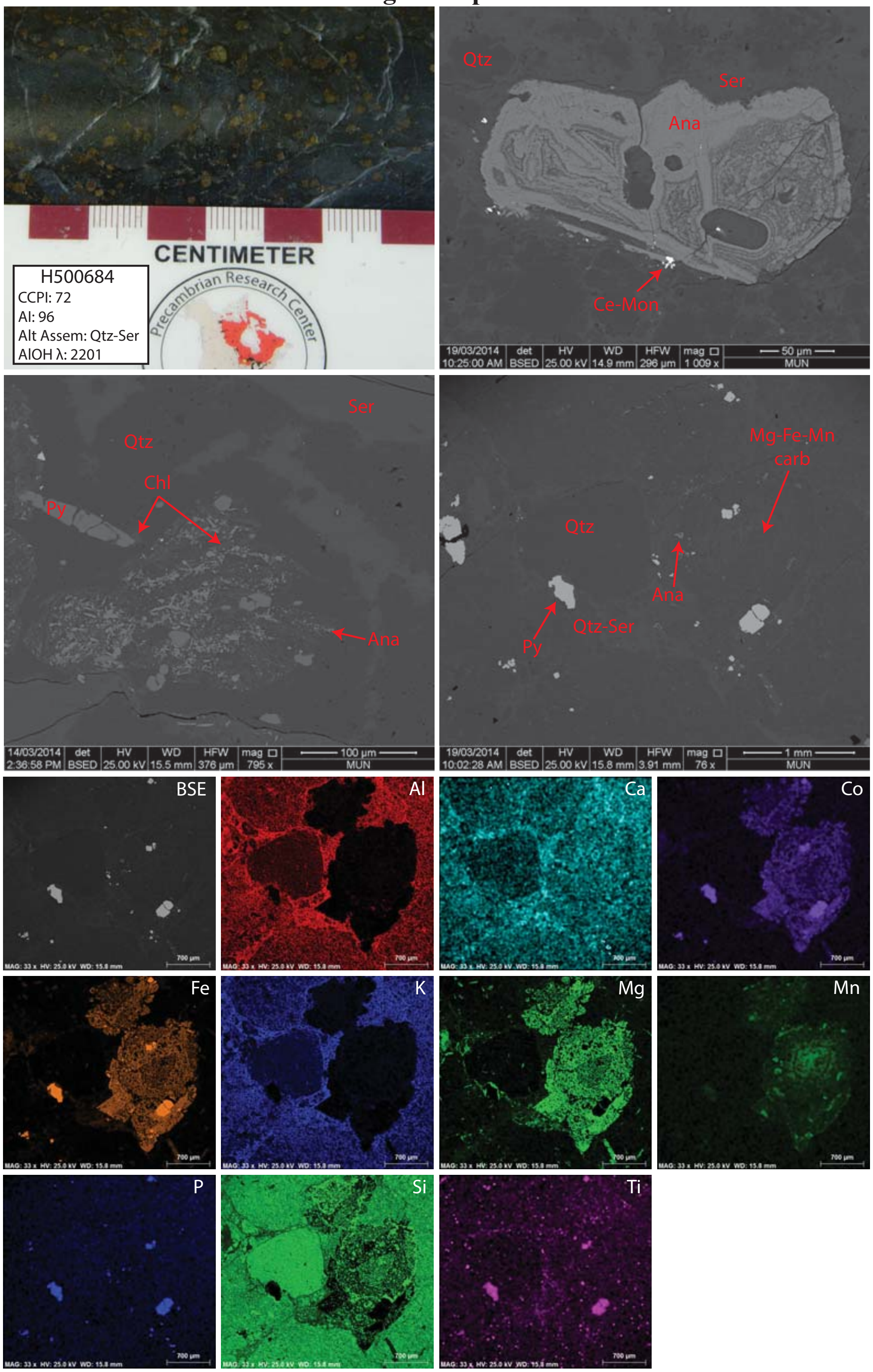

E.1.2 SEM Image Compilation: H500686

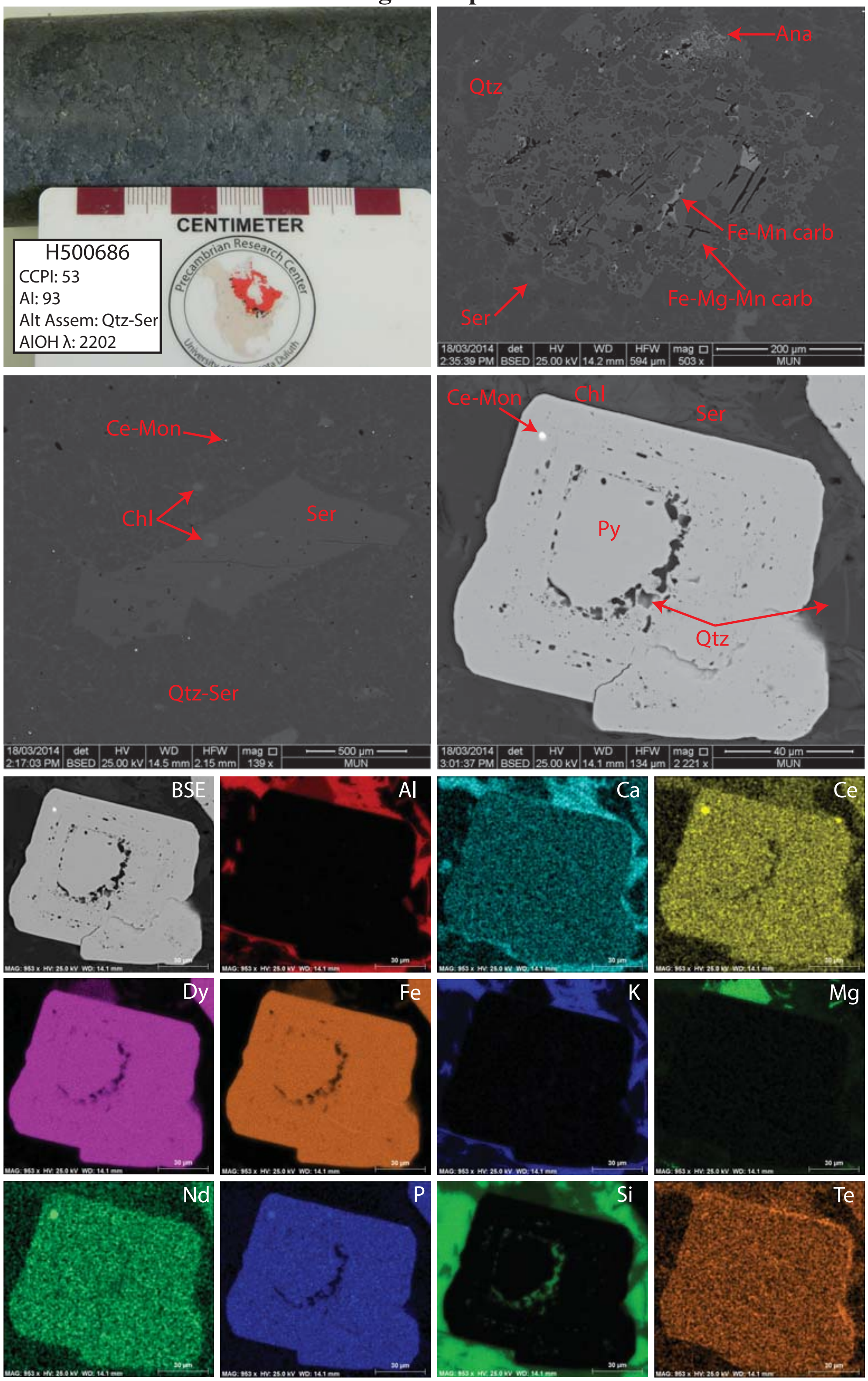

E.1.2 SEM Image Compilation: H501259

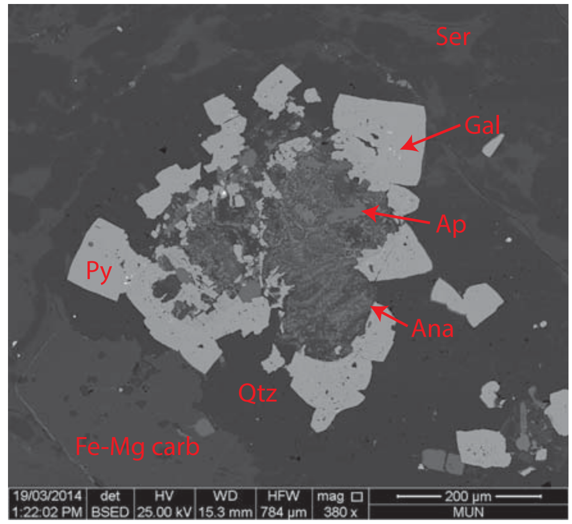

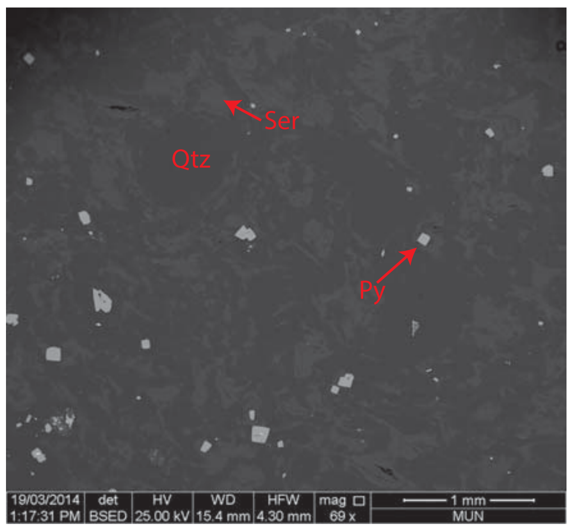

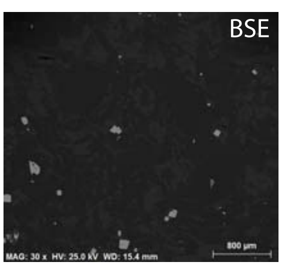

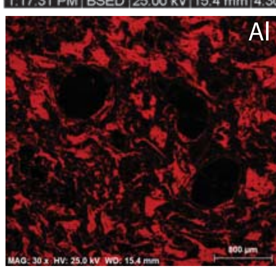

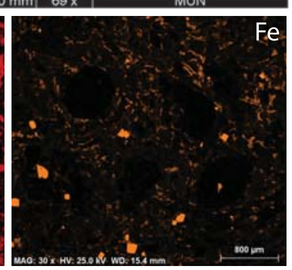

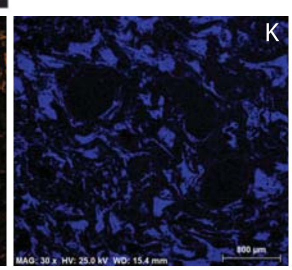

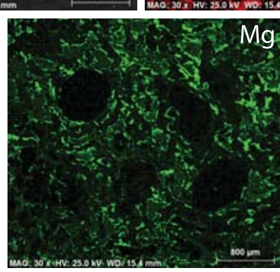

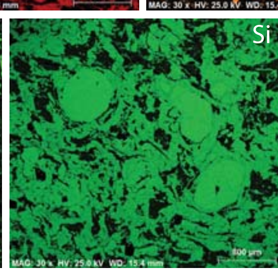

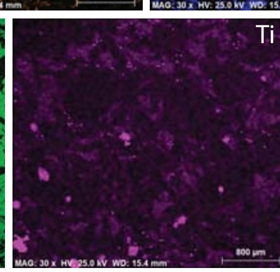

E.1.2 SEM Image Compilation: H501297

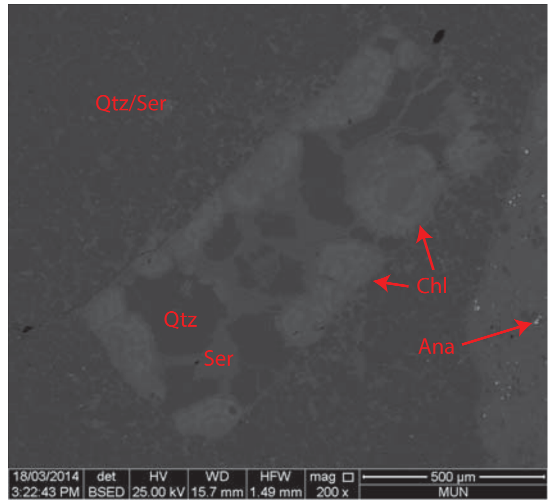

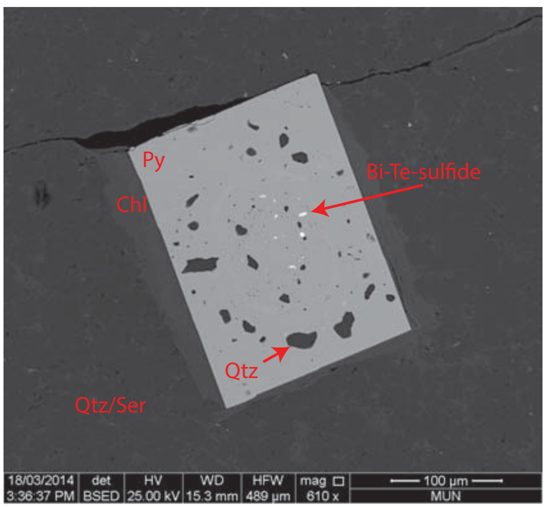

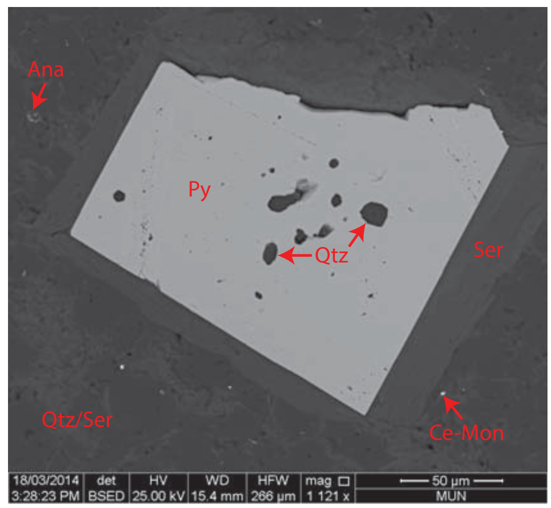

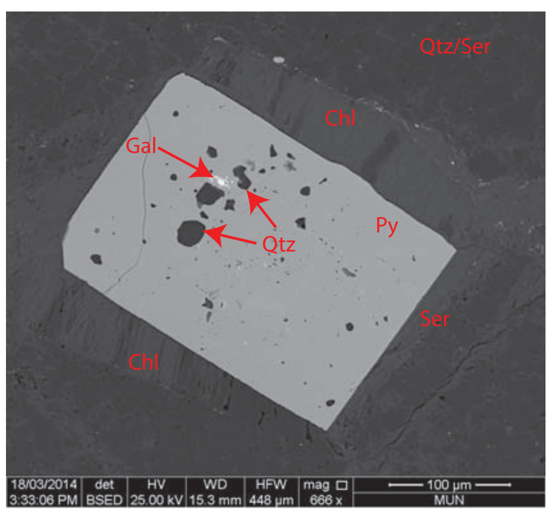

E.1.2 SEM Image Compilation: H501332

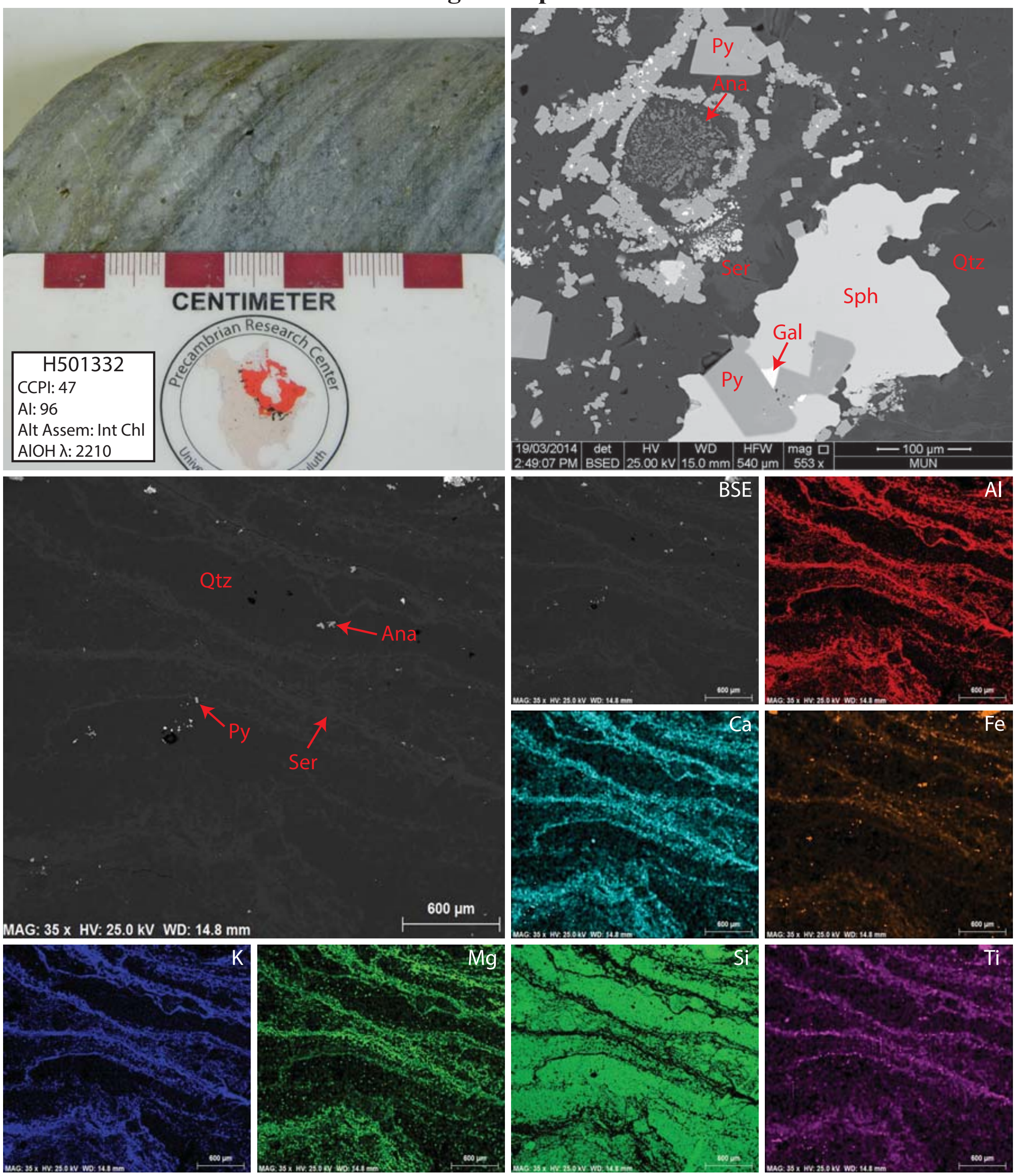

E.1.2 SEM Image Compilation: H501332 Cont.

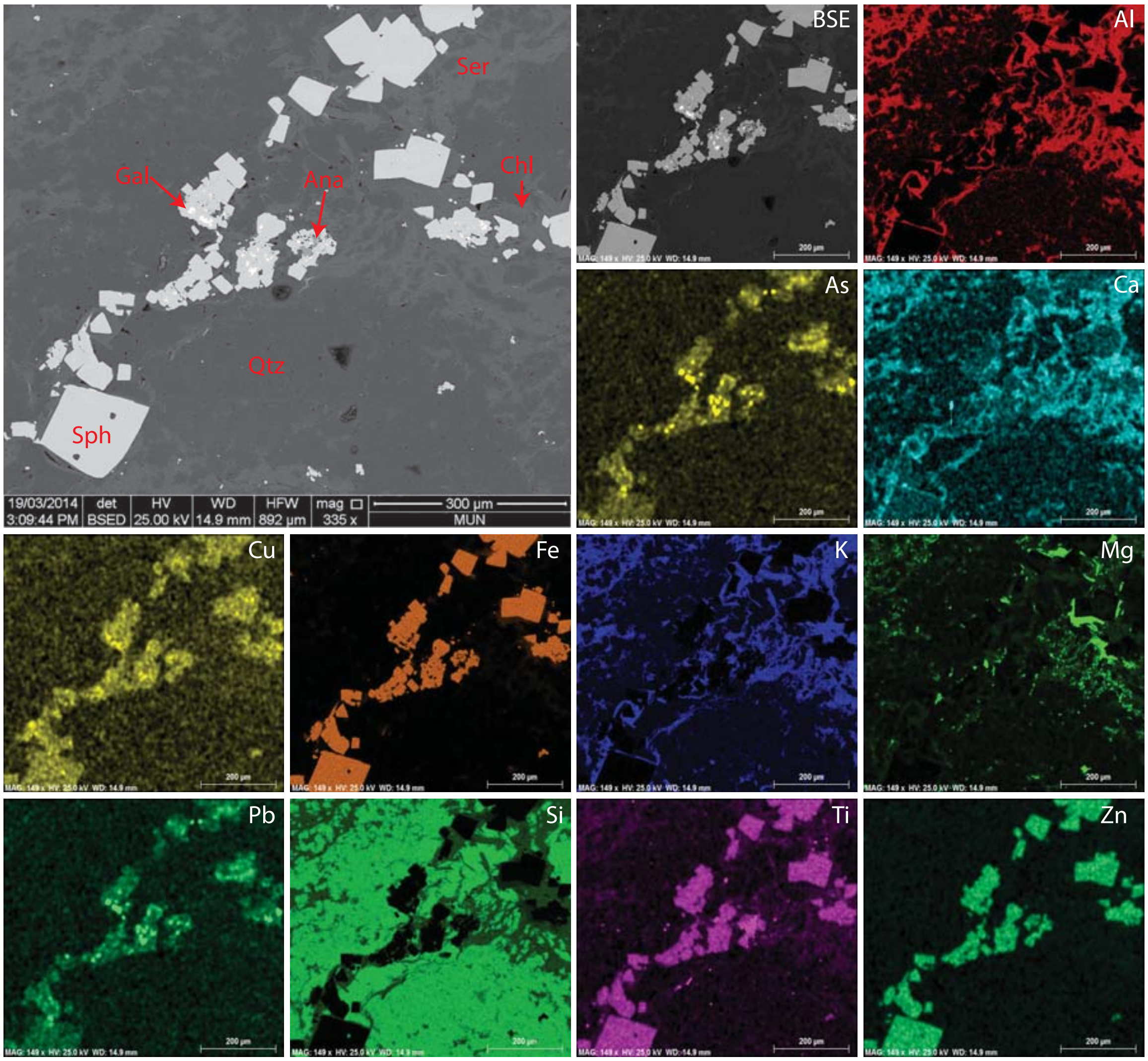

E.1.2 SEM Image Compilation: H501203

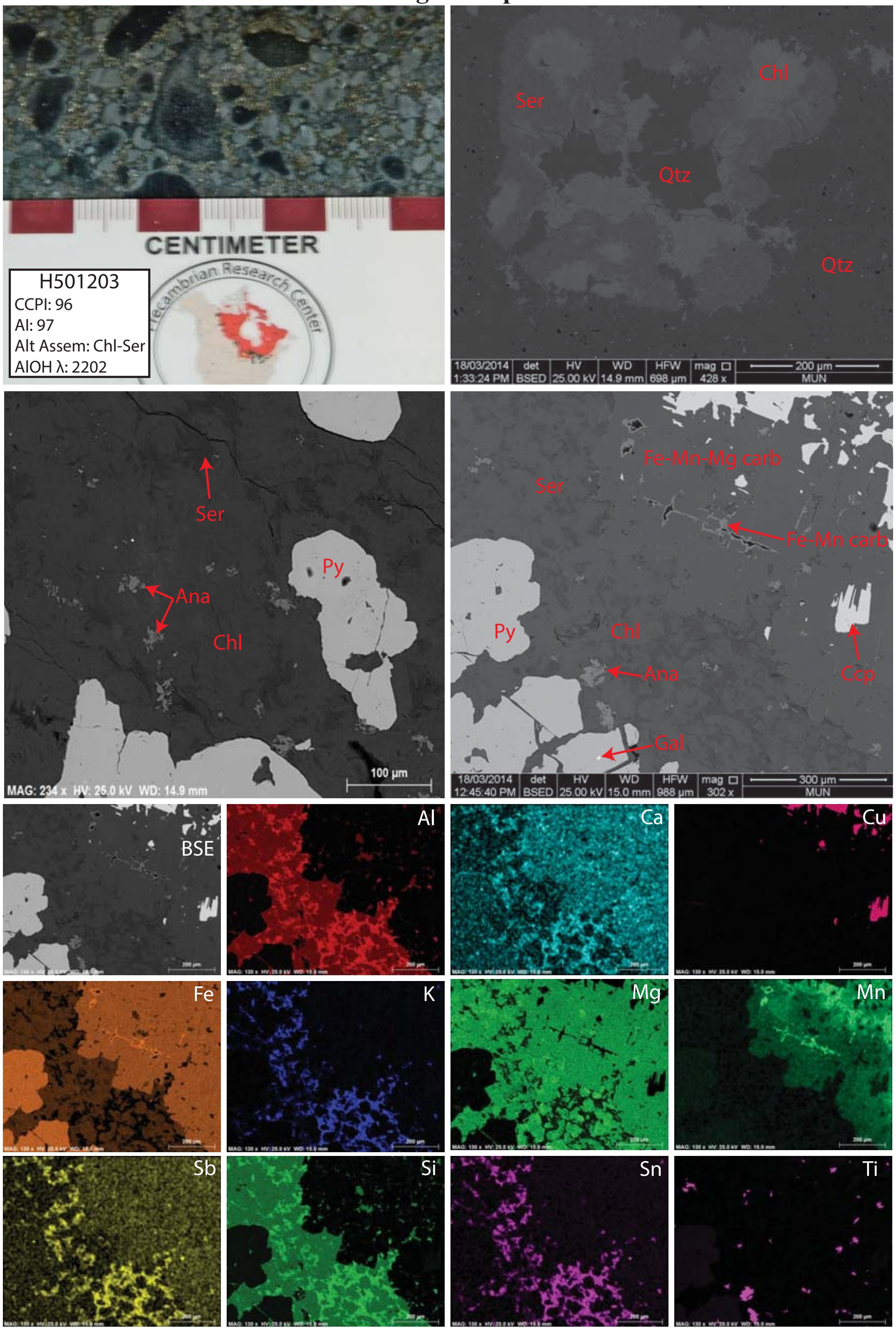

E.1.2 SEM Image Compilation: H501206

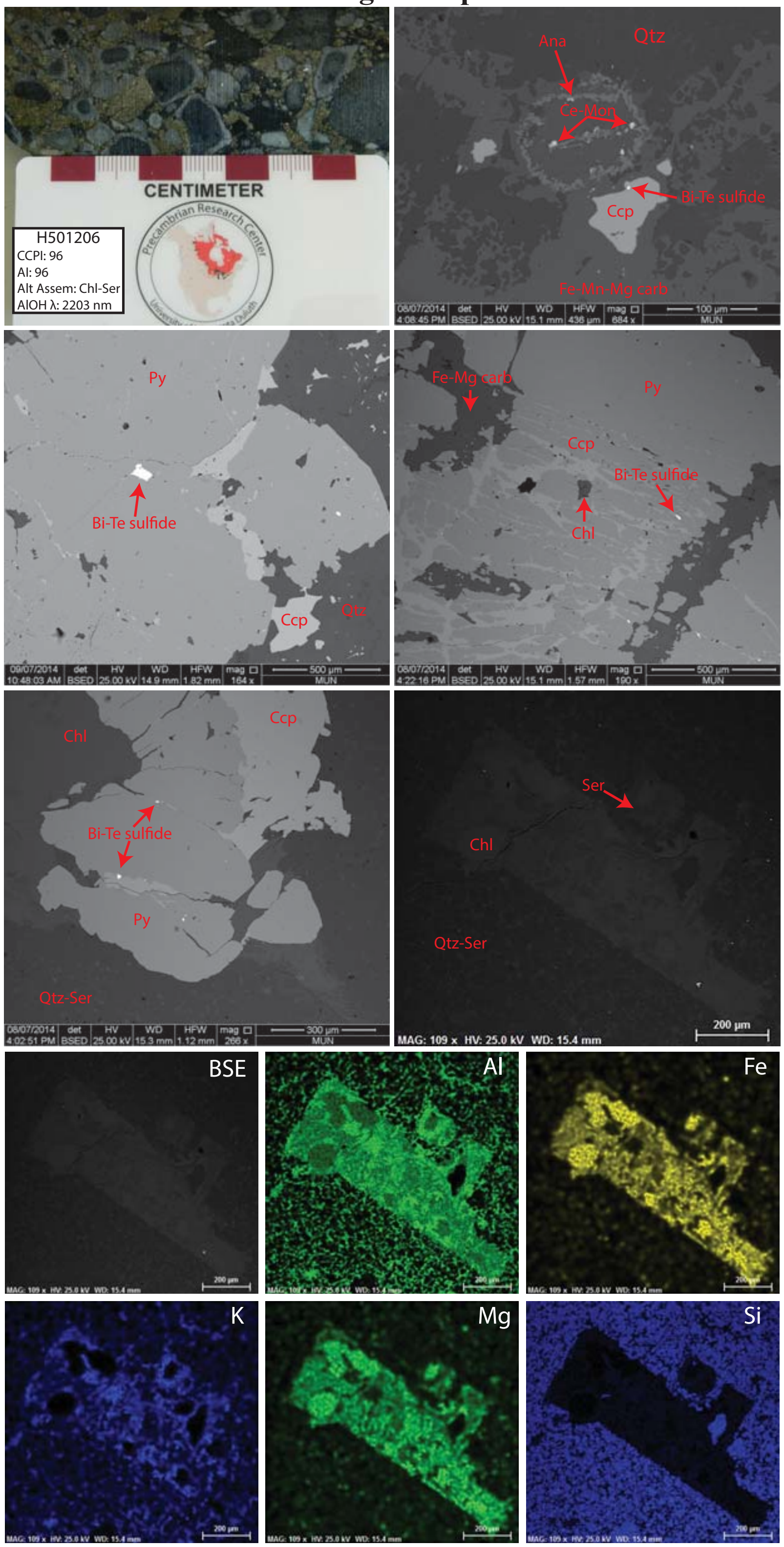

E.1.2 SEM Image Compilation: H501206 Cont.

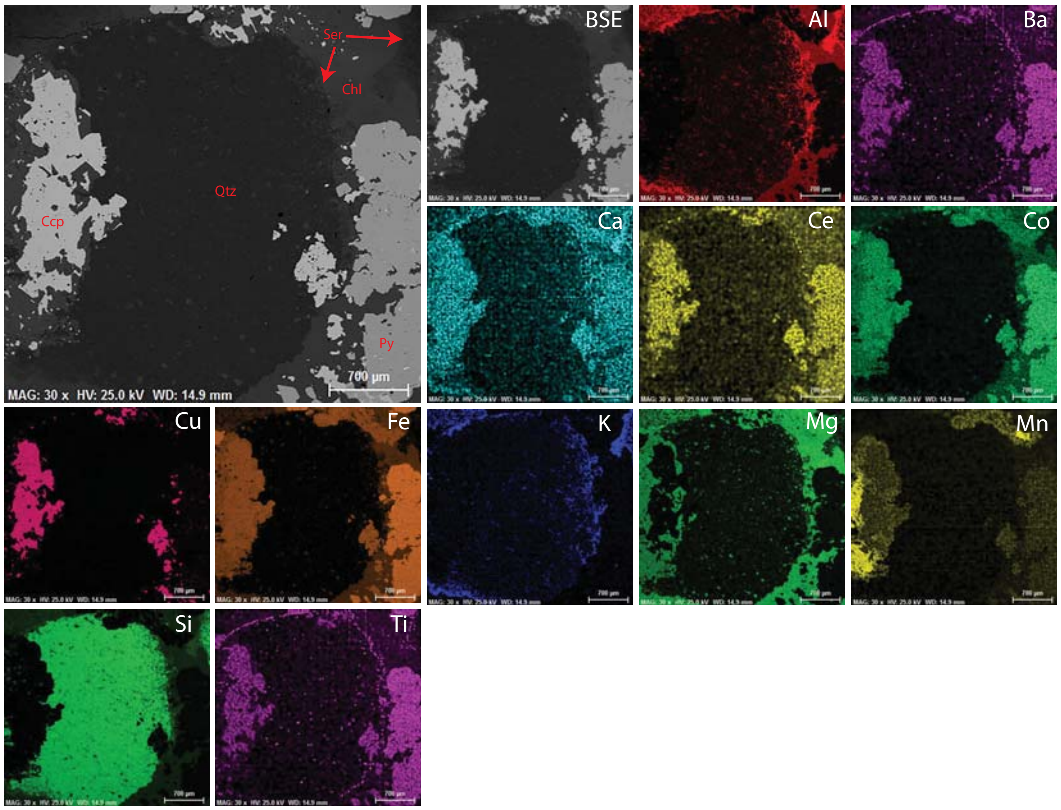

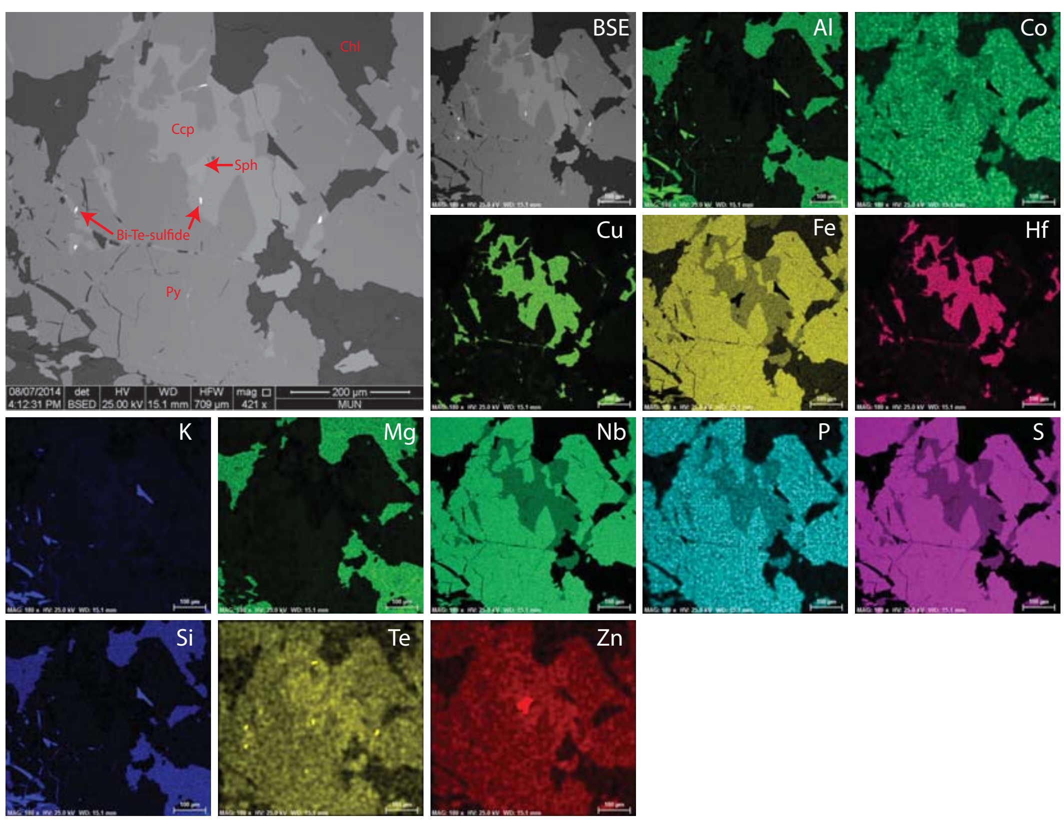

E.1.2 SEM Image Compilation: H501206 Cont.

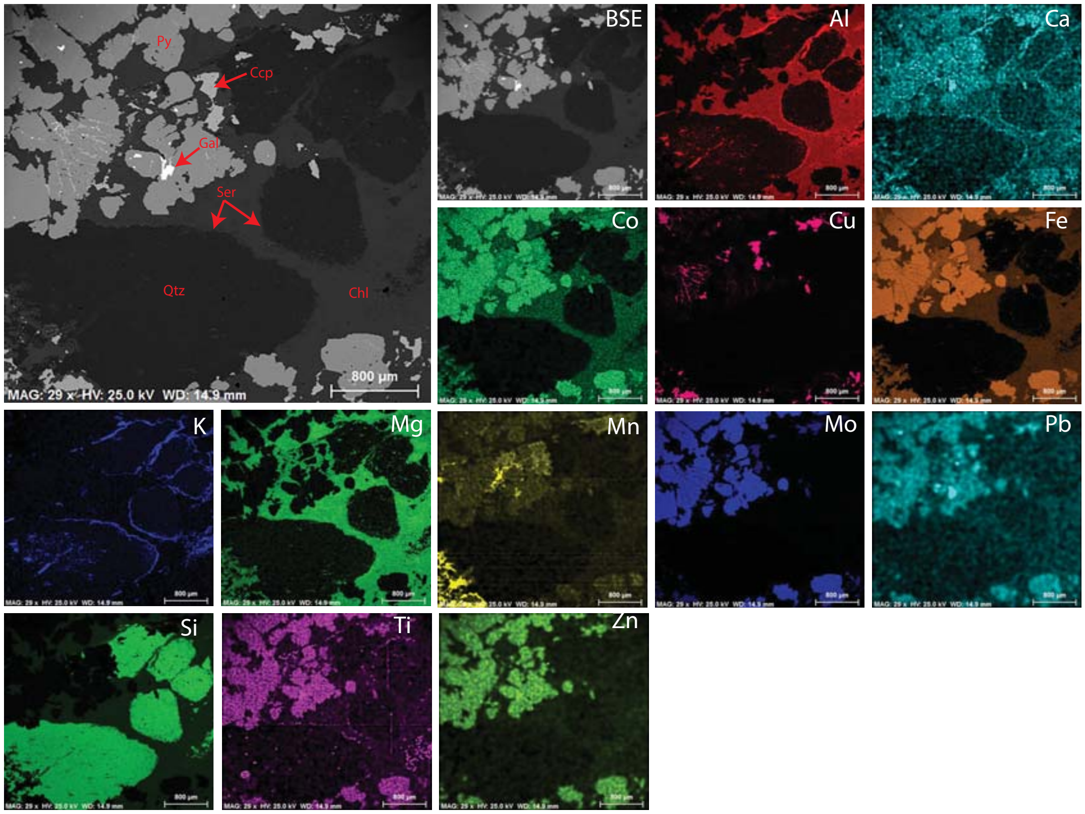

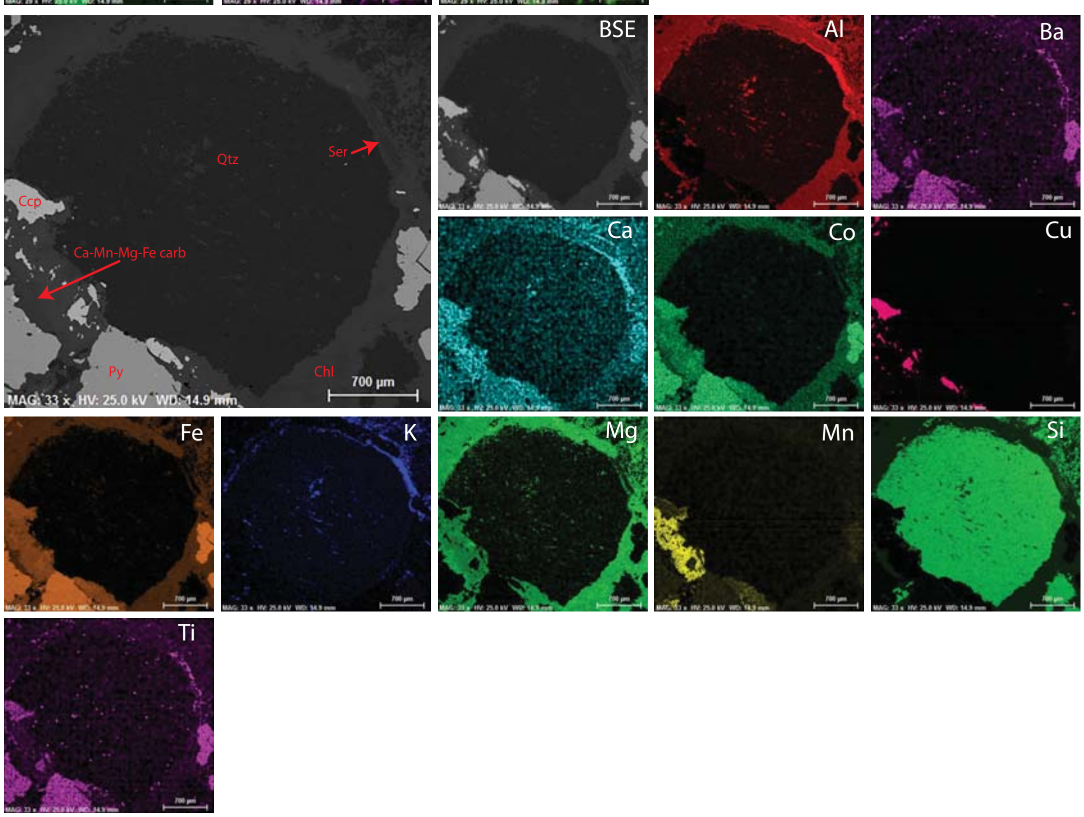

E.1.2 SEM Image Compilation: H501317

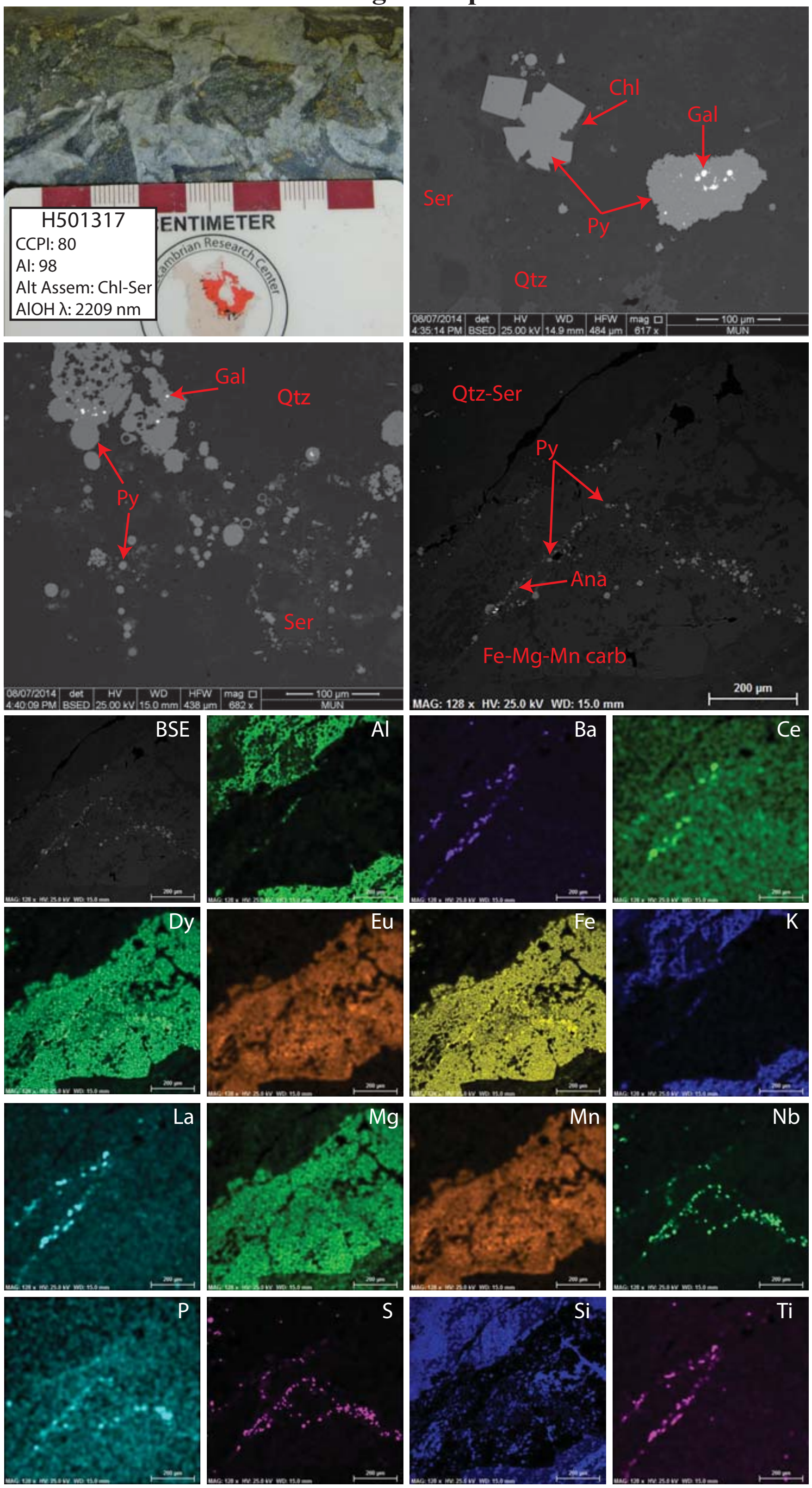

E.1.2 SEM Image Compilation: H500662

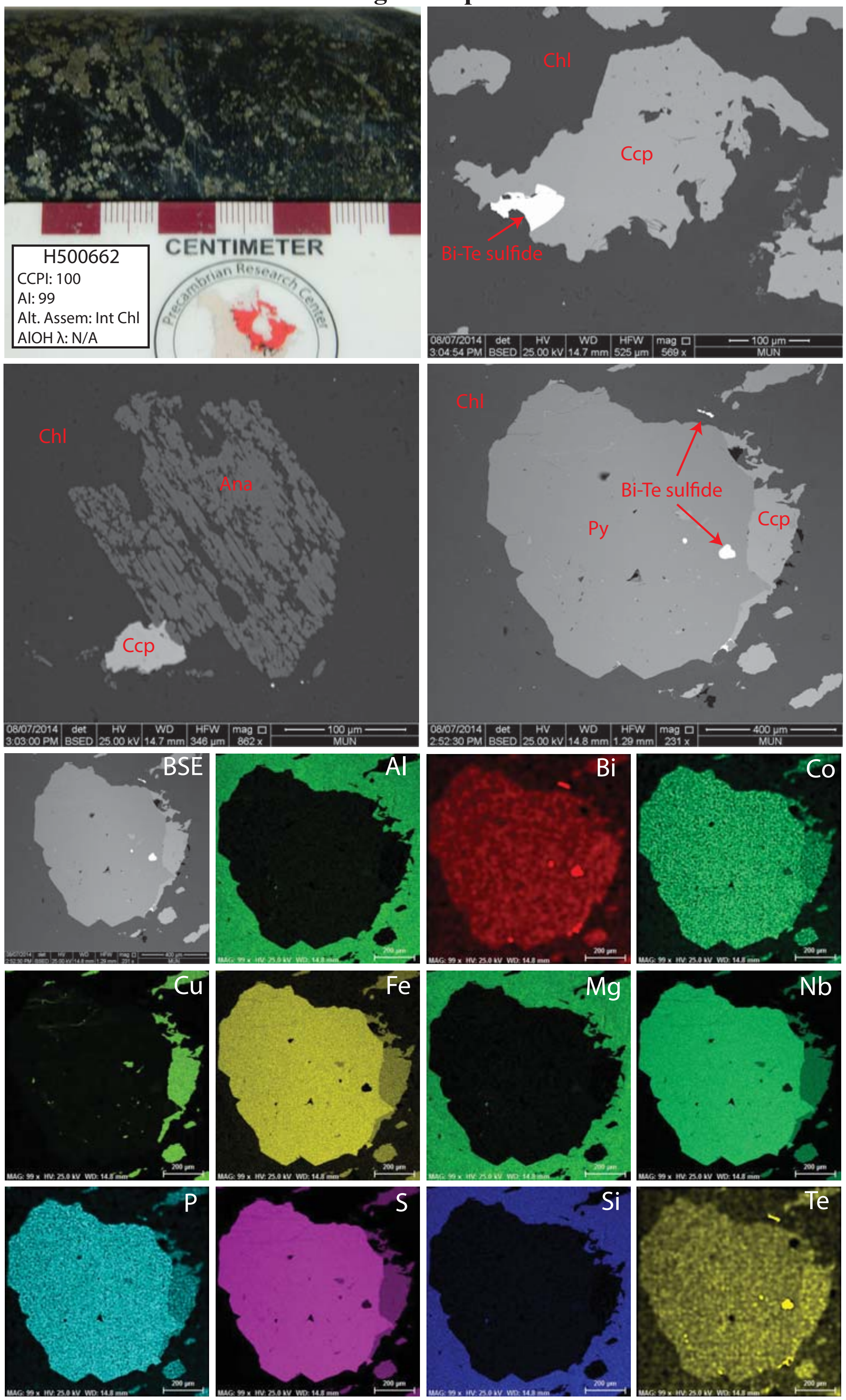

E.1.2 SEM Image Compilation: H500663

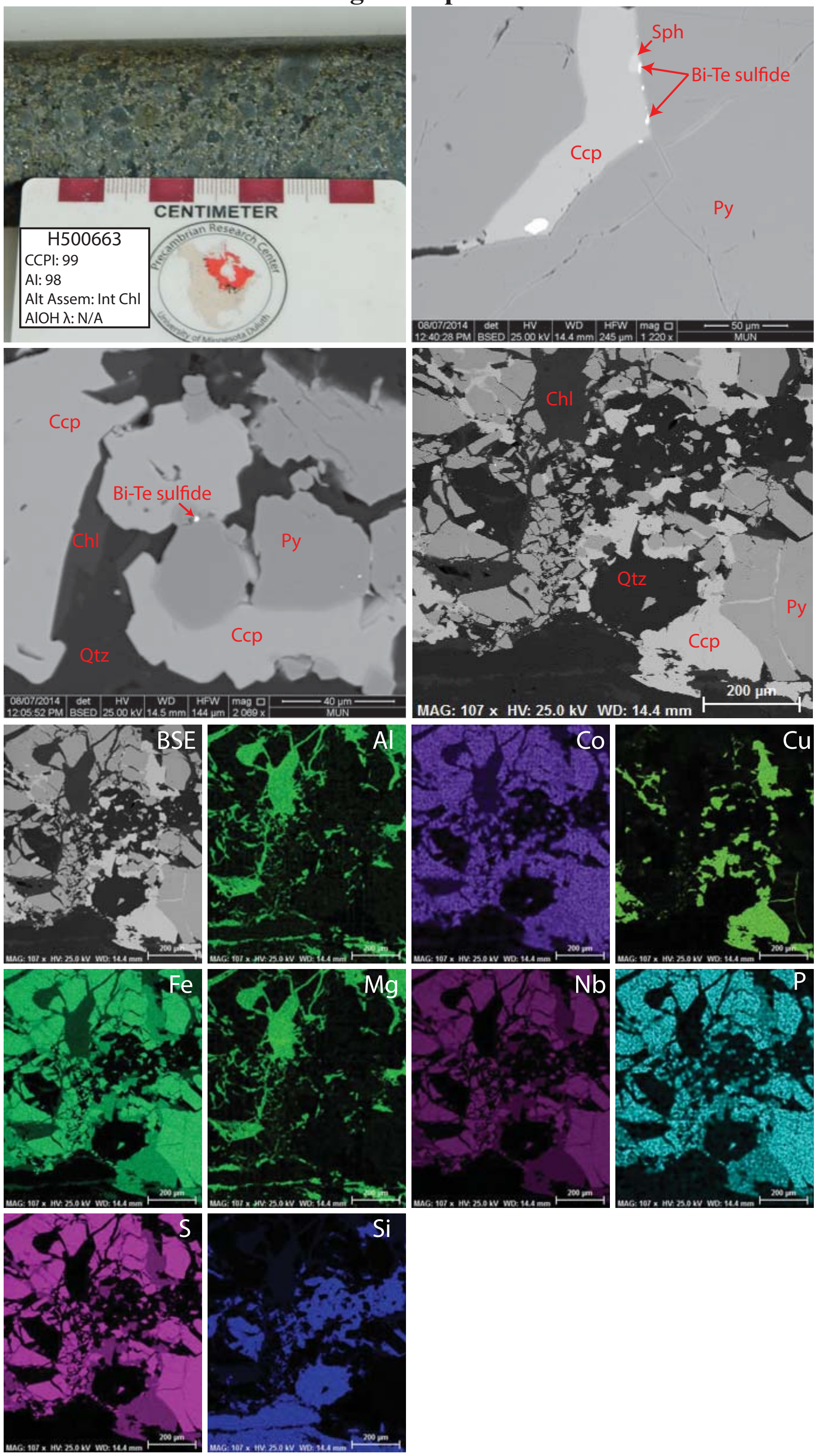

E.1.2 SEM Image Compilation: H501306

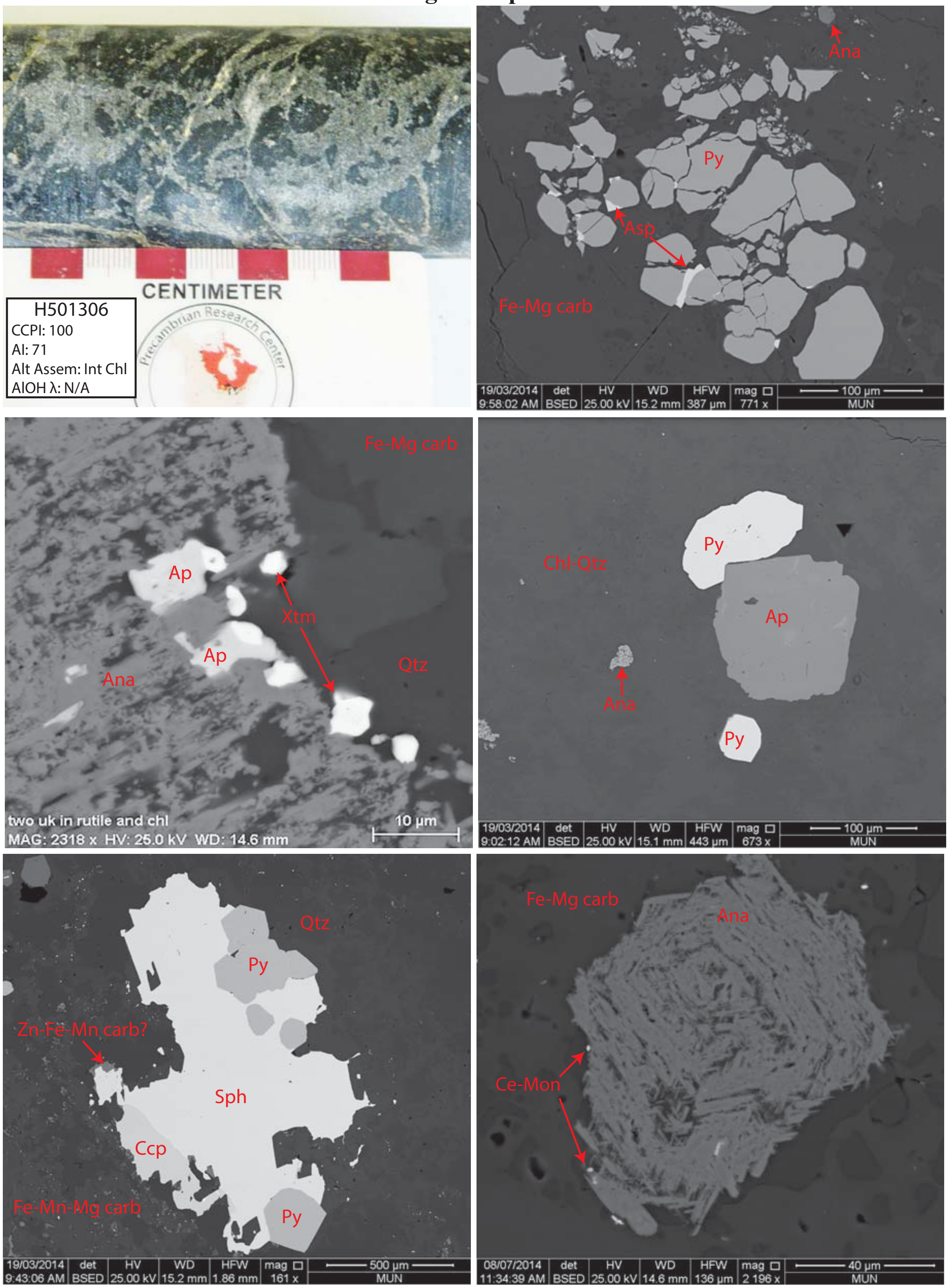

E.1.2 SEM Image Compilation: H501306 Cont.

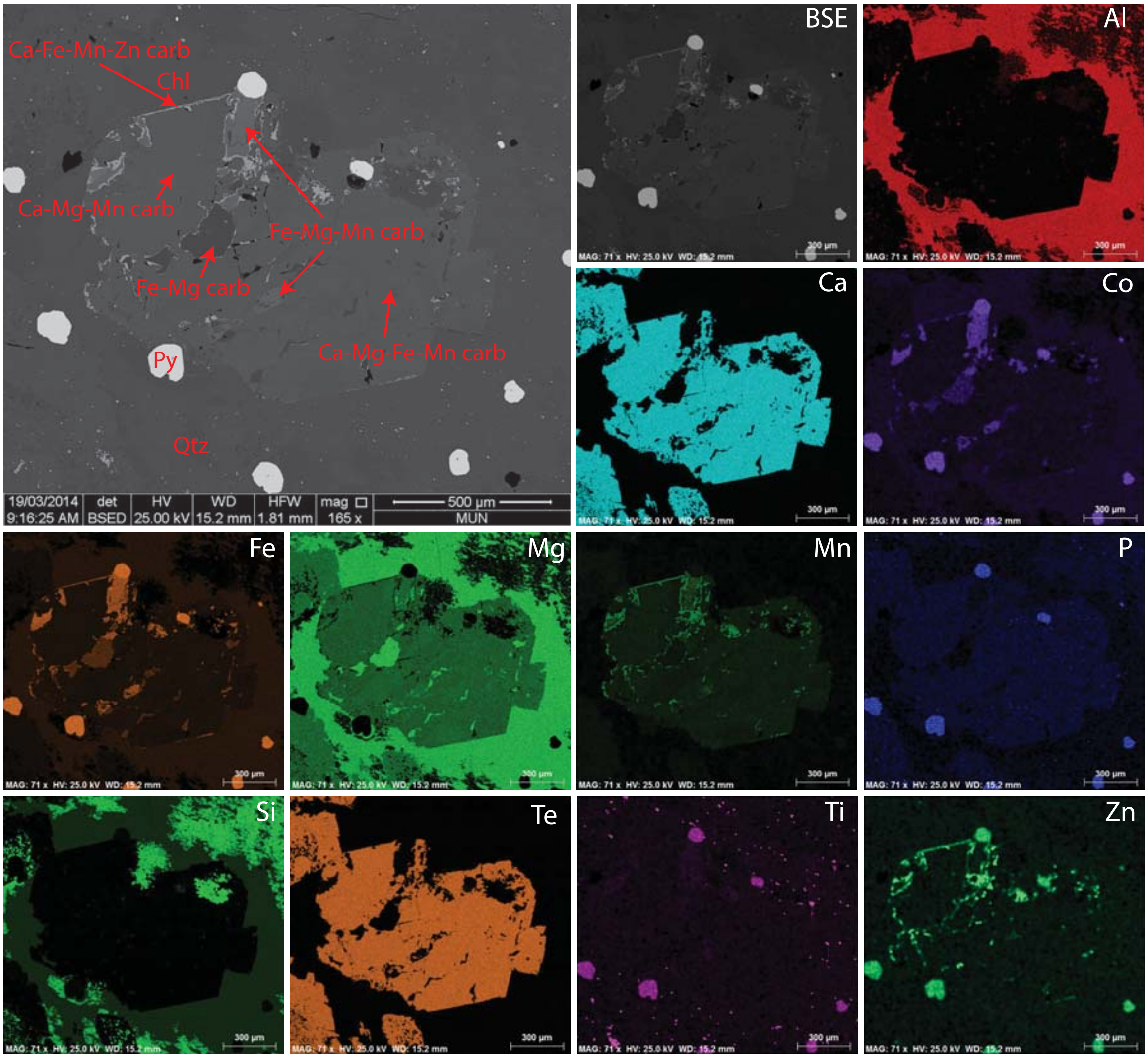

E.1.2 SEM Image Compilation: H501306 Cont.

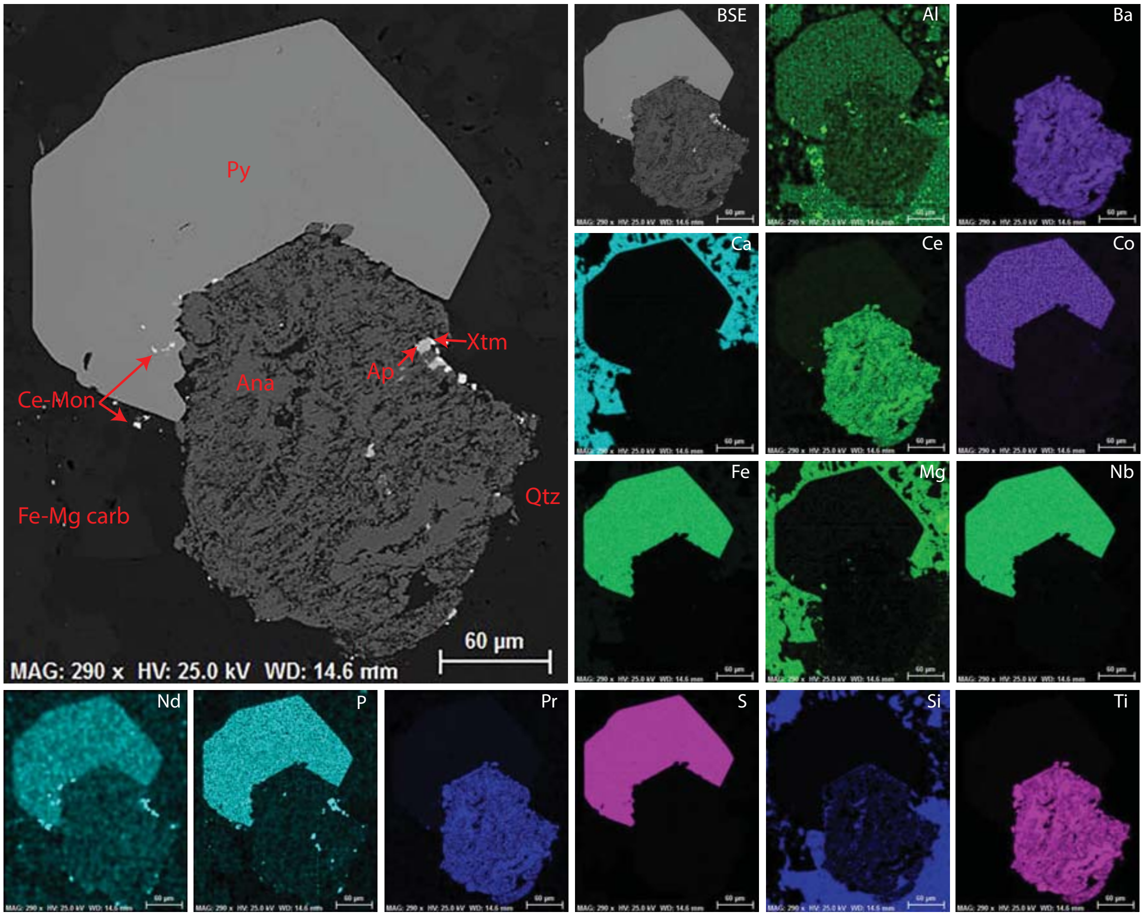

E.1.2 SEM Image Compilation: H501336

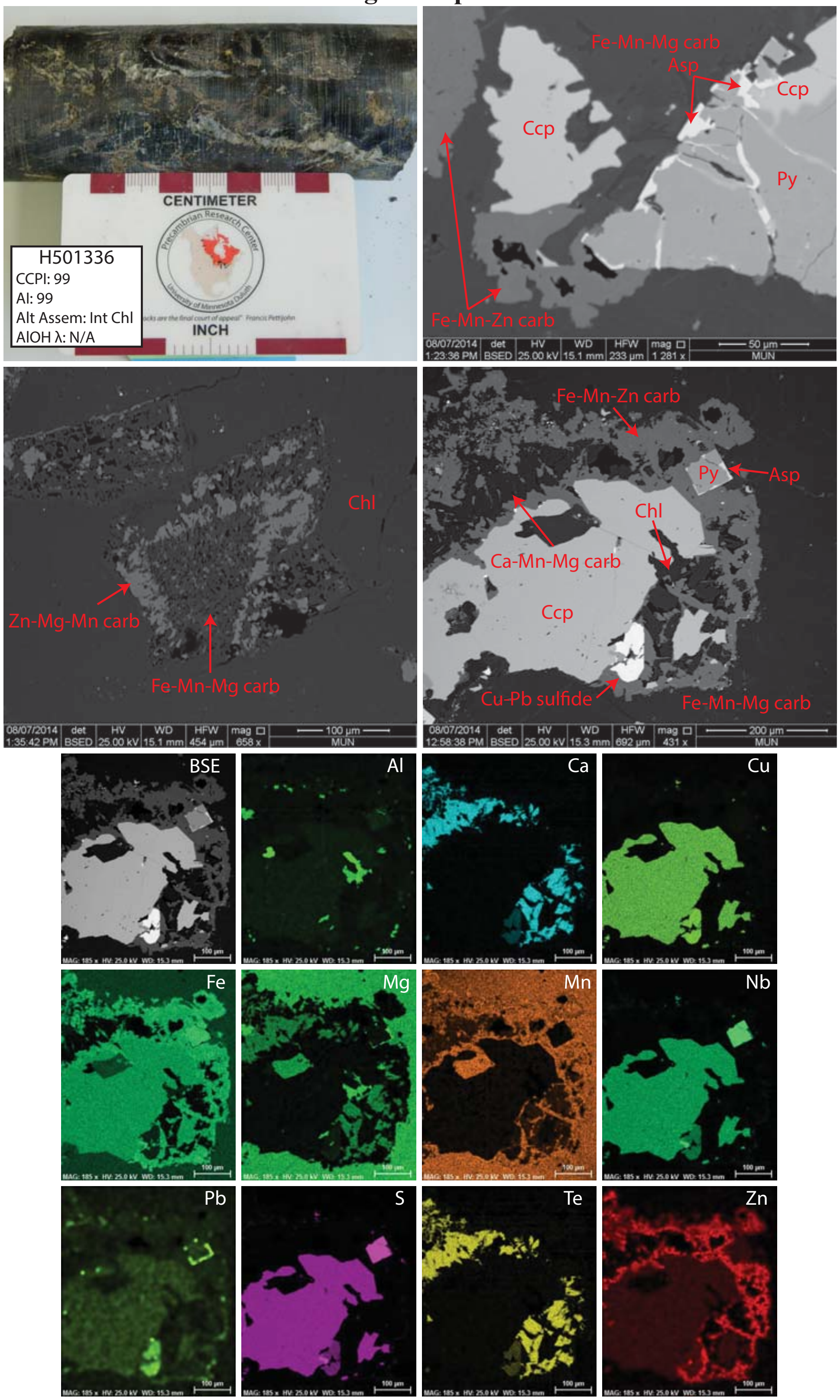

Appendix F.1.1 Chapter 2 Figure 2.19A and 2.19B

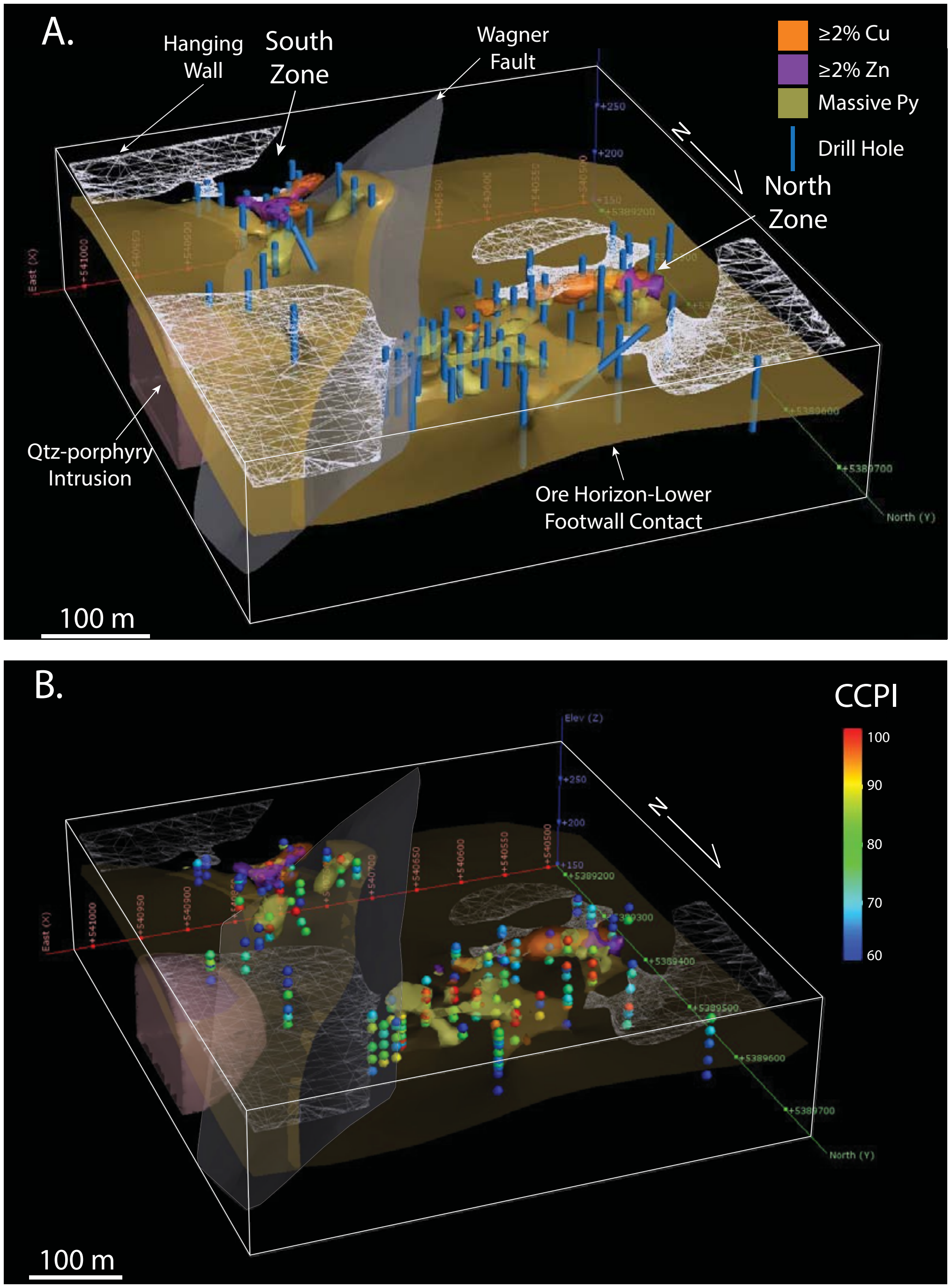

Figure 2.19 Series of 3D models of the Boundary deposit. A) Model showing key lithological contacts, major sulfide zones, and drill holes used to determine alteration extents. Ore zones are defined by assays from additional drill holes not shown. B) Model showing CCPI values in relationship to major ore zones.

Appendix F.1.2 Chapter 2 Figure 2.19C and Figure 2.19D

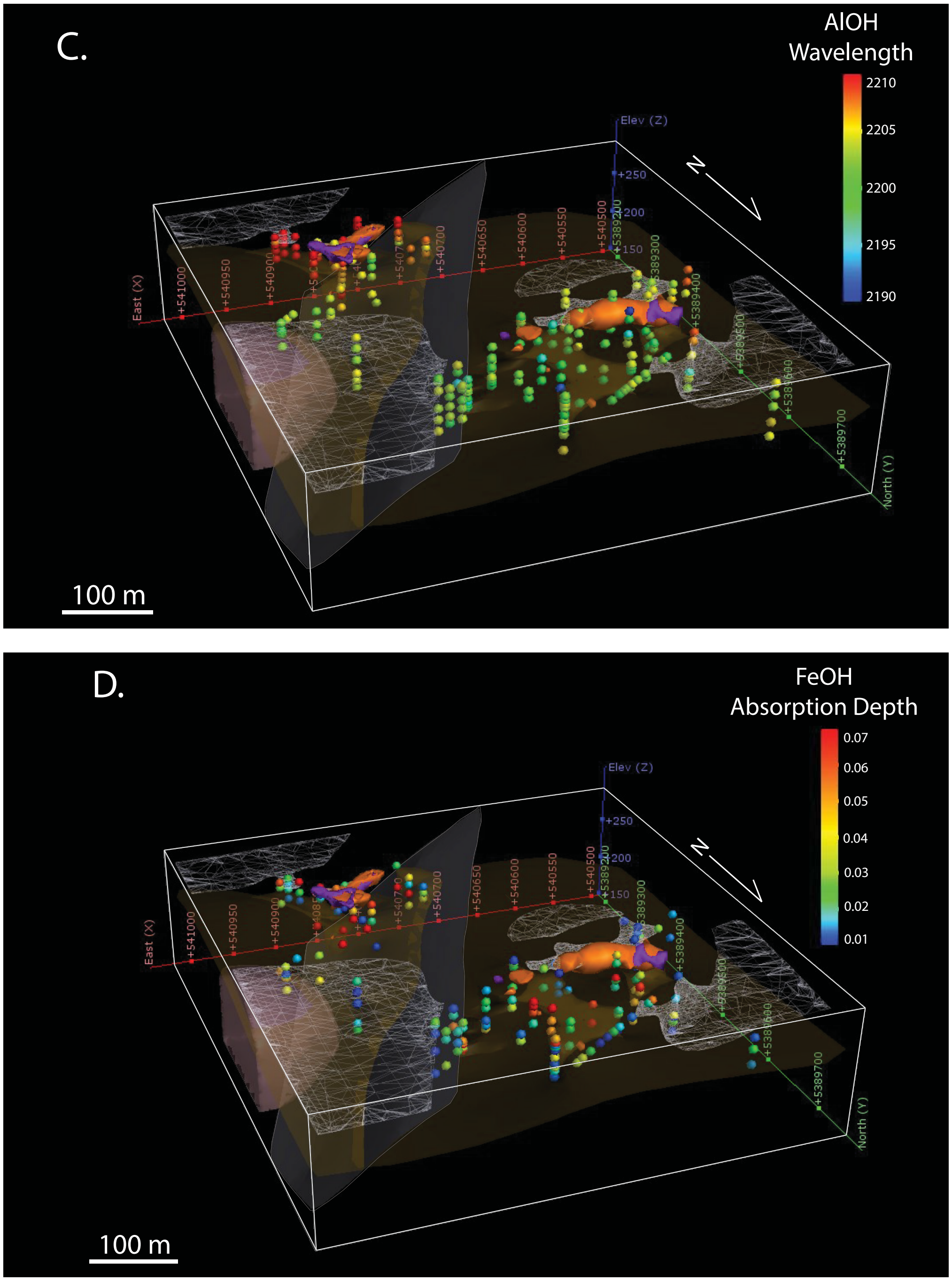

Figure 2.19 Series of 3D models of the Boundary deposit. C) Model showing AlOH wavelengths. Note that wave-lengths are significantly longer in the South zone. Long wavelengths in the North zone only occur on the western end of the deposit. D) Model showing FeOH absorption depth. The higher values occur within the same samples of the high CCPI samples from Figure 19B.

Appendix F.1.3 Chapter 2 Figure 2.19E

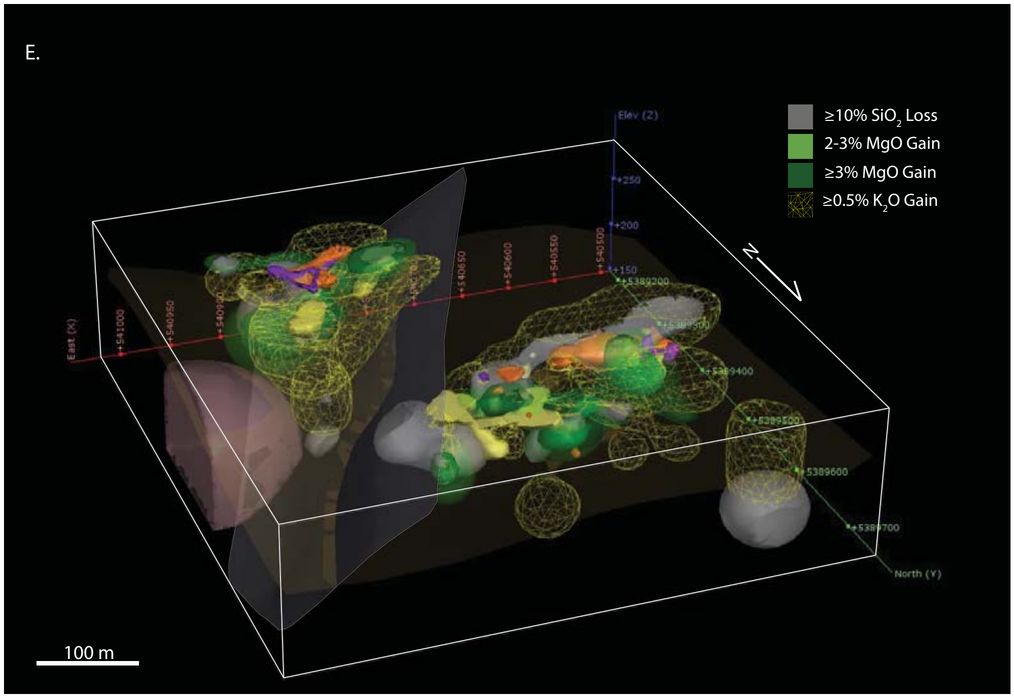

Figure 2.19 Series of 3D models of the Boundary deposit. E) Alteration model of the Boundary deposit based on mass balance changes. The major chlorite gains correlate with the high CCPI values (2.19B) and FeOH absorption values (2.19D).